Investigating mechanisms of sensitivity and resistance to immunomodulatory thalidomide analogues in multiple myeloma

Matteo Costacurta

ORCID: 0000-0003-4605-7427

Doctor of Philosophy

January 2021

Gene Regulation Laboratory
Department of Cancer Research
Peter MacCallum Cancer Centre
The University of Melbourne
Faculty of Medicine, Dentistry and Health Sciences

This thesis is being submitted in total fulfilment of the degree

Abstract

Multiple myeloma (MM) is an incurable plasma cell neoplasm. The incorporation of immunomodulatory imide drugs (IMiDs) – thalidomide, lenalidomide and pomalidomide - into clinical practice has improved survival and quality of life of MM patients. However, most patients develop therapeutic resistance to IMiDs, representing a significant clinical problem. IMiDs exert anti-MM effects by engaging Cereblon (CRBN), a ligand of the E3 ligase complex CUL4-DDB1-RBX1. By binding CRBN, IMiDs promote ubiquitination and proteasomal degradation of important MM cell transcription factors, IKZF1 (Ikaros) and IKZF3 (Aiolos). Degradation of such *neosubstrates* has also been shown to augment an anti-cancer immune response by activation of cytotoxic effector cells against MM plasma cells. Finally, it has been demonstrated that IMiDs modulate events occurring within the bone marrow microenvironment with negative impact on the MM-sustaining niche. Despite these recent advances in the characterisation of IMiD mechanism of action, the precise molecular events underpinning the anti-MM activity of IMiDs remain incompletely understood. Further insight is required to improve clinical responses to IMiDs and overcome therapy resistance in MM.

In this work, genome-wide approaches such as RNA-sequencing and CRISPR-based functional genomics screening were employed to dissect the molecular mechanisms of IMiD-sensitivity and -resistance in models of acquired resistance to lenalidomide. RNA-sequencing revealed a strong interferon-like transcriptional response and increased transcription of genes downstream the MAPK pathway, together with downregulation of MYC-responsive genes, following IMiD treatment of IMiD-sensitive MM cells. Conversely, IMiD-resistant cells displayed reduced transcriptional changes following IMiD exposure as a likely consequence of CRBN downregulation and subsequent attenuation of neosubstrate degradation. Genome-wide CRISPR screening demonstrated that loss of *CRBN* and other genes regulating protein degradation, such as subunits of the COP9 signalosome, but also loss of genes that are not implicated in protein turnover, such as *NCOR1* and *EDC4,* is sufficient to cause resistance to IMiDs in IMiD-sensitive cells. CRIPSR screening also demonstrated that resensitisation of IMiD-resistant cells to IMiDs can occur through loss of *ATXN7*, *TOP2B* and other genes implicated in several distinct biological processes, such as glucose metabolism, cell cycle progression and RNA processing. Dexrazoxane, a pan-TOP2 inhibitor and TOP2B-selective degrader, was discovered to possess anti-proliferative properties and combinatorial activity with lenalidomide in certain MM cell lines.

To develop a deeper understanding of the biology of CRBN and IMiDs, proximity labelling with BioID2 was employed to characterise the interactome of CRBN in the presence and absence of an IMiD. Co-treatment of BioID2-CRBN-expressing OPM2 cells with IMiDs and/or the proteasome inhibitor bortezomib, followed by liquid chromatography mass spectrometry proteomics, allowed identification of known CRBN interactors (COP9 signalosome subunits) and neosubstrates (IKZF1, IKZF3 and CK1α). This approach enabled further characterisation of CRBN-associated proteome and identification of new CRBN and CRBN-IMiD interacting partners, such as MEF2C, DVL1, DVL2, MYH9, PRRC2C and EDC4. This data led to the hypothesis that CRBN may be implicated in several novel biological processes, such as RNA processing and protein translation regulation. Additionally, some of the newly identified interacting partners may modulate the MM niche in the bone marrow and may help understand the occurrence of side effects to IMiD therapy.

This work has further defined transcriptional signatures of IMiD treatment and of acquired IMiD-resistance. TOP2B was found to be a potential druggable vulnerability of MM cells with acquired IMiD-resistance. The unbiased study of the CRBN-interacting proteome has helped broaden the knowledge on its biological activities both in presence and absence of an IMiD. Collectively, this thesis provides new and important insight into IMiD mechanism of action and further expands knowledge of IMiD biology.

Declarations

All the work here presented is original work except when indicated in the text. This thesis is below the maximum word limit for a PhD thesis (100000 words).

This thesis includes some experiments and analyses performed by other members of the Johnstone Laboratory and Dr. Jarrod Sandow (Walter and Eliza Hall Institute, Melbourne).

I would like to thank the following members of the Johnstone Laboratory for their contribution to this work: the Molecular Genomics Core at Peter MacCallum Cancer Centre for performing Next Generation Sequencing experiments; Dr Stephin Vervoort and Dr Simon Hogg for their contribution in Next Generation Sequencing data processing and analysis; Dr Olga Motorna for providing experimental validation of *NCOR1* deleted cells; Mr Benjamin Martin for his help with genome-wide CRISPR screening; Dr Jarrod Sandow for his fundamental contribution with mass spectrometry proteomics experiments; Associate Professor Jake Shortt and Professor Ricky Johnstone for their supervision.

Here I declare that some of the data presented in chapter 3 has been published by me as first author, in collaboration with Dr Stephin Vervoort, Dr Simon Hogg, Mr Benjamin Martin, Prof. Ricky Johnstone and A/Prof. Jake Shortt, on the journal Haematologica. The manuscript has been included in this thesis as an addendum to chapter 3.

The remainder of the experimental and written work in this thesis is my own. None of the work in this thesis has been submitted for other qualification and was all conducted after enrolment in the degree. No third-party editorial assistance was provided in the preparation of this thesis.

The PhD scholarship, the Melbourne Research Scholarship, was awarded to me by the University of Melbourne.

Matteo Costacurta

_____

Publication arising from this thesis

Matteo Costacurta, Stephin J Vervoort, Simon J Hogg, Benjamin P Martin, Ricky W Johnstone, Jake Shortt, Whole genome CRISPR screening identifies TOP2B as a potential target for IMiD sensitization in multiple myeloma, *Haematologica 2020 (In press)*

Acknowledgements

In this journey I have never been alone, and there are so many people I wish to acknowledge for being there with me during my PhD.

To my supervisors **Ricky** and **Jake**, your mentorship and supervision has been terrific over these past four years. I could not be more grateful to you both for your help from even before I applied for the PhD scholarship. You moulded my *forma mentis* as a scientist: teaching me to focus on the important questions was the most valuable lesson I have learnt from you. Thank you for being kind and generous and to always have time to discuss about any issue I would have.

To the Johnstone Lab, past and present members, I would like to let you know how much I have enjoyed these years as your colleague and how much I am grateful to all of you for being always helpful, supportive and very fun and pleasant people to work with.

I wish to thank three brilliant post-docs in the Johnstone Lab: **Jennifer**, **Simon** and **Stephin**. Thank you for always being keen to suggest how to move my research forward. Your presence has been fundamental for the success of my PhD and the development of my scientific thinking. I wish to especially thank **Stephin** – I could never be more thankful to you for teaching me so much. You have played such a big part in my PhD despite not being my direct supervisor – thanks for keeping me into the right direction and being direct when I needed to correct my path. Thank for the support, scientifically and morally speaking. You represent the scientist I want to become in my future: extremely knowledgeable, "addicted" to learning new things and with rock solid integrity.

To my closest friends in the lab – **Emily, Izabela, Lizzy and Stefan** – it has been so much fun with you guys and I feel so lucky to have you, wonderful people, in my life. Our friendship has been growing day by day during these four years, and I hope it lasts forever.

To my Australian family – you all had met me once, before I moved to Australia, but you made me feel like I always belonged here. With you I was never alone - I love you all.
A special thank goes to **Franca**, my Australian mum. Thank you for taking care of me as one of your children. I will never forget everything you have done for me.

To my family in Italy, my mum **Caterina**, my dad **Emiliano**, my brother **Francesco** and my grandparents **Franca**, **Bortolo** and **Alessia**. I would have loved you to be here and celebrate with me one of the greatest achievements of my life. Thanks for the many, many, many video calls at the weirdest times of the day. Thank you for your unconditional love and support. I miss you so much and I wish to be able to celebrate together soon.

To **Kristine**. You are the best partner I could ever ask for and our relationship has been the highlight of my 2020 - I feel so lucky to be sharing my life with you. The amount of love and support I have received from you cannot be measured. Thanks for teaching me how to be persistent in getting to achieve my career goals, thanks for coaching me every day in how to become successful and fulfilled in life. Thanks for always being there and loving me unconditionally.

I wish to dedicate this whole work to my grandfather **Bortolo**, for being the reason I am now a scientist. Thank you for teaching me the beauty of Knowledge.

Abbreviations

ATAC-seq = Assay for Transposase-Accessible Chromatin using sequencing

ATXN7 = Ataxin-7

BFP = Blue Fluorescent Protein

BM = Bone Marrow

BMME = Bone Marrow Microenvironment

BMSC = Bone Marrow Stromal Cell

CD = Cluster of Differentiation

ChIP-seq = Chromatin Immunoprecipitation with sequencing

CK1α = Casein Kinase 1 alpha

CPM = Count Per Million read

CRBN = Cereblon

CRISPR = Clustered Regular Interspaced Palindromic Repeats

CTD = C-Terminal Domain

CTV = CellTrace Violet

CUL4 = Cullin 4

DDB1 = DNA Damage Binding protein 1

DEG = Differentially Expressed Genes

DEP = Differentially Enriched Proteins

dFBS = dialysed Foetal Bovine Serum

DGE = Differential Gene Expression

DMEM = Dulbecco's Modified Eagle Medium

DMSO = Dimethylsulphoxide

DNA = Deoxyribonucleic Acid

DSB = Double Strand Break

DVL = Dishevelled

DXZ = Dexrazoxane

EDC4 = Enhancer Of mRNA Decapping 4

ETO = Etoposide

FACS = Fluorescent Activated Cell Sorting

FBS = Foetal Bovine Serum

FDR = False Discovery Ratio

GFP = Green Fluorescent Protein

GO = Gene Ontology

GSEA = Gene Set Enrichment Analysis

HDAC = Histone Deacetylase

HRP = Horseradish Peroxidase

HSP90 = Heat Shock Protein 90

IBER = Iberdomide

IC50 = Concentration inducing growth inhibition of 505 of cells

IFN = Interferon

IKZF1 = Ikaros

IKZF3 = Aiolos

IMiDs = Immunomodulatory imide Drugs

IRF4 = Interferon Regulatory Factor 4

KO = Knockout

LEN = Lenalidomide

MEF2 = Myocyte Enhancer Factor 2

MM = Multiple Myeloma

MOI = Multiplicity of Infection

MS = Mass Spectrometry

MYC = Myelocytomatosis

MYH9 = Non-Muscle Myosin Heavy Chain 9

NCOR1 = Nuclear Coreceptor Repressor 1

NER = Nucleotide Excision Repair

NES = Normalised Enrichment Score

nRLE = normalised Relative Log2 Expression

NTD = N-Terminal Domain

ORF = Open Reading Frame

OS = Overall Survival

PBS = Phosphate Buffer Saline

PC = Plasma Cell

PCR = Polymerase Chain Reaction

PI = Propidium Iodide

POM = Pomalidomide

PPI = Protein-Protein Interaction

PRRC2C = Proline Rich Coiled-Coil 2C

RAS = Rat Sarcoma

RBX1 = Ring-Box 1

RIPA = Radioimmunoprecipiation Assay

RNA = Ribonucleic Acid

RPMI-1640 (cell culture medium) = Roswell Park Memorial Institute - 1640

SE = Superenhancer

sgRNA = short guide RNA

SLAM-seq = Thiol(SH)–linked alkylation for the metabolic sequencing of RNA

TBD = Thalidomide Binding Domain

TF = Transcription Factor

TIDE = Tracking of Indel Decomposition

TOP2 = DNA Topoisomerase II

Ub = Ubiquitin

ZIP = Zero Interaction Potency

Table of Contents

Chapter 1: Literature review 25

1.1. Multiple Myeloma 26

1.1.1. Definition and epidemiology 26

1.1.2. Aetiology and risk factors 26

1.1.3. Clinical history and presentation of multiple myeloma 26

1.1.3.1 Paraprotein behaviour in multiple myeloma 27

1.1.3.2 Multiple myeloma is a multistep disease 27

1.1.3.3 Risk stratification of myeloma patients 27

1.1.3.4 Clinical presentation of end-organ damage in multiple myeloma 28

1.1.3.5 Other types of plasma cell malignancy 28

1.1.3.5.1 Extramedullary Myeloma 28

1.1.3.5.2 Plasma cell leukemia 29

1.1.3.5.3 Solitary plasmacytoma 29

1.1.3.5.4 AL amyloidosis 29

1.1.4 Pathogenesis of multiple myeloma 29

1.1.4.1 Cell of origin: the malignant plasma cell 29

1.1.4.1.1 From haematopoietic stem cells (HSC) to mature B-cells 30

1.1.4.1.2 Antigen encountering and B-cell maturation into memory B-cells or antibody-secreting plasma cells 30

1.1.4.1.3 *IRF4*, *PRDM1* and *XBP1* as master regulators of plasma cell differentiation and antibody secretion 31

1.1.4.2 The transcription factors Ikaros (IKZF1) and Aiolos (IKZF3) in the lymphoid lineage 31

1.1.4.2.1 The structure of IKZF transcription factors 31

1.1.4.2.2 The double activity of IKZF1/3-mediated transcriptional regulation 32

1.1.4.2.3 IKZF1 and IKZF3 in the lymphoid lineage development 32

1.1.4.2.4 IKZF1 and IKZF3 as regulators of the T-cell response 33

1.1.4.2.5 IKZF1 and IKZF3 in mature B-cells and PCs 33

1.1.4.3 Molecular pathogenesis of multiple myeloma 34

1.1.4.3.1 Disease initiation in multiple myeloma 34

1.1.4.3.2 *IRF4* addiction in multiple myeloma 35

1.1.4.3.3 The *MYC* gene is dysregulated in multiple myeloma 35

1.1.4.4 Molecular Classification of Multiple Myeloma 36

1.1.4.5 Genetic abnormalities and disease progression 37

1.1.4.6 Multiple Myeloma and the Microenvironment 39

1.1.5 Treatment of Multiple Myeloma 41

1.1.5.1 Eligibility to stem cell transplantation defines the initial strategy in tackling MM 41

1.1.5.2 Novel compounds: immunomodulatory thalidomide analogues and proteasome inhibitors 41

1.1.5.3 Other therapies 42

1.1.5.3.1 Monoclonal antibodies 42

1.1.5.3.2 Small-molecule inhibitors 42

1.1.5.3.3 Cellular therapies 43
1.2. The Immunomodulatory imide drugs, IMiDs, in multiple myeloma 44
1.2.1 The impact of IMiDs in the therapy of multiple myeloma 44
1.2.1.1 A snapshot of the pre-thalidomide era and the advent of thalidomide 44
1.2.1.2 Thalidomide and its analogues 44
1.2.1.3 Toxicity profile of immunomodulatory drugs 45
1.2.2 Mechanism of action of IMiDs 45
1.2.2.1 IMiDs and MM pathobiology 46
1.2.2.2 Cereblon is an IMiD target 47
1.2.2.3 Expression of CRBN predicts response to IMiD treatment 48
1.2.2.4 The discovery of CRBN neosubstrates 51
1.2.2.4.1 The biochemistry of ubiquitin and protein degradation 51
1.2.2.4.2 IMiDs induce CRBN-mediated degradation of Ikaros and Aiolos to mediate anti-myeloma effect 51
1.2.2.4.3 Lenalidomide-induced degradation of CK1α in 5q- refractory anaemia 52
1.2.2.4.4 IMiDs disrupt the CRBN chaperone-like activity on MCT1-CD147 55
1.2.2.5 Structural insight into the engagement of neosubstrates by the CRBN complex 55
1.2.2.5.1 The structure of IMiDs and CRBN in complex with CUL4-DDB1-RBX1 55
1.2.2.5.2 The thalidomide binding pocket of CRBN and the interaction with neosubstrates 57
1.2.2.5.3 Novel murine models for the study of IMiDs *in vivo* 57
1.2.2.6 A complex machinery is required for IMiD-dependent degradation of CRBN neosubstrates 58
1.2.2.6.1 The COP9 Signalosome 58
1.2.2.6.2 A continuous assembly/disassembly cycle of CUL4-DDB1-RBX1-CRBN is required for efficient protein degradation of CRBN substrates and neosubstrates 59
1.2.2.6.3 The COP9 signalosome prevents CUL1-SCF^{Fbox1}-dependent CRBN degradation 59
1.3 Hypotheses and aims 61
Chapter 2: Materials and methods 63
2.1 Cell culture techniques 64
2.1.1 Cell lines and culture methods 64
2.1.2 Preparation of cell culture dishes for proteomics assays 64
2.1.3 Viral transduction 65
2.1.3.1 Generation of MM.1S-Cas9 and MM.1Sres-Cas9 FgH1T-UTG cells 66
2.1.4 Dialysis of Foetal Bovine Serum 66
2.2 Cell death and cell proliferation assays 66
2.2.1 Anti-cancer agents 66
2.2.2 CellTrace™ Violet – propidium iodide proliferation assay 67
2.2.3 DNA content/Cell cycle analysis with Nicoletti staining 67
2.2.4 Cell death assay with propidium iodide 67
2.2.5 Lenalidomide-dexrazoxane synergy assays 68
2.2.6 Competitive proliferation assays 68

2.3 Protein techniques 68
2.3.1 Cell lysis 68
2.3.1.1 Lysis in RIPA 69
2.3.1.2 Lysis in Laemmli (solubilisation of chromatin-bound proteins) 69
2.3.2 Quantification of sample protein concentration 69
2.3.3 Western Blotting 70
2.3.3.1 Western blotting antibodies 70
2.3.3.2 Western Blotting Sample Preparation 70
2.3.3.3 Western Blotting 71
2.3.4 Enrichment of biotinylated proteins 71
2.3.4.1 Sample preparation for Mass Spectrometry 71
2.3.4.2 Sample preparation for Western blotting 72
2.3.5 Liquid Chromatography – Mass Spectrometry (LC-MS/MS) 72
2.3.6 Peptide Database Search 73
2.3.7 Statistical analysis of proteomics data 73
2.4 Molecular Biology Techniques 73
2.4.1 Generation of MM.1S CRBN KO cells via electroporation of ribonucleocomplexes 73
2.4.2. Cloning of sgRNAs into *FgH1T-UTG* vector for inducible gene knockout via CRISPR/Cas9 74
2.4.2.1 Preparation of agarose gel for DNA electrophoresis 74
2.4.2.2 Digestion of *FgH1T-UTG-GFP* vector 74
2.4.2.3 Cloning of sgRNAs into *FgH1T-UTG* using single strand DNA oligos 75
2.4.2.4 Bacterial Transformation 75
2.4.2.5 Starting culture, minipreps and sequencing validation 76
2.4.3 Cloning of *CRBN* ORF into the *pBABE-mycBioID2-puroR* vector via Gibson assembly 76
2.4.3.1 Gibson assembly reaction preparation and performance 76
2.4.3.2 Validation of successful assembly via colony PCR 76
2.4.4 Preparation of PCR products for validation of *ATXN7* deletion with TIDE 77
2.5 Next Generation Sequencing (NGS) techniques 78
2.5.1 3'-RNA sequencing 78
2.5.2 Genome-wide CRISPR knockout screening 78
2.5.2.1 Generation of viral library 78
2.5.2.2 Generation of Cas9-expressing MM.1S lines 79
2.5.2.3 Assessment of transduction efficiency of viral library 79
2.5.2.4 Bulk cell transduction with Brunello human viral sgRNA library for genome-scale CRISPR KO screens 79
2.5.2.5 CRISPR Screening for drug resistance or re-sensitisation 80
2.5.2.6 Sequencing library preparation 80
2.5.2.7 Clean-up of libraries for sequencing 81
2.5.2.8 Sequencing and data analysis 81
2.6 Software and webtools 81

Chapter 3: transcriptome analysis and CRISPR screening for the identification of transcriptional signatures and genetic vulnerabilities of multiple myeloma in the context of IMiD sensitivity and resistance 82

3.1 Introduction 83

3.1.1 Background 83

3.1.2 Aims 84

3.2 Results 84

3.2.1 MM.1S/MM.1Sres and U266/U266res cells are models of acquired *in vitro* lenalidomide resistance 84

3.2.2 Transcriptional characterisation of MM.1S and U266 isogenic cell line pairs in presence and absence of IMiD treatment 88

3.2.2.1 Induction of interferon signalling and suppression of MYC target genes as transcriptional response following acute exposure to IMiD 93

3.2.2.2 Interferon, MAP kinase and MYC signatures are perturbed in cells with acquired lenalidomide resistance 94

3.2.2.3 Global attenuation of transcriptional response following IMiD treatment in IMiD-resistant cells correlates with *CRBN* downregulation 103

3.2.2.3.1 Analysis of the transcriptional response to IMiDs in U266/U266res and MM.1S/MM.1Sres isogenic cell line pairs 103

3.2.2.3.2 mRNA expression of *CRBN*, *CUL4*, *DDB1* and *RBX1* in in U266/U266res and MM.1S/MM.1Sres isogenic cell line pairs 104

3.2.3 Statistical correlation studies between the transcriptional responses to IMiDs in MM.1S/MM.1Sres and U266/U266res 106

3.2.3.1 Genes implicated in IFN- and cell-to-cell signalling are differentially expressed in both MM.1Sres and U266res 111

3.2.3.2 Pearson's correlation testing defines the levels of similarity in the response to IMiDs in isogenic cell line pairs U266/U266res and MM.1S/MM.1Sres 111

3.2.4 Genome-wide CRISPR screening identifies genes that are essential for the response to IMiDs 118

3.2.4.1 The gain-of-representation CRISPR screen workflow in IMiD-treated MM.1S cells 118

3.2.4.2 Defining the dependency of MM.1S cells on the *IKZF1/3-IRF4-MYC* axis 118

3.2.4.3 Defining the factors required for IMiD sensitivity 121

3.2.4.4 Validation of the IMiD-resistant phenotype induced by loss of *NCOR1* 125

3.2.5 Genome-wide CRISPR dropout screening defines genes limiting the response to IMiDs. 125

3.2.5.1 MM.1Sres cells are sensitive to deletion of *IKZF1/3, IRF4* and *MYC* despite prolonged treatment with IMiDs 126

3.2.5.2 The sensitivity of MM.1S cells to gene loss does not markedly change following continuous LEN treatment and acquired LEN-resistance 126

3.2.5.3 Defining factors of additional resistance to IMiDs 131

3.2.5.4 Defining IMiD-resensitisation factors in MM.1Sres cells 131

3.2.5.4.1. Genes and pathways limiting IMiD activity 131
3.2.5.4.2. Interference with DNA homeostasis as possible mechanism of resensitisation to IMiDs 135
3.2.5.5 Loss of TOP2B and ATXN7 results in synthetic lethality with IMiDs in MM.1Sres cells... 135
3.2.5.5.1 Validation of *TOP2B* and *ATXN7* deletion 138
3.2.5.5.2 Validation of *ATXN7*- and *TOP2B*-mediated resensitisation of MM.1Sres cells to IMiD treatment 138
3.2.5.5.3 *TOP2B* loss resensitises MM.1Sres cells to IMiDs via a CRBN-independent mechanism 139
3.2.6 Resensitisation of MM.1Sres cells to IMiDs is likely independent of DNA damage..... 139
3.2.6.1 Induction of p53 transcriptional signatures by lenalidomide is independent of DNA damage..... 140
3.2.6.2 The activity of lenalidomide in combination with the TOP2 poison etoposide 143
3.2.7 The cardioprotective agent dexrazoxane is a TOP2 inhibitor, TOP2B degrader, and exerts anti-MM activity 143
3.2.7.1 Kinetics of dexrazoxane-induced TOP2B degradation 145
3.2.7.2 TOP2B degradation by dexrazoxane is independent of CRBN expression 145
3.2.8 Characterisation of dexrazoxane activity as single agent and in combination with lenalidomide 146
3.2.8.1 Dexrazoxane interferes with cell cycle progression and causes apoptosis in MM cells.. 146
3.2.8.2 The activity of dexrazoxane in combination with lenalidomide in MM.1S cells 152
3.2.8.3 The activity of dexrazoxane in combination with lenalidomide on the IKZF1/3-IRF4-MYC axis 152
3.2.8.4 The activity of dexrazoxane in combination with lenalidomide on MM cells proliferation 152
3.2.8.5 Combinatorial effects of dexrazoxane and lenalidomide in MM cell lines OPM2, RPMI-8226 and JJN3..... 156
3.3 Discussion 156
3.3.1 Neosubstrate degradation and sensitivity to IMiDs highly correlate with CRBN expression 156
3.3.2 The magnitude of transcriptional response to IMiD correlates with CRBN expression.... 158
3.3.3 Correlating the transcriptional response to different IMiDs in isogenic sensitive/resistant MM cell lines..... 159
3.3.3.1 Correlation studies reveal similarities in the transcriptional response to IMiDs despite baseline discrepancies between MM.1S and U266 cell lines..... 160
3.3.3.2 The impact of *CRBN* downregulation in the transcriptional response IMiDs in resistant cells..... 161
3.3.4 Transcriptional regulators and DNA repair genes as novel players in IMiD mechanism of action 162
3.3.4.1 Continuous IMiD exposure could increase genomic instability..... 163
3.3.4.2 Bridging TOP2B- and NCOR1-dependent transcriptional regulation to the activity of IKZF1/3 164

3.3.5 TOP2 inhibition as potentially novel MM therapeutic approach in combination with IMiDs 165
3.3.5.1 IMiD treatment and the perturbation of DNA homeostasis: still an open question 166
3.3.5.2 Considerations upon employment of dexrazoxane in the treatment of MM 167
3.3.6 Concluding remarks 168
Addendum to chapter 3: publication in Haematologica 169
Chapter 4: Investigating the CRBN interactome via BioID2-dependent proximity labelling . 188
4.1 Introduction 189
4.1.1 Background 189
4.1.2 Aims 191
4.2 Results 191
4.2.1 Experimental planning for the generation of a chimeric BioID2-CRBN fusion protein 191
4.2.2 BioID2 induces biotinylation of proteins 194
4.2.3 Preparation of PCR products for Gibson assembly of mycBioID2-CRBN 196
4.2.4 Gibson assembly of mycBioID2 and CRBN 196
4.2.5 Validation of protein expression of mycBioID2-CRBN 200
4.2.6 Fusion of CRBN with mycBioID2 reduces promiscuous biotinylating activity of BioID2 ... 201
4.2.7 Basal BioID2 activity is strongly reduced in cells cultured with biotin-depleted media ... 202
4.2.8 Validation of biotinyl-proteome enrichment protocol using surrogate myctag detection: BioID2 undergoes self-biotinylation 205
4.2.9 Liquid Chromatography - Mass Spectrometry Proteomics of biotinyl-protein enrichment 208
4.2.10 Generation of OPM2 cells expressing mycBioID2 and mycBioID2-CRBN and optimisation of culturing conditions for MS proteomics 211
4.2.11 Mass Spectrometry Proteomics of biotinyl-protein enrichment in OPM2-BioID2-CRBN cells (Experiment 1) 216
4.2.12 Generation of IKZF similarity score to define *neosubstrate-like* protein enrichment profiles 217
4.2.12.1 Identification of putative neosubstrates that are essential for viability and proliferation of MM cells 221
4.2.12.2 The transcription factor MEF2C is a CRBN-IMiD *neointeractor* 227
4.2.13 The study of the CRBN interactome in the context of treatment with different IMiDs (Experiment 2) 227
4.2.13.1 Detection of putative neosubstrates IKZF1 and CK1α occurs in cells treated with any BORT/IMiD combination 230
4.2.13.2 Correlative studies and data clustering define sources of variability and identify similarities in the CRBN interactome across treatment conditions 230

4.2.14 BioID2-CRBN induces biotinylation of proteins involved in RNA processing, protein translation and cell motility 231
4.2.15 Dishevelled proteins are putative CRBN interactors and Myosin-9 is a putative neosubstrate for CRBN ubiquitination 245
4.2.16 PRRC2C scores as potential CRBN neosubstrate suggesting that CRBN might regulate stress granule formation 252
4.3 Discussion 255
4.3.1 Rationale for the study of IMiD-dependent modulation of CRBN interactome 255
4.3.2 Development and optimisation of experimental conditions for BioID2-CRBN MS proteomics 256
4.3.3 The BioID2-CRBN system and identification of *bona fide* and novel CRBN-binding proteins 258
4.3.3.1 Considerations on CRBN overexpression and bortezomib toxicity 258
4.3.3.2 Experimental quality control, contaminants and caveats of proteomics datasets analysis 260
4.3.3.3 MEF2C is a novel CRBN *neointeractor* 261
4.3.4 CRBN is a potential regulator of cell migration, RNA processivity and protein homeostasis 262
4.3.4.1 Bortezomib is a major determinant in modulating the CRBN interactome 263
4.3.4.2 EDC4, a lenalidomide sensitivity factor, is a putative CRBN interactor 265
4.3.4.3 CRBN is a potential modulator of events occurring in the MM niche and might be implicated in the occurrence of side effects of IMiD therapy 265
4.3.4.4 The putative CRBN neosubstrate PRRC2C and stress granules 266
4.3.4 Concluding remarks 267
Chapter 5: Discussion 268
5.1 From “Immune-modulating” to “E3 ligase-modulating” drugs 269
5.2 IMiDs: more than just IKZ1, IKZF3, IRF4 and MYC 269
5.3 Technical limitations of *in vitro* models of acquired IMiD resistance 270
5.4. IMiDs, TOP2B and DNA homeostasis 272
5.5. IMiDs potentially affect multiple pathways by modulating CRBN activity in a global fashion 273
5.5.1 Introducing the concept of “transcriptional resistance” to IMiDs 275
5.5.2 Proximity labelling indicates CRBN as possible regulator of RNA processing 275
5.5.3. Novel CRBN interactors and substrates could be associated with PC dynamics and changes within the bone marrow microenvironment 276
5.6 Conclusion 278
Appendix 1: Tables of differentially expressed genes in RNA-seq experiments 280
A1.1 Top 100 differentially expressed genes in U266res vs U266 cells 281

A1.2 Top 100 differentially expressed genes in LEN-treated vs DMSO-treated U266 cells..... 284
A1.3 Top 100 differentially expressed genes in POM-treated vs DMSO-treated U266 cells.... 287
A1.4 Top 100 differentially expressed genes in LEN-treated vs DMSO-treated U266res cells. 290
A1.5 Top 100 differentially expressed genes in LEN-treated vs DMSO-treated U266res cells. 293
A1.6 Top 100 differentially expressed genes in MM.1Sres vs MM.1S cells..... 296
A1.7 Top 100 differentially expressed genes in LEN-treated vs DMSO-treated MM.1S cells... 299
A1.8 Top 100 differentially expressed genes in POM-treated vs DMSO-treated MM.1S cells. 302
A1.9 Top 100 differentially expressed genes in LEN-treated vs DMSO-treated MM.1Sres cells 305
A1.10 Top 100 differentially expressed genes in POM-treated vs DMSO-treated MM.1Sres cells 308
Appendix 2: Tables of gene fold-change in MM.1S and MM.1Sres cells CRISPR screens 311
A2.1: Tables of top 50 enriched and top 50 depleted genes in DMSO-treated MM.1S cells at T-End vs MM.1S cells at T-0 312
A2.2. Tables of top 50 enriched and top 50 depleted genes in LEN-treated vs DMSO-treated MM.1S cells at T-End 315
A2.3. Tables of top 50 enriched and top 50 depleted genes in POM-treated vs DMSO-treated MM.1S cells at T-End 318
A2.4: Tables of top 50 enriched and top 50 depleted genes in DMSO-treated MM.1Sres cells at T-End vs MM.1Sres cells at T-0 321
A2.5. Tables of top 50 enriched and top 50 depleted genes in LEN-treated vs DMSO-treated MM.1Sres cells at T-End 324
A2.6. Tables of top 50 enriched and top 50 depleted genes in POM-treated vs DMSO-treated MM.1Sres cells at T-End 327
Appendix 3: Tables of significantly enriched proteins in proteomics assays 330
A3.1 Significantly enriched proteins in HEK293T BioID2-CRBN expressing cells vs HEK293T BioID2 expressing cells 331
A3.2 Significantly enriched proteins in OPM2-BioID2-CRBN (Experiment 1) 333
A3.3 Significantly enriched proteins in OPM2-BioID2-CRBN (Experiment 2) 335
References 338

Table of figures

Figure 1.1	Genetic abnormalities and multistep pathogenesis of Multiple Myeloma	40
Figure 1.2	Biochemistry of protein ubiquitination and degradation	49
Figure 1.3	A basic model for the mechanism of action of IMiDs in MM	53
Figure 1.4	Structure of immunomodulatory drugs (IMiDs).	56
Figure 3.1	MM.1Sres and U266res cells are refractory to IMiD treatment.	85
Figure 3.2	Transcriptional response to IMiDs in U266 cells	89
Figure 3.3	Transcriptional response to IMiDs in MM.1S cells	91
Figure 3.4	Transcriptional profiling of U266 and U266res cells	95
Figure 3.5	Transcriptional profiling of MM.1S and MM.1Sres cells	97
Figure 3.6	Differential gene expression in LEN resistant MM cells upon IMiD treatment	99
Figure 3.7	GSEA of transcriptional response in U266res cells	101
Figure 3.8	GSEA of transcriptional response in MM.1Sres cells	102
Figure 3.9	Differential Gene Expression of the CRBN E3 ligase complex in LEN sensitive and resistant cells	105
Figure 3.10	Overlap of differentially expressed genes between U266res and MM.1Sres	107
Figure 3.11	Overlap of genes upregulated and downregulated between cells treated with IMiDs	109
Figure 3.12	Correlation analysis of the transcriptional response between LEN and POM in U266 and MM.1S lines	112
Figure 3.13	Correlation analysis of the transcriptional response between U266 and MM.1S in the same treatment conditions	113
Figure 3.14	Correlation analysis of the transcriptional response between isogenic pairs in the same condition	115
Figure 3.15	Genome-wide CRISPR resistance screening identifies genes required for IMiD sensitivity	117
Figure 3.16	Analysis of the pathways and genes involved in sensitivity to IMiDs	119
Figure 3.17	Loss of NCOR1 causes resistance to IMiDs	122

Figure 3.18 CRISPR dropout screening detects sgRNAs capable of restoring IMiD sensitivity 124
Figure 3.19 Protein-Protein interaction network of unique MM.1S and MM.1Sres dependencies 127
Figure 3.20 Gene Ontology terms of unique and mutual MM.1S and MM.1Sres dependencies 128
Figure 3.21 Detection of sgRNA causing additional IMiD-resistance or resensitisation to IMiDs 130
Figure 3.22 Loss of genes TOP2B and ATXN7 resensitises MM.1Sres cells to IMiDs 132
Figure 3.23 Validation of ATXN7 and TOP2B deletion. Loss of TOP2B does not affect CRBN expression 133
Figure 3.24 Competitive proliferation assays validates loss of TOP2B and ATXN7 as IMiDs re-sensitisation factors in MM.1S cell lines 136
Figure 3.25 IMiD treatment increases p53 and ionizing radiation induced transcriptional response without synergizing with DNA damaging agents 141
Figure 3.26 Dexrazoxane induces MM cell death and TOP2B degradation by a CRBN- independent mechanism 144
Figure 3.27 DNA content analysis with Nicoletti Staining 147
Figure 3.28 Consequences of LEN and DXZ exposure on cell cycle phases in MM.1S lines 148
Figure 3.29 Phenotypical and biochemical dissection of synergy between LEN and DXZ in MM.1S lines 150
Figure 3.30 Dexrazoxane elicits anti-proliferative effect in sensitive and resistant MM cell lines 153
Figure 3.31 Dexrazoxane elicits pro-apoptotic effect in IMiD sensitive and resistant MM cell lines 154
Figure 4.1 Experimental planning for the employment of BioID2 in the characterisation of CRBN interactome 192
Figure 4.2 Testing of pBABE-mycBIoID2-puroR expression and functionality in HEK293T cells 195
Figure 4.3 Gibson Assembly of mycBioID2-CRBN (1) 197
Figure 4.4 Gibson Assembly of mycBioID2-CRBN (2) 199

Figure 4.5 Validation and optimisation of BioID2-CRBN activity in HEK293T cells 203
Figure 4.6 MS proteomics validation of mycBioID2-CRBN biotinylating activity 206
Figure 4.7 Generation and optimisation of OPM2-BioID2 and OPM2-BioID2-CRBN cells 209
Figure 4.8 MS proteomics validation of BioID2-CRBN activity in OPM2-BioID2-CRBN cells 213
Figure 4.9 PPI networking of CRBN interactome 215
Figure 4.10 Differentially expressed proteins in LEN only and combo-treated OPM2-BioID2- CRBN 218
Figure 4.11 IKZF-similarity profiling of purified proteins across different conditions 219
Figure 4.12 Identification of IKZF-similar MM dependencies 222
Figure 4.13 DepMap repository data of MEF2C in MM and non-MM cancer cell lines 223
Figure 4.14 Validation of MEF2C as IMiD neointeractor or neosubstrate 224
Figure 4.15 MS proteomics of OPM2-BioID2-CRBN cells with three different IMiDs 228
Figure 4.16 IKZF1, CK1a and EDC4 z_norm plots 232
Figure 4.17 Analysis of variance and correlation across different treatment conditions 234
Figure 4.18 Proteins enriched in presence of bortezomib 236
Figure 4.19 PPI and GO analyses of proteins enriched upon bortezomib treatment 238
Figure 4.20 Proteins losing interaction with CRBN following BORT or IMiD exposure 239
Figure 4.21 Proteins with increased interaction with CRBN upon IMiD treatment 241
Figure 4.22 PPI and GO analyses of mutual CRBN interactors between the two experiments performed in OPM2-BioID2-CRBN cells 243
Figure 4.23 Dishevelled proteins are CRBN interactors 246
Figure 4.24 MYH9 is a CRBN-IMiD neointeractor and neosubstrate for ubiquitination 248

Figure 4.25 LEN treatment of MM.1S cells induces ubiquitination of MYH9 250
Figure 4.26 IKZF similarity profiling identifies PRRC2C as putative CRBN-IMiD neosubstrate 253
Figure 5.1 New proposed model for IMiD-related perturbation of CRBN activity. 274

Table of tables

Table 1.1	Molecular classification of cytogenetic aberrations in MM	38
Table 2.1	Table of cell lines derived from parental MM cell lines via viral transduction	64
Table 2.2	Table of the anti-cancer compounds employed	66
Table 2.3	Composition of lysis buffers	69
Table 2.4	Table of antibodies used for Immunoblotting	70
Table 2.5	Composition of Solutions 1 and 2 for delivery of ribonucleocomplexes via electroporation of cells	74
Table 2.6	sgRNAs employed for validation of CRISPR dropout screen	75
Table 2.7	Gibson Reaction protocol (*FgH1T-UTG*)	75
Table 2.8	Gibson Reaction protocol (*pBABE-mycBioID2-puroR*)	76
Table 2.9	PCR primers employed for amplifications of regions targeted by sgATXN7 #1 and #4	77
Table 2.10	Polymerase Chain Reaction protocol for preparation of sequencing libraries	80
Table 2.11	Thermal cycling conditions for library preparation PCR	80

Chapter 1: Literature review

1.1. Multiple Myeloma

1.1.1. Definition and epidemiology

Multiple myeloma (MM) is a malignant disorder of the plasma cell (PC) that develops within the bone marrow microenvironment and is associated with multiorgan disfunction. MM represents 1% of all cancers and it is the second most frequent haematological malignancy after non-Hodgkin Lymphomas (NHL)[1]. MM is a disease of the elderly (median age of diagnosis is 70 years) and it is still considered an incurable malignancy[1].

1.1.2. Aetiology and risk factors

The aetiology of MM is believed to be multifactorial, and it is poorly understood. It is unclear whether common risk factors for other cancers (for instance tobacco and/or alcohol consumption) are also risk factors for MM[2]. However, different studies report that other risk factors such as family history of MM, African American ethnicity, viral infections and obesity can increase the risk of developing MM[2–6]. Recent studies on MM patients' sera have also raised the hypothesis that post-translational modifications of endogenous proteins might produce immunogenicity and chronic antigen stimulation, with increased neoplastic potential in patient subsets, highlighting an interesting possible etiopathogenetic mechanism[7–10]. Genome-wide association studies (GWASs) have revealed SNPs and chromosomal alterations associated with increased risk in genes and loci with strong relevance for MM pathogenesis, such as *CCND1, IGH, MYC*, *PRDM1* (the role of translocations and key MM drivers will be further discussed)[11–13]. Finally, within the context of inherited/congenital risk of MM onset, a germline truncating mutation of *LSD1/KDM1A* (an H3K4 demethylase that regulates hematopoietic stem cell self-renewal) has been recently identified as responsible for a familial early-onset form of MM[14].

1.1.3. Clinical history and presentation of multiple myeloma

MM is a complex, progressive and multistep disease, characterised by the accumulation of oncogenic events over time. Malignant MM PCs usually infiltrate the BM and release high levels of an aberrant, monoclonal Ig called paraprotein or M-protein. The consequence of BM infiltration and paraproteinemia is multi-organ dysfunction and damage with hypercalcemia, renal insufficiency, anaemia, bone disease and immune suppression (CRAB-I criteria, to be discussed)[1]. In this section, clinical presentation of MM and its different types will be briefly reviewed.

1.1.3.1 Paraprotein behaviour in multiple myeloma

Paraprotein is a monoclonal immunoglobulin or light chain detected in the serum or urine, and it can be produced not only by MM PC, but also by other types of mature B-cell malignancies. It is identified by protein electrophoresis and is usually recognised as a single, intense, homogeneous band in the gamma region of the spectrum[15]. Patterns of paraprotein secretion from the malignant MM PC can be very heterogeneous. There exist four types of secretion patterns: heavy chain Ig and free light chain (FLC) MM, FLC only, non-secretory MM and oligosecretory MM. Heavy chain IgG MMs are the most frequent amongst all MM types (52%), followed by IgA (21%) and FLC MM (16%). In terms of prognosis, IgG MM patients have the best outcome, followed by IgA and then FLC MMs, which show worse prognosis[16,17].

1.1.3.2 Multiple myeloma is a multistep disease

Clonal PCs with early genetic abnormalities are found in the bone marrow of a small percentage of otherwise healthy individuals (3%) over 50 years of age[18]. This condition is called Monoclonal Gammopathy of Undetermined Significance (MGUS). MGUS is a premalignant, asymptomatic disorder with paraprotein serum level < 3g/dL and absence of end-organ damage[19]. Generally, it progresses to MM with a rate of approximately 1% per year[20]. In some patients, the progression from MGUS to MM is preceded by an intermediate syndrome called Smoldering Multiple Myeloma (SMM), which is defined by levels of serum paraprotein > 3g/dL and/or urinary paraprotein 500mg/24h and/or 10-60% PCs infiltrating the BM in the absence of end-organ damage[21]. In general, SMM progresses to frank MM with a rate of 10% in the 5 years following detection of SMM.

1.1.3.3 Risk stratification of myeloma patients

Given the heterogeneity of MM, it is necessary to stratify patients with different survival probability and chance of better response relatively to their ability to sustain certain therapeutic regimens rather than others. Risk stratification for MM depends on how host characteristics, tumour burden, biology of the disease and response to therapy influence the overall survival[21]. To this end, two classification systems have been adopted. The Durie-Salmon staging system (DSS) takes into consideration many different parameters including clinical data (serum LDH – lactate dehydrogenase, haemoglobin, imaging, etc.), whilst the International Staging System (ISS) uses only the levels of both serum albumin and serum β2-microglobulin to predict survival. Recently, the ISS has been incorporated with LDH and cytogenetics (revised-ISS or R-ISS)[22]. Both staging systems are currently used in the clinic and they provide different, valid, complementary

information in predicting outcomes[23]. The other two major factors defining risk in MM are the biological characteristics (i.e. cytogenetics, see section 1.1.4.6) of the disease and the response to therapy.

1.1.3.4 Clinical presentation of end-organ damage in multiple myeloma

Multiple myeloma is a debilitating disease with a wide range of clinical manifestations. These are the direct (or indirect) consequence of the two key features of MM PC biology: the secretion of paraprotein by malignant PCs and their adaptation within the bone marrow (BM) microenvironment. The acronym used to summarise end-organ damage is CRAB-I, and refers to hyperCalcemia, Renal disease, Anaemia, Bone lesions and Immunodeficiency.

The first and possibly most relevant sequela of BM PC infiltration in MM is the onset of a destructive bone disease, affecting 70-80% of patients at diagnosis, and hypercalcemia is the natural consequence of bone infiltration and resorption[24,25]. The third type of infiltration-related complication is represented by anaemia, which is sustained by a multiplicity of mechanisms (anaemia of chronic disease and apoptosis of erythroid progenitors)[26,27]. The fourth implication of BM infiltration is immunodeficiency and hypogammaglobulinemia, or immunoparesis, which is defined by the reduction of one or more uninvolved classes of Ig. It has been documented that 85-90% of patients present reduction in normal Ig levels at diagnosis time[28,29]. It is believed that the causes of immunoparesis are tied to the inhibitory effect on both the humoral and cellular arms of the immune response caused by the proinflammatory cytokine *milieu*[30].

The other two typical syndromes in MM relate to the synthesis and release of paraprotein and are serum hyperviscosity syndrome (HVS) and renal insufficiency. HVS is caused by the rheologic abnormalities of blood in the context of a severe hypergammaglobulinemia[31]. Renal insufficiency in MM can be either acute (cast nephropathy) or chronic (Ig deposition disease - MIDD - or AL amyloidosis)[32].

1.1.3.5 Other types of plasma cell malignancy

1.1.3.5.1 Extramedullary Myeloma

Most commonly, MM presents as intramedullary (i.e. bone marrow) disease. However, in 7-18% of diagnosis, it can present as Extramedullary Myeloma (EMD), where an intramedullary myeloma spreads or develops outside the bone marrow. EMD can occur by local spreading (85% of EMDs[33]), or by haematogenous spreading. This type of “metastasis” can be confined to the blood stream compartment or infiltrate soft tissues in distal localisations (e.g. skin)[33].

1.1.3.5.2 Plasma cell leukemia

Plasma cell leukemia (PCL) is an aggressive and rare disease that is characterised by the presence of more than 20% circulating clonal plasma cells or more than $2x10^6$ per mL. It is defined primary PCL when it occurs at the time of initial diagnosis, and secondary as extramedullary progression from primary MM. Primary PCL is generally more frequent than secondary PCL[34]. The clinical presentation of primary PCL is more severe than that of MM and therapy is based on aggressive polychemotherapy regimens, stem cell transplantation, bortezomib and IMiD-containing combinations[34].

1.1.3.5.3 Solitary plasmacytoma

Solitary Plasmacytoma (SP) is defined as a single mass of clonal plasma cells, with absence or minimal bone marrow involvement and no other symptoms than those related to the primary lesion. Currently, SP diagnosis is imposed in the presence of documented soft tissue or bone plasmacytoma with minimal or no bone marrow infiltration, absence of end organ damage and no other skeletal lesions[35]. SP can be subdivided into extramedullary plasmacytoma (or extraosseous, EMP, more aggressive[36]), and solitary bone plasmacytoma (intraosseous, SBP)[37]. The choice for treatment is still controversial and sees the use of both local radiotherapy and chemotherapy[35,38–40].

1.1.3.5.4 AL amyloidosis

AL Amyloidosis (ALA) can be the consequence of a plasma cell dyscrasia producing a monoclonal component[41]. The pathogenesis of ALA sees deposition of misfolded FLC (frequently lambda) accumulating in the extracellular space as insoluble fibrils which are poised to provoke tissue damage[41]. In ALA, tissue involvement can be systemic or localised. Systemic ALA can affect several organs, such as kidney, heart, gastrointestinal trait, spleen[42].

1.1.4 Pathogenesis of multiple myeloma

1.1.4.1 Cell of origin: the malignant plasma cell

The plasma cell (PC) is the final stage of B cell development. The process of differentiation from haematopoietic stem cell (HSC) to PC is a multi-step and highly regulated process that involves a multiplicity of factors.

1.1.4.1.1 From haematopoietic stem cells (HSC) to mature B-cells

Initially, the HSC differentiates into a multipotent progenitor (MPP), that can give rise to two distinct lineages, the lymphoid and the myeloid lineage (it is not in the scope of this thesis to discuss the myeloid development – this paragraph will focus specifically on the lymphoid lineage). The MPP differentiates into the early lymphoid progenitor (ELP)[43] and begins D_H-J_H loci recombination[44]. The ELP differentiates into a common lymphoid progenitor CLP, and then into early pro-B cell, where successful D_H-J_H and subsequently V_H-DJ_H recombination is followed by expression of the pre-B cell receptor (pre-BCR, constituted by the Igμ chain and the surrogate light chains λ5 and VPREB). Signalling from the pre-BCR induces differentiation of late pro-B into pre-B cells and their clonal expansion[45]. When the surrogate light chains are replaced by mature light chains Igκ and Igλ, the BCR is complete and immature B cells expressing IgM migrate to the secondary lymphoid organs (spleen, lymphnodes, Peyer patches, etc)[45]. Here, they begin the expression of IgD immunoglobulins[46] and complete their differentiation into naïve cells[47].

1.1.4.1.2 Antigen encountering and B-cell maturation into memory B-cells or antibody-secreting plasma cells

The B cell can encounter antigens by direct binding through the BCR. Upon antigen recognition, BCR signalling and the costimulatory action of T-follicular helper cells drive proliferation of B cells in the follicule as centroblasts in the dark zone[48]. Here, they undergo somatic hypermutation (SH) and/or class switch recombination (CSR), negative selection of self-reactive clones[48] and subsequently migrate to the GC light zone for BCR affinity selection[49,50]. The success of both CSR and SH depend on *AICDA*, a gene codifying for the cytidine deaminase AID[51], whose expression is tightly regulated by *IRF4* in cooperation with *PU.1*[52]. Notably, *IRF4* is amongst those factors that are involved in maintaining the plasma cell transcriptional program and has been identified as an example of "non-oncogene addiction" in MM (see section 1.1.4.3.2)[53]. It is interesting to note the behaviour of *MYC* in this context, as this proto-concogene is also implicated in myeloma pathogenesis (discussed in section 1.1.4.3.3). In the dark zone, *MYC* transcription is repressed by BCL6, a gene essential for B cells when transitioning into centroblasts. *MYC* is then re-expressed in subsets of B cells within the light zone - where B cells undergo affinity maturation - together with important genes for MM pathogenesis, such as *CCND2*, *CDK4/6*, and again, *IRF4*[54]. Depending on the type of antigen and response, B cells eventually exit the follicle to generate memory B cells and antibody secreting cells (ASCs), such as short-lived plasma blasts (PBs) and long-lived plasma cells (PCs)[55].

1.1.4.1.3 *IRF4*, *PRDM1* and *XBP1* as master regulators of plasma cell differentiation and antibody secretion

IRF4, PRDM1 and *XBP1* are transcription factors involved in priming differentiation of centrocyte and memory B cells into PCs and into maintaining PC transcriptional program once differentiated. *IRF4* is essential for GC formation[56]. However, *IRF4* expression is reduced during early stages of the GC[56,57], as promotion of GC fate, SH and CSR require low expression of *IRF4*[52]. Conversely, when *IRF4* becomes highly expressed, it represses *BCL6* in cooperation with PU.1[53], *PRDM1* and *XBP1* loci are de-repressed[58]. The PC transcriptional program is thus activated[52], in a process that sees the exiting of the centrocyte from the follicle and the full differentiation into PC or that of memory B cells into PC[59]. A key consequence of *PRDM1* induction is not only the downregulation of many genes that promote the B cell program, such as *MYC, AID, BTK, EBF*, and genes involved in DNA repair (and thus CSR), but also the upregulation of genes promoting PC functions, such as *XBP1* and *IGJ*[60]. The demonstration that B cell precursors with deletion of *PRDM1* fail to differentiate into PC provides with additional insight into to the fundamental role of this TF into PC maturation[61]. *XBP1* is important for later stages of PC development, and it is under the control of *PRDM1*. XBP1 is largely implicated into the unfolded protein response (UPR) that follows endoplasmic reticulum (ER) stress in PCs, which are naturally poised to synthesise large amounts of immunoglobulins and they require adequate fine tuning of events occurring in the ER. Additionally, *XBP1* is required for controlling intracellular trafficking of secretory organelles. It is interesting to note that once PC are fully mature, deletion of *IRF4* is detrimental for PCs, whilst deletion of *PRDM1* and/or *XBP1* is not[62]. This feature has been shown also in MM, where patients can exhibit loss of function mutations/deletions of both *PRDM1* and *XBP1*[63,64], whilst *IRF4* is a known dependency of MM cells (to be further discussed)[65].

1.1.4.2 The transcription factors Ikaros (IKZF1) and Aiolos (IKZF3) in the lymphoid lineage

The IKZF1 and IKZF3 transcription factors are part of a larger family of TF containing C_2H_2 zinc-finger (ZF) motifs, the Ikaros TF family (IKZF1-5, in order Ikaros, Helios, Aiolos, Eos and Pegasus)[66]. This section will solely focus on Ikaros and Aiolos, which are the most relevant in the context of PC biology and IMiD therapeutic action.

1.1.4.2.1 The structure of IKZF transcription factors

IKZF family members possess a DNA binding region in their N-termini and a dimerisation domain in their C-termini. IKZF1/3 DNA-binding region contains four distinct ZF groups, and recognises specifically the core motif AGGAA through the second and third ZF groups[67]. The C-terminal

domain, on the contrary, contains only two ZF groups, it does not bind DNA and its sole purpose is to allow dimerisation with other TF of the IKZF family. Eleven IKZF1 splicing variants have now been discovered. These can lack one or all ZF groups in the DNA binding domain[68]. Amongst these splicing variants, those that lack of ZF DNA-binding groups can act as dominant negative (especially Ik-5, Ik-6, Ik-7, Ik-8) by dimerising with DNA-binding Ikaros isoforms (Ik-1, Ik-2 commonly) and thus reducing their affinity for DNA. These dominant negative isoforms are relevant in the context of B and T lymphoblastic leukemia, both in children and adults[69–71]. This is an important observation, as it suggests that the loss of IKZF transcriptional activity confers to cells characteristics of de-differentiation.

1.1.4.2.2 The double activity of IKZF1/3-mediated transcriptional regulation

Ikaros and Aiolos can both act as transcriptional activators or repressors. In work by Zhang et al.[72], IKZF1 was found to associate with the Nucleosome Repressor Deacetylase (NuRD) complex and Mi-2β in thymocycte as a transcriptional repressor. Firstly, they discovered that IKZF1, together with Mi-2β, binds accessible chromatin and contributes to increase transcription of target genes. Conversely, when IKZF1 and Mi-2β are associated with NuRD, gene expression is repressed as IKZF1 blocks NuRD activity. Secondly, in their IKZF1 null model, they described an increase in a leukaemogenesis transcriptional program driven by Mi2-β-NuRD target genes. Moreover, in the absence of IKZF1, IKZF3 associated with Mi-2β, indicating high degree of redundancy in the IKZF TF family, especially between IKZF1 and 3. Overall, their paper provides evidence that IKZF1 can either activate or repress transcription and it is fundamental for cell differentiation. Interestingly, IKZF1 in association with NuRD can also activate transcription, within a complex that sees the involvement of PP1α and P-TEFb[73]. Another mechanism by which IKZF1 can regulate transcription is through the engagement with Polycomb Repressor Complex 2 (PRC2) and by inducing trimethylation of H3K27 in those chromatin regions not modulated by NuRD[74]. Finally, IKZF1 can repress gene expression by suppressing SWI/SNF activity together with SIN3 and HDACs, or by directly interacting with the transcriptional repressor CtBP[75].

1.1.4.2.3 IKZF1 and IKZF3 in the lymphoid lineage development

IKZF1 and IKZF3 are frequently associated on chromatin and they are required for efficient haemo-lymphopoiesis[76]. In the case of lymphopoiesis, IKZF1 and 3 are essential at different stages. Firstly, as reviewed by Georgopoulos[77], IKZF1 is essential in priming the HSC towards the lympho-myeloid progenitor by repressing transcription of myeloid-related genes. Furthermore, the expression of IKZF1 gradually increases along lymphoid cell maturation. Secondly, IKZF1

promotes maturation of pre-B cells - in cooperation with the master regulators PAX5 and IRF4 - repressing non-lymphoid lineage specific genes[78]. IKZF1 plays a functional role in thymocytes as pre-T cells rely on IKZF1 to switch off expression of *NOTCH1* in order to limit expansion of pre-T cell and fully mature into T-cells thus avoiding malignant transformation.

1.1.4.2.4 IKZF1 and IKZF3 as regulators of the T-cell response

The role of IKZF1 and IKZF3 extends to regulation of mature B- and T-cell. As reviewed by Powell et al.[79], IKZF1/3 can positively or negatively regulate several subsets of T cells – T_{h1}, T_{h2}, T_{h17}, T_{fh} and T_{reg}. T_{h1} cell differentiation is limited by IKZF1 and IKZF3, as they repress IL-12/IFNγ signalling and IL-2 production at regulatory regions of the *IL2* and *IFNG* genes, promoting a T_{h2} phenotype switch. IKZF1-mediated repression of *IL2* locus seems to be involved in T $CD4^+$ anergy - in the absence of CD28 costimulation - a key mechanism in maintenance of immune tolerance[80]. Both IKZF1 and IKZF3 may also promote T cell switching into T_{h17}, a subset of T cells that has been associated with chronic inflammation and tumour progression[81]. IKZF1 also regulate T_{reg} lymphocytes, a subset of T cells involved into tolerance and suppression of autoimmunity. Deletion of IKZF1 in naïve $CD4^+$ T cells blocks differentiation into T_{regs} by abolishing TGFβ-dependent expression of *FOXP3*[82]. Finally, IKZF1/3 can increase T follicular helper (T_{fh}) cells activity by repressing *IL2* and by upregulating *BCL6*[83].

Overall, these observations suggest that IKZF1/3 play an important role in modulating T cell functions, including cytokine signalling and antigen-dependent responses, and are involved in limiting auto-inflammatory/auto-immune reactions[84].

1.1.4.2.5 IKZF1 and IKZF3 in mature B-cells and PCs

In contrast to IKZF1, IKZF3 is not expressed in the haematopoietic compartment, but becomes critical in the post-GC mature B cell stage. A seminal paper by Wang and colleagues[85] demonstrated that a lack of IKZF3 augments CD40-mediated activation of B cell sustained by BCR signalling. Importantly, in $IKZF3^{null}$ mice, there was a dramatic increase in levels of serum Ig and autoantibodies, suggesting that IKZF3 plays a key role in mediating the response upon antigenic stimulation. IKZF3 is also required to generate long term immunity[86]. As IKZF1 and IKZF3 drive cell differentiation[68,77], loss of function of one of these TFs is sufficient to induce leukemogenesis (see also paragraph 1.2.4.2.3). Hence, it is not surprising that IKZF1 and IKZF3 have been identified as key regulators of PC development and that also MM PCs rely on IKZF3 and IKZF1 activity. In fact, IKZF3 has been demonstrated to cooperate with PRDM1 to repress target genes, and its loss can impair chromatin binding of PRDM1, but not vice versa[87]. It has

also been reported that IRF4 cooperates with IKZF1/NuRD in gene repression and, in doing so, promotes PC differentiation[88]. Finally, IKZF1/3 are MM PCs dependencies (to be further discussed)[89,90]. Taken together, these observations highlight the vital role of IKZF1/3 in differentiation of precursors into PCs and into maintenance of the PCs transcriptional program.

1.1.4.3 Molecular pathogenesis of multiple myeloma

1.1.4.3.1 Disease initiation in multiple myeloma

It is believed that MM is initiated by genetic aberrations, which can arise in naïve B cells before encountering the antigen (pre-GC stages, e.g. during B cell maturation) or after, when the naïve B cell undergoes genetic and phenotypic changes in the GC. There are three key events in which DNA damage, followed by DNA repair, becomes essential and could potentially cause genetic instability with malignancy onset in the B-cell[91]: 1) *V(D)J* recombination (driven by RAG1 and RAG2 during B cell maturation), 2) CSR and 3) SH in the GC (both regulated by AID). It has been hypothesised that the initiation process of malignancy in a PC occurs in the germinal centre[92]. Early sequencing-based studies on the variable regions of the immunoglobulin heavy chain revealed that the malignant MM precursor has undergone somatic hypermutation. In fact, a non-malignant pre-CSR B-cell clone in the bone marrow was found to possess the same sequence in the variable regions as the post-switch MM PC[93]. Thus, it is likely that the malignant MM PC has encountered the antigen, and that MM is probably a post-GC disease (for GC dynamics, see paragraph 1.1.4.1.2). Secondly, MM cells and their precursors (MGUS clones, paragraph 1.1.4.6), are usually IgG or IgA, but rarely IgM or IgD[92,94] suggesting that the MM cell arises following errors during CSR or SH. The proof of concept for a role of SH in MM initiation was provided in 2008 by Chesi et al., in a study where, with an elegant system, *MYC* was sporadically activated through SH only in presence of AID. Strikingly, this murine model spontaneously develops a PC tumour that recapitulates many of the clinical features of MM in humans[95]. With regards to CSR, the hypothesis is further supported by the observation that about 30% of the MM-driving translocations involve the *IGH* gene[96]. Fascinatingly, a 2013 paper reports the finding of MM subsets with translocation involving the D_H-J_H region, and proposes that these MM could also arise from abnormalities acquired during the pro-B-cell stage[97]. The question remains open for those 40% of MMs which do not exhibit *IGH* translocation events, but rather hyperdiploidy. Hyperdiploid MMs (HMM) are difficult to study mainly because there is a lack of appropriate models, as 90% of MM cell lines are derived from non-HMMs[98]. Some authors have hypothesised that hyperdiploid MMs (HMMs) could arise from errors during

chromosome segregation in highly proliferative centroblasts[99]. As for now, the exact mechanisms by which MM initiation occurs remain mostly undefined.

1.1.4.3.2 *IRF4* addiction in multiple myeloma

Interferon Regulatory Factor 4 (*IRF4*) is an essential transcription factor (TF) in B cells and it is required for the terminal differentiation of active B cells into Ig-secreting PCs. Fine tuning of IRF4 levels has been demonstrated to control a transcriptional program required for B-cell fate upon antigen presentation. IRF4 promotes CSR by upregulating AID and increasing *PRDM1* and *XBP1* expression, TFs involved in PC maturation and lineage maintenance. Moreover, IRF4 interacts with PU.1 and members of the Ikaros transcription factor family (IKZFs), especially IKZF1 (Ikaros) and IKZF3 (Aiolos) in driving transcription of *PRDM1*[88]. IRF4 controls the expression of a plethora of genes, including *MYC*, an important proto-oncogene for many MM. The seminal paper of Shaffer et al.[65] provided evidence that, in the specific context of MM, IRF4 establishes a positive feedback loop with MYC, where they mutually enhance their expression. The dependency of MM on *IRF4* has been as an example of "non-oncogene addiction". In other words, whereas IRF4 activity is normally required for healthy PCs, it becomes aberrant in the context of the cancer as it sustains MM cells proliferation. In recent work, Jin et al.[100] dissect the transcriptional co-regulatory network[101] of MM through the analysis of TFs located at superenhancers (SE) and confirmed the contribution of IRF4 to be essential for MM. Moreover, the study revealed that the *IRF4*-driven transcriptional program in MM was abnormal as compared to healthy PCs although partially overlapping with that of antigen-stimulated B-cells (both memory B-cell and normal PCs). Remarkably, they observed that the *MYC*- and *IRF4*-regulated SEs, as part of the same transcriptional network, were present only in MM cells. This result elegantly aligns with the discovery that the targeting of the acetyltransferase CBP/EP300 bromodomain results into repression of *IRF4* and *MYC* transcriptional programs in MM[102]. In summary, the "non-oncogene addiction" of MM for *IRF4* sees the interplay between many factors including IKZF1, IKZF3, MYC and chromatin remodelers. Deeper insight into the cooperation between these genes in sustaining malignant PC survival is the key to understanding the action of IMiDs in the context of MM.

1.1.4.3.3 The *MYC* gene is dysregulated in multiple myeloma

The dysregulation of *MYC* is a common feature in cancer[103,104]. Interestingly, MYC can either enhance or suppress transcription. Transcriptional activation by MYC is dependent on the activity and association with histone acetyltransferases (HATs). A seminal paper in 1998

demonstrated that MYC exerts its function in complex with the HAT TRRAP, also a cofactor for E2F activity[105]. Later on, other studies reported that MYC also partners with another HAT, EP300/CBP, and with several components of the transcriptional machinery, such as pTEFB and the mediator complex, in order to enhance transcription[106–108]. Conversely, suppression of transcription by MYC depends on the presence of MIZ1, which binds directly to the DNA and MYC/MAX function as cofactors for gene repression[109,110]. An early genome-wide study in Burkitt Lymphoma lines indicated that MYC can bind up to around 15% of the genes in the genome, and suggested that MYC could globally regulate transcription[111]. MYC is capable of modulating several distinct biological functions, and the effects of *MYC* overexpression strictly depend on the cellular setting. As reviewed by Jovanovic and colleagues, MYC has been found to modulate apoptosis, cell cycle progression, protein translation, cell proliferation and the cross-talk between tumour cells and their microenvironment[112]. As review by others, MYC itself is cannot initiate tumorigenesis probably by virtue of its double role in regulating apoptosis and cell cycle[103,104]. Initiation is possible only in presence of other malignant events (e.g. abrogation of cell cycle arrest checkpoints, overexpression of *BCL2*, loss of *TP53* or *CDKN2A*)[103]. Therefore, the current belief is that MYC hyperactivation leads to tumorigenesis by the removal of cell growth control mechanisms.

MYC rearrangements in early stages of MM are relatively rare (around 10%)[113] and they preferentially occur in advanced stages of the disease. *MYC* was found overexpressed in around 40% of MMs consequent to translocations, extra copies and activation by transcriptional axis such as the *IRF4-MYC* feedback loop (see previous paragraph). A very recent genome-wide study also identified MYC amongst the key factors in MM maintenance and progression[114]. This result confirms previous data reporting a detrimental effect of MYC knockdown and pharmacological inhibition in several MM cell lines[65,115]. It is evident that *MYC* has a primary role in MM and its implications in several biological processes of malignant PCs could make of MYC a strategic target in PC malignancies.

1.1.4.4 Molecular Classification of Multiple Myeloma

Multiple Myeloma can be classified based on molecular aberrations demonstrated through conventional cytogenetic testing and fluorescent *in situ* hybridisation (FISH) studies. These aberrations separate MM in two main entities: hyperdiploid MMs (HMMs) and non-hyperdiploid MMs (NHMMs). The first group is represented by MMs that gain extra copies of chromosomes (typically the odd-numbered chromosomes), whilst the second group is characterised by

translocation involving the *IGH* locus. These genetic abnormalities are considered initiating (or primary) events that are found as early as in the MGUS stage[96–98].

The largest group of MMs is represented by HMMs. Generally, HMMs have a more favourable prognosis[116] and they respond better to IMiDs (e.g. lenalidomide), possibly explaining the better OS of these patients[117]. The other large cytogenetic group of MMs is represented by NHMMs. These are generally associated with poorer OS and high-risk cytogenetics as compared to HMM, which usually bear low-risk genetic abnormalities. Other rearrangements often present at the time of diagnosis also include monosomy of chromosome 13 or 14, 1q21 gain and del17p[118]. The latter is documented in 10% of newly diagnosed MM (NDMM), it sees the loss of p53 and it is associated with very poor prognosis[119]. Genetic subsets of MM are summarised in Table 1.1.

Although MM genetic classification is strictly based on the type of initiating event, other abnormalities are commonly found in MM. In fact, genetic instability promotes the occurrence of secondary genetic rearrangements which are required for tumour progression. *MYC* rearrangements are paradigmatic of MM secondary events[120]. *MYC* can be either overexpressed or translocated. *MYC* translocation can be Burkitt-like – t(8;14), representing the 85% – or involving Ig light chains – t(8;22), mostly lambda[120]. Other secondary events with prognostic value include mutations in RAS and NF-kB pathways[121]. Primary events require additional dysregulation of other genes or pathways, to progress into advanced stages. Furthermore, the combination of primary and secondary events can define the risk of progression and the outcome for the patient.

1.1.4.5 Genetic abnormalities and disease progression

Intratumoral heterogeneity in MM depends on the dominance of some clones over others during progression, which seems to follow a Darwinian type of evolution[122]. The relationship between molecular pathogenesis and progression of MM is represented in Figure 1.1. MGUS, the pre-malignant stage that precedes MM, is established when an initiating event, such as *IGH* translocations or trisomy of some chromosomes, provides the PC with a proliferative advantage. As reviewed by others[121,123], the MGUS clone (the premalignant stage of MM) accumulates additional genetic abnormalities, such as secondary Ig translocations or mutations activating RAS and/or increasing MYC expression, thus progressing into predominantly intramedullary MM. Here, MM PCs can acquire further malignant properties by entering the final and most aggressive stage of the disease, including extramedullary MM. At this point, MM PCs have lost dependency on the bone marrow stroma.

As in most tumours, MM progressive nature is reflected by genetic instability and increasing aggressiveness along disease progression. Recent studies have highlighted the complexity of the genetic landscape of MM and how these change with progression. Single Nucleotide Variant (SNV) analyses following whole exome sequencing have showed that the number of SNVs is much higher in newly diagnosed MM (NDMM, median > 120) as compared to MGUS (median = 89)[124]. The same study also demonstrated that copy number changes (or Copy Number Alterations, CNA) are fewer in MGUS (median CNA = 2) as compared to NDMM (median CNA = 16). This study further supports the notion that MM is a genetically unstable entity. Another study on CNAs also demonstrated that the highest number of CNAs is seen in HMM rather than NHMM (HMM CNA median = 10 vs NHMM CNA median = 3), pinpointing significant differences in the genetic landscape between the two MM subgroups[125]. Given the complexity of the interplay between genotype and phenotype in MM, it is fundamental to integrate molecular and clinical data to better understand the mechanisms of progression in order to improve current therapeutic strategies.

Table 1.1. Molecular classification of cytogenetic aberrations in MM (adapted from Rajkumar[21])

Subtype	Gene(s)/chromosomes affected[a]	Percentage
Trisomic multiple myeloma	Recurrent trisomies involving odd-numbered chromosomes with the exception of chromosomes 1, 13, and 21	42
IgH translocated multiple myeloma		30
t(11;14) (q13;q32)	*CCND1* (cyclin D1)	15
t(4;14) (p16;q32)	*FGFR3* and *MMSET*	6
t(14;16) (q32;q23)	*C-MAF*	4
t(14;20) (q32;q11)	*MAFB*	<1
Other IgH translocations [a]	*CCND3* (cyclin D3) in t(6;14) multiple myeloma	5
Combined IgH translocated/trisomic multiple myeloma	Presence of trisomies and any one of the recurrent IgH translocations in the same patient	15
Isolated Monosomy 14	Few cases may represent 14q32 translocations involving unknown partner chromosomes	4.5
Other cytogenetic abnormalities in absence of IgH translocations or trisomy or monosomy 14		5.5
Normal		3

[a] Includes the t(6;14)(p21;q32) translocation, and rarely, other IgH translocations involving uncommon partner chromosome.

1.1.4.6 Multiple Myeloma and the Microenvironment

The BM microenvironment (BMME) in MM is a complex biological entity, and is represented by a cellular and a non-cellular component. Several types of cells derive from the mesenchymal compartment, such as fibroblastic bone marrow stromal cells (BMSCs), adipose cells and osteoblasts (OBs), and many others from the myeloid and lymphoid lineages, such as osteoclasts (OCs), myeloid-derived suppressor cells (MDSCs), dendritic cells (DCs), B- and T-lymphocytes, Natural Killer cells (NKs), and of course MM PCs. The non-cellular component is represented by the extra cellular matrix (ECM). The BMME is of extreme importance in promoting tumour progression by providing with pro-survival, pro-angiogenic, immune-suppressive signalling, structural support and protection to MM PCs.

During intramedullary disease stage, the contact between BMSCs and MM PCs fosters MM survival and proliferation, angiogenesis and bone destruction. Mechanisms of physical interaction between BMSCs and MM cells are represented by contact between VLA4 and/or α4β1 integrin with VCAM-1. Such adhesion mediates the release of diverse pro-survival cytokines from both BMSCs and MM cells, such as IL-1, IL-3, IL-6, TNFα, VEGF, DKK1, MIP1α/β, RANKL[126–130]. These factors from BMSCs and MM cells have both autocrine and paracrine functions and promote MM cells growth, angiogenesis and bone resorption.

Bone resorption is the cause of the typical bone disease that manifests with MM. Several cytokines are involved in OC stimulation. However, it is believed that the main mechanisms of impaired bone homeostasis are the secretion of WNT inhibitors (DKK1) and the imbalance within the RANK/RANKL/OPG system[128–131]. Angiogenesis is a hallmark of MM progression and has prognostic implications in terms of response to treatment, PFS and OS[132–134]. The formation of new vessels results from the combined action of several cytokines - however, VEGF seems to play a major role[135,136]. Immune suppression is thought to be driven mostly by M2 MPs and MDSCs[137,138]. Both cell types promote a pro-inflammatory environment by secreting cytokines (e.g. IL-10, IL-12, TNFα) that inhibit the activity of T helper CD4 and cytotoxic CD8. Moreover, MDSCs were found to dramatically impair NK cell-mediated killing. In summary, the proinflammatory environment created by distinct cell populations allows MM to benefit from neovasculogenesis, reduced immune surveillance, and it is responsible for clinically relevant features such as the characteristic MM-related bone disease.

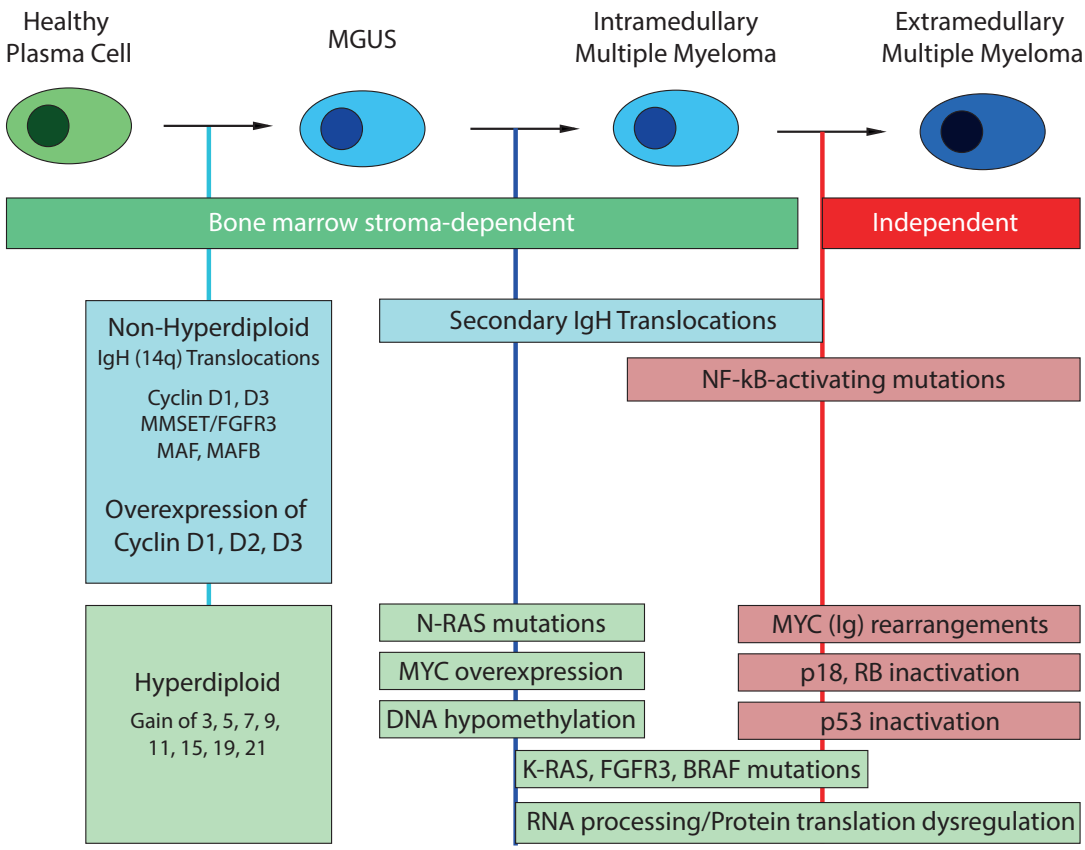


Figure 1.1. Genetic abnormalities and multistep pathogenesis of Multiple Myeloma (adapted from Kuehl and Bergsagel, 2012; Furukawa and Kikuchi, 2012[356])

1.1.5 Treatment of Multiple Myeloma

Multiple myeloma treatments include several types of approach, such as autologous or allogeneic stem cell transplantation (ASCT), alkylating agents (cyclophosphamide, melphalan), anthracyclines, corticosteroids (dexamethasone, prednisone), IMiDs, proteasome inhibitors, epigenetic compounds, monoclonal antibodies and cellular therapies.

1.1.5.1 Eligibility to stem cell transplantation defines the initial strategy in tackling MM

According to the latest guidelines, the first step into MM treatment sees the allocation of patients into transplant eligible (usually <65yo or fit patients <70yo with in good clinical condition) or non-eligible[139]. Transplant eligible patients typically undergo induction therapy with a bortezomib-dexamethasone (Vd) based regimen. The addition of a third agent, such as and IMiD or doxorubicin, has been demonstrated to increase the initial response[140]. The combination of lenalidomide, bortezomib and dexamethasone (VRd) prolongs PFS relative to 'doublet' based inductions but the OS is unaffected[141]. Triplets with other proteasome inhibitors such as carfilzomib and ixazomib are utilised as treatment in refractory/relapsed MM, and they are now included amongst the treatment options for NDMM[142,143]. High dose melphalan (200mg/m^2) is typically utilised as conditioning therapy for ASCT. After ASCT, patients undergo maintenance therapy with either bortezomib or lenalidomide. Both drugs have been successful in prolonging PFS and OS as maintenance therapy[144,145]. Transplant ineligible patients are usually administered with bortezomib- or lenalidomide-containing induction regimens. A recent study has assessed the outcome of VRd in these patients, resulting in overall benefit in terms of PFS and OS[146].

Eligibility to SCT represents itself an important prognostic factor, as eligible patients are usually younger, with better performance status and they can undergo high dose therapy regimens. On the contrary, older patients are likely to also have a worse performance status, which implicates reduced ability to sustain heavy therapeutic schemes. Transplantation in patients over 70 years of age is currently under discussion and needs further investigation[147,148].

1.1.5.2 Novel compounds: immunomodulatory thalidomide analogues and proteasome inhibitors

IMiDs and proteasome inhibitors were introduced in the early 2000s as novel therapies for the treatment of MM and they have proven effective in terms of prolonging survival[149]. These drugs are considered cornerstones in the treatment of MM. Subsequently, newer analogues of the same class have been developed. Pomalidomide has shown therapeutic benefit in lenalidomide-

refractory MMs. Other IMiDs, such as iberdomide (CC-220) have also been developed and are showing promising early clinical results[150]. Novel proteasome inhibitors have been tested and recently approved for clinical use. For example, carfilzomib is an irreversible inhibitor of the 26S subunit of the proteasome, and it has showed benefit in patients with MM who have become refractory to bortezomib containing drug regimens[151]. The mechanism of action and clinical use of IMiDs will be widely discussed in section 1.2.

1.1.5.3 Other therapies

In addition to IMiDs and proteasome inhibitors, other novel anti-myeloma therapies have been introduced into clinical practice. These drugs include monoclonal antibodies (and bispecific engagers), small molecules and cellular therapies.

1.1.5.3.1 Monoclonal antibodies

Monoclonal antibodies that specifically target SLAMF7 and CD38, elotuzumab and daratumumab respectively, have been proven to be effective in combination with bortezomib and lenalidomide[152–154]. Daratumumab is active as monotherapy in refractory/relapsed MM[155]. A recent study has also highlighted the mechanism by which IMiDs increase expression of CD38 on MM PCs cell surface, thus increasing the response to daratumumab[156]. Another anti-CD38 monoclonal antibody, isatuximab, has undergone early clinical studies, with encouraging results in combination with IMiDs[157,158]. A novel interesting target in MM is represented by B-cell maturation antigen (BCMA). An anti-BCMA monoclonal antibody conjugated with the microtubule toxin auristatin F has provided interesting results[159,160]. An anti-BCMA/anti-CD3 bispecific mAb has also been tested in order to enhance immune tumoricidal effect by increasing contact between MM cells and T-cells. Clinical studies with this bispecific mAb are ongoing on the basis of solid pre-clinical data[161–163].

1.1.5.3.2 Small-molecule inhibitors

Novel small molecules are represented by panobinostat, venetoclax and aplidin. Panobinostat, a pan-HDAC inhibitor, improved the outcome of patients with relapsed or relapsed/refractory (R/R) MM in combination with bortezomib and dexamethasone[164]. Panobinostat was also combined successfully with dexamethasone and lenalidomide instead of bortezomib, documenting less gastrointestinal toxicity[165]. Venetoclax, an anti-BCL2 agent, is currently on trial for MM, and it has shown encouraging results in patients with t(11;14) that were refractory to previous treatments[166]. Aplidin, a molecule derived from the marine tunicate *Aplidium albicans,*

has activity as a single agent or in combination with dexamethasone in R/R MM[167]. Beside its anti-MM action, aplidin is active also in limiting bone resorption[168,169].

1.1.5.3.3 Cellular therapies

Cellular therapies mainly include such as chimeric antigen receptor T-CD8 cells (CAR-T) with demonstrable efficacy in MM. A recent study has reported that anti-BCMA CAR-T cells have shown anti-MM responses with persistence of remission at one year following the infusion[170]. Interestingly, small subsets of MM patients can express CD19 and anti-BCMA in combination with anti-CD19 CAR-T cells have shown promising results in R/RMM. However, these clinical trials with CAR-T cells in MM are still ongoing and routine employment in the clinical practice will require further investigation.

1.2. The Immunomodulatory imide drugs, IMiDs, in multiple myeloma

1.2.1 The impact of IMiDs in the therapy of multiple myeloma

1.2.1.1 A snapshot of the pre-thalidomide era and the advent of thalidomide

Towards the year 2000, the gold standard for MM therapy was based on alkylating agents and/or corticosteroids, such as melphalan and prednisone. In some cases, patients were able to receive autologous stem cell transplantation (ASCT) following high-dose chemotherapy[171]. In 1998, the Myeloma Trialists' Collaborative Group showed that three-chemotherapy-drug based regimen was no superior to the already well-established melphalan and prednisone (MP)[172]. A seminal paper in 1996[173] reported the success of high-dose chemotherapy supported by ASCT in patients with less than 65 years of age who had Durie-Salmon stage II or III MM. Other strict criteria in selecting the candidates were applied to ensure sustainability of the chemotherapeutic regimen. Novel effective therapeutic strategies against MM were therefore urgently needed in order to improve the outcome of MM patients.

The story of thalidomide is very controversial, but it represents an example of extremely successful drug repurposing. Thalidomide was initially introduced during the 1950s as a sedative and antiemetic for morning sickness[174], but was subsequently withdrawn from the market as it was found responsible for causing malformations in newborns[175–179]. In later years, thalidomide was demonstrated to be effective in the treatment of erythema nodosum leprosum[178,180]. In the late 1990s, in light of evidence of thalidomide's anti-angiogenic activity[181], it was successfully deployed in advanced MM[182]. The success of this trial changed MM therapeutic strategies over the following decades.

1.2.1.2 Thalidomide and its analogues

The realisation of thalidomide's therapeutic potential led to the synthesis of more potent analogues, such as lenalidomide and pomalidomide. Data collected in early clinical trials demonstrated a clear superiority of thalidomide-containing regimens versus non-thalidomide regimen. In a study conducted by Rajkumar et al. in 2006, patients were randomly assigned to thalidomide plus dexamethasone or dexamethasone only[183]. The response rate in the thalidomide-dexamethasone group was superior to that of dexamethasone only, although the incidence of adverse events such as deep venous thrombosis and neuropathy was also higher with thalidomide. An improvement in overall survival with thalidomide was seen in another study[184] aiming to compare melphalan, prednisone and thalidomide with melphalan and prednisone only. Lenalidomide and pomalidomide have both demonstrated superiority to

thalidomide in more recent clinical trials. In 2009, Gay et al. compared lenalidomide plus dexamethasone (LD) vs thalidomide and dexamethasone (TD). The adverse events in LD were mainly neutropenia, and in TD were thromboembolism and peripheral neuropathy[185]. The more recent OPTIMISMM trial[186], compared pomalidomide, dexamethasone and bortezomib to dexamethasone and bortezomib only in relapsed/refractory MMs previously treated with lenalidomide. The pomalidomide regimen demonstrated superiority in terms of overall survival and no additional toxicity/adverse events against the non-pomalidomide containing scheme.

1.2.1.3 Toxicity profile of immunomodulatory drugs

IMiD-induced toxicity can be categorised into haematological and non-hematological[187,188]. The incidence of each adverse reaction is largely chemotype dependent, as the different analogues possess distinct and overlapping toxicity profiles. Haematological toxicity includes neutropenia, thrombocytopenia and deep venous thrombosis with thromboembolism (VTE). Non-haematological toxicity is commonly represented by peripheral neuropathy.

Thalidomide-induced peripheral neuropathy (TiPN) affects a significant portion of patients. Some authors have proposed that it could be the consequence of thalidomide interference with TNF-α signalling and inhibition of angiogenesis[189]. With regards to lenalidomide and pomalidomide, neuropathy is a much less frequent event[190,191].

Myelosuppression is a typical side effect of lenalidomide and pomalidomide treatment and is less frequent with thalidomide. It has been reported that around 50% of patients can develop myelosuppression[192]. It is thought that IMiD-dependent IKZF1 degradation (see below) disrupts the transcriptional network driving haematopoiesis by interfering with PU.1 and GATA2 activity within the myeloid compartment[193,194].

Another side effect of IMiDs is venous thromboembolism (VTE). Cancer patients, especially those with haematological malignancies, are more likely to develop VTE as compared to the healthy population[195]. Moreover, reduced mobility of MM patients consequent to bone destruction represents an additional risk factor to that of VTE, making adequate anticoagulant prophylaxis imperative in MM patients treated with IMiDs[196].

1.2.2 Mechanism of action of IMiDs

Lenalidomide and its analogues are responsible for a plethora of different biological effects within the MM PC and its microenvironment. From a cell intrinsic point of view, IMiDs activity is mostly that of a cytostatic drug, as they inhibit the progression of the cell cycle with cells accumulating in the G0-G1 phase. On the other hand, the non-cell intrinsic functions are

believed to be the consequence of IMiDs modulating the functions of the different cells that compose the MM niche. The discovery of CRBN-induced degradation of IKZF1 and IKZF3 has helped to answer several questions with regards to IMiD biology from both a cell autonomous and non-cell autonomous perspective.

1.2.2.1 IMiDs and MM pathobiology

In the "pre-neosubstrate" era (the concept of "neosubstrate" will be discussed in the following paragraphs) and prior to the identification of CRBN as IMiD-binding protein, IMiD molecular mechanism was mostly obscure and limited to the description of the phenotypic effects on MM cells and the tumour microenvironment. Despite significant advances and discoveries in the field, many of these observations are still poorly understood. In this paragraph they will be described because of their relevance in the biology of MM and its therapy.

Mechanistically, and from a cell intrinsic perspective, it has been shown that IMiD treatment results in concomitant downregulation of MYC and IRF4[197]. This observation was then associated with IMiD-dependent degradation of the transcription factors IKZF1 and IKZF3 (this will be discussed in the next paragraphs). Treatment with IMiDs has also been associated with upregulation of several tumour suppressor genes, such as *CDKN1A* and B (p21 and p27), *CDKN2AB* (p27), *EGR1*, *EGR2*, *EGR3*. Moreover, IMiDs can inhibit CDK2, 4 and 6 causing reduction of phosphorylated pRB and subsequent cell cycle blockade[198]. Induction of apoptosis represents another cell-intrinsic effect of IMiD on MM cells. IMiDs promote downregulation of anti-apoptotic factors cIAP-2 and FLIP, with subsequent activation of TRAIL/Apo2L, and also increase activation of caspase-8, with sensitisation to FAS-induced apoptosis[199]. Modulation of NF-kB signalling is also a consequence of IMiD treatment. Suppression of IGF-1 induced by IMiDs has a negative impact on the NF-kB pathway, mitigating the pro-inflammatory environment and interfering with MM cells proliferation[200]. Furthermore, blockade of the NF-kB pathway in MM has been shown to raise pro-apoptotic signalling (release of cytochrome c) and to suppress expression of pro-apoptotic factors (mainly members of the *BCL2* family)[200]. These observations indicate that IMiDs possess both pro-apoptotic and cytostatic properties.

From a non-cell intrinsic perspective, IMiDs possess a broad activity against several cancer-sustaining processes (see paragraph 1.2.4). Firstly, IMiDs mitigate MM bone disease by reducing the release of RANKL[201]. Secondly, thalidomide and its analogues can inhibit angiogenesis. In particular, thalidomide can deplete VEGF, one of the most important cytokines in neovasculogenesis[202]. Other thalidomide analogues can also interfere with this process, as well. It has been shown that lenalidomide blocks sprouting of new vessels by reducing the release of

VEGF and other angiogenic factors such as bFGF and IL-6[203]. IMiDs are capable of disrupting physical interaction with the bone marrow stroma. Lenalidomide can impede association of adhesion proteins such as β-catenin, cadherin-5 and CD31, and diminish the expression of multiple surface proteins, such as integrins, ICAM-1, VCAM-1 and E-selectin, etc., that are key mediators of the interactions between MM PCs and BMSCs[204,205]. The upregulation of these molecules is thought to be the consequence of NF-kB activation via stimulation by TNFα[200], which release is significantly reduced by the action of thalidomide and its analogues[203].

The effect of IMiDs is not limited to the stromal compartment. IMiDs, as the name "Immunomodulatory drugs" suggests, are widely active on immune cells within the microenvironment. Firstly, IMiDs are capable of activating immune effector cytotoxic cells against tumour cells. It has been established that both lenalidomide and pomalidomide can enhance antigen uptake and cross-presentation by dendritic cells to T helper cells[206], increase activation of T CD8 cells and to augment their production of IFNγ, perforin and granzyme B, which are mediators of T cell dependent cytotoxicity[207], and inhibit the activation of T regulatory cells (T_{regs}) by reducing *FOXP3* expression[208,209]. Innate immunity also benefits from therapy with IMiDs[210]. It has been demonstrated that lenalidomide enhances NK-mediated tumour toxicity – although concurrent administration of dexamethasone can severely impact this process[211]. On the other hand, lenalidomide augments the activity of NK cells when combined with monoclonal antibodies such as elotuzumab and daratumumab in MM[152,155], and also rituximab in non-Hodgkin Lymphoma[212]. Finally, some authors have demonstrated that lenalidomide can boost CAR-T cell activity against MM and lymphoma[213,214].

All these findings are key to understanding IMiD activity within the tumour microenvironment in a global fashion. Some of the processes by which IMiDs exert anti-tumour action could be successfully leveraged to potentiate available therapeutic approaches against MM and other cancers.

1.2.2.2 Cereblon is an IMiD target

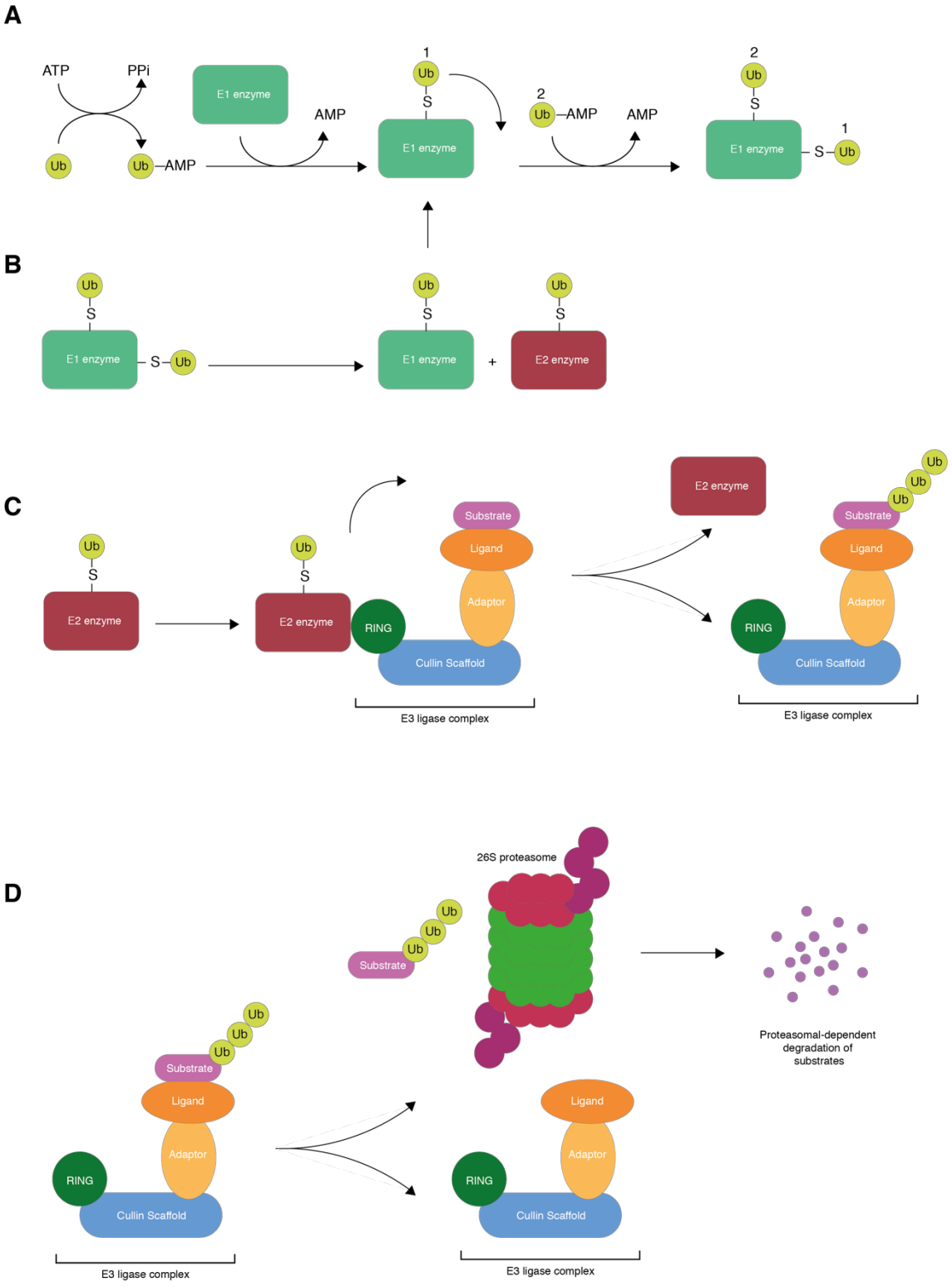
Cereblon (CRBN) is a gene encoding for a 50kDa protein and it is located on chromosome 3p. It was firstly identified to be responsible of a mild type of autosomal recessive non-syndromal mental retardation due to a nonsense mutation (R419X) and proved to regulate conductance of Ca^{2+} and K^{+} ions through neuronal cell surface[215]. In 2010, a Japanese group identified CRBN as the primary target of thalidomide by incubating crude cell lysate with thalidomide immobilised in ferriteglycidyl methacrylate (FG) beads, resulting in the identification of CRBN as an IMiD-binding protein. In the same paper, DNA Damage binding protein 1 (DDB1), Cullin 4A (CUL4A)

and Ring-Box 1 (RBX1) were also co-immunoprecipitated with CRBN and confirmed as CRBN interactors[216]. With this paper, the first step towards the discovery of thalidomide's mechanism of action was made, although the consequences of thalidomide interaction with CRBN-DDB1-CUL4-RBX1 were still largely unknown.

1.2.2.3 Expression of CRBN predicts response to IMiD treatment

The identification of CRBN as primary target of thalidomide and its analogues highlighted the role that CRBN might have in response to IMiD treatment. Soon after, CRBN expression was investigated *in vitro* and within patient cohorts to assess its role in the context of IMiD activity. In 2011, RNA interference was employed to demonstrate that reduced CRBN expression in IMiD sensitive myeloma cells abolishes IMiD inhibitory effect on cell cycle and IMiD killing[217]. In the same paper, lenalidomide resistant MM.1S cells were generated by prolonged exposure to increasing concentrations of lenalidomide. These cells displayed reduced CRBN expression. This observation was associated with deletion of one copy of *CRBN* which resulted in downregulation of *CRBN* mRNA and CRBN protein levels, again confirming the relevance of CRBN in this setting. Furthermore, Zhu et al. showed that expression of *CRBN* in patient MM samples collected pre- and post-lenalidomide therapy was significantly diminished at the time of relapse[217]. In another study, higher expression of CRBN was associated with better response to lenalidomide-dexamethasone regimens by real time quantitative PCR[218]. More recent studies adopting Next Generation Sequencing (NGS)-based technologies have helped characterise genetic abnormalities associated with resistance to IMiD therapy in MM patients. A 2016 study demonstrated that patients with refractory MM who had received LEN treatment showed increased mutations in *TP53,* genes of the *RAS* family and in genes of the CRBN pathway[219]. In particular, 12% of these patients had mutations in the *CRBN* gene, especially at the level of the Thalidomide Binding Domain (the structure of CRBN in relation to thalidomide binding will be discussed in section 1.2.2.5), whilst 6% displayed mutations in *CUL4B*. Another work identified additional genes as possibly involved into IMiD resistance (*TP53*, *PRDM1*, *IRF4*, *MYC*, *DDB1* and *IKZF1)*[220]. The most recent study on CRBN mutational landscape demonstrated that almost one third of patients refractory to pomalidomide, a potent lenalidomide analogue, show genetic alterations in *CRBN*. These include single nucleotide mutations, copy loss, structural variants and the splicing of exon 10[221]. The presence of these mutations also correlated with shorter progression free survival. These observations, taken together, strongly suggest that sensitivity to IMiDs is dependent on the status of CRBN (wild-type or mutated), and that CRBN

Figure 1.2 Biochemistry of protein ubiquitination and degradation. (A) The ubiquitination cascade commences with conjugation of ubiquitin (Ub) with ATP and release of inorganic pyrophosphate. Subsequently, AMP-Ub is conjugated to a cysteine of an E1 enzyme through a thioester bond and, after that, another Ub is again conjugated to AMP. (B) Once E1 are double Ub-loaded, they interact with E2 enzyme and catalyse the Ub transfer to E2[357]. Then, the E2 enzyme carries Ub to an E3 ligase complex (C) which functions as a scaffold by bringing the substrate in proximity to E2-Ub for ubiquitination[357]. (D) Once Ub-conjugated, the substrate is degraded by the 26S proteasome[224].


A
ATP
PPi
Ub
Ub—AMP
E1 enzyme
AMP
1
Ub
S
E1 enzyme
2
Ub—AMP
AMP
2
Ub
S
E1 enzyme
S
1
Ub
B
Ub
S
E1 enzyme
S
Ub
Ub
S
E1 enzyme
+
Ub
S
E2 enzyme
C
Ub
S
E2 enzyme
Ub
S
E2 enzyme
RING
Substrate
Ligand
Adaptor
Cullin Scaffold
E3 ligase complex
E2 enzyme
Ub
Ub
Ub
Substrate
Ligand
Adaptor
RING
Cullin Scaffold
E3 ligase complex
D
26S proteasome
Ub
Ub
Ub
Substrate
Proteasomal-dependent
degradation of
substrates
Ub
Ub
Ub
Substrate
Ligand
Adaptor
RING
Cullin Scaffold
E3 ligase complex
Ligand
Adaptor
RING
Cullin Scaffold
E3 ligase complex

downregulation and/or mutation represent the main mechanisms by which MM cells escape IMiDs anti-cancer effects in patients.

1.2.2.4 The discovery of CRBN neosubstrates

1.2.2.4.1 The biochemistry of ubiquitin and protein degradation

Protein degradation is a fundamental event for the maintenance of cell homeostasis, it is mediated by the action of proteases and it is ATP-dependent. In the late 80s it was discovered that degradation of the bulk cell proteome depends largely on the ubiquitin-proteasome system (Figure 1.2)[222]. The ubiquitin-proteasome machinery becomes essential also in the context of misfolded protein accumulation. In fact, a functional deficiency in this pathway has been identified in the pathogenesis of neurodegenerative diseases[223]. Moreover, as ubiquitination of protein is a key post-translational modification that serves to modulate several other pathways, malfunctioning of this tightly regulated system can lead to dysregulation of essential processes such as cell cycle or gene expression[222]. Ub tagging can result in different outcomes for the substrate. For example, polyubiquitination in Lys48 or Lys11 is a marker for proteasomal degradation, whereas poly-Ub is Lys63 serves DNA repair. On the other hand, a single Ub (mono-Ub) can influence localisation and function of specific proteins[224].

The aforementioned CUL4-RBX1-DDB1 complex is a cullin-RING ligase which participates in the canonical reaction of substrate Ub-conjugation for proteasomal degradation[225,226]. Cullin-RING Ub ligases are E3s possessing a scaffold protein (cullins, 1 to 7), a RING protein (RBX1) that is responsible for binding E2s, and an adaptor (DDB1) that confers substrate specificity. Additionally, cullin-RING receptor ligands, such as CRBN or DDB2, are capable of docking cullin-RING adaptors and they ensure the loading of the target substrate onto the E3 complex[226,227].

1.2.2.4.2 IMiDs induce CRBN-mediated degradation of Ikaros and Aiolos to mediate anti-myeloma effects

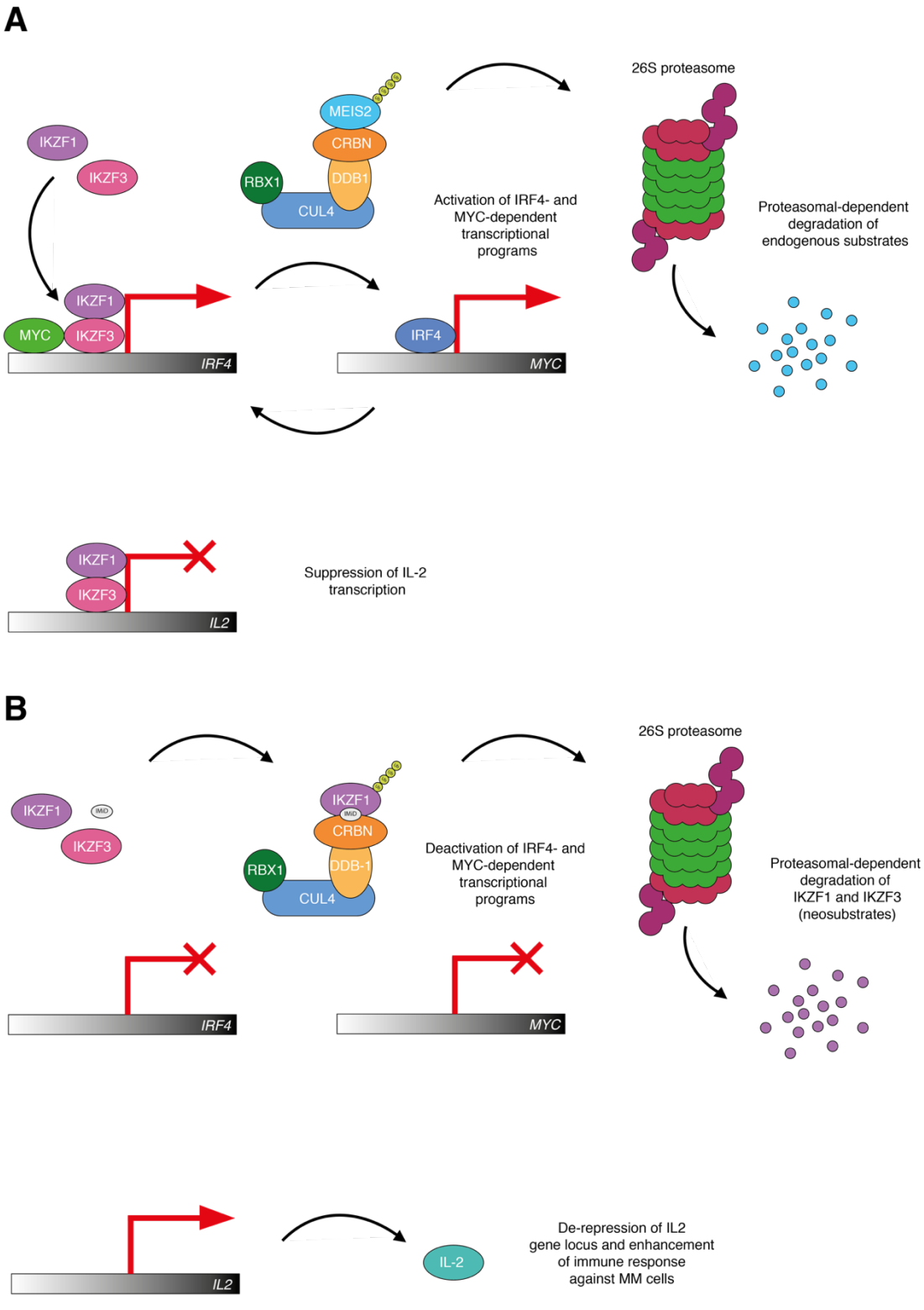
In 2014, based on the findings of Ito et al.[216], two independent groups investigated whether the anti-MM effects of lenalidomide were the consequence of modulating CRBN E3 ligase activity[89,90]. In these papers, Lu et al. and Kronke et al. demonstrated, through a luciferase reporter assay and a proteomic-based assay respectively, that lenalidomide is capable of binding CRBN, inducing ubiquitination and subsequent proteasomal-dependent degradation of Ikaros (or IKZF1) and Aiolos (or IKZF3). Previous papers had reported the importance of *IRF4* in MM, defining this dependency as an example of "non-oncogene addiction"[65], and shown that

expression of IRF4 is significantly downregulated following IMiD treatment[197]. For these reasons, Kronke et al. aimed to provide evidence of a mechanistic link between IRF4 suppression and lenalidomide treatment[90]. Having identified IKZF1 and IKZF3 as lenalidomide targets, they hypothesised that degradation of these TFs would impact *IRF4* transcription. Using RNA interference, they demonstrated that knockdown of IKZF3 induces a reduction in *IRF4* transcription, depicting a possible cell intrinsic molecular mechanism of action of IMiDs in MM cells[90]. Based on the notion that IKZF1 and IKZF3 repress transcription at the *IL2* locus (as discussed in section 1.1.4.2.4), Kronke and colleagues also demonstrate that knockdown of IKZF1/3 or treatment with lenalidomide increase the transcription of *IL2*. Since IRF4 modulates the expression of MYC[65,197], some authors hypothesised that the detrimental effect produced by IMiDs on MM cells is due to the IRF4-MYC axis shut-down via IKZF1/3 degradation[228]. In summary, a molecular mechanism for IMiDs was finally depicted, thus highlighting the importance of the IKZF1/3-IRF4-MYC axis in MM and the capability of IMiDs to interfere with its signalling (a schematic of IMiDs mechanism of action is provided in Figure 1.3).

1.2.2.4.3 Lenalidomide-induced degradation of CK1α in 5q- refractory anaemia

Multiple myeloma is not the only disease for which IMiDs are indicated. In the era prior to the discovery of neosubstrates, lenalidomide was proven to be effective in 5q- myelodysplastic syndrome. Del(5q) is often associated with refractory anaemia, a clinical condition which may require frequent blood transfusions[187]. The idea of a tumour suppressor being deleted within the missing region in the chromosome 5q had been hypothesised to explain the link between loss of 5q and the refractory phenotype[229]. After the discovery of IKZF1/3 CRBN-dependent ubiquitination and degradation, Ebert and colleagues have made the seminal discovery that lenalidomide is capable of inducing apoptosis of 5q- cells via CRBN-dependent CK1α degradation in the context of haploinsufficiency[230]. Their paper clearly delineated very important aspects of IMiD biology. Firstly, they highlighted the existence of differential substrate specificity between IMiDs, as lenalidomide, but not thalidomide or pomalidomide, engages CK1α upon CRBN binding. Secondly, they observed that CK1α degron region does not align with that of IKZF1/3, meaning that substrate binding to CRBN-IMiD is not dependent solely on a single aminoacidic motif. These observations, taken together, suggest that IMiD "degradomes" only partially overlap between each other. In the clinical context, the existence of differential degradomes could explain the diversity of side effects between analogues and their efficacy in counteracting tumour growth.

Figure 1.3. A basic model for the mechanism of action of IMiDs in MM. (A) The CUL4-DDB1-RBX1-CRBN E3 ubiquitin ligase catalyses the ubiquitination of endogenous substrates (e.g. MEIS2) to promote their proteasomal-dependent degradation. Normally, within MM cells, IKZF1 and IKZF3 are poised to induce transcription of *IRF4*, the plasma cell master regulator. Then, IRF4 stimulates the transcription of *MYC*, which triggers a positive feedback loop by augmenting *IRF4* transcription. IKZF1 and IKZF3 also repress transcription of IL-2, a T-cell activating cytokine. (B) In the presence of an IMiD, CRBN substrate specificity is redirected towards "neosubstrates", such as IKZF1 and IKZF3, with loss of affinity for endogenous substrates, as IMiDs would modify the surface of CRBN that interfaces with substrates. The loss of IKZF1 and IKZF3 causes the shutdown of the *IRF4-MYC* transcriptional loop, with subsequent anti-MM effect. Simultaneously, de-repression of the *IL2* locus with production of IL-2 would trigger an anti-MM immune response (adapted from Licht et al., 2014[228]).


A
IKZF1
IKZF3
MEIS2
CRBN
RBX1
DDB1
CUL4
26S proteasome
Activation of IRF4- and
MYC-dependent
transcriptional
programs
Proteasomal-dependent
degradation of
endogenous substrates
IKZF1
MYC
IKZF3
IRF4
IRF4
MYC
IKZF1
IKZF3
IL2
Suppression of IL-2
transcription
B
IKZF1
IMiD
IKZF3
IKZF1
IMiD
CRBN
RBX1
DDB-1
CUL4
26S proteasome
Deactivation of IRF4- and
MYC-dependent
transcriptional
programs
Proteasomal-dependent
degradation of
IKZF1 and IKZF3
(neosubstrates)
IRF4
MYC
IL2
IL-2
De-repression of IL2
gene locus and enhancement
of immune response
against MM cells

1.2.2.4.4 IMiDs disrupt the CRBN chaperone-like activity on MCT1-CD147

In 2016, a German group employed tandem affinity purification (TAP) of CRBN and screened for potential CRBN interaction partners via mass spectrometry. They discovered that CRBN interacts with MCT1 (or SLC16A1) and Basigin, (BSG or EMMPRIN or CD147)[231]. These proteins are implicated in several mechanisms such as transport of nutrients, migration of inflammatory cells and induction of metalloproteinases[232]. All of these pathways and mechanisms can ultimately be advantageous for cancer cells, for MM cells can hijack processes such as angiogenesis, cell proliferation, and metabolism at their own benefit to escape cell growth control and to metastasise both locally and/or distantly (as discussed in paragraph 1.2.4). In this context, CRBN promotes maturation of MCT1 in complex with CD147 independently of ubiquitinylation, and CRBN binding to CUL4 and MCT1-CD147 is mutually exclusive. However, similarly to IKZF1/3 and CK1α degradation, exposure to IMiD inhibited maturation of MCT1-CD147 in a dose-dependent manner and suppressed pro-survival signalling. With this work, Eichner and colleagues have provided important additional data that could potentially explain effects on microenvironment following IMiD treatment and proved the existence of an alternative pathway by which IMiDs exert antitumoral effects.

1.2.2.5 Structural insight into the engagement of neosubstrates by the CRBN complex

1.2.2.5.1 The structure of IMiDs and CRBN in complex with CUL4-DDB1-RBX1

The backbone of thalidomide and analogues is represented by glutarimide and phtalimide moieties, where the latter is modified with an amino group at the fourth carbon in lenalidomide and pomalidomide (isoindolinone group). In simple terms, pomalidomide structures appears as a combination of those of thalidomide and lenalidomide (Figure 1.4)[233]. Crystal structure studies have provided precise information regarding CRBN in complex with DDB1 and lenalidomide. CRBN possesses three domains – an N-terminal domain, a helical bundle domain that mediates the interaction with DDB1, and a C-terminal domain where the thalidomide pocket is located (TBD, thalidomide binding domain). Within the CUL4-DDB1-RBX1-CRBN complex, CRBN represents the DCAF (DDB1- and CUL4-Associated Factor) element, i.e. the cullin ring ligand for CUL4-DDB1-RBX1. The variety of CUL4-DDB1-RBX1 substrates is the consequence of the existence of several DCAFs for the same complex[225]. Ubiquitination of substrates occurs when CUL4-RBX1 rotates around DDB1 and CRBN creating a ubiquitination zone, where any lysine within the zone is likely to be ubiquitin-conjugated[225,234].

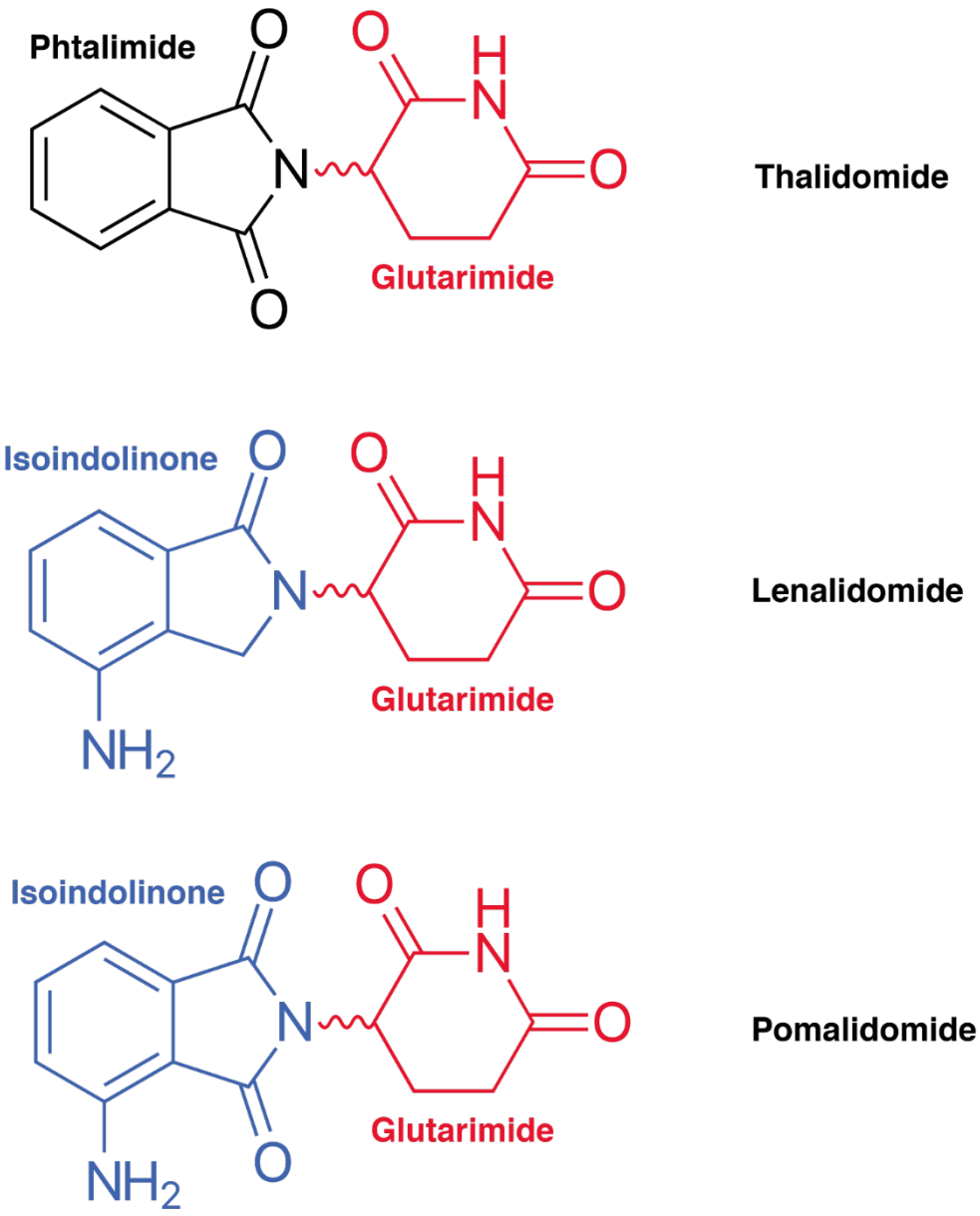


Figure 1.4 Structure of immunomodulatory drugs (IMiDs). (A) Thalidomide structure. Highlighted in red, the glutarimide group. The phtalimide group is represented in black. (B) Lenalidomide structure: in red the glutarimide group, in blue the isoindolinone group. (C) The structure of pomalidomide has mutual characteristics with those of both thalidomide and lenalidomide.

1.2.2.5.2 The thalidomide binding pocket of CRBN and the interaction with neosubstrates

An interesting feature of the TBD is the presence of a conserved Zn^{2+}-binding site in the thalidomide binding pocket. The TBD is constituted by three key Trp aminoacids (residues 380, 386 and 400). Mutations at Trp 380 and 386 together abolish the contact between thalidomide and CRBN[235]. It is now accepted that when an IMiD binds CRBN, the glutarimide moiety docks into the TBD, whilst the isoindolinone (or phtalimide) group is extruded outside the TBD and provides with a surface for the recruitment of neosubstrates. Fischer and colleagues[225], in their work, propose a simple model, where the endogenous CRBN substrate MEIS2 is normally degraded, and its degradation is impaired in the presence of an IMiD. At the same time, in IMiD-exposed cells, degradation of neosubstrates (such as IKZF1 and IKZF3) and stabilisation of endogenous CRBN targets will occur. Moreover, in the work of Petzold and colleagues[234], it has been demonstrated that recruitment of IKZF1 and CK1α at the CRBN carboxy-terminal domain (CTD) is mutually exclusive. In IKZF1, the "degron", or the region involved into CRBN-IMiD binding, is located in the ZF2 motif. Sievers and colleagues have demonstrated that the ZF2 motif is the minimal element required for IKZF3 degradation, and that the presence of another ZF motif, such as ZF3, provides with additional affinity for CRBN-pomalidomide[236].

Fascinatingly, the tertiary structure of the CRBN-binding region of CK1α shares a very high level of homology with that of IKZF1, indicating that not only the sequence directly, but also the tertiary structure, influences the binding of CRBN to neosubstrates[234].

1.2.2.5.3 Novel murine models for the study of IMiDs *in vivo*

The lack of activity of thalidomide and analogues in rodents has been known for decades. In 1965, Fratta and colleagues demonstrated that, with the exception of rabbits, rodents were not susceptible to thalidomide teratogenicity[179]. A 2015 paper proved that mouse Crbn and human CRBN differs of five residues in the CTD, where the thalidomide binding pocket sits[230]. These five residues are thus possible candidates for insensitivity to thalidomide analogues in rodents. One of them, precisely CRBN V387, which corresponds to Crbn I391 was demonstrated to cause complete resistance to IMiDs. In fact, the substitution of Isoleucin with Valine in position 391 was sufficient to cause degradation of Ck1α in mouse cells. Despite this understanding, a murine model was not yet available to fully explore the phenotype produced by thalidomide analogues *in vivo*. However, recent advances in genetic engineering allow quick and efficient editing of DNA at a nucleotide-precision level. In the paper of Fink and colleagues, CRISPR homology directed repair was employed to successfully generate an IMiD-sensitive mouse strain by substituting I391 with a Valine[237]. With Crbn I391V, known CRBN target were now degraded upon

lenalidomide treatment. The inhibitory effect on the haematopoietic compartment were evident, with reductions of the white blood cell count. Furthermore, lenalidomide induced release of IL-2 by T cells and produced foetal malformation in litters. Although this model provides an important tool for *in vivo* IMiDs studies and an essential proof of concept for their mechanism of action, many questions remain to be addressed. Other research groups have focussed on the benefit of IMiDs in other diseases, such as inflammatory bowel syndromes. It has been reported that IMiD treatment is beneficial for colitis in both WT mice or mice bearing *Crbn* I391V, suggesting alternatives pathways by which IMiD positively impact the immune system[238].

1.2.2.6 A complex machinery is required for IMiD-dependent degradation of CRBN neosubstrates

In two recent papers with similar findings[239,240], MM1.S-Cas9 cells (an IMiD sensitive patient-derived MM cell line) were employed to identify genes causing resistance to IMiDs. The methodology involved lentiviral transduction of cells with a genome-wide CRISPR knockout (KO) library[241], with several sgRNAs specific for each gene in the genome followed by application of a selective pressure with IMiD treatment for several weeks. Ideally, at the end of the screen, only resistant clones should be viable and/or proliferating in culture. With the use of Next Generation Sequencing (NGS), it is then possible to sequence the genomic DNA of remaining cells at the end of the screen to assess enrichment or depletion of sgRNAs integrated in the genome. In this specific case, the authors identified enriched sgRNAs that caused resistance to IMiDs. SgRNAs specific for *CRBN* were the most significant and enriched, followed by subunits of the COP9 Signalosome, *DDB1*, *CAND1*, E2 ubiquitin ligating enzymes (*UBE2M*, *UBE2G1*, *UBE2D3*), *GLMN* and others interesting genes, such as *NCOR1*. Most of these proteins are essential for the recycling of CUL4-DDB1-CRBN following substrate ubiquitination.

1.2.2.6.1 The COP9 Signalosome

The COP9 Signalosome (CSN) is a multi-subunit protein complex which serves for numerous functions. The main role of the CSN is that of regulation of cullins, a family of scaffold protein that are poised to promote ubiquitination of substrates in the context of protein degradation, DNA stability, signal transduction and other important mechanisms[224,242,243]. An important regulator of cullin activity is NEDD8. This ubiquitin-like protein is required for cullins to exert their action of scaffolding cofactors in polyubiquitylation of substrates[244]. In particular, CSN inactivates cullins by removal of NEDD8 through its catalytic subunit, COPS5 or CSN5. NEDD8

removal by CSN5 causes inability of the E3 ubiquitin ligase enzyme to induce ubiquitinylation of substrates. However, cullin functions are extended to other mechanisms such as DNA repair response, including nucleotide excision repair (NER) and double-strand break repair (DBSR). In fact, it has been shown that CUL4 and DDB1 are required for both NER, transcription-coupled NER and DSBR, and that CSN fine-tune their activity in the context of the DNA damage response[245,246].

Although CSN5 is strictly required for de-neddylation, the deletion of other subunits can affect cellular homeostasis at various levels. Another layer of complexity is consequential to the existence of "Mini-CSN" in which only some of the subunit are present, although their functions remain poorly characterised. Single CSN subunit can elicit biological effects on their own, such as COPS2/CSN2, which participates into regulating transcription together with CREB[247]. It is interesting to note that, as reported by Chamovitz[248], in *Drosophila* the knockout of some CSN subunits leads to a broad transcriptional dysregulation (around the 20% of the transcriptome) and larval lethality. The CSN is essential for various functions: development, transcriptional regulation, protein degradation and DNA homeostasis. Its key role in the context of IMiD treatment is the result of CUL4 activity modulation. From this point of view, it is not excluded that IMiD could potentially impact many of these biological processes.

1.2.2.6.2 A continuous assembly/disassembly cycle of CUL4-DDB1-RBX1-CRBN is required for efficient protein degradation of CRBN substrates and neosubstrates

The work of Sievers et al.[239] highlighted some fundamental insights into IMiDs mechanism of action. The knockout of *CRBN*, *UBE2M*, *UBE2G1*, *UBE2D3* and *COPS5/CSN5* synthetically produced resistance to lenalidomide. Further experiments demonstrated that E2 enzymes UBE2D3 and UBE2G1 are required for polyubiquitylation of CRBN substrates. Moreover, whilst heterozygous loss of *UBE2M* results in reduced NEDDylation and inhibition of CUL4 activity, deletion of *COPS5/CSN5* causes missing removal of NEDD8 from CUL4. The latter is necessary to allow physiological re-cycling of the CUL4-DDB1-RBX1 complex. In fact, NEDDylation prevents CAND1 from disassembling CUL4-DDB1-RBX1-CRBN prior to another round of substrate ubiquitinylation[249]. Thus, inhibition of NEDDylation or de-NEDDylation both impact on CUL4-DDB1-RBX1-CRBN ubiquitin-ligase activity, annihilating *de facto* IMiD anti-MM action.

1.2.2.6.3 The COP9 signalosome prevents CUL1-SCF^{Fbox1}-dependent CRBN degradation

As previously mentioned, Liu et al. obtained similar findings to those of Sievers and colleagues – CRBN, DDB1, CSN subunits and NCOR1 were hit in their resistance screen with pomalidomide.

However, in Liu's paper, a different aspect of CRBN biology was explored[240]. Firstly, pomalidomide resistance was validated in MM.1S cells with deletion of CRBN and each single CSN subunits independently. Secondly, they provided with evidence that CSN prevents CRBN degradation. In the absence of COPS2/CSN2, COPS4/CSN4, COPS6/CSN6, COPS7B/CSN7B or COPS8/CSN8, CRBN levels were lower than in WT cells. The same group had previously discovered that CRBN's proteasomal degradation follows ubiquitination by CUL1-$SCF^{Fbox1250}$; thus, they explored and then confirmed the hypothesis that CSN controls CRBN levels via de-NEDDylation of CUL1 by employing CSN2-deleted cells. The authors then explored the possibility of increasing CRBN protein levels by inhibiting the proteasome. In doing so, CRBN levels were increased, with subsequent increased efficiency of IKZF1 and IKZF3 degradation.

1.3 Hypotheses and aims

IMiDs have significantly improved survival and quality of life of MM patients and they represent a cornerstone of MM therapy. Their biological activity impacts MM PCs survival and proliferation, affects the MM-sustaining bone marrow microenvironment and potentiates anti-MM immune response. Unfortunately, patients ultimately develop therapy resistance to these drugs. Despite advances in the characterisation of the molecular mechanisms underpinning IMiD anti-MM effect (such as the discovery of IMiD-induced degradation of IKZF1/3 with the subsequent downregulation on the *IRF4-MYC* axis), the pathways implicated in IMiD resistance and the biochemistry underlying CRBN functions in MM cells are still largely unknown. Given the complexity of MM and its impact as an incurable and debilitating disease, a deeper understanding of the mechanisms driving disease progression and development of therapy resistance is urgently required.

Hypothesis 1. Acquired resistance to IMiDs is a process of adaptation to prolonged IMiD exposure and does not solely depend on downregulation of CRBN. Alternative mechanisms of resistance exist, and resistance can be rescued by modulation of unknown pathways.

Aim 1. To employ novel, unbiased technologies, such as RNA-sequencing and genome-wide CRISPR screening to 1) explore transcriptional signatures of IMiD therapy and those of acquired resistance to IMiDs in MM; 2) clarify mechanisms of sensitivity and resistance to IMiDs in MM and 3) identify vulnerabilities and mechanisms of resensitisation to IMiDs in cells with acquired IMiD-resistance.

Significance. Novel insight obtained with these approaches may translate into the clinic with development of novel strategies for potentiation of IMiD therapy, significant improvement in the response to IMiD therapy and better overall survival for the MM patient.

Hypothesis 2. Beside the known mechanisms of action, other factors are important for the anti-MM effects of IMiDs and are consequential to the fate of endogenous CRBN substrates, *neosubstrates*, interactors and *neointeractors* upon treatment with IMiDs.

Aim 2. To utilise BioID2-dependent proximity labelling to better characterise the CRBN interactome in the context of IMiD treatment, with the employment of different IMiD analogues and the addition of the proteasome inhibitor bortezomib to inhibit degradation of the pool of CRBN substrates/neosubstrates.

Significance. Findings in this area may provide a better understanding of CRBN substrates and both stable and transient interacting proteins. A more comprehensive map of the CRBN

interactome (in the presence or the absence of an IMiD) might improve the current understanding of IMiD mechanism of action and highlight the biochemistry underpinning the side effects of IMiD therapy.

Chapter 2: Materials and methods

2.1 Cell culture techniques

2.1.1 Cell lines and culture methods

All myeloma lines were cultured in RPMI-1640 media (Gibco) supplemented with 10% FBS (HyClone), 1mM Sodium Pyruvate (Gibco, 11360070), 2mM GlutaMAX (Gibco, 35050061) and Penicillin 100 U/mL plus Streptomycin 100 mg/mL (Pen/Strep). MM.1S, MM.1Sres, U266, U266res and OPM2 cells were split twice a week, RPMI-8226 and JJN3 cells were split three times a week. MM.1Sres and MM.1Sres-derived cell lines were spiked with 10μM lenalidomide twice a week. Lenalidomide was washed out at least 3 days before experiments. All MM lines were kept at 37° C, 5% CO_2. MM.1S, MM.1Sres, U266 and U266res cell line (lenalidomide-resistant MM.1S) were a gift from Prof. Keith Stewart (Mayo Clinic, Scottsdale, AZ). JJN3 cells were a gift from Prof. Andrew Spencer (Alfred Hospital, Melbourne). All cell lines derived by viral transduction were cultured in the same fashion to that of their relative parental line and are listed in Table 2.1.

HEK293T cells were cultured in DMEM supplemented with 10% FBS, 2mM GlutaMAX and Pen/Strep, split three times a week and kept at 37° C, 10% CO_2.

Cell line fidelity was verified by STR-profile and regularly tested and free of mycoplasma contamination. Viable cell counts were performed employing Bio-Rad TC10 automated cell counter following resuspension of cells in a 1:1 ratio with 0.4% trypan blue in PBS.

2.1.2 Preparation of cell culture dishes for proteomics assays

For proteomics assays, HEK293T cells were cultured in 10 cm or 15 cm cell culture dishes (Greiner Bio-One). Pre-coating with poly-L-lysine was performed to ensure cell adhesion on culture dishes surfaces. For coating of cell culture dishes, poly-L-lysine was diluted 1:9 with ultrafiltered sterile water and 5ml of diluted Poly-L-lysine (Sigma-Aldrich) were poured into culture dishes, followed by 1-hour incubation at room temperature. After that, poly-L-lysine was discarded. Cell culture dish surfaces were dried in sterile environment for 20 minutes at room temperature and subsequently rinsed twice with sterile Phosphate Buffer Saline solution (PBS) prior to cell seeding.

Table 2.1. Table of cell lines derived from parental MM cell lines via viral transduction.

Cell line	Transduction type	Vector	Cell line of origin
MM.1S-Cas9-mCherry	Lentiviral	*FUCas9-mCherry*	MM.1S
MM.1Sres-Cas9-mCherry	Lentiviral	*FUCas9-mCherry*	MM.1Sres

MM.1S-Cas9-SCR-GFP	Lentiviral	*FGH1T-UTG-SCR-GFP*	MM.1S-Cas9-mCherry
MM.1S-Cas9-SCR-BFP	Lentiviral	*FGH1T-UTG-SCR-BFP*	MM.1S-Cas9-mCherry
MM.1S-Cas9-sgTOP2B#1	Lentiviral	*FGH1T-UTG-GFP-sgTOP2B#1*	MM.1S-Cas9-mCherry
MM.1S-Cas9-sgTOP2B#4	Lentiviral	*FGH1T-UTG-GFP-sgTOP2B#4*	MM.1S-Cas9-mCherry
MM.1Sres-Cas9-SCR-GFP	Lentiviral	*FGH1T-UTG-SCR-GFP*	MM.1Sres-Cas9-mCherry
MM.1Sres-Cas9-SCR-BFP	Lentiviral	*FGH1T-UTG-SCR-BFP*	MM.1Sres-Cas9-mCherry
MM.1Sres-Cas9-sgTOP2B#1	Lentiviral	*FGH1T-UTG-GFP-sgTOP2B#1*	MM.1Sres-Cas9-mCherry
MM.1Sres-Cas9-sgTOP2B#4	Lentiviral	*FGH1T-UTG-GFP-sgTOP2B#4*	MM.1Sres-Cas9-mCherry
MM.1Sres-Cas9-sgATXN7#1	Lentiviral	*FGH1T-UTG-GFP-sgATXN7#1*	MM.1Sres-Cas9-mCherry
MM.1Sres-Cas9-sgATXN7#4	Lentiviral	*FGH1T-UTG-GFP-sgATXN7#4*	MM.1Sres-Cas9-mCherry
MM.1S-Luc2-GFP	Retroviral	*MSCV-Luc2-GFP*	MM.1S
MM.1Sres-Luc2-GFP	Retroviral	*MSCV-Luc2-GFP*	MM.1Sres
OPM2-BioID2	Retroviral	*pBABE-myc-BioID2-puroR*	OPM2
OPM2-BioID2-CRBN	Retroviral	*pBABE-myc-BioID2-CRBN-puroR*	OPM2

2.1.3 Viral transduction

On day 0, $12x10^6$ HEK293T cells were plated 24 hours prior to transfection in a T175 flask (CELLSTAR®, Greiner Bio-One, Germany). On day 1, target DNA was added with a cocktail of packaging vectors suitable for production of lentiviral particles or retroviral particles in presence of polyethylenimine (PEI, Sigma-Aldrich, 9002-98-6). For lentiviral transduction, 7 µg *pMDL*, 4.2 µg *pVSV*, 3.5 µg *pRSV-REV*, 14 µg target DNA and PEI at a PEI to DNA ratio of 5:1 were resuspended in DMEM (up to 1 mL) with no supplements. For retroviral transduction, 30µg of *pCL-Ampho*, 30µg of target DNA and PEI at a PEI to DNA ratio of 3:1 were resuspended in DMEM (up to 1 mL) with no supplements. Following addition of plasmids in media, the solution was thoroughly vortexed. After that, PEI was added, the mix vortexed again and then incubated at room temperature for 10 minutes. Finally, DNA-PEI mix in DMEM was pipetted dropwise in the flask with growing HEK293T cells.

On day 2, supernatant was discarded and replaced with fresh DMEM with supplements (as previously described in paragraph 2.1.1). On day 3, supernatant was discarded and replaced with fresh MM cell media (RPMI-1640 with supplements). On day 4, supernatant was collected, replaced with fresh MM cell media and filtered with a 0.45 µm strainer (Greiner Bio-One, Germany). Target cells were then plated at 500000/mL in a 6-well plate (CELLSTAR®, Greiner Bio-One, Germany) and cultured with collected media containing lentiviral particles. 4 µg/mL Sequabrene (Sigma-Aldrich, S2667) was added to each well. On day 5, cells were harvested, washed and replated with fresh viral media (with sequabrene 4 µg/mL) for a second transduction hit. On day 6, cells were washed and re-plated with fresh media.

2.1.3.1 Generation of MM.1S-Cas9 and MM.1Sres-Cas9 FgH1T-UTG cells

MM.1Sres-Cas9 cells were transduced via lentiviral infection with either *FgH1T-UTG-GFP* expressing sgTOP2B#1, sgTOP2B#2, sgATXN7#1, sgATXN7#4 or a scrambled guide, or with *FgH1T-UTG-BFP* expressing a scrambled guide. Double positive mCherry^{bright} and GFP or BFP^{bright} cells were FACS-sorted to obtain a pure population (FACSAria Fusion V, BD Biosciences). Subsequently, guide expression was triggered upon activation of tetracycline responsive element with 1µg/mL doxycycline (Doxycyline Hyclate, Sigma-Aldrich) to induce gene knockout (KO). For MM.1Sres-Cas9 cells with *TOP2B* and *ATXN7* deletion, lenalidomide was not spiked into the growth medium. Gene deletion was validated via detection of insertion/deletion in the guide targeting region with Tracking of Indel Decomposition (TIDE) or via probing for protein expression through Western blotting.

2.1.4 Dialysis of Foetal Bovine Serum

To perform dialysis, 25 cm of SnakeSkin dialysis tube (ThermoFisher Scientific) were filled with FBS, sealed and immersed for 72 hours at 4°C in PBS. PBS was changed twice a day. After 72 hours, dialysed FBS (dFBS) was filter-sterilised and stored at -20°C.

2.2 Cell death and cell proliferation assays

2.2.1 Anti-cancer agents

Each compound was added in cell growth medium at the appropriate concentration as described in the result chapters. All anti-cancer agents employed for this thesis are listed in Table 2.2.

Table 2.2. Table of the anti-cancer compounds employed

Compound Name	Solvent	Final Stock Concentration	Storage	Catalogue #	Provider
Lenalidomide	DMSO	100mM	-20° C /-80° C	901558	Sigma-Aldrich
Pomalidomide	DMSO	10mM	-20° C /-80° C	P0018	Sigma-Aldrich
Iberdomide	DMSO	10mM	-20° C /-80° C	S8760	Selleckchem
Etoposide Phosphate	0.9% NaCl	3mM	4° C (dark)	NA	PeterMac Pharmacy
Dexrazoxane (ICRF-187)	DMSO	100mM	-80° C	S1222	Selleckchem
Puromycin	PBS	1mg/mL	-20° C	P8833	Sigma-Aldrich
Velcade (Bortezomib)	0.9% NaCl	910µM	4° C (dark)	NA	PeterMac Pharmacy

2.2.2 CellTrace™ Violet – propidium iodide proliferation assay

One vial of desiccated CellTrace™ Violet (CTV) dye (Invitrogen, C34557) was reconstituted with 20 µL of DMSO provided within the kit. Cells were harvested, centrifuged at 300rcf for 4 minutes. Media was discarded and cells resuspended at 10^7/mL in PBS into a 50 mL tube. 1 µL of CTV was added for each mL of cell suspension. Cells were then incubated in a water bath at 37° C for 20 minutes, gently mixing up and down the suspension every 5 minutes. Cells were successively centrifuged at 300rcf for 4 minutes and the supernatant was discarded. Cells were washed with 50 mL of PBS and centrifuged again at 300rcf for 4 minutes. After that, supernatant was discarded and cells were resuspended at 10^7/mL in FACS buffer (100 mM EDTA, 2% Foetal Bovine Serum in PBS), stained with Propidium Iodide (PI) at a final concentration of 1µg/mL and sorted for highly CTV^+ (Pacific Blue) and viable (PI negative) cells (BD, Fusion V Aria). CTV^+ cells were plated in a 6-well plate and cultured in drug or vehicle as long as CTV dye resulted detectable through FACS analysis (BD, LSR II). FACS analyses were performed every 3-4 days measuring CTV peaks (In the Pacific Blue channel) of PI^- cells (FL3 channel).

2.2.3 DNA content/Cell cycle analysis with Nicoletti staining

MM.1S and MM.1Sres cells were initially seeded at 10^5/mL in a 48-well plate (CELLSTAR®, Greiner Bio-One, Germany). To measure DNA content, MM.1S and MM.1Sres cells were harvested after treatment with LEN and/or DXZ for 7 days. 3 technical replicates were set up for each condition. LEN was refreshed every day, whilst DXZ was added at day 0 (T0) and day 3. After treatment with LEN and/or DXZ, myeloma cells were harvested, spun at 300rcf for 4 minutes and washed with ice cold PBS twice. Subsequently, cells were fixed with -20°C ethanol 50% in PBS and incubated in ice for at least 2 hours. Then, cells were washed with ice cold PBS to dilute ethanol and spun at 300rcf for 4 minutes. Supernatant was discarded and cells resuspended in Sodium Citrate/PI buffer (0.1% w/v sodium citrate, 40 mg of PI each litre of deionized water) with addition of 100µg/mL of RNAse A. DNA content at different cell cycle phases was assessed through flow cytometry (BD, LSR II) at low acquisition speed.

2.2.4 Cell death assay with propidium iodide

MM cells were plated at day 0 at a fixed density in a 48-well plate (10^4 for MM.1S and MM.1Sres, $5x10^4$ for OPM2, RPMI-8226 and JJN3 cells) in a total volume of 1mL. 3 technical replicates were set up for each condition for the day 3 and day 7 harvest timepoints. LEN was refreshed every day, whilst DXZ was added at day 0 (T0) and day 3. Viable cell count was performed alongside at day 3 and day 7. After treatment with LEN and/or DXZ for 3 and 7 days, myeloma cells were

harvested, spun at 300rcf for 4 minutes and washed with ice cold PBS twice. After that, cells were resuspended in FACS buffer (100 mM EDTA, 2% Foetal Bovine Serum in PBS) and PI 1μg/mL. Cell death at day 3 and day 7 was assessed by measurement of PI^+ cells by flow cytometry analysis (BD, LSR II).

2.2.5 Lenalidomide-dexrazoxane synergy assays

MM.1S and MM.1Sres cells were plated at day 0 at a fixed density in a 96-well plate ($5x10^4$) in a total volume of 0.2 mL. Cells were treated with combination of 0, 0.5, 1, 2, 5, and 10 μM LEN and 0, 5, 10, 20, 50 and 100 μM DXZ. LEN was refreshed every day, whilst DXZ was added at day 0 (T0) and day 3. After 7 days, cells were harvested, spun at 300rcf for 4 minutes and washed with ice cold PBS twice. After that, cells were resuspended in FACS buffer (100 mM EDTA, 2% Foetal Bovine Serum in PBS) and 1 μg/mL PI. Cell death at day 7 was assessed by measurement of PI^+ cells by flow cytometry analysis. The average cell viability (% of PI negative cells) for each condition of three independent experiments was used to compute the Zero Interaction Potency (ZIP) synergy score using the R package synergyfinder (v1.8.0).

2.2.6 Competitive proliferation assays

MM1Sres-Cas9 cells transduced with *FgH1T-UTG-GFP* (expressing non targeting/scrambled sgRNA, sgTOP2B#1 or sgTOP2B#2) or *FgH1T-UTG-Scramble-BFP* were cultured for 1 week in media containing doxycycline 1μg/ml to induce the expression of sgRNAs. Scramble-BFP cells and sgTOP2B-GFP cells were seeded at a 1:1 ratio, with a total number of 1 million cells in 3 mL of media in a 6-well plate. Cells were treated with DMSO, LEN 2μM or POM 500nM for 21 days refreshing drugs every day. Cells were split twice a week and always seeded at 1 million cells in 3 mL of media. GFP^+ and BFP^+ fractions of each sample were measured by FACS analysis through gating on $mCherry^+$ cells every twice a week, every 3-4 days. Scrambled-BFP cells in competition with Scramble-GFP cells were used as control and cultured as described above.

2.3 Protein techniques

2.3.1 Cell lysis

Radio Immuno Precipitation Assay (RIPA) buffer supplemented with protease inhibitor (cOmplete protease inhibitor cocktail, Roche, 11697498001) or in Laemmli buffer for solubilisation of chromatin-bound proteins. To lyse 1 million cells, either 20μL of RIPA buffer or

50µL of Laemmli sample buffer were used. Composition of both RIPA and Laemmli buffer is described in Table 2.3.

Table 2.3 Composition of lysis buffers

Lysis buffer	Percentage or Molarity	Reagent
RIPA buffer	150 mM	NaCl
	1%	Nonidet P-40
	0.5%	Sodium Deoxycholate
	0.1%	Sodium Dodecyl Sulphate
	50mM	Tris pH 7.4
	-	ddH_2O
Laemmli buffer (2x)	4%	Sodium Dodecyl Sulphate
	20%	Glycerol
	0.1%	Tris pH 6.8
	-	ddH_2O

2.3.1.1 Lysis in RIPA

Cells were harvested, spun at 300g for 4 min. Subsequently, cells were resuspended in PBS and spun at 300g at 4°C - this step was repeated once more. 20 µL of RIPA buffer were used for lysis of 10^6 cells. For proteomics assays, HEK293T cells were harvested by direct on-dish lysis with 3mL of buffer and transferred on a 15mL falcon tube. Cells were incubated at 4°C for 30 minutes and vortexed every 10 minutes. After that, insoluble chromatin fraction in the lysates was pelleted by spinning at top speed for 10 minutes, pellet discarded and supernatant kept for protein quantification.

2.3.1.2 Lysis in Laemmli (solubilisation of chromatin-bound proteins)

Cells were harvested, spun at 300g for 4 min. Subsequently, cells were resuspended in PBS and spun at 300g at 4°C - this step was repeated once more. 50µL of 1X Laemmli buffer were used for lysis of 10^6 cells. Cells were incubated at room temperature for 5 minutes and then for 15 minutes at 95°C. Lysates were then used for protein quantification.

2.3.2 Quantification of sample protein concentration

Pierce BCA (Bicinchoninic Acid) Protein Assay Kit (ThermoFisher Scientific, 23225) was employed for sample protein quantification. Serial dilution of Bovine Serum Albumin (BSA) in ddH_2O (2, 1, 0.5, 0.25, 0.125, 0.0625 and 0 mg/mL) were used as a standard reference for quantification of samples. Quantification solution (BCA + buffer) was made accordingly to the manufacturer's

instruction. In a 96 well plate, 190µL of quantification solution were added to either 10µL of each standard or 10µL of each sample (diluted 1:10). An iMark Microplate Reader (Bio-Rad, CA, USA) was employed for measurement of absorbance (l = 565nM) in each sample to determine protein concentration.

2.3.3 Western Blotting

2.3.3.1 Western blotting antibodies

Antibodies utilised for immunoblotting are summarised in Table 2.4.

Table 2.4. Table of antibodies used for Immunoblotting

Name*	Species	Dilution	Manufacturer	Catalogue #
Anti-HSP90	Mouse	1:10000	Enzo Biochem	ADI-SPA-830
Anti-b-Actin (clone AC-74)	Mouse	1:10000	Sigma-Aldrich	A5316
Anti-a-Tubulin (clone B-5-1-2)	Mouse	1:10000	Sigma-Aldrich	T5168
Anti-CRBN	Rabbit	1:1000	Celgene Corp	NA
Anti-TOP2B	Rabbit	1:500	Abcam	ab72334
Anti-IKZF1 (clone H-100)	Rabbit	1:500	Santa Cruz Biotechnologies	sc-13039
Anti-IKZF3	Rabbit	1:1000	Abcam	ab139408
Anti-IRF4 (clone 3E4)	Rat	1:1000	Santa Cruz Biotechnologies	sc-130921
Anti-MYC (clone Y69)	Rabbit	1:1000	Abcam	ab32072
Anti-phospho-S139-H2AX (clone 20E3)	Rabbit	1:1000	Cell Signaling Technologies	9718
Anti-MEF2C	Rabbit	1:1000	Abcam	ab211493
Anti-myctag (clone 9B11)	Mouse	1:1000	Cell Signaling Technologies	2276
Anti-p53 (clone FL-393)	Rabbit	1:500	Santa Cruz Biotechnologies	sc-6243
Anti-Mouse IgG HRP	Swine	1:5000	Agilent Dako	P0260
Anti-Rabbit IgG HRP	Rabbit	1:5000	Agilent Dako	P0217
Anti-rat IgG HRP	Rabbit	1:5000	Agilent Dako	P0450
* If monoclonal, clone number is specified				

2.3.3.2 Western Blotting Sample Preparation

For preparation of RIPA-lysed samples, 6X SDS sample buffer. 6X SDS sample buffer was made with 6X Laemmli buffer, 0.5% bromophenol blue (Sigma-Aldrich) and 6% fresh β-mercaptoethanol (Sigma-Aldrich), and was added to each sample at a 1:6 ratio. For Laemmli-lysed samples, β-mercaptoethanol with bromophenol blue was added to each sample at a 1:20 ratio.

2.3.3.3 Western Blotting

30 to 60 µg of protein (in sample buffer) were loaded into 15-well or 10-well precast 4-15% gradient acrylamide gels (Bio-Rad) for protein electrophoresis. Protein separation in acrylamide gels was performed by electrophoresis at 120-160V in Running Buffer (14.4g Glycine, 3g Tris base, 1g SDS, in 1 L ddH_2O) for 45-90 minutes. Invitrogen PageRuler Plus Protein Ladder (Invitrogen) was used as reference for protein molecular weight. Proteins were transferred from gels to PVDF membranes (Immobilon-P, Merck Millipore) via semi-dry transfer (Semi-dry transfer cell, Bio-Rad) with semi-dry Transfer Buffer (7.3g Tris, 3.65g Glycine, 0.4g SDS in 1 L of ddH_2O) for 100-120 minutes at 70mA. Following transfer, membranes were blocked for 1 hour in blocking buffer (5% w/v skim milk powder in TBS-Tween), washed with TBS-Tween and incubated overnight at 4°C with a primary antibody (diluted with 5% BSA in TBS-Tween). The following day, membranes were washed in TBS-Tween, incubated with an anti-mouse or anti-rabbit secondary antibody (diluted respectively with 5% w/v skim milk powder in TBS-Tween) and washed with TBS-Tween. Finally, membranes were probed for immunoreactive bands using an ECL reagent (Amersham ECL or ECL Prime, GE Healthcare) and revealed by film exposure (Fujifilm Super RX, Fujifilm) with an AGFA CP1000 developer.

2.3.4 Enrichment of biotinylated proteins

OPM2-BioID2 or OPM2-BioID2-CRBN cells were expanded and cultured for 8 hours in biotin-free RPMI-1640 with 10% dFBS. Cells were then spun at 300rcf and replated at the density of $15x10^6$ per flask in 20mL of biotin-free media. Each flask represented a single technical replicate. Each experiment was performed with five technical replicates per treatment condition. After overnight treatment with 50µM biotin (Sigma-Aldrich) and DMSO, IMiDs, bortezomib or combination of bortezomib/IMiDs, all technical replicates were harvested on ice, spun at 300rcf, washed with ice-cold PBS twice and transferred in Eppendorf 1.5mL tubes. Cells were spun again at 300rcf and supernatant discarded. Then, cell pellets were resuspended in 500µL of RIPA buffer and incubated at 4°C rotating for 30 minutes. Subsequently, lysates were spun at 20000rcf, supernatant collected and quantified through a BCA assay. An equal amount of protein (1mg) across samples was taken for processing. After that, samples were either snap-frozen at -80°C or prepared for purification of biotinylated proteins.

2.3.4.1 Sample preparation for Mass Spectrometry

10µL of High-Capacity Streptavidin-Agarose resins (in 50% slurry, Pierce, Thermo-Fisher) per sample were used. Resins were initially spun at 2000rcf for 1 minute washed with 400µL of RIPA

buffer twice. Thus, 5µL of beads were resuspended in each sample prior to incubation for 30-45 minutes at 4°C rotating. Resins were spun at 2000rcf, supernatant discarded and resins washed with 400µL of RIPA buffer (x2, 4°C). Then, resins were spun a 2000rcf and washed with 400µL of PBS-SDS (0.5% w/v SDS in PBS) at room temperature (x3), followed by incubation for 20 minutes with 100µL of 100mM dithiothreitol (DTT) SDS-PBS. Resins were subsequently washed with UC buffer (6M urea, 100mM Tris-HCl pH8.5 in ddH_2O) twice in Spin-Cap columns (Pierce, 69725). After that, samples were incubated with 100µL UC buffer with 50mM iodoacetamide in the dark for 20 minutes prior to several washing steps (400µL UC buffer – 6 washes, 400µL PBS – 4 washes, 400µL ddH_2O – 3 washes). Protein immobilised in resins were digested overnight at 37°C in 100ul 50mM NH_4HCO_3 (AMBIC) containing 2µg of Trypsin Gold. The next day, peptides were centrifuged at 1000rcf for 1 minute in Eppendorf Protein LoBind® 1.5mL tubes (Eppendorf, 0030108116), resins washed again in 50µL of 50mM AMBIC and acidified with 1% formic acid (FA) prior to freeze-dry and lyophilisation.

2.3.4.2 Sample preparation for Western blotting

40µL of High-Capacity Streptavidin-Agarose resins (in 50% slurry, Pierce, Thermo-Fisher) per sample were used. Resins were initially spun at 2000rcf for 1 minute washed with 400µL of RIPA buffer four times. Following protein quantification with a BCA assay, 40µg of protein were collected as input fraction. Thus, 20µL of beads were resuspended in each of sample prior to incubation for 30-45 minutes at 4°C rotating. Following incubation, resins were spun at 2000rcf, supernatant discarded and resins washed with 400µL of RIPA buffer (five times at 4°C). After that, both input and enriched fraction were resuspended in sample buffer and boiled for 15 minutes at 95°C.

2.3.5 Liquid Chromatography – Mass Spectrometry (LC-MS/MS)

All LC-MS/MS runs and following analyses (excluding data visualisation and interpretation) were performed by Dr. Jarrod Sandow (WEHI, Melbourne, AUS).

An M-class UPLC (Waters, USA) coupled to a timsTOF Pro (Bruker, Germany) with a CaptiveSpray source was employed for LC-MS/MS analysis. Peptides were lyophilised and subsequently resuspended in 1% formic acid (FA) plus 2% acetonitrile (ACN) and therefore separated on a 25cm Aurora Series emitter column (25cm X 75µm, 1.6µm C18, IonOpticks, Australia). An integrated column oven (Sonation GmbH, Germany) was used to maintain the temperature of the column at 50°C. The column was equilibrated with a volume corresponding to 5 columns prior to loading sample in 100% buffer A (0.1% FA in MilliQ water). Separation of samples was

performed at 400nL/min by employing a linear gradient with serial increases in concentration of buffer B (0.1% FA in ACN). The timsTOF Pro was run in PASEF mode (Compass Hystar 5.0.36.0).

2.3.6 Peptide Database Search

MaxQuant 1.6.17 was adopted to process MS raw files. Common proteomics contaminants specific for trypsin digestion were allowed, with a maximum of 2 missed cleavages, when running the peptide search within the *Homo sapiens* database. The minimum peptide length as criteria for inclusion in the search function was 7 aminoacids. Cysteine carbamidomethylation was set as fixed peptide modification. Protein N-terminal domains N-acetylation and methionine oxidation of were set as variable peptide modifications. A precursor ion mass error tolerance was set to 6ppm when performing the main search. A target-decoy approach was adopted to filter PSM and protein identifications at a false discovery rate (FDR) of 1% with enabling of match between runs.

2.3.7 Statistical analysis of proteomics data

The output file proteinGroups.txt from MaxQuant was used for further data processing and analysis on a customised pipeline developed in R. The peptide sequence, together with its charge and modification, was defined as a feature. Features not found in at least 50% of the replicates in one group were discarded. Volume variability was corrected by normalisation following log2 transformation of the intensity of each feature. Log2 intensity values were normalised by multiplying each value with the ratio of maximum median intensity of all replicates over median replicate intensity. Intensity values were imputed when missing to avoid infinite log2(fold-change) using a randomly generated normal distribution of values. This distribution was generated with the following parameters: mean = $mean_{(intensities\ distribution)}$ - 1.8 standard deviations (stdev), stdev = 0.3 x $stdev_{(intensities\ distribution)}$. The Limma R package was employed for differential protein enrichment between different treatment conditions and probability was corrected with Benjamini-Hochberg false discovery ratio (FDR).

2.4 Molecular Biology Techniques

2.4.1 Generation of MM.1S CRBN KO cells via electroporation of ribonucleocomplexes

Solution 1 was incubated for 20 min at room temperature and then mixed with Solution 2 (composition of both Solutions 1 and 2 is described in table 2.5). In the meantime, $5x10^5$ of target cells were spun at 300rcf and washed with PBS twice. Cell pellets were resuspended in 20µL of

Solution 1 + Solution 2 mix and pipetted into a 16-well nucleocuvette provided within the Amaxa Nucleofector kit. Cells were electroporated with an Amaxa 4D-Nucleofector (Cell line SG program, EO100). Following electroporation, cells were incubated at 37° C for 10 minutes and then resuspended in 1 mL of pre-warmed media in a 48-well plate and kept in culture at 37° C, 5% CO_2.

Table 2.5 Composition of Solutions 1 and 2 for delivery of ribonucleocomplexes via electroporation of cells

	Volume and/or Moles	Reagent
Solution 1	300 pmol (in 1.5μL)	CRBN specific sgRNA reconstituted with ddH_2O
	100 pmol (in 1.67μL)	recombinant Alt-R *S. pyogenes* HiFi Cas9 nuclease V3
	0.83μL	ddH_2O
	1μL	Electroporation Enhancer
Solution 2	16.4μL	SG buffer
	3.6μL	Supplement 1
Recombinant Alt-R *S. pyogenes* HiFi Cas9 nuclease V3 and Alt-R Electroporation Enhancer were purchased from Integrated DNA Technologies (IDT, San Jose, CA, USA). SG buffer and Supplement 1 were included in the Amaxa SG Cell Line 4D-Nucleofector X Kit (Lonza, Basel, Switzerland, V4XC-3032). Synthetic CRBN-targeting sgRNA (sequence: TGTATGTGATGTCGGCAGAC) was purchased from Synthego Corporation (California, USA).		

2.4.2. Cloning of sgRNAs into *FgH1T-UTG* vector for inducible gene knockout via CRISPR/Cas9

2.4.2.1 Preparation of agarose gel for DNA electrophoresis

1g agarose was added to 100mL of Tris-Borate-EDTA (108g of Tris base, 55g boric acid, 40mL of 0.5M EDTA pH 8.0, up to 1 L of ddH_2O) and microwaved until solubilisation of agarose in the buffer. 10μL of Sybr Safe (Invitrogen) were added to 100mL of TBE-agarose for DNA staining. Subsequently, TBE-agarose was poured into a casting tray and left at room temperature to allow cooling and polymerisation until complete solidification.

2.4.2.2 Digestion of *FgH1T-UTG-GFP* vector

2μg of *FgH1T-UTG-GFP* or *BFP* (a gift from Dr. Marco Herold, WEHI) was digested for 4 hours or overnight at 55°C with 20 units of the restriction enzyme BsmBI (NEB) in 3.1 Buffer (NEB). After digestion, DNA was loaded and run in a 1% agarose Tris-Borate-EDTA (TBE) gel with 1:10000 Sybr Safe (Invitrogen) for DNA electrophoresis at 120V for 45-60 minutes. The DNA band correspondent to digested *FgH1T-UTG-GFP* was identified upon fluorescence with UV light and cut off the gel for DNA clean-up with NucleoSpin Gel and PCR Clean-up columns (Macherey-

Nagel) by following the manufacturer's instructions. Purified DNA yield was measured via UV spectrophotometry with a NanoDrop 2000 (ThermoFisher Scientific).

2.4.2.3 Cloning of sgRNAs into *FgH1T-UTG* using single strand DNA oligos

Sequence of sgRNAs were extracted from the Brunello sgRNA library and purchased as single stranded DNA (ssDNA) oligos from Sigma-Aldrich (Table 2.6).

Table 2.6 sgRNAs employed for validation of CRISPR dropout screen

Target gene (sgRNA)*	Sequence (20bp)
TOP2B (sgTOP2B #1)	CACATGTGACTATAATTGTC
TOP2B (sgTOP2B #4)	TAGGCTACATGGCTTACCAG
ATXN7 (sgATXN7 #1)	CATACTCACATTCTACCATG
ATXN7 (sgATXN7 #4)	TGTCCGGTGAGGAATACGTG
Non targeting control sgRNA	GTCATGTCACTTATCAAGTC
*Each sgRNA was ordered as ssDNA between 5' and 3' ends complementary to the *FgH1T-UTG* vector following digestion with BsmBI: 5'-TCCCTATCAGTGATAGAGAT-[sgRNA 20bp sequence]-TAGAGCTAGAAATAGCAAGT-3'	

Gibson Assembly was employed to clone the guide into the *FgH1T-UTG* vector. ssDNA oligos were designed having the 5' and 3' ends with 20bp complementary to both ends of the digested vector to allow recombination of oligos in the target vector via Gibson Assembly.

For Gibson Assembly of sgRNA into the *FgH1T-UTG* vector, reaction mix (Table 2.7) was incubated for 30 minutes at 50°C, then on ice for 5 minutes. Subsequently, 5µL of reaction were taken for bacterial transformation.

Table 2.7 Gibson Reaction protocol (*FgH1T-UTG*)

Reagent	Quantity
Digested (linearised) backbone	50ng
0.45µM ssDNA oligo	1µL
NEBuilder HiFi DNA Assembly mix	5µL
ddH_2O	Up to 10µL

2.4.2.4 Bacterial Transformation

50µL of Stbl3 *E. coli* were thawed in ice and 5µl of the Gibson reaction added into bacterial suspension. Following a 30-minute incubation in ice, the mixture was immerged in a water bath

at 42°C for 90 seconds (heat shock) to transform bacteria with plasmidic DNA. After that, transformed bacteria were put in ice for 2 minutes and then recovered in 500µL of Luria Bertani (LB) broth shaking for 30-60 minutes at 37°C. Then, bacteria were pelleted by centrifugation at 11000g for 30 seconds and plated on a petri dish containing agar-LB supplemented with 100µg/mL ampicillin and incubated overnight at 37°C.

2.4.2.5 Starting culture, minipreps and sequencing validation

The next day, colonies on the plate were picked using a pipette tip and resuspended into 5mL of LB with 50 µg/mL ampicillin for starting culture. Bacteria were incubated for 16 hours or until saturation shaking at 37°C. Subsequently, plasmidic DNA extracted with the NucleoSpin Plasmid DNA Purification (Macherey-Nagel) for miniprep as per the manufacturer's instructions. Once extracted, integration of sgRNA sequence in the backbone was validated via Sanger Sequencing.

2.4.3 Cloning of *CRBN* ORF into the *pBABE-mycBioID2-puroR* vector via Gibson assembly

2.4.3.1 Gibson assembly reaction preparation and performance

Fragment preparation for Gibson assembly of CRBN into *pBABE-mycBioID2-puroR* is described in chapter 4, section 4.3.4. The reaction mix (see Table 2.8) was incubated for 30 minutes at 50°C, then on ice for 5 minutes. Subsequently, 10µL of reaction were taken for bacterial transformation.

Table 2.8 Gibson Reaction protocol (*pBABE-mycBioID2-puroR*)

Reagent	Quantity
pBABE-mycBioID2-puroR	50ng
CRBN ORF	100ng (1:10 vector:insert molar ratio)
NEBuilder HiFi DNA Assembly mix	5µL
ddH_2O	Up to 10µL

2.4.3.2 Validation of successful assembly via colony PCR

TOP10F *E. coli* were transformed (see paragraph 2.4.2.4); bacteria were plated and incubated overnight (~16 hours) on Luria Bertani Broth-Agar (supplemented with ampicillin) petri dish at 37°C. The next day, colonies were picked with a pipette tip and immersed in 20µL of ultrapure water for storage at 4°C until colony PCR validation. 10µL of water-bacteria suspension and Taq polymerase mix (Promega) were employed for detection of colonies containing plasmids with

successful assembly by PCR. Primers for the colony PCR are described in section 4.2.4 in chapter 4. Colony PCR with Taq polymerase mix was performed as per manufacturer's instructions. PCR amplicons were separated via DNA electrophoresis in a 1% agarose Tris-Borate-EDTA (TBE) gel with 1:10000 Sybr Safe (Invitrogen) at 120V for 45-60 minutes. The DNA band correspondent to the molecular weight of *mycBioID2* plus that of *CRBN* ORF was identified upon fluorescence with UV light. The corresponding colony stored at 4°C was then started in culture and validated via Sanger sequencing (paragraph 2.4.2.5).

2.4.4 Preparation of PCR products for validation of *ATXN7* deletion with TIDE

Each guide was aligned to the genome to identify the targeted regions by browsing the UCSC Genome Browser (https://genome.ucsc.edu/). A region of ± 300bp around the target region of each guide was selected for PCR amplification. After that, the online suite Primer3web (v4.1.0) (https://primer3.ut.ee/primer3/) was employed to design highly efficient PCR primers (Table 2.9).

Table 2.9 PCR primers employed for amplifications of regions targeted by sgATXN7 #1 and #4

Target gene (sgRNA)	Direction	Sequence
ATXN7 (sgATXN7 #1)	Forward	CCGTTCCTCCCACTTCAGTA
ATXN7 (sgATXN7 #1)	Reverse	AGGGTTGTTGTGATAAGTGACA
ATXN7 (sgATXN7 #4)	Forward	CAATAGCAGCGGGGAGTTG
ATXN7 (sgATXN7 #4)	Reverse	GTGGAAGGGGATGAGGATGA

Genomic DNA from cell pellets of $5x10^6$ MM.1Sres-Cas9 SCR GFP, SCR BFP sgATXN7#1 and sgATXN7#4 cells was extracted with DNeasy Blood & Tissue Kit (Qiagen) and quantified via UV spectrophotometry with a NanoDrop 2000. Subsequently, KAPA HiFi polymerase was employed to run PCR according to the manufacturer's instructions. After the PCR, each product was loaded and run into a 1% agarose-TBE gel for DNA electrophoresis at 120V for 45 minutes. The DNA band corresponding to the PCR product was cut off the gel and clean-up performed with NucleoSpin Gel and PCR Clean-up columns (Macherey-Nagel) by following the manufacturer's instructions. Purified DNA yield was measured via UV spectrophotometry with a NanoDrop 2000.

Finally, Sanger sequencing samples were prepared for the sequencing reaction. 18ng of each PCR product were mixed with 1µL of each primer at 10µM concentration in separate Eppendorf 1.5mL tubes (i.e. 1 PCR product, 1 primer). The volume in each tube was normalised with ddH_2O

up to 12µL and sample submitted for Sanger Sequencing at the Australian Genome Research Facility (AGRF, Melbourne)

2.5 Next Generation Sequencing (NGS) techniques

2.5.1 3'-RNA sequencing

MM.1S and MM.1Sres cells were treated for 16 hours with DMSO, 2µM LEN or 500nM POM and harvested for RNA extraction. Fresh RNA was obtained by lysing cells with TRIzol reagent (Invitrogen) and purified by using the Direct-zol RNA Miniprep extraction kit (Zymo Research) accordingly to manufacturer's instruction. The concentration of RNA in each sample was assessed by UV spectrophotometry with a NanoDrop 2000. RNA was then stored at -80° C or handed to the Molecular Genomic Core (Peter MacCallum Cancer Centre) for cDNA library preparation and single-end 75 bp sequencing. Sequencing library preparation was performed by the Molecular Genomics Core (Peter MacCallum Cancer Centre) with the QuantSeq 3'mRNA-Seq Library Prep Kit for Illumina accordingly to manufacturer's instructions and sequencing was executed with an Illumina NextSeq. Data generated from the sequencing run were demultiplexed using CASAVA (v1.8) and FASTQ files obtained were quality-controlled with FastQC. The software cutadapt (v1.5) was employed to trim at 3' ends to remove biases introduced by random primers and at 5' to delete poly-A tails. After that, alignment of reads with the hg19 human reference genome was performed using HISAT2 (v2.1.0). Subsequently, reads were counted using the algorithm featureCounts (from Subread, v1.5). Differential gene expression analysis was performed with R Studio using the limma-voom R package. The R packages ggplot2 and pheatmap were employed for data visualisation.

2.5.2 Genome-wide CRISPR knockout screening

2.5.2.1 Generation of viral library

To generate the Brunello human sgRNA viral library for the CRISPR screen carried in the study, 25 T175 flasks with HEK293T cells were adopted. Lentiviral transduction was performed as described above with the Brunello human sgRNA plasmid library (Addgene). To concentrate viral media, supernatant from each flask was collected at day 4 and day 5 and spun at 2000g for 20 minutes in Amicon Ultracentrifugal Filter Units (Merck Millipore). For each T175 flask containing 20 to 25 mL of viral media, a final volume of 1 to 1.5mL was obtained. Filtrated media was discarded and the concentrated fraction was snap-frozen in aliquots of 1 mL in cryovials at -80°C.

2.5.2.2 Generation of Cas9-expressing MM.1S lines

MM.1S-Cas9 and MM.1Sres-Cas9 cells were generated transducing MM.1Sres and MM.1S cells as described above (lentiviral transduction section) with FUCas9Cherry (Addgene 70182). The bulk population was FACS-sorted for $mCherry^+$ cells. Cells were kept in culture at 10 millions/30 mL of media in each T175 flask.

2.5.2.3 Assessment of transduction efficiency of viral library

MM.1S-Cas9 and MM.1Sres-Cas9 cells were seeded at 10^6 in 3 mL each well on 6-well plates. Cells were then transduced with 0, 2, 5, 10, 20 or 50 µL by addition of concentrated virus and 4µg/mL of sequabrene in the growth medium (day 0). For both MM.1S-Cas9 and MM.1Sres-Cas9 cells, a sequabrene only sample was also plated as control. At day 3, cells were spun and washed twice to remove sequabrene and were subsequently re-plated. 0.5µg/mL puromycin was added to each sample (excluding the control) for selection of transduced cells. Viable cell count was measured for each sample at day 3 and day 7 post-puromycin treatment (day 6 and day 10 respectively) to identify the amount of virus inducing a growth inhibition of 60 to 80% (Multiplicity of Infection ~0.2-0.4).

2.5.2.4 Bulk cell transduction with Brunello human viral sgRNA library for genome-scale CRISPR KO screens

The number of cells to transduce was chosen on the basis of the representation aimed for each guide in the library, the number of conditions in the screen and the MOI. A 500-fold representation with ~80000 sgRNAs (4 each gene plus non-targeting sgRNAs) by transducing with a low MOI (~0.2-0.4) was aimed for. The number of cells to transduce with a theoretic MOI of 1 was: 500 (-fold representation) x 80000 (sgRNA number in the Brunello library) = $40x10^6$. We aimed for a low MOI (~0.2-0.4) to ensure one viral integration per cell (at an average MOI of 0.3). Thus, $(40x10^6)/0.3 = 120x10^6$ was the total number of cells to transduce for a single condition. Having four conditions (i.e. T_0, DMSO, DMSO, 2µM LEN and 500nM POM), the number of cells to be transduced was $(120x10^6) \times 4 = 480x10^6$.

Thus, a total number of ~500 million cells (for each cell line) was transduced via lentiviral transduction (as previously described), with the required amount of concentrated Brunello genome-wide sgRNA viral library required. To obtain this value, the volume of concentrated viral media that infects 10^6 cells was multiplied by 500 (to infect $500x10^6$ cells) At day 3, sequabrene was washed out from the growth medium, cells were re-plated and grown in 0.5µg/mL puromycin containing medium for 7 days.

2.5.2.5 CRISPR Screening for drug resistance or re-sensitisation

Subsequent to puromycin selection, cells were split in four populations each (T_0, DMSO, 2μM LEN, 500nM POM) and re-plated at a density of 10^6/3mL of medium with at least 40x10^6 cells per condition to maintain a 500-fold guide representation. At this point, cells of the T_0 population were harvested, pellets snap-frozen and stored at -80° C until the end of the screen. MM.1S-Cas9 cells were cultured in DMSO, LEN or POM for 7 weeks and 3 days, refreshing drug daily. MM.1Sres-Cas9 cells were cultured for 3 weeks in DMSO, LEN or POM, refreshing drug daily. Both MM.1S-Cas9 and MM.1Sres-Cas9 cells were split twice weekly and at least 40x10^6 cells re-plated (when possible) to maintain guide representation for the duration of the screen. At the end of the screen, cells were harvested and pelleted for DNA extraction.

2.5.2.6 Sequencing library preparation

Genomic DNA extraction from cell pellets was performed using the DNeasy Blood & Tissue Kit (Qiagen). DNA in each sample was quantified employing a QuBit 3.0 fluorometer (Invitrogen). All the DNA extracted was used for library preparation to maintain representation of the guide library. Each Polymerase Chain Reaction (PCR) sample was set up by following the protocol in table 2.10. Thermal cycling conditions are described in table 2.11.

Table 2.10 Polymerase Chain Reaction protocol for preparation of sequencing libraries

Reagent	Quantity
ExTaq DNA polymerase (TaKaRa Bio)	0.75 μL
10X reaction buffer (TaKaRa)	10 μL
100uM P5 primer mix	0.5 μL
5uM P7 primer*	10 μL
Sample Genomic DNA	7.5 μg
ddH2O	Up to 100 μL
*For each condition, a different P7 primer was assigned in order to allow separation and identification of single libraries (condition) in the Illumina flowcell.	

Table 2.11 Thermal cycling conditions for library preparation PCR

Stage	Time	Temperature
1- Initial denaturation	1 minute	95° C
2- Denaturation	30 seconds	95° C
3- Annealing	30 seconds	53° C

4- Extension	30 seconds	72° C
5- Back to step 2 (x28)		
6- Final extension	10 minutes	72° C
7- Incubation	∞	4° C

2.5.2.7 Clean-up of libraries for sequencing

After library prep PCR, samples were cleaned up for isolation of guide libraries for each sample. PCR products within each sample were pooled to obtain 100μL of pooled product. Then, AMPure XP beads (Beckman Coulter) were employed for isolation of the 350bp PCR product containing the guide, the adaptors and the sequencing library index. The quality of sequencing products was checked for each sample with a TapeStation (Agilent Technologies).

2.5.2.8 Sequencing and data analysis

After library multiplexing, the sequencing was run with an Illumina NextSeq 500 and 75 base pair single-end reads were generated. Sequencing data were demultiplexed using CASAVA (v1.8) and the 20bp guides extracted through cutadapt (v1.7) with removal of reads derived from the vector. MAGeCK (v0.5.6) was used to perform sgRNA enrichment and statistical analysis. The R package ggplot2 was employed for data visualisation.

2.6 Software and webtools

SnapGene Viewer (v2.6.2) was adopted to visualise and design DNA sequence, plasmids and cloning strategies. RStudio v4.0.2 (RStudio, Boston, MA) was employed to analyse and visualize data from the CRISPR screens data. InteractiVenn (interactivenn.net) was used to generate Venn diagrams. STRING (string-db.org), metascape (metascape.org) and ToppFun (toppgene.cchmc.org) were adopted to study protein-protein interaction networks and gene ontology data. FlowJo 10 was employed to analyse FACS data. Prism 8 (GraphPad Software, La Jolla, CA, USA) was used to graph data from the competition assays, cell cycle analysis and cell death assay results.

Chapter 3: transcriptome analysis and CRISPR screening for the identification of transcriptional signatures and genetic vulnerabilities of multiple myeloma in the context of IMiD sensitivity and resistance

3.1 Introduction

3.1.1 Background

Immunomodulatory drugs represent a cornerstone in the therapy of MM. These compounds have had remarkable success in improving survival and quality of life of MM patients. Nevertheless, patients ultimately develop resistance to treatment. IMiDs engage the E3 ligase CRBN and subsequently degrade IKZF1 and IKZF3, two key transcription factors for cells of the B-lineage. Degradation of IKZF1 and IKZF3 can suppress the *IRF4-MYC* transcriptional axis with consequent negative impact on MM PC proliferation and survival[251]. However, the discovery of other neosubstrates, such as CK1a, ZFP91 and SALL4, and the activity of CRBN as a chaperone of the protein BSG, suggested that this model might be oversimplified[230,231,252,253]. Although recent studies provided new insight into IMiD mechanism of action against MM PCs[239,240], the complexity of IMiDs biological effect on MM PCs has not been fully characterised yet. It has been demonstrated that loss of CRBN determines resistance to IMiD treatment[217,219]. However, multiple pathways could be involved in IMiD resistance, and the mechanisms by which resistance occurs are poorly understood. Deeper understanding of MM and IMiD biology could identify vulnerabilities that can be targeted to potentiate IMiD efficacy and overcome IMiD resistance.

The availability of next generation sequencing technologies allows dissection of transcriptional profiles, identification of functional dependencies of tumour cells and of drug mechanism of action at a molecular level. In this study, RNA-sequencing was employed to characterise the transcriptional signatures of IMiD-sensitivity and IMiD-resistance cells in the presence or absence of an IMiD. Moreover, whole-genome functional genomics screening by Clustered Regular Interspaced Palindromic Repeats (CRISPR) was adopted to identify mechanisms by which IMiD-sensitive cells can potentially acquire IMiD resistance and those by which IMiD-resistant cells can be resensitised to IMiD treatment.

Characterisation of U266/U266res and MM.1S/MM.1Sres isogenic pairs of MM cell lines as models of acquired IMiD-resistance demonstrated that U266res and MM.1Sres cells are indeed IMiD-resistant. The resistant phenotype in U266res and MM.1Sres cells correlated with downregulation of CRBN and attenuation of neosubstrate degradation. Analysis of the transcriptional signatures of these cells in the presence and absence of IMiD treatment showed perturbation of genes mainly associated with IFN and MYC signalling. This response, however, was virtually abrogated in IMiD-treated resistant cells. In MM.1S cells, a genome-wide CRISPR

resistance screen identified genes required for IMiD sensitivity, including CRBN. Conversely, a dropout screen in MM.1Sres cells identified loss of *TOP2B* (DNA topoisomerase II β), *ATXN7* (Ataxin-7) and other genes as IMiD-resensitisation factors. The loss of *TOP2B* also enhanced the response to IMiD in MM.1S cells. Dexrazoxane (DXZ), a cardioprotective agent that inhibits TOP2 and specifically degrades TOP2B[254], was employed with the aim of mimicking genetic loss of TOP2B. Although DXZ did not phenocopy the synergy observed in the screen - as it was toxic for MM.1S and MM.1Sres cells even in absence of IMiD treatment - it proved to be effective as an antiproliferative agent across several MM cell lines and to increased lenalidomide responses, especially in IMiD-sensitive cells. Collectively, this work provides with important information with regards to the effects of IMiD treatment in MM cells, a detailed genetic dissection of acquired IMiD resistance and ultimately identifies TOP2 as a genetic vulnerability in MM and a putative druggable target.

3.1.2 Aims

In this study, isogenic pairs of IMiD-sensitive and -resistant MM cell lines were used with the aim of:

1. Characterising the transcriptional signatures of IMiD sensitivity and IMiD resistance and that of acute transcriptional response to IMiDs via RNA-sequencing
2. Exploring functional dependencies of IMiD-sensitive and -resistant MM cells and, ultimately, to define mechanisms of IMiD sensitivity and resistance by employing genome-wide CRISPR-screening;
3. Identifying genetic vulnerabilities of MM cells and potentiate the therapeutic effect of IMiDs *in vitro* and *in vivo.*

3.2 Results

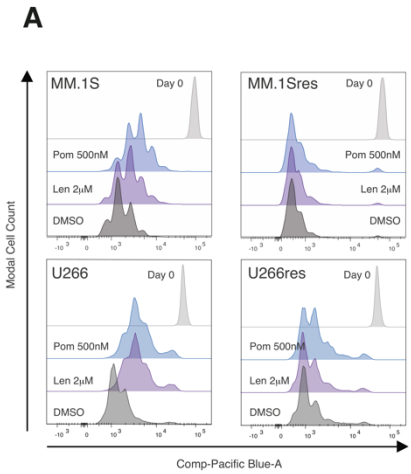
3.2.1 MM.1S/MM.1Sres and U266/U266res cells are models of acquired *in vitro* lenalidomide resistance

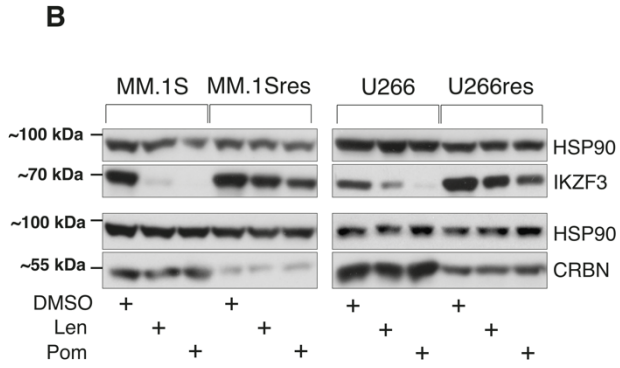
To explore features of IMiD sensitivity and resistance, pairs of isogenic cell lines with acquired IMiD resistance, designated U266/U266res and MM.1S/MM.1Sres, were employed. The resistant cell lines were generated by culturing MM.1S and U266 cells over time in growth medium containing increasing concentrations of LEN (up to 10μM)[217].

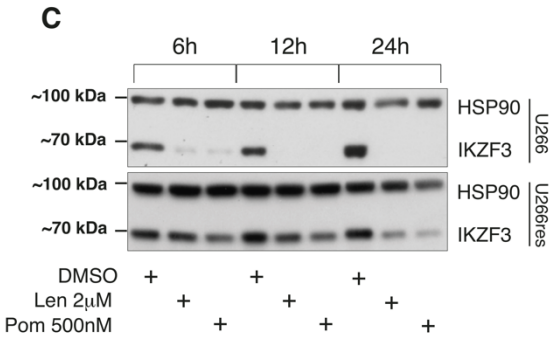
The resistant phenotype of U266res and MM.1Sres cells was validated by performing a CellTrace Violet/Propidium Iodide (CTV/PI) combined proliferation/cell death assay in MM cells exposed

Figure 3.1. MM.1Sres and U266res cells are refractory to IMiD treatment.

(A) CellTrace Violet histograms of MM.1S, MM.1Sres, U266 and U266res cells at day 9 and 7 of treatment, respectively, with DMSO, 2μM LEN and 500nM POM. (B) Immunoblot showing expression of IKZF3 and CRBN in MM.1S, MM.1Sres, U266 and U266res cells treated with DMSO, 2μM LEN or 500nM POM for 16 hours. HSP90 expression was employed as loading control. (C) Immunoblot displaying IKZF3 levels following 6, 12 and 24 hours of DMSO, 2μM LEN or 500nM POM exposure in U266 and U266res cells. HSP90 was used as loading control.


A
MM.1S
Day 0
Pom 500nM
Len 2μM
DMSO
MM.1Sres
Day 0
Pom 500nM
Len 2μM
DMSO
U266
Day 0
Pom 500nM
Len 2μM
DMSO
U266res
Day 0
Pom 500nM
Len 2μM
DMSO
Modal Cell Count
Comp-Pacific Blue-A


B
MM.1S
MM.1Sres
U266
U266res
~100 kDa
~70 kDa
HSP90
IKZF3
~100 kDa
~55 kDa
HSP90
CRBN
DMSO
Len
Pom


C
6h
12h
24h
~100 kDa
~70 kDa
HSP90
IKZF3
U266
~100 kDa
~70 kDa
HSP90
IKZF3
U266res
DMSO
Len 2μM
Pom 500nM

to LEN, POM or the vehicle, dimethylsulfoxide (DMSO). MM.S/MM.1Sres and U266/U266res cell lines were stained with CTV and seeded in culture in the presence of either DMSO, 2μM LEN or 500nM POM. At the timepoints indicated, LEN and POM showed antiproliferative effects as compared to DMSO-treated MM.1S and U266 cells (Figure 3.1A). In these cells, LEN treatment delayed the loss of CTV fluorescence relative to DMSO. POM also delayed the loss of CTV fluorescence relative to both LEN and DMSO, suggesting that POM is be more effective than LEN in reducing cell proliferation in MM.1S cells. The highest peak in the MM.1S cells histogram plot of CTV intensity indicates that MM.1S cells treated with LEN were one division behind to those exposed to DMSO. MM.1S cells treated with POM were one division behind those exposed to LEN, therefore two division behind MM.1S cells cultured in the vehicle control. In U266 cells, loss of CTV fluorescence was similar between LEN- and POM-treated cells. Both LEN- and POM-treated cells demonstrated to delay the rate at which the CTV dye is lost as compared to DMSO control in U266 cells. Furthermore, U266 cells treated with IMiDs appeared to be at least one division behind the DMSO control. As expected, both MM.1Sres and U266res cells were refractory to the growth inhibitory effects of either LEN or POM, since no marked difference in the loss of CTV fluorescence was detected as compared to vehicle-treated control and there seemed to be no difference in the number of cell division over time across the treatment conditions (Figure 3.1A).

Since IMiDs induce CRBN-dependent degradation of Ikaros (IKZF) family proteins via CRBN-dependent ubiquitination[89,90], CRBN expression in both isogenic pairs and relative IKZF3 degradation efficiency upon IMiD treatment were assessed (Figure 3.1B). MM.1S, MM.1Sres, U266 and U266res cells were treated for 16 hours with either DMSO, 2μM LEN or 500nM POM. CRBN downregulation had been previously documented via cytogenetic characterisation of LEN-resistant MM.1S by Zhu and colleagues as the result of the loss of one CRBN gene copy[217]. Whole cell lysate immunoblots confirmed that CRBN protein levels were lower in U266res and MM.1Sres cells as compared to U266 and MM.1S cells. Additionally, expression of CRBN did not change in LEN- and POM-treated cells as compared to their DMSO-treated control. The efficiency of IKZF3 degradation was much greater in sensitive cells as compared to resistant cells, where it was virtually abrogated. In MM.1S cells, treatment with LEN induced marked loss of IKZF3 and virtually complete absence of IKZF3 in POM-treated cells. U266 cells exposed to LEN also exhibited considerable loss of IKZF3 as compared to the vehicle control. U266 cells treated with POM also demonstrated nearly complete degradation of IKZF3 protein. Conversely, LEN- and POM-induced degradation of IKZF3 relative to the DMSO control resulted attenuated in

MM.1Sres cells when compared to LEN- and POM-treated MM.1S cells. In particular, POM also caused greater loss of IKZF3 relative to LEN in MM.1Sres cells. U266res cells showed abrogation of IMiD-induced IKZF3 degradation when compared to IMiD-naïve U266 cells. POM displayed greater activity in reducing IKZF3 level as compared to LEN in U266res cells. Overall, POM resulted in more efficient IKZF3 degradation, even at a lower concentration, suggesting greater potency of POM as compared to LEN (Figure 3.1B).

These data confirmed that MM.1S and U266 cells are sensitive to IMiDs, whilst MM.1Sres and U266res cells are refractory to these drugs. Moreover, the resistant phenotype correlated with low levels of CRBN and reduced IKZF3 degradation upon IMiD treatment.

3.2.2 Transcriptional characterisation of MM.1S and U266 isogenic cell line pairs in presence and absence of IMiD treatment

Having validated the resistant phenotype of MM.1Sres and U266res cells, the response to acute exposure to IMiD and the transcriptional signature of IMiD resistance were explored. In a time-course study, U266 and U266res cells were treated with DMSO, 2μM LEN or 500nM POM for 6, 12 and 24 hours, and IKZF3 degradation upon LEN and POM treatment was tested by Western blot, aiming to assess the best timepoint for whole-genome transcriptome sequencing (Figure 3.1C). In U266 cells, both LEN and POM caused marked downregulation of IKZF3 as compared to baseline IKZF3 expression in DMSO-treated cells already at 6 hours. However, in U266res cells, degradation of IKZF3 mediated by LEN and POM resulted abolished at 6 hours. In particular, LEN did not induce degradation of IKZF3, whilst POM-treated cells exhibited demonstrated a mild reduction of IKZF3 levels. At 12 and 24 hours, U266 cells treated with LEN and POM showed complete loss of IKZF3 as compared to DMSO-treated U266 cells. Conversely, LEN and POM treatment of U266res cells resulted in little degradation of IKZF3. At these timepoints, POM demonstrated a slightly higher efficiency in degrading IKZF3 as compared to LEN. These data indicated that most of the IKZF3 pool was lost at 6-12 hours of treatment in U266 cells and that IMiD-induced neosubstrate degradation was abolished in U266res cells at the same timepoints. In addition, prior experiments (Figure 3.1B) consistently showed strong reduction in IKZF3 protein levels within 16-hour IMiD treatment. Therefore, it was hypothesised that a 16-hour IMiD treatment would have been an ideal timepoint for transcriptional studies in both U266/U266res and MM.1S/MM.1Sres cell lines.

Figure 3.2 Transcriptional response to IMiDs in U266 cells

(A) Volcano plot representing differentially expressed genes (DEGs) in U266 cells upon 16 hours treatment with 2μM LEN or 500nM POM relative to DMSO-treated U266 cells. Blue dots represent hits significant for adjusted p-value < 0.05.(B) and (C) GSEA plots of top positively and negatively enriched gene sets, respectively, in U266 cells following LEN treatment.

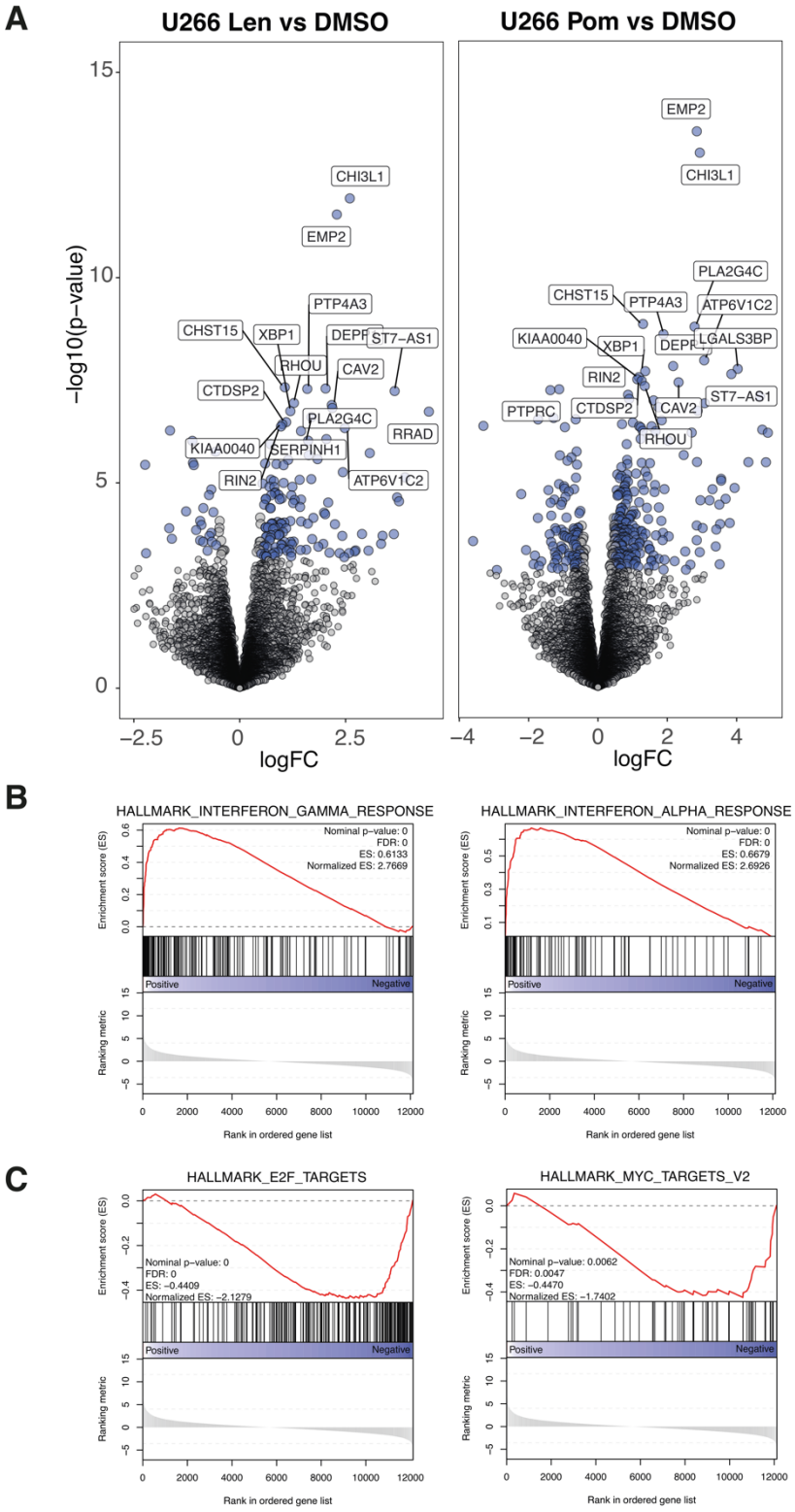
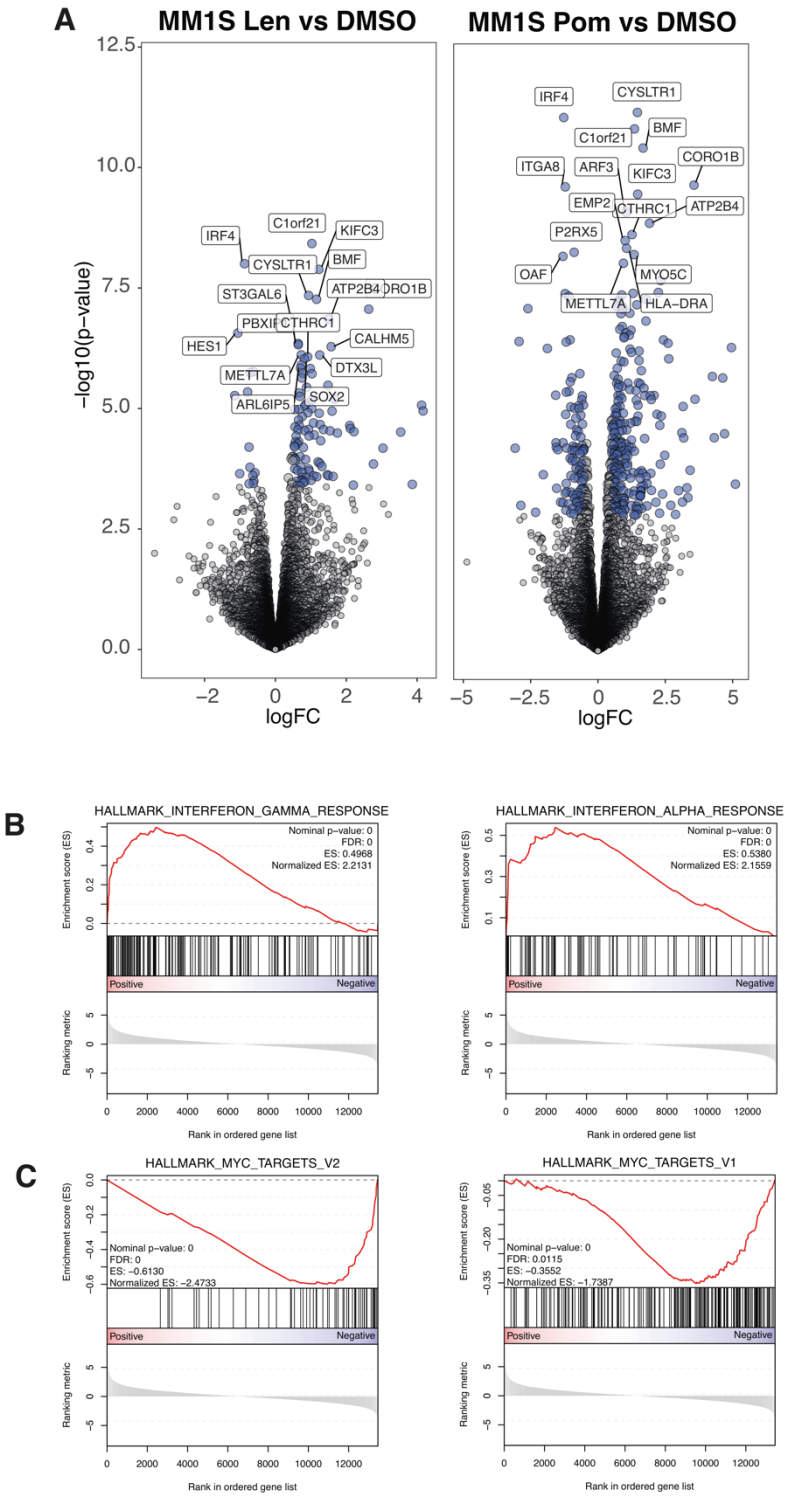

A
U266 Len vs DMSO
U266 Pom vs DMSO
−log10(p−value)
logFC
logFC
CHI3L1
EMP2
PTP4A3
CHST15
XBP1
ST7−AS1
RHOU
CAV2
CTDSP2
PLA2G4C
RRAD
KIAA0040
SERPINH1
RIN2
ATP6V1C2
PLA2G4C
CHST15
PTP4A3
ATP6V1C2
KIAA0040
XBP1
LGALS3BP
RIN2
ST7−AS1
PTPRC
CTDSP2
CAV2
RHOU
B
HALLMARK_INTERFERON_GAMMA_RESPONSE
Nominal p−value: 0
FDR: 0
ES: 0.6133
Normalized ES: 2.7669
HALLMARK_INTERFERON_ALPHA_RESPONSE
Nominal p−value: 0
FDR: 0
ES: 0.6679
Normalized ES: 2.6926
Enrichment score (ES)
Positive
Negative
Ranking metric
Rank in ordered gene list
C
HALLMARK_E2F_TARGETS
Nominal p−value: 0
FDR: 0
ES: −0.4409
Normalized ES: −2.1279
HALLMARK_MYC_TARGETS_V2
Nominal p−value: 0.0062
FDR: 0.0047
ES: −0.4470
Normalized ES: −1.7402

Figure 3.3 Transcriptional response to IMiDs in MM.1S cells

(A) Volcano plot representing DEGs in MM.1S cells upon 16 hours treatment with 2μM LEN or 500nM POM relative to DMSO-treated MM.1S cells. Blue dots represent hits significant for adjusted p-value < 0.05. (B) and (C) GSEA plots of top positively and negatively enriched gene sets, respectively, in MM.1S cells following LEN treatment.


A
MM1S Len vs DMSO
MM1S Pom vs DMSO
−log10(p−value)
logFC
logFC
IRF4
C1orf21
KIFC3
CYSLTR1
BMF
ST3GAL6
ATP2B4
CTHRC1
HES1
CALHM5
METTL7A
DTX3L
ARL6IP5
SOX2
CYSLTR1
IRF4
BMF
C1orf21
CORO1B
ITGA8
ARF3
KIFC3
EMP2
CTHRC1
ATP2B4
P2RX5
OAF
MYO5C
METTL7A
HLA−DRA
B
HALLMARK_INTERFERON_GAMMA_RESPONSE
Nominal p−value: 0
FDR: 0
ES: 0.4968
Normalized ES: 2.2131
HALLMARK_INTERFERON_ALPHA_RESPONSE
Nominal p−value: 0
FDR: 0
ES: 0.5380
Normalized ES: 2.1559
Enrichment score (ES)
Positive
Negative
Ranking metric
Rank in ordered gene list
C
HALLMARK_MYC_TARGETS_V2
Nominal p−value: 0
FDR: 0
ES: −0.6130
Normalized ES: −2.4733
HALLMARK_MYC_TARGETS_V1
Nominal p−value: 0
FDR: 0.0115
ES: −0.3552
Normalized ES: −1.7387

3.2.2.1 Induction of interferon signalling and suppression of MYC target genes as transcriptional response following acute exposure to IMiDs

U266, U266res, MM.1S and MM.1Sres cells were treated with DMSO, 2μM LEN and 500nM POM and harvested after 16 hours for RNA extraction and next generation sequencing, aiming to define pathways and transcriptional signatures that could be associated with IMiD sensitivity and acquired IMiD resistance in these cell lines.

Differential gene expression (DGE) analysis was performed with read count from RNA-seq of LEN- and POM-treated U266 cells in order to define genes whose expression changed following acute exposure to IMiDs, as compared to DMSO (Figure 3.2A). In U266 cells exposed to LEN, 32 genes were significantly downregulated and 137 genes significantly upregulated as compared to DMSO-treated U266 cells. In POM-exposed U266 cells, 108 genes were significantly downregulated and 246 genes significantly upregulated as compared to DMSO-treated U266 cells. Treatment with POM induced a similar response to that of cells treated with LEN, but with higher magnitude, as there were more differentially expressed genes (DEGs) in POM-treated cells relative to LEN-exposed cells. In addition, many of the genes downregulated or upregulated by LEN were also found differentially expressed in POM-exposed cells. Next, Gene Sets Enrichment Analysis (GSEA) was performed in order to define transcriptional signatures that may be associated with IMiD treatment. A gene set is a ranked list of genes that regulate specific biological processes. In GSEA, the degree of variation of gene expression in a certain gene set is represented by the Normalised Enrichment Score (NES)[255]. GSEA produced similar results between LEN- and POM-exposed cells (relative to the DMSO-treated control U266 cell population) (Figure 3.2B-C). IFNγ and IFNα responsive genes were predominantly enriched in both LEN- and POM-exposed cells. The NES was 2.77 and 2.69 in IFNγ- and IFNα-responsive gene sets, respectively, in LEN-treated cells. In POM-treated cells, the NES was 2.68 and 2.71 in IFNγ- and IFNα-responsive gene sets, respectively (Figure 3.2B; only GSEA plots of LEN-treated cells are shown). Conversely, negative enrichment of E2F and MYC target genes was observed, in both LEN and POM, again with almost identical enrichment scores and profiles. The NES of E2F- and MYC-regulated gene sets was -2.13 and -1.74, respectively, in LEN-treated cells. In U266 cells treated with POM, the NES was -2.3 and -1.76 for E2F- and MYC-regulated gene sets, respectively (Figure 3.2C; only GSEA plots of LEN-treated cells are shown).

DGE analysis from RNA-seq of IMiD-treated MM.1S cells displayed similar results to those of U266 cells (Figure 3.3A). In these cells, 13 genes were significantly downregulated and 103 genes significantly upregulated following LEN treatment. In MM.1S cells treated with POM, 146 genes

were significantly downregulated and 300 genes were significantly upregulated. Treatment of MM.1S cells with IMiDs reduced the expression of *IRF4*, which has a pivotal role in the maintenance of the PC transcriptional program (Figure 3.3A). Similar to U266 cells, POM induced a stronger response relative to LEN in MM.1S cells. This was evident as the number of differentially expressed genes was markedly higher in POM as compared to LEN, relative to DMSO-treated cells. Both IMiDs induced transcription of IFNγ- and IFNα-regulated genes, with a NES of 2.21 and 2.16, respectively, in LEN-exposed cells (Figure 3.3B; only GSEA plots of LEN-treated cells are shown). In POM-treated cells, the NES of IFNγ- and IFNα-regulated genes was 1.87 and 1.8, respectively. Suppression of MYC-responsive genes was demonstrated also in MM.1S cells. In LEN-treated MM.1S cells, the NES was -2.47 for the MYC_TARGET_V2 gene set, and -1.74 for the MYC_TARGET_V1 gene set. In POM-treated cells, the NES for the MYC_TARGET_V1 and V2 gene sets resulted -1.71 and -2.02, respectively (Figure 3.3C; only GSEA plots of LEN-treated cells are shown).

Taken together, these findings showed that IMiDs can suppress *IRF4* in MM.1S cells and consistently induce a strong IFN-like response in both IMiD-sensitive U266 and MM.1S cells. Additionally, downregulation of E2F- and MYC- target genes was demonstrated in U266 cells following acute exposure to IMiDs. In MM.1S cells, acute treatment with IMiDs also caused downregulation of MYC-responsive genes, but did not affect genes regulated by E2F. Finally, although POM caused differential expression of more genes in both U266 and MM.1S cells as compared to LEN, treatment with LEN induced higher enrichment of IFN-related gene sets and E2F- and MYC-related gene sets as compared to POM-exposed cells.

3.2.2.2 Interferon, MAP kinase and MYC signatures are perturbed in cells with acquired lenalidomide resistance

To understand which transcriptional changes are associated with prolonged IMiD treatment, the transcriptome of U266res cells was compared to that of U266 cells, and the transcriptome of MM.1Sres cells was compared to that of parental MM.1S cells. This approach aimed to define which specific genes and/or pathways could potentially drive and could be associated with a status of IMiD resistance. Analysis of DEGs demonstrated marked discrepancies between the transcriptome of U266 cells and that of LEN-resistant U266 cells in the absence of IMiD treatment (Figure 3.4A-B). In U266res cells, 695 genes were significantly downregulated, whilst 729 were found significantly upregulated, as compared to U266 cells. Gene Set Enrichment

Figure 3.4 Transcriptional profiling of U266 and U266res cells

(A) Heatmap showing the average normalised log2 count per million (LogCPM) of three replicates of differentially expressed genes from 3'RNA-seq in U266 and U266res cells treated with DMSO, 2μM LEN and 500nM POM for 16 hours. (B) Volcano Plot of differentially expressed genes between U266res and U266 cells in untreated conditions. Blue dots represent genes significant for adjusted p-value < 0.05. (C) Gene Set Enrichment Analysis (GSEA) of differentially expressed genes between U266res and U266 cells in untreated conditions, showing the most positively enriched gene set. (D) Gene Set Enrichment Analysis (GSEA) of differentially expressed genes between U266res and U266 cells in untreated conditions, showing the most negatively enriched gene set.

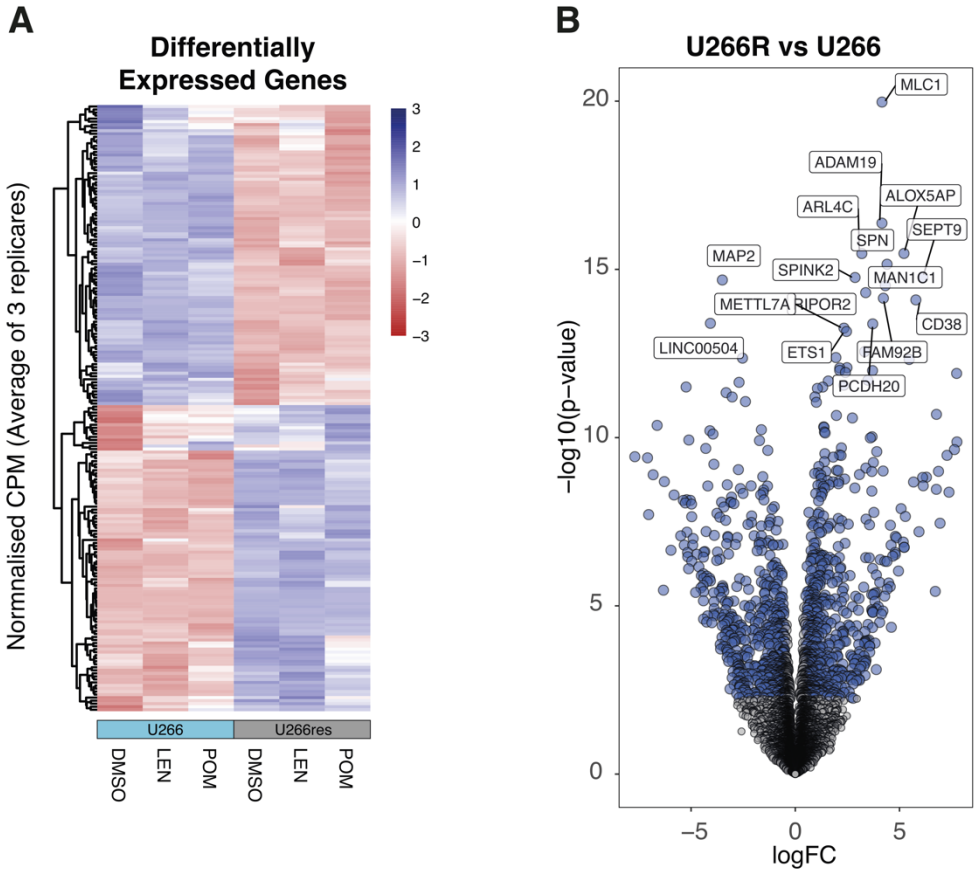

A
Differentially Expressed Genes
Normalised CPM (Average of 3 replicares)
3
2
1
0
−1
−2
−3
U266
U266res
DMSO
LEN
POM
DMSO
LEN
POM
B
U266R vs U266
−log10(p−value)
logFC
MLC1
ADAM19
ALOX5AP
ARL4C
SEPT9
SPN
MAP2
SPINK2
MAN1C1
METTL7A
RIPOR2
CD38
LINC00504
ETS1
RAM92B
PCDH20
C
HALLMARK_INTERFERON_GAMMA_RESPONSE
Nominal p−value: 0
FDR: 0
ES: 0.5276
Normalized ES: 2.0759
Enrichment score (ES)
Positive
U266R vs U266
Negative
Ranking metric
Rank in ordered gene list
D
HALLMARK_OXIDATIVE_PHOSPHORYLATION
Nominal p−value: 0
FDR: 0.0244
ES: −0.4257
Normalized ES: −1.8057
Enrichment score (ES)
Positive
U266R vs U266
Negative
Ranking metric
Rank in ordered gene list

Figure 3.5 Transcriptional profiling of MM.1S and MM.1Sres cells

(A) Heatmap showing the average normalised log2 count per million (LogCPM) of three replicates of DEGs from 3'RNA-seq in MM.1S and MM.1Sres cells treated with DMSO, 2μM LEN and 500nM POM for 16 hours. (B) Volcano Plot of differentially expressed genes between MM.1S res and MM.1S cells in untreated conditions. Blue dots represent genes significant for adjusted p-value < 0.05. (C) Gene Set Enrichment Analysis (GSEA) of differentially expressed genes between MM.1Sres and MM.1S cells in untreated conditions, showing the most positively enriched gene sets. (D) Gene Set Enrichment Analysis (GSEA) of differentially expressed genes between MM.1Sres and MM.1S cells in untreated conditions, showing the most negatively enriched gene sets.

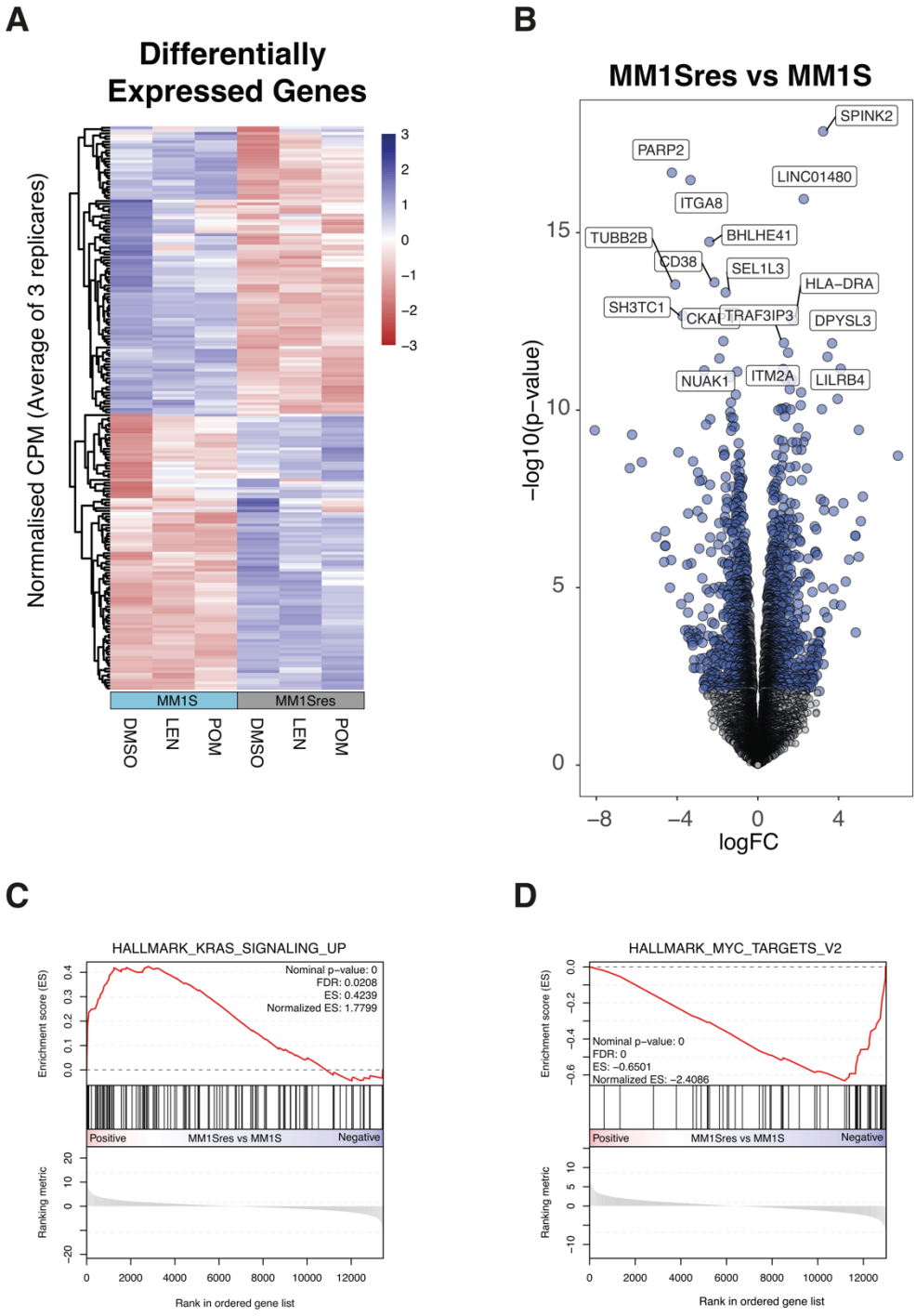
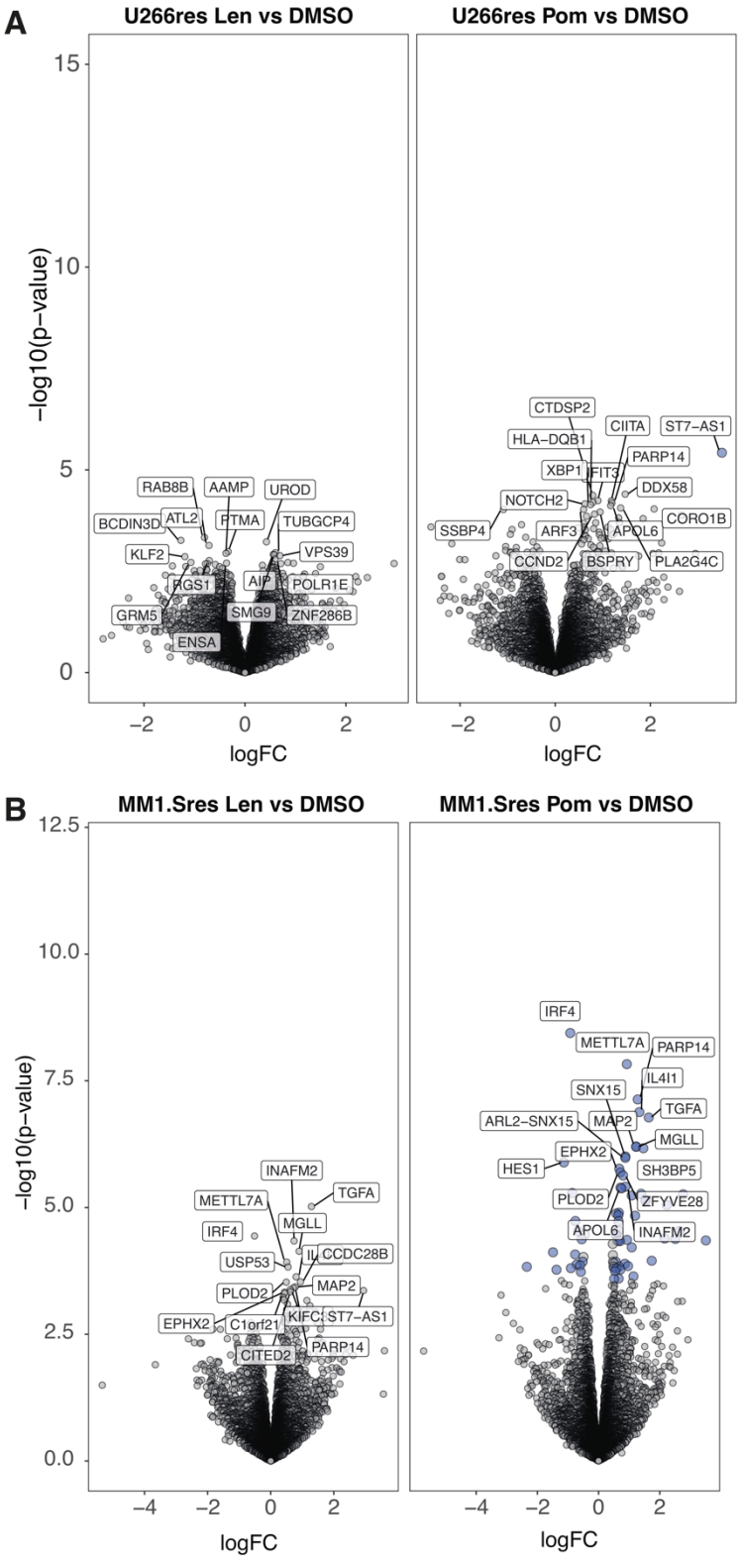

A
Differentially Expressed Genes
Normnalised CPM (Average of 3 replicares)
3
2
1
0
−1
−2
−3
MM1S
MM1Sres
DMSO
LEN
POM
DMSO
LEN
POM
B
MM1Sres vs MM1S
SPINK2
PARP2
LINC01480
ITGA8
TUBB2B
BHLHE41
CD38
SEL1L3
HLA−DRA
SH3TC1
TRAF3IP3
DPYSL3
NUAK1
ITM2A
LILRB4
−log10(p−value)
15
10
5
0
−8
−4
0
4
logFC
C
HALLMARK_KRAS_SIGNALING_UP
Nominal p−value: 0
FDR: 0.0208
ES: 0.4239
Normalized ES: 1.7799
Enrichment score (ES)
Positive
MM1Sres vs MM1S
Negative
Ranking metric
Rank in ordered gene list
D
HALLMARK_MYC_TARGETS_V2
Nominal p−value: 0
FDR: 0
ES: −0.6501
Normalized ES: −2.4086
Enrichment score (ES)
Positive
MM1Sres vs MM1S
Negative
Ranking metric
Rank in ordered gene list

Figure 3.6 Differential gene expression in LEN resistant MM cells upon IMiD treatment
(A) Volcano plots showing DEGs in U266res cells treated with 2μM LEN or 500nM POM for 16 hours. Blue dots represent hits significant for adjusted p-value < 0.05. (B) Volcano plots showing DEGs in MM.1Sres cells treated with 2μM LEN or 500nM POM for 16 hours. Blue dots represent hits significant for adjusted p-value < 0.05.


A
U266res Len vs DMSO
U266res Pom vs DMSO
−log10(p−value)
logFC
RAB8B
AAMP
UROD
BCDIN3D
ATL2
FTMA
TUBGCP4
KLF2
VPS39
RGS1
AIP
POLR1E
GRM5
SMG9
ZNF286B
ENSA
CTDSP2
CIITA
ST7−AS1
HLA−DQB1
PARP14
XBP1
FIT3
DDX58
NOTCH2
CORO1B
SSBP4
ARF3
APOL6
CCND2
BSPRY
PLA2G4C
B
MM1.Sres Len vs DMSO
MM1.Sres Pom vs DMSO
INAFM2
TGFA
METTL7A
MGLL
IRF4
USP53
CCDC28B
PLOD2
MAP2
EPHX2
C1orf21
KIFC
ST7−AS1
CITED2
PARP14
IRF4
METTL7A
PARP14
IL4I1
SNX15
TGFA
ARL2−SNX15
MAP2
MGLL
EPHX2
HES1
SH3BP5
PLOD2
ZFYVE28
APOL6
INAFM2

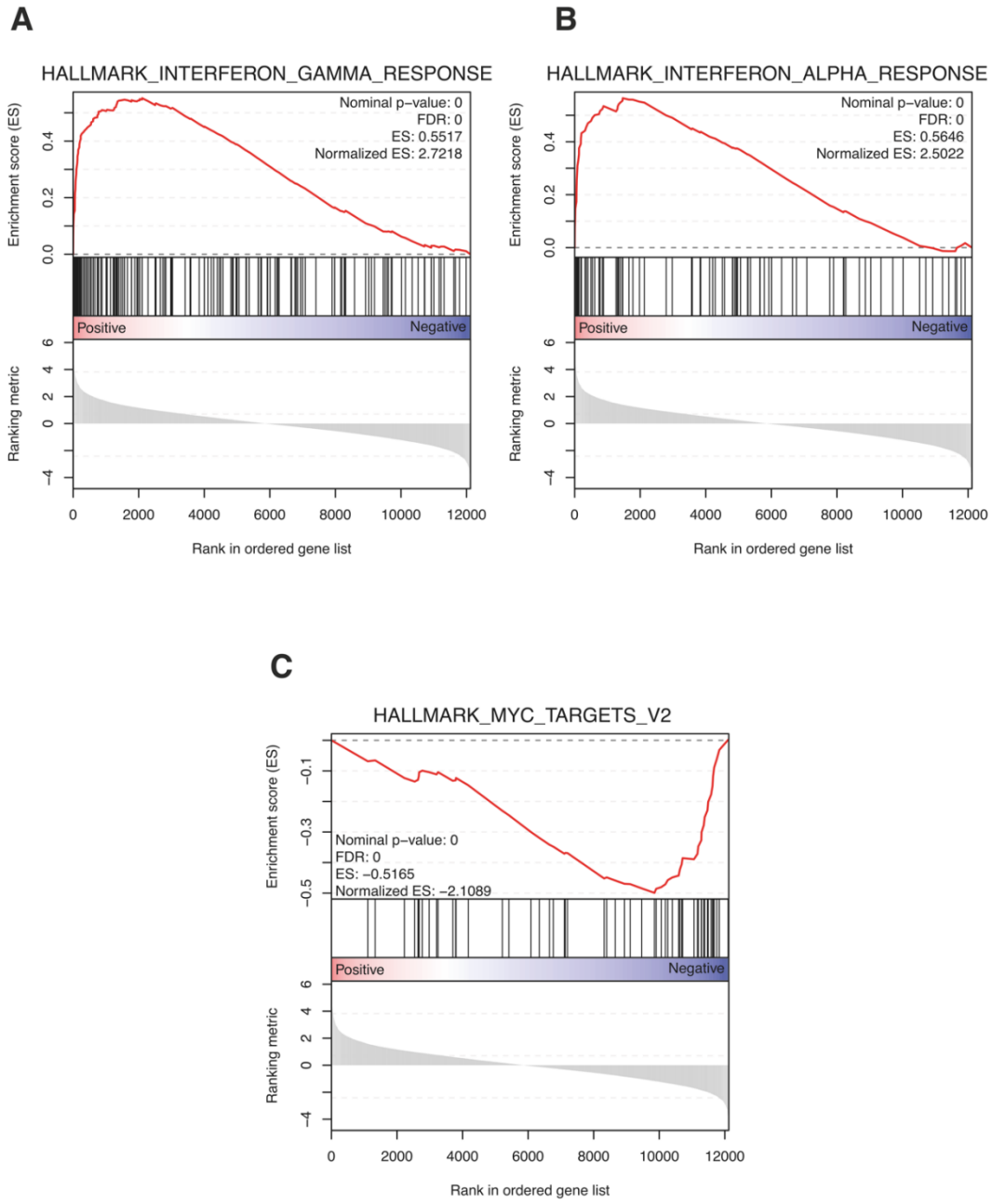


Figure 3.7 GSEA of transcriptional response in U266res cells

(A) and (B) GSEA plots displaying positively enriched gene sets in U266res cells exposed to LEN for 16 hours. (C) GSEA plots showing the negative enriched gene set in U266res cells upon 16-hour POM treatment.

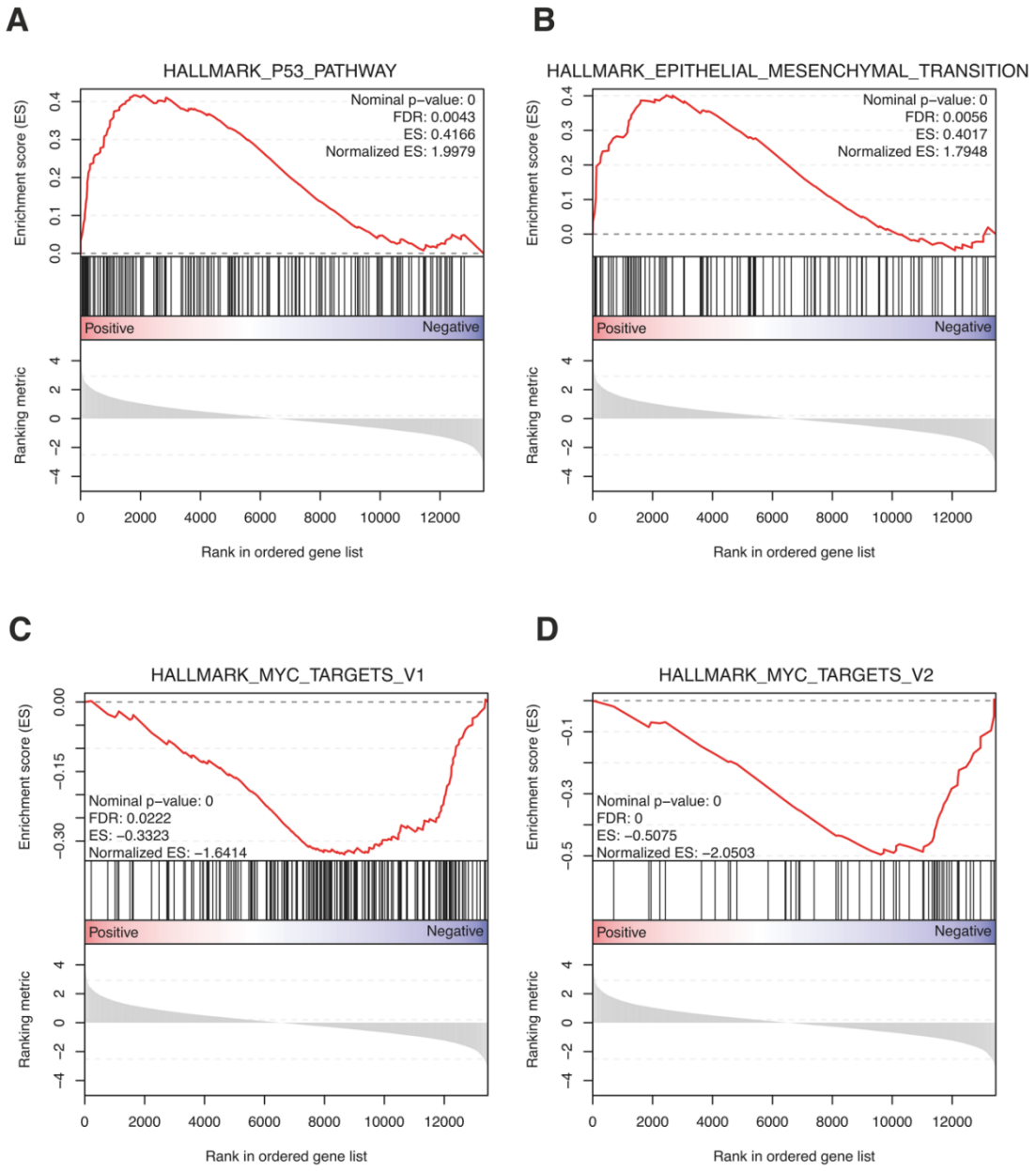


Figure 3.8 GSEA of transcriptional response in MM.1Sres cells

(A) and (B) GSEA plots displaying positively enriched gene sets in MM.1Sres cells exposed to LEN for 16 hours. (C) and (D) GSEA plots showing the negative enriched gene sets in MM.1Sres cells upon 16-hour LEN treatment.

Analysis (GSEA) revealed increased expression of IFNγ-responsive genes in resistant cells as compared to sensitive U266 cells, with a NES of 2.07 (Figure 3.4C). Conversely, genes involved in oxidative phosphorylation were downregulated, as the NES for these gene set was -1.81 (Figure 3.4D).

RNA-seq of MM.1S/MM.1Sres cells revealed substantial changes in the transcriptional landscape of MM.1Sres cells as compared to MM.1S cells, with numerous significant DEGs (Figure 3.5A-B). In particular, 1163 genes were significantly downregulated and 1227 significantly upregulated. GSEA demonstrated enrichment in *KRAS* signalling (but not IFN-related gene sets) with a NES of 1.78 in MM.1Sres cells relative to MM.1S cells, whereas *MYC* target genes were less transcribed, displaying a NES of -2.4 (Figure 3.5C-D).

These results indicate that chronic exposure to IMiDs in U266 and MM.1S cells could be associated with induction of either IFN-responsive genes or genes that are upregulated upon KRAS signalling. Conversely, suppression of *MYC* responsive genes seemed to be a feature of prolonged IMiD treatment in both U266res and MM.1Sres cells. These data suggest that these pathways might be implicated in maintaining an IMiD-resistance phenotype.

3.2.2.3 Global attenuation of transcriptional response following IMiD treatment in IMiD-resistant cells correlates with *CRBN* downregulation

Differential gene expression analysis was performed with read counts from the RNA-seq data of both U266res and MM.1Sres cells treated with LEN and POM relative to DMSO-treated U266res and MM.1S cells. This analysis aimed to assess whether IMiD resistant cells would exhibit the same, similar or different changes in gene expression following IMiD treatment compared to isogenic wild type cells.

3.2.2.3.1 Analysis of the transcriptional response to IMiDs in U266/U266res and MM.1S/MM.1Sres isogenic cell line pairs

In U266res and MM.1Sres cells, a global reduction of the transcriptional response to LEN and POM treatment (as compared to DMSO) was observed relative to U266 and MM.1S cells (Figures 3.2A, 3.3A, 3.6A-B). No significant gene was differentially expressed in U266res cells treated with LEN, while, only one, *ST7-AS1* was significantly upregulated in U266res cells treated with POM (Figure 3.6A). In MM.1Sres cells, treatment with LEN did not significantly increase expression of any gene. Conversely, treatment with POM caused a minor response with downregulation of

fewer genes relative to POM-treated MM.1S. Notably, *IRF4* was found significantly reduced even in POM-treated MM.1Sres (Figure 3.6B).

Despite the overall absence of differentially expressed genes meeting statistical significance, GSEA was performed with the dataset obtained in IMiD-treated U266res and MM.1Sres cells, with the hypothesis that similar patterns of transcriptional perturbations could occur but with reduced magnitude. U266res cells, showed enrichment in IFN responsive gene sets following treatment with LEN and POM (NES = 2.72 for IFNγ and NES = 2.5 for IFNα, Figure 3.7A-B; only GSEA plot of U266res cells treated with LEN are shown) and downregulation of *MYC* targets following POM treatment (HALLMARK_MYC_TARGETS_V2, NES = -2.1, Figure 3.7C; only the GSEA plot of U266res cells treated with POM is shown). Negative enrichment of MYC targets was not significant in U266res cells treated with LEN. In MM.1Sres cells, however, there was not a significant IFN-like transcriptional response. Instead, MM.1Sres cells treated with either LEN or POM showed increased expression of genes that are transcribed following p53 induction and genes that are involved in epithelial to mesenchymal transition. The NES of these gene sets was 2.0 and 1.8 in LEN-exposed MM.1Sres cells, respectively, and 1.9 and 1.8 in POM-exposed MM.1Sres cells, respectively (Figure 3.8A-B; only GSEA plots of MM.1Sres cells treated with LEN are shown). With regards to downregulated gene sets, MM.1Sres cells treated with LEN or POM also demonstrated suppression of *MYC*-induced genes. In particular, for MYC_TARGETS_V1 and MYC_TARGETS_V2, the NES was -1.64 and -2.05, respectively, in MM.1Sres cells treated with LEN. In MM.1Sres cells treated with POM, the NES was -2.15 and -2.46 for MYC_TARGETS_V1 and MYC_TARGETS_V2, respectively (Figure 3.8C-D; only GSEA plots of MM.1Sres cells treated with LEN are shown). These results suggest consistency in the subset of genes that are suppressed following IMiD treatment, in both IMiD-sensitive and cells with acquired IMiD-resistance.

3.2.2.3.2 mRNA expression of *CRBN*, *CUL4*, *DDB1* and *RBX1* in in U266/U266res and MM.1S/MM.1Sres isogenic cell line pairs

The RNA-seq dataset was then further interrogated to assess expression of genes composing the CRBN complex, i.e. *CRBN*, *RBX1*, *CUL4* and *DDB1*. Although not statistically significant, downregulation of *CRBN* was detected in U266res and MM.1Sres cells as compared to U266 and MM.1S cells respectively (Figure 3.9), consistent with the data obtained by immunoblotting and the cytogenetic profiling performed by Zhu and colleagues[217]. In particular, in both U266 and MM.1S cells, treatment with IMiDs did not seem to cause changes in the mRNA levels of *CRBN* (Figure 3.9A-B). U266res cells and MM.1Sres cells did not show marked variations in expression

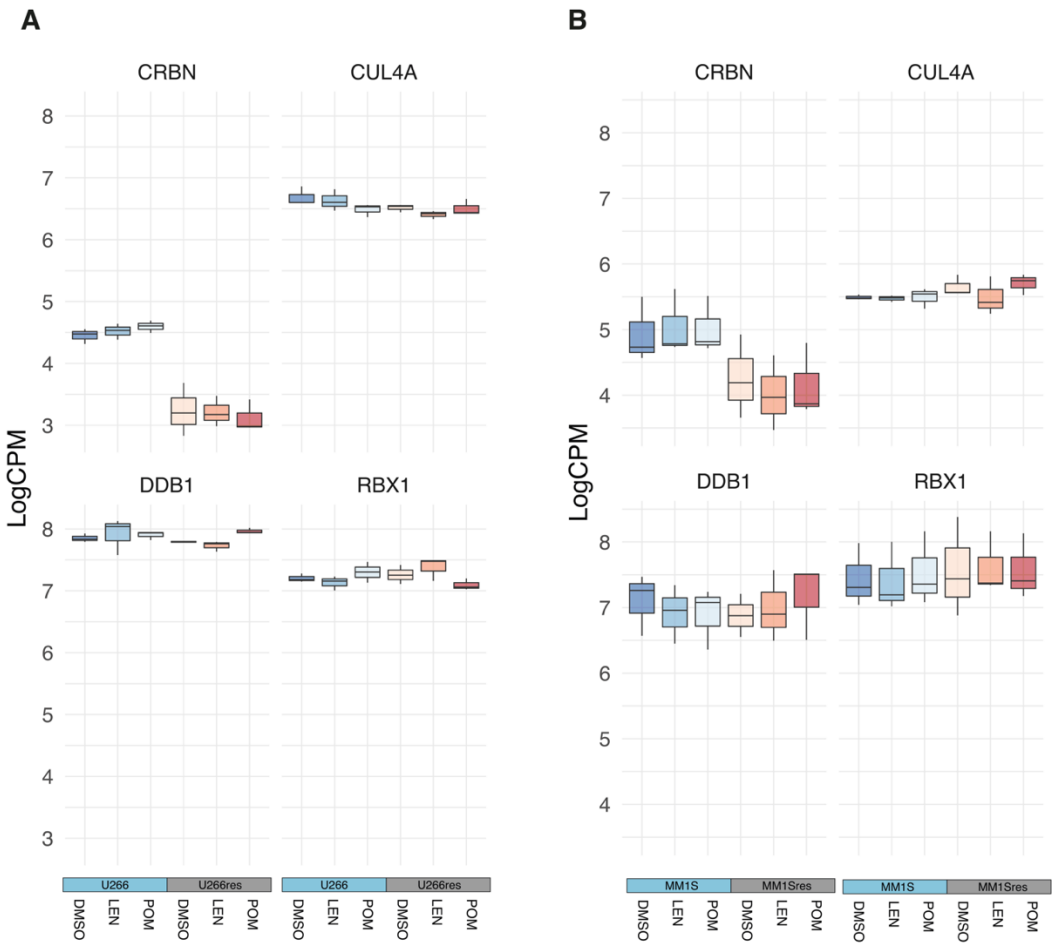


Figure 3.9 Differential Gene Expression of the CRBN E3 ligase complex in LEN sensitive and resistant cells

Boxplots representing differential gene expression (in log2 fold change of normalised count per million reads) of genes in the CRBN E3 ligase complex (*CRBN*, *CUL4A*, *DDB1* and *RBX1*) in U266/U266res (A) and MM.1S/MM.1Sres cells (B), treated with vehicle (DMSO), 2μM LEN or 500nM POM for 16 hours.

of *CRBN* in presence of LEN or POM, as compared to DMSO (Figure 3.9B). *CUL4A* did not show marked changes in mRNA levels in U266res cells relative to U266 cells, and treatment with IMiDs also did not change its expression (Figure 3.9A). In MM.1S cells, only POM demonstrated some activity in upregulating *CUL4A*, relative to both DMSO and LEN-treated MM.1S cells (Figure 3.9B). In MM.1Sres cells, *CUL4A* was not overall differentially expressed as compared to MM.1S cells in DMSO-treated samples (Figure 3.9B). Treatment with IMiDs also did not induce substantial alteration in the mRNA expression of CUL4A as compared to DMSO (Figure 3.9A-B). Expression of the *DDB1* gene was unmodified between U266 and U266res cells. Moreover, in both cell lines, LEN- and POM did not cause variation of *DDB1* expression as compared to DMSO (Figure 3.9A). Again, in MM.1S cells, the *DDB1* expression pattern was similar to that of U266 and U266res cells, and no marked change was observed in MM.1S or MM.1Sres cells treated with LEN and POM as compared to DMSO. Moreover, *DDB1* expression was unmodified between MM.1S and MM.1Sres cells (Figure 3.9B). Similar to *DDB1*, *RBX1* mRNA levels were not substantially altered in U266 cells as compared to U266res, nor they were in U266 or U266res cells treated with LEN and POM relative to DMSO (Figure 3.9A). RBX1 also did not change between MM.1S and MM.1Sres cells. In these lines, exposure to IMiDs did not cause variation in RBX1 expression as compared to DMSO (Figure 3.9B). These data indicate that, in U266res and MM.1Sres cells, CRBN is the member of this complex showing downregulation as compared to U266 and MM.1S cells, respectively. Overall, mRNA expression of *CUL4A* and *DDB1* relative to CRBN in U266 cell lines was greater than that of MM.1S cell lines.

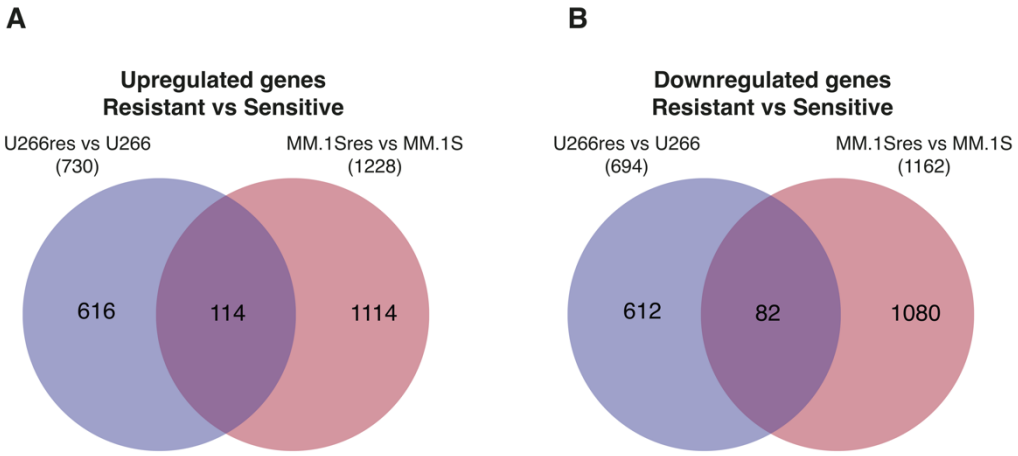
Taken together with the Western data showing reduced CRBN and IKZF3 degradation (Figure 3.1B), these data suggest that *CRBN* downregulation might contribute to IMiDs resistance in U266res and MM.1Sres cells, with consequential attenuation of neosubstrate degradation and the transcriptional response that follows IMiD treatment.

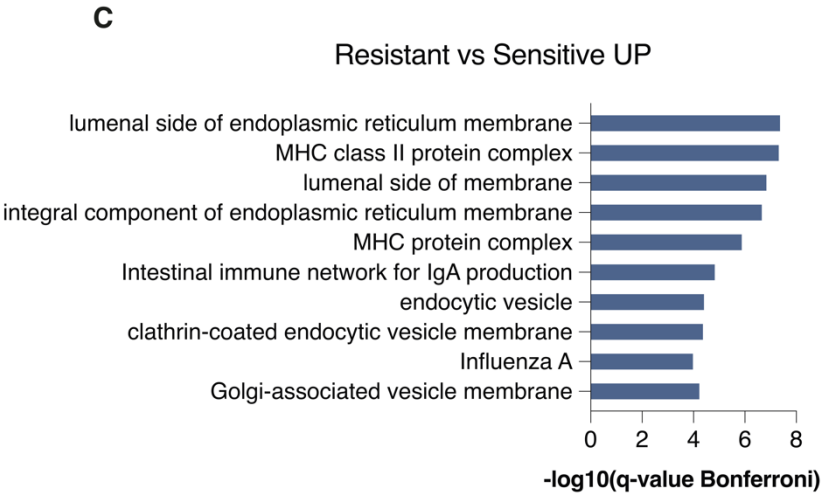
3.2.3 Statistical correlation studies between the transcriptional responses to IMiDs in MM.1S/MM.1Sres and U266/U266res

Statistical tests were used to explore the correlation in the transcriptional response between MM.1S/MM.1Sres and U266/U266res cells treated with an IMiD. The aim of these correlative studies was to ultimately define whether the type of transcriptional response to LEN and POM was cell line-dependent, and to assess the degree of correlation between the transcriptional response of LEN and that of POM (relative to DMSO).

Figure 3.10 Overlap of differentially expressed genes between U266res and MM.1Sres

(A) and (B) Venn diagram overlapping DEGs between U266res vs U266 cells and MM.1Sres vs MM.1S cells (upregulated and downregulated, respectively). (C) GO analysis (ToppFun) showing statistically significant (in -log10 of p-value subjected to the Bonferroni correction) overlaps of GO terms with mutual U266res and MM.1Sres cells upregulated genes. (D) GO analysis (ToppFun) showing statistically significant (in -log10 of p-value subjected to the Bonferroni correction) overlaps of GO terms with mutual U266res and MM.1Sres cells downregulated genes.


A
Upregulated genes
Resistant vs Sensitive
U266res vs U266
(730)
MM.1Sres vs MM.1S
(1228)
616
114
1114
B
Downregulated genes
Resistant vs Sensitive
U266res vs U266
(694)
MM.1Sres vs MM.1S
(1162)
612
82
1080


C
Resistant vs Sensitive UP
lumenal side of endoplasmic reticulum membrane
MHC class II protein complex
lumenal side of membrane
integral component of endoplasmic reticulum membrane
MHC protein complex
Intestinal immune network for IgA production
endocytic vesicle
clathrin-coated endocytic vesicle membrane
Influenza A
Golgi-associated vesicle membrane
0
2
4
6
8
-log10(q-value Bonferroni)

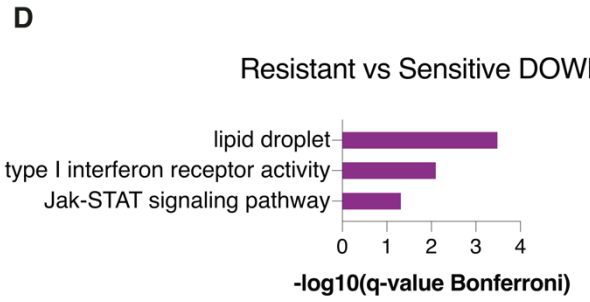
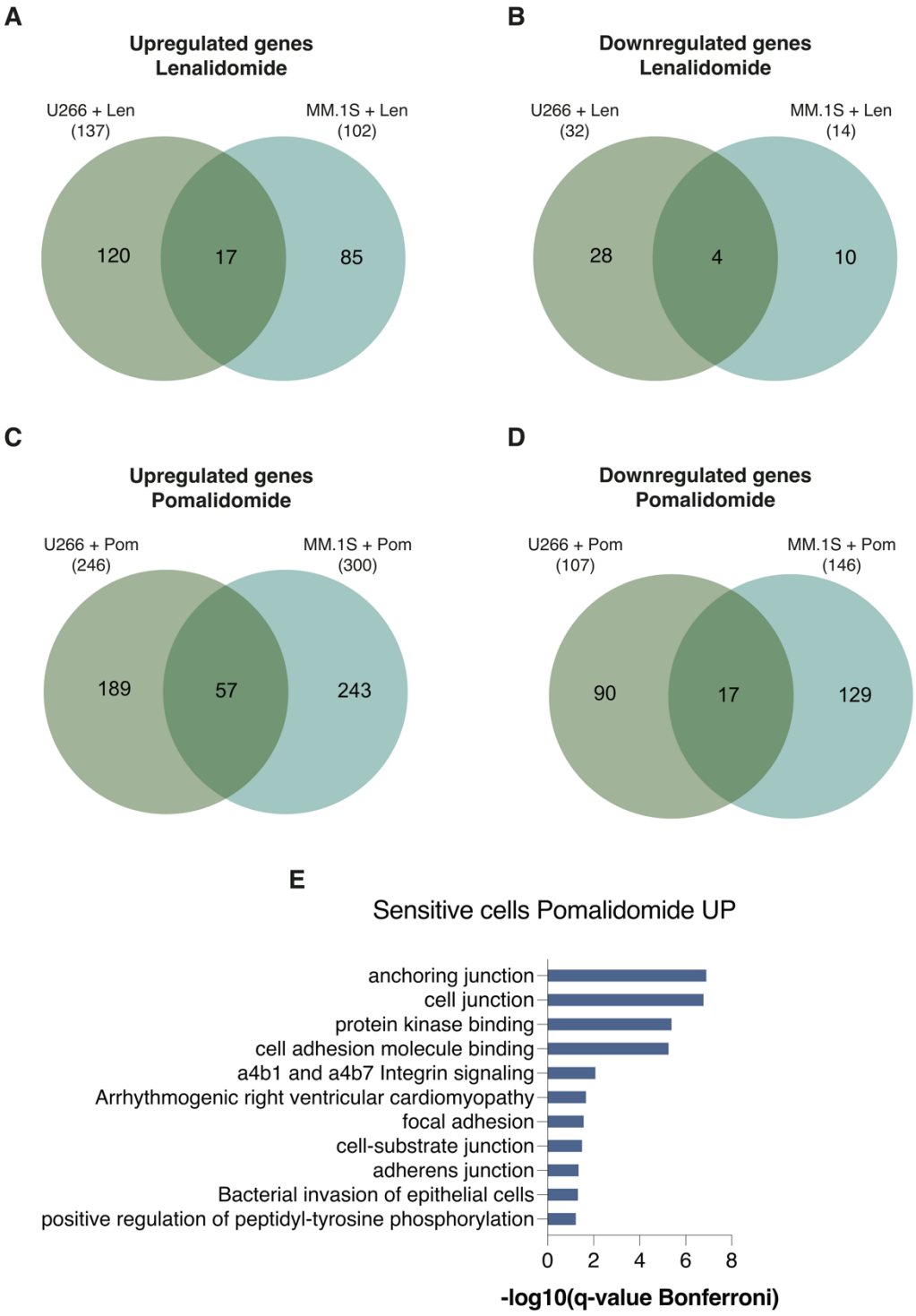

D
Resistant vs Sensitive DOWN
lipid droplet
type I interferon receptor activity
Jak-STAT signaling pathway
0
1
2
3
4
-log10(q-value Bonferroni)

Figure 3.11 Overlap of genes upregulated and downregulated between cells treated with IMiDs

(A) Venn diagrams displaying overlaps between DEGs of U266 and MM.1S cells that are upregulated or downregulated after treatment with 2μM LEN for 16 hours. (B) Venn diagrams displaying overlaps between DEGs of U266 cells and MM.1S cells that are downregulated after treatment with 2μM LEN for 16 hours. (C) Venn diagrams displaying overlaps between DEGs of U266 and MM.1S cells that are upregulated after treatment with 500nM POM for 16 hours. (D) Venn diagrams displaying overlaps between DEGs of U266 and MM.1S cells that are downregulated after treatment with 500nM POM for 16 hours. (E) Bar chart representing overlaps with GO terms of mutual DEGs in U266 and MM.1S cells treated with POM.


A
Upregulated genes
Lenalidomide
U266 + Len
(137)
MM.1S + Len
(102)
120
17
85
B
Downregulated genes
Lenalidomide
U266 + Len
(32)
MM.1S + Len
(14)
28
4
10
C
Upregulated genes
Pomalidomide
U266 + Pom
(246)
MM.1S + Pom
(300)
189
57
243
D
Downregulated genes
Pomalidomide
U266 + Pom
(107)
MM.1S + Pom
(146)
90
17
129
E
Sensitive cells Pomalidomide UP
anchoring junction
cell junction
protein kinase binding
cell adhesion molecule binding
a4b1 and a4b7 Integrin signaling
Arrhythmogenic right ventricular cardiomyopathy
focal adhesion
cell-substrate junction
adherens junction
Bacterial invasion of epithelial cells
positive regulation of peptidyl-tyrosine phosphorylation
0
2
4
6
8
-log10(q-value Bonferroni)

3.2.3.1 Genes implicated in IFN- and cell-to-cell signalling are differentially expressed in both MM.1Sres and U266res

Upregulated and downregulated genes in DMSO-treated MM.1Sres cells were overlapped with those of DMSO-treated U266res cells, in each case relative to MM.1S and U266 cells, respectively (Figure 3.10A-B). 114 genes were mutually upregulated in both U266res and MM.1Sres cell lines, corresponding to 15.6% of total upregulated genes in U266res cells (vs U266 cells) and 9.3% of MM.1Sres cells (vs MM.1S cells). 11.8% of downregulated genes in U266res cells and 7% of downregulated genes in MM.1Sres cells were overlapping (a total of 82 downregulated genes). GO analysis on mutual up- and down-regulated genes showed increased expression of HLA genes and diminished IFN-related signalling, with downregulation of IFN receptors and genes responsive to the JAK2-STAT5 axis (Figure 3.10C-D). These data show that there is stable induction of the expression of IFN-responsive genes in both U266res and MM.1Sres cells, with simultaneous downregulation of IFN receptors expression as compared to U266 and MM.1S cells, respectively.

To assess the existence of a common response to IMiDs between U266 and MM.1S cells, genes upregulated or downregulated in MM.1S and U266 cells following IMiD treatment were overlapped (Figure 3.11A-B). In cells exposed to LEN, 17 genes were co-upregulated, corresponding to 12.4% of U266 and 16.7% of MM.1S cells upregulated genes, and 4 were co-downregulated, corresponding to 12.5% of U266 and 28.5% of MM.1S cells downregulated genes. In parental MM.1S and U266 cells treated with POM, 57 genes were co-upregulated and 17 co-downregulated (Figure 3.11C-D). These 57 genes represented 23.1% of U266 cells and 19% of MM.1S cells upregulated genes. The 17 downregulated genes represented 15.9% of U266 and 11.6% of MM.1S cells downregulated genes. Subsequently, GO analysis was preformed using co-upregulated genes following POM treatment (Figure 3.11E). Treatment with POM increased the expression of genes involved in cell adhesion and cell-to-cell signalling. GO analysis of co-upregulated genes following LEN treatment was similar to that of POM genes, but with fewer significant overlapping gene sets, whilst GO analysis on co-downregulated genes produced no statistically significant overlapping gene sets.

3.2.3.2 Pearson's correlation testing defines the levels of similarity in the response to IMiDs in isogenic cell line pairs U266/U266res and MM.1S/MM.1Sres

Given the low number of overlapping genes between MM.1S, MM.1Sres, U266 and U266res cell lines, Pearson's correlation tests between RNA-seq datasets were performed to assess whether a statistical correlation between LEN- and POM- dependent responses existed. Statistical

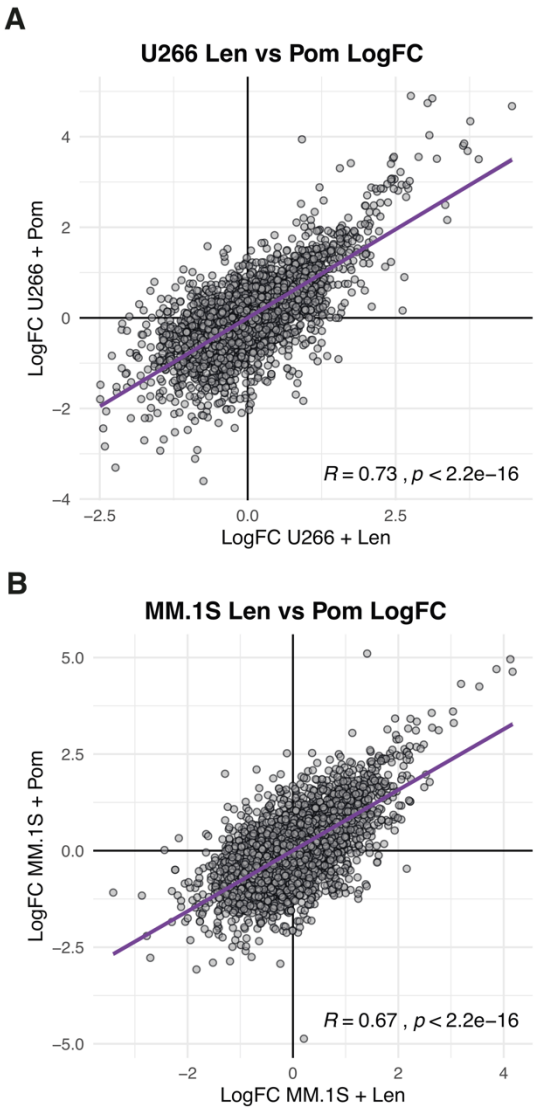
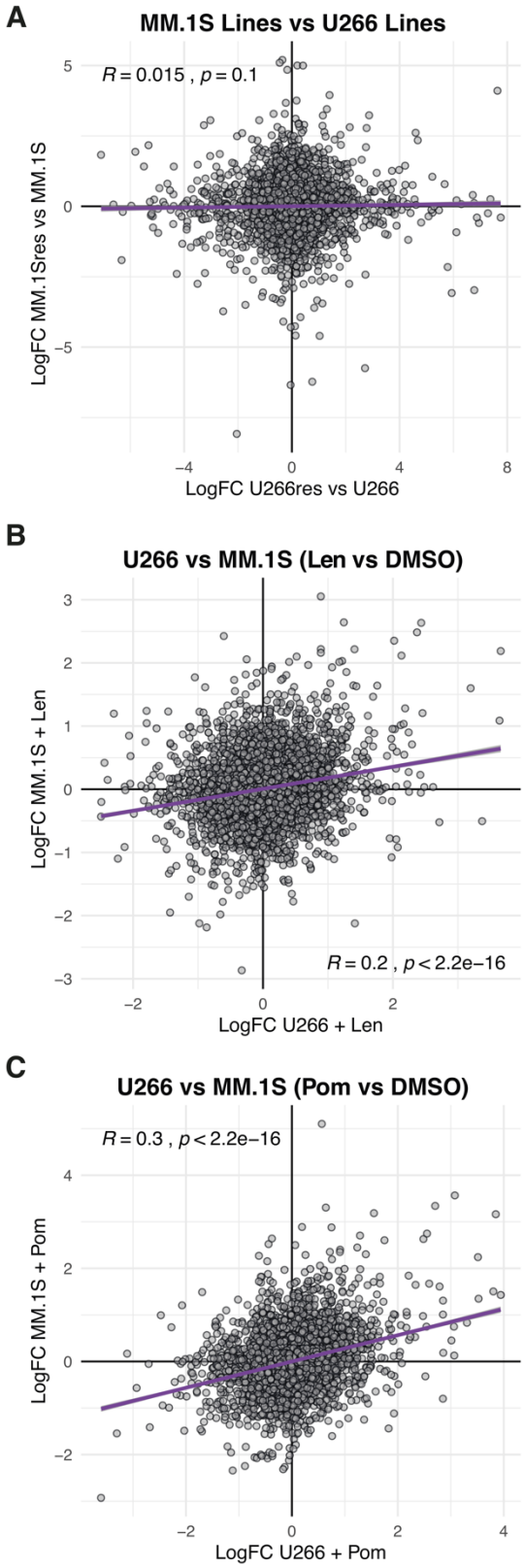


Figure 3.12 Correlation analysis of the transcriptional response between LEN and POM in U266 and MM.1S lines

(A) Pearson's correlation test between log2 of fold change in CPM (LogFC) of U266 cells treated with LEN and POM vs U266 cells exposed to DMSO only. (B) Pearson's correlation test between LogFC in MM.1S cells treated with LEN and POM vs MM.1S cells exposed to DMSO only.

Figure 3.13 Correlation analysis of the transcriptional response between U266 and MM.1S in the same treatment conditions

(A) Pearson's correlation test between LogFC in U266res vs U266 cells and MM.1Sres vs MM.1S cells in untreated (vehicle) condition. (B) Pearson's correlation test between LogFC U266 and MM.1S cells treated with LEN vs vehicle. (C) Pearson's correlation test between LogFC U266 and MM.1S cells treated with POM vs vehicle.


A
MM.1S Lines vs U266 Lines
R = 0.015 , p = 0.1
LogFC MM.1Sres vs MM.1S
LogFC U266res vs U266
B
U266 vs MM.1S (Len vs DMSO)
R = 0.2 , p < 2.2e−16
LogFC MM.1S + Len
LogFC U266 + Len
C
U266 vs MM.1S (Pom vs DMSO)
R = 0.3 , p < 2.2e−16
LogFC MM.1S + Pom
LogFC U266 + Pom

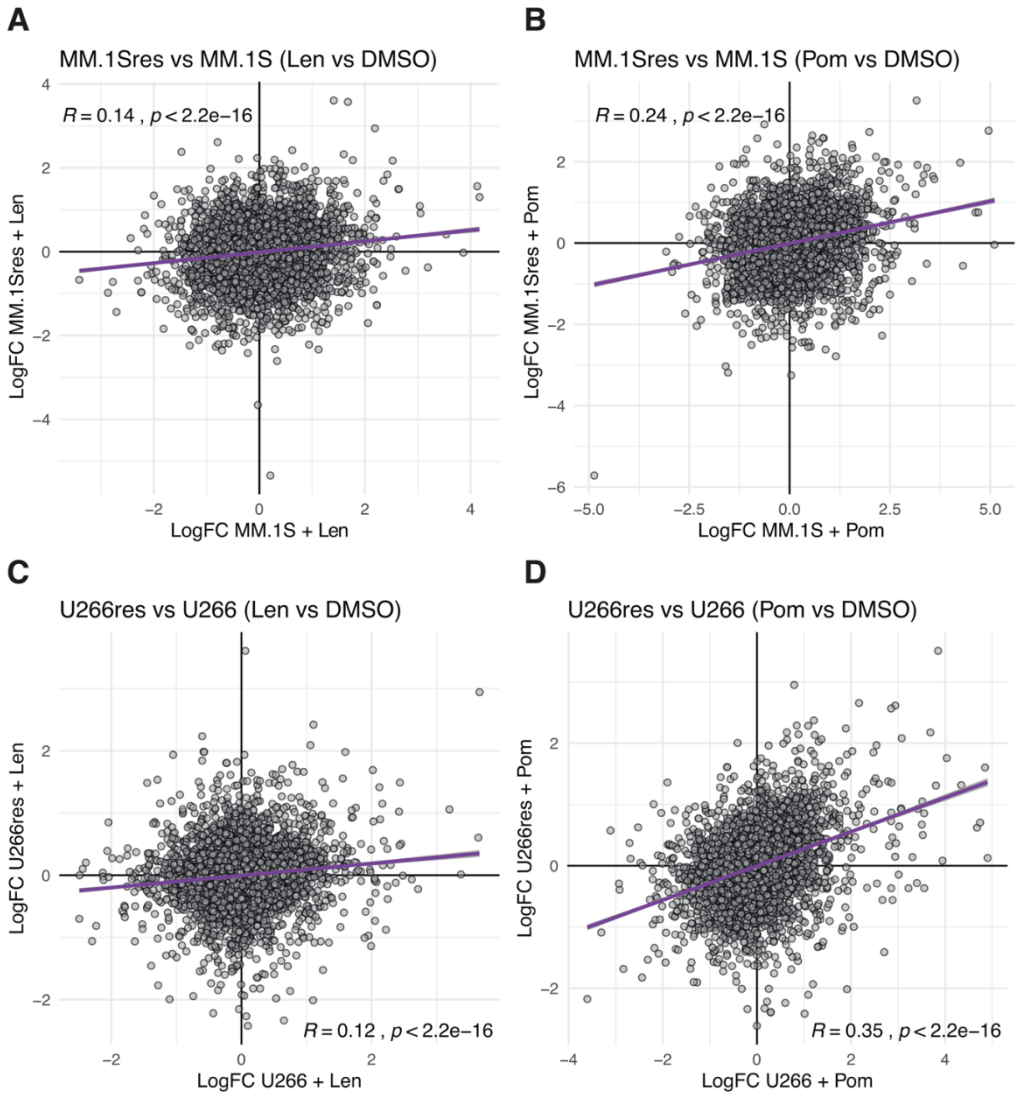


Figure 3.14 Correlation analysis of the transcriptional response between isogenic pairs in the same condition

(A) Pearson's correlation test between LogFC in MM.1Sres cells treated with LEN in comparison to DMSO and MM.1S cells treated with the same IMiD. (B) Pearson's correlation test between LogFC in MM.1Sres cells treated with POM in comparison to DMSO and MM.1S cells treated with the same IMiD. (C) Pearson's correlation test between LogFC in U266res cells treated with LEN in comparison to DMSO and U266 cells treated with the same IMiD. (D) Pearson's correlation test between LogFC in U266res cells treated with POM in comparison to DMSO and U266 cells treated with the same IMiD.

correlation between the transcriptional response to LEN and POM was tested within the same cell line. In both MM.1S and U266 cells, perturbations in the transcriptome were very similar, as there was a high degree of correlation (U266 R=0.73, MM.1S R=0.67) between the effect induced by LEN and that induced by POM (Figure 3.12). Next, it was assessed whether prolonged LEN treatment would cause similar long-term transcriptional perturbations in U266 and MM.1S cell lines. Pearson's correlation test demonstrated no correlation (R=0.015) between DMSO-treated U266res/U266 cells and DMSO-treated MM.1Sres/MM.1S cells (Figure 3.13A). Correlation between the response to IMiDs in U266 cells and MM.1S cells was also verified, aiming to define whether treatment with IMiDs would induce a similar transcriptional response in both U266 and MM.1S cells. U266 and MM.1S cells exhibited some degree of positive correlation when treated with the same IMiD (R = 0.2 with LEN, R = 0.3 with POM), indicating that LEN and POM might induce similar transcriptional responses in different cell lines. Next, correlation of the transcriptional response between cells of the same isogenic pair to the same IMiD was tested with the aim of quantifying the magnitude of the response to IMiDs between sensitive and resistant cell lines. In both MM.1S and U266 cell lines, sensitive and resistant cells treated with LEN showed little correlation (R=0.14 and R=0.12 respectively, Figure 3.14A, 3.14C), whilst transcriptomes the same cells treated with POM were slightly more correlated (R=0.24 and R=0.35 respectively, Figure 3.14B,3.14D). This data indicates that in U266res and MM.1Sres the transcriptional response to IMiDs was virtually abolished as compared to U266 and MM.1S cells, respectively.

These observations indicate that the transcriptional responses are similar between IMiDs in the same cell line, although less correlated between different cell lines. A similarity in the transcriptional response was documented by a minor correlation between cell lines of the same isogenic pair treated with the same IMiD. A correlation between sensitive and resistant cells of the same isogenic pair was also seen, supporting the observation that transcriptional responses in resistant cells are globally reduced as compared to those of sensitive cells. Taken together, these correlation studies indicate the presence of similarities in the transcriptional response to sensitive cells acutely treated with the different IMiDs and suggest that the baseline transcriptional landscape might determine the type of transcriptional response observed upon IMiD treatment.

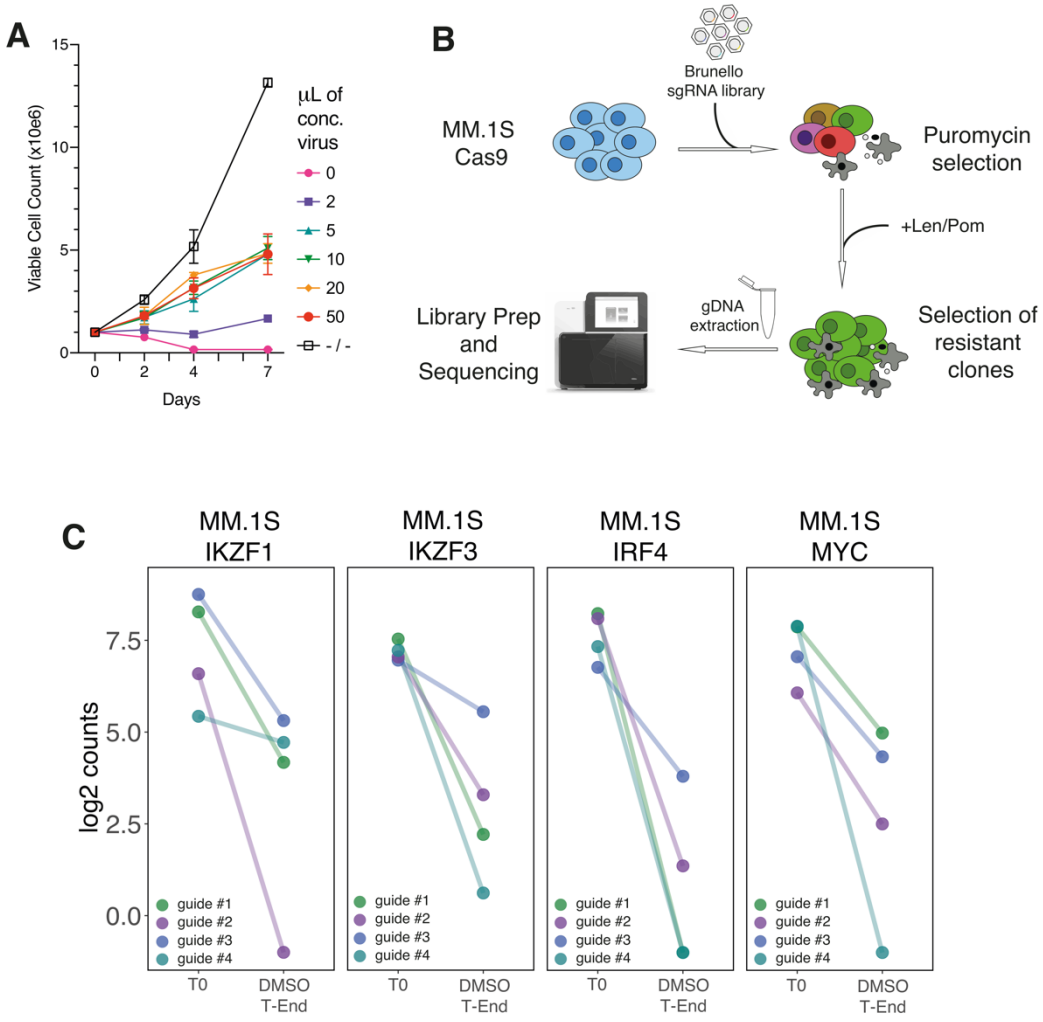


Figure 3.15. Genome-wide CRISPR resistance screening identifies genes required for IMiD sensitivity

(A) Viral library titration assay evaluating number of viable cells growing in puromycin containing media following transfection with different concentrations of the Brunello genome-wide library in MM.1S-Cas9 cells. In the legend, ” -/-“ is the no-puromycin/no-virus control. (B) Summary of the workflow for a genome-wide CRISPR resistance screen. (C) Line plot showing log2 fold change in representation of *IKZF1*, *IKZF3*, *IRF4* and *MYC* sgRNAs in DMSO-treated cells at the end of the screen relative to the T-0 reference.

3.2.4 Genome-wide CRISPR screening identifies genes that are essential for the response to IMiDs

Although RNA-seq provided data with regards to the acute response to IMiDs and the mechanisms of adaptation to prolonged exposure to LEN, it did not fully explain what could drive resistance to IMiDs. Therefore, genome-wide CRISPR screening was employed to identify those genes that are required for IMiD sensitivity.

3.2.4.1 The gain-of-representation CRISPR screen workflow in IMiD-treated MM.1S cells

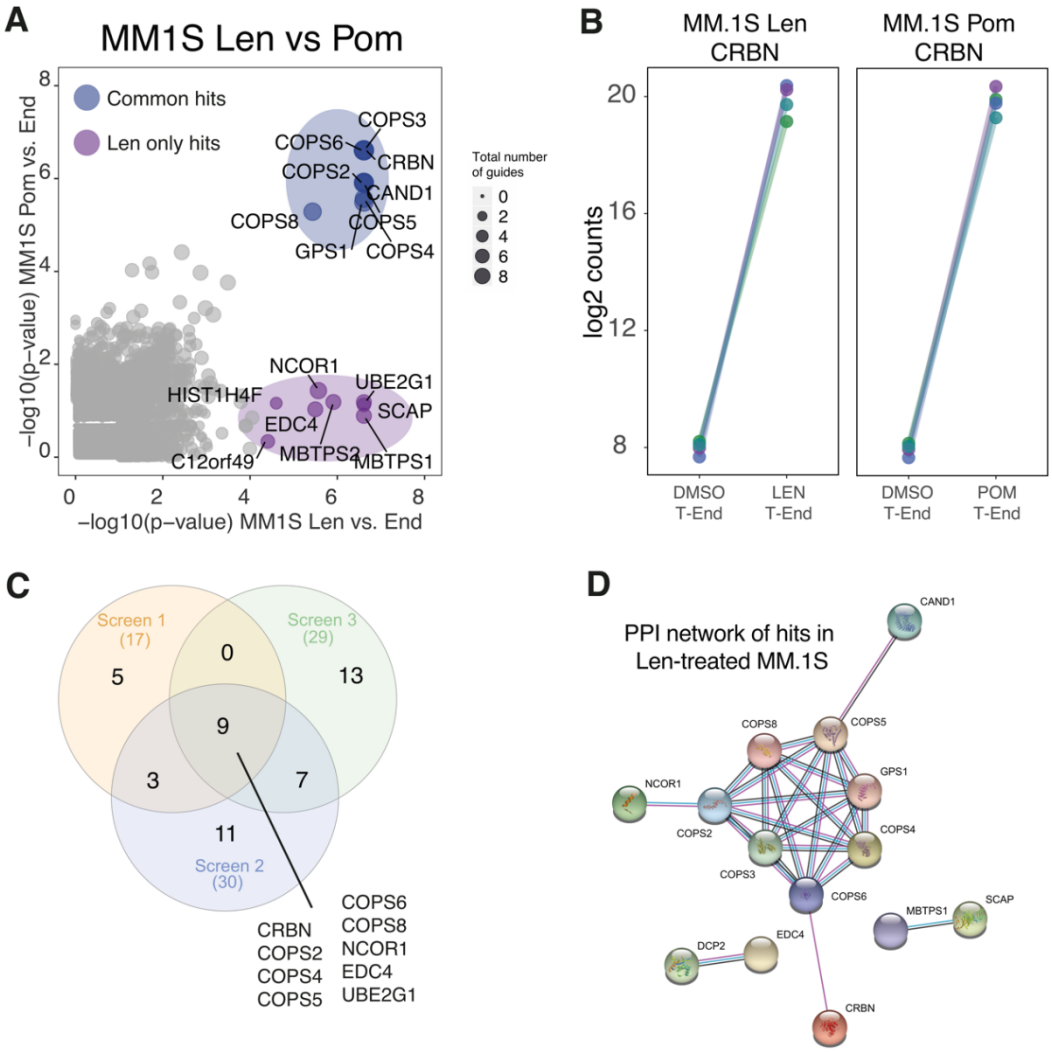
The Brunello human genome-wide library (4 sgRNAs per gene, for a total of ~80000 sgRNAs) was adopted to perform a screen in MM.1S cells expressing Cas9 (MM.1S-Cas9) over ~8 weeks. To ensure only a single viral integration per MM.1S-Cas9 clone, cells needed to be transduced with a low Multiplicity of Infection (MOI). This is a necessary condition to individually knockout genes by viral transduction with a sgRNA library in a cell population[241,256]. The ideal MOI for achieving one viral integration per cell is 0.2 to 0.4. The amount of concentrated viral medium necessary for a MOI within the 0.2-0.4 range was assessed by titration. MM.1S-Cas9 were transduced with different concentration of viral media and treated with puromycin for 7 days. Non-transduced cells and cells grown in media without puromycin were used as controls for the experiment (Figure 3.15A). The amount of virus conferring puromycin resistance to ~20 to ~40% of cells, relative to the non-treated non-transduced control, was subsequently chosen for transduction of MM.1S-Cas9 cells in the genome-wide screen. Puromycin treatment induced cell death in ~60% of the cells in presence of 5mL of concentrated virus (for a detailed explanation of experimental condition for the screen, refer to chapter 2, section 2.5.2). Finally, ~500 million cells were transduced in media with the appropriate viral concentration selected to achieve a MOI between 0.2 and 0.4, and selected with puromycin for 7 days. At day 8, 25% of the cells were taken as a timepoint zero (T-0) reference for initial library representation, while the remaining cells were seeded in culture with DMSO, 2µM LEN or 500nM POM. The gain-of-representation screen was performed over ~8 weeks, at which timepoint only LEN- and POM-resistant clones remained viable and proliferating. Following cell harvest and DNA extraction, samples were sequenced using the Illumina platform (Figure 3.15B).

3.2.4.2 Defining the dependency of MM.1S cells on the *IKZF1/3-IRF4-MYC* axis

The sequencing data was analysed with the aims of 1) confirming the dependency of MM.1S cells on genes that are involved in the response to IMiDs and 2) defining additional gene and pathways which MM.1S cells are dependent on. The difference in *IKZF1*, *IKZF3*, *MYC* and *IRF4*

Figure 3.16 Analysis of the pathways and genes involved in sensitivity to IMiDs

(A) Scatterplot displaying sgRNAs enriching in MM.1S-Cas9 cells after 8 weeks (T-end) of selection with LEN and or POM, as compared to the vehicle control (DMSO at T-end). (B) Line plot showing log2 fold change of read counts of *CRBN* sgRNAs in LEN and POM (at the end of the screen) relative to the DMSO control. (C) Venn diagram overlapping sgRNA hit in this screen with those of Liu and colleagues and Sievers and colleagues. (D) Protein-Protein Interaction network (STRING) and (E) Gene Ontology analysis of sgRNAs selected at the end of the screen in the presence of LEN (metascape).


A
MM1S Len vs Pom
Common hits
Len only hits
COPS3
COPS6
CRBN
COPS2
CAND1
COPS8
COPS5
GPS1
COPS4
NCOR1
UBE2G1
HIST1H4F
SCAP
EDC4
MBTPS2
C12orf49
MBTPS1
Total number of guides
0
2
4
6
8
−log10(p−value) MM1S Pom vs. End
−log10(p−value) MM1S Len vs. End
B
MM.1S Len CRBN
MM.1S Pom CRBN
log2 counts
DMSO T-End
LEN T-End
DMSO T-End
POM T-End
C
Screen 1 (17)
Screen 3 (29)
Screen 2 (30)
5
0
13
9
3
7
11
CRBN
COPS2
COPS4
COPS5
COPS6
COPS8
NCOR1
EDC4
UBE2G1
D
PPI network of hits in Len-treated MM.1S
CAND1
COPS8
COPS5
GPS1
NCOR1
COPS2
COPS4
COPS3
COPS6
MBTPS1
SCAP
EDC4
DCP2
CRBN
E
GO analysis on enriched hits of Len-treated MM.1S
-log10(fdr)
protein deneddylation
NER, DNA damage recognition
transcription-coupled NER
DNA repair
response to DNA damage
chromosome organization
COP9 signalosome assembly
ER-nucleus signaling pathway
ATF6-mediated UFP

sgRNAs representation was calculated between sgRNA read counts in DMSO-treated MM.1S-Cas9 cells at the end timepoint and sgRNA read counts at the initial timepoint, as these are genes that known to be implicated in the response to IMiDs. In addition, *MYC* and *IRF4* have been demonstrated to be essential genes for the proliferation and survival of MM cells[65,115]. It was established that, for a gene to be essential for MM.1S cells, 4/4 sgRNA needed to be less represented at the end of the screen, in the vehicle-treated condition, as compared to the timepoint zero. 4/4 of the sgRNA specific for *IKZF1*, *IKZF3*, *MYC* and *IRF4* were less represented at the end of the screen, confirming their importance for MM.1S cells growth and viability (Figure 3.15C). Although all four sgRNAs were less represented in both *IKZF1* and *IKZF3*, one sgRNA each for *IKZF1* and *IKZF3* did not meet the significance cut-off (with adjusted p-value > 0.05). This data indicates that the loss of *IKZF1/3, IRF4* and *MYC* is disadvantageous for MM.1S cells.

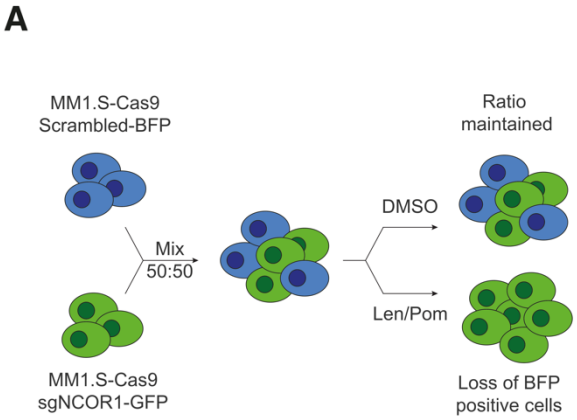
3.2.4.3 Defining the factors required for IMiD sensitivity

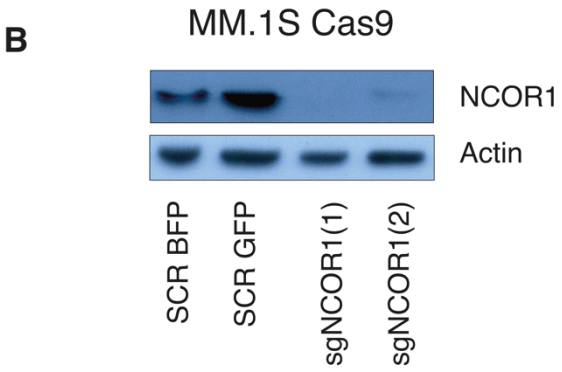
To explore which genes are required for a state of sensitivity to IMiDs, sequencing data was analysed to determine which sgRNAs were enriched in MM.1S-Cas9 cells treated with LEN or POM at the end of the screen as compared to DMSO-treated cells at the same timepoint. Several sgRNAs enriched in MM.1S Cas9 cells treated with LEN or POM. SgRNAs specific for *CRBN*, *CAND1* and COP9 signalosome subunits *GPS1*, *COPS2*, *COPS3*, *COPS4*, *COPS5*, *COPS6* and *COPS8* were enriched in MM.1S Cas9 cells treated with LEN or POM (Figure 3.16A) at the end of the screen. Additionally, other sgRNAs specific for *NCOR1*, *UBE2G1*, *HIST1H4F*, *EDC4*, *SCAP*, *MBTPS1/2* and *C12orf49* were significantly enriched solely in cells exposed to LEN (Figure 3.16A). The most enriched sgRNAs in all the screens were specific for *CRBN* (Figure 3.16B). As previously published by Sievers and colleagues[239], deletion of *CRBN* causes complete resistance to IMiDs. This finding strongly suggests that the downregulation of *CRBN* observed in U266res and MM.1Sres cells is most likely a strong and common driver of IMiD resistance.

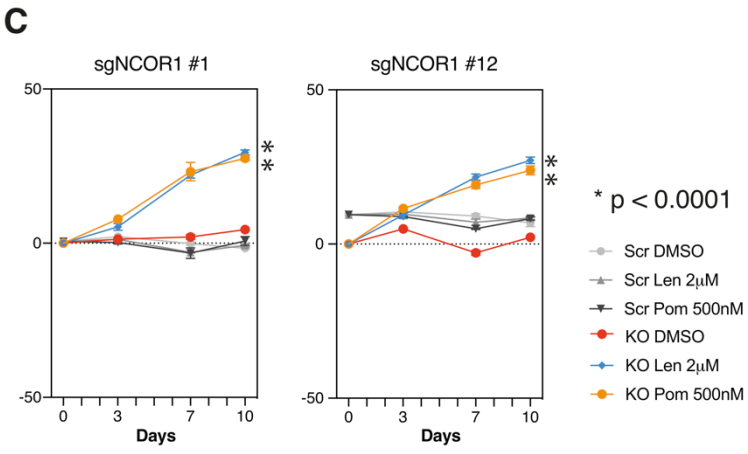
SgRNAs specific for genes that were identified as IMiD sensitivity factors in this screen (screen 1) were then overlapped with those of the studies of Sievers and Liu (screen 2 and screen 3, respectively)[239,240]: *CRBN*, *COPS2*, *COPS4*, *COPS5*, *COPS6*, *COPS8*, *NCOR1*, *EDC4* and *UBE2G1* sgRNAs were the most consistently identified throughout screen 1, screen 2 and screen 3 (Figure 3.16C). Protein-protein interaction and gene ontology analyses of these genes indicated that the COP9 signalosome is involved in protein turnover and ubiquitination, protein neddylation and in the regulation of nucleotide excision repair (NER) (Figure 3.16D-E).

Figure 3.17 Loss of NCOR1 causes resistance to IMiDs

(A) Schematic representation of competition assays workflow for validation of resistance screens. (B) Western Blot showing CRISPR-induced knockout of *NCOR1* with two independent sgRNAs in MM.1S-Cas9 cells, as compared to two independent non-targeting sgRNAs (SCR BFP, SCR GFP). Experiment performed by Dr Olga Motorna, Johnstone Laboratory (C) Graphs representing one of three independent competitive proliferation assays showing change in the fraction of MM.1S-Cas9 GFP (scramble or *NCOR1* KO) cells growing in competition with scramble MM.1S-Cas9 BFP cells, treated with DMSO, 2μM LEN or 500nM POM. Statistical significance (p) was calculated using two-way ANOVA testing and adjusted with Benjamini and Hochberg correction.


A
MM1.S-Cas9
Scrambled-BFP
Mix
50:50
MM1.S-Cas9
sgNCOR1-GFP
DMSO
Len/Pom
Ratio
maintained
Loss of BFP
positive cells


B
MM.1S Cas9
NCOR1
Actin
SCR BFP
SCR GFP
sgNCOR1(1)
sgNCOR1(2)


C
sgNCOR1 #1
sgNCOR1 #12
50
0
-50
0
3
7
10
Days
**
**
* p < 0.0001
Scr DMSO
Scr Len 2μM
Scr Pom 500nM
KO DMSO
KO Len 2μM
KO Pom 500nM

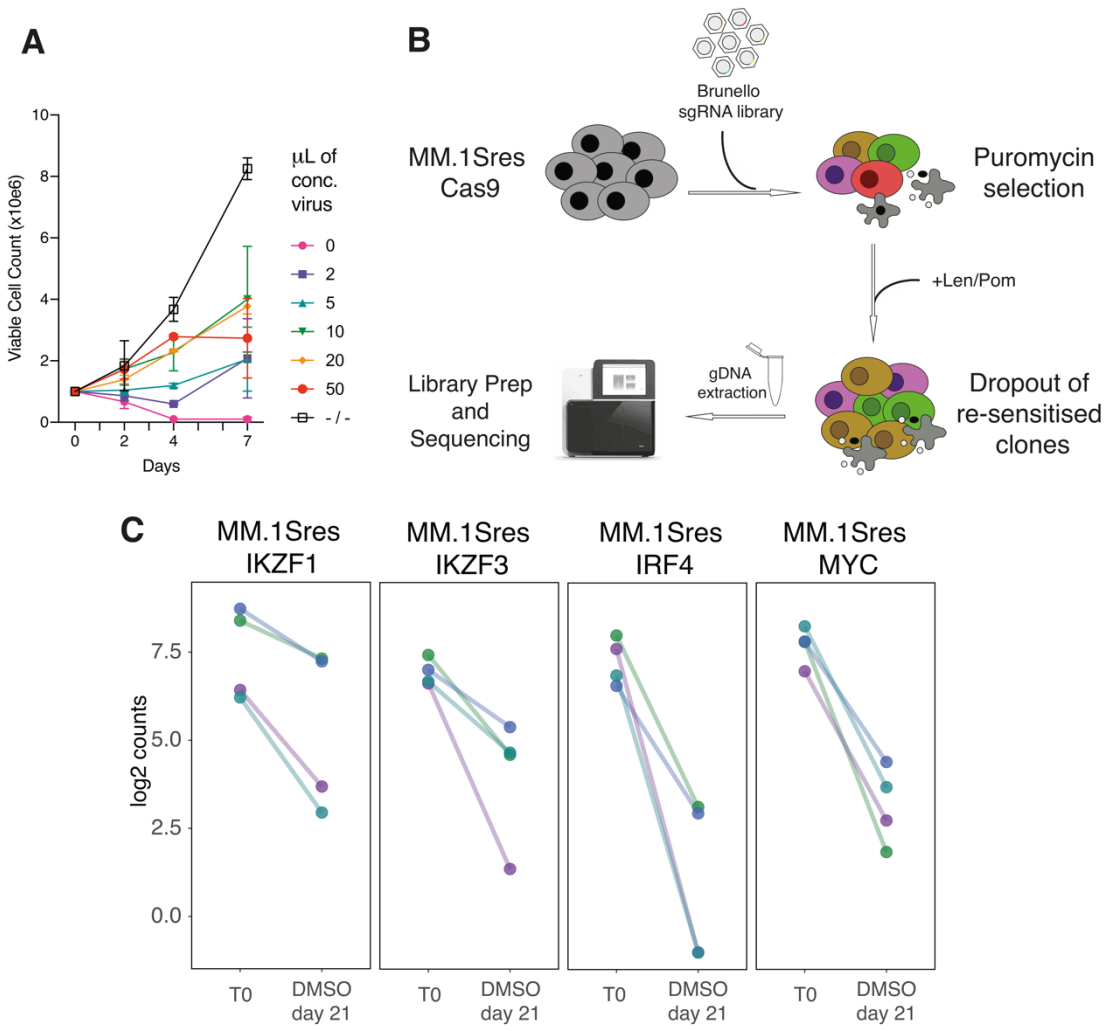


Figure 3.18 CRISPR dropout screening detects sgRNAs capable of restoring IMiD sensitivity

(A) Viral library titration assay evaluating number of viable cells growing in puromycin containing media following transfection with different concentrations of the Brunello genome-wide library in MM.1Sres-Cas9 cells. In the legend, " -/-" is the no-puromycin/no-virus control. (B) Summary of the workflow for a genome-wide CRISPR loss-of-representation screen. (C) Line plot showing log2 fold change of read counts of *IKZF1*, *IKZF3*, *IRF4* and *MYC* sgRNAs in DMSO treated cells at the end of the screen relative to the T-0 reference.

3.2.4.4 Validation of the IMiD-resistant phenotype induced by loss of *NCOR1*

The effect of CRBN and COP9 signalosome deletion in the context of IMiD treatment had already been widely explored in the works of Sievers and Liu[239,240]. Therefore, these genes were not further investigated. Instead, the role of *NCOR1* as a gene important for the response of MM cells to IMiDs was validated using an orthogonal method. Competitive proliferation assays were conducted to verify whether deletion of *NCOR1* would produce a resistant phenotype when cultured in presence of LEN and possibly induce cross-resistance when cells deleted of NCOR1 were cultured in presence of POM (Figure 3.17A). Two independent cell lines with *NCOR1* deletion, MM.1S-Cas9 sgNCOR1(1) and MM.1S-Cas9 sgNCOR1(2), were employed for validation of NCOR1 as a gene important for the response to IMiDs. To confirm *NCOR1* deletion by CRISPR based gene editing, NCOR1 protein expression was analysed by Western blot (Figure 3.17B). A loss of NCOR1 was evident when compared to control MM.1S-Cas9 cell lines expressing non targeting sgRNAs (SCR BFP and SCR GFP). To determine whether these lines would validate the result of the CRISPR screen, MM.1S-Cas9 sgNCOR1(1) and MM.1S-Cas9 sgNCOR1(2) cells expressing a GFP reporter were cultured in DMSO, 2mM LEN, or 500nM POM for 10 days in competition with cells expressing a non-targeting sgRNA (scrambled) and a BFP reporter (MM.1S-Cas9 SCR BFP) at a 1:1 ratio. In parallel, MM.1S-Cas9 SCR GFP cells in competition with MM.1S-Cas9 SCR BFP cells were cultured together with DMSO, 2μM LEN, or 500nM POM at the same time as a control for the assay. Over 10 days, *NCOR1* deleted cells (expressing GFP) outgrew the BFP cells in cell culture media containing either LEN and POM, but not DMSO. In contrast, the BFP/GFP ratio was maintained in the control assay in all treatments, demonstrating that deletion of *NCOR1* produces an IMiD-resistant phenotype (Figure 3.17C).

Collectively, these results provide evidence that IMiD resistance can occur upon the loss of several genes, either implicated in protein ubiquitination and degradation, such as *CRBN*, subunits of the COP9 signalosome, *CAND1* and *UBE2G1*, or in other processes, such as transcriptional regulation (*NCOR1*) or RNA processing (*EDC4*).

3.2.5 Genome-wide CRISPR dropout screening defines genes limiting the response to IMiDs

To define potential mechanisms of resensitisation to IMiDs in MM.1Sres cells, a genome-wide CRISPR dropout screen was performed. A viral titration similar to that for MM.1S Cas9 was performed to assess the optimal amount of concentrated virus in order to maintain a MOI between 0.2 and 0.4. The 5μL condition was chosen to be scaled up to proportionally infect the number of cells required for the screen (Figure 3.18A). 500 million cells were transduced with

the Brunello genome-wide library and selected for 7 days in puromycin and 25% of the cells were harvested as T-0 timepoint (initial library representation). The remaining cells were cultured with either DMSO, 2μM LEN or 500nM POM for 21 days. A shorter timepoint (8 weeks for MM.1S vs 3 weeks for MM.1Sres) was chosen with the purpose of identifying sgRNAs inducing early IMiD resensitisation. At the end timepoint, cells were harvested and genomic DNA extracted. Following DNA extraction, the sgRNA library was prepared and submitted for sequencing (Figure 3.18B).

3.2.5.1 MM.1Sres cells are sensitive to deletion of *IKZF1/3, IRF4* and *MYC* despite prolonged treatment with IMiDs

Simil

ar to MM.1S-Cas9 cells, read count of *IKZF1/3, MYC* and *IRF4* specific sgRNAs at the end of the screen in DMSO-treated MM.1Sres-Cas9 cells was compared to that of MM.1Sres-Cas9 cells at the T-0 timepoint. This approach was aimed to assess whether prolonged treatment with LEN resulted in resistance to the deletion of *IKZF1/3, MYC* and *IRF4*, which are important genes for the response to IMiDs. As for MM.1S-Cas9 cells, loss-of-representation of 4/4 sgRNAs was the primary criteria for defining a genetic dependency. For these genes, 4/4 sgRNAs specific for each of *IKZF1/3, MYC* and *IRF4* genes were less represented at the end of the screen, as compared to the T-0 timepoint (Figure 3.18C). This result indicates that MM.1Sres cells, despite having acquired resistance to LEN, are still sensitive to the deletion of these important genes.

3.2.5.2 The sensitivity of MM.1S cells to gene loss does not markedly change following continuous LEN treatment and acquired LEN-resistance

Loss-of-representation of sgRNAs in DMSO-treated MM.1S-Cas9 and MM.1Sres-Cas9 was performed with the aim of understanding whether prolonged treatment with IMiD would induce changes in the sensitivity to gene loss in MM.1Sres cells relative to MM.1S cells. This approach could potentially identify genes and/or pathways that correlate with a status of IMiD-sensitivity or IMiD-resistance. If MM.1Sres cells have acquired resistance or sensitivity to the loss of certain genes or pathways following prolonged treatment with IMiDs, it could be hypothesised that the modulation of these genes or pathways might contribute to sustain a status of IMiD-resistance and might represent acquired vulnerabilities. This specific information was obtained by comparing representation of sgRNAs at the end timepoint of the screen (T-end, ~8 weeks for MM.1S, 21 days for MM.1Sres) with that at timepoint 0 (T-0), i.e. post-selection with puromycin

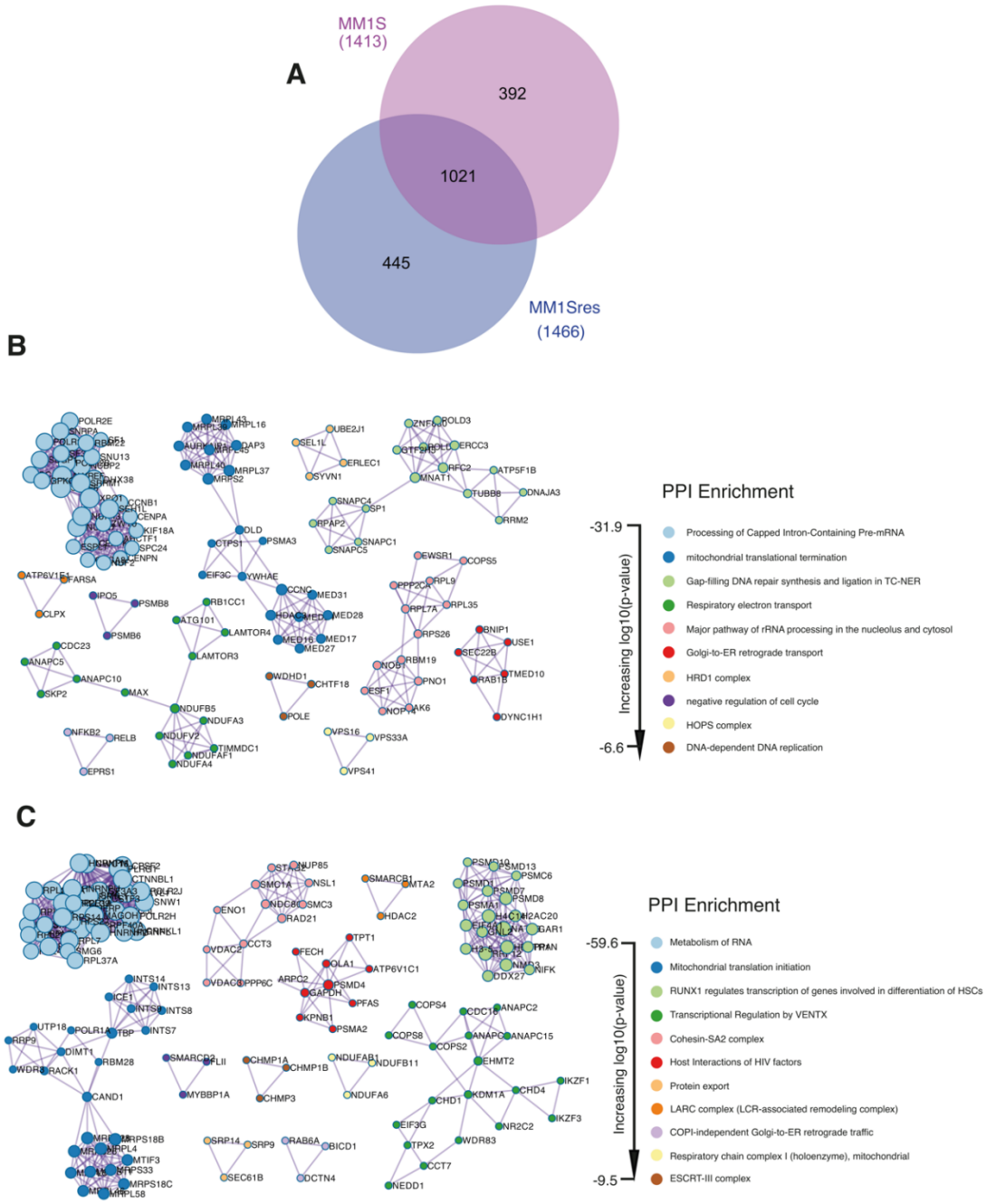


Figure 3.19 Protein-Protein interaction network of unique MM.1S and MM.1Sres dependencies

(A) Venn diagram demonstrating partial overlap between MM.1S and MM.1Sres cells dependencies. (B) and (C) Protein-protein interaction network of unique dependencies of MM.1S and MM.1Sres cells, respectively. The legend represents the colour code for different interaction clusters with their relative level of significance.

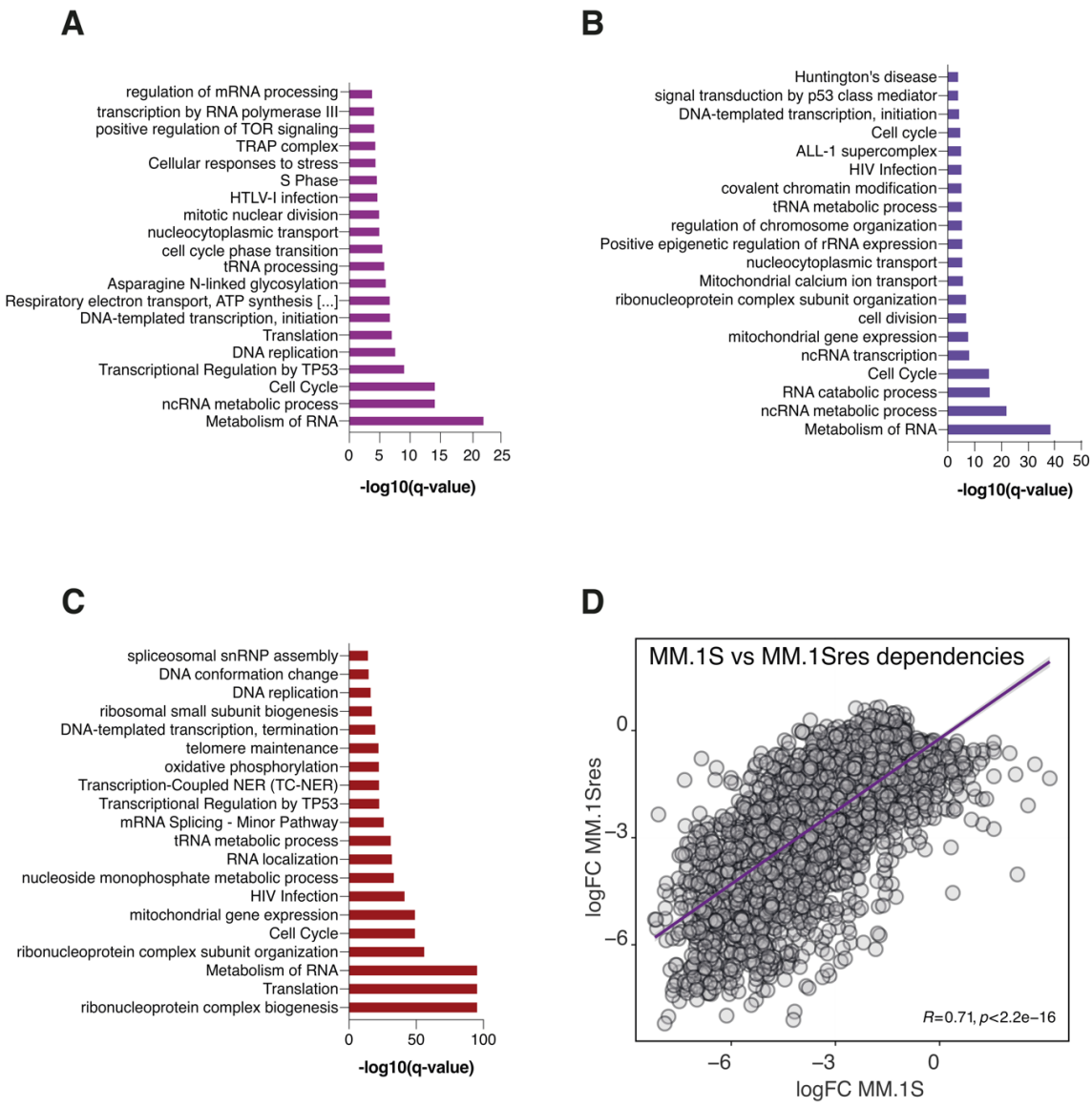


Figure 3.20 Gene Ontology terms of unique and mutual MM.1S and MM.1Sres dependencies

(A), (B) and (C) Gene Ontology analysis of unique MM.1S cells dependencies, unique MM.1Sres cells dependencies and mutual MM.1S/MM.1Sres cells dependencies. (D) Pearson's correlation between MM.1S and MM.1Sres cells dependencies. R = Pearson correlation coefficient, p=level of significance.

and pre-treatment. For each of the screens, guides with a false discovery ratio (FDR) < 0.05 and with a negative log2 fold change were selected. Loss of 1413 and 1466 different genes caused depletion of MM.1S-Cas9 and MM.1Sres cells, respectively. Loss of 392 different genes caused depletion exclusively of MM.1S-Cas9 cells and loss of 445 different genes caused depletion exclusively of MM.1Sres-Cas9 cells. The number of genes whose loss caused depletion of both MM.1S-Cas9 and MM.1Sres-Cas9 cells was 1021 (Figure 3.19A). Protein-protein interaction (PPI) networking and gene ontology (GO) analysis of these 1021 genes demonstrated that MM.1S and MM.1Sres cells are mostly sensitive to genes implicated in RNA processing and protein translation (Figure 3.19B-C). This analyses also highlighted specific pathways to which MM.1S and MM.1Sres cells are uniquely dependent. For instance, MM.1S cells appeared dependent on DNA repair, whilst MM.1Sres seemed to rely, amongst the other pathways, on the activity of genes related to transcriptional regulation (RUNX1 program, VENTX program, cohesin-SA2 activity) (Figure 3.19B-C). GO analyses also showed similarities between genes uniquely essential for MM.1S and MM.1Sres cells, with enrichment in GO terms for RNA metabolism, transcriptional regulation, cell cycle progression and translation (Figure 3.20A-B). GO analysis of genes to which MM.1S and MM.1Sres cells are mutually dependent suggests that MM.1S and MM.1Sres cells are extremely sensitive to the loss of genes involved in ribosome biogenesis (Figure 3.20C). These studies provided evidence that RNA processing and protein translation are fundamental for the survival of both MM.1S and MM.1Sres cells.

The approach outlined above is only qualitative and did not take into account the extent of sgRNA depletion. Therefore, it was assessed whether there was a correlation between genes whose loss is disadvantageous for MM.1S cells and those whose loss is disadvantageous for MM.1Sres cells. Pearson's correlation test was performed between the log2(fold change) of these genes in MM.1S-Cas9 cells and MM.1Sres-Cas9 cells. This statistical test therefore included quantitative information with regards to sgRNA depletion. Pearson's correlation coefficient was 0.71, with a p-value < 2.2^{-16}. This data indicated a substantial degree of correlation between the dependencies of MM.1S and MM.1Sres cells (Figure 3.22D).

Taken together, these data suggest that MM.1S and MM.1Sres cells are dependent on essential processes such as RNA processing and protein translation. Most of the genes, when deleted, are detrimental for both MM.1S and MM.1Sres cells. Finally, Pearson's correlation test indicated that prolonged treatment with LEN did not markedly change the landscape of genetic vulnerabilities of MM.1S cells.

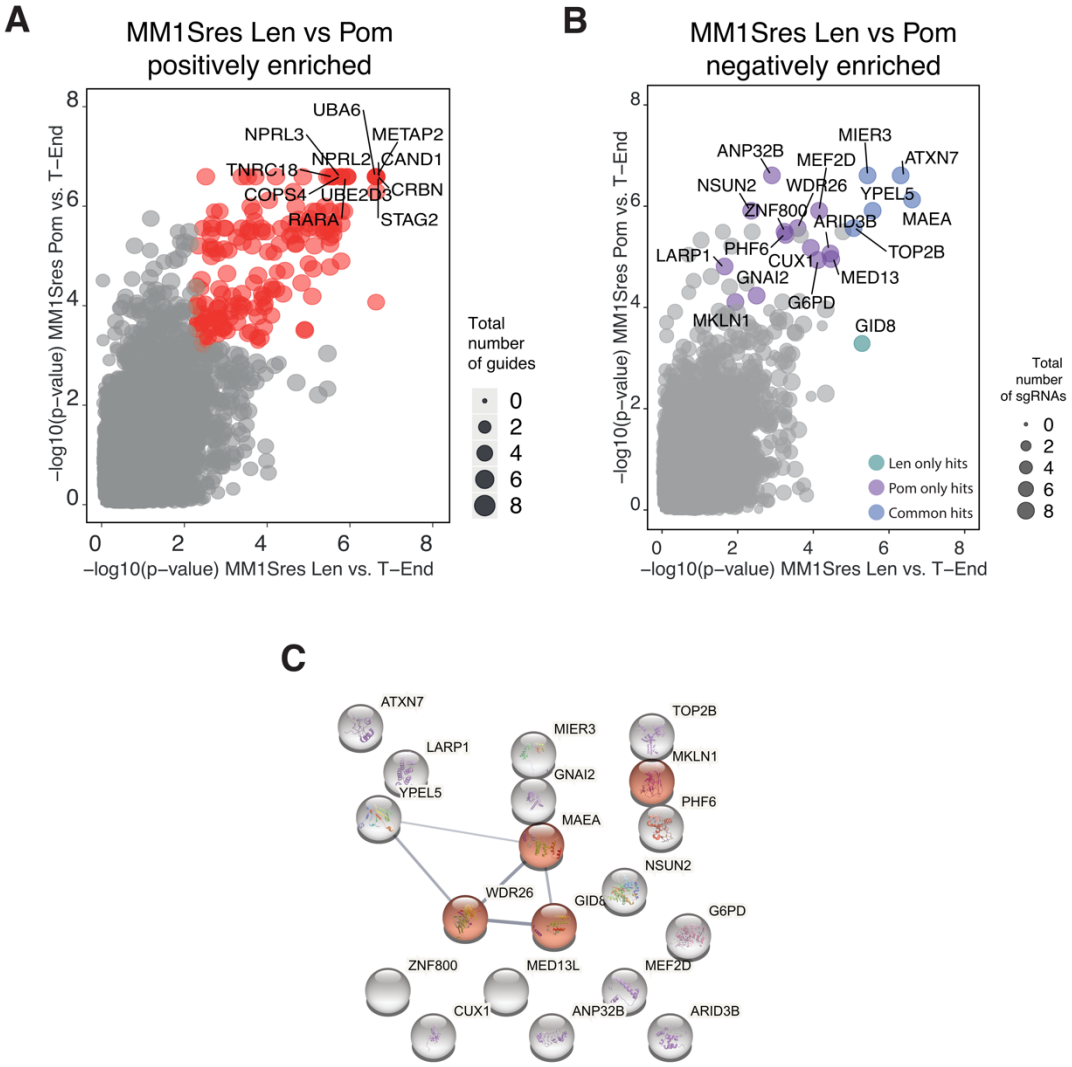


Figure 3.21 Detection of sgRNA causing additional IMiD-resistance or resensitisation to IMiDs

(A) Scatterplot displaying sgRNAs enriching in MM.1Sres-Cas9 cells after 3 weeks (T-end) of selection with LEN and or POM, as compared to the vehicle control (DMSO at T-end). (B) Scatterplot displaying sgRNAs lost in MM.1Sres-Cas9 cells after 3 weeks (T-end) of treatment with LEN (LEN vs T-end) and or POM (POM vs T-end), as compared to the vehicle control (DMSO vs T-0). (C) PPI networking of significantly depleted sgRNAs highlighted in panel (B).

3.2.5.3 Defining factors of additional resistance to IMiDs

To verify whether MM.1Sres cells could potentially develop further resistance to IMiDs, gain-of-representation of sgRNAs in MM.1Sres-Cas9 cells, treated with LEN and POM (at the end of the screen), was assessed relatively to DMSO-treated MM.1Sres-Cas9 cells (at the end of the screen). Deletion of *CRBN*, *CAND1* and *COPS4* (enriched also in the MM.1S resistance screen), and other genes such as *METAP2*, *UBA6*, *UBE2D3* and *STAG2*, conferred additional resistance to IMiDs in MM.1Sres cells (Figure 3.21A). This result suggests that despite already having an IMiD-resistant phenotype, MM.1Sres cells can still gain a proliferative advantage in the presence of IMiDs following deletion of key genes for protein degradation.

3.2.5.4 Defining IMiD-resensitisation factors in MM.1Sres cells

To identify IMiD resensitisation factors, only sgRNAs depleted in MM.1Sres-Cas9 treated cells with either LEN or POM, but not DMSO, were chosen. SgRNAs depleted at the end timepoint in the IMiD treatment conditions were compared to the DMSO-treated controls at the same timepoint. Importantly, sgRNAs depleted at the end timepoint in DMSO-treated cells relative to the timepoint zero were not considered, as these would score as genes that are essential for cell growth and viability.

3.2.5.4.1. Genes and pathways limiting IMiD activity

Several genes were identified as IMiD resensitisation factors when deleted in MM.1Sres cells (Figure 3.21B) and some sgRNAs scored with both LEN and POM, such as *ATXN7*, *TOP2B*, *MED13L*, *MIER3*, *YPEL5* and *MAEA*. SgRNAs specific for *MKLN1, WDR26* and *GID8* were also significantly depleted in POM- and LEN-treated cells, respectively, at the end of the screen. Other sgRNAs were depleted solely in the presence of POM: *ANP32B, GNAI2*, *ARID3B, MEF2D, PHF6, ZNF800, CUX1*, *LARP1*, *NSUN2* and *G6PD*. To characterise possible functional and/or physical interaction between the genes identified in this screen, PPI analysis was employed. SgRNAs depleted in IMiD-only conditions at the end of the screen revealed that YPEL5, MAEA, WDR26 and GID8 are members of an E3 ubiquitin ligase (CTLH complex) that promotes degradation of enzymes required for gluconeogenesis in presence of adequate intracellular glucose levels[257]. G6PD is also implicated in glucose metabolism. Finally, the CTLH complex also promotes degradation of MKLN1, a protein implicated in cell motility (Figure 3.21C)[258].

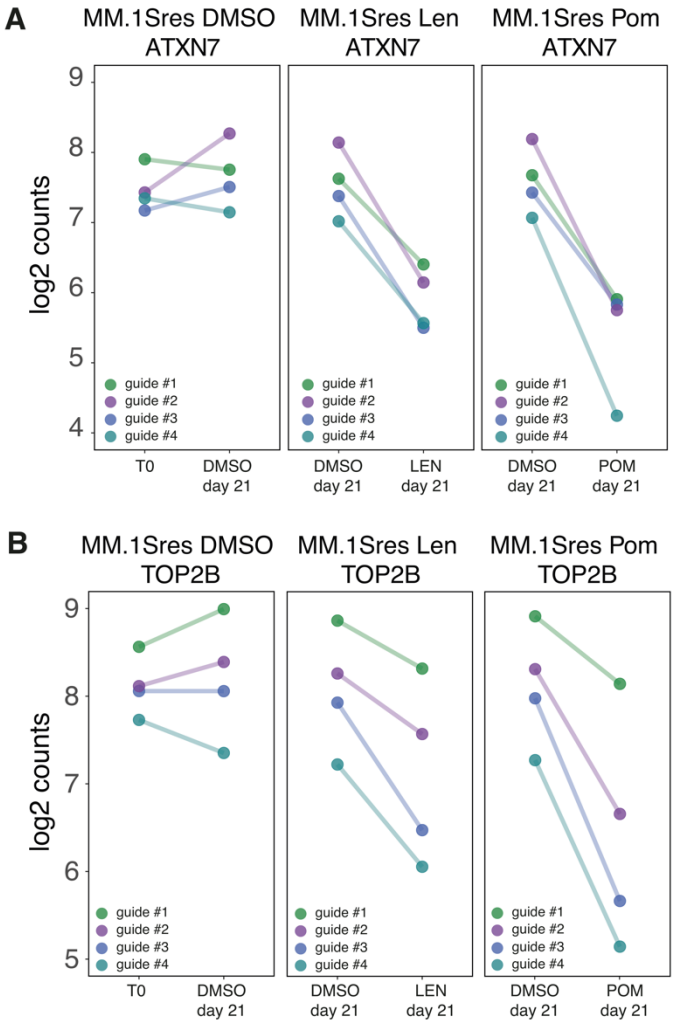
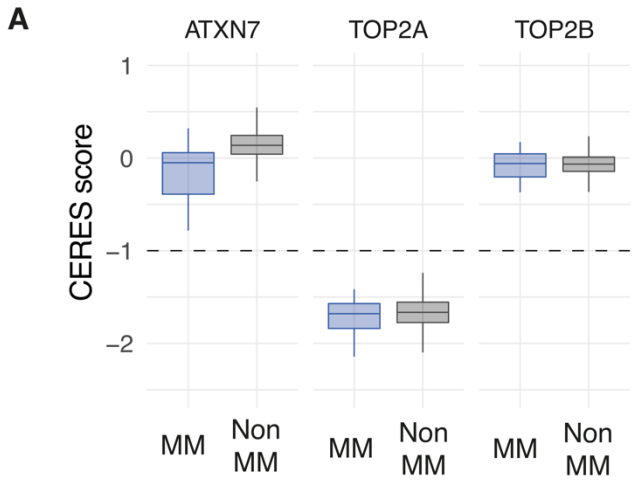


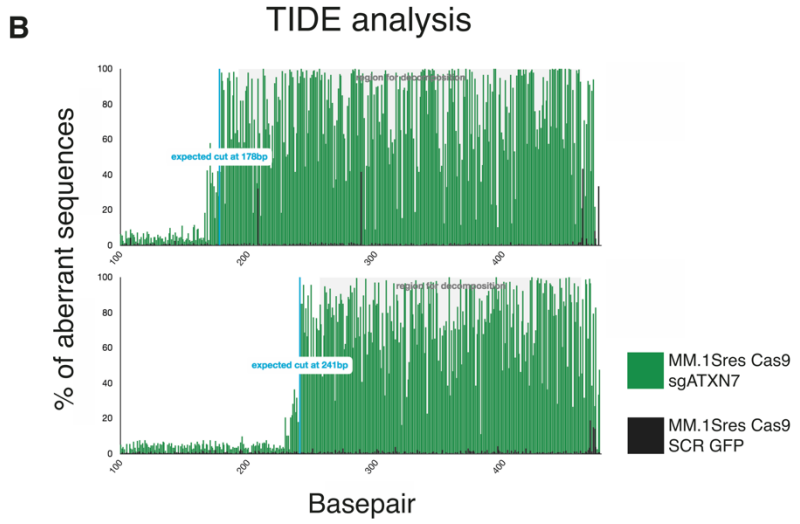
Figure 3.22 Loss of genes TOP2B and ATXN7 resensitises MM.1Sres cells to IMiDs

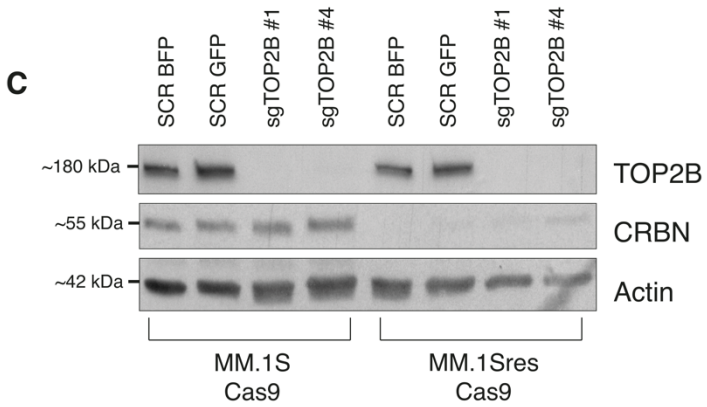
(A) Line plot showing LogFC of read counts of *ATXN7* targeting sgRNAs in MM.1Sres-Cas9 cells treated with LEN and POM relative to the DMSO condition, at the end of the screen. The dropout in DMSO-treated cells was assessed by the log2 fold change between sgRNAs in DMSO at T-end (3 weeks) and at the T-0 timepoint. (B) Line plot showing LogFC of read counts of *TOP2B* targeting sgRNAs in MM.1Sres-Cas9 cells treated with LEN and POM relative to the DMSO condition, at the end of the screen. The dropout in DMSO-treated cells was assessed by the log2 fold change between sgRNAs in DMSO at T-end (3 weeks) and at the T-0 timepoint.

Figure 3.23 Validation of ATXN7 and TOP2B deletion. Loss of TOP2B does not affect CRBN expression

(A) CERES score (dependency score) of *ATXN7*, *TOP2A* and *TOP2B* in MM cell lines and Non-MM cell lines. A value of 0 represents a non-dependency on the gene, a value below -1 represents a dependency on the gene. (B) TIDE analysis for the validation of MM.1Sres-Cas9 *ATXN7* KO cells. The histogram represents the reading frame of the region targeted by sgATXN7 #1 and #4 as compared to the same region in scrambled GFP cells. (C) Immunoblot displaying expression of *TOP2B* and *CRBN* in MM.1Sres-Cas9 scrambled BFP and GFP cells as compared to MM.1Sres-Cas9 *TOP2B* KO cells. Actin was employed as loading control.


A
ATXN7
TOP2A
TOP2B
CERES score
1
0
−1
−2
MM
Non MM
MM
Non MM
MM
Non MM


B
TIDE analysis
% of aberrant sequences
expected cut at 178bp
expected cut at 241bp
Basepair
MM.1Sres Cas9 sgATXN7
MM.1Sres Cas9 SCR GFP


C
SCR BFP
SCR GFP
sgTOP2B #1
sgTOP2B #4
SCR BFP
SCR GFP
sgTOP2B #1
sgTOP2B #4
~180 kDa
~55 kDa
~42 kDa
TOP2B
CRBN
Actin
MM.1S Cas9
MM.1Sres Cas9

3.2.5.4.2. Interference with DNA homeostasis as possible mechanism of resensitisation to IMiDs

ATXN7 is a subunit of the deubiquitination module of the STAGA complex, a multisubunit entity that is involved in transcriptional regulation and DNA repair[259,260]. *TOP2B* is a gene encoding DNA topoisomerase II β, an enzyme capable of relaxing the DNA double helix in presence of topological constraints. In order to release torsional stress, TOP2B produces a double strand breaks, allows unwinding of DNA and it subsequently repairs the gap. This protein is particularly important in processes such as replication, transcription and DNA repair, together with its paralog TOP2A[261–264]. However, whereas TOP2B is not essential for cells, expression of its paralog TOP2A is required for cell viability (see below, paragraph 3.2.5.5). Since CUL4, DDB1 and RBX1, together with the COP9 signalosome, have a role in genomic stability (i.e. DNA repair), sgRNA specific for genes that also promote DNA homeostasis, *ATXN7* and *TOP2B*, were chosen for further data validation.

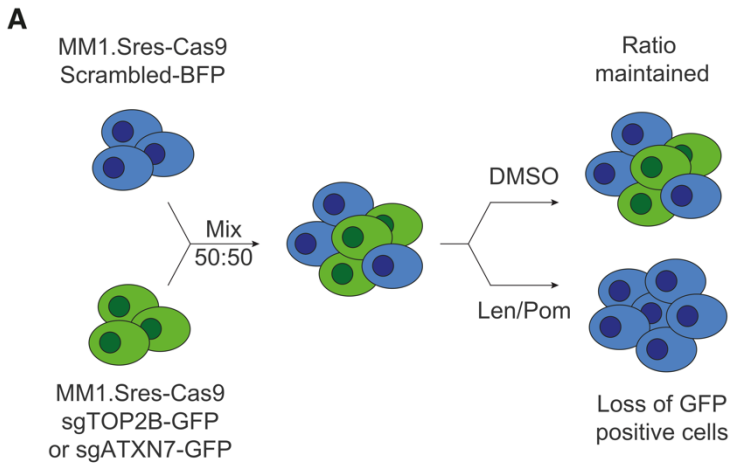
These observations provide with proof of concept that IMiD sensitivity can be restored via loss of genes and molecular pathways that are different to that of the *IKZF1/3-IRF4-MYC* transcriptional axis. SgRNAs causing resensitisation to IMiDs in MM.1Sres cells were specific for genes that are known to regulate DNA repair (*ATXN7*, *TOP2B*)[260,262,263], gene transcription (*ATXN7, TOP2B, MIER3, MED13L*, *ARID3B, MEF2D, PHF6, ZNF800, CUX1*)[259,261,264–271], cell cycle progression (*ANP32B*, *GNAI2*)[272,273], RNA processing (*NSUN2*, *LARP1*)[274,275], glucose metabolism (*YPEL5, MAEA, WDR26, GID8* and *G6PD*)[257,276] and cell motility (*MKLN1*)[258]. Taken together, these results indicate that several distinct biological pathways are capable of limiting IMiD activity in MM.1Sres cells and that modulation of these biological processes can potentiate the response to IMiD in MM.1Sres cells.

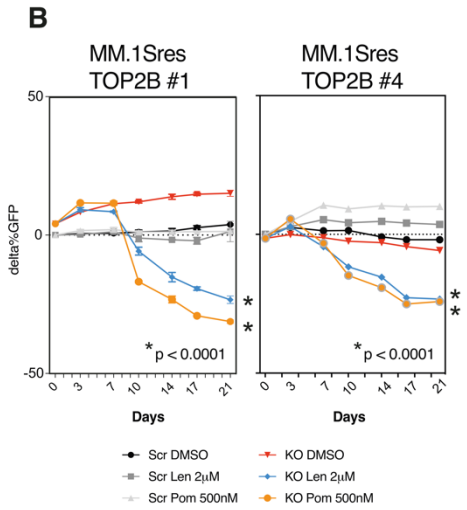
3.2.5.5 Loss of TOP2B and ATXN7 results in synthetic lethality with IMiDs in MM.1Sres cells

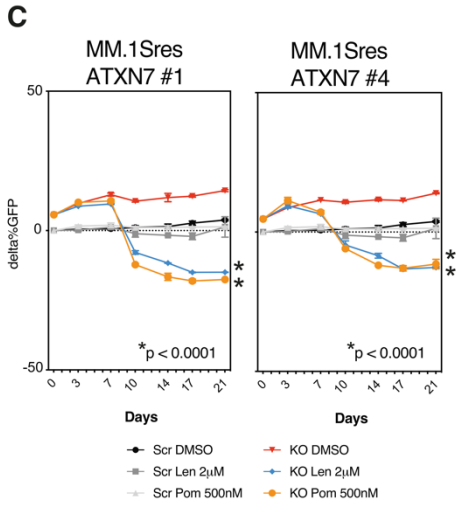
As shown in the single guide plots, deletion of *ATXN7* and *TOP2B* did not impair cell growth in MM.1Sres, because the read count of each sgRNA at the end of the screen in DMSO-treated cells is not significantly lower than that at the timepoint zero (Figure 3.22A-B). This result is supported by data extracted from the DepMap repository (https://depmap.org/portal/), where dependency of cell lines to the expression of specific genes is measured by the CERES score[277]. This score standardises the magnitude of gene dependency between all the cell lines characterised in the DepMap repository by taking into account the average sgRNA efficiency, the copy number effect and the gene knockout effect within each cell line. The CERES

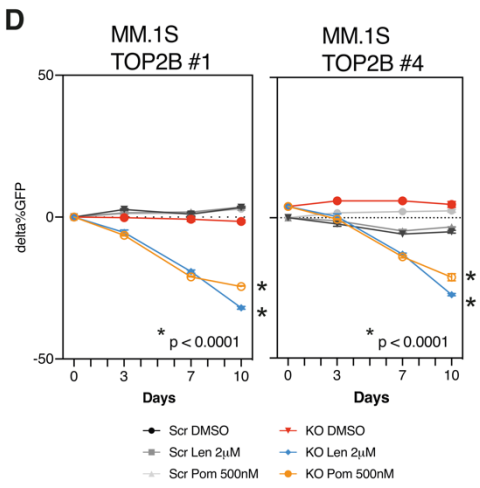
Figure 3.24 Competitive proliferation assays validates loss of TOP2B and ATXN7 as IMiDs re-sensitisation factors in MM.1S cell lines

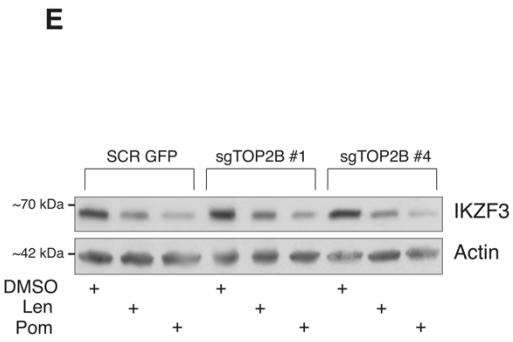
(A) Schematic representation of competition assays workflow for validation of dropout screens. (B) Graphs representing one of three independent competitive proliferation assays showing change in the fraction of GFP cells growing in competition with scramble BFP cells, treated with DMSO, 2μM LEN or 500nM POM, in MM.1Sres-Cas9 *ATXN7* KO cells. (C) Graphs representing one of three independent competitive proliferation assays showing change in the fraction of GFP cells growing in competition with scramble BFP cells, treated with DMSO, 2μM LEN or 500nM POM, in MM.1Sres-Cas9 TOP2B KO cells. (D) Graphs representing one of three independent competitive proliferation assays showing change in the fraction of GFP cells growing in competition with scramble BFP cells, treated with DMSO, 2μM LEN or 500nM POM, in MM.1S-Cas9 *TOP2B* KO cells. In (B), (C), (D), statistical significance (p) was calculated using two-way ANOVA testing and adjusted with Benjamini and Hochberg correction. (E) Immunoblot showing IKZF3 degradation in scrambled GFP cells and MM.1Sres-Cas9 *TOP2B* KO cells following 16 hours of DMSO, 2μM LEN or 500nM POM. Actin was used as loading control.


A
MM1.Sres-Cas9
Scrambled-BFP
Mix
50:50
MM1.Sres-Cas9
sgTOP2B-GFP
or sgATXN7-GFP
DMSO
Len/Pom
Ratio
maintained
Loss of GFP
positive cells


B
MM.1Sres
TOP2B #1
MM.1Sres
TOP2B #4
delta%GFP
Days
*p < 0.0001
Scr DMSO
Scr Len 2μM
Scr Pom 500nM
KO DMSO
KO Len 2μM
KO Pom 500nM


C
MM.1Sres
ATXN7 #1
MM.1Sres
ATXN7 #4
delta%GFP
Days
*p < 0.0001
Scr DMSO
Scr Len 2μM
Scr Pom 500nM
KO DMSO
KO Len 2μM
KO Pom 500nM


D
MM.1S
TOP2B #1
MM.1S
TOP2B #4
delta%GFP
Days
*p < 0.0001
Scr DMSO
Scr Len 2μM
Scr Pom 500nM
KO DMSO
KO Len 2μM
KO Pom 500nM


E
SCR GFP
sgTOP2B #1
sgTOP2B #4
~70 kDa
~42 kDa
IKZF3
Actin
DMSO
Len
Pom

dependency score for both MM and non-MM tumours demonstrated that all cancers are strongly dependent on *TOP2A* (CERES < -1). Conversely, *TOP2B* and *ATXN7* do not score as essential genes (CERES > -1) (Figure 3.23A).

3.2.5.5.1 Validation of *TOP2B* and *ATXN7* deletion

To selectively delete *TOP2B* and *ATXN7* in MM.1Sres cells, MM.1Sres cells expressing Cas9 were individually transduced with two different sgRNAs specific for *TOP2B* and two sgRNAs specific for *ATXN7*. Tracking of Indel Decomposition (TIDE)[278] was employed for detection of insertions/deletions at the locus of *ATXN7*. The *ATXN7* locus in MM.1Sres-Cas9 SCR GFP, sgATXN7#1 and sgATXN7#4 cells was obtained via PCR amplification and Sanger-sequenced. Alignment between the ATXN7 locus sequence of MM.1Sres-Cas9 SCR GFP cells and that of the MM.1Sres-Cas9 sgATXN7#1 and sgATXN7#4 cells displayed a high percentage of aberrant sequences downstream the region of expected sgRNA cut in MM.1Sres-Cas9 sgATXN7#1 and sgATXN7#4 cells, demonstrating a successful cut and editing of the ATXN7 locus (Figure 3.23B). TOP2B immunoblotting of whole cell lysates from MM.1Sres-Cas9 *TOP2B* KO cells was employed for *TOP2B* KO validation (Figure 3.23C). Expression of TOP2B in MM.1Sres-Cas9 cells expressing a non-targeting sgRNA (SCR BFP or SCR GFP) were compared to those of MM.1Sres-Cas9 sgTOP2B#1 and MM.1Sres-Cas9 sgTOP2B#4 cells. Both MM.1Sres-Cas9 sgTOP2B#1 and MM.1Sres-Cas9 sgTOP2B#4 cells displayed a virtually complete loss of TOP2B protein as compared to the MM.1Sres-Cas9 SCR BFP and GFP cells.

3.2.5.5.2 Validation of *ATXN7*- and *TOP2B*-mediated resensitisation of MM.1Sres cells to IMiD treatment

To validate that the loss of *ATXN7* and *TOP2B* resensitises MM.1Sres cells to IMiDs, competitive proliferation assays with two independent guides each specific for *ATXN7* and *TOP2B* were conducted. MM.1Sres-Cas9 cells independently expressing two sgRNAs specific for *ATXN7* or *TOP2B* with a GFP reporter were grown in competition with MM.1Sres-Cas9 cells expressing a non-targeting sgRNA with a BFP reporter at a 1:1 ratio. As a control, MM.1Sres-Cas9 cells expressing a non-targeting sgRNA and BFP were grown in competition with MM.1Sres-Cas9 cells expressing a non-targeting sgRNA and GFP at the same ratio. Both assays were conducted for 21 days treating cells with either DMSO, 2μM LEN or 500nM POM (Figure 3.24A). In this case, a reduction of the GFP to BFP cells ratio would validate the result of the screen. Treatment with IMiDs caused loss of GFP cells in the context of MM.1Sres-Cas9 cells with *ATXN7* or *TOP2B* KO. Conversely, in the control samples the ratio between GFP and BFP positive cells did not

significantly change (Figure 3.24B-C). The effect of *TOP2B* loss on IMiD sensitivity was tested in MM.1S cells, to determine whether loss of TOP2B would increase sensitivity to IMiD (Figure 3.24D). MM.1S-Cas9 cells independently expressing two sgRNAs specific for *TOP2B* with a GFP reporter were grown in competition with MM.1S-Cas9 expressing a non-targeting sgRNA with a BFP reporter at a 1:1 ratio. Again, MM.1Sres-Cas9 cells expressing a non-targeting sgRNA and BFP grown in competition with MM.1Sres-Cas9 cells expressing a non-targeting sgRNA and GFP at the same ratio were employed as control. Both cell populations were treated with either DMSO, 2μM LEN and 500nM POM for 10 days. Following *TOP2B* deletion, depletion of GFP cells with increase in representation of BFP positive cells was observed in IMiD-treated cells, whereas the DMSO-treated control population maintained the BFP/GFP ratio of day zero.

3.2.5.5.3 *TOP2B* loss resensitises MM.1Sres cells to IMiDs via a CRBN-independent mechanism

To verify whether the loss of TOP2B altered CRBN protein levels with subsequent restoration of neosubstrate degradation, CRBN levels were studied by immunoblotting in MM.1S-Cas9 SCR GFP, SCR BFP, sgTOP2B#1, sgTOP2B#4 cells and in MM.1Sres-Cas9 SCR GFP, SCR BFP, sgTOP2B#1, sgTOP2B#4 cells. IKZF3 levels in MM.1Sres-Cas9 SCR GFP sgTOP2B#1, sgTOP2B#4 cells treated with DMSO, 2μM LEN and 500nM POM for 16 hours were also assessed. In MM.1Sres-Cas9 sgTOP2B cells, CRBN expression was not markedly augmented as compared to the SCR control. (Figure 3.23C). To further confirm this result, IKZF3 levels were also assessed via immunoblot in MM.1Sres-Cas9 SCR GFP sgTOP2B#1, sgTOP2B#4 cells treated with DMSO, 2μM LEN and 500nM POM for 16 hours to explore whether deletion of TOP2B would modulate neosubstrates expression via a CRBN independent mechanism (Figure 3.24E). Deletion of *TOP2B* in MM.1Sres cells did not augment degradation of neosubstrates in presence of an IMiD when compared to cells expressing a non-targeting guide.

This data validates that loss of *TOP2B* or *ATXN7* potentiates IMiD activity, that loss of *TOP2B* also synergises with IMiDs in MM.1S cells and that this mechanism is probably not the consequence of increased CRBN expression or neosubstrate degradation. Most importantly, these observations indicate that potentiation of IMiD-mediated anti-MM properties via loss of *TOP2B* occurs in both IMiD-sensitive and IMiD-resistant contexts.

3.2.6 Resensitisation of MM.1Sres cells to IMiDs is likely independent of DNA damage

As a well-characterised gene and a potential drug target, TOP2B was chosen for further experimental testing with TOP2 small-molecule inhibitors. Whereas ATXN7 is part of a poorly characterised protein complex, TOP2 (A and B) is considered a druggable target, and TOP2

poisons, such as etoposide or doxorubicin, are widely used as chemotherapeutic agents[279]. In presence of topological constraints in the DNA, TOP2B produces a double strand break and covalently binds to DNA (TOP2 cleavage complex, TOP2cc) and subsequently rejoins the two strands. Etoposide (ETO) or doxorubicin are capable of trapping TOP2cc and impeding a successful repair, with consequent DNA damage and induction of cell death via p53 stabilisation[280]. Hence, it is possible that: 1) IMiDs might alter the DNA repairing functions of CUL4, DDB1 and RBX1 via an unknown CRBN-mediated mechanism that does not necessarily involve degradation of neosubstrates; and/or 2) As TOP2B participates in DSB repair, its absence might be sufficient to trigger apoptosis in the context of IMiD-induced perturbations of CUL4-DDB1-RBX1 DNA repair activity.

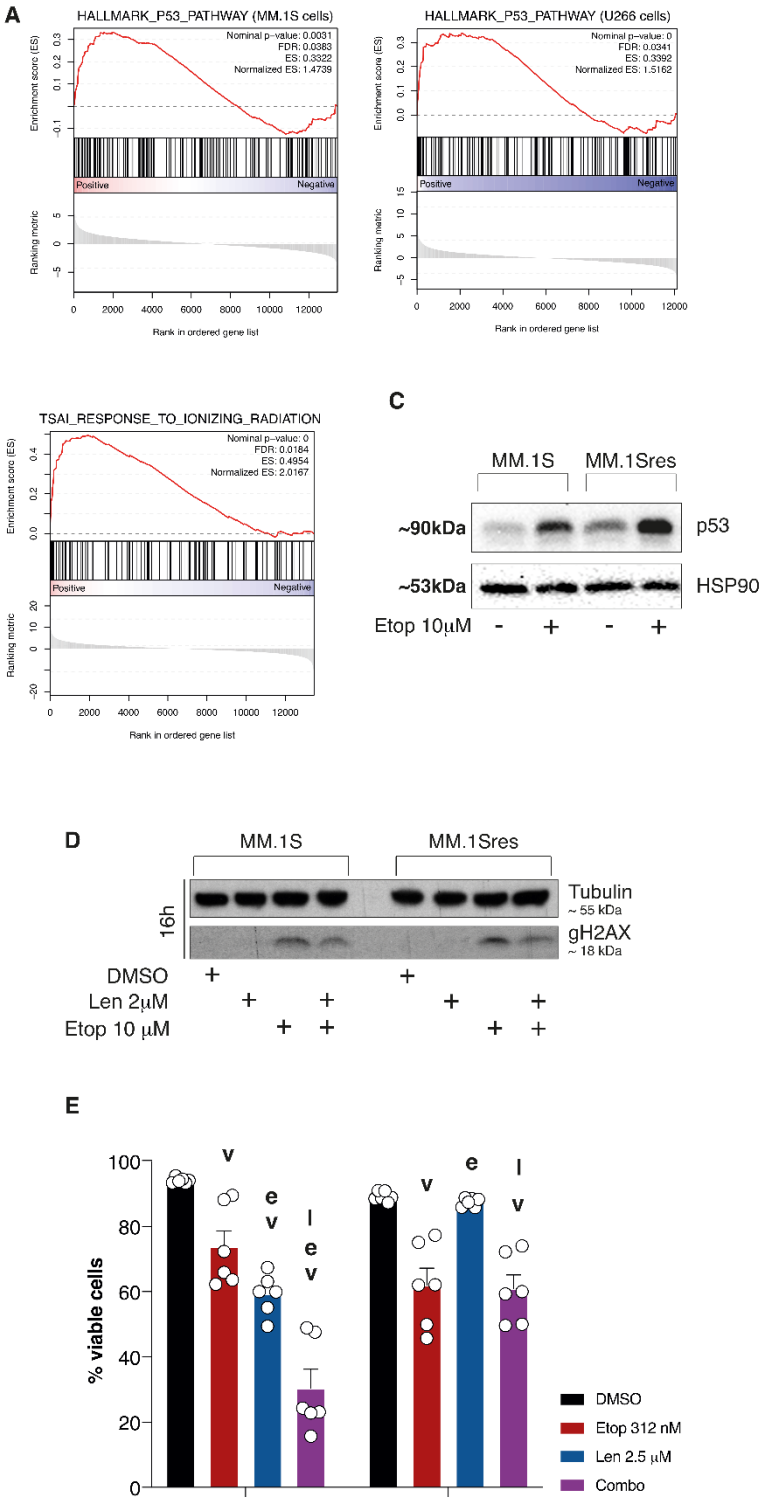
3.2.6.1 Induction of p53 transcriptional signatures by lenalidomide is independent of DNA damage

GSEA of MM.1S cells (*TP53* wild-type) and U266 cells (mutated *TP53*) RNA-seq datasets showed that acute treatment with LEN or POM produces enrichment in p53-dependent signalling (Figure 3.25A). In particular, NES of HALLMARK_P53_PATHWAY gene set in MM.1S cells treated with LEN and POM was 1.47 and 1.66, respectively (in Figure 3.25A, only GSEA plot of MM.1S cells treated with LEN is shown). In U266 cells treated with LEN and POM, NES of the same gene set was 1.52 and 1.52, respectively (only GSEA plot of U266 cells treated with LEN is shown). Moreover, MM.1Sres cells exclusively displayed enrichment in a gene signature specific for response to radiation therapy, with a NES of 2.01 (Figure 3.25B). These observations raised the possibility that, in MM cells with acquired LEN resistance, p53 expression could differ from that of its sensitive counterpart and that MM.1Sres cells might be more sensitive to DNA damage. Thus, MM.1S and MM.1Sres cells were cultured in the presence or absence of 10µM ETO for 16 hours to induce p53 stabilisation. Firstly, immunoblot for p53 showed that MM.1Sres cells have a higher baseline expression of p53. Secondly, the magnitude of p53 stabilisation following ETO treatment was slightly greater in MM.1Sres cells when compared to that of MM.1S cells (Figure 3.25C). This result suggested that treatment with ETO might induce greater DNA damage in MM.1Sres cells relative to MM.1S cells.

To test whether LEN itself could induce DNA damage, MM.1S and MM.1Sres cells were treated with DMSO, LEN, 10µM ETO or in combination for 16 hours (Figure 3.25D). Immunoblotting for phospho-S139-H2AX, a marker for DNA damage[281], displayed no phosphorylation of histone protein H2AX following LEN treatment, as compared to ETO-treated cells, where phosphorylation of H2AX was evident. Furthermore, no increase in phospho-S139-H2AX was

Figure 3.25 IMiD treatment increases p53 and ionizing radiation induced transcriptional response without synergizing with DNA damaging agents

(A) GSEA plots displaying enrichment in p53 response gene set in MM.1S and U266 cells, respectively, following treatment with LEN. (B) GSEA plot showing enrichment in the transcriptional response that follows exposure to radiation therapy in MM.1Sres cells relative to MM.1S cells. (C) Immunoblot demonstrating induction of p53 after exposure to DNA damaging agent etoposide (ETO) for 16 hours in MM.1S and MM.1Sres cells. (D) Immunoblot displaying phosphorylation of H2AX at S139 following exposure to DMSO, 2.5μM LEN, 10μM ETO or combination LEN/ETO for 16 hours (E) Bar plot of percentage of viable (PI negative) MM.1S and MM.1Sres cells treated with DMSO, 312nM ETO, 2.5μM LEN or with LEN/ETO in combination. Error bars represent the mean ± SEM of three independent experiments with two technical replicates each. v= significant vs vehicle (DMSO), l=significant vs LEN, e=significant vs ETO ($p<0.05$ or less).


A
HALLMARK_P53_PATHWAY (MM.1S cells)
Nominal p-value: 0.0031
FDR: 0.0383
ES: 0.3322
Normalized ES: 1.4739
HALLMARK_P53_PATHWAY (U266 cells)
Nominal p-value: 0
FDR: 0.0341
ES: 0.3392
Normalized ES: 1.5162
Enrichment score (ES)
Positive
Negative
Ranking metric
Rank in ordered gene list
B
TSAI_RESPONSE_TO_IONIZING_RADIATION
Nominal p-value: 0
FDR: 0.0184
ES: 0.4954
Normalized ES: 2.0167
C
MM.1S
MM.1Sres
~90kDa
p53
~53kDa
HSP90
Etop 10μM - + - +
D
MM.1S
MM.1Sres
16h
Tubulin
~ 55 kDa
gH2AX
~ 18 kDa
DMSO
Len 2μM
Etop 10 μM
E
% viable cells
MM1S
MM1Sres
DMSO
Etop 312 nM
Len 2.5 μM
Combo

observed in cells treated with LEN and ETO. This result indicates that LEN is not a DNA damaging agent.

3.2.6.2 The activity of lenalidomide in combination with the TOP2 poison etoposide

The effect of combining LEN and ETO was tested to verify whether combinatorial treatment would increase the response to LEN in MM.1S and MM.1Sres cells. Both MM.1S and MM.1Sres cells were treated with either DMSO, single agent 2.5µM LEN or low-dose ETO (312nM), or a combination LEN/ETO for 7 days (Figure 3.25E). An additive rather than synergistic effect of the two drugs was observed in MM.1S cells. In MM.1Sres cells, treatment with ETO did not sensitize these cells to LEN. Moreover, MM.1Sres cells were not differentially sensitive to ETO relative to MM.1S cells.

Collectively, these results suggest that the enrichment in gene sets of p53-dependent transcriptional signatures and transcriptional response to ionizing radiation, together with the increased p53 induction, could be isolated observations or the consequences of other unclear mechanisms. Moreover, LEN did not display activity as DNA damaging agent and MM.1Sres cells did not show
increased sensitivity to ETO alone or in double treatment with LEN. Ultimately, these observations argue against DNA damage as possible mechanism of resensitisation to IMiDs of MM1.Sres cells in the context of TOP2B loss.

3.2.7 The cardioprotective agent dexrazoxane is a TOP2 inhibitor, TOP2B degrader, and exerts anti-MM activity

Treatment with ETO did not result in re-sensitisation of MM.1Sres cells to lenalidomide, but enhanced the effect of lenalidomide in MM.1S cells. Since the induction of DNA damage via ETO treatment was believed to represent a confounding factor, a different pan-TOP2 inhibitor, dexrazoxane (DXZ), was adopted. DXZ is an FDA-approved drug for the prevention of doxorubicin-induced cardiac toxicity, and it is an EDTA derivative with iron-chelating properties. Although the mechanism of cardioprotection is still unclear, it has been hypothesised that DXZ chelates the pool of free iron in the intracellular space, reducing the oxidative stress that follows doxorubicin exposure[254,279,282]. Importantly, it has been demonstrated that treatment with DXZ induces selective degradation of TOP2B (but not TOP2A), with a reduction of DNA damage following co-treatment with ETO[254]. Given this observation, DXZ could be an appropriate

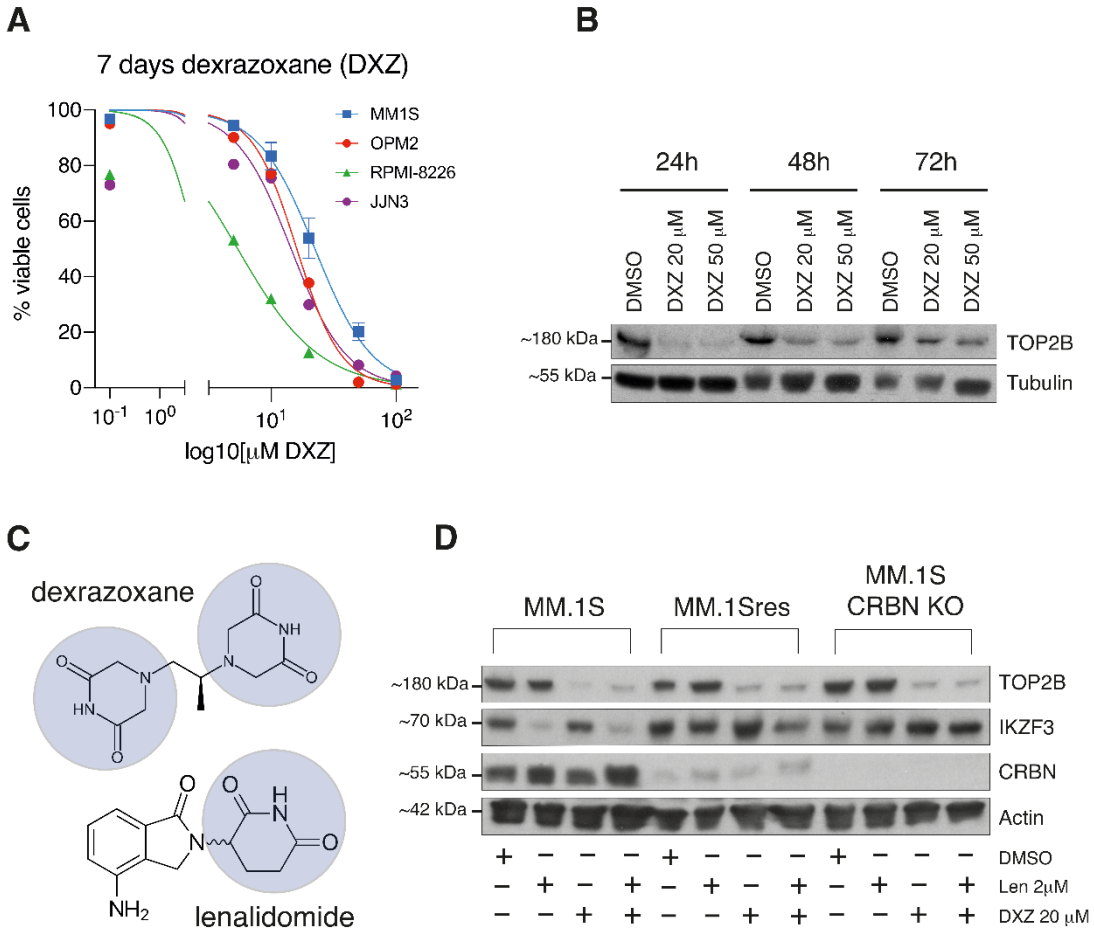


Figure 3.26 Dexrazoxane induces MM cell death and TOP2B degradation by a CRBN-independent mechanism

(A) Dose-response curve of increasing concentrations of DXZ in MM.1S, OPM2, RPMI-8226 and JJN3 cells in function of cell viability. (B) Immunoblot displaying TOP2B expression in MM.1S cells following treatment with DMSO, 20μM or 50μM DXZ for 24, 48 and 72 hours. Tubulin was used as loading control. (C) Structural analogies between DXZ and lenalidomide. (D) Immunoblot for expression of TOP2B, IKZF3, CRBN in MM.1S, MM.1Sres and MM.1S CRBN KO cells treated with DMSO, LEN, DXZ or double treatment LEN-DXZ for 16 hours. Expression of actin was employed as loading control.

chemical probe for inducing acute loss of TOP2B and a possible candidate in combination with IMiDs from a translational perspective.

3.2.7.1 Kinetics of dexrazoxane-induced TOP2B degradation

The IC50 of DXZ was defined and amongst the four MM cell lines tested, two were IMiD-sensitive (MM.1S, OPM2), and two were IMiD-resistant (RPMI-8226 and JJN3)[283]. In these cell lines, DXZ IC50 spanned between 5μM to 20μM (Figure 3.26A). It was then verified whether degradation of TOP2B would occur at those concentrations (Figure 3.26B). MM.1S cells were cultured with DMSO, 20μM or 50μM DXZ and harvested at 24, 48 and 72 hours to assess TOP2B protein levels by immunoblot. DXZ was able to induce almost complete degradation of TOP2B at 24 hours. At 48 hours, levels of TOP2B were less reduced as compared to the 24 hours timepoint (with both DXZ concentrations). At 72 hours, TOP2B expression in cells treated with DXZ was further increased as compared to the 48-hour and 24-hour timepoints.

3.2.7.2 TOP2B degradation by dexrazoxane is independent of CRBN expression

The structure of DXZ is similar to that of the glutarimide group of IMiDs (Figure 3.26C). Since the glutarimide group of IMiDs is reported to bind the CRBN Tri-Trip pocket in the thalidomide binding region, it was hypothesised that DXZ might bind CRBN, induce TOP2B degradation and/or interfere with IMiD interactions in the context of co-treatment with IMiDs. To test these hypotheses, MM.1S, MM.1Sres (with reduced CRBN expression) and MM.1S CRBN KO cells (*CRBN null* control) were treated overnight with DMSO, 2μM LEN, 20μM DXZ or LEN/DXZ in combination and levels of TOP2B evaluated by Western blot (Figure 3.26D). In addition to MM.1S and MM.1Sres cells, a CRBN *null* MM.1S cell line was generated to ensure the presence of a control with no residual expression and therefore CRBN activity.

MM.1S CRBN KO cells were generated via electroporation of a CRBN sgRNA in complex with recombinant Cas9 (for a detailed protocol, refer to Material and Methods, section 2.4.1). Prior to electroporation, the ribonucleocomplex was prepared: recombinant Cas9 and a CRBN-specific sgRNA were mixed together and incubated a room temperature for 20 minutes to allow binding of Cas9 with the sgRNA. MM.1S cells were resuspended in deionized water in the nucleocuvette provided within the manufacturer's electroporation kit. Cells were electroporated and subsequently cultured. Expression of CRBN in MM.1S CRBN KO cells was tested by immunoblotting, together with that of MM.1S and MM.1Sres (Figure 3.26D).

The reduction (MM.1Sres cells) and absence (MM.1S CRBN KO cells) of CRBN did not affect TOP2B degradation by DXZ but reduced (MM.1Sres cells) or abolished (MM.1S CRBN KO cells) LEN-induced degradation of IKZF3. Treatment with DXZ did not interfere with LEN-dependent

IKZF3 degradation. As expected, IKZF3 degradation correlated with CRBN expression in the three isogenic lines. Interestingly, combinatorial treatment in MM.1S cells showed a slight decrease of IKZF3 as compared to LEN only, suggesting that DXZ might cause additional reduction of IKZF3 proteins levels.

Collectively, these observations suggest that DXZ is an active anti-MM compound and causes degradation of TOP2B at concentrations causing MM cell death, although DXZ seemed to progressively lose efficiency over time in inducing degradation of TOP2B. Despite the structural similarities with IMiDs, DXZ probably does not interfere with LEN activity but seems to cooperate with LEN to reduce IKZF3 levels. Finally, TOP2B degradation following DXZ treatment is likely independent of CRBN.

3.2.8 Characterisation of dexrazoxane activity as single agent and in combination with lenalidomide

3.2.8.1 Dexrazoxane interferes with cell cycle progression and causes apoptosis in MM cells

The effect of DXZ on the different phases of the cell cycle was characterised both as a single-agent and in combination with LEN. It has been reported that LEN typically blocks MM cells in the G0-G1 phase with consequent reduction of cells in the S phase[198], and DXZ inhibits type 2 topoisomerases, which are involved into segregation of sister chromatids[263]. MM.1S and MM.1Sres cells were treated for 7 days with either DMSO, 2μM LEN, 20μM DXZ or both drugs, and Nicoletti staining was employed to assess DNA content for cell cycle phases analysis by FACS (exemplified in Figure 3.27). In MM.1S cells (Figure 3.28A-B), DXZ induced an increase in cell death (SubG1) and accumulation of hyperdiploid cells, whilst LEN blocked cells in G0-G1 with subsequent reduction of the percentage of events in the S phase. A clear combinatorial effect was observed in MM.1S cells treated with both drugs in the SubG1 phase. Cells in S-phase were significantly reduced in presence of LEN, but no significant difference was observed in MM.1S cells treated with LEN and DXZ in combination. DXZ alone also induced a mild reduction of the percentage of cells in S-phase. MM.1S cells showed an increase in hyperdiploidy in presence of DXZ. However, this effect seemed to be attenuated by concomitant treatment with LEN. In MM.1Sres cells (Figure 3.28A, 3.28C), although LEN did not exert any significant effect, DXZ alone was able to increase the fraction of cells in SubG1 and that of hyperdiploid cells, but no significant combinatorial effect was observed. A reduction in DXZ-treated MM.1Sres cells in S-phase was documented, as compared to MM.1Sres cells treated without DXZ. DXZ also

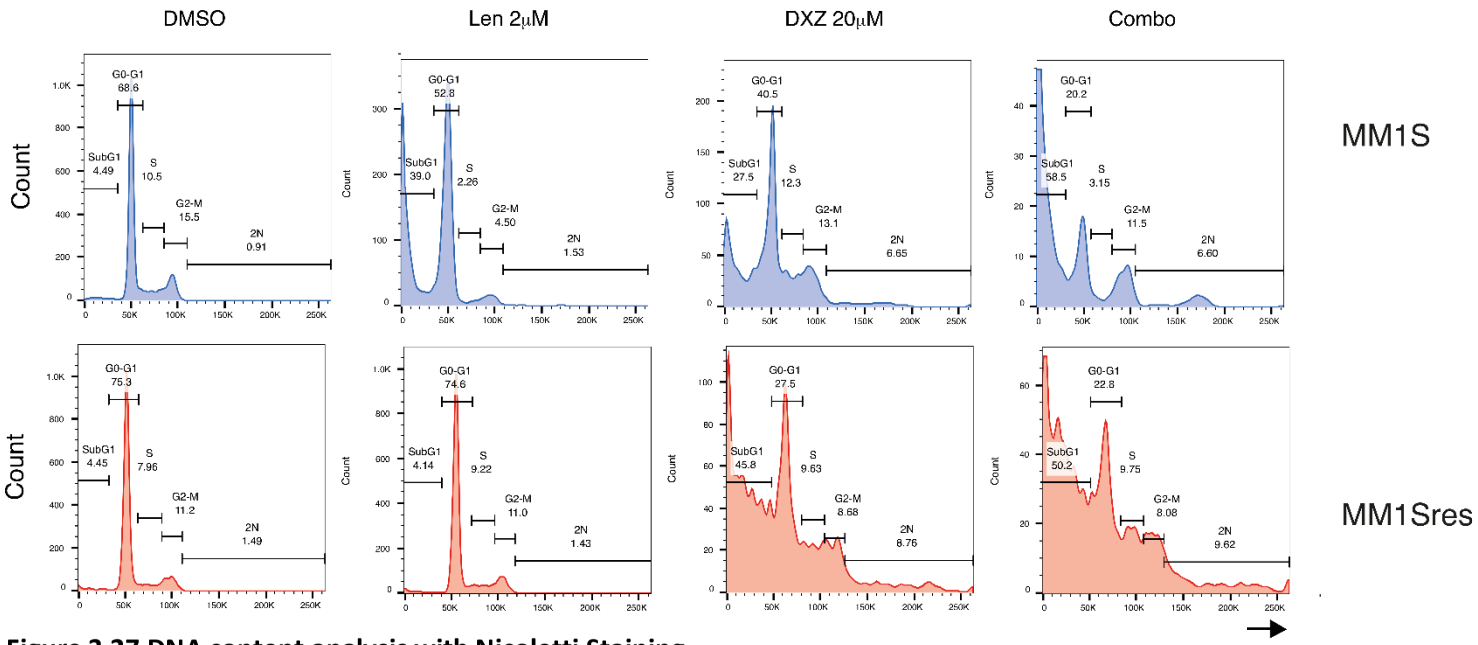
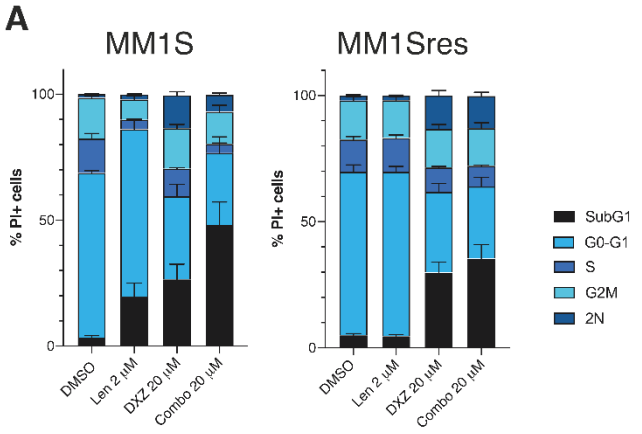
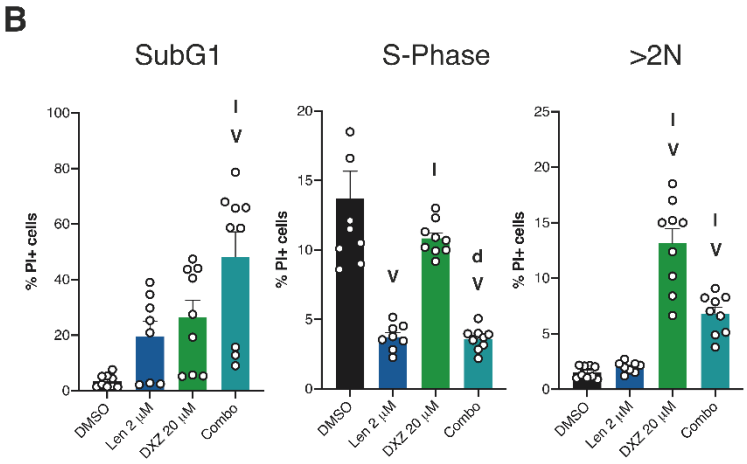


Figure 3.27 DNA content analysis with Nicoletti Staining

Representative FACS histograms of PI intensity for DNA content analysis in MM.1S and MM.1Sres cells treated with DMSO, LEN 2μM, DXZ 20μM, or in combination LEN-DXZ, for 7 days.

Figure 3.28 Consequences of LEN and DXZ exposure on cell cycle phases in MM.1S lines
(A) Summary of DNA content analysis in all the cell cycle phases of MM.1S and MM.1Sres cells (3 independent experiments, with at least 2 technical replicates each). Both MM.1S and MM.1Sres were treated for 7 days with DMSO, 2μM LEN, 20μM DXZ or a combination with LEN and DXZ. (B) Bar charts showing fraction of cells in SubG1, S phase and >2N across the 4 different treatment conditions of the experiment in panel (A), for MM.1S. V=significant vs vehicle (DMSO), l=significant vs LEN, d=significant vs DXZ. (C) Bar charts showing fraction of cells in SubG1, S phase and >2N across the 4 different treatment conditions of the experiment in panel (A), for MM.1Sres. V=significant vs vehicle (DMSO), l=significant vs LEN, d=significant vs DXZ.


A
MM1S
MM1Sres
% PI+ cells
100
50
0
DMSO
Len 2 μM
DXZ 20 μM
Combo 20 μM
SubG1
G0-G1
S
G2M
2N


B
SubG1
S-Phase
>2N
% PI+ cells
DMSO
Len 2 μM
DXZ 20 μM
Combo

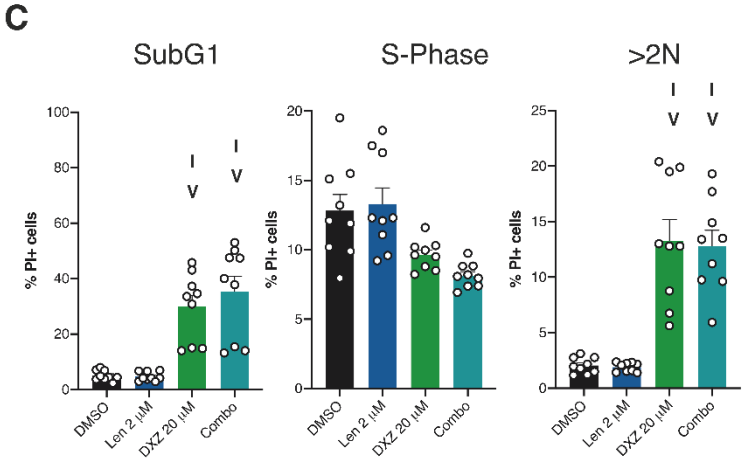
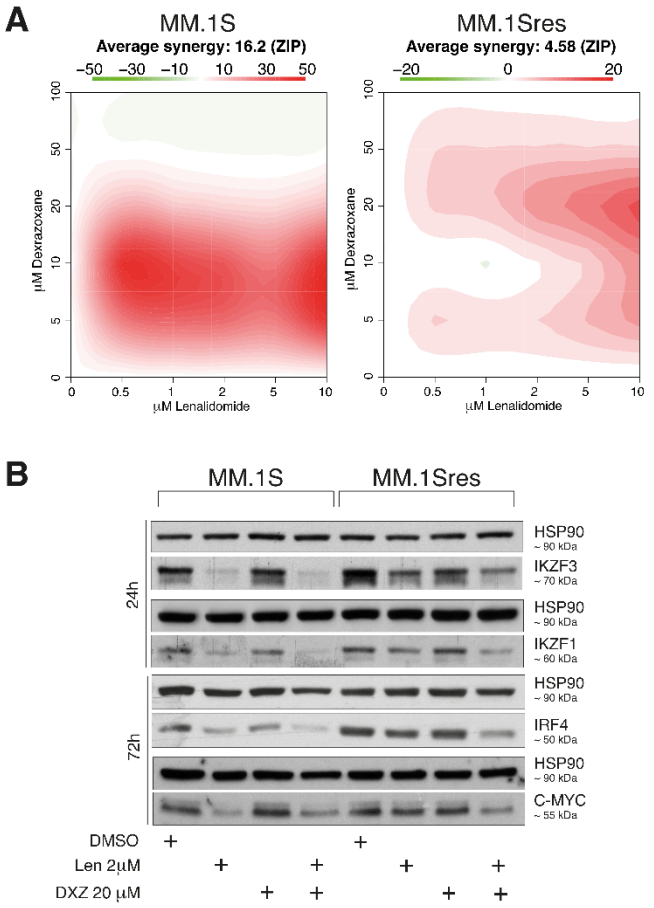

C
SubG1
S-Phase
>2N
% PI+ cells
DMSO
Len 2 μM
DXZ 20 μM
Combo

Figure 3.29 Phenotypical and biochemical dissection of synergy between LEN and DXZ in MM.1S lines

(A) Synergy plots of cell death in MM.1S and MM.1Sres cells treated with the combination of increasing concentrations of LEN and DXZ for 7 days. The colours in the heatmap indicate variations of the ZIP score in the different conditions. (B) Western blot displaying expression of IKZF1, IKZF3 at 24 hours and IRF4 and MYC at 72 hours in MM.1S and MM.1Sres cells treated with DMSO, LEN, DXZ or combination LEN/DXZ. Expression of HSP90 is provided as control for equivalent loading across samples. (C) Average viable cell count at 3 and 7 days for MM.1S and MM.1Sres cells treated with DMSO, LEN, DXZ or combined LEN/DXZ (Combo).


A
MM.1S
Average synergy: 16.2 (ZIP)
−50 −30 −10 10 30 50
MM.1Sres
Average synergy: 4.58 (ZIP)
−20 0 20
µM Dexrazoxane
µM Lenalidomide
0 0.5 1 2 5 10
0 5 10 20 50 100
B
MM.1S
MM.1Sres
24h
72h
HSP90 ~ 90 kDa
IKZF3 ~ 70 kDa
IKZF1 ~ 60 kDa
IRF4 ~ 50 kDa
C-MYC ~ 55 kDa
DMSO
Len 2µM
DXZ 20 µM
C
MM1S
MM1Sres
Viable Cell Count (x10e6)
DMSO
Len 2µM
DXZ 20 µM
Combo
Day 0
Day 3
Day 7

incremented the fraction of hyperdiploid MM.1Sres cells as compared to those treated with no DXZ.

3.2.8.2 The activity of dexrazoxane in combination with lenalidomide in MM.1S cells

In order to assess whether the combinatorial effect of LEN and DXZ is synergistic, MM.1S and MM.1Sres cells were treated with increasing concentration of LEN each combined with increasing concentration of DXZ for 7 days (Figure 3.29A). Cell death was assessed by PI labelling via FACS analysis. The average Zero Interaction Potency score[284] revealed strong synergy between the two agents in MM.1S cells (average ZIP score = 16.2). Maximum synergy was observed in MM.1S cells in the DXZ concentration range between 5 and 10μM, whilst in MM.1Sres cells synergy scored lower overall (average ZIP score = 4.58), with a small peak in the area corresponding to 10μM LEN.

3.2.8.3 The activity of dexrazoxane in combination with lenalidomide on the IKZF1/3-IRF4-MYC axis

Next, the impact of combinatorial LEN/DXZ treatment on the IKZF1/3-MYC-IRF4 axis was studied (Figure 3.29B). MM.1S and MM.1Sres cells were treated with either DMSO, 2μM LEN, 20μM DXZ or both drugs. IKZF1 and IKZF3 levels were assessed at a 24-hour timepoint. Expression of both IKZF1 and IKZF3 were greatly reduced following LEN treatment (as compared to DMSO- and DXZ-treated MM.1S cells) in MM.1S cells but not in MM.1Sres, as expected. Moreover, DXZ alone did not affect IKZF1/3 degradation in either cell lines. In MM.1Sres, however, combinatorial activity was observed with both drugs, as IKZF1/3 levels were reduced following co-treatment with LEN and DXZ as compared to LEN alone. MYC and IRF4 levels were studied after 72 hours of drug exposure. As expected, in MM.1S, downregulation of IRF4 and MYC in LEN-treated cells correlated with the magnitude of IKZF1 and IKZF3 degradation. Furthermore, in MM.1S cells, IRF4 suppression was more accentuated in LEN/DXZ relatively to LEN only, whilst DXZ alone did not affect its levels. Surprisingly, MYC was slightly higher in MM.1S cells exposed to both drugs as compared to cells treated with LEN only. However, in MM.1Sres cells, both IRF4 and MYC were found to be downregulated in cells exposed to the combination LEN/DXZ, in line with the suppression of IKZF1 and IKZF3 observed at 24 hours.

3.2.8.4 The activity of dexrazoxane in combination with lenalidomide on MM cells proliferation

The effect on cell proliferation of DXZ, alone and in combination with LEN, was also investigated. MM.1S and MM.1Sres cells were treated for 7 days with either DMSO, 2μM LEN, 20μM DXZ or

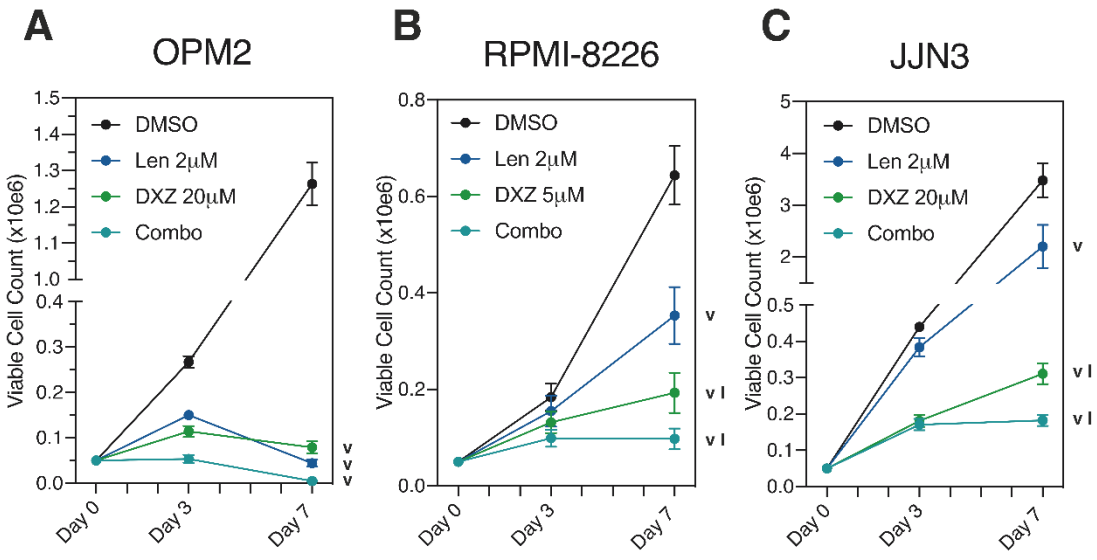
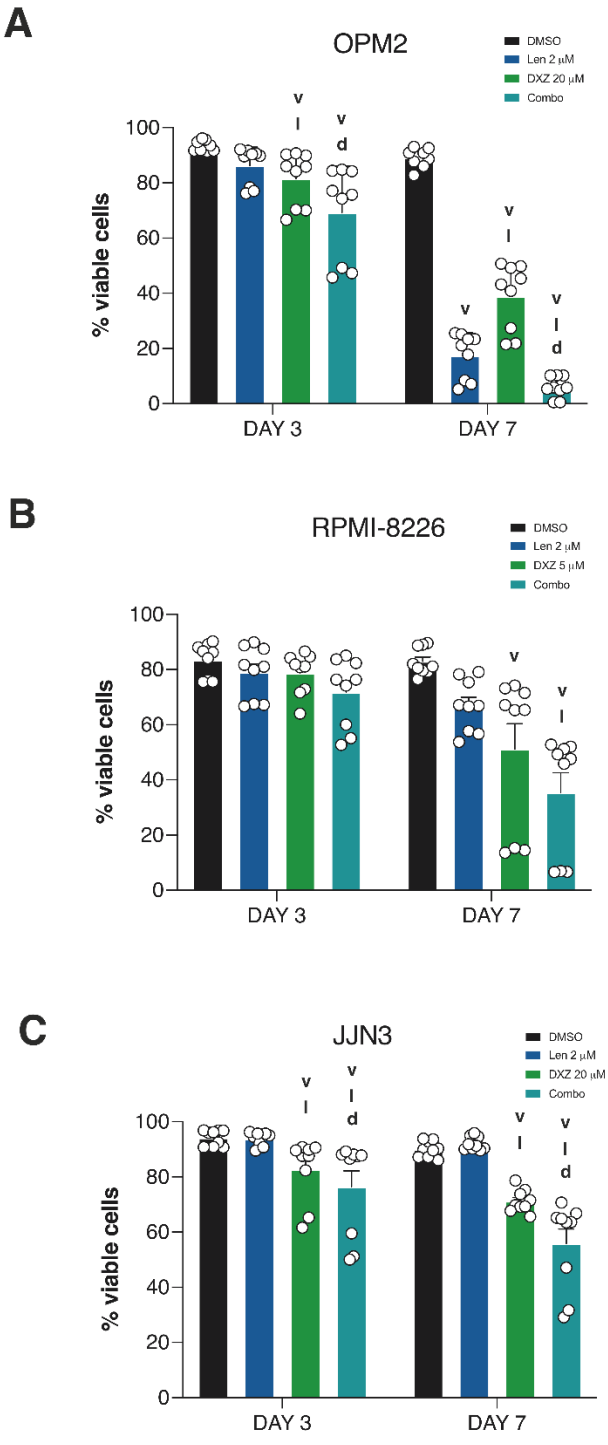


Figure 3.30 Dexrazoxane elicits anti-proliferative effect in sensitive and resistant MM cell lines

(A) Viable cell count at 3 and 7 days of OPM2 cells treated with DMSO, LEN (2μM), DXZ (5 or 20μM) or combination LEN/DXZ. (B) Viable cell count at 3 and 7 days of RPMI-8226 cells treated with DMSO, LEN, DXZ or combination LEN/DXZ. (C) Viable cell count at 3 and 7 days of JJN3 cells treated with DMSO, LEN (2μM), DXZ (5 or 20μM) or combination LEN/DXZ. In all panels, error bars represent mean ± SEM of n = 3 independent experiments. v= significant vs vehicle (DMSO), l=significant vs LEN, d=significant vs DXZ ($p<0.05$ or less).

Figure 3.31 Dexrazoxane elicits pro-apoptotic effect in IMiD sensitive and resistant MM cell lines

(A) Percentage of PI negative (viable) OPM2 cells treated with DMSO, LEN (2µM), DXZ (20µM or combination LEN/DXZ and assessed by flow cytometry. (B) Percentage of PI negative (viable) RPMI-8226 cells treated with DMSO, LEN (2µM), DXZ (5 µM) or combination LEN/DXZ and assessed by flow cytometry. (C) Percentage of PI negative (viable) JJN3 cells treated with DMSO, LEN (2µM), DXZ (20µM) or combination LEN/DXZ and assessed by flow cytometry. In (A), (B) and (C), error bars represent mean ± SEM of n = 3 independent experiments. v= significant vs vehicle (DMSO), l=significant vs LEN, d=significant vs DXZ ($p<0.05$ or less).


A
OPM2
DMSO
Len 2 μM
DXZ 20 μM
Combo
% viable cells
100
80
60
40
20
0
DAY 3
DAY 7
B
RPMI-8226
DMSO
Len 2 μM
DXZ 5 μM
Combo
% viable cells
DAY 3
DAY 7
C
JJN3
DMSO
Len 2 μM
DXZ 20 μM
Combo
% viable cells
DAY 3
DAY 7

both drugs and viable cell count obtained at day 3 and day 7 (Figure 3.29C). As expected, LEN significantly impacted MM.1S cell proliferation, but not that of MM.1Sres cells. DXZ, however, exhibited an anti-proliferative action in both cell lines. Strikingly, in MM.1S cells (but not MM.1Sres cells), combination treatment LEN/DXZ completely blocked proliferation and killed all cells. In summary, these observations indicate that DXZ also displays combinatorial activity with LEN as pro-apoptotic and cytostatic and that combination treatment could potentially impact MM cells by interfering with the IKZF1/3-IRF4-MYC transcriptional axis.

3.2.8.5 Combinatorial effects of dexrazoxane and lenalidomide in MM cell lines OPM2, RPMI-8226 and JJN3

The action of DXZ in combination with LEN in other MM lines was studied. OPM2, RPMI-8226 and JJN3 (Figure 3.30A) were cultured in DMSO, 2µM LEN, 20µM DXZ (or 5µM DXZ in RPMI-8226 cells) or both drugs for 3 and 7 days. All lines were sensitive to prolonged treatment with DXZ, whereas LEN alone profoundly inhibited cell growth of OPM2 but only partially affected RPMI-8226 and JJN3 cells. However, in RPMI-8226 and JJN3, the dual treatment of LEN and DXZ had an additive effect compared to the single-agent conditions, as it was able to arrest proliferation. Cell death was assessed at 3 and 7 days in OPM2, RPMI-8226 and JJN3 in the same setting (Figure 3.31A-C), demonstrating high toxicity of DXZ as single agent or in combination with LEN in OPM2 cells, and lower but still significant activity of DXZ alone in RPMI-8226 and JJN3. Furthermore, in IMiD-resistant cells, a mild additivity in the combinatorial treatment was observed.

Taken together, these observations demonstrated that MM cells are sensitive to DXZ, which had little effect on the IKZF1/3-IRF4-MYC axis in MM.1S cells. Conversely, DXZ seemed to have an impact on this axis in MM.1Sres cells when in combination with LEN. DXZ demonstrated pro-apoptotic and anti-proliferative effects both as a single agent and in combination with LEN in several MM cell lines. LEN also increased DXZ toxicity to various degrees across different cell lines.

3.3 Discussion

3.3.1 Neosubstrate degradation and sensitivity to IMiDs highly correlate with CRBN expression

This work focused on the characterisation of IMiD sensitivity and acquired IMiD resistance by employing isogenic pairs of IMiD-sensitive/resistant cell lines U266/U266res and

MM.1S/MM.1Sres cells. Using CTV/PI assays, an IMiD-resistant phenotype in MM.1Sres and U266res cells was substantiated by the absence of IMiD-induced growth inhibition. The study of protein expression in both cells revealed reduced IKZF3 degradation upon LEN or POM exposure. In U266 cells, after just 6 hours of LEN and POM treatment, IKZF3 level were significantly reduced, displaying the typical kinetics of acute protein degradation. In U266res cells, IMiD-induced IKZF3 degradation was almost absent at any timepoint studied. Both the magnitude and the rate at which neosubstrates are degraded following IMiD exposure highly correlated with CRBN levels. CRBN is known to be the primary target of IMiD drugs, and the CRISPR screen demonstrated that deletion of CRBN causes complete resistance to IMiDs. Moreover, the *CRBN* gene is downregulated in patients with MM refractory to IMiD treatment[217,249]. Collectively, these data indicated that the main mechanism of acquired resistance to IMiDs in MM.1Sres cells is likely the result of reduced CRBN expression.

To confirm that CRBN loss is the main driver of IMiD-resistance, re-expression of adequate CRBN levels with rescue of IKZF1/3 degradation upon treatment with IMiDs would be required. If in MM.1Sres and U266res cells the resistant phenotype is caused solely by suppression of CRBN, its overexpression would supposedly be sufficient to completely rescue an IMiD-responsive phenotype. The cytogenetic characterisation by Zhu et al. of MM.1Sres and MM.1S cells proved that MM.1Sres cells lack one copy of the *CRBN* gene compared to its sensitive counterpart[217]. However, the involvement of other mechanisms sustaining CRBN downregulation cannot be excluded, because generally gene/protein expression is finely tuned by several processes occurring from chromatin accessibility to protein degradation[285,286]. For example, the occurrence of MMs expressing CRBN splicing variants lacking of exons 10/11, which contain the TBD (Thalidomide Binding Domain), has been associated with refractoriness to IMiD therapy[221,287,288]. A recent study aiming to explore epigenetic mechanisms of IMiD-resistance demonstrated that CRBN downregulation is independent of epigenetic modifications as its promoter shows epigenetic marks of transcriptional activation despite documenting reduced CRBN expression. In that study, the authors demonstrated that IMiD resistance was associated with global changes in DNA methylation and chromatin accessibility and that IMiD-sensitivity could be restored with epigenetic therapy[289]. This observation would have to be kept in consideration if CRBN overexpression studies were to be conducted, as it indicates that overexpressing CRBN might not be sufficient to restore sensitivity to IMiDs.

3.3.2 The magnitude of transcriptional response to IMiD correlates with CRBN expression

3'-RNA sequencing was employed to investigate transcriptional signatures of MM isogenic cell lines in response to IMiDs. Acute treatment with IMiDs in sensitive cells provoked significant alterations in the transcriptome. In particular, GSEA revealed strong enrichment in IFNγ and IFNα signature and downregulation of MYC-related genes in both U266 and MM.1S cells. It has been reported that IKZF1 regulates transcription of the IFN locus[80]. This could potentially explain the induction of IFN-like responses following acute exposure to IMiDs. A high number of differentially expressed genes was detected in both MM.1Sres and U266res cells as compared to their sensitive counterparts, indicating that prolonged culturing in LEN has induced significant transcriptional changes in these cells. GSEA revealed that IFN-and KRAS-induced genes were upregulated in U266res and MM.1Sres cells, respectively. Conversely, genes required for oxidative phosphorylation and MYC-responsive genes were downregulated, in U266res and MM.1Sres cells. Moreover, the enrichment in IFN-like signatures observed in U266res cells could be the result of sustained induction of IFN-related genes. A mechanism that potentially explains sustained enrichment of IFN transcriptional signatures following prolonged IMiD treatment might be epigenetic adaptation to drug exposure. Epigenetic-mediated drug resistance is a well-known phenomenon by which cancer cells escape drug-induced toxicity[290]. As IMiD resistance has been associated with global modification of the epigenome[289], and acute IMiD treatment induced transcription of IFN-related gene, one could argue that sustained IFN transcriptional signature in U266res cells might also be the result of adaptation to prolonged LEN treatment - along with the several epigenetic changes occurring in these cells in order to adapt to LEN. It remains to be explained, however, why IFN-like signalling was not significantly enriched in GSEA analysis of MM.1Sres cells, which rather displayed induction of KRAS signalling.

From this perspective, studying chromatin accessibility using genome-wide approaches such as bisulphite sequencing and/or ATAC-seq could help understanding the occurrence of enduring epigenetic modifications possibly driving expression of genes related to IFN and RAS transcriptional signatures, and acquired IMiD resistance from the perspective of epigenetic commitment. However, RAS is generally activated by point mutations that render it constitutively active in cancer[291]. Interestingly, patients that become refractory to IMiDs bear significantly more mutations in members of the *MAPK (NRAS, KRAS, BRAF)* family, *CRBN* and *TP53* as compared to responders[219]. Whole-exome sequencing would address whether *MAPK* genes or *TP53* are mutated in MM.1Sres cells and help exploring further resistance mechanisms (e.g. point mutation in genes required for protein degradation, such as CUL4A/B or DDB1). With

regards to IFN response signatures in these two isogenic pairs, it would also be informative to investigate the differential response of MM cells in the context of IFN signalling modulation (e.g. phenotypical, biochemical and transcriptomic studies in presence of exogenous IFN or other stimuli such as lipopolysaccharide, or treatment with IMiDs in cells with loss of IFN receptors). Further studies with regards to IMiD-induced IFN responses could be useful for understanding the effect of IFN (either alpha or gamma) on MM cells, as IFN is currently being developed in fusion with mAb for targeted therapies in MM[292].

GSEA of DEGs in MM.1Sres and U266res cells revealed treatment with IMiDs induces positive or negative enrichment of the same gene signatures of IMiD-exposed MM.1S and U266 cells. In fact, downregulation of MYC target genes was found in both MM.1Sres and U266res cells acutely exposed to IMiDs and upregulation of KRAS and IFN signalling related genes in MM.1Sres and U266res cells, respectively, when drug-treated. This observation suggests that, in cells with acquired IMiD-resistance, the response to IMiD is similar to that of the sensitive counterpart, but it is globally reduced. Moreover, this result correlates with both downregulation of CRBN and attenuation of neosubstrates degradation, indicating that the impairment of CRBN-dependent neosubstrates degradation is likely the cause of unresponsiveness.

3.3.3 Correlating the transcriptional response to different IMiDs in isogenic sensitive/resistant MM cell lines

Similarities in the transcriptional status between MM.1S/MM.1Sres cells and U266/U266res cells were assessed by identifying mutual DEGs and the presence of statistical correlation between RNA-seq datasets. In MM.1Sres and U266res cells, GO term analysis showed upregulation of HLA genes and downregulation of IFN receptors. This data is consistent with GSEA analysis showing upregulation of IFN genes. One could speculate that, if IFN impacts cell growth, both MM.1S and U266 cells might have adapted to its presence by downregulating IFN receptors over time. The upregulation of HLA genes also indicates that these cells have undergone exposure to IFN[293,294]. This is potentially relevant in the clinical context, as antigen presentation could increase the activity of T-cell. Moreover, IFN enhances the activity of T CD4 and T CD8 by inducing a T_{h1}-like response, whereas IKZF1 promotes a pro-inflammatory T_{h2}-like response[79]. So, it is possible that from a therapeutic perspective, IKZF1 degradation induces release of IFN with concomitant enhancement of a T_{h1} response and a suppression of the T_{h2} response. To explore this aspect, *in vivo* studies are required. A murine model on a C57BL/6 background has recently been engineered by Fink and colleagues to respond to LEN[237]. In these

mice, a point mutation on the IMiD-binding pocket of Crbn, Crbn^{I391V}, was introduced. This point mutation on *Crbn* was sufficient to induce a response to LEN with Crbn-dependent ubiquitinylation and therefore proteasomal degradation of Ikzf1 and and Ck1α upon LEN treatment. This model would be ideal for the study of immune enhancing properties of IMiDs if cross-bred with Vk*MYC mice[95]. Vk*MYC mice spontaneously develop plasmacytomas which recapitulate many aspects of human MMs. GO terms of sensitive cells treated with POM demonstrated upregulation of genes that are associated with cell adhesion and extracellular and intercellular signalling, such as integrins. This is an interesting result, as these are genes involved in the interaction of MM cells with the tumour microenvironment, and IMiDs are known to be modulators of these interactions. It is not clear why these genes were found to be upregulated and not suppressed. It is plausible that IMiDs reduce expression of these genes at a protein level, and their transcriptional upregulation is the outcome of a compensatory feedback loop. To test the hypothesis of a feedback loop, the study of the cell surface proteome would represent an elegant approach. A loss of surface expression of adhesion molecules with concurrent upregulation of their transcript would be suggestive of the presence of a feedback loop and provide the basis for more hypothesis testing.

3.3.3.1 Correlation studies reveal similarities in the transcriptional response to IMiDs despite baseline discrepancies between MM.1S and U266 cell lines

Some of the differentially expressed genes in DMSO-treated U266res cells were also differentially expressed in MM.1Sres cells, as compared to their relative sensitive counterpart. However, these two datasets displayed complete absence of correlation. Transcriptional responses to different IMIDs strongly correlated in the same cell line, whilst little correlation was seen between different cell lines treated with the same IMiDs. Also, some correlation was observed between sensitive and resistant cells treated with the same IMiD. The almost complete lack of statistical correlation between MM.1Sres and U266res cells reflects either inherited differences in U266 and MM.1S cells transcriptomes and/or distinct mechanisms of adaptation to prolonged LEN treatment. Moreover, the presence of a mild correlation between sensitive cells of different isogenic lines exposed to the same IMiD, and the correlation between sensitive and resistant lines of the same isogenic pair exposed to the same IMiD, corroborate the observation that the perturbations induced upon IMiD treatment are similar. Collectively, these data support the observation that the transcriptional response to IMiD is similar but greatly reduced in resistant cells and it is partially comparable across different MM cell lines.

3.3.3.2 The impact of *CRBN* downregulation in the transcriptional response IMiDs in resistant cells

Assessing the differential expression of *CRBN, CUL4A, DDB1* and *RBX1* between sensitive and resistant lines demonstrated that no other subunit of the *CRBN* complex was downregulated, at least transcriptionally. This observation suggests that in the presence of continuous selective pressure by LEN, downregulation of other genes of the *CRBN* complex might cause a proliferative disadvantage for MM.1S or U266 cells. However, to confirm that CUL4A, DDB1 and RBX1 are not downregulated, protein expression would have to be assessed. Again, to fully understand the role of CRBN in the context of transcriptional response to IMiDs, RNA-sequencing in MM.1S and U266 cells with complete loss of *CRBN,* and MM.1Sres and U266res cells with *CRBN* re-expression would be necessary. It is not clear whether the sole *CRBN* downregulation would be responsible for such profound changes in the transcriptional landscape between isogenic pairs. Given that numerous gene sets were upregulated or downregulated, the question is whether suppression of CRBN directly impacted on a multitude of pathways or induced relatively small perturbations but with consequential propagation of secondary responses. Transcriptional studies in the context of acute or stable loss of CRBN would help clarifying this aspect, perhaps with the aid of more novel approaches such as sequencing of nascent RNA by labelling with 4S-Uridine (SLAM-seq) following acute CRBN degradation (employing the AID-degron system)[295,296]. The advantage of studying nascent RNA following acute loss of a gene is the possibility of specifically identify which genes are directly affected by the loss of the gene/protein studied. By doing this, it could be possible to define which genes are primarily susceptible to loss of CRBN and discriminate from those which levels change as a secondary effect or as a result of change in expression of other genes following IMiD treatment. Deeper understanding of CRBN-independent transcriptional changes in cells with acquired resistance may inform with regards to additional mechanisms of adaptation to prolonged IMiD treatment. An interesting perspective is provided by the fact that prolonged treatment with LEN not only induces continuous neosubstrates proteolysis, but also inhibits turnover of CRBN endogenous substrates, which can accumulate and supposedly impact several biological processes. Although the complete pool of substrate and neosubstrates directly regulated by CRBN has not been fully defined yet, this observation raises the hypothesis that differential gene expression in MM.1Sres and U266res cells (relative to their sensitive isogenic) is probably the outcome of both CRBN endogenous target accumulation and persistent degradation of CRBN neosubstrates. With regards to the latter, another unanswered question is how much of IKZF1/3 degradation accounts for the observed transcriptional changes. The use of an AID-degron (and SLAM-seq, to

define genes which are directly impacted by the loss of IKZF1 and IKZF3) would help isolating the specific effect of acute IKZF1/3 loss thus avoiding degradation of other IMiD neosubstrates. Conversely, generation of clones with single point mutations that prevent IMiD-induced IKZF1/3 degradation ($IKZF1^{Q126H}$ and $IKZF3^{Q147H}$)[89,90] by introduction of point mutations with CRISPR/Cas9 Homology Directed Repair would allow dissection of the transcriptional response that follows degradation of non-IKZFs neosubstrates.

3.3.4 Transcriptional regulators and DNA repair genes as novel players in IMiD mechanism of action

Although RNA sequencing has clearly provided important insight with regards to the relationship between phenotype and transcriptional response to IMiDs, it was not informative in terms of which pathways could have been implicated in the acquired IMID resistance. For this reason, CRISPR screening for genes that when deleted confer IMID resistance was performed. Several genes involved in IMiD biochemistry were discovered, some of which directly related to degradation of neosubstrates. As primary IMiD target, a strong CRBN enrichment was observed, meaning that knockout of CRBN confers full resistance to IMiD. Again, this result is concordant with the literature, as loss of CRBN, its mutation or expression of splicing variants lacking domains important for the response to IMiDs have been described[219,221,288]. Loss of other genes, including those encoding subunits of the COP9 signalosome and *CAND1,* induced resistance to IMiDs. Recent work has also been published showing exceptionally similar findings[239,240]. The COP9 signalosome and CAND1 are both regulators of CUL4 functions[297]. In particular, COP9 signalosome subunits have been found dysregulated in patients by analysis of MM transcriptomes, indicating potential clinical relevance of these genes in the response to IMiDs[240]. Other genes, however, such as *NCOR1,* might be responsible for regulating the transcriptional response that follows IMiD treatment rather than degradation of substrates, as NCOR1 is a transcriptional repressor[298]. In fact, there is no existing evidence of NCOR1 involvement in protein degradation. IMiD-resistance induced by *NCOR1* deletion in MM.1S cells was clearly demonstrated by loss of representation of SCR cells and increase in *NCOR1* deletion cells by competitive proliferation in presence of an IMiD.

Whereas the CRISPR resistance screen identified genes that mediate IMiD sensitivity in MM.1S cells, the CRISPR dropout screen in MM.1Sres cells revealed potential mechanisms of IMiD resensitisation in the context of IMiD resistance. In particular, loss of genes such as *TOP2B*, *ATXN7*, subunits of the CTLH complex, in addition to *MED13L* and *MIER3,* restored sensitivity in

MM.1Sres cells in presence of an IMiD. Both *TOP2B* and *ATXN7* KO did not negatively impact cell proliferation. On the contrary, *TOP2B* paralog *TOP2A* is an essential gene in all types of cancer. Importantly, loss of *TOP2B* did not markedly change CRBN levels or the rate at which IKZF3 is degraded. Dependency pathway analysis revealed that, in these cell lines, dependencies are similar. This was demonstrated by Pearson's correlation and by GO analysis. These cells were highly dependent on ribosome biogenesis, mRNA processing, and on other pathways, such as DNA repair (MM.1S cells) or transcriptional regulation (the RUNX program, the VENTX program and the cohesin complex activity). In MM.1S cells, *IKZF1*, *IKZF3*, *IRF4* and *MYC* were demonstrated to be genes that are essential for survival, as expected. Furthermore, MM.1Sres cells were dependent on the expression of these genes even after prolonged treatment with IMiDs.

3.3.4.1 Continuous IMiD exposure could increase genomic instability

These results raise several hypotheses. CRBN is the top-enriched hit in the resistance screen - this recapitulates CRBN downregulation in MM.1Sres and U266res cells, indicating that, in these cells, loss of CRBN is probably the main mechanism of resistance to IMiD treatment. The primary role of COP9 signalosome is to remove NEDD8 from CUL4 to inactivate the E3 complex, with CAND1 proceeding with its disassembly. As demonstrated by Sievers and colleagues, loss of these genes is thought to block the complex in an inactive state[239]. Interestingly, COP9 signalosome is also implicated into DNA repair following damaging of the double helix together with CUL4-DDB1-RBX1, which led to the hypothesis that IMiDs could modulate the response to DNA damage.

One could also speculate that the mechanism of resentisation might involve a DNA damage response, as TOP2B and ATXN7 might be required together with CUL4, DDB1, RBX1 and the COP9 signalosome for NER and/or DSB repair. In this scenario, CUL4- and DDB1-mediated DNA repair might be modulated via CRBN-IMiD binding and that could be toxic for MM.1Sres cells in absence of genes such as *TOP2B* or *ATXN7.* Interestingly, genes involved in NER are found to be essentialities in MM.1S cells but not in MM.1Sres cells. This would indicate that MM.1Sres cells might have been desensitised to DNA damage. However, further experiments with etoposide argue against the possibility of LEN being a DNA-damaging agent. A baseline increment in transcription of genes involved in DNA damage and response to DNA damage was observed in MM.1Sres cells (p53 pathway genes and genes implicated in the response to UV exposure), and also in MM.1S cells treated with IMiDs (genes upregulated following radiation therapy),

therefore in absence of apparent DNA damaging events. Genes indexed in these gene sets are also involved in epithelial-to-mesenchymal transition, which could represent a confounding factor. Nevertheless, the possibility of LEN inducing desensitisation to DNA damage via upregulation of genes of the aforementioned pathways cannot be *a priori* excluded. In addition, MM.1Sres cells appeared dependent on the function of the cohesin complex, which regulates chromatin looping in the context of transcriptional. TOP2B has been found essential component of this machinery[299]. Interestingly, loss of STAG2, another cohesin complex subunit[299], resulted in resistance to IMiDs in MM.1Sres cells. This observation further reinforces the hypothesis that cohesins might participate in the response to IMiDs. The increased dependency of MM.1Sres cells on cohesin activity also suggests that MM.1Sres cells could have augmented genomic instability compared to MM.1S cells. In this context, desensitisation to DNA damage would be possibly required to escape apoptosis upon DNA damaging levels above sustainable thresholds.

3.3.4.2 Bridging TOP2B- and NCOR1-dependent transcriptional regulation to the activity of IKZF1/3

The synergistic effect of *TOP2B* loss and IMiD treatment documented in MM.1S-Cas9 cells raised the possibility that this synergy could be conserved across other MM cell lines. To further investigate this combinatorial mechanism, testing IMiD activity in CRBN/TOP2B double knockout cells would inform whether synergy occurs via a CRBN-dependent mechanism. Moreover, employment of AID-degron on IKZF1/3 could demonstrate whether resensitisation is the consequence of IKZF1 and/or IKZF3 loss. An interesting aspect emerges from recent studies on TOP2B, which seem to be a key regulator of RNA Pol II driven transcription. TOP2B has been detected in promoters of actively transcribed genes, and it produces double strand breaks in order to allow RNA Pol II elongation during transcription[300]. TOP2B has been found to associate with CTCF-cohesin complexes in proximity of transcriptionally active sites[299,301]. Given that IMiDs induce degradation of the two key TFs (IKZF1 and IKZF3), it is plausible that loss of TOP2B might impact transcription of genes that are normally repressed by IKZF1/3 and transcribed upon degradation of IKZF1/3.

As reported by a seminal paper in 2006, TOP2B and NCOR1 (with HDAC3) are both required for transcription of estrogen responsive genes[264]. Therefore, there is a potential association of TOP2B activity on transcriptionally active sites with NCOR1-mediated IMiD sensitivity. Since NCOR1 is involved in transcriptional repression, it is possible that NCOR1 co-represses loci where IKZF1 and IKZF3 also suppress gene transcription. Loss of *NCOR1* could also determine increased

transcription of genes that can overcome inhibition of the *IKZF1/3-IRF4-MYC* axis. The mechanism by which loss of *NCOR1* confers resistance to IMiDs is still obscure and will require further investigation. Also, both NCOR1 and TOP2B could potentially cooperate in regulating the transcriptional response upon IMiD exposure. Although in MM.1Sres cells the CRBN ubiquitin-ligase machinery is impaired and degradation of neosubstrates attenuated, it is possible that a prolonged treatment (more than 7-10 days) is enough to significantly deplete IKZF1/3 within cells, and to produce a detrimental phenotype in the context of TOP2B deletion. Arguably, MM.1Sres cells would have enough time to adapt and undergo epigenetic commitment with a reduced IKZF1/3 degradation ratio and residual protein levels, which would explain the reason why CRISPR deletion – i.e. a relatively rapid and theoretically total loss - of IKZF1 and IKZF3 is still capable of significantly impairing cell growth. In fact, the rate at which neosubstrates are degraded has been correlated to the degree of IMiD sensitivity[251]. Characterisation of loci regulated by TOP2B could be studied by defining actively transcribed genes upon IMiD treatment via RNA Pol II, TOP2B, NCOR1 and IKZF1/3 ChIP-seq. Moreover, the study of the transcriptional landscape (RNA-seq and SLAM-seq) in *TOP2B* KO cells and that of cells with acute loss of TOP2B (e.g. with a TOP2B-AID degron system) could be extremely informative to understand which genes are mostly affected by loss of TOP2B in presence and absence of an IMiD, without affecting TOP2A expression. These approaches would help understanding the role of TOP2B in the transcriptional response to IMiDs.

3.3.5 TOP2 inhibition as potentially novel MM therapeutic approach in combination with IMiDs

Finally, a therapeutic angle for TOP2B loss in combination with IMiDs was defined using a TOP2 poison, etoposide phosphate, and then a TOP2B degrader, dexrazoxane. Treatment with ETO induced DNA damage and strong stabilisation of p53 in both MM.1S and MM.1Sres cells. In MM.1Sres cells, baseline levels and stabilisation upon ETO treatment was higher than that documented in MM.1S cells. Phosphorylation of histone protein H2AX (a marker of DNA damage) in cells treated with ETO and LEN demonstrated that LEN does not appear to induce DNA damage. Subsequently, *in vitro* experiment displayed combinatorial activity of ETO with LEN in MM.1S cells but not in MM.1Sres cells.

Dexrazoxane (DXZ) is a compound used in the clinic to counteract the toxicity of doxorubicin at a cardiac level[302]. In this study, DXZ was employed to induce acute loss of TOP2B to test whether DXZ phenocopies *TOP2B* deletion in IMiD-treated cells. DXZ promoted degradation of TOP2B for

up to 72 hours. Analogies in the structure of DXZ and the glutarimide moiety of IMiDs (which binds the thalidomide binding pocket of CRBN CTD) were found, but DXZ did not seem to have an effect on IKZF3 degradation in co-treatment with IMiDs, neither IMiDs seemed to induce TOP2B degradation. Furthermore, deletion of *CRBN* did not impair activity of DXZ, excluding CRBN as E3 ligase required for TOP2B turnover. DXZ displayed anti-MM action alone across several IMiD-sensitive and IMiD-resistance (acquired and *de novo*) cell lines. Cell cycle profiling of DXZ alone and in combination with LEN suggests that DXZ is likely to induce apoptosis following blockage of cells in cytokinesis. In MM.1S cells, DXZ showed strong synergy with LEN. Study of the IKZF1/3-IRF4-MYC axis indicates that DXZ downregulates IKZF1/3, IRF4 and MYC in MM.1Sres cells, and IKZF1/3 and IRF4 but not MYC in MM1.S cells. Combinatorial LEN/DXZ action was also observed in OPM2 and at a lower magnitude in *de novo* IMiD-resistant RPMI-8226 and JJN3 cells.

3.3.5.1 IMiD treatment and the perturbation of DNA homeostasis: still an open question

Etoposide phosphate is a DNA damaging agent. Normally, TOP2 unwinds DNA during essential processes (e.g. replication, transcription) by producing a DSB and repairing it when the double helix is relaxed[262,263]. ETO mechanism of action consists of trapping of TOP2 in its covalent complex with DNA (TOP2cc) with blockage of TOP2-dependent DNA re-ligation. Thus, the DSB is not repaired with subsequent p53 activation and apoptosis ensues. Since CUL4-DDB1-RBX1 and the COP9 signalosome are essential in DNA repair, it was hypothesised that, mechanistically, loss or inhibition of TOP2B could render DNA repair defective thus rescuing IMiD toxicity. However, data obtained did not validate this hypothesis, as LEN did not induce increase of DNA damage in combination with ETO and ultimately does not potentiate its effect in MM.1Sres cells.

Prolonged LEN exposure has increased baseline p53 levels, and exposure to ETO demonstrated that stabilisation of p53 is higher in MM.1Sres cells as compared to MM.1S cells. It has been demonstrated that IMiDs are capable of stabilizing MDM2 with consequent p53 reduction in Namalwa cells, a model of Burkitt Lymphoma with loss of 5q[303], which seems in contrast with the enrichment of p53-related genes obtained by computing GSEA on RNA-sequencing data. In this case, the model adopted might account for differences. A recent paper also showed that CRBN indirectly modulates DNA damage response via disruption of the crosstalk between p53 and proteins of the BCL2 family in mouse fibroblasts and neurons[304]. In this paper, the authors demonstrated that treatment with etoposide and cisplatin induces significantly more cell death when *Crbn* is deleted as compared to wild-type cells, and that *Crbn* KO mice mortality rate is

higher following etoposide challenge. However, these data were obtained in non-tumour models. In MM.1Sres cells, treatment with the IMiD in combination with the TOP2 poison etoposide did not phenocopy the synergy between LEN or POM and deletion of *TOP2B*. Further study with regards of DNA damage and repair in the context of IMiD treatment were not pursued. However, the baseline increment of p53 levels documented by western blotting and the enrichment of p53-related gene sets again support the observation that MM.1Sres cells might be characterised by higher genomic instability. Importantly, it has been reported that patients with prolonged lenalidomide exposure and DNA damaging agents (oral melphalan specifically) have a higher risk of developing secondary neoplasia as compared to patients receiving lenalidomide or melphalan as single agent, which is also indicative of a potential genotoxic activity of LEN[305]. Such potential side effect of IMiD treatment should be kept into consideration for future studies.

3.3.5.2 Considerations upon employment of dexrazoxane in the treatment of MM

DXZ iron-chelating properties are thought to be the main reason of its beneficial effect in co-treatment with anthracyclines, but it has been proposed that inactivation of TOP2 and degradation of TOP2B could have a protective role, as well[254]. In this work, DXZ-induced TOP2B degradation was explored. Increasing levels of TOP2B over from 24 to 72 hours indicated that DXZ could be subjected to intracellular metabolism or increased expression as a compensatory mechanism following acute degradation. Although some authors demonstrated that metabolism of DXZ to ADR-925 occurs via dihydropyrimidase and dihydroorotase in hepatocytes and cardiomyocytes[306], Jirkovsky and colleagues provide with evidence that DXZ can be rapidly metabolised to its iron-chelating isoform ADR-925 by spontaneous hydrolysis in rat cardiomyocytes *in vitro*[282]. *In vivo* drug metabolism studies have revealed that DXZ drug metabolism also occurs in cardiomyocytes and hepatocytes. However, the liver seems to account for the majority of its transformation into ADR-925. This active isoform is then eliminated via urinary excretion[282]. It is not clear whether DXZ or ADR-925 promote TOP2B degradation. The sustained loss of TOP2B along 72 hours would suggest that DXZ is likely responsible for TOP2B proteasomal-dependent degradation. As the kinetics of conversion to ADR-925 suggests, DXZ concentration diminishes over time, correlating with the increase of TOP2B protein observed along the time course for TOP2B degradation, whilst that of ADR-925 raises proportionally. In terms of potential toxicity in a clinical context, it has been reported that the mean peak plasma concentration after 15 minutes post 500mg/m^2 DXZ infusion is 36.5 mg/L, which corresponds to 135µM, a much higher concentration than those showing anti-MM activity

in vitro (5 to 20μM). Since DXZ exerts anti-proliferative and pro-apoptotic action as a single agent, inhibition of TOP2A is probably the underlying mechanism of action as TOP2B is not an essential gene and its deletion does not affect cell proliferation. Moreover, treatment with DXZ increases cells in hyperdiploidy, suggesting failure of cytokinesis, a process in which TOP2A is implicated. The combinatorial activity with LEN in IMiD sensitive cells could be the result of both TOP2A inhibition and the synergy between TOP2B loss and LEN. In the context of MM.1Sres cells, however, a more prolonged TOP2B loss would be required, which would be technically impossible, as treatment longer than 7 days with DXZ largely impact cell survival with abrogation of a dynamic range required for observing synergy.

3.3.6 Concluding remarks

Overall, this work provides interesting insights into IMiD biology, by partially confirming previously published data and by defining TOP2B as a potential vulnerability in the context of IMiD resistance. Although DXZ seems to be active as a single agent, the lack of preclinical and clinical data in cancer does not make it suitable for cancer therapy as yet. Further pre-clinical *in vivo* investigation is needed to test drug tolerability and sustainability of regimens with repeated dosing and assessment of toxicity (e.g. haematological, gastrointestinal, etc). Efficacy against MM should be demonstrated with DXZ as a single agent and in combination with IMiDs. Response to DXZ and LEN/DXZ of MM xenograft in irradiated Crbn wild-type and $Crbn^{I391V}$ knock-in mice would be the ideal experimental setting for exploring the impact of an IMiD-responsive microenvironment. In the case of successful outcome of pre-clinical experimentation, clinical testing of DXZ in MM patients would be required, with strict monitoring of pharmacokinetics, toxicity profile and response to therapy at least in terms of overall survival. Collectively, these data represent important information for dealing with the clinical management of the drug, especially if considering a hypothetical combination therapy of IMiDs and DXZ. The clinical use of DXZ, if beneficial, could represent an interesting advance in the treatment of MM or other blood malignancies. These preliminary data could also serve as a rationale for the development of more specific and more potent TOP2A and TOP2B inhibitors.

Addendum to chapter 3: publication in Haematologica

Whole genome CRISPR screening identifies TOP2B as a potential target for IMiD sensitization in multiple myeloma

Authors

Matteo Costacurta[1,2], Stephin J Vervoort[1,2], Simon J Hogg[1,2], Benjamin P Martin[1,2], Ricky W Johnstone[1,2*], Jake Shortt[1,2,3,4*]

Affiliations

[1]Translational Haematology Program, Peter MacCallum Cancer Centre, Melbourne. [2]Sir Peter MacCallum Department of Oncology, The University of Melbourne, Parkville. [3]Monash Haematology, Monash Health, Clayton. [4]Blood Cancer Therapeutics Laboratory, School of Clinical Sciences at Monash Health, Monash University, Clayton, Australia. *equal contributions

Correspondance : Ricky W. Johnstone (ricky.johnstone@petermac.org)

: Jake Shortt (jake.shortt@monash.edu)

Author contributions

M.C. conducted experimental work, planned experiments, analyzed the data and wrote the manuscript. S.V. helped with experimental planning, analyzed sequencing data and contributed with manuscript writing. S.H. analyzed sequencing data. B.M. helped with screening experiments. R.J. and J.S. supervised the project, planned experiments and wrote the manuscript.

Acknowledgments

We acknowledge the FACS facility and the Molecular Genomic Core at the Peter MacCallum Cancer Centre for contributing to this work.

Funding

JS is supported by an Australian Medical Research Future Fund Next Generation Clinician Researcher Fellowship. This research was funded by NHMRC Project Grant 1127387. R.W.J was supported by the Cancer Council Victoria, National Health and Medical Research Council of Australia (NHMRC), and The Kids' Cancer Project. The Victorian Centre for Functional Gnomics, the Molecular Genomics Core and the Flow Cytometry Core Facilities at the Peter MacCallum Cancer Center provided excellent technical support. The Peter MacCallum Foundation and

Australian Cancer Research Foundation provide generous support for equipment and core facilities.

Data availability

To be provided upon request

Conflict of interests

JS: advisory boards and received speaker's fees from Celgene and BMS outside of the published work. The Johnstone laboratory receives funding support from Roche, BMS, Astra Zeneca, and MecRx. RWJ is a paid scientific consultant and shareholder in MecRx.

Thalidomide analogues (IMiDs), such as lenalidomide (LEN) and pomalidomide (POM) have significantly improved survival in patients with multiple myeloma (MM)[304]. However, many patients relapse despite continued IMiD exposure, and IMiD resistance remains a significant clinical problem. IMiDs engage Cereblon (CRBN), an adaptor for the CUL4A-DDB1-RBX1 E3 ligase complex to promote proteasome-dependent degradation of neosubstrates IKZF1 (Ikaros) and IKZF3 (Aiolos). The degradation of these transcription factors is both directly toxic to MM cells and immunostimulatory to T-cells[305]. Interrogation of the molecular events driving IMiD-mediated engagement of CRBN neosubstrates has greatly improved our mechanistic understanding of these agents. Acquired or intrinsic IMiD-resistance may occur through several mechanisms including loss of expression of CRBN and/or associated E3 ligase factors[90]. However, deeper insight into IMiD-resistance mechanisms may inform novel therapeutic approaches. Here, genome-wide CRISPR-Cas9 screening was employed to characterize resistance mechanisms and resensitization factors in isogenic IMiD-sensitive and -resistant MM lines. Loss of DNA Topoisomerase II beta (TOP2B) resensitized IMiD-refractory cells to IMiDs and its inhibition with the cardioprotective drug, dexrazoxane (DXZ), potentiated IMiD activity. Collectively, these findings identify TOP2B as a potential new therapeutic target in MM.

LEN-resistant MM1.S (MM.1Sres) cells were previously derived by culturing MM.1S cells in presence of increasing doses of LEN[7]. MM.1Sres cells displayed no significant increase in cell death upon prolonged (7 days) LEN exposure, while isogenic MM.1S cells were sensitive to LEN-induced cell death (Figure 1A). MM.1Sres cells also exhibited resistance to the anti-proliferative effects of LEN and POM as demonstrated by CellTrace Violet (CTV) labelling (Figure 1B). As previously reported[306], MM.1Sres cells showed reduced CRBN expression and reduced IKZF3 degradation upon IMiD treatment as compared to MM.1S (Figure 1C).

To determine genes and pathways required for IMiD anti-myeloma activity in MM.1S cells, a genome-scale CRISPR knockout screen was performed in MM.1S-Cas9 cells treated with LEN, POM or DMSO (Figure 1D). Genetic dependencies of MM.1S-Cas9 cells were identified by loss-of-representation of short guide RNA (sgRNA) in DMSO-treated cells and identified genes such as *MYC, IRF4, IKZF1* and *IKZF3* (Figure *S1A*). MM.1S-Cas9 cells were dependent on essential processes such as RNA metabolism and DNA-damage related pathways (*Figure S1B-C*). Deletion of CRBN and members of the COP9 signalosome (CSN), a 9-protein complex involved in protein turnover regulation, were the most significantly enriched sgRNAs in the presence of continued IMiD exposure (Figure 1E, *S1D-E*), validating previously published data[307]. Gene ontology (GO)

analysis and protein-protein interaction (PPI) networking revealed that CSN may also modulate CUL4-DDB1 functions in response to DNA damage (*Figure S1F-G*). Notably, some sgRNAs (*NCOR1*, *EDC4*, *SCAP*, *UBE2G1*, *MBTPS1/2*) conferred selective resistance to LEN but not POM (Figure 1E), reflecting either a difference of potency and/or discrepant substrate specificity between the two IMiDs.

The identification of genes that when deleted restore IMiD-sensitivity in MM.1Sres cells was achieved by a loss-of-representation CRISPR screen in 21-day LEN and POM-treated MM.1Sres-Cas9 cells relative to DMSO control (Figure 2A). The dependencies of DMSO-treated MM.1Sres-Cas9 cells partially overlapped and correlated with those of MM.1S-Cas9 cells, suggesting that acquired IMiD-resistance did not globally alter gene dependencies in these cells (*Figure S2A-F*). To identify selective resentitisation mechanisms in the presence of IMIDs, the DMSO endpoint was compared with the matched timepoint in IMiD-treated MM.1Sres-Cas9 cells. This revealed that deletion of *ATXN7, TOP2B*, *MIER3*, *YPEL5*, *MAEA* and *MED13L* sensitized MM.1Sres cells to both LEN and POM (Figure 2B-C). *ATXN7* is part of the deubiquitination module of STAGA, a multisubunit entity involved in transcriptional regulation and DNA repair[308]. *MED13L* and *MIER3* also modulate transcription[127,309–311]. Interestingly, *YPEL5* and *MAEA* cooperate in an E3 ligase complex targeting gluconeogenesis enzymes[100]. However, *TOP2B* was selected for further study due to its potential tractability as a drug target. *TOP2B* is an enzyme which resolves topological DNA constraints during replication, transcription and repair[90]. To validate that *TOB2B* loss resensitises to IMiDs, competitive proliferation assays were performed in the presence and absence of LEN and POM (Figure 2D). MM.1Sres-Cas9 cells expressing two independent *TOP2B* sgRNAs with a GFP reporter were mixed at a 1:1 ratio with MM.1Sres-Cas9 cells expressing a non-targeting sgRNA with a BFP reporter *(Figure 2D-E, Figure S2G).* Consistent with the CRISPR-screen results, a competitive loss of GFP^+ relative to BFP^+ cells was observed following IMiD treatment (Figure 2E) confirming that *TOP2B* deletion confers IMiD-sensitivity in MM.1Sres-Cas9 cells. Analogous assays in MM.1S-Cas9 cells revealed that *TOP2B* loss further sensitized these cells to the anti-tumour effects of IMiDs (Figure 2F), indicating that *TOP2B* deletion enhances IMiD activity in both IMiD-naïve and resistant contexts. *TOP2B* deletion had little or no effect on CRBN expression or subsequent IKZF3 degradation following IMiD treatment (*Figure S3A-B*). MYC levels appeared to be modestly more downregulated in IMiD-treated MM.1Sres-Cas9 compared to MM.1S-Cas9 cells while the IMiD-induced downregulation of IRF4 was similar in MM.1Sres-Cas9 compared to MM.1S-Cas9 cells (*Figure S3C*). These observations indicate that

the resensitization to IMiD treatment following deletion of *TOP2B* likely does not depend on further effects on the IKZF1/3-IRF4-MYC axis.

Having discovered the IMiD-sensitizing effects of genetic *TOP2B* depletion in MM.1Sres-Cas9 cells, orthogonal assays using DXZ, a chemical inhibitor of TOP2 that induces selective degradation of TOP2B protein, were used to validate this observation. DXZ also posseses iron-chelating activity and is FDA-approved for prevention of anthracycline-induced cardiotoxicity[312]. To investigate whether DXZ-mediated TOP2B degradation would phenocopy genetic deletion, MM.1Sres and MM.1S cells were treated with DXZ alone or in combination with LEN. TOP2B degradation in DXZ-treated MM.1S cells was evident 24hr after drug exposure and remained low in treated cells for up to 72hrs (Figure 3A) at clinically relevant concentrations[313]. Cell cycle analysis demonstrated that concentrations of DXZ sufficient to induce TOP2B degradation were cytostatic in MM.1S and MM.1Sres cells, with accumulation of cells in SubG1 and >2N, suggesting apoptosis-induction and failure of cytokinesis (Figure 3B, *S3D-F*). Combinatorial effects of LEN and DXZ were observed in MM.1S and MM.1Sres cells with DXZ alone inducing cytostasis in MM.1Sres cells (Figure 3C-D). Similar to the effects observed following TOP2B deletion, DXZ did not modulate CRBN expression or alter IKZF3 degradation (*Figure S3G*). However, an effect of the LEN and DXZ combination on cMYC, IKZF1, IKZF3 and IRF4 expression (Figure 3E) was evident. These findings may indicate that the effects of LEN and DXZ converge on the IRF4-MYC axis in MM.1Sres cells downstream or in parallel to canonical CRBN-neosubstrate interactions. Subsequently, DXZ combination treatments were performed in IMiD-sensitive OPM2 cells and IMiD-resistant RPMI-8226 and JJN3 MM cell lines (Figure 3D). In OPM2 cells, DXZ and LEN alone induced robust growth inhibition with a combinatorial effect observed following treatment with both agents (Figure 3F-G). DXZ induced death of RPMI-8226 and JJN3 cells, with mild additivity in presence of LEN (Figure 3F,H-I).

CRISPR-based dissection of the genetic dependencies of MM.1S cells provided additional insight into IMiD biology and acquired IMiD resistance. Consistent with the initial description of MM.1Sres[314], downregulation of CRBN expression and attenuation of neosubstrate degradation appears to be the major mechanism of IMiD resistance in these cells. Synthetic generation of IMiD resistance using gene deletion in MM.1S cells recapitulated prior studies identifying CRBN and elements of the CSN[234,235]. Gene ontology analysis of these hits revealed their importance in transcription-coupled nucleotide excision repair (TC-NER). Moreover, CUL4 and DDB1 have been demonstrated to participate with CSN in DNA repair pathways such as NER and TC-NER[90]. IMiD-sensitivity in MM.1Sres cells was rescued by knockout of *TOP2B*, a gene that modulates

DNA repair, chromatin stability and gene expression[315]. However, LEN did not induce a DNA damage response or synergise with etoposide in MM.1Sres cells, suggesting that DNA damage induction is not the primary re-sensitization mechanism (*Figure S3H-I*). Genetic deletion of *TOP2B* was not lethal to MM.1Sres cells, however these cells were sensitized to IMiD-induced death. This phenotype seemed to be independent of an increase in CRBN activity or expression changes within the IKZF1/3-IRF4-MYC axis. The biology underpinning re-sensitization of MM.1Sres cells to IMiDs through loss of TOP2B remains to be defined.

DXZ had demonstrable anti-MM properties and additional activity in combination with LEN, especially in IMiD-sensitive cells. Since *TOP2B* deletion did not induce growth inhibition, the single-agent activity of by DXZ may depend upon TOP2A inhibition rather than TOP2B degradation or through other effects. Deletion or depletion of TOP2A can have deleterious effects on the growth and/or survival of cancer cells (*Figure S3J*) but we do not have evidence clearly demonstrating that the anti-MM activity of DXZ is through effects on TOP2A. Given that DXZ did not appear to demonstrably impinge on the IKZF1/3-IRF4-MYC axis, exactly how DXZ confers anti-MM activity, either alone or in combination with IMiDs, remains unknown. The IC_{50} of DXZ across the MM lines tested spanned from 5 to 20mM (data not shown), which is significantly lower than peak plasma concentration reached after a cardioprotective 500mg/m^2 dose (36.5mg/mL or 135mM)[316–318]. This suggests that DXZ could be repurposed as a TOP2-targeting anti-MM agent as part of a combinatorial approach, however its posology is not well suited to recurrent or chronic administration. We are unaware of any other selective small-molecule TOP2B inhibitors. Greater understanding of the structure-activity relationship between DXZ and TOP2B may allow the rational development of related chemotypes for drug therapy. Further investigation of these mechanisms by which TOP2B inhibition leads to anti-MM activity could reveal alternative pathways to IMiD potentiation.

References

1. Kumar SK, Rajkumar SV, Dispenzieri A, et al. Improved survival in multiple myeloma and the impact of novel therapies. Blood 2008;111(5):2516–2520.
2. Lu G, Middleton RE, Sun H, et al. The Myeloma Drug Lenalidomide Promotes the Cereblon-Dependent Destruction of Ikaros Proteins. Science 2014;343(6168):305–309.
3. Licht JD, Shortt J, Johnstone R. From Anecdote to Targeted Therapy: The Curious Case of Thalidomide in Multiple Myeloma. Cancer Cell 2014;25(1):9–11.
4. Krönke J, Udeshi ND, Narla A, et al. Lenalidomide Causes Selective Degradation of IKZF1 and IKZF3 in Multiple Myeloma Cells. Science 2014;343(6168):301–305.
5. Liu J, Song T, Zhou W, et al. A genome-scale CRISPR-Cas9 screening in myeloma cells identifies regulators of immunomodulatory drug sensitivity. Leukemia 2019;33(1):171–180.
6. Sievers QL, Gasser JA, Cowley GS, Fischer ES, Ebert BL. Genome-wide screen identifies cullin-RING ligase machinery required for lenalidomide-dependent CRL4CRBN activity. Blood 2018;132(12):1293–1303.
7. Zhu YX, Braggio E, Shi C-X, et al. Cereblon expression is required for the antimyeloma activity of lenalidomide and pomalidomide. Blood 2011;118(18):4771–4779.
8. Ramachandran S, Haddad D, Li C, et al. The SAGA Deubiquitination Module Promotes DNA Repair and Class Switch Recombination through ATM and DNAPK-Mediated γH2AX Formation. Cell Reports 2016;15(7):1554–1565.
9. Poss ZC, Ebmeier CC, Taatjes DJ. The Mediator complex and transcription regulation. *Critical Reviews in Biochemistry and Molecular Biology* 2013;48(6):575–608.
10. Derwish R, Paterno GD, Gillespie LL. Differential HDAC1 and 2 Recruitment by Members of the MIER Family. PLOS ONE 2017;12(1):e0169338.
11. Lampert F, Stafa D, Goga A, et al. The multi-subunit GID/CTLH E3 ligase promotes proliferation and targets the transcription factor Hbp1 for degradation. eLife 2018;7e35528.
12. Chen SH, Chan N-L, Hsieh T. New Mechanistic and Functional Insights into DNA Topoisomerases. Biochemistry 2013;82(1):139–170.
13. Lyu YL, Kerrigan JE, Lin C-P, et al. Topoisomerase II Mediated DNA Double-Strand Breaks: Implications in Doxorubicin Cardiotoxicity and Prevention by Dexrazoxane. Cancer Research 2007;67(18):8839–8846.

14. Brier ME, Gaylor SK, McGovren JP, Glue P, Fang A, Aronoff GR. Pharmacokinetics of Dexrazoxane in Subjects With Impaired Kidney Function. The Journal of Clinical Pharmacology 2011;51(5):731–738.
15. Fischer ES, Scrima A, Böhm K, et al. The Molecular Basis of CRL4DDB2/CSA Ubiquitin Ligase Architecture, Targeting, and Activation. Cell 2011;147(5):1024–1039.

Figure Legends

Figure 1. Resistance to LEN and POM is mediated by loss of CRBN and the COP9 signalosome.
(A) Bar plot representing the percentage of Propidium Iodide negative (PI^-, viable) MM.1S and MM.1Sres cells treated with DMSO or LEN (2μM) for 7 days. Results are aggregated from 3 independent experiments with 2 technical replicates per experiment. Error bars represents the mean ± SEM of the 3 biological replicates with their respective technical replicates. * $p < 0.0001$ (B) CellTrace™ Violet/Propidium Iodide proliferation assay comparing proliferation of MM.1S and MM.1Sres cells in presence of LEN (2μM) or POM (500nM) (day 7 timepoint) in comparison to vehicle (DMSO). Results are representative of 3 independent experiments (C) Immunoblot of IKZF3 and CRBN levels in DMSO-, LEN (2μM) - or POM (500nM)-treated MM.1S and MM.1Sres cells for 16 hours (blots are representative of 3 independent experiments). (D) Schematic representation of the CRISPR genome-scale resistance screen workflow. ~500e6 MM.1Sres-Cas9 cells were transduced with the Brunello genome-wide library, selected with puromycin and then treated with DMSO, LEN (2μM) or POM (500nM) for ~8 weeks. gDNA was extracted for library prep and Illumina sequencing. (E) Scatter plots showing hits overlapping between LEN and POM that are significant for adjusted p-value<0.05 and hits unique to LEN-treated cells significant for adjusted p-value<0.05.

Figure 2. *TOP2B* deletion synergizes with IMiDs in MM.1S and MM.1Sres cells.

(A) Schematic representation of the CRISPR genome-scale dropout screen workflow. ~500e6 MM.1Sres-Cas9 cells were transduced with the Brunello genome-wide library, selected with puromycin and then treated with DMSO, LEN (2μM) or POM (500nM) for 3 weeks. gDNA was extracted for library prep and Illumina sequencing. (B) Scatter plot overlapping the -log10(p-value) of negatively enriched guides in MM.1Sres-Cas9 cells treated with LEN and POM at the end of the screen. (C) Normalized counts (in log2) at the end of the screen (T-End) of sgRNAs specific for *TOP2B* in MM.1Sres. In the DMSO condition, the counts in T-End are compared to a timepoint zero (T-0) reference. In the LEN and POM conditions, the counts for sg*TOP2B* in T-End are plotted relatively to the average counts in the DMSO T-End condition. (D) Schematic representation of the competitive proliferation assay workflow. MM.1S- or MM.1Sres-Cas9 Scramble-BFP cells were grown in competition with MM.1Sres-Cas9 sg*TOP2B*-GFP at a 1:1 ratio in DMSO, LEN (2μM) or POM (500nM) to replicate the data observed in the genome-wide dropout screen. (E) Representative experiment of three independent replicates showing the change in percentage of MM.1Sres-Cas9 Scramble- or sgTOP2B-GFP^+ cells grown in competition with MM.1Sres-Cas9 Scramble-BFP^+ cells treated with DMSO, LEN (2μM) or POM (500nM) for

21 days. Each dot with relative error bars represents the mean ± SD of values from two technical replicates. (F) Representative experiment of three independent replicates showing the change in percentage of MM.1S-Cas9 Scramble- or sgTOP2B-GFP$^+$ cells grown in competition with MM.1S-Cas9 Scramble-BFP$^+$ cells (at a 1:1 ratio) treated with DMSO, LEN (2μM) or POM (500nM) for 10 days. Each dot with relative error bars represents the mean ± SD of values from two technical replicates.

Figure 3. TOP2 inhibitor dexrazoxane displays anti-myeloma properties and combinatorial activity with lenalidomide.

(A) Immunoblot showing TOP2B expression in MM.1S cells treated with DMSO or DXZ (20uM or 50uM) across 24, 48 and 72 hours. Tubulin expression is provided as a loading control. The experiment is representative of three biological replicates. (B) Bar graphs demonstrating Nicoletti cell cycle profiling of MM.1S and MM1Sres cells exposed to DMSO, LEN (2μM), DXZ (20μM) or combined LEN/DXZ (combo). The plot represents an aggregate of three independent experiments with three technical replicates each. Error bars represents mean+SEM of n = 3 independent experiments. v=significant vs vehicle (DMSO), l=significant vs LEN, d=significant vs DXZ ($p<0.05$ or less). (C) Heatmaps representing the variation of Zero Interaction Potency (ZIP) synergy score in MM.1S and MM.1Sres cells treated with increasing concentration of LEN and DXZ in combination. The average percentage of PI negative cells (viable) in each drug combination of three independent experiments was employed to compute synergy. The R package synergyfinder v2.2.4 was employed to perform the analysis. (D) Average viable cell count at 3 and 7 days for MM.1S and MM.1Sres treated with DMSO, LEN (2μM), DXZ (5μM or 20μM depending on the cell line) or combined LEN/DXZ (Combo). (E) Immunoblot showing expression of IKZF1, IKZF3 after 24h of treatment with DMSO, 2μM LEN, 20μM DXZ or combined treatment and expression of IRF4 and MYC after 72h of treatment in the same conditions. HSP90 is provided as loading control. The experiment is representative of three biological replicates. (F) Viable cell count at 3 and 7 days of OPM2, RPMI-8226 and JJN3 cells treated with DMSO, LEN (2μM), DXZ (20μM) or Combo. (G) Percentage of PI negative (viable) OPM2 cells treated with DMSO, LEN (2μM), DXZ (20μM) or Combo and assessed by flow cytometry. (H) Percentage of PI negative (viable) RPMI-8226 cells treated with DMSO, LEN (2μM), DXZ (5uM) or Combo and assessed by flow cytometry. (I) Percentage of PI negative (viable) JJN3 cells treated with DMSO, LEN (2μM), DXZ (20μM) or Combo and assessed by flow cytometry. In (D, (F), (G), (H) and (I), error bars represents mean+SEM of n = 3 independent experiments. v= significant vs vehicle (DMSO), l=significant vs LEN, d=significant vs DXZ ($p<0.05$ or less).

Figure 1

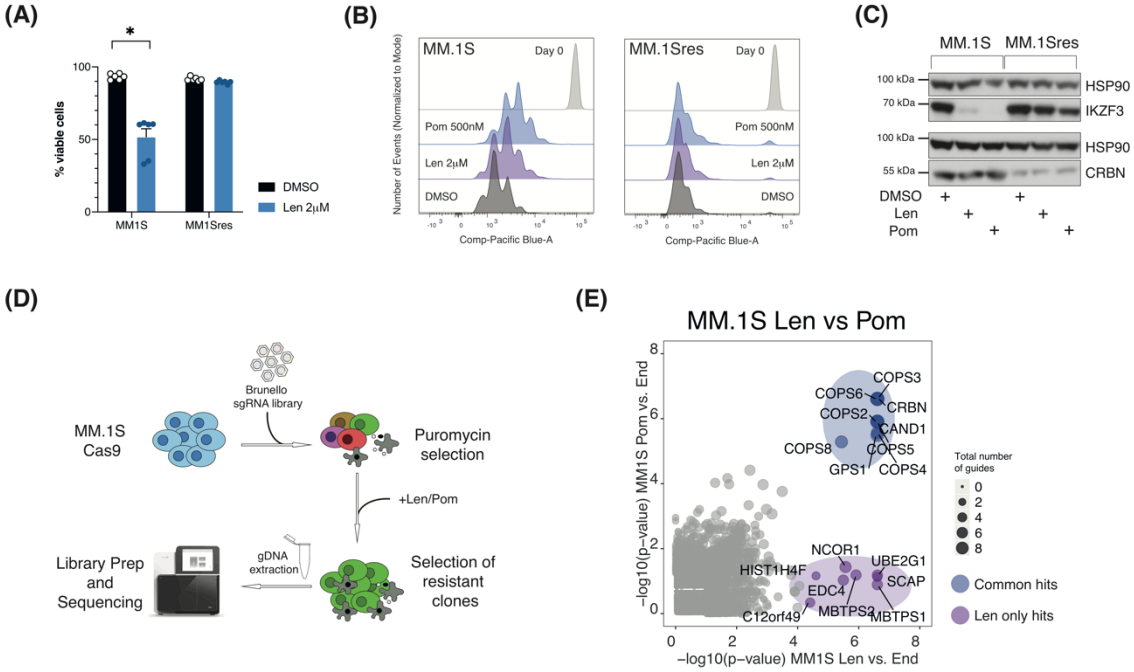

(A)
% viable cells
100
50
0
*
MM1S
MM1Sres
DMSO
Len 2μM
(B)
MM.1S
Day 0
Pom 500nM
Len 2μM
DMSO
MM.1Sres
Day 0
Pom 500nM
Len 2μM
DMSO
Number of Events (Normalized to Mode)
Comp-Pacific Blue-A
Comp-Pacific Blue-A
(C)
MM.1S
MM.1Sres
100 kDa
HSP90
70 kDa
IKZF3
100 kDa
HSP90
55 kDa
CRBN
DMSO
Len
Pom
(D)
Brunello
sgRNA library
MM.1S
Cas9
Puromycin
selection
+Len/Pom
Selection of
resistant
clones
gDNA
extraction
Library Prep
and
Sequencing
(E)
MM.1S Len vs Pom
−log10(p−value) MM1S Pom vs. End
−log10(p−value) MM1S Len vs. End
COPS3
COPS6
CRBN
COPS2
CAND1
COPS8
COPS5
GPS1
COPS4
NCOR1
UBE2G1
HIST1H4F
SCAP
EDC4
MBTPS2
C12orf49
MBTPS1
Total number
of guides
0
2
4
6
8
Common hits
Len only hits

Figure 2

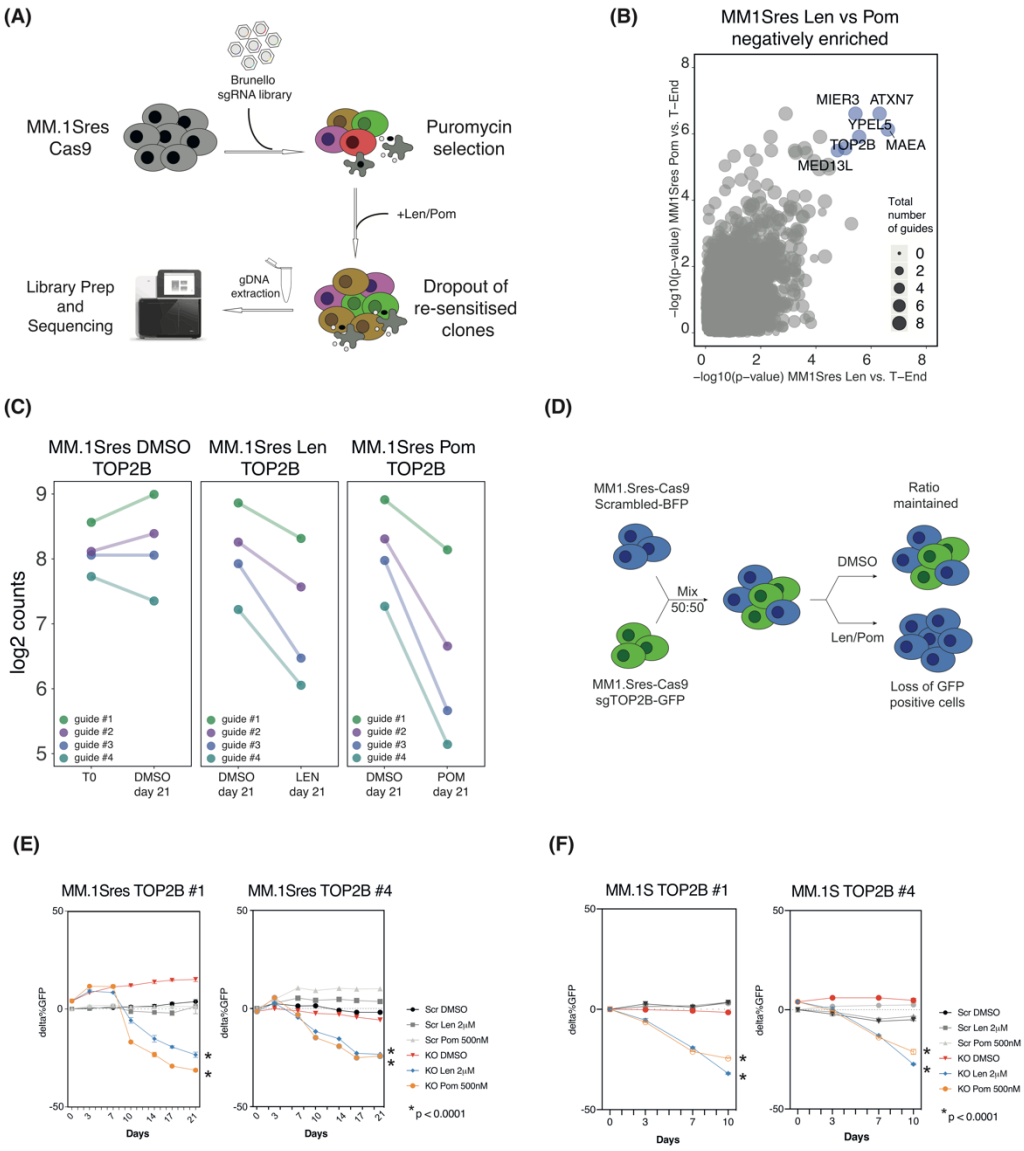
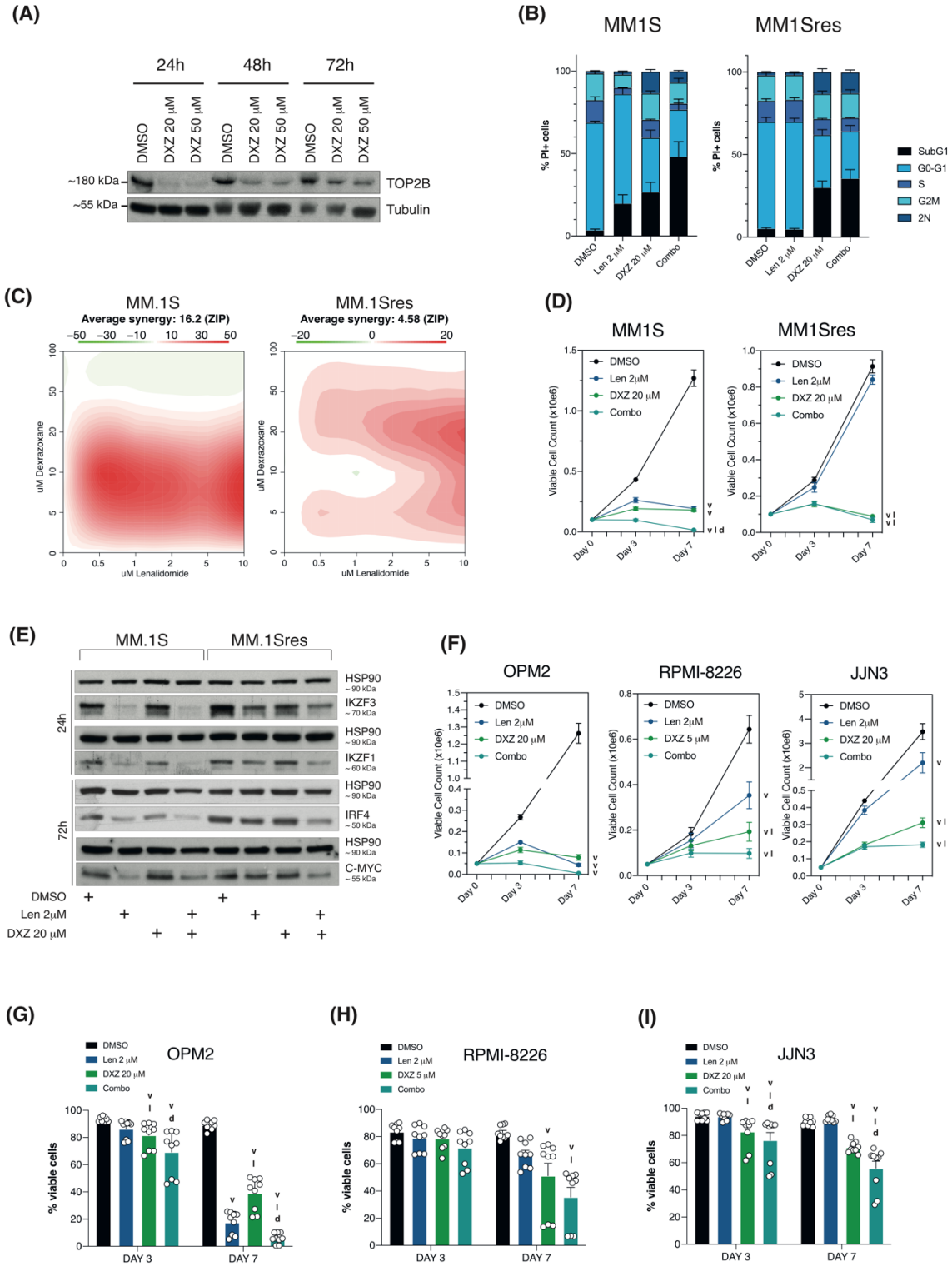

(A)
Brunello sgRNA library
MM.1Sres Cas9
Puromycin selection
+Len/Pom
Library Prep and Sequencing
gDNA extraction
Dropout of re-sensitised clones
(B)
MM1Sres Len vs Pom negatively enriched
MIER3
ATXN7
YPEL5
TOP2B
MAEA
MED13L
Total number of guides
−log10(p−value) MM1Sres Pom vs. T−End
−log10(p−value) MM1Sres Len vs. T−End
(C)
MM.1Sres DMSO TOP2B
MM.1Sres Len TOP2B
MM.1Sres Pom TOP2B
log2 counts
guide #1
guide #2
guide #3
guide #4
T0
DMSO day 21
LEN day 21
POM day 21
(D)
MM1.Sres-Cas9 Scrambled-BFP
Mix 50:50
MM1.Sres-Cas9 sgTOP2B-GFP
DMSO
Len/Pom
Ratio maintained
Loss of GFP positive cells
(E)
MM.1Sres TOP2B #1
MM.1Sres TOP2B #4
delta%GFP
Days
Scr DMSO
Scr Len 2μM
Scr Pom 500nM
KO DMSO
KO Len 2μM
KO Pom 500nM
*p < 0.0001
(F)
MM.1S TOP2B #1
MM.1S TOP2B #4
delta%GFP
Days
*p < 0.0001

Figure 3


(A)
24h
48h
72h
DMSO
DXZ 20 μM
DXZ 50 μM
~180 kDa
~55 kDa
TOP2B
Tubulin
(B)
MM1S
MM1Sres
% PI+ cells
SubG1
G0-G1
S
G2M
2N
(C)
MM.1S
MM.1Sres
Average synergy: 16.2 (ZIP)
Average synergy: 4.58 (ZIP)
uM Dexrazoxane
uM Lenalidomide
(D)
MM1S
MM1Sres
Viable Cell Count (x10e6)
DMSO
Len 2μM
DXZ 20 μM
Combo
Day 0
Day 3
Day 7
(E)
MM.1S
MM.1Sres
24h
72h
HSP90
~90 kDa
IKZF3
~70 kDa
IKZF1
~60 kDa
IRF4
~50 kDa
C-MYC
~55 kDa
DMSO
Len 2μM
DXZ 20 μM
(F)
OPM2
RPMI-8226
JJN3
DXZ 5 μM
(G)
OPM2
% viable cells
DAY 3
DAY 7
(H)
RPMI-8226
(I)
JJN3

Supplementary Figures

Figure S1. GO and PPI analysis of genome-wide CRISPR resistance KO screen

(A) Normalized read counts (in log2) at the end of the screen of sgRNAs specific for *IRF4*, *MYC*, *IKZF1* and *IKZF3* in DMSO-treated MM.1S-Cas9 cells at the end of the screen. The average counts in DMSO T-End are compared to the T-0 reference, respectively. (A) PPI network of MM.1S-Cas9 cells unique dependencies (metascape). (B) GO analysis of MM.1S unique dependencies. (C) PPI network of MM.1S-Cas9 cells unique dependencies (metascape). (D) Venn diagram of overlapping hits between our CRISPR resistance screen and those of Sievers et al. and Liu et al[5,6]. (E) Normalized read counts (in log2) at the end of the screen of sgRNAs targeting CRBN in MM.1S-Cas9 cells in the LEN and POM conditions. The average counts in LEN and POM T-End are compared to the DMSO T-End condition, respectively. (F) PPI network of hits in MM.1S-Cas9 cells treated with LEN at the end of the resistance screen (STRING). (G) GO analysis of hits in MM.1S-Cas9 cells treated with LEN at the end of the resistance screen (ToppFun). FDR values are represented as -log10.

Figure S2. GO and PPI analysis of MM.1S and MM.1Sres dependencies

(A) PPI network of MM.1Sres-Cas9 cells unique dependencies (metascape). (B) GO analysis of MM.1Sres-Cas9 cells unique dependencies. (C) Venn diagram of MM.1S-Cas9 and MM.1Sres-Cas9 cells dependencies (adj.p-value<0.05). (D) GO analysis of MM.1S-Cas9 and MM.1Sres-Cas9 cells mutual dependencies. (E) Scatter plot representing the log2 fold change of sgRNAs (dependencies) that are significant for adj.p-value<0.05. The regression line represents Pearson's correlation with relative Pearson's coefficient value R and the level of significance p. (F) Normalized read counts (in log2) at the end of the screen of sgRNAs specific for *IRF4*, *MYC*, *IKZF1* and *IKZF3* in DMSO-treated MM.1Sres-Cas9 cells at the end of the screen. The average counts in DMSO T-End are compared to the T-0 reference, respectively. (G) Immunoblot validating CRISPR-mediated *TOP2B* KO in MM.1S and MM.1Sres cells expressing Cas9.

Figure S3. Impact of genetic TOP2B deletion or TOP2 inhibition on the expression of CRBN, the IKZF1/3-IRF4-MYC axis and the cell cycle, upon IMiD treatment

(A) Immunoblot showing expression of TOP2B and CRBN in MM.1S-Cas9 and MM.1Sres Cas9 TOP2B KO cells relative to their controls (MM.1S-Cas9 and MM.1Sres Cas9 SCR BFP and SCR GFP cells). Actin is provided as loading control. (B) Western blot displaying degradation of IKZF3 in MM.1Sres-Cas9 TOP2B KO cells in comparison to MM.1Sres SCR GFP cells after 16h of treatment

with DMSO, 2µM LEN or 500nM POM. Actin is provided as loading control. (C) Immunoblot showing expression of IRF4 and MYC in MM.1Sres-Cas9 TOP2B KO cells in comparison to MM.1Sres SCR GFP cells after 72h of treatment with DMSO, 2µM LEN or 500nM POM. HSP90 is provided as loading control. (D) FACS histogram plots of PI^+ cells showing the effect on MM.1S and MM.1Sres cells of DMSO, LEN, DXZ and the combination treatment (histograms are representative of one of 3 independent experiment). (E) and (F) Bar plots showing proportion of Nicoletti-stained MM1S and MM1Sres cells, respectively, in SubG1, S-Phase and >2N (DNA content higher than that in G2M) as aggregate of three independent biological replicates with three technical replicates each. Error bars represent mean±SEM of n = 3 independent experiments. v=significant vs vehicle (DMSO), l=significant vs LEN, d=significant vs DXZ ($p < 0.05$ or less). (G) Immunoblot showing expression of TOP2B, IKZF3 and CRBN in MM.1S and MM.1Sres cells treated for 16 hours with DMSO, LEN (2µM), DXZ (20µM) or combined treatment for 16 hours. Actin is provided as loading control (H) Immunoblot displaying expression of gamma H2AX as marker of DNA damage in MM.1S and MM.1Sres cells treated with DMSO, LEN (2µM), etoposide (10µM) or combo for 16 hours. Tubulin is provided as loading control. (I) Bar plot representing percentage of viable cells (PI negative, by FACS analysis) of MM.1S and MM.1Sres exposed to prolonged treatment (7 days) with DMSO, LEN (2µM), etoposide (312nM) and Combo. (J) Dependency score (from the DepMap repository) of the genes *TOP2A* and *TOP2B* in MM cell lines (MM) and other tumours (Non-MM). A value of 0 represents a non-dependency, a value of -1 or below represents a dependency.

Figure S1

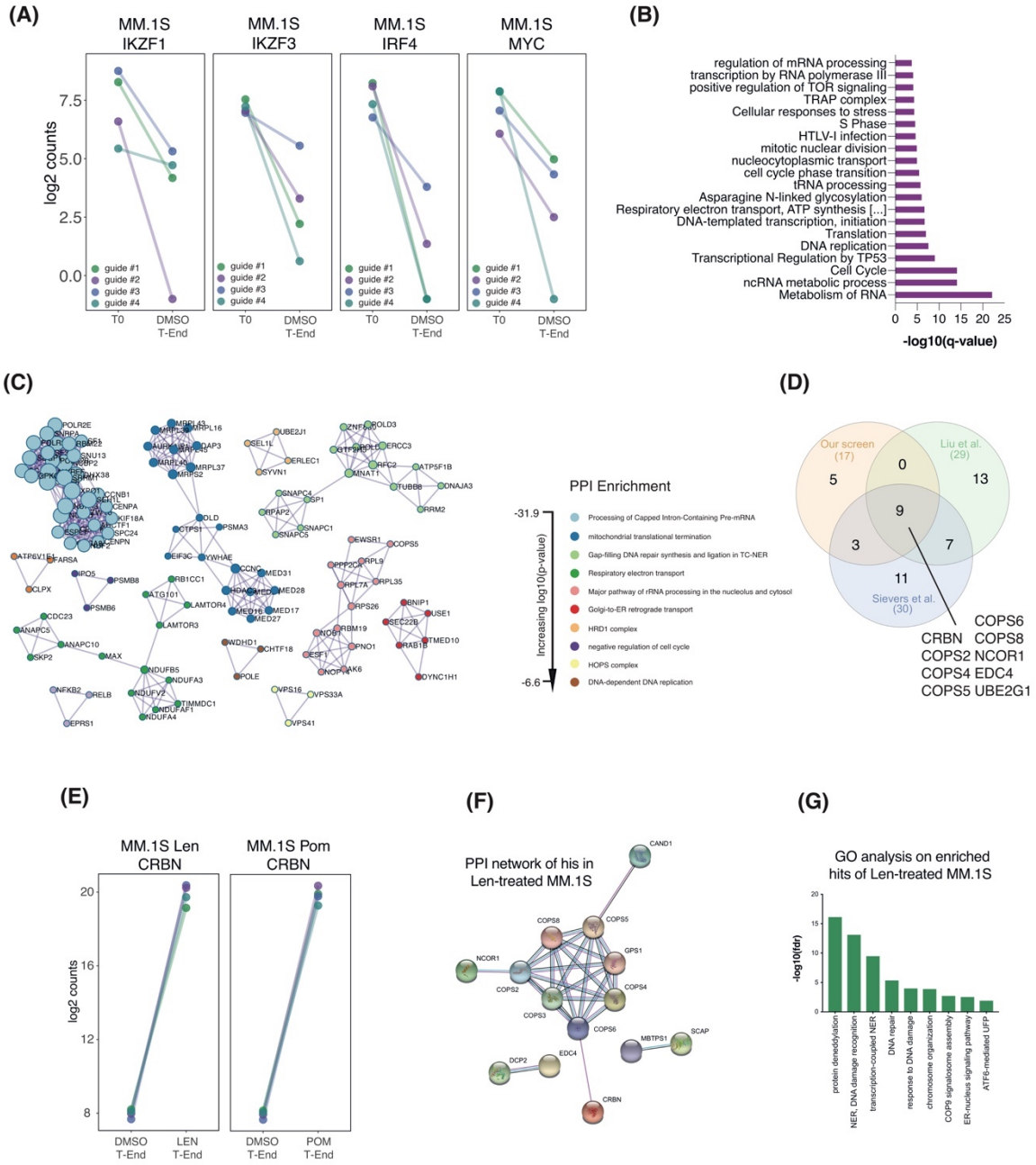

(A)
MM.1S IKZF1
MM.1S IKZF3
MM.1S IRF4
MM.1S MYC
log2 counts
guide #1
guide #2
guide #3
guide #4
T0
DMSO T-End
(B)
regulation of mRNA processing
transcription by RNA polymerase III
positive regulation of TOR signaling
TRAP complex
Cellular responses to stress
S Phase
HTLV-I infection
mitotic nuclear division
nucleocytoplasmic transport
cell cycle phase transition
tRNA processing
Asparagine N-linked glycosylation
Respiratory electron transport, ATP synthesis [...]
DNA-templated transcription, initiation
Translation
DNA replication
Transcriptional Regulation by TP53
Cell Cycle
ncRNA metabolic process
Metabolism of RNA
-log10(q-value)
(C)
PPI Enrichment
Increasing log10(p-value)
Processing of Capped Intron-Containing Pre-mRNA
mitochondrial translational termination
Gap-filling DNA repair synthesis and ligation in TC-NER
Respiratory electron transport
Major pathway of rRNA processing in the nucleolus and cytosol
Golgi-to-ER retrograde transport
HRD1 complex
negative regulation of cell cycle
HOPS complex
DNA-dependent DNA replication
(D)
Our screen (17)
Liu et al. (29)
Sievers et al. (30)
COPS6
CRBN COPS8
COPS2 NCOR1
COPS4 EDC4
COPS5 UBE2G1
(E)
MM.1S Len CRBN
MM.1S Pom CRBN
log2 counts
DMSO T-End
LEN T-End
POM T-End
(F)
PPI network of his in Len-treated MM.1S
(G)
GO analysis on enriched hits of Len-treated MM.1S
-log10(fdr)
protein deneddylation
NER, DNA damage recognition
transcription-coupled NER
DNA repair
response to DNA damage
chromosome organization
COP9 signalosome assembly
ER-nucleus signaling pathway
ATF6-mediated UFP

Figure S2

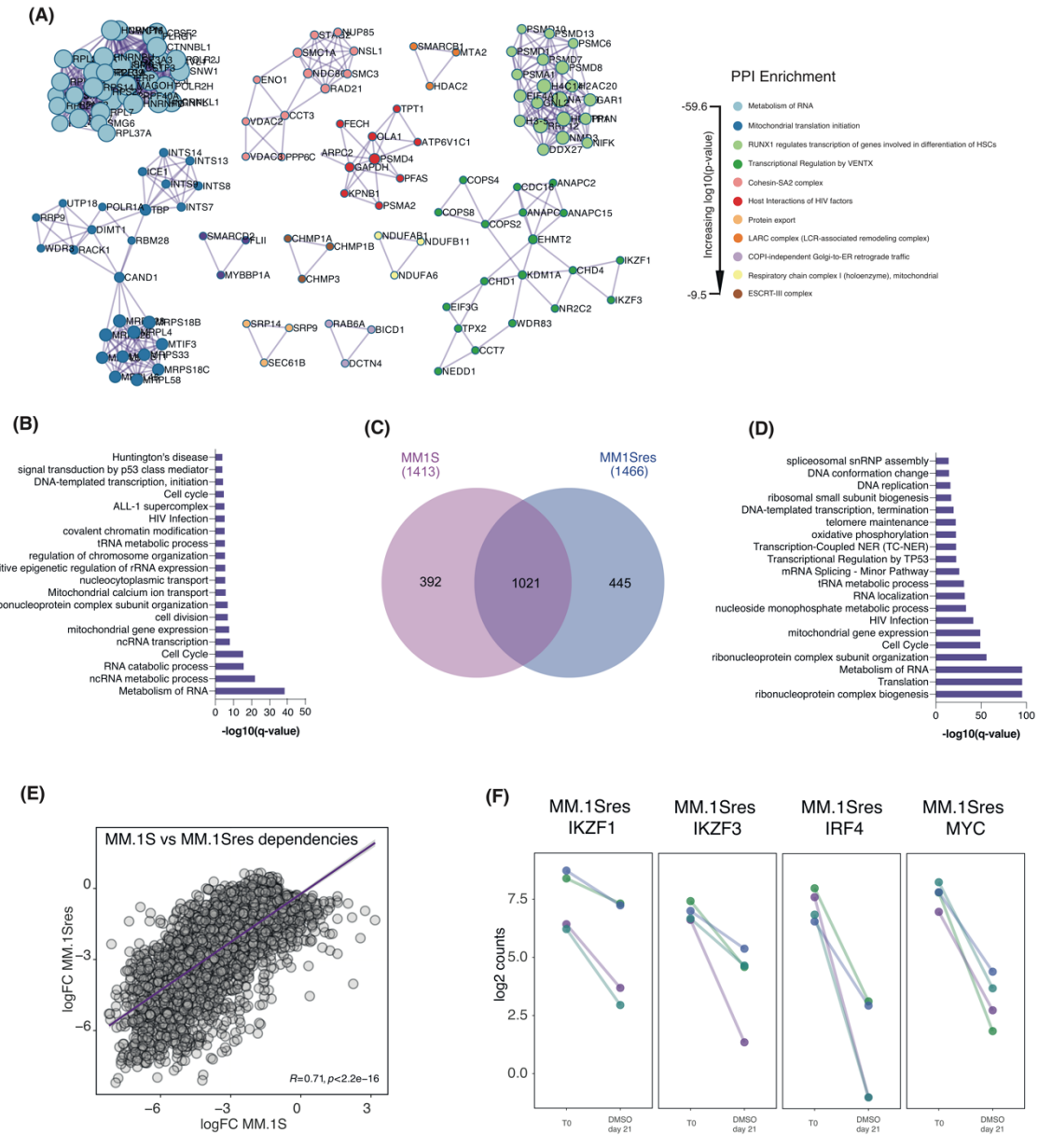
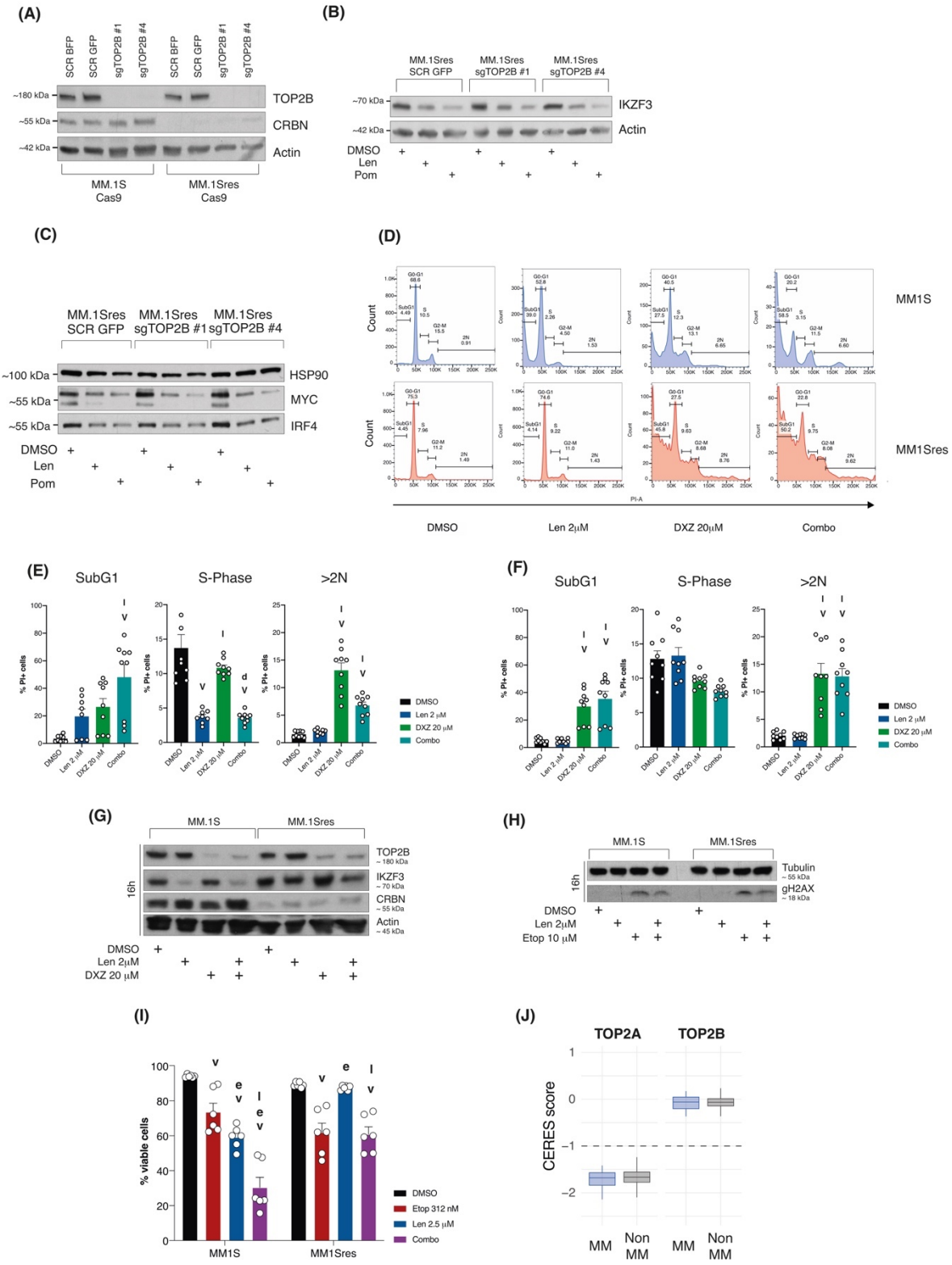

(A)
PPI Enrichment
-59.6
-9.5
Increasing log10(p-value)
Metabolism of RNA
Mitochondrial translation initiation
RUNX1 regulates transcription of genes involved in differentiation of HSCs
Transcriptional Regulation by VENTX
Cohesin-SA2 complex
Host Interactions of HIV factors
Protein export
LARC complex (LCR-associated remodeling complex)
COPI-independent Golgi-to-ER retrograde traffic
Respiratory chain complex I (holoenzyme), mitochondrial
ESCRT-III complex
(B)
Huntington's disease
signal transduction by p53 class mediator
DNA-templated transcription, initiation
Cell cycle
ALL-1 supercomplex
HIV Infection
covalent chromatin modification
tRNA metabolic process
regulation of chromosome organization
Positive epigenetic regulation of rRNA expression
nucleocytoplasmic transport
Mitochondrial calcium ion transport
ribonucleoprotein complex subunit organization
cell division
mitochondrial gene expression
ncRNA transcription
Cell Cycle
RNA catabolic process
ncRNA metabolic process
Metabolism of RNA
0 10 20 30 40 50
-log10(q-value)
(C)
MM1S
(1413)
MM1Sres
(1466)
392
1021
445
(D)
spliceosomal snRNP assembly
DNA conformation change
DNA replication
ribosomal small subunit biogenesis
DNA-templated transcription, termination
telomere maintenance
oxidative phosphorylation
Transcription-Coupled NER (TC-NER)
Transcriptional Regulation by TP53
mRNA Splicing - Minor Pathway
tRNA metabolic process
RNA localization
nucleoside monophosphate metabolic process
HIV Infection
mitochondrial gene expression
Cell Cycle
ribonucleoprotein complex subunit organization
Metabolism of RNA
Translation
ribonucleoprotein complex biogenesis
0 50 100
-log10(q-value)
(E)
MM.1S vs MM.1Sres dependencies
logFC MM.1Sres
logFC MM.1S
R=0.71, p<2.2e−16
(F)
MM.1Sres IKZF1
MM.1Sres IKZF3
MM.1Sres IRF4
MM.1Sres MYC
log2 counts
T0
DMSO day 21

Figure S3


(A)
SCR BFP
SCR GFP
sgTOP2B #1
sgTOP2B #4
~180 kDa
~55 kDa
~42 kDa
TOP2B
CRBN
Actin
MM.1S Cas9
MM.1Sres Cas9
(B)
MM.1Sres SCR GFP
MM.1Sres sgTOP2B #1
MM.1Sres sgTOP2B #4
~70 kDa
~42 kDa
IKZF3
Actin
DMSO
Len
Pom
(C)
MM.1Sres SCR GFP
MM.1Sres sgTOP2B #1
MM.1Sres sgTOP2B #4
~100 kDa
~55 kDa
~55 kDa
HSP90
MYC
IRF4
DMSO
Len
Pom
(D)
MM1S
MM1Sres
Count
PI-A
DMSO
Len 2μM
DXZ 20μM
Combo
(E)
SubG1
S-Phase
>2N
% PI+ cells
DMSO
Len 2 μM
DXZ 20 μM
Combo
(F)
SubG1
S-Phase
>2N
% PI+ cells
DMSO
Len 2 μM
DXZ 20 μM
Combo
(G)
MM.1S
MM.1Sres
16h
TOP2B ~ 180 kDa
IKZF3 ~ 70 kDa
CRBN ~ 55 kDa
Actin ~ 45 kDa
DMSO
Len 2μM
DXZ 20 μM
(H)
MM.1S
MM.1Sres
16h
Tubulin ~ 55 kDa
gH2AX ~ 18 kDa
DMSO
Len 2μM
Etop 10 μM
(I)
% viable cells
DMSO
Etop 312 nM
Len 2.5 μM
Combo
MM1S
MM1Sres
(J)
TOP2A
TOP2B
CERES score
MM
Non MM
MM
Non MM

Chapter 4: Investigating the CRBN interactome via BioID2-dependent proximity labelling

4.1 Introduction

4.1.1 Background

The discovery of IMiD-induced CRBN-dependent degradation of IKZF1 and IKZF3 encouraged the identification of novel IMiD neosubstrates. Identification of CK1α, ZFP91 and SALL4 as novel targets resulted in the following observations[230,252,253]: (i) IKZF1 and IKZF3 were not the only neosubstrates, and the exact number remained to be determined; (ii) lenalidomide's specificity for CK1α indicated that different IMiDs exhibit different substrate specificity[230,234]. This divergence across IMiDs has not been fully characterised yet. The work of Fischer and colleagues[225] demonstrated stabilisation of MEIS2 in cells treated with thalidomide, lenalidomide and pomalidomide. However, it remains to be determined which CRBN endogenous substrates would be stabilised when CRBN is bound to an IMiD, and no unbiased study has ever been conducted with the aim of defining the CRBN "degradome" in the absence of CRBN modulating drugs. In the literature, there is a lack of data with regards to proteins that are neither substrates nor neosubstrates but still interact with CRBN, either in the absence or presence of an IMiD. The work of Eichner and colleagues[231] showed that CRBN elicits a chaperone-like function in stabilising the CD147-MCT1 complex independently of ubiquitination. This finding represents the proof of concept that a CRBN-IMiD interaction does not necessarily induce ubiquitination and degradation of neosubstrates. The existence of proteins that are directly ubiquitinated by CRBN-IMiD but not degraded is yet to be demonstrated. No study has yet discovered CRBN or CRBN-IMiD targets whose function is modulated by CRBN-dependent ubiquitination without being subjected to proteasomal degradation. To this end, it is important to explore all the aspects of IMiD activity on CRBN in order to fully understand the mechanism of action if IMiDs.

The BioID2 enzyme is a modified prokaryotic biotin ligase capable of biotinylating lysine residues in close proximity[307,308]. This enzyme was initially generated by introducing an R40G substitution in *A. aeolicus* BirA, a biotin ligase for Acetyl-CoA Carboxylase that regulates the expression of the biotin synthesis operon. Roux and colleagues have developed this tool to study the interactome and the localisation of LaminA by conjugating it with BioID2[307,308]. This strategy provided BioID2 with specificity for LaminA interacting partners. Biotinylated proteins were then purified with streptavidin-conjugated resins. Once purified, samples were prepared for mass spectrometry. The main advantage of the BioID2 system relative to standard immunoprecipitation is the ability to capture interactions that are not stable in time, weak

interactions which would be lost with standard immunoprecipitation and proteins that are located in proximity of the target and do not physically interact with it. However, this technique does not completely substitute standard antibody-mediated immunoprecipitation. Immunoprecipitation allows to define more precisely which proteins stably interact with the protein studied. By enriching for proteins that are biotinylated in a proximity-dependent manner, it is impossible to discriminate transient interactors from stable interactors[309].

In this chapter, a BioID2-CRBN chimeric protein was generated. This chimera was tested in both HEK293T cells and OPM2 cells, was shown to efficiently mediate biotinylation and enabled the purification of known CRBN interacting partners such as CUL4A, CUL4B and subunits of the COP9 signalosome. OPM2 MM cells expressing BioID2-CRBN were treated with LEN and/or the proteasome inhibitor bortezomib (BORT), and *bona fide* neosubstrates IKZF1 and IKZF3, CK1a and CRBN interactors were selectively enriched in cells treated with both agents. The transcription factor MEF2C, an important regulator within the MM transcriptional core regulatory network[100], was enriched in purified lysates of cells treated with LEN in one of the experiments. However, MEF2C proved not to be a neosubstrate targeted for degradation, but rather a *neointeractor* (here, a CRBN *neointeractor* is defined as a protein that is bound by CRBN only following treatment with an IMiD, but is not necessarily ubiquitinated or degraded upon interaction with CRBN). Subsequently, the same system was employed to test the effects of different IMiDs - LEN, POM and Iberdomide (IBER) on the CRBN interactome in combination with the proteasome inhibitor bortezomib (BORT), aiming to explore differences in neosubstrate/neointeractor identification following treatment with these diverse thalidomide analogues. Proteins such as DVL1, DVL2 were consistently found to be CRBN interactors. MYH9 was the most significantly enriched protein in presence of any IMiD. Protein-protein interaction analysis of purified biotinylated proteins (therefore CRBN putative interactors) also suggested that CRBN might be involved in fundamental processes such as RNA splicing, transport and translation. A gene that was identified as essential for the response to IMiD, EDC4, was also identified as a CRBN interactor. PRCC2C was found as a potential novel neosubstrate, indicating CRBN might regulate formation of stress granules.

This technology could represent an important tool in defining the interactome of CRBN in the presence or absence of IMiDs. The detection of novel putative interactors such as MEF2C, members of the DVL family, MYH9, EDC4 and PRRC2C might lead to the identification of

previously un-discovered factors which are implicated in modulation of both anti-MM activity and regulation of the MM surrounding microenvironment following IMiD treatment.

4.1.2 Aims

Given the lack of understanding of CRBN, the biology underpinning IMiD-dependent modulation of CRBN interactome and the intracellular biological responses which follow IMiD treatment, this project was aimed to:

1. Generate a functional CRBN-BioID2 fusion protein with biotinylating activity;
2. Once generated, validate the system by identification of *bona fide* neosubstrates biotinylated in cells exposed to an IMiD;
3. With the use of different IMiDs, identify novel interaction partners and/or substrates of CRBN and/or IMiD-bound CRBN (CRBN-IMiD).

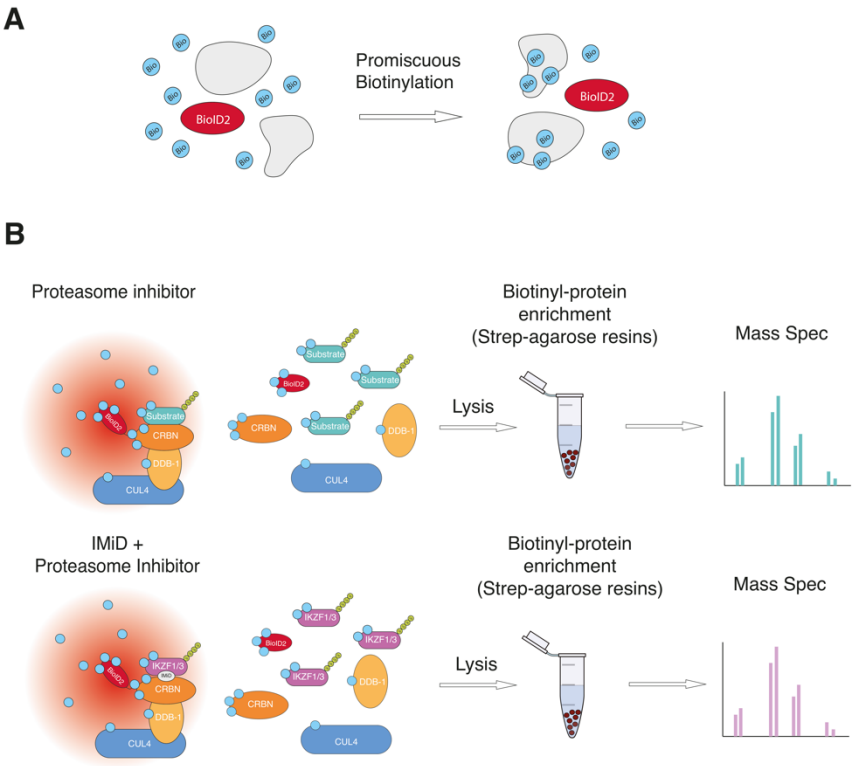
4.2 Results

4.2.1 Experimental planning for the generation of a chimeric BioID2-CRBN fusion protein

The biotin-conjugating enzyme BioID2 is capable of biotinylating proximal proteins at their lysine residues through ATP hydrolysis (Figure 4.1A)[307–309]. It was hypothesised that, in appropriate culture conditions, the fusion of BioID2 with CRBN would provide BioID2 with specificity for CRBN interactors and proteins that are in close proximity with CRBN. Under basal conditions, endogenous interactors of BioID2-CRBN, cultured in medium with exogenous biotin, would be biotinylated by BioID2. In the presence of a proteasome inhibitor, it might be possible to purify endogenous substrates of CRBN that are no longer degraded by the proteasome. With single agent IMiD-exposure (Figure 4.1B), new interacting partners of CRBN upon IMiD treatment could be identified. However, in order to detect undiscovered CRBN neosubstrates, a double treatment with a proteasome inhibitor and an IMiD would be required, to protect ubiquitinated neosubstrates from degradation by a functional proteasome. In the work of Fischer et al.[225], the structure of CRBN was studied by employing the chicken (*G. gallus*) isoform (Figure 4.1C). Within CRBN, there exist three main structural domains: the N-terminal domain (NTD), the helical bundle domain (HBD), which is poised to bind DDB1, and the C-terminal domain (CTD), which contains the thalidomide binding domain (TBD). In order to avoid possible steric hindrance with

Figure 4.1. Experimental planning for the employment of BioID2 in the characterisation of CRBN interactome

(A) Schematic representation of the non-specific biotinylating activity of *A. aeolicus* BirA*R40G (BioID2) in presence of free biotin. (B) Experimental planning for discovery of novel substrates and interactors of CRBN via BioID2 proximity labelling. (C) Secondary structure of *G. gallus* CRBN and its domains. (D) Strategy for cloning CRBN open reading frame into the *pBABE-mycBIoID2-puroR* vector at BioID2 C-terminal domain with a Gly-Gly-Gly linker.


A
BioID2
Promiscuous
Biotinylation
BioID2
B
Proteasome inhibitor
Biotinyl-protein
enrichment
(Strep-agarose resins)
Mass Spec
Substrate
CRBN
DDB-1
CUL4
Lysis
IMiD +
Proteasome Inhibitor
IKZF1/3
C
G. gallus CRBN domains
NTD
HBD
CTD
1
46
185
317
445
helical bundle
domain (DDB-1)
IMiD- and substrate-
binding domain
Adapted from Fischer et al., 2014
D
#
CRBN
5'-LTR
pBABE
*
BioID2
PuroR
3'-LTR
Cloning of CRBN into
pBABE-BioID2-PuroR
* myc-tag
# GGG linker

neosubstrate engagement at the CTD of CRBN, it was decided to clone the 5' of CRBN open reading frame (ORF) at the 3' end of BioID2. In doing so, BioID2 CTD would be linked to CRBN NTD (Figure 4.1D).

4.2.2 BioID2 induces biotinylation of proteins

Firstly, the functionality of the *pBABE-mycBioID2-puroR* construct was validated. This vector was used in the paper of Kim et al. to generate several fusion proteins, such as BioID2-LaminA or BioID2-Sun2 (Figure 4.2A). This vector contains a myc-tagged *BioID2* ORF under the control of *pBABE* and *MSCV* promoters for constitutive mycBioID2 expression. In 5'-to-3'-UTR direction, the SV40 promoter is downstream of BioID2 ORF and controls the expression of a puromycin resistance cassette, which allows selection of transduced cells.

To test the functionality of BioID2, transient transfection with polyethinylimmine (PEI) in HEK293T cells was employed (Figure 4.2B). HEK293T cells were seeded overnight to allow cell adhesion. After 16 hours, cells were transfected with *pBABE-mycBioID2-puroR* vector DNA with PEI (at a DNA to PEI ratio of 1:5) or with a mock control (water plus an equivalent volume of PEI). After 24 hours, 50µM biotin was added to the media in one of the mock and one of the *pBABE-mycBioID2-puroR* (or *mycBioID2*) samples. After 24 hours, cells were harvested by direct on-dish lysis in RIPA buffer. Protein biotinylation and BioID2 expression were tested (Figure 4.2C). Immunoblotting for myctag demonstrated successful transfection with expression of BioID2 in transfected cells (lanes 3 and 4), which was undetected in the mock controls in both the presence and absence of exogenous biotin (lanes 1 and 2). When probing with streptavidin-HRP, HEK293T cells subjected to a mock transfection (lanes 1 and 2) showed the presence of biotinylated proteins of different molecular weight, either in presence and absence of exogenous biotin. This result suggests the presence of endogenous biotinylated proteins. In mycBioID2-transfected cells (lanes 3 and 4), a smear was detected when probing with streptavidin-HRP, which is indicative of protein biotinylation, even in absence of exogenous biotin (lane 3). Enhanced biotinylation was documented with detection of stronger signal in biotin-spiked HEK293T mycBioID2 cells, indicating that BioID2 activity depends on biotin concentration (lane 4). This result indicates that, in the presence of BioID2, the proteome in HEK293T cells is subjected to non-specific biotinylation, but some proteins seem to be endogenously biotinylated on a baseline level. Moreover, the presence of exogenous biotin in the growth media increases the biotinylating activity of BioID2.

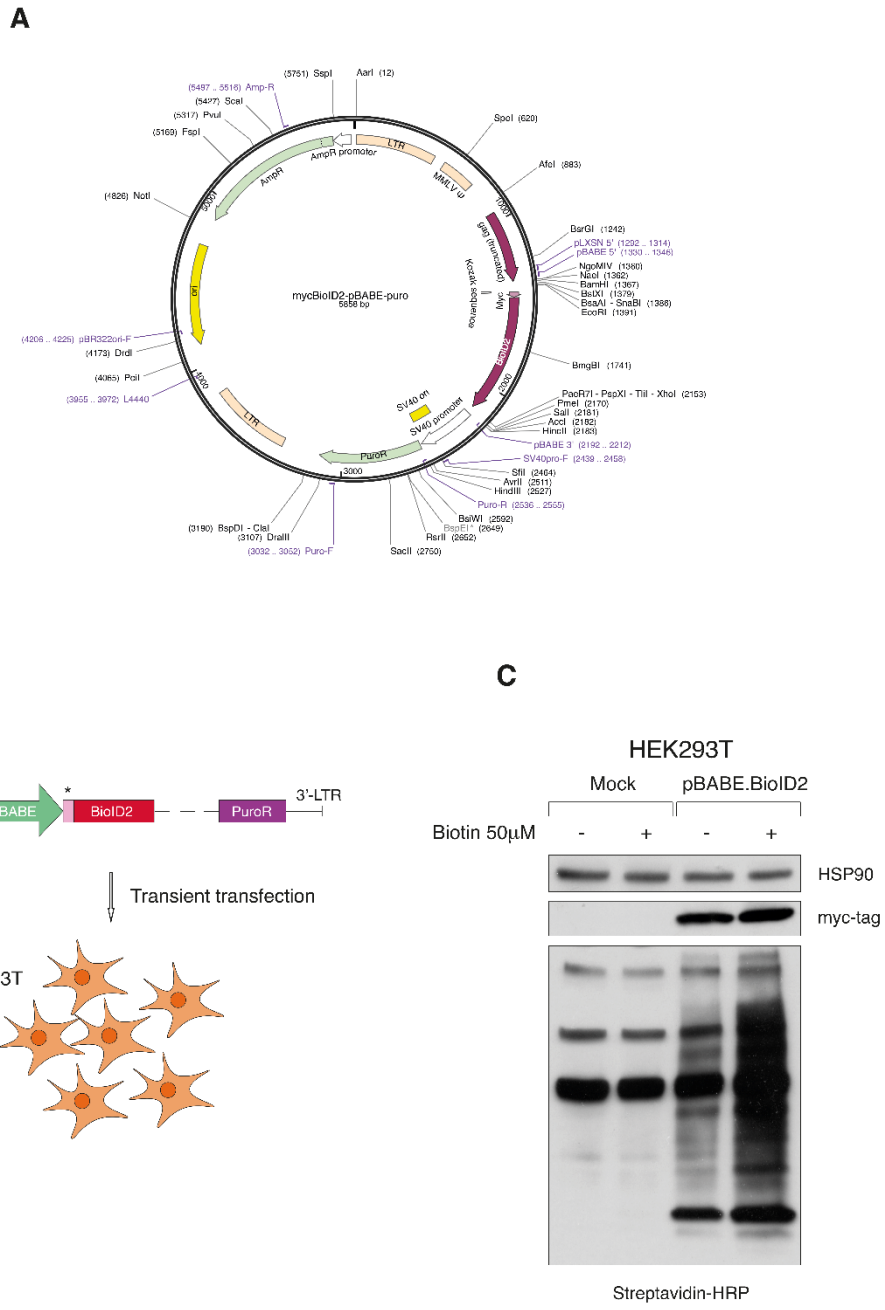


Figure 4.2. Testing of pBABE-mycBioID2-puroR expression and functionality in HEK293T cells

(A) Vector map of *pBABE-mycBioID2-puroR*. (B) Schematic overview of the overexpression experiment to test BioID2 functionality in transiently transfected HEK293T cells. (C) Western blot representing HEK293T cells transfected or non-transfected with *pBABE-mycBioID2-puroR*, in presence or absence of 50μM biotin in the media. Anti-myctag was used to validate the expression of the construct in the cells. Streptavidin-HRP was employed to probe for biotinylated species in the cells. HSP90 was used as loading control.

4.2.3 Preparation of PCR products for Gibson assembly of mycBioID2-CRBN

Next, a strategy to clone CRBN ORF at the 3' end of BioID2 was defined. Gibson Assembly[310], a cloning technique that does not require the use of restriction enzymes, was adopted. This cloning strategy requires 1) the vector to be linearised, 2) the insert to possess a 5' end complementary to the 3' end of the linearised vector and 3) a 3' end complementary to the 5' end of the linearised vector.

Polymerase chain reaction (PCR) was employed to linearise the vector (Figure 4.3A). The forward primer was complementary to the sequence downstream the 3' end of BioID2 (region B). The reverse primer corresponded to the reverse complement of the sequence upstream the 3' end of BioID2 (region A) with the addition of 9 nucleotides translating for 3 Glycines downstream the BioID2 3' end. The Gly-Gly-Gly sequence represents the linker between BioID2 and CRBN. A high-fidelity DNA polymerase (KAPA HiFi DNA polymerase, Roche) was employed to minimise the chance of introducing errors in the reading frame. Following amplification by PCR, the amplicon was loaded and run in an agarose gel for DNA electrophoresis. Subsequent UV imaging revealed a strong band around 6000 bp, corresponding to the expected molecular weight of *pBABE-mycBioID2-puroR* (5858 bp). The PCR product was extracted and purified for the Gibson reaction (Figure 4.3B).

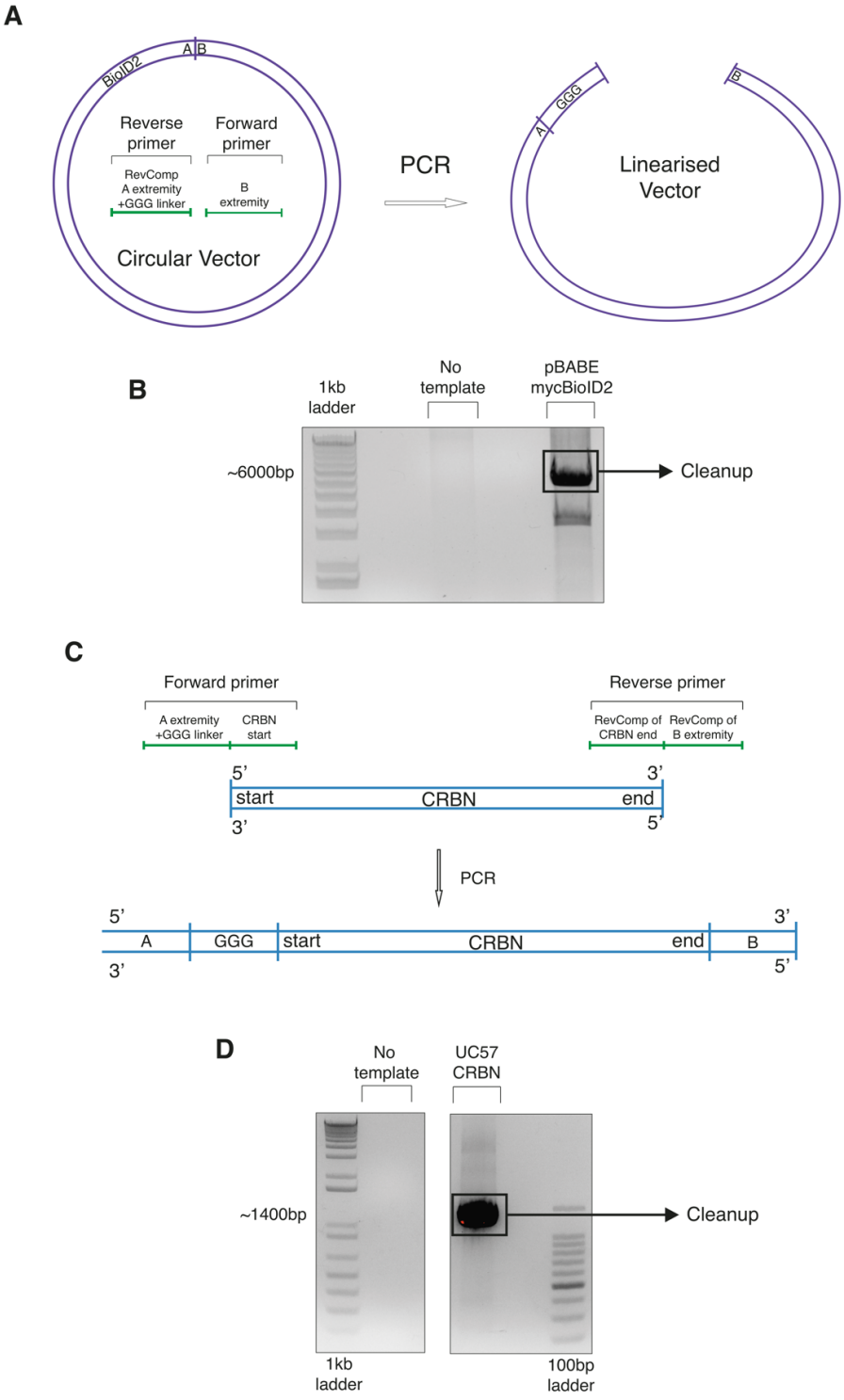
The CRBN ORF sequence was purchased in a UC57 vector (Biomatik Corp, Cambridge, Ontario) and amplified via PCR using KAPA polymerase. The forward primer was complementary to extremity A plus the GGG linker of the linearised vector, the reverse primer corresponded to the reverse complement of CRBN 3' end and extremity B (Figure 4.3C). The PCR product was subsequently loaded and run in an agarose gel and a DNA band detected via UV imaging at around 1400bp, matching the size of *CRBN* ORF. The PCR product was extracted from the gel and cleaned-up for Gibson reaction (Figure 4.3D).

4.2.4 Gibson assembly of mycBioID2 and CRBN

The Gibson reaction works through four main steps (Figure 4.4A). The first step sees incubation of the linearised vector at adequate ratio with the insert (generally vector to insert ratio 1:3). It is essential that the 5' and 3' ends of the linearised vector (mycBioID2 with the addition of a GGG linker, in this case) correspond exactly to that of the 5' and 3' ends of the insert (CRBN). The maximum reaction efficiency is reached if the ends of the two fragments overlap of 25-30 bp[305]. In the second step, the exonuclease T5 removes the 5' ends of both strands in each

Figure 4.3. Gibson Assembly of mycBioID2-CRBN (1)

(A) *pBABE-mycBIoID2-puroR* linearisation via PCR in preparation of Gibson reaction. The DNA strands are represented in purple. The PCR primers are represented in green. (B) Agarose gel showing amplification of the linearised *pBABE-mycBIoID2-puroR* DNA obtained through PCR. At the centre, the control PCR sample with no vector. (C) Strategy for amplification of CRBN open reading frame with 5' and 3' ends complementary to those of the linearised vector. The DNA strands are represented in blue. The PCR primers adopted are represented in green. (D) Agarose gel demonstrating PCR amplification of CRBN as compared to the "No template" control in preparation for Gibson Assembly.


A
BioID2
A
B
Reverse primer
Forward primer
RevComp A extremity +GGG linker
B extremity
Circular Vector
PCR
A
GGG
B
Linearised Vector
B
1kb ladder
No template
pBABE mycBioID2
~6000bp
Cleanup
C
Forward primer
A extremity +GGG linker
CRBN start
Reverse primer
RevComp of CRBN end
RevComp of B extremity
5'
3'
start
CRBN
end
3'
5'
PCR
5'
3'
A
GGG
start
CRBN
end
B
3'
5'
D
No template
UC57 CRBN
~1400bp
Cleanup
1kb ladder
100bp ladder

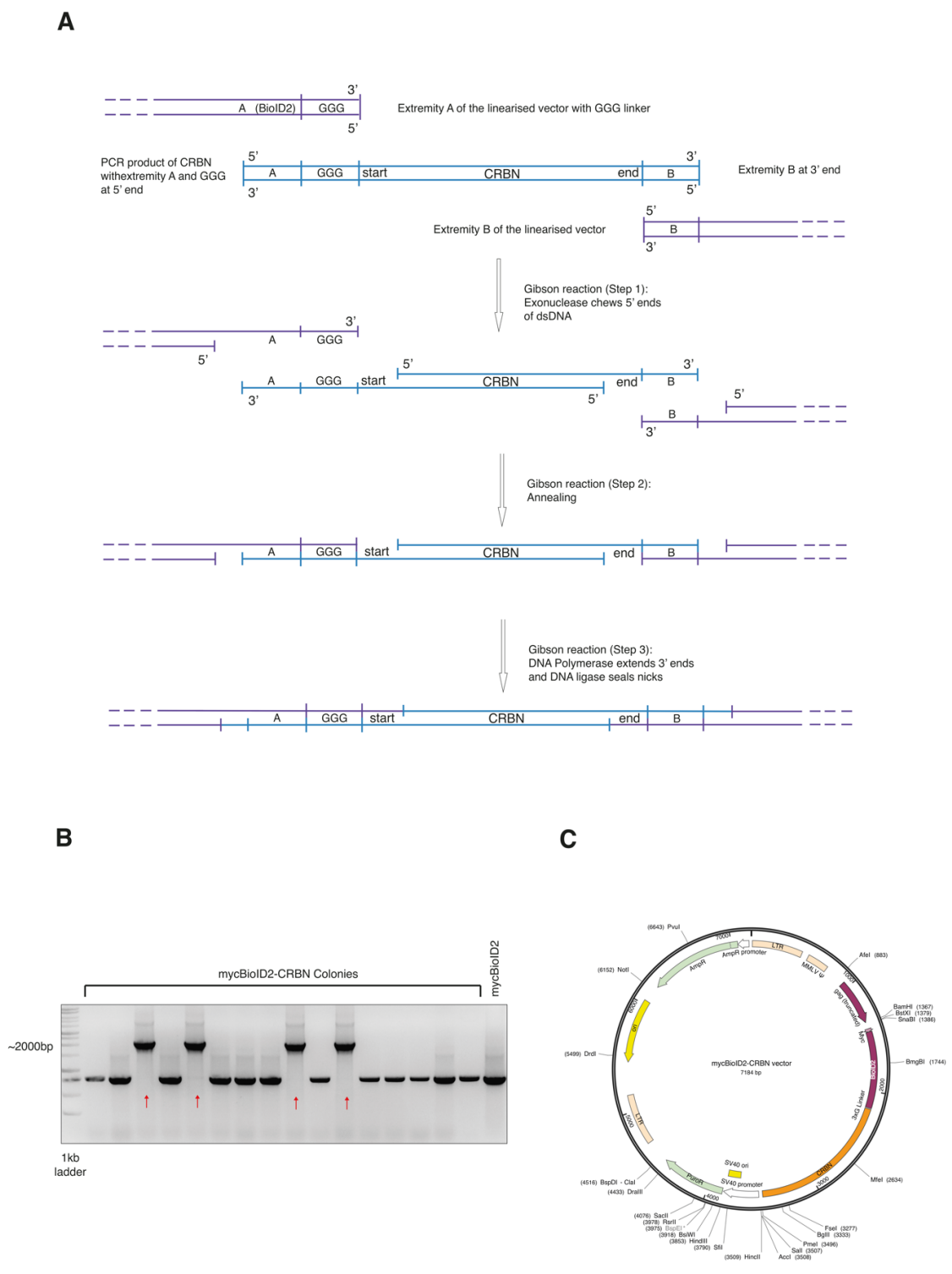


Figure 4.4. Gibson Assembly of mycBioID2-CRBN (2)

(A) Schematic representation of the four steps of the Gibson reaction. (B) Agarose gel displaying amplification of BioID2-CRBN via colony PCR of transformed TOP10F cells bacterial colonies. (C) Vector map of newly cloned *pBABE-mycBIoID2-CRBN-puroR.*

fragment, exposing complementary ends that anneal together. Subsequently, a DNA polymerase extends the 3' ends to fill the gaps left by the exonuclease T5 digestion of 5' ends. Finally, a DNA ligase seals the nicks between base pairs after the polymerase reaction. Collectively, these steps take 15 to 60 minutes (depending on the number of fragments to assemble) and are performed at 50°C (one-step reaction). To perform the Gibson reaction, 100 ng of vector and 300 ng of insert were incubated together (molar ratio of 1:10) in a volume of 10μL (diluted with RNAse and DNAse free distilled water) with 10μL of NEB HiFi DNA (NEBiolabs) assembly mix for 15 minutes at 50°C.

Next, TOP10F *E. coli* were transformed with 10μL of the Gibson reaction and successful assembly validated by PCR (colony PCR, Figure 4.4B, see materials and methods paragraph 2.4.3). The forward primer for colony PCR corresponded to the *myctag* sequence, whilst the reverse primer corresponded to the reverse complementary of the *pBABE* promoter at the 3' of *mycBioID2* ORF, with an expected product of ~2000bp. 4 out of 15 colonies amplified a ~2000bp product. Overnight expansion of these colonies was followed by DNA purification via miniprep (paragraph 2.4.2.5). Two colonies were chosen for Sanger sequencing validation. Three different primers were utilised to cover the ORF from *myctag* to the 3' end of CRBN, included the assembly sites: 5'-pMSCV-forward (CCCTTGAACCTCCTCGTTCGACC) upstream of *myctag*, 5'-BioID2-end-forward (AGTTCAGCCTGAGAAGAAGC) before the GGG linker, and 3'-pBABE-reverse (CCTTACACACAGTCAATCCCA), downstream of the stop codon for *CRBN* ORF. One colony with the correct sequence was further expanded for maxiprep. The validated vector now consisted of a unique ORF, *mycBioID2-CRBN*, under the control of *pBABE* and *MSCV* promoters. (Figure 4.4C)

4.2.5 Validation of protein expression of mycBioID2-CRBN

After sequencing validation, the functionality of the construct was tested by transient transfection of HEK293T cells in a similar manner to that adopted to test the *mycBioID2* vector (section 4.2.2). $5x10^5$ cells were seeded in a 6-well plate in 5 mL of medium per sample. The next day, cells were transfected with an empty *pBABE-puroR*, *mycBioID2* or *mycBioID2-CRBN* vectors using PEI. After 48h, cells were harvested by on-dish lysis with RIPA buffer and protein concentration assessed with a BCA assay and expression of myctag and CRBN was assessed via immunoblotting (Figure 4.5A). When probing for CRBN, endogenous CRBN was detected in all three samples, while a strong band was detected also at ~90 kDa in cells transfected with *mycBioID2-CRBN*. To ensure that this band corresponded to the mycBioID2-CRBN fusion protein,

a technical replicate was probed with an anti-myctag antibody. In cells transfected with the empty *pBABE-puroR* vector, myctag was not detected. In cells transfected with *mycBioID2*, a strong band was detected at ~25kDa, corresponding to the molecular weight (MW) of mycBioID2. In cells transduced with the *mycBioID2-CRBN* vector, myctag was detected at the same MW of the 90kDa-CRBN band in the first replicate (in cells transduced with the *mycBioID2-CRBN* vector), confirming that the CRBN band identified at ~90kDa was mycBioID2-CRBN.

4.2.6 Fusion of CRBN with mycBioID2 reduces promiscuous biotinylating activity of BioID2

The occurrence of selective biotinylating activity of mycBioID2-CRBN was tested by transient transfection of *mycBioID2-CRBN* in HEK293T cells. $5x10^5$ cells were seeded in a 6-well plate (in 5 mL of DMEM). The following day, *mycBioID2* and *mycBioID2-CRBN* vectors were transiently transfected to achieve overexpression of BioID2 and BioID2-CRBN as previously performed. After 24 hours, media was supplemented with vehicle or 50µM biotin. 24 hours later, cells were harvested by on-dish lysis with RIPA buffer. BCA assay was employed for protein quantification. Immunoblot analysis of cells transfected with *mycBioID2* or *mycBioID2-CRBN*, in presence or absence of exogenous biotin, demonstrated that streptavidin-HRP signal was much stronger in HEK293T expressing mycBioID2 in absence of exogenous biotin as compared to HEK293T expressing mycBioID2-CRBN. BioID2-CRBN displayed a reduced capability of inducing protein biotinylation as compared to BioID2 (Figure 4.5B). In fact, the biotinylation pattern observed in HEK293T cells transfected with *myBioID2-CRBN* differed to that of cells transfected with *mycBioID2* only, suggesting that mycBioID2-CRBN might be more specific in biotinylating proteins.

Next, the possibility of enriching biotinylated proteins via incubation of lysate with streptavidin-agarose resins was assessed. $4x10^6$ HEK293T cells (in 10 mL of media) were seeded in a 10 cm cell culture dish (for details see paragraph 2.1.2, materials and methods). The following day, *mycBioID2* and *mycBioID2-CRBN* vectors were transiently transfected to achieve overexpression of BioID2 and BioID2-CRBN. After 24 hours, media was supplemented with DMSO vehicle or 50µM biotin. 24 hours later, cells were harvested and lysed. 40µg of lysate were taken as input control for each sample, whereas the remainder were incubated with streptavidin resins, washed and subsequently boiled in sample buffer to break the streptavidin-biotin bonds to separate biotinylated proteins from the resins. Non-specific biotinylation in inputs and enriched fractions was studied by Western blot. Probing the membrane with HRP-conjugated streptavidin showed strong chemiluminescence in the purified fraction, confirming enrichment of

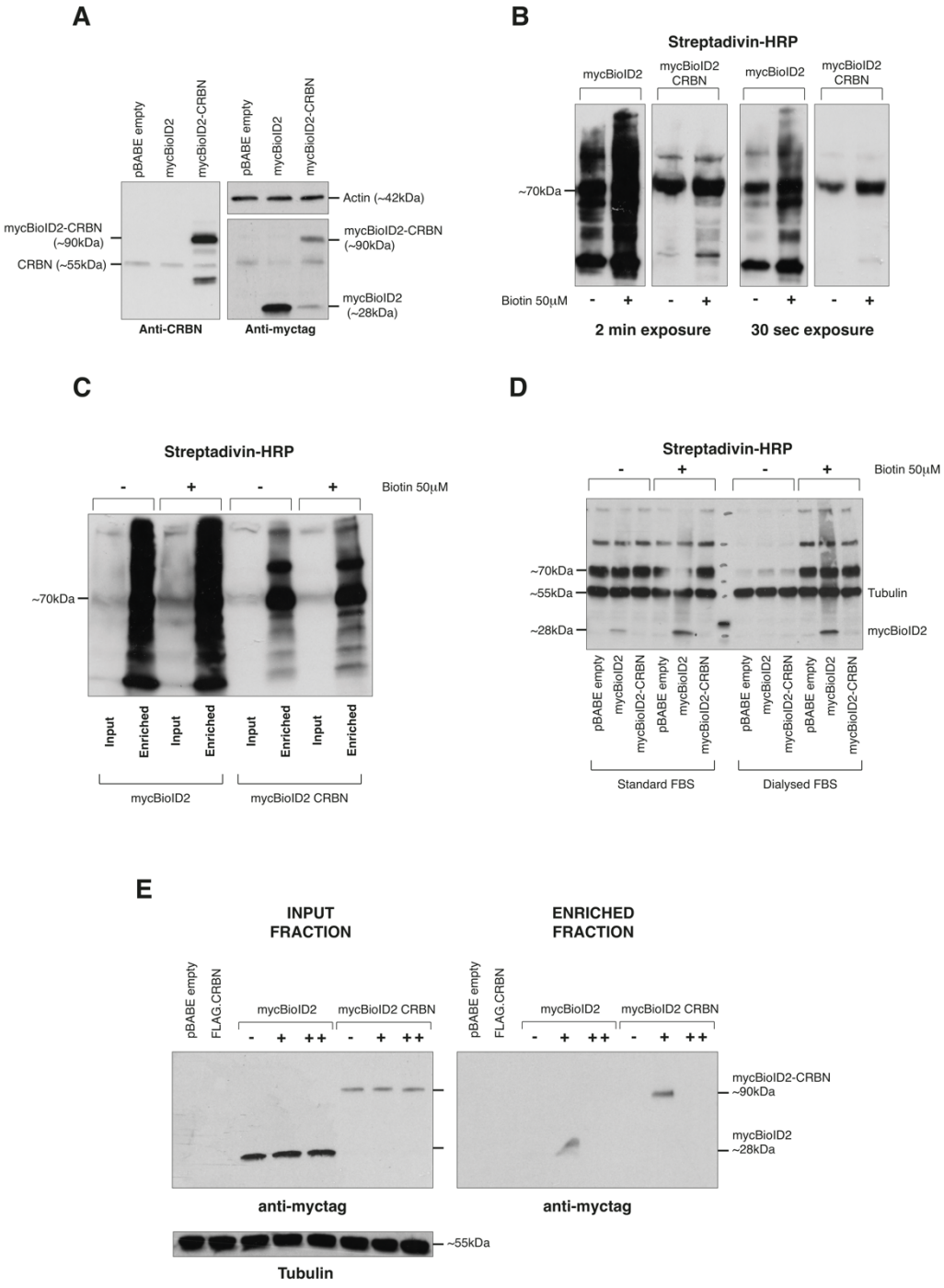
biotinylated proteins (Figure 4.5C). Biotinyl-protein enrichment was greater in HEK293T mycBioID2-expressing cells relative to HEK293T mycBioID2-CRBN, further supporting the observation that mycBioID2-CRBN-induced biotinylation might be more specific and/or less efficient.

4.2.7 Basal BioID2 activity is strongly reduced in cells cultured with biotin-depleted media

Preliminary data demonstrated that it is possible to enrich and then detect BioID2-biotinylated proteins via immunoblotting. However, significant amounts of biotinylated proteins were still detectable in non-biotin-spiked cells. This could be caused by biotin being already present in the cell culture medium. When performing mass spectrometry of the biotinyl-proteome, this "background noise" could affect sensitivity of the experiment by reducing the resolution between samples. Thus, small changes in the biotinyl-proteome would be harder to detect. Since DMEM medium contains no biotin, it was hypothesised that the source of biotin was the foetal bovine serum (FBS) supplemented in the media. Thus, dialysis was employed to deplete small molecules (such as biotin) from the FBS. To test the occurrence of biotin depletion in dFBS, HEK293T cells were transfected with either *pBABE-puroR*, *mycBioID2* or *mycBioID2-CRBN* vectors as in 4.2.6. Cells were cultured in either DMEM-FBS or DMEM-dFBS, with or without addition of exogenous 50µM biotin 24 hours prior to harvest. Western blotting and incubation with strep-HRP (followed by re-probing with an anti-tubulin antibody as loading control) clearly demonstrated that, with dFBS, "background noise" was reduced as compared to the FBS control in the absence of exogenous biotin (Figure 4.5D). This reduction of non-specific activity in cells cultured with dFBS can be observed as: (i) in cells cultured with FBS but without exogenous biotin, several non-specific bands were detected (from ~70kDa and above), together with a dim smear and a dim ~28kDa-band correspondent to mycBioID2 (lane 2); (ii) in cells cultured with FBS and exogenous biotin, the pattern of non-specific bands was highly similar to that of cells cultured in FBS and no biotin, showing also a brighter smear and stronger biotinylation of mycBioID2 (lane 5). This indicates that the addition of exogenous biotin in the growth media increases BioID2 activity; (iii) in cell cultured with dFBS, non-specific bands and the smear expected in cells expressing mycBioID2 were almost undetectable. The band at ~28kDa corresponding to mycBioID2 was also not detected, suggesting absence of significant BioID2 activity; (iv) in cells cultured with dFBS and additional biotin, the signal correspondent to biotinylated myctag (~28kDa) was strong and the non-specific biotinylating activity of BioID2 was restored. This result indicates that FBS is a source of biotin that could affect the activity of BioID2 and that dialysis of FBS is sufficient to significantly reduce BioID2 baseline activity. In cells

Figure 4.5. Validation and optimisation of BioID2-CRBN activity in HEK293T cells

(A) Western blots showing expression of CRBN and myctag in HEK293T cells transiently transfected with *pBABE-puroR, pBABE-mycBIoID2-puroR* or *pBABE-mycBIoID2-CRBN-puroR*. Actin was employed as loading control. The experiment is representative of three independent biological replicates. (B) Western Blot displaying protein biotinylation, in presence or absence of exogenous 50μM biotin for 24 hours, by probing with Streptavidin-HRP, in HEK293T cells transiently transfected with *pBABE-mycBIoID2-puroR* or *pBABE-mycBIoID2-CRBN-puroR*. On the left, chemiluminescent signal after 2-minute exposure with ECL substrate. On the right, signal after 30-second exposure. (C) Western blot demonstrating biotinylated protein enrichment (input vs pulldown) in presence or absence of exogenous 50μM biotin for 24 hours, by probing with Streptavidin-HRP, in HEK293T cells transiently transfected with *pBABE-mycBIoID2-puroR* or *pBABE-mycBIoID2-CRBN-puroR*. (D) Immunoblot displaying biotinylated proteins in HEK293T cells transiently transfected with *pBABE-puroR, pBABE-mycBIoID2-puroR* or *pBABE-mycBIoID2-CRBN-puroR*, cultured in either standard FBS or dialysed FBS, in presence or absence of exogenous 50μM biotin for 24 hours. Tubulin is provided as loading control. The experiment is representative of three independent biological replicates. (E) Immunoblot showing expression of myctag in input and biotinylated (enriched) fractions, in HEK293T cells transiently transfected with *pBABE-puroR, pCMV-FLAG-CRBN, pBABE-mycBIoID2-puroR* or *pBABE-mycBIoID2-CRBN-puroR*, in presence (+) or absence (-) of exogenous 50μM biotin for 24 hours and free biotin in cell lysate prior to enrichment (++). Tubulin is provided as loading control. The experiment is representative of three independent biological replicates.


A
pBABE empty
mycBioID2
mycBioID2-CRBN
mycBioID2-CRBN (~90kDa)
CRBN (~55kDa)
Actin (~42kDa)
mycBioID2-CRBN (~90kDa)
mycBioID2 (~28kDa)
Anti-CRBN
Anti-myctag
B
Streptadivin-HRP
mycBioID2
mycBioID2 CRBN
~70kDa
Biotin 50μM
2 min exposure
30 sec exposure
C
Streptadivin-HRP
Biotin 50μM
~70kDa
Input
Enriched
mycBioID2
mycBioID2 CRBN
D
Streptadivin-HRP
Biotin 50μM
~70kDa
~55kDa
~28kDa
Tubulin
mycBioID2
Standard FBS
Dialysed FBS
E
INPUT FRACTION
ENRICHED FRACTION
pBABE empty
FLAG.CRBN
mycBioID2
mycBioID2 CRBN
mycBioID2-CRBN ~90kDa
mycBioID2 ~28kDa
anti-myctag
~55kDa
Tubulin

cultured with dFBS, BioID2 activity was restored with the addition of exogenous biotin. This observation suggests that BioID2 activity is dependent of biotin concentration in the growth medium.

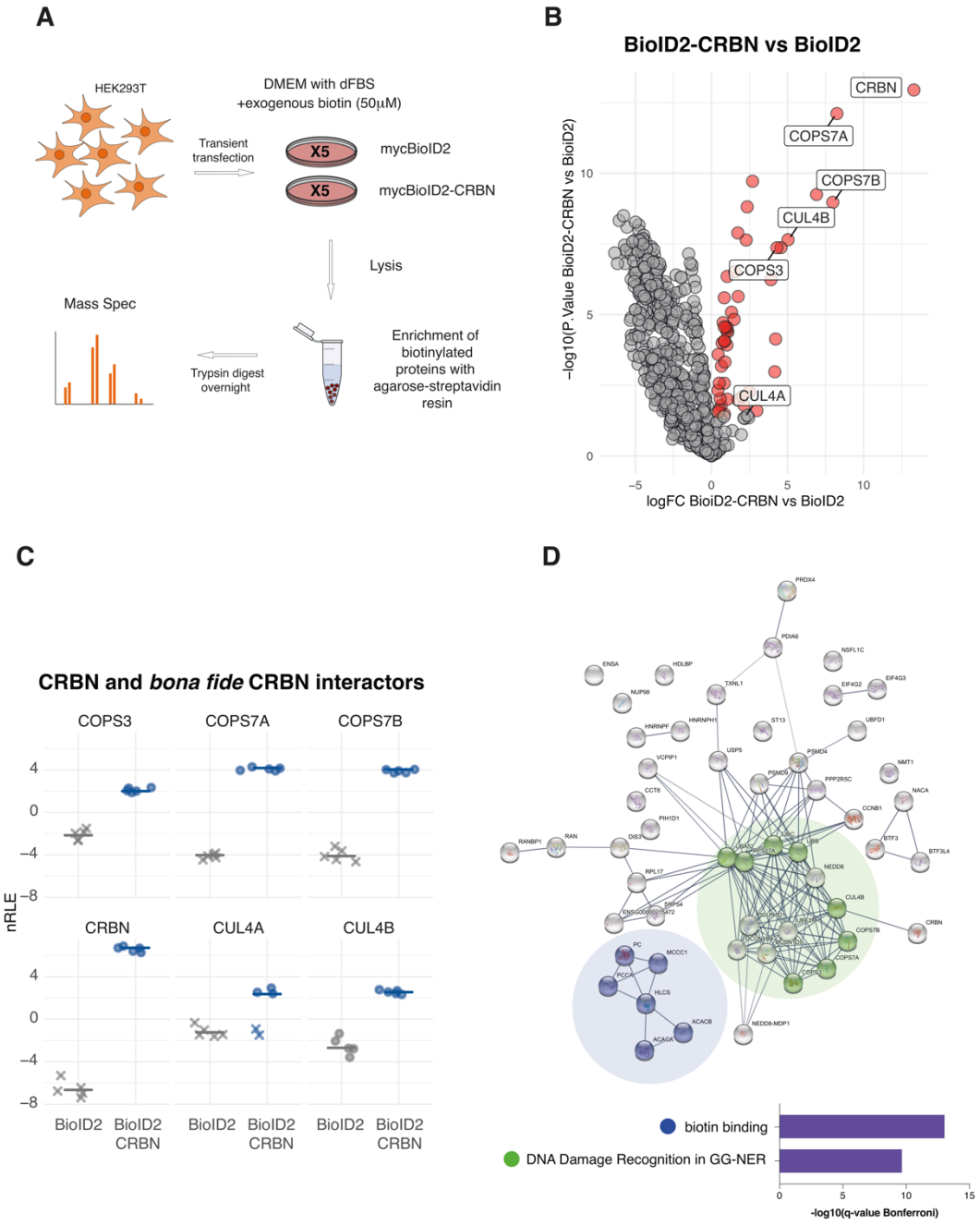
4.2.8 Validation of biotinyl-proteome enrichment protocol using surrogate myctag detection: BioID2 undergoes self-biotinylation

To optimize the enrichment for biotinylated proteins, an assay similar to that of section 4.2.6 was performed with the addition of saturating amounts of biotin in the lysate prior to incubation with resins as control for residual carryover input in the enriched fraction following purification of biotinylated proteins. $4x10^6$ HEK293T cells were seeded in a 10 cm cell culture dish pre-coated with poly-L-lysine to ensure adhesion of cells on the dish surface overnight. 24 hours later, cells were transfected with *pBABE-puroR*, *pCMV-FLAG-CRBN*, *pBABE-mycBioID2* (3 samples) or *mycBioID2-CRBN* (3 samples) vectors. After 24 hours, two of each of mycBioID2 and mycBioID2-CRBN samples were spiked with 50μM biotin; one of each with DMSO. Input controls were taken before incubation with strep-agarose resins. Before incubation one of each mycBioID2 and mycBioID2-CRBN samples was incubated with an additional amount of free biotin equal to 1000x the molar binding capacity of the resins. The amount of free biotin to add prior to incubation was calculated in the following manner. Given the binding capacity of resins (10μg of biotin-BSA/μL, according to manufacturer's product description) and the amount of resins in each sample (20μL), the total binding capacity is 200μg of biotin-BSA in each sample. The molecular weight of biotin-BSA is approximately that of BSA only, ~66.5 kDa. Thus, in 200μg, there are ~3nmol of biotin-BSA. Aiming to a 1000-fold excess of biotin in the carryover control sample, ~3μmol of free biotin had to be added. The mass of biotin that contains 3μmol is 732μg, which were added to the carryover control samples.

After incubation with Streptavidin-Agarose resins, inputs and enriched samples were studied via immunoblot analysis (Figure 4.5E). Both Western of inputs and enriched fraction were probed with anti-myctag. In the input control, myctag was detected in cells transduced with *mycBioID2* or *mycBioID2-CRBN*, but not in cells transfected with *pBABE-puroR* and *pCMV-FLAG-CRBN*. In the enriched fraction, myctag was found only in cells spiked with exogenous biotin. There was no band in the untreated sample, meaning that there was no BioID2 activity in the absence of exogenous biotin, and the addition of free biotin saturated the binding capacity of the resins, with no carryover input left in the enriched fraction after the washing steps. These results indicate that streptavidin agarose resins allow efficient enrichment of biotinylated proteins.

Figure 4.6. MS proteomics validation of mycBioID2-CRBN biotinylating activity

(A) Schematic representation of biotinyl-proteomics workflow in HEK293T cells transiently transduced with *pBABE-mycBIoID2-puroR* or *pBABE-mycBIoID2-CRBN-puroR* in presence of 50μM biotin for 24 hours. (B) Differentially enriched proteins in HEK293T cells transiently transduced with *pBABE-mycBIoID2-puroR* or *pBABE-mycBIoID2-CRBN-puroR* obtained through MS proteomics. (C) Plots displaying enrichment of known CRBN interactors purified with enrichment of biotinylated species in the experiment in panel B. nRLE is the normalised Relative Log2 Expression of intensities of proteins specific for each protein shown. (D) PPI network and GO terms of proteins identified in the experiment in panel B.


A
HEK293T
DMEM with dFBS
+exogenous biotin (50μM)
Transient
transfection
X5
mycBioID2
X5
mycBioID2-CRBN
Lysis
Mass Spec
Trypsin digest
overnight
Enrichment of
biotinylated
proteins with
agarose-streptavidin
resin
B
BioID2-CRBN vs BioID2
CRBN
COPS7A
COPS7B
CUL4B
COPS3
CUL4A
−log10(P.Value BioiD2-CRBN vs BioID2)
logFC BioiD2-CRBN vs BioID2
C
CRBN and bona fide CRBN interactors
COPS3
COPS7A
COPS7B
CRBN
CUL4A
CUL4B
nRLE
BioID2
BioID2
CRBN
D
biotin binding
DNA Damage Recognition in GG-NER
-log10(q-value Bonferroni)

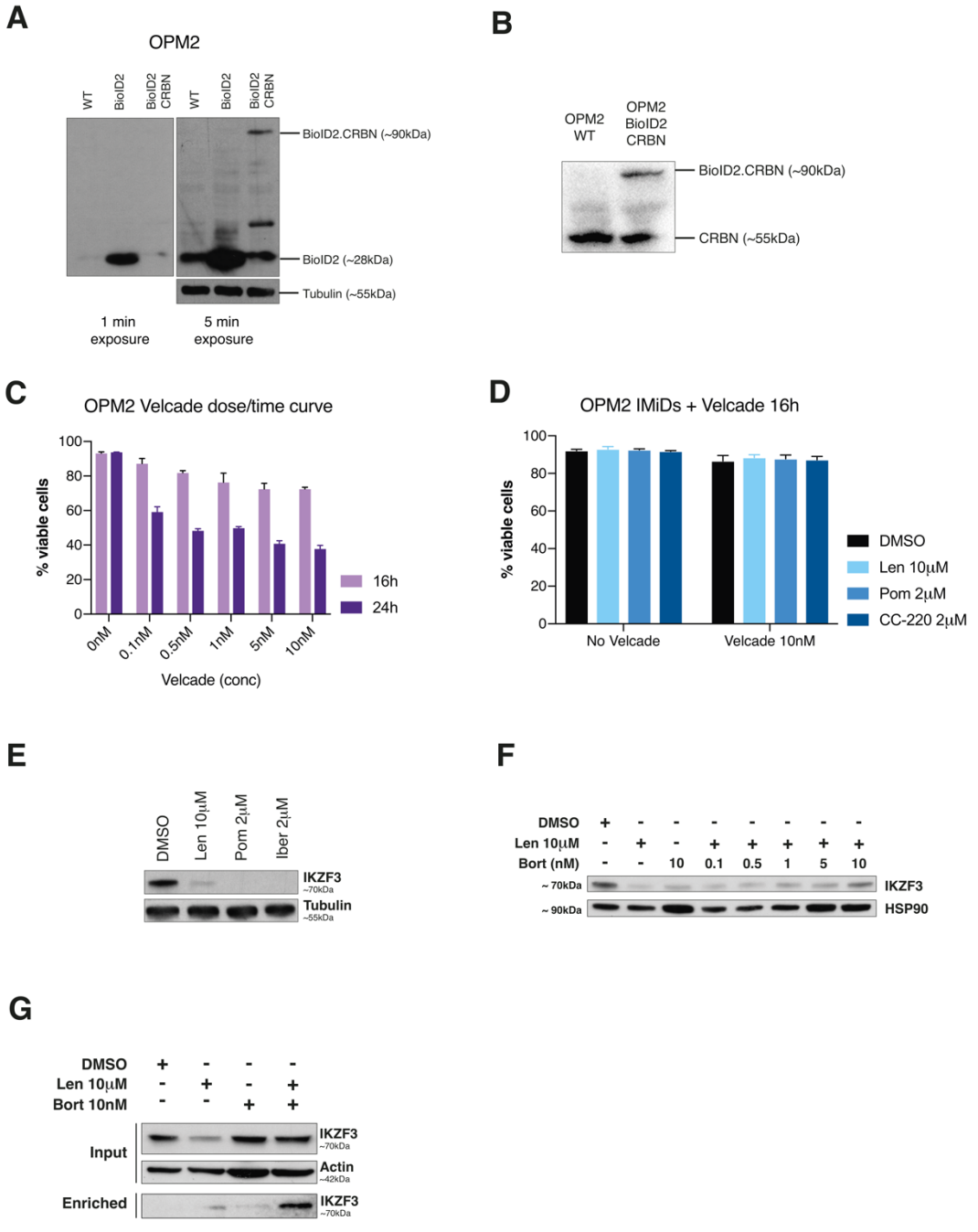
Moreover, identification of BioID2 via surrogate myctag expression in the enriched fraction indicates that BioID2 undergoes self-biotinylation.

4.2.9 Liquid Chromatography - Mass Spectrometry Proteomics of biotinyl-protein enrichment

Next, the capability of this system to purify known CRBN interactors was tested in HEK293T BioID2-CRBN expressing cells via liquid chromatography - mass spectrometry (LC-MS/MS). A schematic workflow of the experiment is represented in Figure 4.6A. 10^7 HEK293T cells were seeded on 15 cm cell culture dishes pre-coated with poly-L-lysine to promote cell adhesion for 16 hours (overnight) in DMEM supplemented with dFBS. The next day, cells were transduced with 30μg of *mycBioID2* or *mycBioID2-CRBN* (5 technical replicate each). After 24 hours, 50μM biotin was spiked in the media. 24 hours later, cells were harvested by on-dish lysis with RIPA buffer. Protein concentration was determined with a BCA assay. Cell growth did not seem to be affected by dFBS. Following cell harvest, lysates were enriched with High-Capacity Streptavidin-Agarose resins and prepared for label-free quantitative MS proteomics (see materials and methods section, section 2.3.4). This approach clearly showed that fusion of BioID2 with CRBN confers BioID2 with specificity for CRBN interactors. Only 47 protein resulted significantly enriched in HEK293T cells expressing BioID2-CRBN as compared to those expressing BioID2 only. Moreover, known CRBN interactors were only identified in HEK293T cells expressing BioID2-CRBN (Figure 4.6B). Proteins identified solely in cells transfected with BioID2-CRBN included CRBN (the most enriched protein) and subunits of the CSN (COPS7A and COPS7B in particular), CUL4A/B, proteins involved in nuclear transport, ubiquitin-like proteins, DCAFs and others. In most of the BioID2 only samples, these proteins were not detected. This is demonstrated by the presence of imputed data (represented by crosses in the plots), meaning that the protein matched peptide intensity was 0. In this case, the algorithm normally introduces imputed *a priori* data to allow statistical testing[311]. COPS3, COPS7A, COPS7B and CRBN intensities were imputed in all the four replicates of HEK293T BioID2 cells and were conversely all detected in HEK293T BioID2-CRBN cells. CUL4A also was undetected and therefore the matched peptides intensities were imputed in HEK293T BioID2 cells. However, for CUL4A, 2/5 of the replicates had their intensity imputed also in HEK293T BioID2-CRBN cells samples. CUL4B intensity was measured in all samples of both conditions. Finally, Protein-Protein Interaction (PPI) network and gene ontology (GO) term analyses demonstrated that the proteins purified in the enriched fraction, i.e. CRBN stable or transient interactors, are involved in DNA repair (Figure 4.6C-D). Mitochondrial proteins that are covalently bound to biotin were also found enriched (Acetyl-CoA Carboxylases – ACACA and ACACB, Pyruvate Carboxylase - PC[312,313]). This result confirmed the efficiency of this approach in identifying CRBN interactors.

Figure 4.7. Generation and optimisation of OPM2-BioID2 and OPM2-BioID2-CRBN cells

(A) Immunoblot displaying myctag expression in OPM2 WT, OPM2-BioID2 and OPM2-BioID2-CRBN cells (1-minute and 5-minute film exposure). Tubulin is provided as loading control. (B) Immunoblot displaying expression of endogenous CRBN and BioID2-CRBN in OPM2 WT and OPM2-BioID2-CRBN cells. (C) Bar plot showing OPM2-BioID2-CRBN cells viability following 16 or 24 hours of treatment with bortezomib at different concentrations. Error bars represent the mean SD (standard deviation) of two technical replicates. (D) Bar plot showing OPM2-BioID2-CRBN cell viability following 16 hours of treatment with 10nM bortezomib in combination with DMSO, LEN, POM or CC-220 (IBER). Error bars represent the mean SD (standard deviation) of two technical replicates. The experiment is representative of two independent biological replicates. (E) Immunoblot displaying IKZF3 expression in OPM2-BioID2-CRBN cells treated with DMSO, LEN, POM or IBER. Tubulin is provided as loading control. (F) Immunoblot displaying IKZF3 expression in OPM2-BioID2-CRBN cells treated with LEN, BORT and combinations of LEN plus different BORT concentrations. HSP90 is provided as loading control. (G) Western blot displaying IKZF3 levels in input and enriched fraction of OPM2-BioID2-CRBN cells treated with LEN, BORT and combo LEN/BORT. For the input fraction, actin is provided as loading control.


A
OPM2
WT
BioID2
BioID2 CRBN
WT
BioID2
BioID2 CRBN
BioID2.CRBN (~90kDa)
BioID2 (~28kDa)
Tubulin (~55kDa)
1 min exposure
5 min exposure
B
OPM2 WT
OPM2 BioID2 CRBN
BioID2.CRBN (~90kDa)
CRBN (~55kDa)
C
OPM2 Velcade dose/time curve
% viable cells
100
80
60
40
20
0
16h
24h
0nM
0.1nM
0.5nM
1nM
5nM
10nM
Velcade (conc)
D
OPM2 IMiDs + Velcade 16h
% viable cells
100
80
60
40
20
0
DMSO
Len 10μM
Pom 2μM
CC-220 2μM
No Velcade
Velcade 10nM
E
DMSO
Len 10μM
Pom 2μM
Iber 2μM
IKZF3
~70kDa
Tubulin
~55kDa
F
DMSO + - - - - - - -
Len 10μM - + - + + + + +
Bort (nM) - - 10 0.1 0.5 1 5 10
~ 70kDa
IKZF3
~ 90kDa
HSP90
G
DMSO + - - -
Len 10μM - + - +
Bort 10nM - - + +
Input
IKZF3
~70kDa
Actin
~42kDa
Enriched
IKZF3
~70kDa

4.2.10 Generation of OPM2 cells expressing mycBioID2 and mycBioID2-CRBN and optimisation of culturing conditions for MS proteomics

Generation of a MM cell line expressing mycBioID2-CRBN followed MS validation of the system in transiently transfected cells, with the aim of further test the BioID2-CRBN protein in a more IMiD-relevant setting. OPM2 cells were retrovirally transduced with *mycBioID2* or *mycBioID2-CRBN* vectors. After transduction, OPM2-BioID2 and OPM2-BioID2-CRBN cells were selected in 1μg/mL puromycin. To validate BioID2-CRBN expression, cell lysates of OPM2 cells, either wild-type or transduced with *mycBioID2* or *mycBioID2-CRBN,* were probed for myctag expression (Figure 4.7A). Whereas OPM2 wild-type cells did not show myctag expression, OPM2-BioID2 cells displayed a band corresponding to the molecular weight of myc-tagged BioID2 (~25kDa), and OPM2-BioID2-CRBN cells one at the molecular weight of BioID2 plus that of CRBN (~90kDa). With a CRBN specific antibody, immunoblotting of OPM2-BioID2-CRBN cell lysate demonstrated overexpression of exogenous BioID2-CRBN (with a MW of ~90kDa) in addition to endogenous CRBN (~55kDa). The additional band at 90kDa (Figure 4.7B) was present only in OPM2-BioID2-CRBN cell lysate, but it was not present in OPM2 wild-type cell lysate, which demonstrated only the presence of endogenous CRBN at ~55kDa. These data demonstrate that OPM2-BioID2 cells express mycBioID2 and that OPM2-BioID2-CRBN cells express mycBioID2-CRBN.

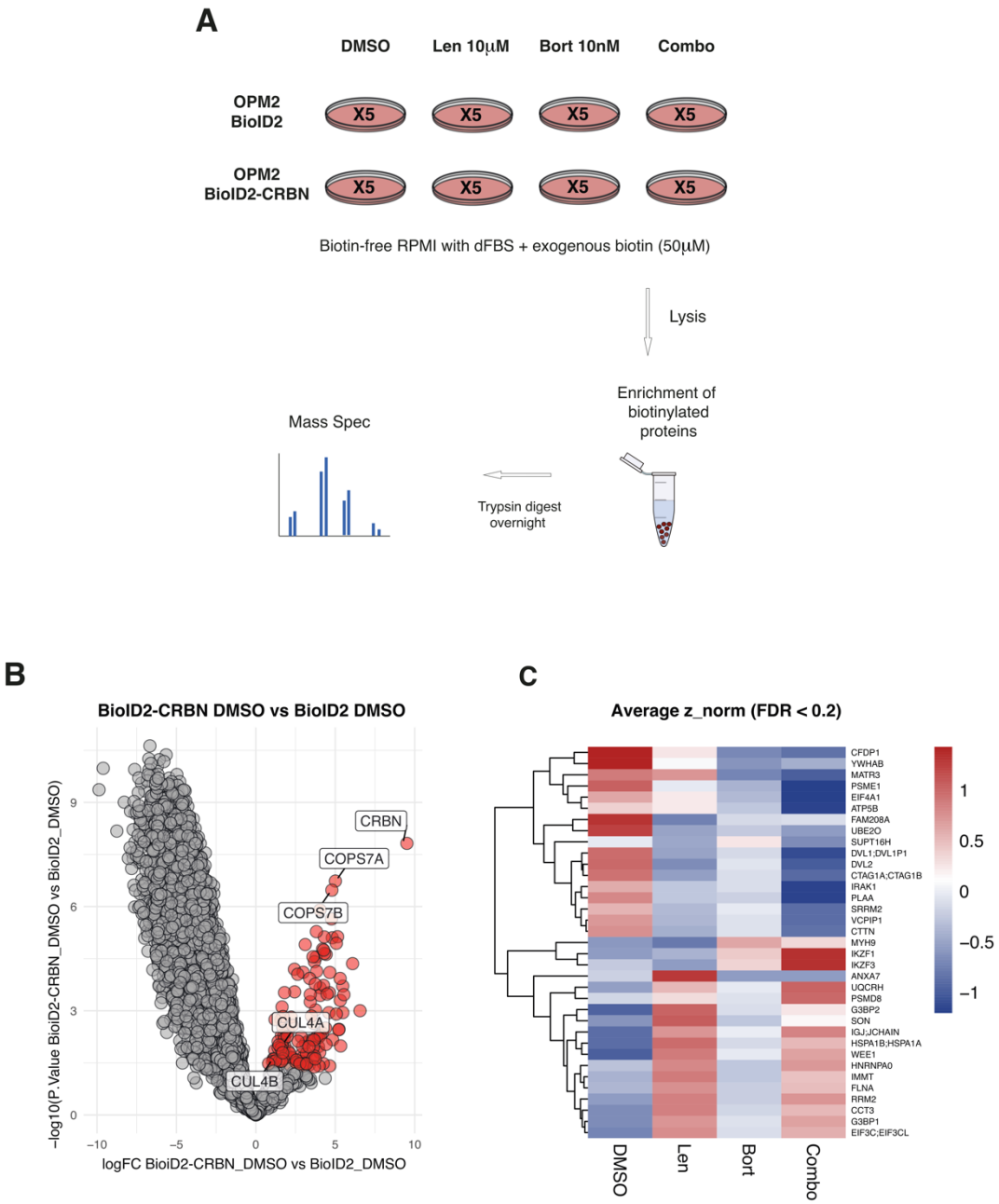
The detection of IMiD neosubstrates requires proteasome inhibition, but proteasome inhibitors are highly toxic for MM cells[314]. Optimal labelling with BioID2 requires incubation with exogenous biotin for at least 16 to 24 hours[307–309]. For this reason, the toxicity of bortezomib in OPM2-BioID2-CRBN cells at 16 and 24 hours was assessed. OPM2-BioID2-CRBN cells were treated with increasing concentrations of bortezomib (0.1, 0.5, 1, 2, 5, and 10 nM; Figure 4.7C). Bortezomib (BORT) cytotoxicity was more time-dependent rather than concentration dependent. However, some degree of concentration-dependent response was seen, but it was not as evident as the difference in cell death between 16 and 24 hours. At 16 hours, none of the concentrations tested were able to kill more than 30% of the cells. Conversely, at 24 hours, all concentrations tested induced the death of 30% or more of the cells. This experiment demonstrates that an exposure of OPM2-BioID2-CRBN cells to BORT longer than 16 hours would likely compromise the outcome of the experiment. Subsequently, combination treatment with BORT and an IMiD was tested in OPM2-BioID2-CRBN cells to verify whether IMiDs enhance BORT toxicity in 16 hours. OPM2-BioID2-CRBN cells were treated with DMSO, LEN, POM or Iberdomide (CC-220, IBER) in presence and absence of 10nM BORT (Figure 4.7D). Cell viability via PI labelling was assessed after 16 hours, documenting no increase in cell death in double agent (BORT/IMiD)

as compared to single agent (IMiD only). Next, the efficacy of IBER in comparison to LEN and POM was evaluated. Both OPM2 and OPM2-BioID2-CRBN cells were treated for 16h with DMSO, 10μM LEN, 2μM POM or 2μM IBER and cell harvested for protein expression analysis via immunoblot. This experiment demonstrated that LEN promotes degradation of IKZF3 in both OPM2 and OPM2-BioID2-CRBN cells. Degradation of IKZF3 induced by POM and IBER was greater than that induced by LEN. Moreover, treatment with POM and IBER induced complete degradation of IKZF3 (Figure 4.7E).

Next, the lowest concentration required to induce stabilization of neosubstrates in OPM2-BioID2-CRBN cells treated with LEN/BORT was determined by exposing OPM2-BioID2-CRBN cells to a high concentration of LEN (10μM) and increasing concentrations of BORT up to 10nM (0, 0.1, 0.5, 1, 5, 10 nM). At the maximum concentration tested (10nM), cells demonstrated reduction of the pool of IKZF3, likely caused by the toxic activity of BORT in these cells. However, only at 10nM was BORT capable of inducing stabilization of IKZF3 (Figure 4.7F). Conversely, in samples with lower BORT concentrations, LEN-induced IKZF3 degradation was not inhibited. Finally, enrichment of biotinylated IKZF3 was tested in OPM2-BioID2-CRBN cells following dual treatment with BORT and LEN as compared to DMSO or each single agent. $60x10^6$ cells were seeded in biotin-free RPMI supplemented with 10% dFBS. After eight hours, media was washed out, cells re-seeded in fresh biotin-free RPMI+dFBS, split in four different flasks ($15x10^6$ cells each) and treated with DMSO, 10μM LEN, 10nM BORT or the combination of both agents, with addition of exogenous biotin (50μM). After 16 hours, cells were harvested, lysed and equal amounts of protein across samples were incubated with streptavidin-agarose resins for biotinyl-protein enrichment. A small aliquot of lysate was taken as input control prior to enrichment. Both inputs and enriched fraction were separated via protein electrophoresis, Western-blotted and probed for IKZF3 (Figure 4.7G). In the input control, degradation was observed in cells treated with 10μM LEN. Treatment with BORT slightly stabilised the levels of IKZF3. In the LEN/BORT combination condition, BORT was able to stabilise IKZF3. In the enriched fraction, IKZF3 was strongly enriched in the double agent condition and virtually absent in the other samples. This experiment demonstrated that this system allows identification of well-described CRBN neosubstrates.

Figure 4.8. MS proteomics validation of BioID2-CRBN activity in OPM2-BioID2-CRBN cells

(A) Schematic representation of the MS proteomics experiment performed with OPM2-BioID2 and OPM2-BioID2-CRBN cells treated with LEN, BORT and combo LEN/BORT (Experiment 1). (B) Volcano plot displaying differentially expressed proteins in DMSO-treated OPM2-BioID2-CRBN cells vs OPM2-BioID2 cells. Red dots correspond to OPM2-BioID2-CRBN cells proteins significantly different from OPM2-BioID2 cells for adjusted p-value < 0.05. (C) Heatmap showing differentially expressed proteins across all samples, significant for false discovery ratio < 0.2 (two-way ANOVA). Differential expression is measured with the average z_norm, which corresponds to the nRLE of each sample normalised by its SD.


A
DMSO
Len 10μM
Bort 10nM
Combo
OPM2 BioID2
OPM2 BioID2-CRBN
X5
Biotin-free RPMI with dFBS + exogenous biotin (50μM)
Lysis
Enrichment of biotinylated proteins
Trypsin digest overnight
Mass Spec
B
BioID2-CRBN DMSO vs BioID2 DMSO
−log10(P.Value BioID2-CRBN_DMSO vs BioID2_DMSO)
logFC BioID2-CRBN_DMSO vs BioID2_DMSO
CRBN
COPS7A
COPS7B
CUL4A
CUL4B
C
Average z_norm (FDR < 0.2)
CFDP1
YWHAB
MATR3
PSME1
EIF4A1
ATP5B
FAM208A
UBE2O
SUPT16H
DVL1;DVL1P1
DVL2
CTAG1A;CTAG1B
IRAK1
PLAA
SRRM2
VCPIP1
CTTN
MYH9
IKZF1
IKZF3
ANXA7
UQCRH
PSMD8
G3BP2
SON
IGJ;JCHAIN
HSPA1B;HSPA1A
WEE1
HNRNPA0
IMMT
FLNA
RRM2
CCT3
G3BP1
EIF3C;EIF3CL
DMSO
Len
Bort
Combo

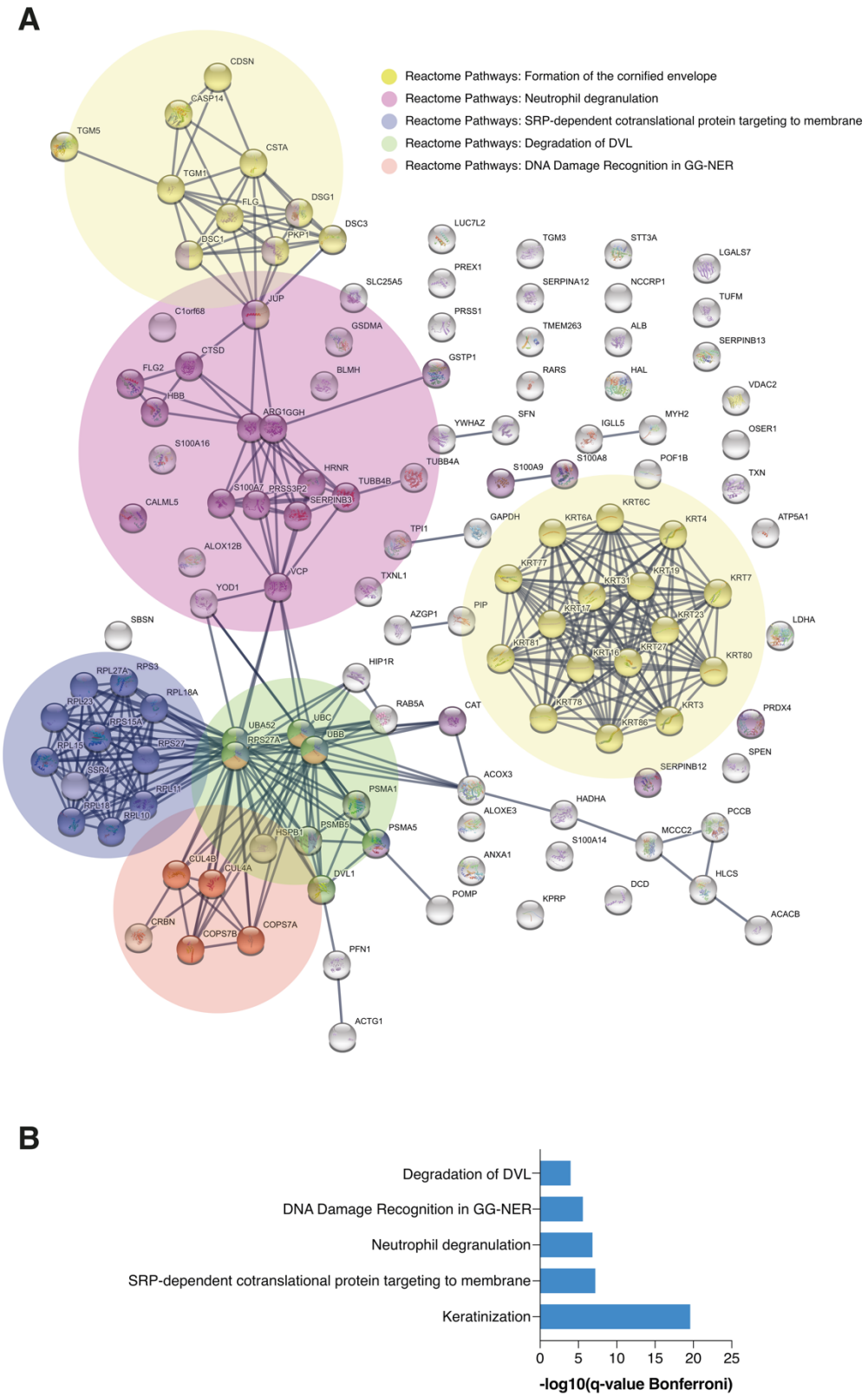


Figure 4.9. PPI networking of CRBN interactome

(A) PPI network and (B) GO terms analysis of newly identified CRBN interactors (refer to Figure 4.8).

4.2.11 Mass Spectrometry Proteomics of biotinyl-protein enrichment in OPM2-BioID2-CRBN cells (Experiment 1)

After validating the OPM2-BioID2-CRBN model, LC-MS/MS proteomics was performed in order to determine CRBN interacting partners and substrates, in presence and absence of an IMiD, in an unbiased manner. OPM2-BioID2 and OPM2-BioID2-CRBN cells were treated for 16 hours with DMSO, 10nM BORT, 10µM LEN or the combination of BORT and LEN, with five technical replicates per condition, in the presence of 50µM biotin. Equal amounts of protein in each sample were subjected to enrichment for biotinylated proteins by incubation with Streptavidin-Agarose resins and washed to obtain a purified fraction. Following overnight protein digest with trypsin, peptides were injected into the mass spectrometer for quantitative proteomics (Figure 4.8A; for detail on the experimental protocol, refer to material and methods, section 2.3.4).

Firstly, enrichment of biotinylated peptides was assessed by comparing differentially enriched proteins (DEPs) between OPM2-BioID2 and OPM2-BioID2-CRBN cells in absence of any treatment (DMSO control) to explore whether OPM2-BioID2-CRBN cells demonstrated enrichment of *bona fide* CRBN interacting partners as compared to OPM2-BioID2 cells (Figure 4.8B). Cells expressing BioID2 displayed biotinylation of a spectrum of proteins. Conversely, in OPM2-BioID2-CRBN cells there was high specificity for CRBN interacting proteins, as CRBN and *bona fide* CRBN interactors were identified (COPS7A, COPS7B, CUL4A/B). Subsequent analysis of differentially enriched proteins was entirely focused on OPM2-BioID2-CRBN, aiming to explore variations of the CRBN interactome following LEN, BORT or double-agent exposure. This experiment identified several novel putative CRBN interactors and/or *neointeractors* (Figure 4.8C). PPI analysis of identified CRBN interactors with STRING (http://string-db.org/) demonstrated that peptides purified in this experiment matched with proteins involved in epidermal development processes, neutrophil granulation, axon guidance, DVL protein degradation, translation and DNA damage response (Figure 4.9A). GO analysis displayed similar results, with keratinization being the most significant overlap (Figure 4.9B).

Subsequently, differences in CRBN interacting proteins following treatment with LEN, BORT or the combination of LEN+BORT was explored. IKZF1 and IKZF3 were the most enriched in BORT/LEN as compared to LEN only (Figure 4.10A). Moreover, the comparison between LEN and DMSO showed that DVL1 and DVL2 (two scaffold proteins implicated into modulation of WNT signaling[323,324]) were significantly depleted. In nRLE plots (nRLE = normalised Relative Log2 Expression of intensity), IKZF1 and IKZF3 were more abundant in the combination treatment as

compared to vehicle and single agents (Figure 4.10C). The median of the replicates in each same treatment condition was used to define the average level of enrichment. BORT-treated OPM2-BioID2-CRBN cells displayed increased enrichment in IKZF1 as compared to DMSO-treated cells. Conversely, LEN did not induce an increase in IKZF1 enrichment overall. In these cells, combination treatment caused significant enrichment of IKZF1. IKZF3 was also found enriched in OPM2-BioID2-CRBN cells treated with both LEN and BORT, whereas in all the other conditions IKZF3 was not detected (with consequent value imputation). Conversely, DVL1 and DVL2 were less enriched in presence of LEN or BORT/LEN (Figure 4.10B,D). In particular, BORT alone did not change the level of DVL1/2 enrichment, whereas LEN as a single agent and in combination with BORT demonstrated to affect DVL1/2 enrichment. In one of the samples treated with combined BORT/LEN, no intensity of peptides matching DVL1/2 was detected, with subsequent intensity value imputation. This data confirmed the ability of this approach in identifying known CRBN neosubstrates IKZF1 and IKZF3, and suggests that DVL proteins are in direct or indirect association with CRBN in baseline conditions. Additionally, LEN exposure seemed to cause CRBN to associate less with DVL1/2.

4.2.12 Generation of IKZF similarity score to define *neosubstrate-like* protein enrichment profiles

The Euclidean distance between the mean of all identified proteins across the four conditions was calculated. This approach allowed the assignment of an "IKZF similarity" score to each protein in order to identify those whose enrichment profile - across the different conditions - was the most similar to IKZF1/3, from 0 (most similar) to 1 (most dissimilar) (Figure 4.11A). The scatterplot of ranked proteins according to their score demonstrated that IKZF1 and IKZF3 had the lowest IKZF similarity score, followed by other peptides unique for proteins such as Myosin Light Chain Kinase (MYLK) and Myocyte Enhancer Factor 2C (MEF2C) (Figure 4.11B). Proteins of the DVL family exhibit an opposite profile to that of IKZF1/3. An efficient way of visualising the enrichment profile of each protein across diverse conditions is represented by line-plotting the mean nRLE value. This plot reflects the IKZF similarity score of MYLK, MEF2C, DVL1 and DVL2 as compared to that of IKZF1/3. DVL1 and DVL2 have an enrichment profile opposite to that of IKZF1 and IKZF3, whereas the profile of MYLK and MEF2C is more similar. DVL1 and DVL2 showed interaction with CRBN, which was maintained in the presence of BORT but lost in the presence of LEN or in combinatorial treatment BORT/LEN. This approach clearly displayed the differences in the enrichment profile between those of IKZF1/3 and those of other hits across the four treatment conditions. The enrichment profile of MEF2C demonstrated that this protein can

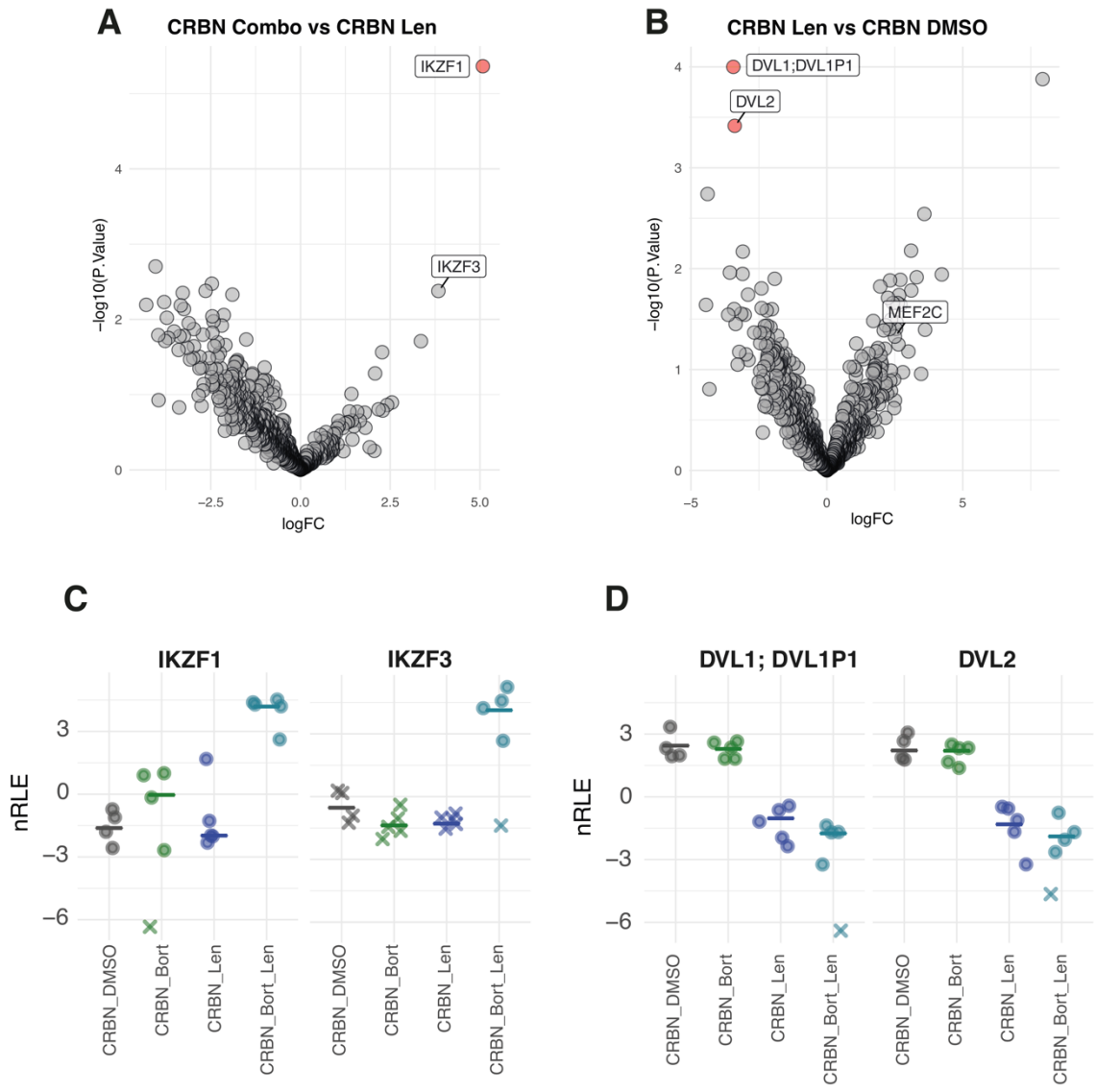
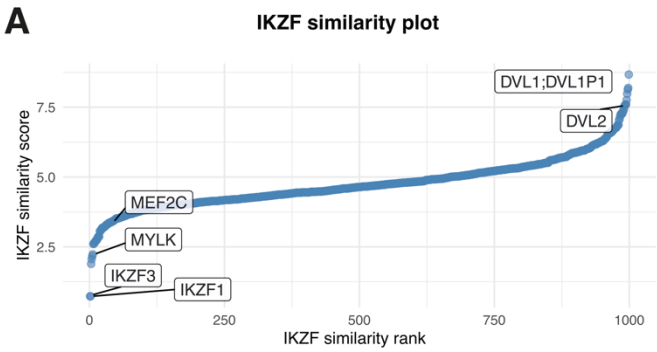


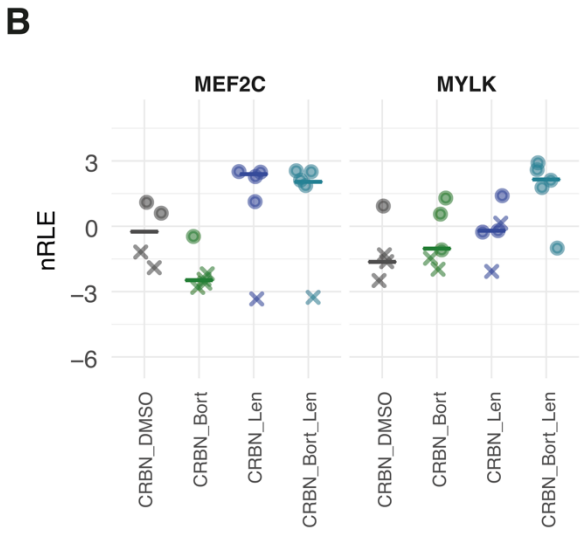
Figure 4.10. Differentially expressed proteins in LEN only and combo-treated OPM2-BioID2-CRBN

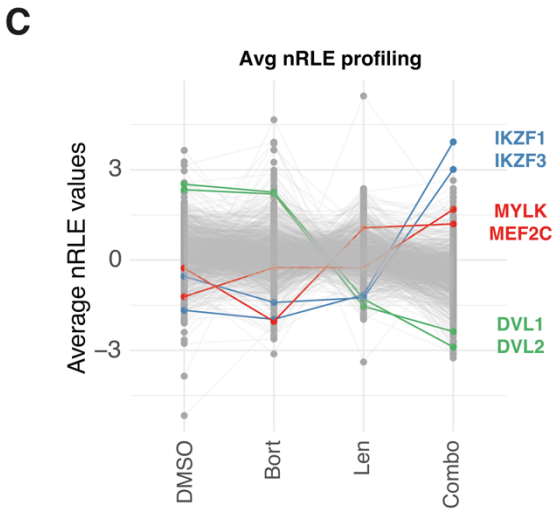
(A) Volcano plot demonstrating differentially enriched proteins between OPM2-BioID2-CRBN cells treated with LEN only and LEN plus BORT. Red dots represent proteins significant for adjusted p-value < 0.05. (B) Volcano plot demonstrating differentially enriched proteins between OPM2-BioID2-CRBN cells treated with LEN and DMSO. Red dots represent proteins significant for adjusted p-value < 0.05. (C) Plots representing nRLE values for IKZF1 and IKZF3 proteins in each technical replicate across all conditions. Dots represent real intensity values, whilst crosses represent imputed values introduced in case of intensity = 0. (D) Plots representing nRLE values for DVL1/DVL1P1 and DVL2 proteins in each technical replicate across all conditions. Dots represent real intensity values, whilst crosses represent imputed values introduced in case of intensity = 0.

Figure 4.11. IKZF-similarity profiling of purified proteins across different conditions

(A) Dotplot representing IKZF similarity score of identified proteins ranked by increasing IKZF similarity score. (B) Line plot displaying average nRLE values profile of each protein in OPM2-BioID2-CRBN cells across the four treatment conditions DMSO, BORT, LEN and combo BORT/LEN. (C) Plot showing the nRLE value of each sample across the four different treatment conditions DMSO, BORT, LEN and combo BORT/LEN for MEF2C and MYLK proteins. Horizontal bars represent the median of each sample within the same conditions. Circles represent real intensity values, whilst crosses represent imputed values.


A
IKZF similarity plot
IKZF similarity score
7.5
5.0
2.5
DVL1;DVL1P1
DVL2
MEF2C
MYLK
IKZF3
IKZF1
0
250
500
750
1000
IKZF similarity rank


B
MEF2C
MYLK
nRLE
3
0
−3
−6
CRBN_DMSO
CRBN_Bort
CRBN_Len
CRBN_Bort_Len
CRBN_DMSO
CRBN_Bort
CRBN_Len
CRBN_Bort_Len


C
Avg nRLE profiling
Average nRLE values
3
0
−3
DMSO
Bort
Len
Combo
IKZF1
IKZF3
MYLK
MEF2C
DVL1
DVL2

interact with CRBN in the absence of IMiDs, but this interaction was virtually lost in the presence of BORT (Figure 4.11C). In this condition, MEF2C was detected in only one sample (out of five). However, MEF2C was found enriched in the presence of LEN, either alone or in combination with BORT. In both conditions, there was one undetected intensity value. MYLK also displayed an enrichment profile similar to that of IKZF1/3 (Figure 4.11C). Interaction of CRBN with MYLK is virtually absent under basal conditions, with only one detected intensity value, but MYLK seemed to interact with CRBN in the presence of BORT. The enrichment of MYLK was greater in OPM2-BioID2-CRBN cells treated with LEN as compared to BORT- and DMSO-treated cells. In the combination BORT/LEN treatment, MYLK was more enriched relative to all the other conditions. These results indicate that MEF2C and MYLK might be CRBN *neointeractors* or *neosubstrates* in the presence of LEN but not CRBN endogenous interactors. Conversely, the enrichment profile of DVL1/2 suggests that these might be CRBN interactors and the interaction of DVL1/2 with CRBN might be lost upon IMiD treatment.

4.2.12.1 Identification of putative neosubstrates that are essential for viability and proliferation of MM cells

Following ranking of identified proteins in relation to their IKZF similarity score, the relevance of proteins identified by MS in the context of MM was explored by interrogation of dependency data from the DepMap respository (http://depmap.org/portal/). Dependency (measured with the CERES score) of genes expressed in MM.1S and OPM2 cells were overlapped with proteins identified in Experiment 1 in order to identify CRBN-IMiD neosubstrates or at least neointeractors that also score as dependencies in MM. It was established that a score below 3.5 would represent IKZF similarity and a score above 5.5 would represent IKZF dissimilarity. 885 proteins identified in Experiment 1 had an IKZF similarity score between 3.5 and 5.5 (in both MM.1S and OPM2 cells). 42 proteins had a similarity score < 3.5 and 138 proteins had a similarity score > 5.5. In MM.1S cells, there were 340 proteins scoring as dependencies (for screening purposes, the minimum CERES score to define a dependency was set to 0.5), and 17 of these had a low IKZF similarity score (< 3.5). MEF2C and IKZF3 were found to be essential for viability and proliferation in MM.1S cells. In addition, MEF2C demonstrated an enrichment profile similar to that of IKZF1/3, as previously discussed (Figure 4.11, 4.12A). Similar results were obtained in OPM2 cells, where 336 of the identified proteins scored as dependencies. In these cells, neither IKZF3 nor MEF2C scored as dependencies, and there were 15 proteins that were IKZF-similar and also dependencies (Figure 4.12B). However, MEF2C was chosen for further validation for three main reasons. Firstly, it has recently been demonstrated that MEF2C plays a vital role in the

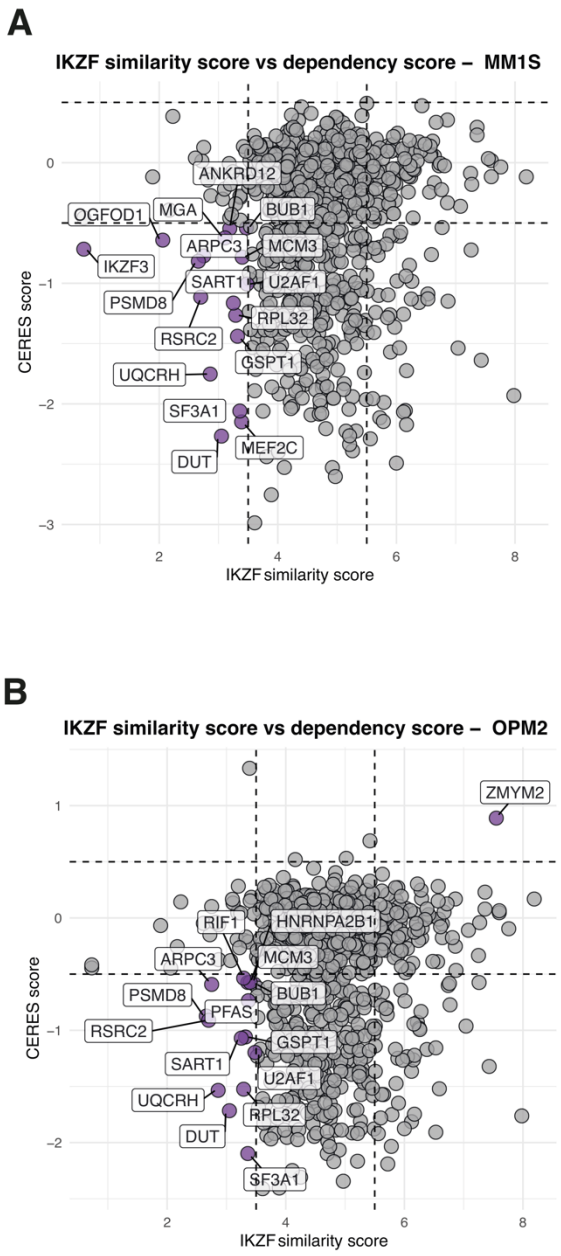


Figure 4.12. Identification of IKZF-similar MM dependencies

(A) and (B) Scatterplots displaying proteins that are IKZF-similar (in increasing order) in function of their relative CERES score in MM.1S cells and OPM2 cells, respectively. The maximum score for IKZF-similar proteins (= 3.5) was chosen as smaller than the mean minus one standard deviation of the IKZF similarity score distribution (SD = 0.89, mean = 4.73, mean – SD = 3.84) and the minimum score for IKZF-dissimilar proteins (= 5.5) was arbitrarily chosen as greater than the mean plus one standard deviation of the IKZF similarity score distribution (mean + SD = 5.62). Genes were defined as dependencies when CERES score < -0.5 and detrimental when CERES score > 0.5.

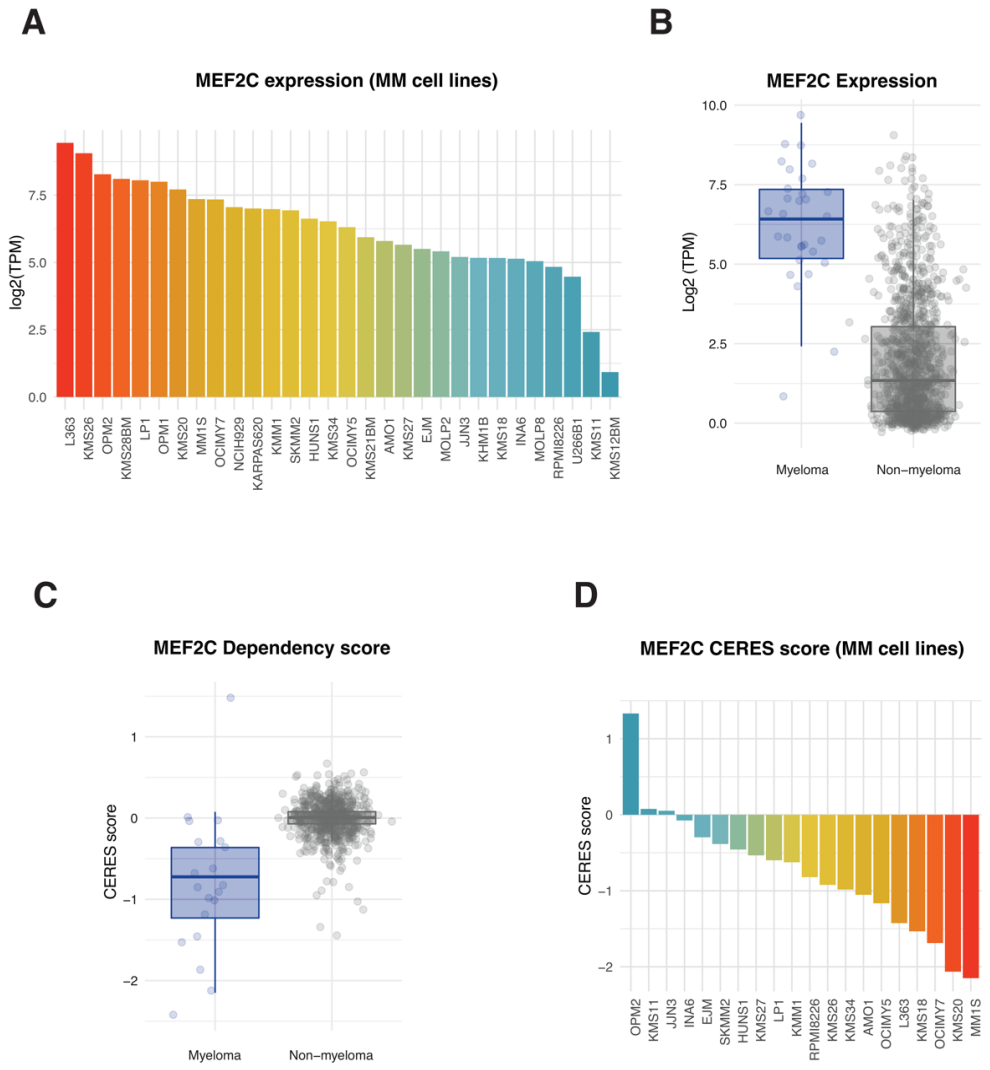
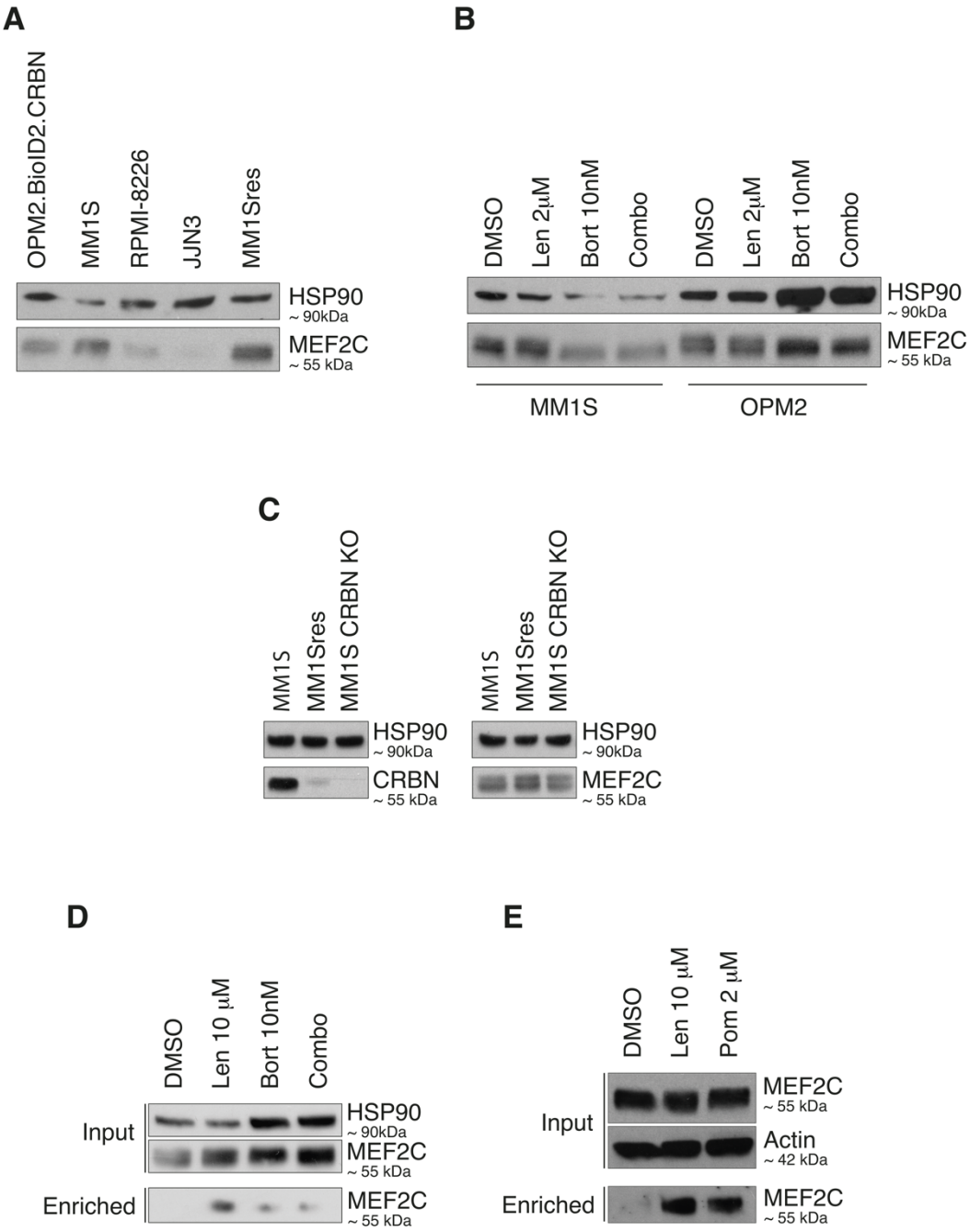


Figure 4.13. DepMap repository data of MEF2C in MM and non-MM cancer cell lines

(A) Expression of MEF2C, in log2 of transcripts per million (log2 TPM), in MM cell lines. (B) Expression of MEF2C, in log2 of transcripts per million (log2 TPM), in MM cell lines as compared to non-MM cell lines. (C) Dependency (CERES) score of MEF2C in MM cell lines. In this repository, a gene is considered a dependency when CERES < -1. (D) Dependency (CERES) score of MEF2C in MM cell lines as compared to non-MM cell lines.

Figure 4.14. Validation of MEF2C as IMiD neointeractor or neosubstrate

(A) Immunoblot demonstrating expression of MEF2C in OPM2-BioID2-CRBN, MM.1S, RPMI-8226, JJN3 and MM.1Sres MM cell lines. HSP90 is provided as loading control. (B) Immunoblot showing MEF2C expression in MM.1S and OPM2 cells treated with DMSO, LEN, BORT or combination BORT/LEN. HSP90 is provided as loading control. (C) Immunoblots displaying CRBN and MEF2C expression in MM.1S, MM.1Sres and MM.1S CRBN KO cells. HSP90 is provided as loading control. (D) Western blot showing MEF2C expression in input and biotinylated (enriched) fraction on lysates of OPM2-BioID2-CRBN cells treated with DMSO, LEN, BORT or combination BORT/LEN. HSP90 is provided as loading control for non-enriched fraction (input). (E) Western blot displaying MEF2C expression in input and biotinylated (enriched) fraction on lysates of OPM2-BioID2-CRBN cells treated with DMSO, LEN or POM. For non-enriched fraction (input), actin is provided as loading control.


A
OPM2.BioID2.CRBN
MM1S
RPMI-8226
JJN3
MM1Sres
HSP90
~ 90kDa
MEF2C
~ 55 kDa
B
DMSO
Len 2μM
Bort 10nM
Combo
DMSO
Len 2μM
Bort 10nM
Combo
HSP90
~ 90kDa
MEF2C
~ 55 kDa
MM1S
OPM2
C
MM1S
MM1Sres
MM1S CRBN KO
HSP90
~ 90kDa
CRBN
~ 55 kDa
MM1S
MM1Sres
MM1S CRBN KO
HSP90
~ 90kDa
MEF2C
~ 55 kDa
D
DMSO
Len 10 μM
Bort 10nM
Combo
Input
HSP90
~ 90kDa
MEF2C
~ 55 kDa
Enriched
MEF2C
~ 55 kDa
E
DMSO
Len 10 μM
Pom 2 μM
Input
MEF2C
~ 55 kDa
Actin
~ 42 kDa
Enriched
MEF2C
~ 55 kDa

core transcriptional regulatory network in MM[100]. Secondly, MEF2C is highly expressed in MM as compared to other cancers types. Gene expression datasets from the DepMap repository shows that this gene is highly expressed in MM cells, especially in L363, KMS26 and OPM2 cells (Figure 4.13A). MEF2C can however be lowly expressed also in some MM cell lines, as it is shown for U266 cells, KMS11 and KSM12BM (Figure 4.13A). MEF2C is also highly expressed as compared to other cancer types (Figure 4.13B). Thirdly, MM cells generally show remarkable dependency on MEF2C. This is particularly evident when comparing the dependency of MM cell lines to all non-MM cell lines (Figure 4.13C). In the cohort of MM cell lines available in the DepMap repository, OPM2, KMS11 and JJN3 are the least dependent on MEF2C (Figure 4.13D). In particular, the dependency score for OPM2 is positive, suggesting that loss of MEF2C might be advantageous for OPM2 cells. On the other hand, MM.1S, KMS20 and OCIMY7 are the most MEF2C-dependent cell lines (Figure 4.13D).

MEF2C expression was therefore evaluated in some of the available MM cell lines in the Johnstone Laboratory. Lysates of OPM2-BioID2-CRBN, MM.1S, MM.1Sres, RPMI-8226 and JJN3 cells were made in RIPA buffer and studied via immunoblotting (Figure 4.14A). OPM2-BioID2-CRBN, MM.1S and MM.1Sres cells displayed higher expression of MEF2C relative to RPMI-8226 and JJN3 cells. Interestingly, IMiD-sensitive cell lines OPM2 and MM.1S cells, together with MM.1Sres cells (the isogenic IMiD-resistant MM.1S cell line), showed elevated expression of MEF2C both at a protein levels, whilst IMiD-resistant RPMI-8226 and JJN3 cells demonstrated lower MEF2C and protein expression. Lower *MEF2C* expression in RPMI-8226 and JJN3 cells, and higher *MEF2C* expression in MM.1S and OPM2 cells, were also demonstrated with data on *MEF2C* expression from the DepMap repository (Figure 4.13A). Thus, there seemed to be a positive correlation between IMiD sensitivity and MEF2C expression. Expression of MEF2C was also assessed in MM.1S and OPM2 cells treated with DMSO, LEN, BORT and BORT/LEN for 16 hours to verify the occurrence of potential LEN-induced MEF2C degradation and subsequent stabilisation in the combo setting (Figure 4.14B). MEF2C did not seem significantly downregulated in either MM.1S or OPM2 cells following LEN treatment. In MM.1S cells, the addition of bortezomib reduced MEF2C expression, but the expression of housekeeping gene HSP90 was also suppressed, possibly suggesting higher toxicity of bortezomib in MM.1S cells as compared to OPM2 cells. Conversely, in BORT and BORT/LEN treated OPM2 cells, MEF2C levels were increased. Next, it was hypothesised that MEF2C might be an endogenous substrate of CRBN. Expression of MEF2C was not substantially different in MM.1S, MM.1Sres or CRBN KO MM.1S cells, indicating that MEF2C is not an endogenous CRBN substrate (Figure 4.14C).

4.2.12.2 The transcription factor MEF2C is a CRBN-IMiD *neointeractor*

Subsequently, enrichment of MEF2C in OPM2-BioID2-CRBN cells was tested in order to validate the MS proteomics data. OPM2-BioID2-CRBN cells were seeded in biotin-free media and cultured in DMSO, 10nM BORT, 10μM LEN or in double treatment for 16 hours in presence of exogenous 50μM biotin. OPM2-BioID2-CRBN cells were then harvested and lysed in RIPA. Cell lysates were incubated with streptavidin-agarose resins for biotinyl-protein enrichment. A small aliquot of lysate was taken as input control prior to enrichment. Expression of MEF2C in inputs and enriched fractions were studied via immunoblot (Figure 4.14D; for details see material and methods, section 2.3.4). No change in MEF2C expression was observed in the input fraction. However, in the enriched fraction, MEF2C was more abundant following treatment with LEN as compared to all other conditions. In BORT-treated cells MEF2C was also detected. This result indicates that MEF2C is a CRBN-LEN *neointeractor*. Next, it was determined if MEF2C is a CRBN-POM *neointeractor*. OPM2-BioID2-CRBN cells were therefore treated with DMSO, 10μM LEN or 2μM POM in presence of exogenous 50μM biotin for 24 hours. This timepoint was chosen because, in the absence of BORT, the labelling time can be prolonged without technical limitation due by the toxicity of proteasome inhibition. The input fraction demonstrated no change in MEF2C expression across cells treated with DMSO, LEN or POM, indicating that MEF2C is not a POM neosubstrate. Purification of biotinylated proteins, however, showed that MEF2C is enriched following treatment with both LEN and POM, but not in the presence of DMSO, indicating that MEF2C is also a CRBN-POM *neointeractor* (Figure 4.14E).

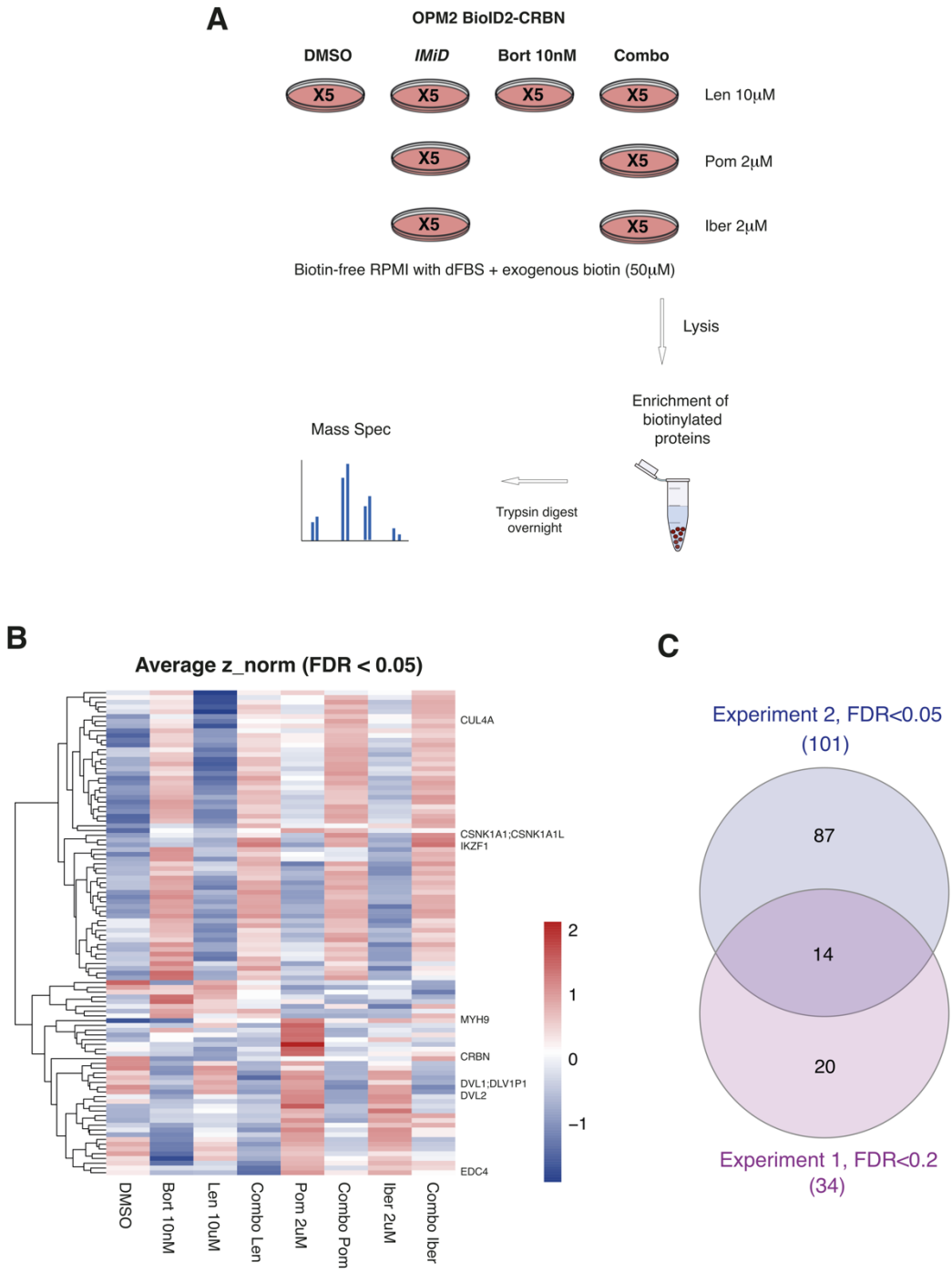
These observations, taken together with publicly available data from the DepMap portal, demonstrated that *MEF2C* is an essential gene in MM and that treatment with IMiDs induces CRBN to interact with MEF2C protein. In addition, a correlation between MEF2C levels and IMiD sensitivity was observed, suggesting that MEF2C might play a role in sensitivity to IMiDs.

4.2.13 The study of the CRBN interactome in the context of treatment with different IMiDs (Experiment 2)

Next, the aim was to extend this approach to OPM2-BioID2-CRBN cells treated POM and IBER (in presence and absence of a proteasome inhibitor) in order to cross-compare the effect of different IMiDs on the CRBN interactome. In a similar experiment to Experiment 1, OPM2-BioID2-CRBN cells were cultured in DMSO, 10nM BORT, 10μM LEN, 2μM POM, 2μM IBER or in a combination of BORT with each IMiD, with five technical replicates per condition, in presence of

Figure 4.15. MS proteomics of OPM2-BioID2-CRBN cells with three different IMiDs

(A) Schematic representation of the workflow for MS proteomics on biotinylated species of OPM2-BioID2-CRBN cells treated with DMSO, BORT, LEN, POM, IBER or a combination of BORT with each IMiD. (B) Heatmap showing differentially expressed proteins across all samples, significant for false discovery ratio < 0.05 (two-way ANOVA). Differential expression is measured with the average z_norm, which corresponds to the nRLE of each sample normalised by its SD. (C) Venn diagram showing overlap of differentially enriched proteins identified in both Experiment 1 (significant FDR < 0.2, two-way ANOVA) and Experiment 2 (significant FDR < 0.05, two-way ANOVA).


A
OPM2 BioID2-CRBN
DMSO
IMiD
Bort 10nM
Combo
X5
Len 10μM
Pom 2μM
Iber 2μM
Biotin-free RPMI with dFBS + exogenous biotin (50μM)
Lysis
Enrichment of biotinylated proteins
Trypsin digest overnight
Mass Spec
B
Average z_norm (FDR < 0.05)
CUL4A
CSNK1A1;CSNK1A1L
IKZF1
MYH9
CRBN
DVL1;DLV1P1
DVL2
EDC4
2
1
0
−1
DMSO
Bort 10nM
Len 10uM
Combo Len
Pom 2uM
Combo Pom
Iber 2uM
Combo Iber
C
Experiment 2, FDR<0.05
(101)
87
14
20
Experiment 1, FDR<0.2
(34)

50μM biotin. After 16 hours, cells were harvested and lysed in RIPA buffer, and protein concentration was measured with a BCA assay. Lysates were enriched with Streptavidin-Agarose resins, digested with trypsin and peptides injected in the mass spectrometer for label-free quantitative proteomics (Figure 4.15A).

4.2.13.1 Detection of putative neosubstrates IKZF1 and CK1α occurs in cells treated with any BORT/IMiD combination

Differential protein enrichment was calculated across all conditions to assess differences in the CRBN interactome in the presence of different IMiDs. 102 of identified proteins were significant for adjusted p-value < 0.05 (two-way ANOVA) (Figure 4.15B). 14 proteins identified in Experiment 2 (significant for adjusted p-value < 0.05, two-way ANOVA) were also present in Experiment 1 (significant for adjusted p-value < 0.2, two-way ANOVA) (Figure 4.15C). These were MYH9, DVL1/DVL1P1, DVL2, IKZF1, G3BP1, CCT3 EIF3C/EIF3CL, RRM2, HNRNPA0, IGJ/JCHAIN, IMMT, CTTN, VCPIP1, PLAA (Figure 4.15C). In addition to CRBN and its scaffold CUL4A, two *bona fide* neosubstrates were identified (IKZF1 and CSNK1A1 – CK1α; Figure 4.16A-B). IKZF1 was not detected in DMSO, LEN, POM and IBER-treated cells, with consequent intensity value imputation. IKZF1 was detected in one replicate of BORT-treated cells, and highly enriched in BORT/LEN, BORT/POM and BORT/IBER cells. CK1α was found enriched in all the combo treatment conditions but not in DMSO and IMiDs, where intensities were imputed. In BORT-treated cells, only two replicates demonstrated enrichment of CK1α, whilst the intensities of the other three replicates were imputed. In this experiment, MEF2C nor IKZF3 were not detected. Interestingly, loss of EDC4 causes resistance to LEN (see chapter 3, paragraph 3.2.4.3) and was identified as a CRBN interactor in this experiment (Figure 4.16C). EDC4, however, did not demonstrate significant enrichment in the double-agent treatment conditions. It was enriched in DMSO-, LEN-, POM-, BORT/POM-, IBER- and BORT/IBER-treated cells. In the Combo/LEN condition, intensities from all replicates were not detected. EDC4 was detected in only one replicate in BORT-exposed cells. These results showed that IKZF1 and CK1α possess an enrichment profile matching that of a neosubstrate. EDC4, however, did not seem to be a neosubstrate but rather a CRBN interactor.

4.2.13.2 Correlative studies and data clustering define sources of variability and identify similarities in the CRBN interactome across treatment conditions

To understand overall variations of the CRBN interactome in the context of different drug treatments, Pearson's correlation, principal component analysis (PCA) and k-mean clustering were applied to the dataset. By calculating a Pearson's correlation (Figure 4.17A), the data

demonstrated a clear separation between cells treated with BORT and without BORT. POM and IBER seemed more correlated to each other as compared to LEN and POM or LEN and IBER. The addition of BORT to IMiDs resulted in increased correlation between IMiDs. Next, PCA was performed in combination with k-mean clustering. 2, 4 or 8 number of k-mean clusters were utilised (Figure 4.17B-D). PCA plots demonstrated that BORT is the major factor of variance in the dataset, which can be observed along component 1 (PCA1). In particular, most of the variability (65.07%) in the dataset was distributed along PC1, followed by PC2 (14.73%), where variations of the CRBN interactome in the presence of different IMiDs is distributed. Again, POM and IBER displayed less variation as compared to LEN-POM or LEN-IBER, suggesting that the effect of POM is probably more similar to that of IBER. In addition, unsupervised k-mean clustering with k = 2 clusters (Figure 4.17B) also showed that differentially enriched proteins separate into two main groups, which distributed along the eigenvector direction of each condition. The first cluster overlaid with samples where BORT was not present, the second overlaid with samples where BORT was added either alone or in combination with IMiDs. Clustering with k = 4 (Figure 4.17C) demonstrated demarcation between BORT, non-BORT, DMSO/LEN and POM/IBER samples. With k = 8 (Figure 4.17D), however, there was overlay of different clusters as variance tended to be smaller. This suggested that the ideal number of clusters sits probably between k = 4 and k = 6. Since cluster overlay occurred in POM and IBER, the data suggests once again high similarities between POM and IBER in modifying CRBN interactome. Finally, PCA and unsupervised clustering were performed on proteins of choice: the neosubstrates IKZF1 and CK1α, CRBN, and proteins identified in Experiment 1, MYH9 and DVL1 (Figure 4.17E-F). PCA demonstrated that IKZF1 and CK1α sit in the direction of combination treatment eigenvectors, MYH9 in that of IMiDs only, CRBN in that of DMSO and DVL1. With k = 2 (Figure 4.17E), clustering showed no clear demarcation of BORT and non-BORT treated samples. Conversely, with k = 4, separation of hits with different enrichment profiles was clear (Figure 4.17F). More detail regarding the roles and activities of these proteins will be further discussed.

4.2.14 BioID2-CRBN induces biotinylation of proteins involved in RNA processing, protein translation and cell motility

Average log2 of intensity values across conditions (average of z_norm) for each protein was subsetted according to differential protein enrichment across samples. The first group to be subsetted was that of protein enriched with BORT and BORT/IMiDs as compared to IMiDs and DMSO only (Figure 4.18). This subset displayed those proteins where the interaction with CRBN

Figure 4.16. IKZF1, CK1α and EDC4 z_norm plots

(A) Plots showing z_norm values of each sample across all treatment conditions for IKZF1. (B) Plots showing z_norm values of each sample across all treatment conditions for CK1α. (C) Plots showing z_norm values of each sample across all treatment conditions for EDC4. In the figure, circles represent real intensity values, whilst crosses represent imputed values. Horizontal bars in (A), (B) and (C) represent the median of the z_norm values in each condition.

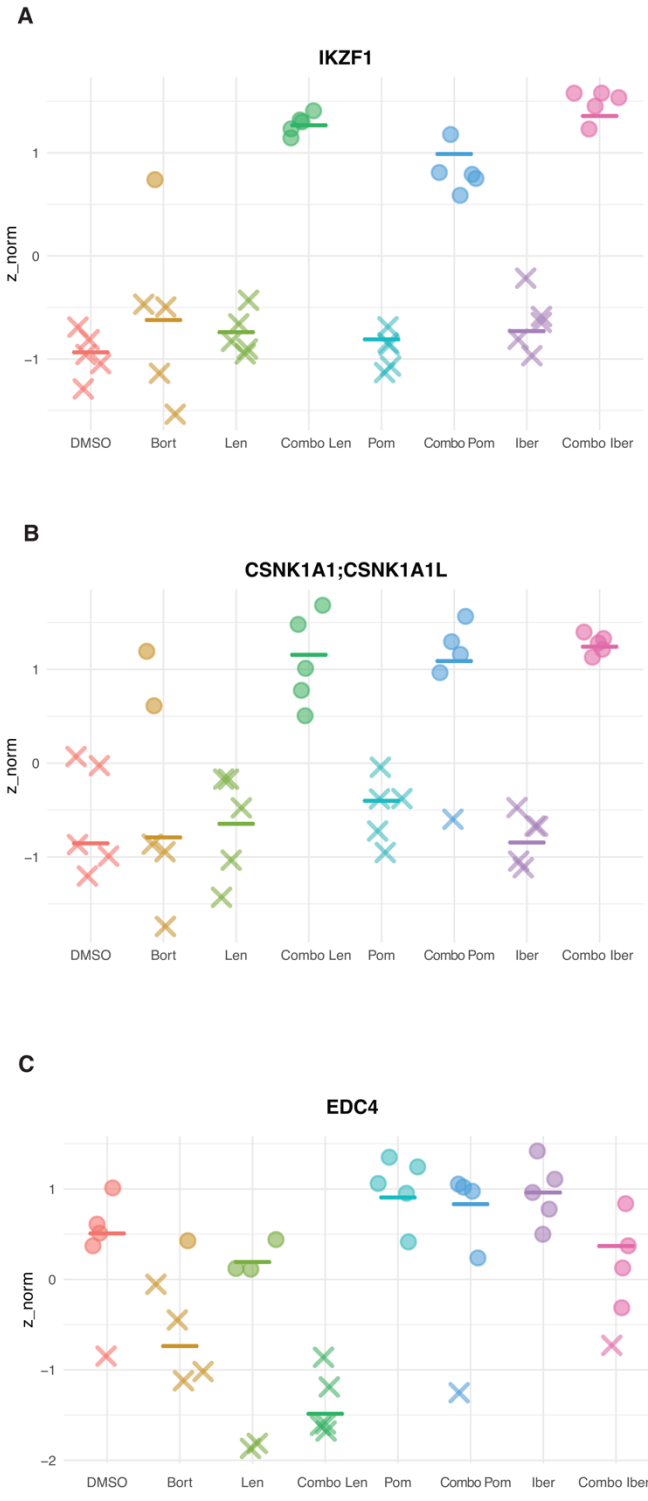

A
IKZF1
z_norm
1
0
−1
DMSO
Bort
Len
Combo Len
Pom
Combo Pom
Iber
Combo Iber
B
CSNK1A1;CSNK1A1L
z_norm
1
0
−1
DMSO
Bort
Len
Combo Len
Pom
Combo Pom
Iber
Combo Iber
C
EDC4
z_norm
1
0
−1
−2
DMSO
Bort
Len
Combo Len
Pom
Combo Pom
Iber
Combo Iber

Figure 4.17. Analysis of variance and correlation across different treatment conditions

(A) Heatmap showing correlation of variance in the proteome across treatment conditions (DMSO, LEN, POM, IBER, BORT, COMBO LEN, COMBO POM, COMBO IBER). (B) Principal component analysis on all differentially enriched proteins significant for false discovery ratio < 0.05 (two-way ANOVA). Arrows represent eigenvectors of each condition. Circles indicate differentially enriched proteins colour-coded based on 2 k-mean clusters. (C) Principal component analysis on all differentially enriched proteins significant for false discovery ratio < 0.05 (two-way ANOVA). Arrows represent eigenvectors of each condition. Circles indicate differentially enriched proteins colour coded based on 4 k-mean clusters. (D) Principal component analysis of all differentially enriched proteins significant for false discovery ratio < 0.05 (two-way ANOVA). Arrows represent eigenvectors of each condition. Circles indicate differentially enriched proteins colour-coded based on 8 k-mean clusters. (E) Principal component analysis on selected proteins (IKZF1, CK1α, CRBN, MYH9, DVL1/DVL1P1). Arrows represent eigenvectors of each condition. Circles indicate differentially enriched proteins colour-coded based on 2 k-mean clusters. (F) Principal component analysis of selected proteins (IKZF1, CK1α, CRBN, MYH9, DVL1/DVL1P1). Arrows represent eigenvectors of each condition. Circles indicate differentially enriched proteins colour-coded based on 4 k-mean clusters.

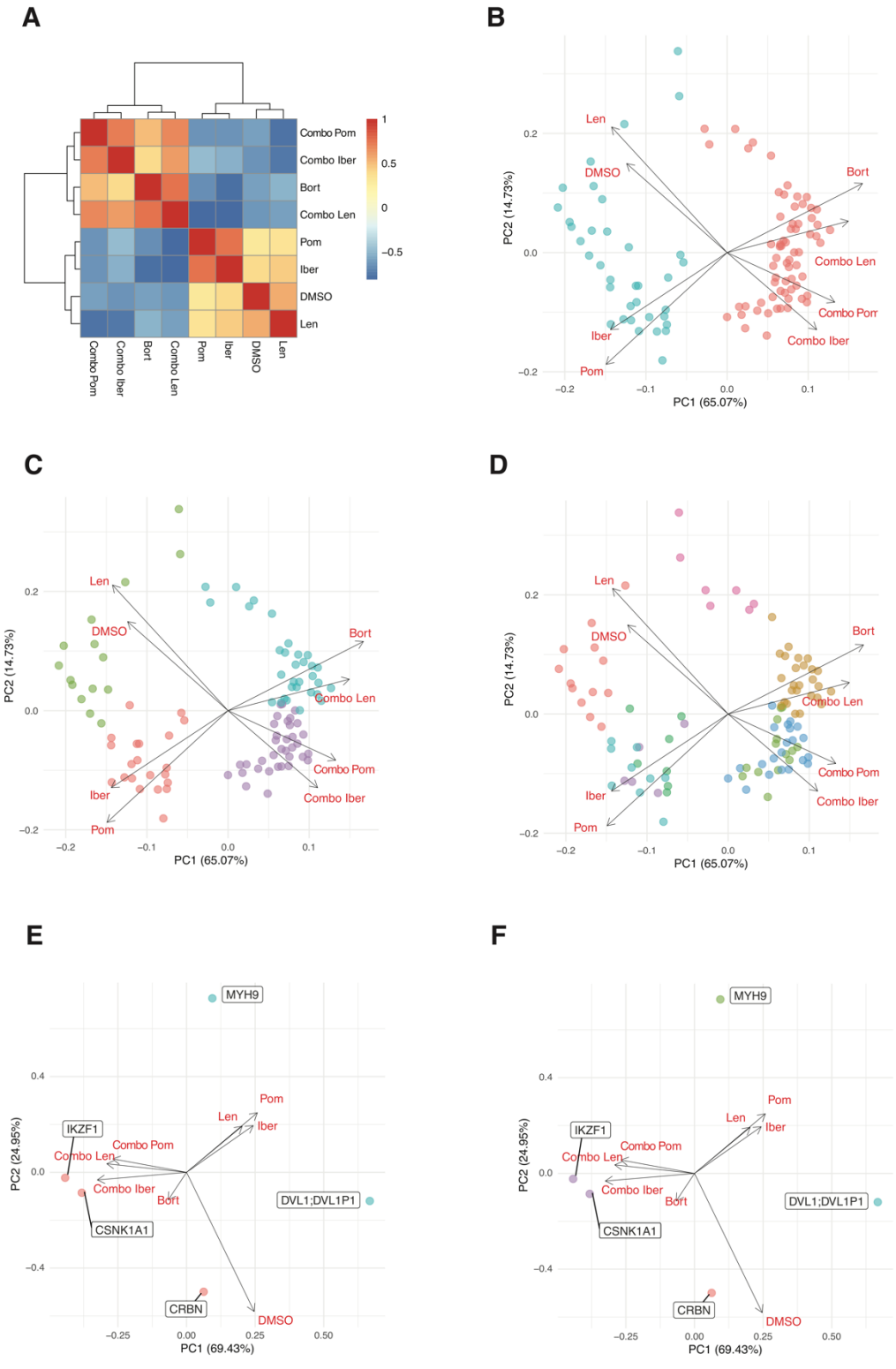
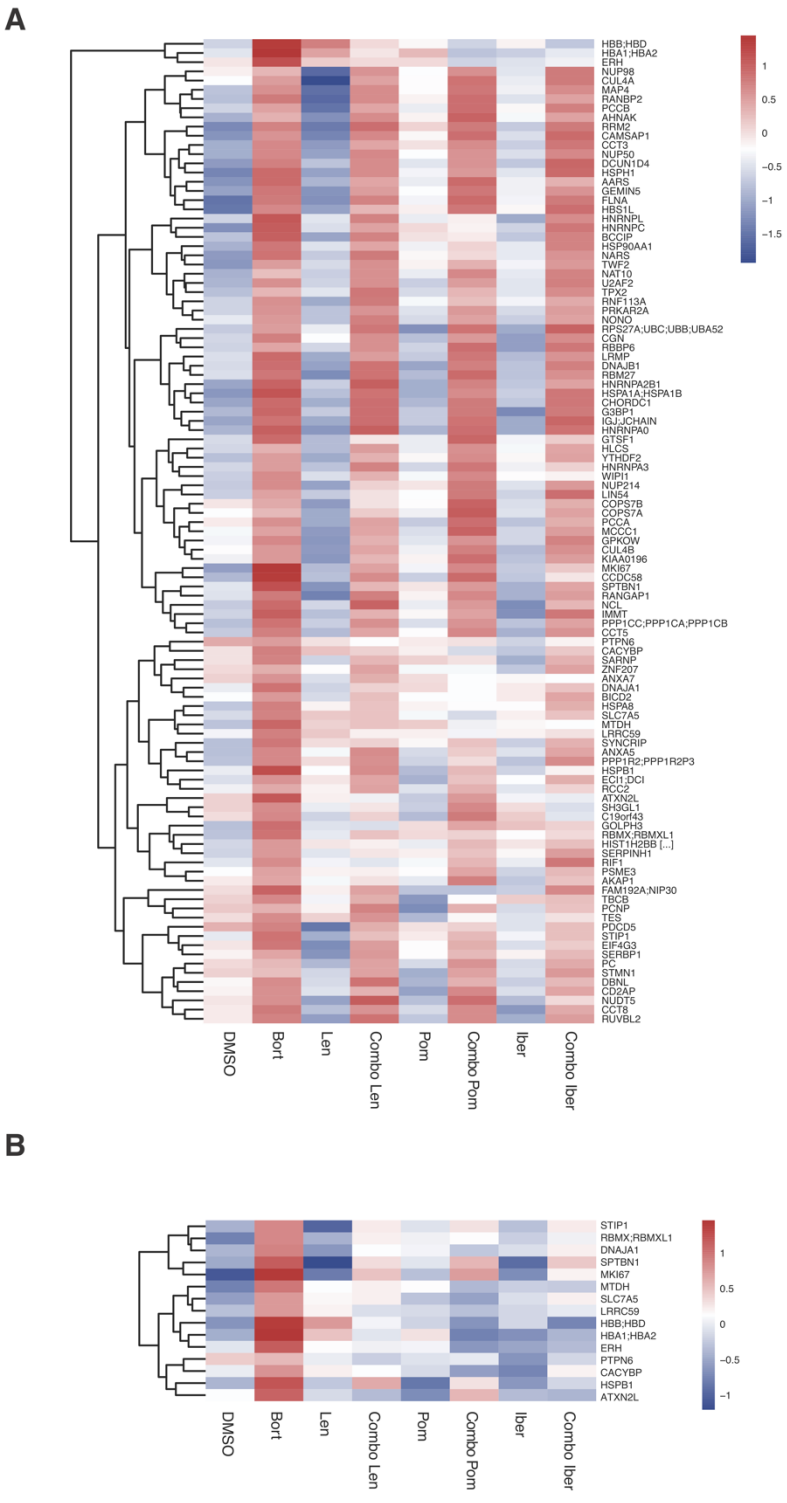

A
Combo Pom
Combo Iber
Bort
Combo Len
Pom
Iber
DMSO
Len
1
0.5
0
−0.5
B
PC2 (14.73%)
PC1 (65.07%)
C
D
E
PC2 (24.95%)
PC1 (69.43%)
MYH9
IKZF1
CSNK1A1
CRBN
DVL1;DVL1P1
F

Figure 4.18. Proteins enriched in presence of bortezomib

(A) Heatmap representing the average z_norm of proteins with increased enrichment in all cells exposed to BORT, including BORT in combination with IMiDs. Subsetting criteria used were: $mean(z_norm)_{BORT} > mean(z_norm)_{All\ IMiDs} + 0.5$ and $mean(z_norm)_{BORT} > mean(z_norm)_{DMSO}$. (B) Heatmap representing proteins with increased enrichment in all cells exposed to BORT, excluding BORT in combination with IMiDs. Subsetting criteria used were: $mean(z_norm)_{BORT} > mean(z_norm)_{All\ IMiDs} + 0.5$, $mean(z_norm)_{BORT} > mean(z_norm)_{All\ Combos}$ and $mean(z_norm)_{BORT} > mean(z_norm)_{DMSO}$.


A
HBB;HBD
HBA1;HBA2
ERH
NUP98
CUL4A
MAP4
RANBP2
PCCB
AHNAK
RRM2
CAMSAP1
CCT3
NUP50
DCUN1D4
HSPH1
AARS
GEMIN5
FLNA
HBS1L
HNRNPL
HNRNPC
BCCIP
HSP90AA1
NARS
TWF2
NAT10
U2AF2
TPX2
RNF113A
PRKAR2A
NONO
RPS27A;UBC;UBB;UBA52
CQN
RBBP6
LRMP
DNAJB1
RBM27
HNRNPA2B1
HSPA1A;HSPA1B
CHORDC1
G3BP1
IGJ;JCHAIN
HNRNPA0
GTSF1
HLCS
YTHDF2
HNRNPA3
WIPI1
NUP214
LIN54
COPS7B
COPS7A
PCCA
MCCC1
GPKOW
CUL4B
KIAA0196
MKI67
CCDC58
SPTBN1
RANGAP1
NCL
IMMT
PPP1CC;PPP1CA;PPP1CB
CCT5
PTPN6
CACYBP
SARNP
ZNF207
ANXA7
DNAJA1
BICD2
HSPA8
SLC7A5
MTDH
LRRC59
SYNCRIP
ANXA5
PPP1R2;PPP1R2P3
HSPB1
ECI1;DCI
RCC2
ATXN2L
SH3GL1
C19orf43
GOLPH3
RBMX;RBMXL1
HIST1H2BB [...]
SERPINH1
RIF1
PSME3
AKAP1
FAM192A;NIP30
TBCB
PCNP
TES
PDCD5
STIP1
EIF4G3
SERBP1
PC
STMN1
DBNL
CD2AP
NUDT5
CCT6
RUVBL2
1
0.5
0
−0.5
−1
−1.5
DMSO
Bort
Len
Combo Len
Pom
Combo Pom
Iber
Combo Iber
B
STIP1
RBMX;RBMXL1
DNAJA1
SPTBN1
MKI67
MTDH
SLC7A5
LRRC59
HBB;HBD
HBA1;HBA2
ERH
PTPN6
CACYBP
HSPB1
ATXN2L
1
0.5
0
−0.5
−1
DMSO
Bort
Len
Combo Len
Pom
Combo Pom
Iber
Combo Iber

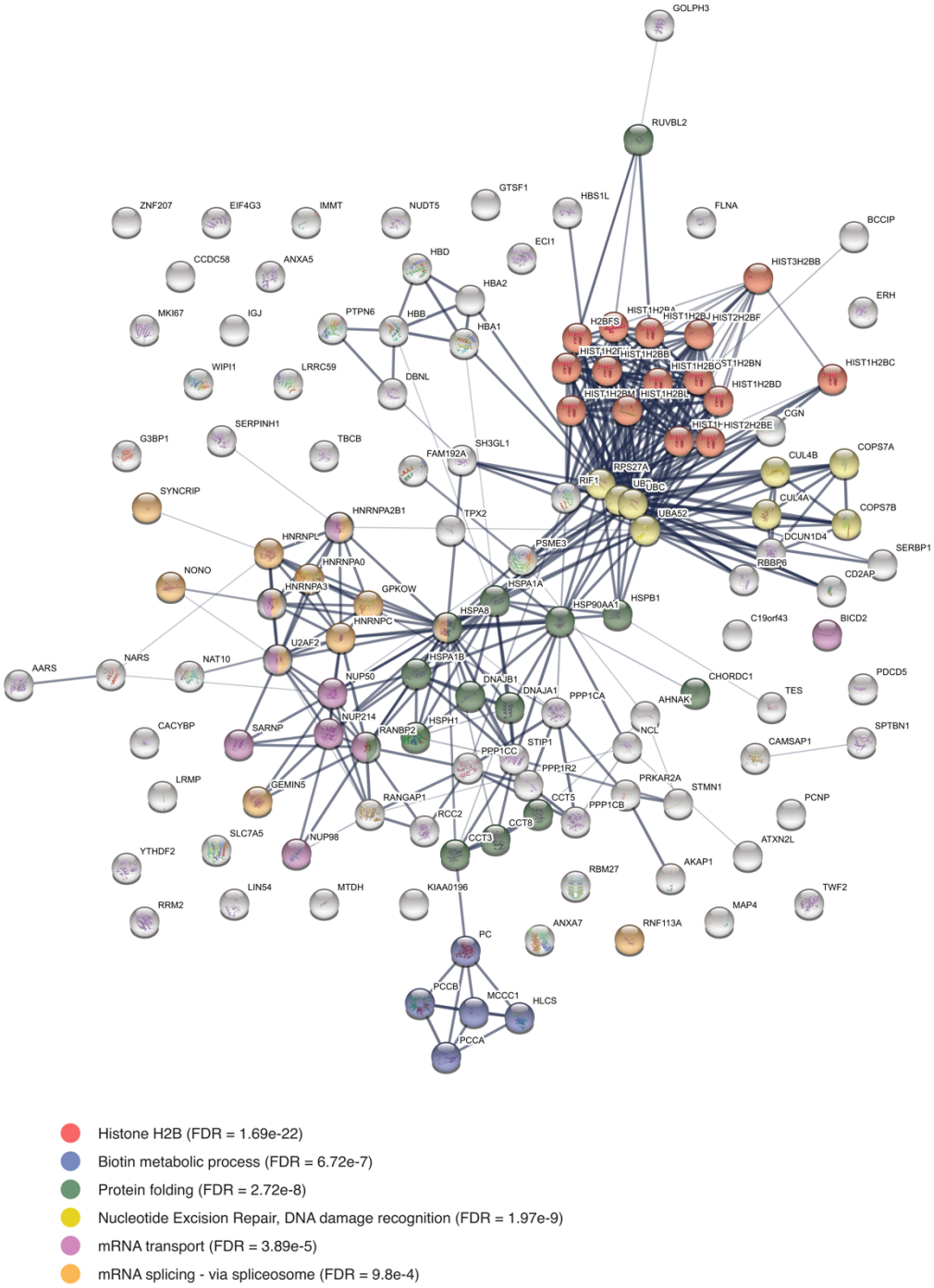


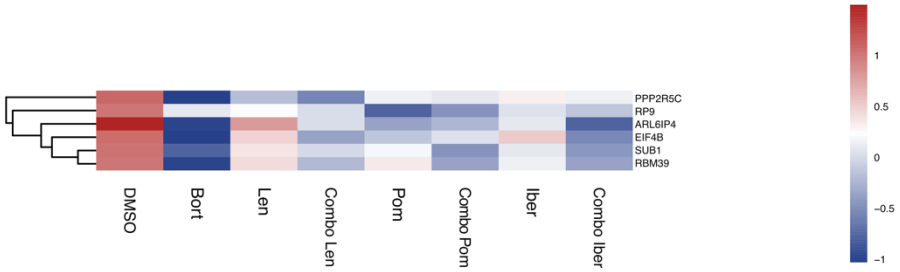
Figure 4.19. PPI and GO analyses of proteins enriched upon bortezomib treatment

Protein-Protein Interaction network of proteins of the subset in Figure 4.18A with relative GO term analysis colour-coded by pathway. FDR = False Discovery Ratio.

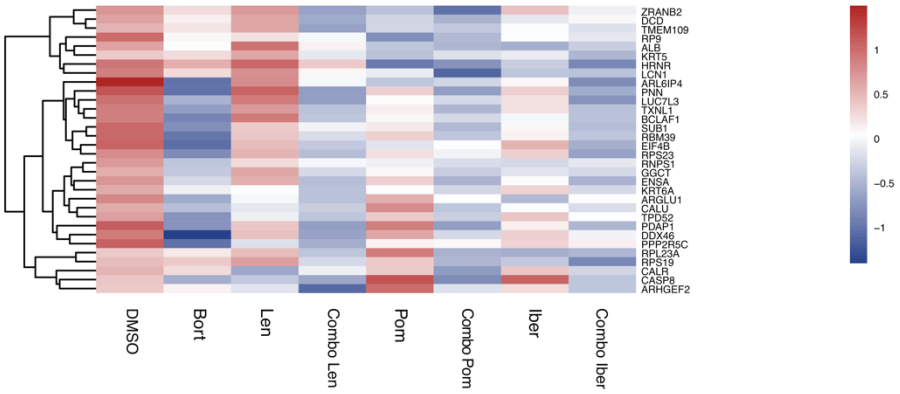
Figure 4.20. Proteins losing interaction with CRBN following BORT or IMiD exposure

(A) Heatmap showing the average z_norm of proteins that are highly enriched in cells treated with vehicle. These proteins lose interaction with CRBN in the presence of either BORT, IMiDs or combo treatment. Subsetting criteria used were: $mean(z_norm)_{DMSO} > mean(z_norm)_{BORT}$, $mean(z_norm)_{DMSO} > mean(z_norm)_{All\ IMiDs} + 0.5$ and $mean(z_norm)_{BORT} > mean(z_norm)_{All\ Combos} + 0.5$. (B) Heatmap showing the average z_norm of proteins that are highly enriched in cells treated with vehicle. These proteins lose interaction with CRBN in the presence of either BORT, at least one IMiD, or combinatorial treatment. Subsetting criteria used were: $mean(z_norm)_{DMSO} > mean(z_norm)_{BORT}$, $mean(z_norm)_{DMSO} > mean(z_norm)_{1+\ IMiDs} + 0.5$ and $mean(z_norm)_{BORT} > mean(z_norm)_{All\ Combos} + 0.5$. (C) Protein-Protein Interaction network of proteins of the subset in (B) with relative GO term analysis colour-coded by pathway. FDR = False Discovery Ratio.

A


PPP2R5C
RP9
ARL6IP4
EIF4B
SUB1
RBM39
DMSO
Bort
Len
Combo Len
Pom
Combo Pom
Iber
Combo Iber
1
0.5
0
−0.5
−1

B


ZRANB2
DCD
TMEM109
RP9
ALS
KRT5
HRNR
LCN1
ARL6IP4
PNN
LUC7L3
TXNL1
BCLAF1
SUB1
RBM39
EIF4B
RPS23
RNPS1
GGCT
ENSA
KRT6A
ARGLU1
CALU
TPD52
PDAP1
DDX46
PPP2R5C
RPL23A
RPS19
CALR
CASP8
ARHGEF2
DMSO
Bort
Len
Combo Len
Pom
Combo Pom
Iber
Combo Iber
1
0.5
0
−0.5
−1

C

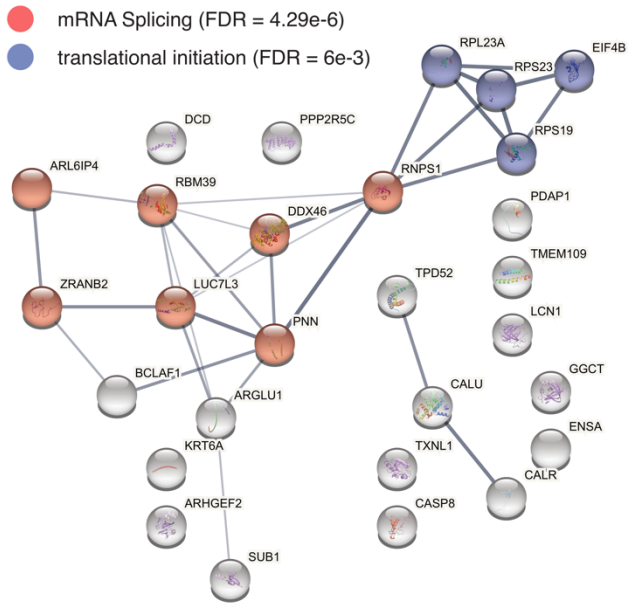

mRNA Splicing (FDR = 4.29e-6)
translational initiation (FDR = 6e-3)
RPL23A
EIF4B
RPS23
DCD
PPP2R5C
RPS19
ARL6IP4
RNPS1
RBM39
PDAP1
DDX46
TMEM109
TPD52
ZRANB2
LUC7L3
LCN1
PNN
GGCT
BCLAF1
CALU
ARGLU1
ENSA
KRT6A
TXNL1
CALR
ARHGEF2
CASP8
SUB1

Figure 4.21. Proteins with increased interaction with CRBN upon IMiD treatment

(A) Heatmap showing the average z_norm of proteins that are highly enriched in cells treated with IMiDs. These proteins do not strongly interact with CRBN in baseline conditions or in the presence of either BORT. These proteins interact with CRBN in the presence of IMiDs or combo treatment. Subsetting criteria used were: $mean(z_norm)_{All\ IMiD} > mean(z_norm)_{DMSO}$, $mean(z_norm)_{All\ IMiDs} > mean(z_norm)_{BORT} + 0.5$ and $mean(z_norm)_{All\ Combos} > mean(z_norm)_{DMSO} + 0.5$. (B) Protein-Protein Interaction network of proteins of the subset in (A) with relative GO term analysis colour-coded by pathway. FDR = False Discovery Ratio.

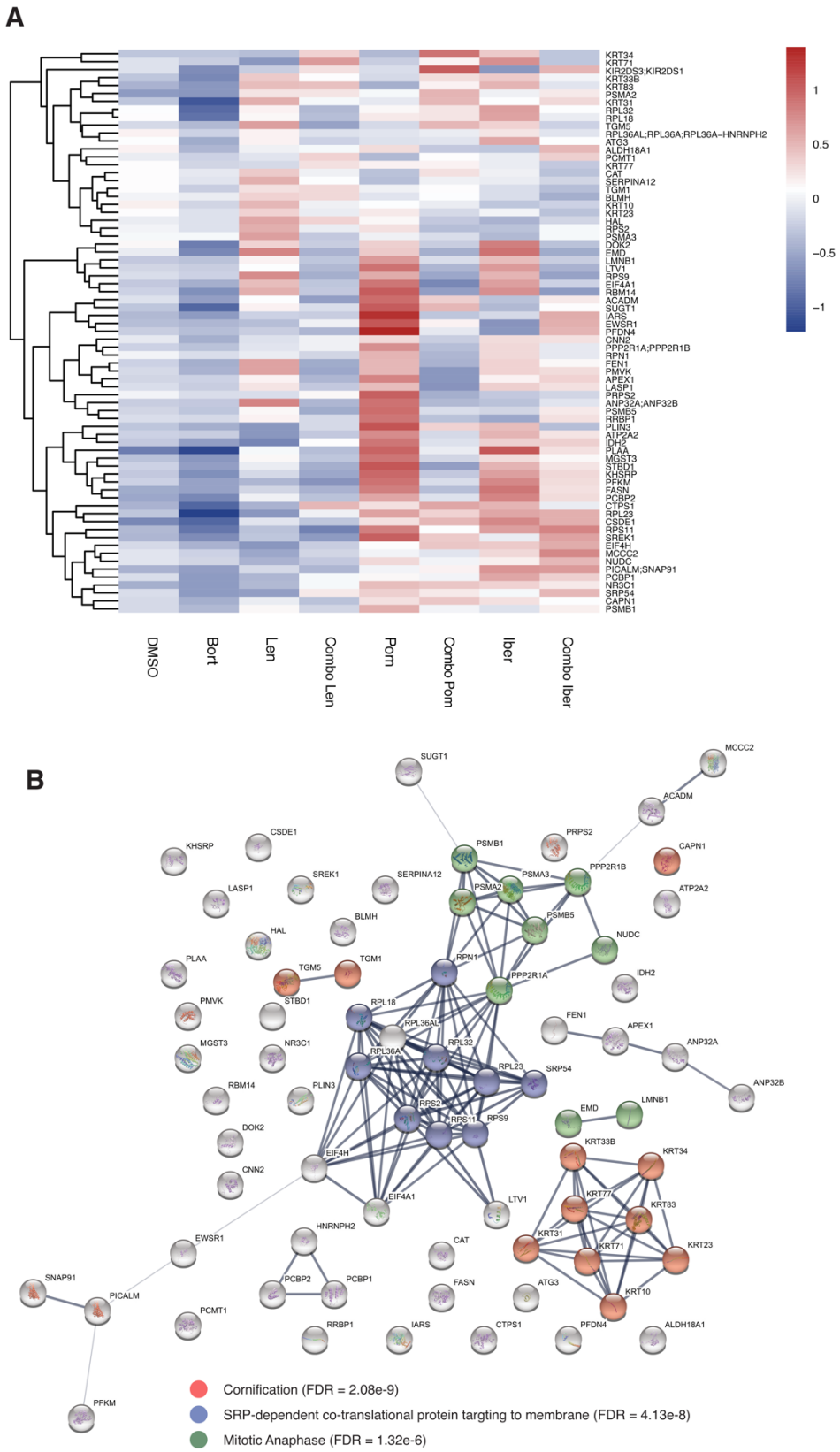
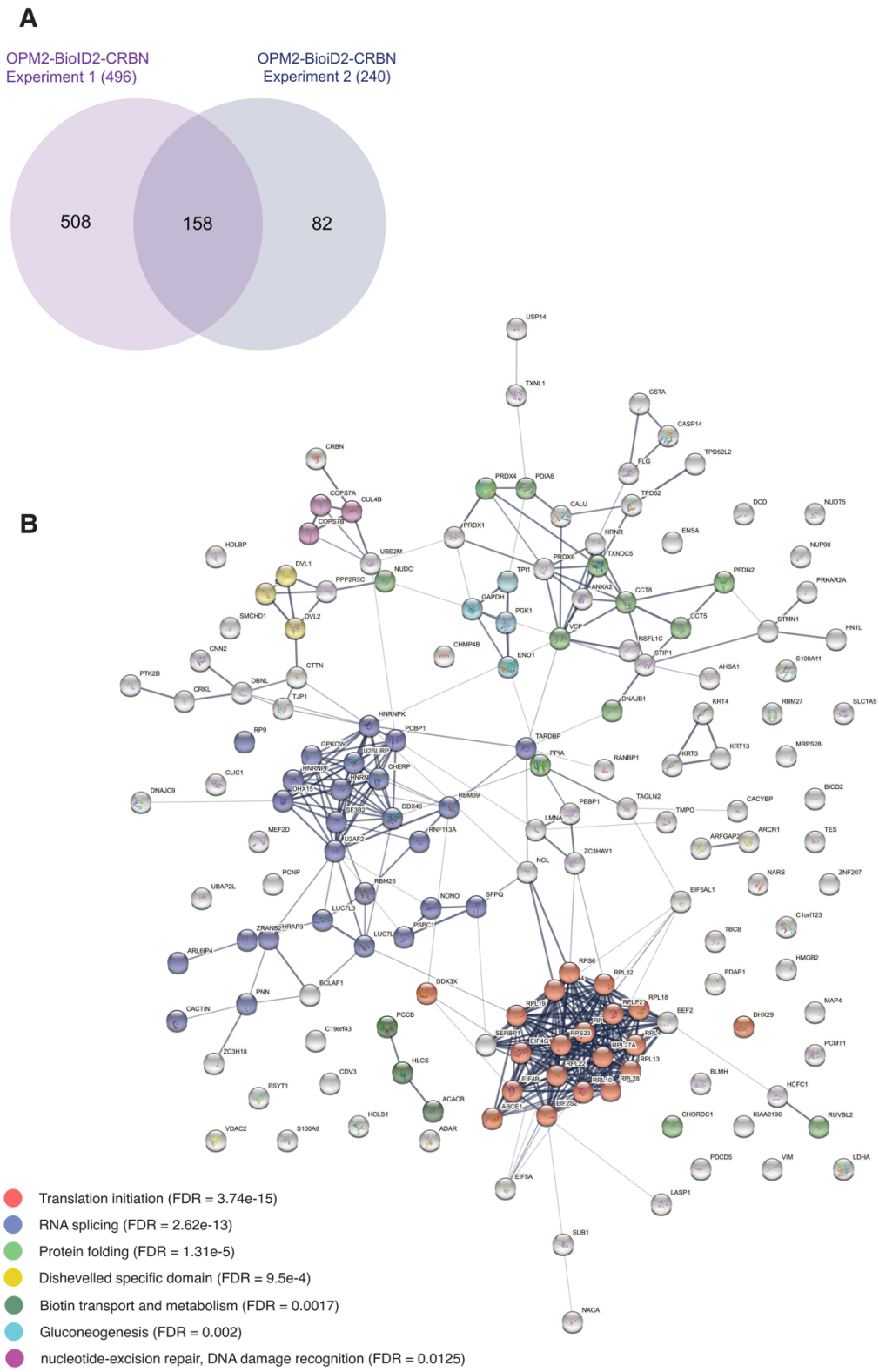

A
KRT34
KRT71
KIR2DS3;KIR2DS1
KRT33B
KRT83
PSMA2
KRT31
RPL32
RPL18
TGM5
RPL36AL;RPL36A;RPL36A−HNRNPH2
ATG3
ALDH18A1
PCMT1
KRT77
CAT
SERPINA12
TGM1
BLMH
KRT10
KRT23
HAL
RPS2
PSMA3
DOK2
EMD
LMNB1
LTV1
RPS9
EIF4A1
RBM14
ACADM
SUGT1
IARS
EWSR1
PFDN4
CNN2
PPP2R1A;PPP2R1B
RPN1
FEN1
PMVK
APEX1
LASP1
PRPS2
ANP32A;ANP32B
PSMB5
RRBP1
PLIN3
ATP2A2
IDH2
PLAA
MGST3
STBD1
KHSRP
PFKM
FASN
PCBP2
CTPS1
RPL23
CSDE1
RPS11
SREK1
EIF4H
MCCC2
NUDC
PICALM;SNAP91
PCBP1
NR3C1
SRP54
CAPN1
PSMB1
1
0.5
0
−0.5
−1
DMSO
Bort
Len
Combo Len
Pom
Combo Pom
Iber
Combo Iber
B
SUGT1
MCCC2
ACADM
KHSRP
CSDE1
PSMB1
PRPS2
CAPN1
SREK1
SERPINA12
PSMA3
PPP2R1B
LASP1
PSMA2
ATP2A2
BLMH
PSMB5
HAL
NUDC
PLAA
TGM5
TGM1
RPN1
PPP2R1A
IDH2
PMVK
STBD1
RPL18
FEN1
RPL36AL
APEX1
MGST3
NR3C1
RPL36A
RPL32
ANP32A
RPL23
SRP54
ANP32B
RBM14
PLIN3
RPS2
EMD
LMNB1
RPS11
RPS9
DOK2
KRT33B
EIF4H
KRT34
CNN2
KRT77
EIF4A1
LTV1
KRT83
HNRNPH2
KRT31
EWSR1
CAT
KRT71
KRT23
SNAP91
PCBP2
PCBP1
FASN
ATG3
PICALM
KRT10
PCMT1
RRBP1
IARS
CTPS1
PFDN4
ALDH18A1
PFKM
Cornification (FDR = 2.08e-9)
SRP-dependent co-translational protein targting to membrane (FDR = 4.13e-8)
Mitotic Anaphase (FDR = 1.32e-6)

Figure 4.22. PPI and GO analyses of mutual CRBN interactors between the two experiments performed in OPM2-BioID2-CRBN cells

(A) Venn diagram demonstrating overlap between proteins identified in the Experiment 1 and Experiment 2 in OPM2-BioID2-CRBN cells. (B) PPI network and GO analyses of mutual CRBN interactors from the two experiments with OPM2-BioID2-CRBN cells.


A
OPM2-BioID2-CRBN
Experiment 1 (496)
OPM2-BioiD2-CRBN
Experiment 2 (240)
508
158
82
B
Translation initiation (FDR = 3.74e-15)
RNA splicing (FDR = 2.62e-13)
Protein folding (FDR = 1.31e-5)
Dishevelled specific domain (FDR = 9.5e-4)
Biotin transport and metabolism (FDR = 0.0017)
Gluconeogenesis (FDR = 0.002)
nucleotide-excision repair, DNA damage recognition (FDR = 0.0125)

is increased upon presence of BORT (Figure 4.18A). When the subset was restricted to proteins highly enriched solely in the presence of BORT and not double agent BORT/IMiDs combinations, only few proteins met the filtering criteria (Figure 4.18B). These proteins are mainly involved in protein folding (HSPB1, DNAJA1) and globin binding (HBB/D, HBA1/2). PPI and GO term analyses of proteins within these subsets demonstrated enrichment for several gene/pathways including histone H2B, RNA splicing, RNA transport and protein folding activity (Figure 4.19). These observations suggest that CRBN interacts with all these proteins and that it might be mediating their ubiquitinylation and/or stability, especially when the proteome is stabilised by proteasomal inhibition. Subsequently, average z_norm for each protein was subset to identify proteins that were highly enriched in DMSO-treated cells and less enriched in the presence of BORT (Figure 4.20A). Amongst these, there were proteins whose interaction with CRBN was decreased or lost in the presence of all IMiDs (Figure 4.20A) or at least one IMiD (Figure 4.20B). These groups included proteins mainly involved in RNA splicing and protein translation (Figure 4.20C). Conversely, subsetting for factors with increased CRBN binding upon IMiD treatment (Figure 4.21A) included proteins involved with translation-related factors, proteasome subunits, keratinisation and other pathways (Figure 4.21B). Finally, CRBN interactors consistently identified across the two experiment were identified by subsetting proteins whose fold change was equal to zero or negative in presence of an IMiD as compared to DMSO only (Figure 4.22A). PPI and GO analysis of proteins in this subset displayed enrichment for processes such as RNA splicing, protein translation and cell polarization/motility (Figure 4.22B). Collectively, these data suggest that CRBN could be involved in RNA processing and protein translation, and that IMiDs treatment could influence RNA processivity.

4.2.15 Dishevelled proteins are putative CRBN interactors and Myosin-9 is a putative neosubstrate for CRBN ubiquitination

Further analysis was performed with proteins that were also significant in Experiment 1: DVL1, DVL2 and MYH9. DVL1 and DVL2 scored as CRBN interactors, and were significantly lost in the presence of BORT (Figure 4.23A). However, in the Experiment 1, DVL1 and DVL2 were lost in the presence of LEN (Figure 4.10B-D). Although in Experiment 2 DVL1 was also less enriched in presence of LEN as compared to DMSO only, the enrichment profile across samples between Experiment 1 and 2 was different. Experiment 2 indicated that DVL1 and DVL2 are stable CRBN interactors because they were not less enriched in presence of any IMiD (Figure 4.23B-C). Similar to Dishevelled proteins, others were found in both Experiments 1 and 2, such as RRM2, IGJ, G3BP1, HNRNPA0, HSPA1A/B (Figure 4.23A). These proteins were found significantly enriched

Figure 4.23. Dishevelled proteins are CRBN interactors

(A) Volcano plot displaying differentially enriched proteins in OPM2-BioID2-CRBN cells treated with BORT as compared to DMSO. Red dots represent hits significant for adjusted p-value < 0.05. The first ten most significant proteins were labelled in the plot. (B) Z_norm plots showing enrichment of DVL1/DVL1P1 in each sample across all treatment conditions. (C) Z_norm plots showing enrichment of DVL2 in each sample across all treatment conditions. In (B) and (C), circles represent real intensity values, whilst crosses represent imputed values. Horizontal bars represent the median of the z_norm values in each condition.

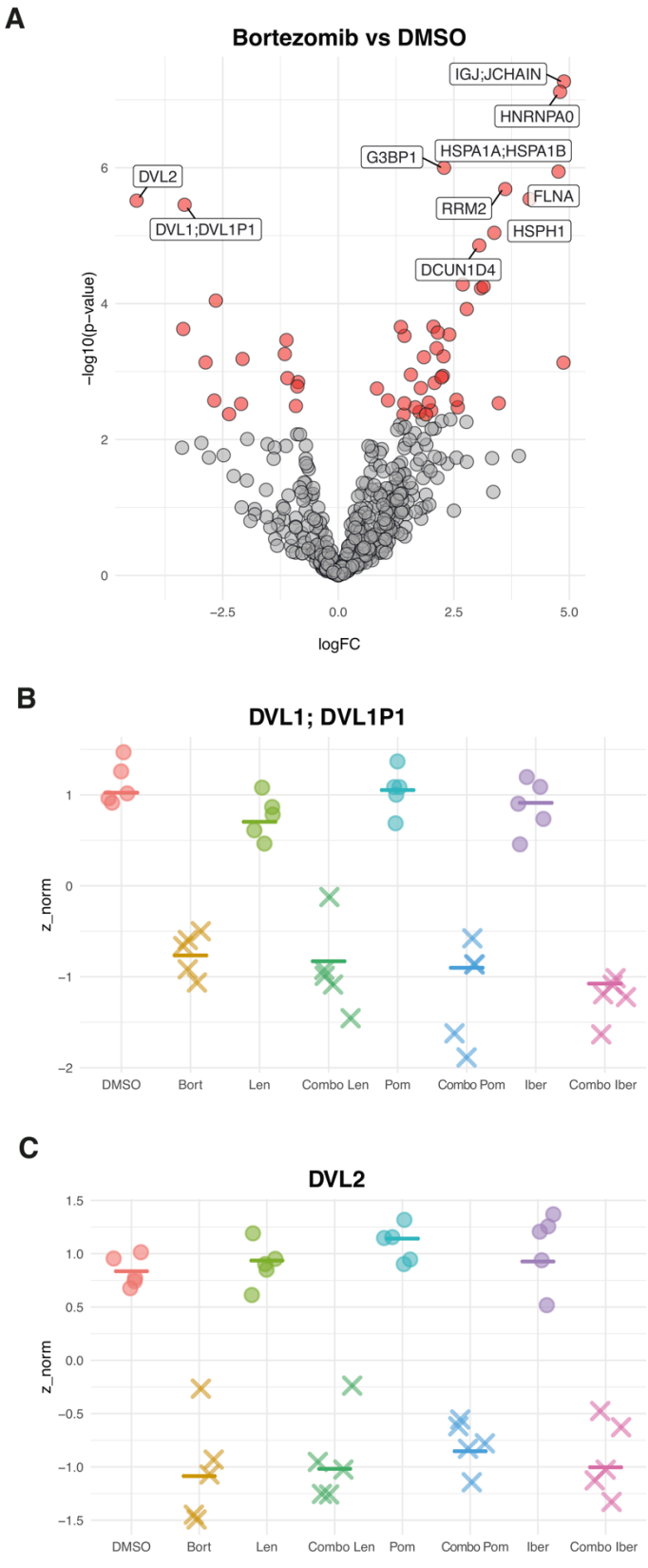

A
Bortezomib vs DMSO
IGJ;JCHAIN
HNRNPA0
G3BP1
HSPA1A;HSPA1B
DVL2
FLNA
RRM2
DVL1;DVL1P1
HSPH1
DCUN1D4
−log10(p−value)
logFC
B
DVL1; DVL1P1
z_norm
DMSO
Bort
Len
Combo Len
Pom
Combo Pom
Iber
Combo Iber
C
DVL2
z_norm
DMSO
Bort
Len
Combo Len
Pom
Combo Pom
Iber
Combo Iber

Figure 4.24. MYH9 is a CRBN-IMiD neointeractor and neosubstrate for ubiquitination

(A) Volcano plot displaying differentially enriched proteins in OPM2-BioID2-CRBN cells treated with LEN as compared to DMSO. Red dots represent hits significant for adjusted p-value < 0.05. (B) Volcano plot displaying differentially enriched proteins in OPM2-BioID2-CRBN cells treated with POM as compared to DMSO. Red dots represent hits significant for adjusted p-value < 0.05. (C) Volcano plot displaying differentially enriched proteins in OPM2-BioID2-CRBN cells treated with IBER as compared to DMSO. Red dots represent hits significant for adjusted p-value < 0.05. (D) Z_norm plots showing enrichment of MYH9 in each sample across all treatment conditions. Circles represent real intensity values, whilst crosses represent imputed values. Horizontal bars represent the median of the z_norm values in each condition.

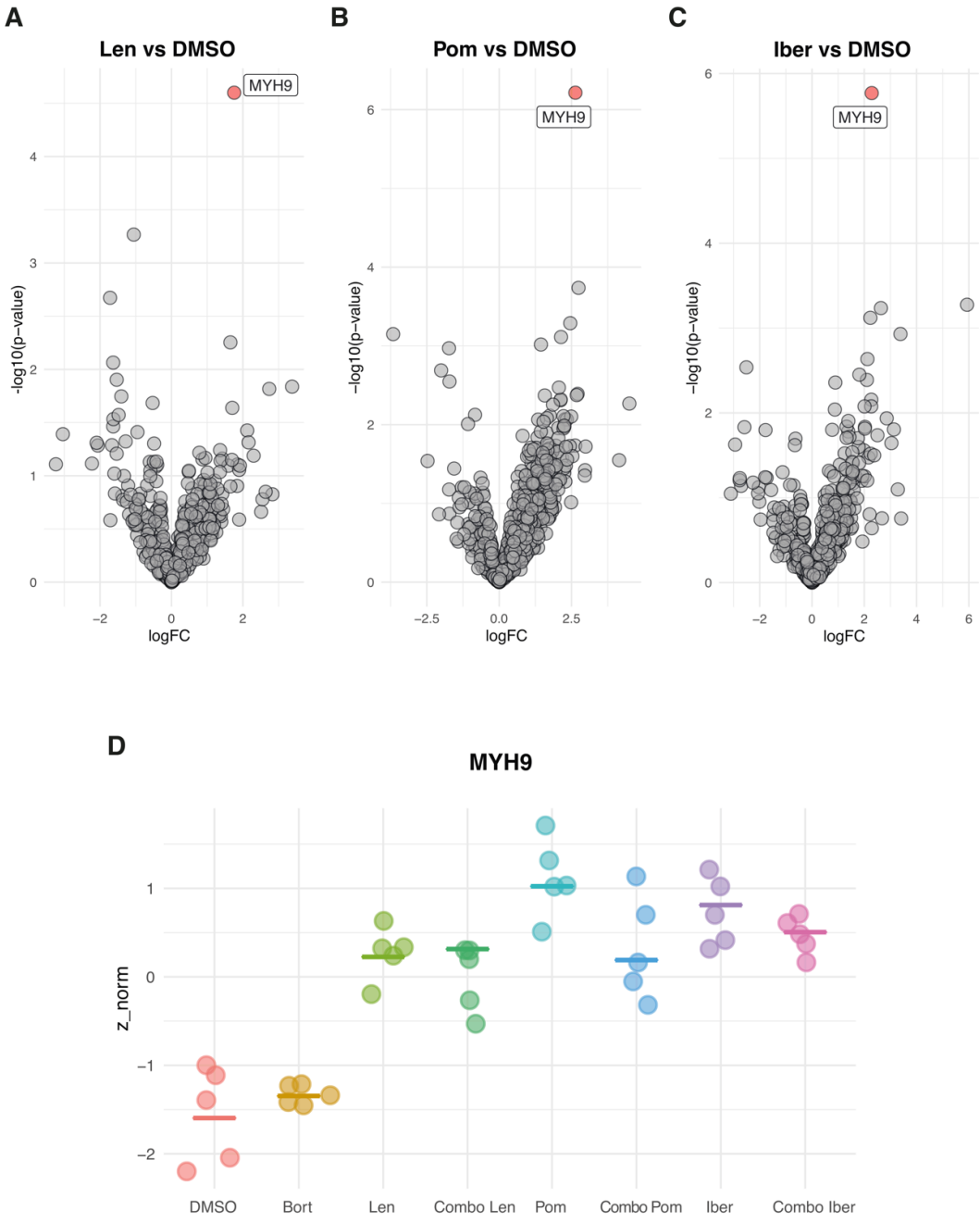
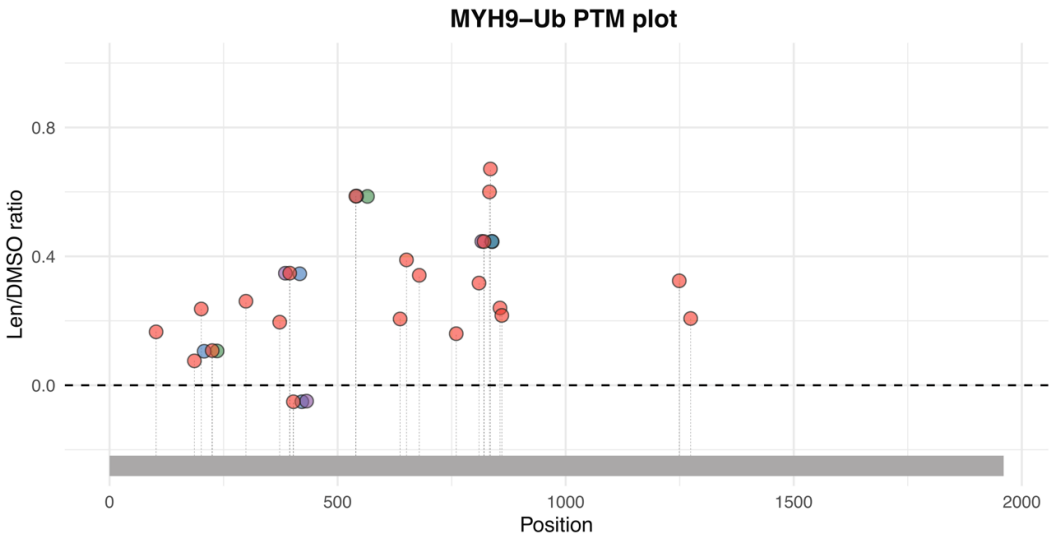

A
Len vs DMSO
MYH9
-log10(p-value)
logFC
B
Pom vs DMSO
MYH9
-log10(p-value)
logFC
C
Iber vs DMSO
MYH9
-log10(p-value)
logFC
D
MYH9
z_norm
DMSO
Bort
Len
Combo Len
Pom
Combo Pom
Iber
Combo Iber

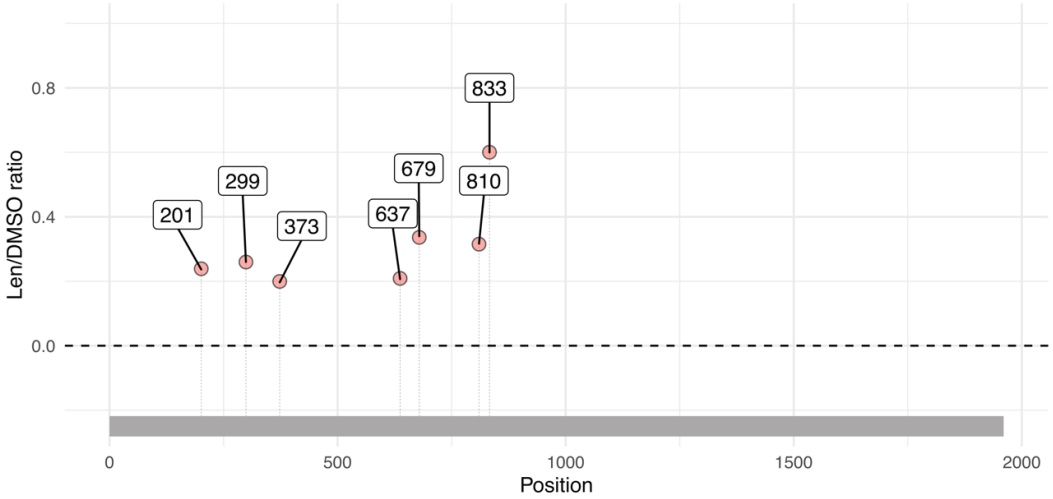
Figure 4.25. LEN treatment of MM.1S cells induces ubiquitination of MYH9

(A) Post-Translational Modification (PTM) plot for MYH9. The plot shows sites that are differentially ubiquitinylated when in presence of LEN. Sites that are specific for other MYH proteins are colour coded as indicated in panel (C). (B) PTM plot for MYH9. The plot shows sites that are differentially ubiquitinylated when in presence of LEN and significant for p-value < 0.05 (t-test). Labels represent the aminoacidic residues where the PTM has occurred.

A


MYH9–Ub PTM plot
Len/DMSO ratio
0.8
0.4
0.0
0
500
1000
1500
2000
Position

B


MYH9–Ub PTM plot, p < 0.05
Len/DMSO ratio
0.8
0.4
0.0
201
299
373
637
679
810
833
0
500
1000
1500
2000
Position

C

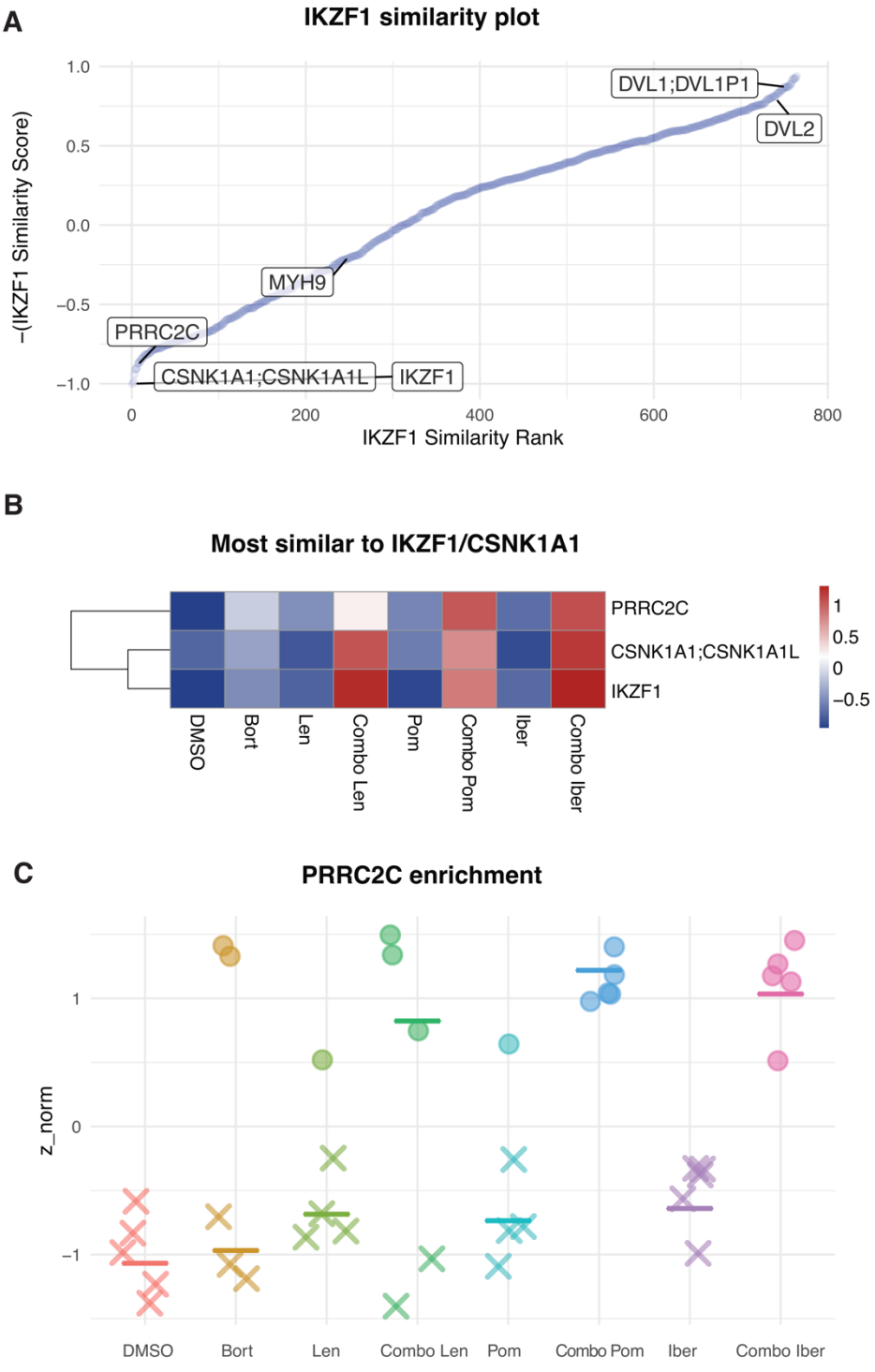

MYH10
MYH11
MYH14
MYH9

but, analogously to Dishevelled proteins, in the presence of BORT rather than LEN. In Experiment 2, MYH9 was found significantly enriched in the presence of IMiDs (Figure 4.24A-C). Treatment with BORT did not seem to markedly modulate the MYH9-CRBN interaction. The interaction between MYH9 and CRBN slightly increased following BORT treatment. With IMiDs, there was strong MYH9 enrichment, which was mildly attenuated by co-treatment with BORT (Figure 4.24D). Similar to DVL1/2, in Experiment 1 MYH9 was enriched in the presence of BORT but not in the presence of LEN (Figure 4.8C). In the work of Kronke and colleagues[90], MS proteomics was performed with the aim of detecting global changes in protein ubiquitination upon treatment with thalidomide or LEN as compared to DMSO. As MYH9 was enriched in IMiD-treated samples, proteomics data with regards to differential ubiquitination of MYH9 upon IMiD treatment was extracted from the aforementioned paper (Figure 4.25). Several aminoacidic residues were found differentially ubiquitinated in MYH9. Some of these sites were not unique for MYH9 but they are also specific for MYH10, MYH11 and MYH14, which represent other isoforms of myosin heavy chain (Figure 4.25A,C). In the dataset, a change in enrichment of ubiquitin-lysine sites was expressed as log2 of IMiD/DMSO ratio. T-testing was used to obtain a p-value for the average of the three measurements for each site. The Post-Translational Modification plot (PTM plot) shows the amino acid positions in the X axis and the enrichment (as average of log2(Len/DMSO ratio)) in the Y axis (Figure 4.25A). Sites significant for p-value < 0.05 were all unique for MYH9, and corresponded to lysines 201, 299, 373, 637, 679, 810 and 833 (Figure 4.25B). Ubiquitinylation occurred preferentially within the region that binds to LIMCH1, a modulator of cell motility[315]. Within this region, there exist three important domains. The first, the N-terminal domain, is an SH3 domain (aminoacids 27-77), the second a myosin motor domain (aminoacids 81-776), and the third an IQ domain for calmodulin-Ca^{2+} binding (aminoacids 779-808). These domains are part of the myosin “head”, whilst the remaining region is represented by the coiled-coil domain[316]. Collectively, these results suggested that CRBN interacts with DVL1 and DVL2, although the purpose of these interactions remains to be determined. CRBN might also interact with MYH9 following treatment of cells with an IMiD and could mediate its ubiquitinylation in key regions for interaction with other factors.

4.2.16 PRRC2C scores as potential CRBN neosubstrate suggesting that CRBN might regulate stress granule formation

To explore whether any potentially novel neosubstrates had been purified, the Euclidean distance of the average log2 intensity of each condition from those of IKZF1 was calculated in order to obtain an IKZF1 similarity score (Figure 4.26A). As expected, the most similar hit was

Figure 4.26 IKZF similarity profiling identifies PRRC2C as putative CRBN-IMiD neosubstrate
(A) IKZF similarity plot of CRBN interactors identified. Labels highlight similarity scores of IKZF1, CK1a, PRRC2C, MYH9, DVL1/DVL1P1 and DVL2. (B) Heatmap of average z_norm of PRRC2C as compared to those of IKZF1 and CK1a. (C) Z_norm plot displaying enrichment of PRRC2C specific protines of all OPM2-BioID2-CRBN samples across the different treatment conditions. Circles represent real intensity values, whilst crosses represent imputed values.


A
IKZF1 similarity plot
1.0
0.5
0.0
−0.5
−1.0
−(IKZF1 Similarity Score)
DVL1;DVL1P1
DVL2
MYH9
PRRC2C
CSNK1A1;CSNK1A1L
IKZF1
0
200
400
600
800
IKZF1 Similarity Rank
B
Most similar to IKZF1/CSNK1A1
PRRC2C
CSNK1A1;CSNK1A1L
IKZF1
1
0.5
0
−0.5
DMSO
Bort
Len
Combo Len
Pom
Combo Pom
Iber
Combo Iber
C
PRRC2C enrichment
z_norm
1
0
−1
DMSO
Bort
Len
Combo Len
Pom
Combo Pom
Iber
Combo Iber

CK1α, representing the other *bona fide* neosubstrate identified in Experiment 1 having an IKZF1 similarity score close to 1 (0.986). In Experiment 2, a score of 1 was assigned to IKZF-similar proteins and a score of -1 to IKZF-dissimilar proteins. The MYH9 similarity score was positive, according to the increased enrichment obtained in presence of any IMiD, but sitting closer to zero than to 1, because it was higher in IMiD-only conditions as compared to BORT/IMiD co-treatments. Conversely, DVL1 and DVL2 were found close to -1 (-0.872 and -0.813 respectively). The most similar to IKZF1 – beside CK1α – and significant for adjusted p-value < 0.05 was PRRC2C (Figure 4.26A-B). The enrichment profile of PRRC2C was also studied by plotting of z_norm values across all conditions (Figure 4.26C). PRRC2C was not detected in the presence of DMSO only. In BORT-treated cells, only 2/5 samples were identified, whereas the other three were imputed. In IMiD-treated cells, no peptides were detected but they were dramatically enriched in BORT-IMiD combinations. Interestingly, PRRC2C is involved in the formation of stress granules and P-bodies, which are constituted from pools of stalling translation complexes[317–320]. Stress granules have been implicated in sustaining cancer and neurodegenerative diseases. G3BP1, another protein that regulates formation of stress granules[321], was found enriched in all BORT-treated and BORT-IMiD treated samples as compared to DMSO or IMiD only. These observations indicate that PRRC2C might be a novel CRBN neosubstrate and that CRBN itself could be implicated in regulating the formation of stress granules.

4.3 Discussion

4.3.1 Rationale for the study of IMiD-dependent modulation of CRBN interactome

The seminal paper of Kronke et al.[90] provided the first ever proteomics dataset of CRBN and CRBN-IMiD interactions. However, the paper focused solely on neosubstrate identification because of the relevance of IKZF1 and IKZF3 in the context of plasma cell biology and their close relationship with the master regulator *IRF4*. The idea of IMiD activity being solely determined by degradation of neosubstrates is likely oversimplified and limited. Beside inducing degradation of IKZF1/3 and other neosubstrates in the presence of an IMiD, CRBN promotes degradation of its endogenous substrate MEIS2 in the absence of an IMiD[225]. CRBN also stabilises MCT1-CD147 by exerting chaperone activity, which is prevented by treatment with IMiDs[231]. These additional functions of CRBN either in presence or absence of an IMiD suggest that IMiDs might perturbate CRBN functions in a global fashion. To date, no study has aimed to discover in an unbiased manner what are CRBN substrates and interacting partners in the presence and absence of an IMiD. Thus, the main goal of this project has been to discover novel neosubstrates and gain

insight into the CRBN interactome – in the presence and absence of an IMiD – with BioID2-dependent proximity labelling, a method which has only recently been applied to E3 ligases[322]. This technology was chosen for two main reasons: 1) BioID2-mediated biotinylation is ideal to identify interacting partners of a protein of interest along a defined period of time, not just at a specific timepoint and 2) since biotin-streptavidin is the strongest non-covalent bond known in nature, BioID2 proximity labelling allows the potential to identify "weak" interactions that could be lost in standard immunoprecipitation protocols with multiple washing steps[309].

4.3.2 Development and optimisation of experimental conditions for BioID2-CRBN MS proteomics

In this study, a method to explore the CRBN interactome was developed based on the concept of proximity labelling. BioID2, a bacterial biotin-ligase, was fused to CRBN and was demonstrated to successfully biotinylate proteins that interact with CRBN in presence and absence of CRBN-specificity modulators (IMiDs). To achieve this, several optimisation steps were required, including testing of mycBioID2 and mycBioID2-CRBN protein expression, the study of their biotinylation efficiency, the assessment of optimal cell culturing conditions in biotin-depleted medium and the efficiency of biotinyl-proteins enrichment with streptavidin-agarose. This process culminated in purification of CRBN and its *bona fide* interacting partners via LC – MS/MS with cell lysates of HEK293T cells transiently transfected with *mycBioID2* and *mycBioID2-CRBN*. This approach confirmed the efficiency of this technology in identifying CRBN interactors.

In HEK293T cells transiently transfected with *pBABE-mycBioID2-puroR,* mycBioID2 showed remarkable biotinylating activity. In the mock control, Western blotting with streptavidin-HRP demonstrated the presence of intense bands, indicating either non-specific signal and/or the presence of endogenous biotinylated species. These bands were detected also in the experiment of Figure 4.5D, where an empty *pBABE-puroR* vector was employed as control. However, the intensity of these bands was dramatically reduced when cells were cultured with dialysed FBS and in absence of exogenous biotin, indicating that the signal likely corresponded to endogenous biotinylated protein. Biotin is involved in fat metabolism, being a cofactor for enzymes such as Acetyl-CoA carboxylases (ACACA/ACC1 and ACACB/ACC2) and Pyruvate (PC)[312]. It is possible that such enzymes are being detected via streptavidin-HRP Western blotting. To further support this observation, these proteins were also found enriched in the proteomic data. With regards to the proteomics data, one should keep in mind that Acetyl-CoA carboxylases represent common contaminants in BioID proteomics datasets, together with keratins and other proteins[309].

For the study of CRBN interactome, it was decided to clone the CTD of BioID2 to the NTD of CRBN with the hypothesis that the presence of mycBioID2 in an excessively close proximity to CRBN CTD, where the thalidomide binding pocket is located[225], could introduce steric hindrance to the process of neosubstrate recruitment. However, it would be interesting to study the proximal interactome of CRBN also with BioID2 at its CTD regardless of the capability of recruiting neosubstrates. CRBN fused with BioID2 at the CRBN C-terminus could serve as a complementary experimental setting to that with BioID2 at the CRBN NTD. With both dataset it might be possible to detect interactors that are outside the biotinylation radius of BioID2 when only at CRBN NTD and vice versa. An additional improvement to the study of CRBN interactome in the presence or absence of an IMiD could be by conjugation with BioID2 of CUL4A/B, extending the study of the interactome at the level of the whole CUL4-DDB1-RBX1-CRBN E3 complex.

Testing of mycBioID2-CRBN expression and functionality involved employment of antibodies against myctag, CRBN and streptavidin-HRP. In Figure 4.5A, probing with anti-CRBN in *mycBioID2-CRBN* revealed high mycBioID2-CRBN expression in transfected cells suggesting high transfection efficiency and/or high promoter activity. The presence of additional bands may indicate truncated isoforms of CRBN with internal start codons are also expressed. The presence of BioID2 in these putative truncated proteins was excluded by the expression pattern of myctag. Additionally, expression of mycBioID2 in *mycBioID2*-transfected HEK293T cells was much higher than that of mycBioID2-CRBN in *mycBioID2-CRBN*-transfected cells. Other bands of unknown nature are also detected and possibly represent non-specific antibody binding. In Figure 4.5D, streptavidin-HRP demonstrated the advantage of adopting dFBS as compared to standard FBS. The signal at 25kDa was strongly suggestive of mycBioID2 detection because it was absent in lysates from cells transfected with empty vector and *mycBioID2-CRBN*-transfected cells. This observation is interesting because it indicates that auto-biotinylation (demonstrated in Figure 4.5E) does not occur in biotin-depleted conditions, making it the ideal condition to reduce background signals. The reduction of background signals was then confirmed in the Figure 4.5E, where, in the absence of exogenous biotin, no mycBioID2 was purified with enrichment with streptavidin-agarose.

Finally, MS proteomics demonstrated that the most statistically significant CRBN interactors were *bona fide* CRBN interactors, i.e. members of the COP9 signalosome COPS7A/B, COPS3, Thioredoxin-like protein 1 (TXNL1)[90,323], CUL4B, DCAFs and newly identified interactors, involved

into RNA transport, translation and other pathways. In the work of Kronke and colleagues[90], the entire COP9 signalosome was co-immunoprecipitated with CRBN. By using BioID2, only COPS7A, COPS7B and COPS3 were purified, meaning that the NTD of CRBN is likely to interact most closely with these subunits. Interestingly, DDB1 was not purified although physically interacting with CRBN. This might indicate that DDB1 is out of the biotinylating radius of BioID2 at CRBN NTD and provides further rationale for a study with BioID2 at the C-terminus of CRBN. Whereas DDB1 was absent, CUL4A/B were purified. This might be caused by CUL4A/B rotation during ubiquitin transfer from the E2 enzyme on RBX1 to CRBN substrates[225]. In this case, one would expect also RBX1 to be tagged with biotin, but RBX1 biotinylation could be prevented by its binding with E2 enzymes. The length of the Gly-Gly-Gly linker between mycBioID2 and CRBN could also be the reason behind limited detection of interactors. For the study of LaminA interactome, Roux and colleagues also conjugated LaminA to BioID2 with a long (25nm) and flexible linker (13x Gly-Ser-Gly-Gly-Gly), providing BioID2 with much more flexibility[308]. A Gly-Gly-Gly linker is unlikey to give BioID2 a significant freedom of moving in the entire space proximal to CRBN. A longer linker could increase the spatial resolution of BioID2 and enable identification of more interactors. With BioID2 at the N-terminus of CRBN, it is plausible to hypothesise that BioID2 would preferentially biotinylate proteins that interact with CRBN at its N-terminus, introducing a bias with respect to proteins interacting with the C-terminus. A longer and flexible linker might allow BioID2 to reach the C-terminus of CRBN and to reduce this bias.

4.3.3 The BioID2-CRBN system and identification of *bona fide* and novel CRBN-binding proteins

4.3.3.1 Considerations on CRBN overexpression and bortezomib toxicity

OPM2 cells were transduced with *mycBioID2* (OPM2-BioID2 cells) or *mycBioID2-CRBN* (OPM2-BioID2-CRBN cells). Validation of transduction was performed via immunoblotting of CRBN and myctag. Similar to HEK293T cells, mycBioID2 appeared much more expressed that mycBioID2-CRBN, and in OPM2-BioID2-CRBN additional bands (possibly non-specific signal) were detected. There could be several reasons explaining the higher expression of BioID2 as compared to BioID2-CRBN. The length of the DNA sequence could require more time to transcribe and translate the whole ORF, or, more likely, expression of CRBN might be tightly regulated by unknown mechanisms, whereas BioID2 alone might be not, possibly because BioID2 is derived from a bacterial protein and might not be subjected to intracellular regulation of gene/protein expression. However, the discrepancy between expression of BioID2 and BioID2-CRBN remains

unclear. To improve the model, CRISPR homology directed repair could have been employed to fuse BioID2 with endogenous CRBN. In doing so, BioID2-CRBN expression would possibly be maintained at a more ''physiological" level. One should keep in mind that overexpression of a gene can significantly alter cell phenotypes[324]. Moreover, fusion with BioID2 might also affect the affinity between exogenous CRBN and IMiDs, with endogenous CRBN competing for IMiDs against BioID2-CRBN.

Cytotoxicity of BORT in OPM2-BioID2-CRBN as single agent and in combination with LEN, POM or IBER was assessed via PI labelling of OPM2-BioID2-CRBN cells to test the toxicity of these drugs prior to proteomics studies. BORT is a very toxic compound for MM and it is active at nanomolar concentrations[314,325]. The cell death profile of OPM2-BioID2-CRBN treated with BORT with different concentrations at 16 or 24 hours suggested that duration of exposure is more important than drug concentration above a certain threshold. In fact, at 5nM, cell viability seemed to reach a plateau, suggesting that, at those concentrations, the proteasome is considerably inhibited and cells require time to undergo apoptosis. It is not clear why such discrepancy in cell death with BORT in different experiments (Figure 4.7C-D) has been observed. One plausible explanation would be that variations in cell confluency kept in culture prior to experimental set up might influence the metabolic state of cells and their proteome[326].
Loading controls in Western blots of Figure 4.7F-G further support the observation that BORT is significantly active at 5nM and may be causing HSP90 and Actin to accumulate. Without a functional proteasome, protein turnover is disrupted and this likely results in the non-specific accumulation of housekeeping genes. Stabilisation of IKZF3 with concomitant LEN treatment is observed with 10nM BORT, possibly because LEN induces rapid target ubiquitination and stabilisation of the bulk neosubstrate pool might require saturating concentration of BORT. Immunoblotting of OPM2-BioID2-CRBN cells treated with a combination of BORT and LEN displayed stabilisation of the IMiD neosubstrate IKZF3 and enrichment of IKZF3 following incubation of OPM2-BioID2-CRBN cell lysates with Streptavidin-Agarose resins. This experiment indicates that neosubstrates can be efficiently stabilised following treatment with 10nM BORT and 10μM LEN and therefore biotinylated and purified via enrichment of biotinylated species. Since BioID2 requires at least 16 hours of incubation to induce substantial biotinylation of proximal substrates[308,309], the use of more advanced, potent and quick biotin ligases such as TurboID or AirID could help reducing significantly the exposure to BORT and thus avoid perturbations of such magnitude in the global cell proteome[322,327].

4.3.3.2 Experimental quality control, contaminants and caveats of proteomics datasets analysis

Many of the interactors found in the pilot experiment with HEK293T cells were also found in DMSO-treated OPM2-BioID2-CRBN cells. Beside CRBN, the other two most significant proteins identified were COPS7A and B, corroborating the hypothesis that these two COP9 signalosome subunits are the closest CRBN interactors at its N-terminus. PPI and GO analyses indicate that CRBN could be involved in neutrophile degranulation. IMiDs could then be implicated in modulation of this process. Modulation of degranulation of myeloid cells by IMiDs could represent one of the unknown molecular mechanisms implicated into regulation of the MM bone marrow microenvironment. However, this has not been reported in the literature. IMiD are known to suppress myelopoiesis via degradation of IKZF1[193,194]. To determine whether IMiDs regulate degranulation of neutrophils, further studies of the effect of IMiD treatment on granulocytes are required. Keratins and other epithelial proteins were also enriched. However, these probably represent contaminants which are often detected in MS proteomics experiments[309]. With regards to proteins specific for ribosomal proteins, it is not clear whether these are contaminants or represent true CRBN interactors, since further experiments highlighted a potential role for CRBN in regulation of post-transcriptional events such as mRNA transport, translation and formation of stress granules.

Analysis of differentially expressed proteins (DEPs) of DMSO, LEN, BORT or combo-treated OPM2-BioID2-CRBN cells revealed only three DEPs significant for false discovery ratio (FDR) < 0.05 (IKZF1 and DVL1/2), so a higher FDR (0.2) was employed with the purpose of screening for novel interactors. However, MS is a very sensitive technique, and replicates of the same sample can be subjected to high variance. This also explains why five replicates were used for each condition. Moreover, some intensity values can be missing in one to all replicates. Inclusion of an “imputed” value when the real intensity is zero becomes necessary, but this can markedly skew the average of intensities. A way to overcome this problem, although partially, is the usage of medians rather than means to calculate the average intensity within replicates. However, this does not always overcome the issue. For instance, IKZF3 matching unique peptides were purified in 4/5 replicates of the combination treatment group, with one intensity value missing, whereas, in all the other conditions, IKZF3 was not enriched (Figure 4.10C). The intensity imputed in the combination treatment group is equal to those of the imputed values the DMSO, BORT and LEN only conditions, which lowers the average and increases the error. Implementation of a more efficient imputing algorithm would provide a better solution. Within this experiment, a higher

FDR (< 0.2) was set as a cut-off. One could argue that such FDR cut-off is rather generous. However, a greater FDR cut-off not only increases false positives, but also true positives, which serves the purpose of screening for novel interactors.

4.3.3.3 MEF2C is a novel CRBN *neointeractor*

MEF2C was identified as potential neointeractor/neosubstrate. However, the MEF2C enrichment profile across the different conditions was not suggestive of that of a neosubstrate, but that of a neointeractor, and this observation was supported also by its IKZF similarity score. On the other hand, Dishevelled proteins DVL1 and DVL2 displayed an enrichment profile opposite to that of IKZF1, IKZF3 and MEF2C. Interestingly, DVL1 and DVL2 are involved in WNT signalling and thus potentially regulate the MM microenvironment (cell adhesion and bone homeostasis)[128,328–330]. Since IMiDs are known to exert a significant effect on the bone marrow microenvironment (as described in section 1.2.2.1 of chapter 1), *in vitro* validation of DVL1/2 interaction with CRBN following IMiD treatment should be followed by *in vivo* studies with murine models that are responsive to IMiDs. MS of the CRBN interactome should be conducted also in bone marrow stromal cells (e.g. HS-5 cells) and other cell types which populate the bone marrow microenvironment. This approach could reveal potential neosubstrates whose expression is cell lineage-dependent. Unknown neosubstrates could be responsible for microenvironmental changes and side effects of IMiD treatment that are well characterised clinically but poorly defined from a biological perspective.

Considering its potential biological importance, MEF2C was chosen for further validation and it was demonstrated to interact with CRBN in the presence of an IMiD. MEF2C was modestly enriched also in presence of BORT. This might be explained by perturbation of the proteome when cells are exposed to BORT, with temporary increase the MEF2C pool. In this case, the MEF2C pool would be represented by misfolded or non-functional protein. Given that a chaperone activity of CRBN has been previously demonstrated[231], CRBN might regulate stability of MEF2C. The importance of MEF2C in MM is clearly presented with data extracted from the DepMap repository. Here, OPM2 are reported as the only non MEF2C-dependent MM cell line (Figure 4.13D). A recent study has demonstrated that MEF2C is one of the transcription factors that drive increased activity of enhancer and superenhancers (SEs) in the context of MM transcriptional co-regulatory network[100]. Interestingly, it was shown that several key genes such as *IRF4*, *MYC*, *IKZF1* and *MEF2C* associate with SEs only in MM and not in healthy PCs. Other genes, however, such as *PRDM1* and *XBP1*, associate with SEs also in normal cells. It was

therefore suggested that this *de novo* SE formation is a consequence of translocations occurring in the process of myelomagenesis, especially t(11;14) and t(4;14). In addition, this represents a solid validation of previously published data with regards to the central role of the *MYC-IRF4* axis in MM. Considering these observations, it is not surprising that many MM cell lines display such remarkable dependency on MEF2C. As an essential TF, it is possible that MEF2C co-localises with IKZF1/3 at promoters and/or enhancers. If this is the case, CRBN-IMiD would be re-directed to those loci where IKZF1 with MEF2C regulate gene expression. This would imply also that CRBN-IMiD binds IKZF1 at a chromatin level, phenomenon that has not been described yet. ChIP-seq of IKZF1/3 and CRBN in presence and absence of an IMiD might answer this question. Moreover, MEF2C ChIP-seq could reveal possible co-localisation with IKZF1/3. A potential improvement of this technique would be represented by ChIP-seq of biotinylated proteins. In doing so, one could explore which loci are directly affected by IMiD treatment. Instead, if MEF2C does not co-localise with IKZF1/3, a study of MEF2C interactome would be required. Moreover, it is possible that MEF2C is ubiquitinated by CRBN in presence of an IMiD. This provides the rationale for MS-based detection of ubiquitinylated MEF2C peptides or those of proteins in close proximity to MEF2C. If MEF2C is not ubiquitinylated and/or its function is not affected, one could hypothesise that CRBN might ubiquitinylate other factors within the chromatin region where MEF2C exerts its regulatory activity (e.g. histone proteins, other TFs, transcriptional co-factor, etc).

The discovery of MEF2C as a novel neointeractor suggests that there might be other pathways regulated by CRBN in the presence of an IMiD. Modulation of MEF2C transcriptional activity following IMiD treatment, if demonstrated, would suggest that IMiDs might globally disrupt MM transcriptional co-regulatory network, since they are already known to have a negative impact on the *IRF4-MYC* axis. To test this hypothesis, ChIP-seq of biotinylated proteins in parallel with that of H3K27Ac (for the study of enhancers or superenhancers[331]) in presence and absence of an IMiD could reveal which loci are directly affected by IMiD treatment and relate them to activity of SEs.

4.3.4 CRBN is a potential regulator of cell migration, RNA processivity and protein homeostasis

The study of the CRBN interactome following treatment with LEN was subsequently extended to other iMiDs – pomalidomide (POM) and Iberdomide (IBER). In this experiment, IKZF3 was not detected, but IKZF1 and CK1α showed an enrichment profile compatible to that of

neosubstrates. Subsetting of the dataset based on the fold-change of the average intensity across different treatment conditions showed enrichment of pathways (via PPI networking and GO analysis) such as mRNA processivity and protein translation. Mutual interactors were found between the two experiments in OPM2-BioID2-CRBN cells, involving mRNA splicing, transport and translation, and proteins regulating cell motility, such as DVL1, DVL2 and MYH9. Treatment with BORT was the main factor for variance in this proteomics dataset. This was particularly evident in DVL1, DVL2 and MYH9 enrichment profile and all those interactors that were identified in the Experiment 1. Analysis of a published proteomics dataset demonstrated increased ubiquitination without degradation of MYH9 in LEN treated cells. Finally, stress granule protein PRRC2C was enriched in a similar way to that of IKZF1 and CK1α, indicating it as a possible candidate IMiD neosusbtrate.

4.3.4.1 Bortezomib is a major determinant in modulating the CRBN interactome

Correlation between samples, PCA plots and unsupervised clustering demonstrated that BORT accounts for most of the variability in the dataset in Experiment 2. Conversely, Experiment 1, LEN seemed to represent the major variability factor. The reason behind this result are unknown. One way to interpret these outcomes might be that BORT had a greater activity in Experiment 2 as compared to Experiment 1. Since the experimental conditions were the same, it is possible that cells used in these two experiments were in a different metabolic state. The density of cultured cells prior to experimental set up could have influenced the intracellular proteome[326]. Another source of variability could be represented by the use of different batches of dialysed FBS or of custom biotin-free RPMI.

One important conclusion from this observation is that even in the presence of BORT, CRBN interactome is significantly modified, even if BORT does not bind CRBN. Correlative analyses also showed that IBER is a more similar drug to POM as compared to LEN overall. This could be explained by the significant difference in potency between LEN/POM and LEN/IBER[236]. By observing IKZF1 and CK1α enrichment profiles, it was noted that cells treated with POM enriched less for IKZF1 as compared to LEN and IBER, indicating that the structure of CRBN-POM binding IKZF1 might keep IKZF1 further away from BioID2. It has been demonstrated that the structure of different IMiDs docking into the CRBN thalidomide binding pocket is unique for each IMiD[225]. Additionally, CK1α is enriched in POM, even if it is known that POM does not induce degradation of CK1α[230]. These observations indicate that an enrichment profile similar to that of IKZF1 and CK1α does not necessarily imply IMiD-induced protein degradation. To identify proteins that are degraded in an unbiased way, it would be necessary to perform MS proteomics of ubiquitinated

species and of the global proteome. The first can be achieved with two methods. Digestion with trypsin leaves ubiquitinated lysine residues conjugated with a glycine dimer. Peptides containing this epitope, called K-ε-GG, can be enriched with specific antibodies[332,333]. A possibly more efficient methods sees the employment of TUBE beads (LifeSensors), magnetic beads for polyubiquitinylated protein enrichment. The latter is simply a snapshot of the global proteome at a given moment – this would indicate whether a certain protein is less expressed following IMiD treatment. Since BioID2-dependent biotinylation of proteins occurs at lysine residues, BioID2 might compete for lysine residues with the E2 ligase enzyme, therefore reducing protein ubiquitination (although the occurrence of this event has not been reported in the literature). In this case, traditional co-immunoprecipitation of CRBN (in parallel to BioID2-CRBN proximity labelling), together with MS-proteomics of ubiquitinated proteins, would possibly improve the identification of CRBN substrates that might be missed with a BioID2-based approach only. Integrating the outcome of these diverse experiments might allow to verify whether putative neosubstrates are real neosubstrates and significantly increase the solidity of the study.

Proteins were also subsetted in order to perform PPI and GO analyses by treatment group. To subset for CRBN interactors, all BORT-containing treatment conditions were allocated into the group. This is because if enrichment with BORT is already very high, the effect induced by an IMiD in combination with BORT is likely negligible. This observation reflects the variability induced by BORT treatment in this experiment. When CRBN putative interactors of the two experiments were overlapped, GO terms in mRNA splicing, transport and translation resulted significant. This possibly suggests a novel role for CRBN in stabilising protein machineries that dictate successful mRNA splicing, then transport and translation in a unique sequence of events. To explore this possibility, total RNA-seq in the context of CRBN knockout or IMiD and bortezomib treatment would reveal, for instance, the occurrence of splicing variants or alternative polyadenylation sites following IMiD treatment[334]. RNA transport could be studied by using fluorescent probes that enable tracking of mRNA molecules movement across the nuclear membrane through nucleopores[335]. If CRBN regulates mRNA transport and/or protein translation, it is possible that CRBN knockout might positively or negatively impact these processes. If so, IMiD treatment could also impact these pathways by modulating CRBN activity. In fact, the CRBN interactome changes radically in presence of an IMiD alone or in combination with BORT. To explore translation dynamics in the presence and absence of IMiDs and proteasome inhibitors, approaches such as Ribo-seq and pulsed-SILAC allow quantification and

sequencing of mRNA bound to ribosomes and quantitative detection of nascent proteins, respectively[336]. This would inform whether and how these drugs affect these processes.

4.3.4.2 EDC4, a lenalidomide sensitivity factor, is a putative CRBN interactor

ECD4 scored as novel putative CRBN interactor in the presence of IMiDs. Although not enriched following treatment with LEN, it was enriched in POM and IBER. EDC4 is an enzyme that induces mRNA decapping to which follows mRNA decay[337]. This enzyme also scored as one of the hits in the genome-wide CRISPR resistance screen described in chapter 3. In addition, EDC4 was identified also in the CRISPR screens of Sievers and Liu[239,240]. Hence, this observation provide evidence that IMiD might regulate mRNA decay via CRBN and loss of EDC4 could disrupt this process and induce an IMiD-resistant phenotype. As discussed in the previous chapter (chapter 3, section 3.2.4.3) a simple hypothesis with regards to EDC4-mediated IMiD-sensitivity would be represented by its RNA-decay promoting activity. If EDC4 is lost, *IKZF1* and *IKZF3* mRNA might become more abundant and synthesis of IKZF1/3 proteins could outpace IMiD-induced IKZF1/3 degradation, with establishment of a "stoichiometric" mechanism of resistance. To explore this hypothesis, resistance mediated by loss of EDC4 would have to be validated by competitive proliferation assays, followed by validation of CRBN interaction with EDC4 upon IMiD treatment. After that, modulation of RNA decay would have to be studied in presence and absence of EDC4 and IMiD treatment, demonstrating whether or not IMiDs have the capability of impacting RNA decay. This finding could also provide further mechanistic insight into a possible role of CRBN in mRNA processing and homeostasis.

4.3.4.3 CRBN is a potential modulator of events occurring in the MM niche and might be implicated in the occurrence of side effects of IMiD therapy

Subsetting for peptides that enriched in the presence of at least one IMiD demonstrated that proteins implicated in RNA processing could represent novel neointeractors. Most importantly, DVL1, DVL2 and CTTN were purified in both experiments. Both DVL1/2 and CTTN have been demonstrated to be implicated into cell polarity and motility during migration[338,339]. The reason why these proteins are interacting less – or not at all – with CRBN in the presence of LEN in the first OPM2-BioID2-CRBN cells experiment and in the presence of BORT in the second OPM2-BioID2-CRBN cells experiment is obscure and factors of variability have been already discussed. However, in both experiments, the interaction of CRBN with DVL proteins and CTTN seems to be very consistent. As modulation of cell adhesion, motility and interaction with the microenvironment are important aspects of IMiD activity, one could argue that CRBN regulates

the biological function of DVL proteins and CTTN, and that IMiD treatment could interfere also with it. In addition to these, MYH9 was identified as the most statistically significant putative IMiD neointeractor in Experiment 2. MYH9 is a non-muscle myosin involved also in cell motility. Analysis of ubiquitinylated protein in the work of Kronke and colleagues[90] documented that MYH9 is ubiquitinylated in the presence of LEN. Although in the same paper the analysis of the global proteome does not display loss of MYH9, one could hypothesise that CRBN might modulate MYH9 activity by ubiquitinylating specific MYH9 domains. For example, ubiquitinylation might prevent or facilitate interaction with other proteins involved in cell motility and migration[224]. Interestingly, there exist a group of diseases related to MYH9 that afflict platelets (e.g. May-Hegglin disease)[316,340]. Since patients treated with IMiDs are subjected to pro-thrombotic events, one could hypothesise that these might be related to IMiD-induced modulation of platelet aggregation. IMiD-induced thrombocytopenia could also partially be the consequence of IMiD modulating the activity of MYH9. In fact, the reduction of platelet numbers is part of the syndromic cohort in patients receiving IMiDs. It is interesting to note that MEF2C transcriptional activity has also been associated with megakaryopoiesis[341]. It could be therefore hypothesised that IMiDs might induce thrombocytopenia also via modulation of MEF2C transcriptional activity. Validation of DVL1/2, CTTN and MYH9 interaction with in both MM PCs and bone marrow stromal cell lines, such as HS-5, followed by functional assays, such as cell migration assays or possibly *in vivo* live imaging, could help understanding whether these proteins control MM cells interaction with the microenvironment and are involved into the occurrence of IMiD side effect.

4.3.4.4 The putative CRBN neosubstrate PRRC2C and stress granules

PRRC2C enrichment profile resulted very similar to those of IKZF1 and CK1α, indicating that this protein might represent a novel neosubstrate. PRRC2C is a factor implicated in the formation of stress granules, which are aggregates of translational complexes (proteins and mRNA) that are stalled upon intracellular stress. Purification of stress granule-associated proteins, such as G3BP1 and G3BP2 and PRRC2C suggests that CRBN might be implicated not only in translation, but also in stress granule formation. Intriguingly, these stress granules can be observed in cells exposed to proteasome inhibitors[342]. This finding suggests a new role for CRBN in the context of bortezomib treatment, and could also represent the reason why these proteins are purified. In other words, BORT-treated cells could trigger stress granules formation. If, as proposed in this work, PRRC2C is a true neosubstrate, this could raise the hypothesis of the existence of a novel

possible functional interaction between the activity of IMiDs and that of bortezomib. This observation provides with the rationale for further investigation of this pathway.

4.3.4 Concluding remarks

Taken together, these results demonstrate that BioID2 represents a valid method to identify CRBN interactors. However, experimental planning has to be accurate and background noise should be reduced with the use of dFBS. The position of BioID2 (on CRBN) and the linker length might also play an important role in defining the space that is susceptible to BioID2-mediated protein biotinylation. Known CRBN interactors and neosubstrates, such as CUL4A/B, COPS7A/B, IKZF1/3 and CK1α were successfully identified. However, prolonged treatment with BORT can introduce significant variability, and the use of newer biotin ligases such as AirID or TurboID should be considered, as these enzymes efficiently biotinylate substrates in a significantly shorter time (< 6 hours). Proximity labelling has the potential to considerably expand the number of potential CRBN interactors and therefore CRBN functions. Complementary assays including enrichment for ubiquitinylated species, analysis of the global proteomics and specific functional assay are key to identify and validate true novel interactors and define novel CRBN roles. The discovery of novel putative interactors and substrates (such as DVL1/2, MEF2C, MYH9, EDC4 and PRRC2C) indicate that CRBN might be involved in several biological processes (such as cell motility, platelet function and maturation, RNA processing, protein folding). Advances in CRBN biochemistry and its modulation with IMiDs will provide with a deeper understanding into IMiDs mechanism of action and possibly side effects of IMiD treatment.

Chapter 5: Discussion

5.1 From "Immune-modulating" to "E3 ligase-modulating" drugs

In the "pre-neosubstrate era" mechanistic understanding of the biological effects of thalidomide analogues was limited. IMiDs were demonstrated to globally affect the tumour niche by disrupting the interplay between MM PCs, BMSCs and other types of cells in the bone marrow microenvironment. Further investigations demonstrated direct anti-MM activity of IMiDs by perturbation of biological and biochemical pathways that are relevant for MM pathogenesis, such as cell cycle progression, the NF-kB pathway, TNF signalling and, most importantly, the IRF4-MYC axis, to which many MMs are considered to be addicted[65,115]. The discovery of the ability of IMiDs to re-direct CRBN substrate specificity towards IKZF1 and IKZF3 ushered in the "neosubstrate era" where IMiDs became not only "immunomodulatory" but also E3 ligase modulators. Historically, there have been significant efforts to develop compounds targeting the proto-oncogene and transcription factor MYC, which is proven to play a pivotal role in several cancers[103,104]. IKZF1 and IKZF3 were further demonstrated to enhance IRF4-MYC axis signalling, indicating that IMiDs have an indirect effect on MYC (and IRF4) transcriptional activity[251]. However, the most critical finding was represented by the possibility of pharmacologically modulating the activity of E3 ligases by modifying their substrate specificities. This has also led to development of small molecule inhibitors that are linked to E3 ligases modulators, also called PROteolysis TArget Chimeras (PROTACs). dBET, a PROTAC constituted by the BET-bromodomain inhibitor JQ1 linked to thalidomide, induces acute degradation of BET-bromodomain proteins such as BRD2/4, which are thus ubiquitinated by CUL4-DDB1-RBX1 and subsequently degraded by the proteasome[343]. This example demonstrates the importance of this discovery and provides with the rationale for developing novel compounds that exploit the ubiquitin-proteasome machinery to target specific tumour vulnerabilities.

5.2 IMiDs: more than just IKZ1, IKZF3, IRF4 and MYC

Given the relevance of IKZF1, IKZF3, MYC and IRF4 in malignant PC biology, the IKZF1/3-IRF4-MYC axis has been the predominantly investigated pathway in MM. It has been recently demonstrated that IRF4, MYC and IKZF1 associate with super-enhancers and are implicated in sustaining the core transcriptional co-regulatory network of MM PCs[100]. These genes are also important for the survival for MM cells. Extensive genome-wide studies of IKZF1, IKZF3, MYC and IRF4 transcriptional activity – i.e. ChIP-seq, ATAC-seq and more advanced transcriptional studies using SLAM-seq in MM cells treated with IMiDs are still lacking. This is surprising as these transcription factors are master regulators of the B-cell lineage and the aberrant MM PC transcriptional program. Integration of data from advanced genome-wide sequencing

techniques in IMiD-treated or untreated cells could reveal how IMiDs impact the core transcriptional regulatory network of MM cells. This would provide with novel insight into IMiD mechanisms of action at a transcriptional level.

IMiD-induced degradation of neosubstrates CK1α, ZFP91, SALL4 indicate that multiple pathways in different cell types might be involved in IMiD sensitivity[230,252,253]. Recent work on primary effusion lymphoma showed that IKZF1/3 degradation is uncoupled from the IRF4-MYC axis and suggested that lenalidomide-induced degradation of CK1α could be the main driver of the response to IMiDs in this disease[344]. Degradation of CK1α may also account for additional anti-MM activity, as inhibition or loss of CK1α has been demonstrated to be disadvantageous for MM[345,346]. Moreover, LEN's efficacy in 5q- refractory anemia has been shown to depend on CK1α degradation in the context of CK1α haploinsufficiency[230]. However, these effects are still probably largely dependent on neosubstrate degradation. In chapter 3 and other work[239,240], the existence of a multiplicity of pathways involved in IMiD sensitivity was demonstrated via genome-scale CRISPR screening. Here, deletion of genes that are either directly or indirectly related to CRBN-mediated protein degradation conferred resistance to IMiDs. Amongst these, the COP9 signalosome and other proteins implicated in the ubiquitin-proteasome cascade play a relevant role in the response to IMiDs. However, other genes that have not been related to protein degradation are also required for IMiD sensitivity, such as *NCOR1* or *EDC4*. Since their loss induces resistance to IMiDs, it can be speculated that pathways regulated by these genes are also implicated in IMiD sensitivity.

5.3 Technical limitations of *in vitro* models of acquired IMiD resistance

In chapter 3, models of *in vitro* acquired resistance to LEN were employed to dissect molecular mechanisms responsible for MM resistance to IMiD therapy, and loss of CRBN represented the major resistance mechanism. This data is corroborated by genetic studies demonstrating that IMiD-refractory MM cells downregulate and/or mutate CRBN[219,221,287,288]. The RNA-sequencing studies performed in this thesis revealed that acquired IMiD-resistance may not be solely attributable to CRBN downregulation. A state of IMiD-resistance was associated with induction of IFN and RAS signalling and suppression of *MYC* target genes, indicating that a number of changes, and not only CRBN levels, likely underpin acquired IMiD resistance. IFN augments expression of HLA molecules and triggers activation of CD8 T-cells and NK cells response against MM cells within the bone marrow microenvironment. In doing so, it potentiates anti-MM immune response[206–210,212,293,294,347]. This represents an important IMiD-dependent anti-MM

mechanism. These *in vitro* models of acquired LEN-resistance were generated by culturing IMiD-sensitive cells with increasing concentrations of LEN, and have the limitation of being generated in the complete absence of additional selective pressure, i.e. cytotoxic immune cells (T CD8, NK), which would normally increase the anti-tumoral response upon IMiD treatment. Co-cultures of isogenic MM cells with cytotoxic immune cells in presence and absence of an IMiD might address whether MM.1Sres cells are still sensitive to T CD8- and NK-mediated killing via IMiD-dependent increase of IFN signalling. An additional tool would be represented by IMiD- and immune-resistant MM cell lines. With this model, CRISPR screening might reveal pathways that mediate resistance to immune-mediated killing both in presence and absence of an IMiD. In the context of the microenvironment, augmented IFN-mediated expression of HLA genes in MM cells might increment T- and NK-cell anti-MM response. Detailed characterisation of the immune population surrounding MM cells could be achieved by *in vivo* studies on murine models with a humanised CRBN. Fink and colleagues have introduced a I391V substitution into the *Crbn* gene of these successfully restoring the biochemical response to IMiDs *in vivo* (Ikzf1, Ck1α degradation, promotion of cytokines secretion and inhibition of haemopoiesis)[237]. Cross-breeding these mice with Vk*MYC mice could represent a valid approach to generate a model of murine myeloma that is potentially IMiD-responsive[95]. NGS methodologies such as single-cell RNA-seq technologies, which have been proven to be essential in the study of immune subpopulations[348,349], could be applied in such murine model to study the transcriptional and phenotypical status of the tumoral immune population in the microenvironment when in presence and absence of an IMiD. Importantly, single-cell RNA-seq also enables tracking of clones from which resistance to drug treatment arises. An additional approach for the *in vivo* study of IMiD mechanism of action could be *in vivo* CRISPR screening[350]. The advantage of this approach would be the investigation of mechanisms of resistance to IMiDs that arise from any of the cells populating the bone marrow MM niche. However, the number of cells that can be injected in animal models can represent a technical limitation when conducting CRISPR screening. For genome-wide libraries, adequate representation of sgRNAs in the cell population tested is required. The use of smaller sgRNA libraries targeting fewer genes but specific for distinct biological processes (protein degradation, epigenetic regulation, transcriptional regulation, protein kinase activity, etc.) could therefore overcome this issue, assuming high permissivity of the cell population tested to viral transduction.

The importance of these type of studies is enabling the identification of IMiDs-resistance mechanisms, clonal evolution and selection of IMiD-resistant clones. Data obtained using these

novel approaches would represent important insight for understanding how MM adapts and escapes IMiD-treatment.

5.4. IMiDs, TOP2B and DNA homeostasis

Genetic loss of *TOP2B* was demonstrated to re-sensitise MM.1Sres cell lines to IMiD treatment, and TOP2 inhibition potentiated responses to IMiDs in MM.1S cells. However, the mechanistic activity of TOP2B in this context remains speculative. In this work, induction of DNA damage via TOP2B poisoning did not re-sensitise MM.1Sres cells to IMiDs. Although NCOR1 has been reported to operate in conjunction with TOP2B[264], its role in this context remains to be defined, as physical and functional interactions between NCOR1 and TOP2B have only been described at the level of loci that are responsive to the estrogen receptor. It was hypothesised that degradation of IKZF1 and IKZF3 induces de-repression of specific loci and in the absence of TOP2B this causes stalling of RNA Pol II. TOP2B has been proven to play a significant role in regulating transcription and TOP2B-mediated DNA double strand breaks have been found to be necessary to prime RNA Pol II processivity[261–264,299]. It has been proposed that rather than inducing relaxation/disentanglement of chromatin, TOP2B activity might promote a more permissive chromatin state at transcriptionally active sites[299]. This hypothesis provides the rationale for further studies with regards to the function of TOP2B inhibition in combination with IMiD treatment. Although TOP2B poisons (e.g. etoposide, doxorubicin, etc.) and degraders (e.g. dexrazoxane) target both TOP2 isoforms, more specific approaches to directly target TOP2B would be necessary (e.g. AID degron system) to isolate the effect of TOP2B loss without affecting TOP2A activity. In the clinic, an advantage of using TOP2 inhibitors rather than poisons would be the absence of DNA damage induction, as demonstrated in previous work by γH2AX assays in cells treated with DXZ[254]. This is expected to mitigate organ toxicity and, possibly, occurrence of genetic rearrangements observed with TOP2 poisons. In fact, DNA double strand breaks in breakpoint clustered regions, triggered by TOP2 poisoning with ETO, seem to be at the basis of secondary genetic events[301,351]. In this thesis, IMiD re-sensitisation via *TOP2B* loss was demonstrated not to be associated with DNA damage induction. Excluding this occurrence further supports the hypothesis that *TOP2B* deletion causes transcriptional stress upon acute loss of transcription factors IKZF1/3 with IMiD treatment. With this premise, it is possible that deletion of *TOP2B* rescues IMiD sensitivity preferentially in cells that were previously IMiD sensitive but have developed IMiD-resistance. To date, no selective TOP2B inhibitor has been described. The clinical use of DXZ as TOP2 inhibitor could be a safer option than ETO or other TOP2 poisoning agents such as doxorubicin. Further studies *in vitro* and *in vivo* with regards of

safety, toxicity profile, dosage and modalities of DXZ administration are required prior to introduce this compound as anti-cancer routine clinical therapy. Trialling DXZ in combination with LEN or any other IMiD would be required in order to assess the impact and clinical efficacy of TOP2B inhibition in the context of IMiD therapy. In the case of ETO-LEN combination therapy, the possibility of IMiD treatment interfering with DNA repair pathways should not be completely excluded *a priori*, as the presence of a modulatory effect of IMiDs on DNA repair is suggested by several lines of evidence. Firstly, IMiDs modify the binding specificity of CRBN, which is a CUL4-DDB1-RBX1 and a COP9 signalosome interacting partner. These proteins play a pivotal role in DNA repair, indicating that IMiDs might interfere with this essential homeostasis control mechanism. Secondly, a statistically significant increase of secondary neoplasia has been reported in patients treated with lenalidomide and oral melphalan, an alkylating agent[305]. For these reasons, further investigations are required to assess the safety of IMiD/DNA-damaging-based combination therapies that might potentially interfere with DNA homeostasis in the long term.

5.5. IMiDs potentially affect multiple pathways by modulating CRBN activity in a global fashion

In chapter 4, proximity labelling was adopted to characterise the CRBN interactome in the presence or absence of CRBN modulating agents. With this study, several novel interactors and putative CRBN substrates/neosubstrates were revealed, suggesting that the current common understanding of IMiDs mechanism of action is oversimplified. This is an important observation that likely applies to both the MM PC itself and other cellular components of the surrounding microenvironment.

A refined model representing the dynamic of CRBN biochemistry could be represented by that illustrated in figure 5.1. IMiDs, by modulating CRBN, are likely to globally alter its functions. In the absence of an IMiD, CRBN exerts both ubiquitinylating and chaperoning activity on endogenous substrates. For example, a well-established CRBN endogenous substrate for degradation is MEIS2[225].

Furthermore, CRBN might be ubiquitinylating proteins that are not destined to proteasomal degradation. In this case, ubiquitinylation would have the role of modulating signalling pathways or regulating protein localisation. In parallel, IMiD-dependent shifts in CRBN substrate specificity might potentially lead to the same outcome. IMiDs may affect multiple pathways not only by triggering neosubstrate degradation, but also by altering protein localisation and function when

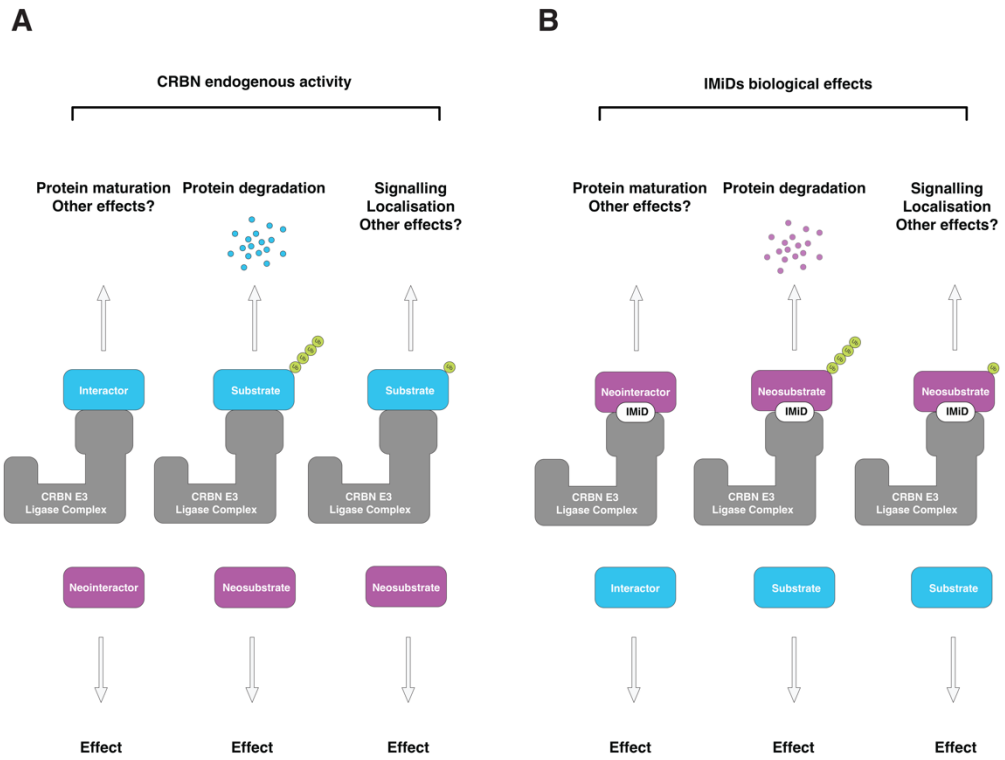


Figure 5.1. New proposed model for IMiD-related perturbation of CRBN activity.

Panel (A) shows the endogenous activity of CRBN in absence of IMiD treatment. CRBN exerts its function of chaperone and ubiquitin E3 ligase on endogenous ligands and substrates, whilst IMiDs neointeractors and neosubstrates are not engaged by the CRBN complex. In the case of IKZF1 and IKZF3, these transcription factor would promote or repress gene transcription as described in chapter 1. Collectively, these mechanisms determine the phenotype of the IMiD untreated cell. In panel (B), it is shown how IMiDs perturb CRBN endogenous activity. In presence of an IMiD, endogenous substrates are stabilised and interactors are no longer regulated by CRBN. Neosubstrates and neointeractors are now regulated by CRBN. This is the case of IKZF1 and IKZF3, now degraded, or BSG (basigin), now unstable. Conversely, CRBN endogenous substrates are now stabilised. IMiDs biological effect is the result of all these singular events occurring simultaneously.

inducing other types of protein ubiquitinylation[224]. This might be the case of MYH9, although further investigation is required. CRBN chaperone activity, demonstrated in the work of Eichner and colleagues[231], might be equally perturbed in the context of other biological processes. This might be the case of other putative neointeractors identified in the dataset, such as MEF2C, DVL proteins or RNA-processing factors.

5.5.1 Introducing the concept of "transcriptional resistance" to IMiDs

MEF2C, a transcription factor implicated in sustaining the PC transcriptional program, was found to be an interactor of CRBN-IMiD (both LEN and POM), but not a neosubstrate for proteasomal degradation. In this study, MEF2C may have been detected if cooperating in conjunction with IKZF1 and/or IKZF3. However, there is no evidence demonstrating MEF2C as IKZF1/3 direct interactor. More evidence would be required to define whether MEF2C is ubiquitinylated upon IMiD treatment and if this event can alter its activity. MEF2C could also be involved in unclear regulatory mechanisms. For instance, it has been reported that members of the MEF2 family are suppressed by HDAC3 and NCOR1. Although this phenomenon has been widely described in skeletal and cardiac muscles, it cannot be excluded as an important process in malignant PCs, where MEF2C is overexpressed and is also essential for cell survival and growth. One could hypothesise that loss of NCOR1 induces resistance to IMiDs because MEF2C responsive loci are no longer repressed. Still, the link that functionally bridges CRBN activity to MEF2C and NCOR1 is obscure and will require more investigation. Biochemical characterization of the interactome of MEF2C and/or NCOR1 via MS proteomics would be required to understand whether these two factors interact with each other and which are their interacting partners. ChIP-seq of MEF2C, NCOR1 and RNA Polymerase II would reveal whether MEF2C and NCOR1 co-localise in the same loci and drive gene transcription. Although this data is at preliminary stage, it can be posited that "transcriptional resistance" caused by lacking of transcriptional repression of genes that promote resistance to IMiD treatment may be at play.

5.5.2 Proximity labelling indicates CRBN as possible regulator of RNA processing

CRBN was also found to interact with multiple proteins implicated in RNA processing and translation, indicating that CRBN might be an important regulator of post-transcriptional events. Some of these proteins were EDC4 and PRRC2C. EDC4 promotes RNA decapping[337], the step that precedes RNA decay, and it is also implicated into formation of P-bodies (PBs). Little is known with regards to the function of PRRC2C, which seems to be involved in formation of stress granules (SGs) as well. Both PBs and SGs are aggregates of stalling translational complexes. The main difference between PBs and SGs is that SGs are exclusively generated upon intracellular

stress, whereas constitution of PBs represents a physiological mechanism of translational regulation[317–319]. The formation of these two types of aggregates represents a strategy for fine-tuning translation ratio and thus constitute important checkpoints in protein synthesis and expression[318]. Interestingly, *EDC4* deletion also caused resistance to LEN, as demonstrated via CRISPR screening; this finding requires validation with appropriate assays comparing SCR and *EDC4*-deleted MM.1S cells, in presence and absence of IMiD treatment. The mechanism by which *EDC4* deletion produces a resistant phenotype is completely obscure. One could hypothesise that the loss of EDC4 might impact RNA decay, prolonging the half-life of the mRNA pool and thus causing increased protein synthesis. If this is the case, cells could be in a status where important factors such as IKZF1, IKZF3, MYC and IRF4 are in excess. In this case, for example, the ratio of newly synthesised IKZF1/3 might overcome that of degraded IKZF1/3, representing a pure stoichiometric mechanism of resistance.

The detection of numerous interactions of CRBN with RNA processing genes is strongly suggestive of a role for CRBN in regulating post-transcriptional events. These include RNA splicing, transport and translation into protein. Again, whole-proteome ubiquitination studies would inform whether any of these interactors are differentially ubiquitinated in presence and absence of an IMiD. These mechanisms could be alternatively supported by CRBN chaperone activity. The use of bortezomib might represent a confounding factor, because proteasome inhibition is followed by accumulation of misfolded proteins that could be subjected to CRBN-mediated chaperoning. However, some of these novel CRBN or CRBN-IMiD interactors (including EDC4) are also detected in bortezomib untreated cells, indicating that the interaction between CRBN and these newly identified putative substrates might occur even in baseline conditions.

5.5.3. Novel CRBN interactors and substrates could be associated with PC dynamics and changes within the bone marrow microenvironment

As reported in chapter 1, IMiDs elicit a significant effect in the MM bone marrow microenvironment, where MM cells interact with the stroma by expressing adhesion molecules. These interactions promote also pro-survival signalling. Another important aspect of IMiDs that needs to be considered is the occurrence of therapy-related haematological toxicity. This includes neutropenia, thrombocytopenia and thrombosis[352]. The study of the CRBN interactome by proximity labelling identified proteins that could be directly or indirectly involved in these events. IMiDs are known to modulate WNT signalling[353]. DVL proteins participate in both canonical and non-canonical WNT signaling. In the canonical pathway, DVL functions as scaffold

to stabilise the beta-catenin degradation complex upon binding of WNT to its receptor FZD. Within the non-canonical WNT pathway, DVL proteins are mainly implicated in regulating cell polarisation and migration. Furthermore, WNT signalling has been demonstrated as a negative regulator of platelet function[354,355]. One could argue that IMiD-dependent modulation of WNT signalling is the consequence of CK1α degradation, although evidence provided within this study now demonstrated that CRBN might physically and functionally interact with DVL proteins independently from IMiD exposure. CRBN could be promoting ubiquitination of DVL, prevent misfolding and/or stabilising other component of the β-catenin degradation complex. DVL also functions as negative regulator of PRICKLE1, whereas CTTN (cortactin) is a downstream effector of the same pathway and PRICKLE1 is the core component of a complex that promotes planar cell polarity[338,339]. Since CRBN has been found to interact with both DVL proteins and CTTN, it can be speculated that CRBN might be involved into this process and IMiDs might interfere with cytoskeleton dynamics during motility. If WNT negatively impacts platelet aggregation, adhesion and granule releasing[354,355], it can be hypothesised that IMiD treatment counteract this effect by increasing platelet function and therefore promoting thrombotic events, which are typical manifestation of IMiD therapy. Other important side effects of IMiD therapy are teratogenicity and neuropathy. WNT signalling has a key role in embryonic development[328]. Although recent work has highlighted the role of IMiD-induced SALL4 degradation in embryonic stem cells[253], it is possible that degradation of CK1α by LEN or modulation of DVL proteins by IMiDs, if experimentally demonstrated, could also result in foetal malformations. Neuropathic pain is another impactful clinical challenge in patients undergoing IMiD therapy. Neuropathic pain has been linked to proinflammatory activity of WNT in rodents. Activation of the WNT/β-catenin pathway at the level of spinal dorsal neurons stimulates the production of TNF-α, regulates the activity of glutamate receptor and calcium flux. Some authors also reported that alteration of TNF-α signalling might be at the basis of thalidomide-induced neuropathy[356]. Modulation of the WNT/β-catenin pathway by IMiDs deserves further investigation and could help discovering the biological mechanisms underpinning specific side effects. Ultimately, defining mechanisms by which IMiDs induce organ toxicity would have a very important impact in the quality of life of patient treated with IMiDs, as these complications could be potentially prevented or treated.

Another important target identified in this study is MYH9. This gene codes for a non-muscle myosin heavy chain isoform. MYH9 is a key component of the cell motility apparatus together with actin filaments and plays a fundamental role in cell adhesion and migration. Furthermore, mutations of this gene are known to cause syndromic platelet disorders (e.g. May-Hegglin

Anomaly) which are associated with thrombocytopenia[316,340]. The results obtained in chapter 4 suggest that MYH9 might be ubiquitinated by CRBN in the presence of an IMiD. The data obtained provide a rational for the study of MYH9 ubiquitination and its downstream effects. It is plausible that IMiDs might induce ubiquitination of MYH9 therefore modifying its interaction with actin or other molecules implicated in motility, such as MYLK (myosin light chain kinase, identified as a CRBN interactor in one of the experiments). To understand whether MYH9 is directly ubiquitinated via a CRBN-IMiD dependent mechanisms, ubiquitination assays (immunoprecipitation and post-translational modification proteomics) in presence and absence of an IMiD and in the context of CRBN loss would be required. These experiments should be conducted in other cell lineages characterising the bone marrow MM niche, such as bone marrow stromal cells, macrophages, endothelial cells, osteoblasts. This would be important because MYH9 is ubiquitously expressed and its ubiquitination might possibly have an effect in different cell populations.

Perturbation of cell adhesion and movement are important aspects of IMiDs biological effect and these data suggest that novel CRBN interactors might be implicated in this complex phenomenon. More investigation is required to verify whether the molecular evidence is associated with modification of the MM PC status within the microenvironment.

5.6 Conclusion

This thesis aimed to define transcriptional signatures of IMiD sensitivity and resistance, and mechanisms of sensitivity and resistance to IMiDs. Moreover, proximity labelling was adopted to better define the changes occurring in the CRBN interactome upon IMiD treatment. In chapter 3, IFN, RAS and MYC signalling were identified as important transcriptional signatures in the context of IMiD sensitivity and resistance. Several genes, such as COP9 signalosome subunit, *NCOR1* and *EDC4*, were identified as essential for IMiD sensitivity, whilst loss of other genes, such as *TOP2B* and *ATXN7*, induced synthetic lethality in presence of an IMiDs in resistant cells. Moreover, a TOP2 inhibitor demonstrated anti-MM activity. The phenotype observed with genetic loss of *TOP2B* and the efficacy of TOP2 inhibitors in MM provides with the rationale for developing novel specific TOP2B inhibitors as therapeutics. Chapter 4 aimed to better characterise the CRBN interactome by proximity labelling. It was demonstrated that BioID2 is a useful tool for the study of CRBN interactome, as IMiDs are CRBN substrate specificity ("E3 ligase") modulators. Newly identified CRBN partners and targets, such as MEF2C, RNA processing factors and protein translation, DVL proteins and MYH9 could potentially provide novel mechanistic insight into IMiDs biological effects. More investigation is required to

understand the consequences of IFN, RAS and MYC modulation, especially in the context of the bone marrow microenvironment. Defining the molecular mechanism of non-protein degradation related factors (NCOR1, MEF2C, TOP2B, ATXN7) might reveal unprecedently described regulatory genetic networks perturbed by IMiDs. Investigating the role of CRBN in RNA processivity and protein translation in presence of an IMiD might also represent a novel important advance in defining the IMiD's biological effects, also in combination with bortezomib. Finally, more studies are required to understand the role of novel CRBN interactors and substrates that are known to be involved in processes occurring in the MM microenvironment and into the aetiology of IMiD-related toxicity.

Appendix 1: Tables of differentially expressed genes in RNA-seq experiments

A1.1 Top 100 differentially expressed genes in U266res vs U266 cells

	logFC	AveExpr	t	P.Value	adj.P.Val	B
MLC1	4.16160292	6.2585394	38.58689	1.06E-20	1.32E-16	36.8564817
ADAM19	4.15877518	4.93992943	25.6000717	4.22E-17	2.62E-13	28.8234386
ALOX5AP	5.214747	4.90773519	23.0712094	3.36E-16	1.05E-12	26.7059217
ARL4C	3.19270665	7.24763872	23.0605494	3.39E-16	1.05E-12	27.2852171
SPN	4.40308149	4.17103206	22.2289598	7.03E-16	1.75E-12	25.8131495
SPINK2	2.8678867	4.80347183	21.2324308	1.74E-15	3.11E-12	25.5337922
SEPT9	6.11664517	4.1978066	21.2264987	1.75E-15	3.11E-12	24.4263215
MAP2	-3.4993333	4.46694163	-21.049307	2.07E-15	3.21E-12	25.1456677
MAN1C1	4.32090041	4.00093922	20.6397686	3.05E-15	4.20E-12	24.3519463
RIPOR2	3.37779564	5.74852844	20.1439827	4.91E-15	6.11E-12	24.6147816
FAM92B	4.22764316	4.75943531	19.7553879	7.20E-15	8.14E-12	24.0800697
CD38	5.78572946	3.52716161	19.6398219	8.08E-15	8.37E-12	22.9020282
LINC00504	-4.0718705	3.52611202	-18.093072	4.01E-14	3.70E-11	21.9299191
PCDH20	3.71521161	3.93137394	18.0576	4.17E-14	3.70E-11	22.3587572
METTL7A	2.33651407	6.07137883	17.7889946	5.57E-14	4.62E-11	22.1932363
ETS1	2.45739603	4.33608635	17.5803967	7.01E-14	5.44E-11	21.9555822
FGR	3.32741807	4.82180074	16.3666178	2.79E-13	2.04E-10	20.607342
HRASLS2	1.94755594	6.58819751	16.0248232	4.17E-13	2.84E-10	20.1436633
AGT	-2.5319534	7.88722418	-15.991078	4.35E-13	2.84E-10	20.0583013
DSEL	5.46359084	3.33102488	15.9147325	4.76E-13	2.96E-10	19.2523475
PPM1L	2.47974383	4.45521667	15.4564506	8.32E-13	4.81E-10	19.5226916
OLR1	2.13366719	4.98393305	15.4382509	8.51E-13	4.81E-10	19.4880052
RAB31	2.12844443	7.28718816	15.3051802	1.00E-12	5.28E-10	19.2263683
CMTM7	3.70624395	3.44400223	15.2921069	1.02E-12	5.28E-10	19.1178867
PSD3	2.40631698	5.36371143	15.1911672	1.16E-12	5.75E-10	19.1779036
RUBCNL	7.7411389	0.6406417	15.137556	1.24E-12	5.91E-10	14.8382692
SELL	3.48379369	4.52213593	14.7728547	1.96E-12	9.03E-10	18.6700585
FAM133A	1.58375398	6.10509101	14.7282049	2.08E-12	9.22E-10	18.5301068
GJC1	-2.6968797	3.37084941	-14.658364	2.27E-12	9.74E-10	18.453915
TMEM52B	2.32679742	5.16432599	14.5071014	2.77E-12	1.15E-09	18.2921549
FOXP1	-5.2383996	3.00754687	-14.411688	3.13E-12	1.22E-09	17.5348912
ALG5	1.3172065	6.33949275	14.4077844	3.15E-12	1.22E-09	18.0920793
RPL21P28	1.0609433	9.65358514	14.3382118	3.45E-12	1.30E-09	17.818222
ADD2	-3.318193	4.34940121	-14.118506	4.61E-12	1.68E-09	17.817026
TPT1	0.94554706	12.0681452	13.9009403	6.16E-12	2.14E-09	17.0606233
LSAMP	-3.0279718	3.58896992	-13.898122	6.19E-12	2.14E-09	17.461592
NLRP7	-2.3910706	4.58908742	-13.664961	8.49E-12	2.85E-09	17.2162783
RPL21	1.01066544	9.80760233	13.6295731	8.91E-12	2.91E-09	16.8307811

FBP1	6.77275256	1.86685884	13.0358764	2.04E-11	6.49E-09	14.2752706
TOX	1.97308835	4.1135678	12.983932	2.19E-11	6.81E-09	16.2705034
PLCL2	2.73986908	3.79850171	12.8622042	2.61E-11	7.90E-09	16.1001437
RIN2	-6.628192	0.47930846	-12.511683	4.33E-11	1.28E-08	12.6895775
IKZF1	1.3638232	5.99405085	12.4441241	4.78E-11	1.38E-08	15.3480021
ITGB7	1.3809577	7.816333	12.4192956	4.96E-11	1.40E-08	15.2043028
MDFIC	-1.6279643	4.57226639	-12.311079	5.82E-11	1.61E-08	15.2505897
PERP	-4.0967585	2.9946321	-12.2638	6.25E-11	1.69E-08	14.981017
MEF2C	1.39658792	5.83581282	12.2075851	6.79E-11	1.80E-08	14.9876616
GFOD1	1.43263192	6.0724123	12.1601616	7.29E-11	1.89E-08	14.9130713
COBLL1	-3.9483407	1.8010388	-12.111746	7.84E-11	1.99E-08	14.4586375
EPB41L2	3.68273017	6.26150935	11.9884373	9.44E-11	2.35E-08	14.6782721
CDH4	3.60199965	3.17468332	11.937327	1.02E-10	2.48E-08	14.7119089
C10orf90	-5.1057706	1.81450107	-11.842398	1.18E-10	2.82E-08	13.664112
PTPRC	-1.7169861	5.24533615	-11.817482	1.22E-10	2.87E-08	14.4236929
PIK3CG	7.75516994	0.76102167	11.7583085	1.34E-10	3.08E-08	12.0015794
CCR1	2.21287112	5.20421187	11.4949861	2.02E-10	4.55E-08	13.9826552
CGA	-4.2950472	2.95899284	-11.46949	2.10E-10	4.65E-08	13.9091394
TLR7	7.63559751	0.48702614	11.4179485	2.27E-10	4.96E-08	11.6361407
HIPK2	-1.3192736	7.22605489	-11.383132	2.40E-10	5.14E-08	13.6109935
ADA2	3.91093979	2.76210396	11.3305779	2.61E-10	5.49E-08	13.6595653
CHST15	1.41941532	6.65151756	11.2433389	2.99E-10	6.20E-08	13.4524397
MZB1	2.11657144	4.07006724	11.1885308	3.27E-10	6.65E-08	13.580094
MFNG	7.28064698	0.54725467	11.1703803	3.36E-10	6.70E-08	11.3588585
LOC100507377	2.19671077	3.08022279	11.1643146	3.40E-10	6.70E-08	13.5727506
PLXNA4	-7.6974401	0.75573764	-11.111679	3.69E-10	7.17E-08	11.3204549
HLA-DRB1	1.81907418	5.98267591	11.0935879	3.80E-10	7.27E-08	13.251324
PPP2R2B	-7.0885025	1.25767522	-11.063236	3.99E-10	7.52E-08	11.6071796
CD52	1.39844578	7.57859872	10.9018572	5.18E-10	9.61E-08	12.7817373
RBMS1	3.74502884	2.71373558	10.8663251	5.49E-10	1.00E-07	12.9618624
ARFGEF3	-3.9048021	3.13965806	-10.793246	6.18E-10	1.11E-07	12.9182327
LITAF	1.12823997	8.2801601	10.6993236	7.21E-10	1.28E-07	12.4180459
ARHGDIB	3.38747076	3.27749758	10.6345886	8.03E-10	1.40E-07	12.7304418
HIVEP3	-2.7294501	2.72368946	-10.567893	8.96E-10	1.55E-07	12.5769458
NT5E	1.98394019	4.21309752	10.53844	9.41E-10	1.60E-07	12.5139242
HEG1	2.0574009	5.45207385	10.5305549	9.54E-10	1.60E-07	12.3838474
NCALD	4.2134416	1.53515249	10.5124973	9.83E-10	1.62E-07	12.0087525
CD247	6.87167992	1.41766188	10.4983358	1.01E-09	1.62E-07	11.2320971
LINC00910	1.4709033	7.01244245	10.4958827	1.01E-09	1.62E-07	12.1426847
NAP1L3	3.67357228	2.5333701	10.4926632	1.02E-09	1.62E-07	12.4078916
MX1	1.09945657	8.61808042	10.4377068	1.11E-09	1.75E-07	11.94731
POMP	0.9325845	8.81227101	10.4116574	1.16E-09	1.81E-07	11.8747438

LINC00689	3.07750394	2.30081737	10.3671897	1.25E-09	1.92E-07	12.2144841
IPCEF1	-6.8193816	0.55903615	-10.359332	1.27E-09	1.92E-07	10.5295593
HLA-DRA	1.22590499	7.90402992	10.3514936	1.29E-09	1.93E-07	11.8492222
VSTM4	-1.5588815	5.49955429	-10.281976	1.45E-09	2.14E-07	11.9128405
ARID5B	6.2915984	0.6996635	10.2605771	1.50E-09	2.19E-07	10.3486913
SYK	6.10978285	-0.5670826	10.2496361	1.53E-09	2.21E-07	10.2160756
SLA	1.25185167	6.2936692	10.2102236	1.63E-09	2.33E-07	11.7073404
MPP6	2.36936535	3.51242143	10.186757	1.70E-09	2.40E-07	11.9703187
SLAMF7	1.55000119	5.87016465	10.1260863	1.89E-09	2.63E-07	11.5935535
FOXP2	2.08307595	3.59073813	10.0947315	1.99E-09	2.75E-07	11.8033146
SEPT11	-6.2821111	1.12480033	-10.082838	2.03E-09	2.77E-07	10.481184
UBL3	1.81164201	3.95586091	10.0757115	2.06E-09	2.78E-07	11.7260184
SH3RF1	5.67355038	1.76574125	10.0668655	2.09E-09	2.79E-07	10.9178044
EDNRB	2.0711601	7.29058095	9.99632002	2.36E-09	3.11E-07	11.2520184
ISG20	1.24198125	7.26677353	9.99183287	2.38E-09	3.11E-07	11.2491335
GLUL	-3.2647607	1.98502321	-9.956907	2.52E-09	3.24E-07	11.4744859
UAP1	1.61981718	6.98993513	9.9557846	2.53E-09	3.24E-07	11.1939563
WARS	1.08540097	7.77483396	9.93465551	2.62E-09	3.32E-07	11.1050883
CCR9	6.1390198	-0.7383089	9.9174219	2.70E-09	3.36E-07	9.81252901
LINC02384	-2.118854	3.62751048	-9.9147327	2.71E-09	3.36E-07	11.4939046

logFC = log2(fold-change), AveExpr = average expression, P.Value= p-value, adj.P.Val = adjusted p-value

A1.2 Top 100 differentially expressed genes in LEN-treated vs DMSO-treated U266 cells

	logFC	AveExpr	t	P.Value	adj.P.Val	B
CHI3L1	2.60013729	1.93525015	15.1787433	1.17E-12	1.46E-08	18.7748632
EMP2	2.29340741	2.02129543	14.4709907	2.90E-12	1.80E-08	17.3561565
CHST15	1.06593795	6.65151756	8.35754829	4.69E-08	0.00011992	8.7069801
DEPP1	2.02814551	2.95446311	8.32166667	5.02E-08	0.00011992	8.66506636
PTP4A3	1.59477323	3.54312369	8.31056582	5.13E-08	0.00011992	8.64762914
ST7-AS1	3.65869757	1.84949254	8.24816574	5.79E-08	0.00011992	7.39106971
RHOU	1.27997952	3.62264305	7.90769268	1.13E-07	0.00019716	7.88628241
CAV2	2.17441217	2.21253439	7.84961342	1.27E-07	0.00019716	7.29923237
PLA2G4C	2.18762228	2.07550974	7.76812147	1.49E-07	0.0002063	6.9380427
XBP1	1.19685681	11.064009	7.67874248	1.79E-07	0.00020753	7.11509733
RRAD	4.46637589	0.50058692	7.66549678	1.84E-07	0.00020753	4.99501689
SERPINH1	1.69435871	5.98756343	7.5121473	2.51E-07	0.00025975	7.05048709
CTDSP2	1.09782272	6.47283681	7.37763624	3.31E-07	0.0003159	6.72585578
KIAA0040	1.00790022	6.23482028	7.32042312	3.72E-07	0.00033009	6.62996903
RIN2	0.97378866	0.47930846	7.25843229	4.23E-07	0.00035029	6.61836283
ATP6V1C2	2.48220046	1.70193611	7.21561071	4.62E-07	0.00035896	6.03185481
CCDC167	-1.6454851	4.8278091	-7.1496242	5.30E-07	0.00037828	6.37539086
LAP3	1.44742378	6.72814382	7.1340242	5.48E-07	0.00037828	6.20674609
PSTPIP2	2.04726078	1.78188579	6.92201986	8.57E-07	0.00055982	5.89857213
BMF	1.61453725	4.4297161	6.88115112	9.34E-07	0.00055982	5.83546919
KCNN3	-1.1168711	6.27590003	-6.8751015	9.46E-07	0.00055982	5.71468102
SOD2	0.73007604	6.40078206	6.78630499	1.14E-06	0.00064576	5.4763562
OTUD5	-0.5680943	10.6320856	-6.5900198	1.74E-06	0.00094218	4.81211237
LGALS3BP	3.07043068	1.51742165	6.55528642	1.88E-06	0.00097348	4.4617808
APOL6	1.62864005	6.9584622	6.50456868	2.10E-06	0.00104335	4.87806593
MTMR11	1.83831411	1.93829444	6.39913101	2.64E-06	0.00126268	4.71293015
BSPRY	1.14326647	5.28037096	6.38055422	2.75E-06	0.00126639	4.69050899
CNTRL	-1.1041441	3.9080274	-6.3067678	3.24E-06	0.0013942	4.65038741
DCAF6	0.60097018	6.95682757	6.28844012	3.37E-06	0.0013942	4.36262236
IFI27	0.86561679	6.2368898	6.27478626	3.47E-06	0.0013942	4.39065998
SSBP4	-2.2339082	2.27053435	-6.2556779	3.62E-06	0.0013942	4.28220529
ZSCAN9	-1.0838343	4.1033748	-6.24675	3.69E-06	0.0013942	4.51294044
MGAT5	1.03622731	4.92027822	6.24558478	3.70E-06	0.0013942	4.47185432
CORO1B	2.43514386	2.54500638	6.06900482	5.48E-06	0.0020021	4.05736969
MYBPH	3.9034886	-1.1314311	5.93999062	7.31E-06	0.00259554	2.44822928
MUC1	1.69004199	4.20257701	5.89448475	8.10E-06	0.00274554	3.75558858
TUBA4A	0.73693244	7.56093183	5.88256319	8.32E-06	0.00274554	3.419773
LINC01485	1.41546253	3.72755897	5.87841678	8.40E-06	0.00274554	3.75014431

RHBDF2	0.80455101	6.49036324	5.847162	9.01E-06	0.00287034	3.42265787
RSPH3	1.03796669	3.96523746	5.80094477	1.00E-05	0.0031064	3.52163296
TRAF3IP3	0.54069378	7.13597689	5.78661258	1.03E-05	0.00313046	3.25518079
ARF3	0.70330255	8.03755376	5.70766662	1.24E-05	0.00357391	3.0064663
TMEM173	1.24439821	4.26304786	5.70480285	1.24E-05	0.00357391	3.325661
STAT4	0.81782271	3.92156289	5.69702312	1.27E-05	0.00357391	3.29145264
CORO1A	-0.6710135	7.68485914	-5.639151	1.44E-05	0.00398624	2.88015724
B4GALT1	0.84410273	6.88060071	5.56970858	1.69E-05	0.00456915	2.74363554
AHNAK	0.82683514	6.46500248	5.54648741	1.78E-05	0.00471581	2.76889514
NOL3	0.91533364	3.75025645	5.5091702	1.94E-05	0.0048828	2.90648207
S100PBP	-0.7252098	6.45447536	-5.5012659	1.98E-05	0.0048828	2.63523114
DGKD	0.74223426	5.09315055	5.49741904	2.00E-05	0.0048828	2.77414067
KCNS3	1.22049498	2.16728979	5.4956363	2.00E-05	0.0048828	2.842189
BATF2	3.71636114	-0.5587911	5.44607856	2.25E-05	0.0053659	1.02836173
IFIT3	0.99279011	7.05385577	5.42000098	2.38E-05	0.00555155	2.42523033
RAB2B	0.61559266	6.9451826	5.40850229	2.45E-05	0.00555155	2.38397461
ITGB7	0.61606454	7.816333	5.40414634	2.47E-05	0.00555155	2.36288163
DDR2	0.94340665	4.70782222	5.39720233	2.51E-05	0.00555155	2.56694449
TNFSF10	1.44757843	2.86826121	5.39139188	2.55E-05	0.00555155	2.70259089
PARP14	1.29777414	6.06016272	5.38083412	2.61E-05	0.00559016	2.41055732
NUPR1	3.76189856	-0.6198107	5.34944122	2.81E-05	0.00590798	1.00066954
IFITM3	2.08893054	1.94487157	5.31998378	3.00E-05	0.00621836	2.24853131
SPR	1.26328758	3.45410771	5.30666966	3.10E-05	0.00630752	2.48310778
FYTTD1	0.57995611	7.62263279	5.26781379	3.39E-05	0.0067894	2.00737922
DDX58	1.42426433	3.70083166	5.21211308	3.85E-05	0.00760225	2.27631892
LILRB4	0.71447992	6.63783132	5.18866947	4.07E-05	0.00782047	1.94701888
ARL4C	-0.8592527	7.24763872	-5.1859206	4.10E-05	0.00782047	1.97762269
CLEC1A	0.73206698	4.95052051	5.17988011	4.15E-05	0.00782047	2.0777488
ITGA8	-1.2662297	3.02637393	-5.1052321	4.94E-05	0.00916436	2.09372733
AP1S2	-0.6220086	6.70061018	-5.0867535	5.16E-05	0.00942678	1.67192718
PTGES3L	1.99227682	1.92222938	5.07508084	5.30E-05	0.00954639	1.96301227
PIPOX	2.01861056	-0.9124392	5.03778908	5.78E-05	0.01026527	1.52862467
CDKN2D	0.48270333	6.64687857	4.95897592	6.95E-05	0.01216764	1.35857721
SPINT1	1.73931339	0.2206684	4.95004116	7.10E-05	0.01225219	1.51549181
PAQR9	-0.9333794	3.32030118	-4.8766434	8.43E-05	0.01407751	1.4536464
RFWD3	-0.4738122	7.06128696	-4.8765143	8.44E-05	0.01407751	1.14608979
STARD5	1.19791854	2.27342126	4.87335787	8.50E-05	0.01407751	1.58318681
CSRNP1	1.45014957	3.22689216	4.86339329	8.70E-05	0.0142209	1.55616766
DUSP5	0.89804933	7.38236464	4.85362583	8.90E-05	0.01436169	1.05903699
TOM1L1	1.05547157	2.18159702	4.83995695	9.19E-05	0.0146399	1.36530541
ZNF219	0.97581736	3.83580674	4.82472288	9.53E-05	0.01465234	1.39386509
FAM200B	0.77176637	3.75223945	4.82168528	9.59E-05	0.01465234	1.35350241

GBE1	0.76005043	4.88656247	4.81702069	9.70E-05	0.01465234	1.19990414
NACAD	1.60708292	1.75430374	4.81101321	9.84E-05	0.01465234	1.45641073
MGST3	0.98497079	6.02176107	4.80589143	9.96E-05	0.01465234	1.0353155
UROD	0.49367935	6.12339533	4.80520939	9.97E-05	0.01465234	1.04031463
RALB	0.74445083	3.55801259	4.80225451	0.00010042	0.01465234	1.23317781
TEX14	2.24771476	2.02814373	4.79803665	0.00010142	0.01465234	1.28159288
UNC13C	-0.9043544	3.57170558	-4.781196	0.00010552	0.01506893	1.20502887
LOC653513	0.61257445	5.69962974	4.72055815	0.00012171	0.01668386	0.84495474
PDE4DIP	0.61257445	5.69962974	4.72055815	0.00012171	0.01668386	0.84495474
SNHG12	0.66734096	5.50287184	4.71779751	0.0001225	0.01668386	0.89688207
IFI44L	0.93141056	4.70928642	4.71106334	0.00012446	0.01668386	0.907074
CDCA4	-0.4777693	5.32746534	-4.710762	0.00012455	0.01668386	0.91834939
CCND2	0.82976175	8.22015305	4.70772748	0.00012544	0.01668386	0.67517014
GEMIN8	-1.6642374	2.14904894	-4.7029786	0.00012685	0.01668386	1.21806053
RSAD2	1.09634835	2.75996819	4.70057742	0.00012757	0.01668386	1.20040546
ERN1	0.78967217	6.23950355	4.68191008	0.00013331	0.01725261	0.78681419
DOK3	-1.027253	2.16322783	-4.6597245	0.00014047	0.01799166	1.11568722
UNG	-0.4906983	6.62428395	-4.6130739	0.00015681	0.0198801	0.55499296
ATP10D	1.02302301	2.39064641	4.60814007	0.00015865	0.01990983	0.98878482
PROK2	-0.6700368	5.19535389	-4.5925735	0.00016459	0.02044866	0.56241203

logFC = log2(fold-change), AveExpr = average expression, P.Value= p-value, adj.P.Val = adjusted p-value

A1.3 Top 100 differentially expressed genes in POM-treated vs DMSO-treated U266 cells

	logFC	AveExpr	t	P.Value	adj.P.Val	B
EMP2	2.8521215	2.02129543	18.4027272	2.88E-14	3.58E-10	21.8311418
CHI3L1	2.93777057	1.93525015	17.3010175	9.55E-14	5.94E-10	21.3688647
CHST15	1.30099575	6.65151756	10.2919903	1.42E-09	5.13E-06	12.1291811
PLA2G4C	2.7875287	2.07550974	10.2037377	1.65E-09	5.13E-06	11.1632202
PTP4A3	1.88969036	3.54312369	9.95863575	2.52E-09	6.25E-06	11.5904508
ATP6V1C2	3.06471331	1.70193611	9.13340622	1.09E-08	2.26E-05	9.60261161
DEPP1	2.16906233	2.95446311	8.9583282	1.51E-08	2.67E-05	9.85766808
LGALS3BP	4.03293563	1.51742165	8.87382144	1.76E-08	2.74E-05	8.69482021
XBP1	1.36334287	11.064009	8.80436025	2.01E-08	2.77E-05	9.19800525
ST7-AS1	3.84921751	1.84949254	8.71832191	2.36E-08	2.93E-05	8.64929962
KIAA0040	1.1799278	6.23482028	8.62614531	2.81E-08	3.17E-05	9.12214596
RIN2	1.13467362	0.47930846	8.56306646	3.16E-08	3.27E-05	9.13150003
CTDSP2	1.26069162	6.47283681	8.52093107	3.43E-08	3.27E-05	8.89694321
CAV2	2.32608003	2.21253439	8.47487395	3.74E-08	3.32E-05	8.67625905
RHOU	1.34835486	3.62264305	8.36501412	4.62E-08	3.83E-05	8.7195792
PTPRC	-1.1181818	5.24533615	-8.2716748	5.53E-08	4.25E-05	8.45633892
KCNN3	-1.3736719	6.27590003	-8.2461928	5.81E-08	4.25E-05	8.42317361
SOD2	0.86839111	6.40078206	8.11445217	7.52E-08	5.19E-05	8.09726906
RRAD	4.67497145	0.50058692	8.06013738	8.36E-08	5.47E-05	6.37162298
ITGB7	0.90200848	7.816333	7.99514883	9.51E-08	5.91E-05	7.82708995
LAP3	1.60491304	6.72814382	7.9538878	1.03E-07	6.10E-05	7.7686435
CORO1B	3.07582027	2.54500638	7.87286696	1.21E-07	6.84E-05	7.67448501
SERPINH1	1.74763051	5.98756343	7.76055668	1.52E-07	8.20E-05	7.45615542
IFITM3	2.87836531	1.94487157	7.66360484	1.84E-07	9.55E-05	6.83723057
TK2	-1.278978	3.90505435	-7.463866	2.77E-07	0.00013761	7.01546911
OTUD5	-0.6422733	10.6320856	-7.4252873	3.00E-07	0.00013843	6.4524855
CCDC167	-1.7292252	4.8278091	-7.4234553	3.01E-07	0.00013843	6.8724264
APOL6	1.84025436	6.9584622	7.40068519	3.15E-07	0.00013987	6.65750402
IFI27	1.00726817	6.2368898	7.34142867	3.56E-07	0.00015259	6.55239388
DCAF6	0.69506049	6.95682757	7.2974059	3.90E-07	0.00016155	6.40139713
SSBP4	-3.3058536	2.27053435	-7.248669	4.32E-07	0.00016646	5.95764933
MGAT5	1.1901191	4.92027822	7.239753	4.40E-07	0.00016646	6.49412387
TMEM173	1.5487177	4.26304786	7.23701765	4.42E-07	0.00016646	6.52621869
CCR2	-0.9541488	6.96967085	-7.2144647	4.63E-07	0.00016714	6.2994681
DDR2	1.23598086	4.70782222	7.20677078	4.71E-07	0.00016714	6.40267266
SIGLEC15	4.7415197	-2.0164678	7.14703241	5.33E-07	0.00018407	4.00783999
IFIT3	1.28990406	7.05385577	7.11674148	5.68E-07	0.00019027	6.03913301
BMF	1.66251419	4.4297161	7.10535047	5.82E-07	0.00019027	6.23464951

PIPOX	2.70510722	-0.9124392	7.06842478	6.29E-07	0.00019712	5.54977018
MAGEA11	4.90031603	-1.965306	7.06406406	6.35E-07	0.00019712	3.93511918
BSPRY	1.23150846	5.28037096	6.90111167	8.95E-07	0.00027132	5.69864871
PSTPIP2	2.0279384	1.78188579	6.85300288	9.92E-07	0.00029339	5.79825272
ARF3	0.82955535	8.03755376	6.76344819	1.20E-06	0.00034695	5.20843588
NFE2L1	-0.6162647	8.02325328	-6.5717807	1.81E-06	0.00051234	4.79602625
PTGES3L	2.47525081	1.92222938	6.48082847	2.21E-06	0.00060736	4.93858921
ARL4C	-1.0988187	7.24763872	-6.4730094	2.25E-06	0.00060736	4.76339726
CORO1A	-0.7673662	7.68485914	-6.421982	2.51E-06	0.00066446	4.49754316
CAV1	0.84151553	6.9732729	6.35713242	2.90E-06	0.00074987	4.37129041
VAMP4	-0.8805214	4.33226877	-6.3341601	3.05E-06	0.00077256	4.61813299
TEX14	2.85803116	2.02814373	6.30227322	3.27E-06	0.00079081	4.43934348
NUPR1	4.34059233	-0.6198107	6.29962651	3.29E-06	0.00079081	3.04275751
MUC4	4.84705643	-1.6531115	6.29651747	3.31E-06	0.00079081	2.92639582
VCL	1.26172162	3.16075606	6.2822929	3.42E-06	0.00080058	4.58549139
PARP14	1.50160574	6.06016272	6.27247724	3.49E-06	0.00080294	4.28328824
RBM47	0.85061027	5.92925295	6.25082602	3.66E-06	0.0008269	4.2447424
CYTIP	-0.604191	6.94088132	-6.235265	3.79E-06	0.00084052	4.11016962
FYTTD1	0.67723758	7.62263279	6.17329085	4.35E-06	0.00094714	3.91904321
LOC730101	1.36955637	3.89110254	6.05627139	5.64E-06	0.00120745	4.09603399
CDKN1A	1.09930775	5.1824711	6.0103333	6.25E-06	0.00131524	3.79006644
CLEC1A	0.83937666	4.95052051	5.99087099	6.52E-06	0.00133598	3.78863182
TRAF3IP3	0.55926886	7.13597689	5.98844015	6.56E-06	0.00133598	3.56609415
RAB2B	0.67603367	6.9451826	5.95281629	7.10E-06	0.00142366	3.4764255
LINC01485	1.42898794	3.72755897	5.93666311	7.37E-06	0.00145278	3.82080258
UNG	-0.6333162	6.62428395	-5.9075059	7.87E-06	0.00152689	3.4038677
LITAF	0.63150207	8.2801601	5.89478806	8.09E-06	0.00154702	3.29007494
IL17RC	3.55328701	-1.78087	5.87784741	8.41E-06	0.00158279	2.10149889
RHBDF2	0.80732418	6.49036324	5.86693887	8.62E-06	0.00159795	3.32534916
CALCA	3.55565815	-2.4032944	5.83296762	9.30E-06	0.0016998	2.04137954
AHNAK	0.86502115	6.46500248	5.81055089	9.79E-06	0.00176214	3.22803593
UNC13C	-1.1220569	3.57170558	-5.7487448	1.13E-05	0.00198164	3.31367306
SLC7A8	1.27792042	1.9959989	5.7460451	1.13E-05	0.00198164	3.45238306
MUC1	1.64762833	4.20257701	5.72542335	1.19E-05	0.00203614	3.29774834
LILRB4	0.7854335	6.63783132	5.72183426	1.20E-05	0.00203614	3.02477314
ZSCAN9	-0.9760056	4.1033748	-5.6921263	1.28E-05	0.00213299	3.20127578
DGKD	0.76703196	5.09315055	5.68947031	1.29E-05	0.00213299	3.08511619
SLC15A3	3.9418163	-2.424854	5.65194317	1.40E-05	0.0022925	1.86396372
CNTRL	-0.9653129	3.9080274	-5.6384241	1.45E-05	0.00233348	3.09473794
CDC6	-0.6870986	5.30266806	-5.6238362	1.50E-05	0.00233692	2.94331755
TSPAN15	1.91789505	-0.0177737	5.62332405	1.50E-05	0.00233692	3.09796648
SLC43A3	3.30448419	-2.0802339	5.62100859	1.50E-05	0.00233692	1.91174285

MFSD12	0.7720735	5.92132798	5.61426611	1.53E-05	0.00234379	2.79169547
SPR	1.32832865	3.45410771	5.60046583	1.58E-05	0.00234379	3.05646772
ITGA8	-1.4274521	3.02637393	-5.5988671	1.58E-05	0.00234379	3.1598234
VPS35	0.54354549	7.33501033	5.59833527	1.58E-05	0.00234379	2.63449947
HBD	-0.8416438	5.67873077	-5.5644351	1.71E-05	0.00242499	2.71083502
CDK5R1	1.03955562	4.70162641	5.56266653	1.72E-05	0.00242499	2.75879914
LOC653513	0.71794447	5.69962974	5.55718639	1.74E-05	0.00242499	2.63257932
PDE4DIP	0.71794447	5.69962974	5.55718639	1.74E-05	0.00242499	2.63257932
CSRNP1	1.6325641	3.22689216	5.55246788	1.76E-05	0.00242499	3.03038805
LOC107987457	0.80649586	6.42625014	5.54840354	1.78E-05	0.00242499	2.59631377
PPP1R18	0.80649586	6.42625014	5.54840354	1.78E-05	0.00242499	2.59631377
MPRIP	0.65040425	5.19008429	5.5414227	1.80E-05	0.00243725	2.67676827
GEMIN8	-2.2122342	2.14904894	-5.501202	1.98E-05	0.00264371	2.92236046
OAS3	0.57742636	7.09453849	5.48724096	2.04E-05	0.00270068	2.41805245
IFI6	0.61500995	8.20334104	5.4821668	2.07E-05	0.00270354	2.33844522
SAMHD1	0.84946591	4.29489159	5.46863663	2.13E-05	0.00275976	2.6651199
KANK1	0.56619114	7.49344437	5.46223535	2.16E-05	0.00277176	2.31679379
CENPM	-0.9376662	4.49776469	-5.4345347	2.31E-05	0.00292378	2.58190199
BATF2	3.6843489	-0.5587911	5.38606834	2.58E-05	0.00323578	1.54076198
TPST2	0.85238663	4.51820858	5.37746614	2.63E-05	0.00326756	2.4268935

logFC = log2(fold-change), AveExpr = average expression, P.Value= p-value, adj.P.Val = adjusted p-value

A1.4 Top 100 differentially expressed genes in LEN-treated vs DMSO-treated U266res cells

	logFC	AveExpr	t	P.Value	adj.P.Val	B
RAB8B	-0.8014838	4.3952367	-4.1539311	0.00046504	0.51948448	-2.3366185
BCDIN3D	-1.2687217	3.3777674	-4.0855789	0.00054685	0.51948448	-3.0746292
UROD	0.42534385	6.12339533	4.04959065	0.00059556	0.51948448	-1.7367967
ATL2	-0.7117599	4.56465146	-3.9626815	0.00073175	0.51948448	-2.5923425
PTMA	-0.3329802	11.3173594	-3.8137408	0.00104094	0.51948448	-1.1304689
TUBGCP4	0.60276125	3.64829523	3.78929617	0.00110283	0.51948448	-2.9470445
AAMP	-0.3760451	7.85828053	-3.7740617	0.00114324	0.51948448	-1.7106051
AIP	0.56144511	5.39409713	3.74768528	0.0012167	0.51948448	-2.2420137
SMG9	0.58242305	4.00854042	3.74072376	0.00123685	0.51948448	-2.767962
VPS39	0.69287072	4.51227106	3.71898502	0.00130194	0.51948448	-2.6901629
KLF2	-1.1892657	5.29129847	-3.6940505	0.00138077	0.51948448	-2.3777086
ZNF286B	0.59545777	3.82852918	3.63441107	0.00158898	0.51948448	-2.9634473
RGS1	-0.7069507	4.26210505	-3.5998217	0.00172364	0.51948448	-2.5641159
GRM5	-1.0692587	0.91982154	-3.5545542	0.00191698	0.51948448	-4.0233164
POLR1E	0.8502353	3.77055158	3.55263225	0.00192565	0.51948448	-3.0746417
ENSA	-0.3649072	8.03997161	-3.5384945	0.00199059	0.51948448	-1.9929938
PTCD1	0.96172332	3.26980594	3.53389493	0.00201217	0.51948448	-3.2604084
RILP	2.9526545	-0.4017495	3.52901751	0.00203532	0.51948448	-4.4598485
BSPRY	0.71169482	5.28037096	3.52552573	0.00205205	0.51948448	-2.7245187
PDCD2L	-0.744953	4.81260357	-3.5244828	0.00205707	0.51948448	-2.838006
OTUD1	-0.7824859	4.7460452	-3.5208253	0.00207478	0.51948448	-2.8950816
ZNF286A	0.54564372	3.98355079	3.51831698	0.00208701	0.51948448	-2.9778639
ZNF22	-0.5873834	5.60990375	-3.5046676	0.00215483	0.51948448	-2.5252601
MX1	0.34641688	8.61808042	3.48479388	0.00225747	0.51948448	-1.8952651
TTYH3	-1.4359321	1.62922452	-3.4685953	0.00234466	0.51948448	-4.1687041
FAHD2A	0.51722582	4.92782129	3.45605747	0.00241442	0.51948448	-2.7094717
PABPC4	-1.1714884	9.08103524	-3.4549705	0.00242056	0.51948448	-2.0098202
CDC42SE1	-0.4998925	7.10141003	-3.4530853	0.00243125	0.51948448	-2.2022536
CCDC194	1.49265833	0.30455759	3.44860633	0.00245683	0.51948448	-4.3105256
RBL1	0.57305547	3.64230254	3.4484095	0.00245796	0.51948448	-3.1201298
NDE1	0.59397237	3.84907147	3.43281197	0.00254917	0.51948448	-3.1579713
FAHD2CP	0.54697073	4.87630711	3.42065739	0.00262253	0.51948448	-2.762613
PGAM5	-0.4479792	5.94188891	-3.4059648	0.00271399	0.51948448	-2.4821964
PDIA4	-0.7655881	7.77984296	-3.3912006	0.00280904	0.51948448	-2.1904346
CDKN1A	0.61581646	5.1824711	3.38721284	0.00283526	0.51948448	-2.7171628
C11orf58	-0.7511368	6.81905534	-3.3732706	0.00292885	0.51948448	-2.4277147
FAM241B	-0.8896838	3.00507736	-3.3598714	0.00302164	0.51948448	-3.8138711
TMEM205	0.35953337	7.2407772	3.35523648	0.0030544	0.51948448	-2.2824581

JADE2	0.56393729	4.5260085	3.35506329	0.00305563	0.51948448	-3.1829504
ABCD4	-1.0050697	3.39278508	-3.353015	0.00307023	0.51948448	-3.5783926
RPL32P3	0.60747028	3.31474667	3.34621892	0.00311914	0.51948448	-3.3843991
TRIP4	-0.5818931	4.34801402	-3.3297864	0.00324058	0.51948448	-3.1511803
TNFRSF13B	0.62453493	1.70596554	3.32850027	0.00325028	0.51948448	-3.1858098
TLNRD1	-0.3719541	8.09451067	-3.3127594	0.00337128	0.51948448	-2.2665232
ZCCHC24	0.64926109	3.81460475	3.3123119	0.00337479	0.51948448	-3.3845588
ENTR1	-0.4803575	5.68801487	-3.2996051	0.00347577	0.51948448	-2.6667851
SENP1	-0.4056797	4.98096612	-3.2920859	0.00353691	0.51948448	-2.8354632
TMEM44-AS1	0.74864141	3.10961604	3.28813537	0.00356945	0.51948448	-3.4884752
HNRNPA1P10	1.39764994	1.22022419	3.28162134	0.00362375	0.51948448	-4.1754127
ATXN1	-0.5506569	5.38985744	-3.2811157	0.003628	0.51948448	-2.679418
DGAT1	1.18046719	1.75812341	3.27331836	0.00369412	0.51948448	-4.0281716
PRSS16	0.59289573	3.13564603	3.27177196	0.00370738	0.51948448	-3.4473093
PFN1	-0.4704957	7.6344447	-3.2619771	0.00379241	0.51948448	-2.3860875
SAMD1	-0.9763186	6.50572139	-3.2599658	0.00381011	0.51948448	-2.6326203
RPL34	-0.3053663	10.8780702	-3.2598624	0.00381102	0.51948448	-2.0556571
KRIT1	0.62196004	2.96650009	3.25768755	0.00383025	0.51948448	-3.5481518
METTL7A	-0.3759242	6.07137883	-3.2562054	0.0038434	0.51948448	-2.4319711
MIF	-1.5745746	4.87131174	-3.2434533	0.00395845	0.51948448	-3.2138028
LMO7	0.50018903	3.63022532	3.2415258	0.00397613	0.51948448	-3.3469747
LOC100507377	0.42852513	3.08022279	3.23077181	0.00407618	0.51948448	-3.1236848
PHF10	-0.6093438	5.32129666	-3.2284099	0.00409848	0.51948448	-2.8716135
NANS	0.35404215	5.83982132	3.22730717	0.00410893	0.51948448	-2.6907439
C5orf15	-0.9854126	5.69028363	-3.2265107	0.0041165	0.51948448	-2.8966091
EPB41L2	-0.7945418	6.26150935	-3.2264679	0.0041169	0.51948448	-2.4072744
TCEA1	-0.7564418	6.85329927	-3.2251884	0.00412909	0.51948448	-2.5513687
SUPT16H	-0.2811937	8.74296625	-3.2227189	0.0041527	0.51948448	-2.307955
RUSC1	0.54998106	4.24080478	3.22124075	0.0041669	0.51948448	-3.1408135
ZNF441	-1.4397818	1.30335812	-3.2152835	0.00422459	0.51948448	-4.1940471
PDE6D	-0.5493519	4.36558521	-3.2147695	0.00422961	0.51948448	-3.1644631
VCL	0.77039627	3.16075606	3.21439163	0.0042333	0.51948448	-3.7533957
APLF	1.15691698	1.67147023	3.21412284	0.00423592	0.51948448	-4.0860079
PROKR1	1.15691698	1.67147023	3.21412284	0.00423592	0.51948448	-4.0860079
EAPP	-0.4584759	5.23825985	-3.2127826	0.00424905	0.51948448	-2.8905266
LOC283335	2.19417211	-0.9125465	3.20898235	0.00428647	0.51948448	-4.4884822
H2AFJ	0.49448321	4.86830577	3.20712528	0.00430487	0.51948448	-3.0521304
PLA2G4C	0.94504899	2.07550974	3.20675395	0.00430856	0.51948448	-4.1289209
WDR75	-0.6130007	5.72043938	-3.2015859	0.00436022	0.51948448	-2.7797162
DGKH	0.6503168	3.40954248	3.19801885	0.00439623	0.51948448	-3.3444079
RPL22L1	-0.5376091	6.72919945	-3.1972743	0.00440378	0.51948448	-2.5556078
TM7SF3	-0.6098686	6.1147584	-3.1906681	0.00447135	0.51948448	-2.7152968

ZNFX1	0.52233954	5.7223452	3.18600275	0.00451967	0.51948448	-2.7466221
MILR1	2.42362077	-1.5944687	3.18596213	0.00452009	0.51948448	-4.460274
TMEM198	0.64572368	3.07959496	3.1835722	0.00454504	0.51948448	-3.4102014
CDCA7	-0.5430356	4.36253138	-3.1792163	0.00459086	0.51948448	-3.0402451
IL6R	-0.460219	8.91238932	-3.1639493	0.00475504	0.51948448	-2.3711919
LRP11	-0.7474644	2.20149032	-3.1531499	0.00487459	0.51948448	-3.8885582
LOC105377348	1.03870081	0.82548816	3.15310365	0.00487511	0.51948448	-4.2023645
SRRM1	-0.5789522	6.41936244	-3.1479793	0.00493286	0.51948448	-2.7207416
DNAAF5	-0.692675	5.00142167	-3.14593	0.00495614	0.51948448	-3.087042
STARD5	0.70667784	2.27342126	3.14125338	0.00500967	0.51948448	-3.8933352
TRUB1	-0.6339332	5.65731762	-3.1396316	0.00502836	0.51948448	-2.878451
TMSB4X	-1.0465403	10.1288634	-3.1355081	0.0050762	0.51948448	-2.3655133
VPS51	0.41168956	6.8501992	3.13162616	0.00512163	0.51948448	-2.6156281
EHBP1L1	0.47915856	5.08189581	3.12834237	0.00516037	0.51948448	-2.9526005
CHKA	-0.6638757	6.56807154	-3.1265033	0.0051822	0.51948448	-2.7256598
CLEC18B	0.86195941	1.68190573	3.1210567	0.00524735	0.51948448	-4.0147853
PIPSL	0.56725852	3.91020803	3.12016795	0.00525805	0.51948448	-3.3017649
DPYSL3	0.60887386	5.54144147	3.11812224	0.00528278	0.51948448	-2.9090496
IARS2	-0.9339683	6.09695345	-3.1114913	0.00536369	0.51948448	-2.899253
CD180	-0.4569639	5.81237846	-3.1007026	0.00549791	0.51948448	-2.8433751

logFC = log2(fold-change), AveExpr = average expression, P.Value= p-value, adj.P.Val = adjusted p-value

A1.5 Top 100 differentially expressed genes in LEN-treated vs DMSO-treated U266res cells

	logFC	AveExpr	t	P.Value	adj.P.Val	B
ST7-AS1	3.50434857	1.84949254	6.23689023	3.77E-06	0.04690036	1.14013667
DDX58	1.47127654	3.70083166	5.19926008	3.97E-05	0.08435532	2.12316506
CTDSP2	0.7888653	6.47283681	5.17171886	4.23E-05	0.08435532	2.22243427
IFIT3	0.89910136	7.05385577	5.04089962	5.74E-05	0.08435532	1.91122806
CIITA	1.18099592	3.88654217	5.03591701	5.81E-05	0.08435532	1.90144066
HLA-DQB1	0.79299114	4.35147621	4.99847511	6.34E-05	0.08435532	1.86176997
PARP14	1.19333856	6.06016272	4.98477716	6.55E-05	0.08435532	1.81999624
NOTCH2	0.62368178	6.96893087	4.96117209	6.92E-05	0.08435532	1.73950884
XBP1	0.74275934	11.064009	4.94273265	7.22E-05	0.08435532	1.50868623
APOL6	1.16677336	6.9584622	4.92071142	7.61E-05	0.08435532	1.6415262
PLA2G4C	1.3762656	2.07550974	4.86407114	8.69E-05	0.08435532	0.6562846
CORO1B	2.07870523	2.54500638	4.83918871	9.21E-05	0.08435532	0.78685215
ARF3	0.59790073	8.03755376	4.82932127	9.42E-05	0.08435532	1.4056249
SSBP4	-1.0890742	2.27053435	-4.8256351	9.51E-05	0.08435532	1.33554589
BSPRY	0.94396376	5.28037096	4.76415842	0.00010984	0.09097354	1.35486003
CCND2	0.82704632	8.22015305	4.71419084	0.00012355	0.09558323	1.13307526
DEPP1	2.65316496	2.95446311	4.69001421	0.00013079	0.09558323	-0.1049459
IFI27	0.65811425	6.2368898	4.66388781	0.0001391	0.09600784	1.10136959
ATP10D	1.33411498	2.39064641	4.62370305	0.00015293	0.09905538	0.47971395
PTGES3L	1.84746703	1.92222938	4.6059892	0.00015946	0.09905538	0.24450244
TEX14	1.35283288	2.02814373	4.50971856	0.00020019	0.11196913	0.54981184
DUSP5	0.85241322	7.38236464	4.50600571	0.00020195	0.11196913	0.69801717
USP18	0.59833469	7.46557631	4.49498855	0.00020728	0.11196913	0.66094975
HOMER3	-0.7061858	9.81329105	-4.4593247	0.00022553	0.11675033	0.47053448
S1PR4	-2.6119168	-2.2402432	-4.4051949	0.00025636	0.11704012	-2.1511533
IL4I1	1.11199338	5.44567232	4.40227028	0.00025815	0.11704012	0.56197779
KIAA0040	0.60560554	6.23482028	4.39885183	0.00026024	0.11704012	0.50158608
HLA-DRA	0.48507021	7.90402992	4.38502964	0.0002689	0.11704012	0.36992757
GADD45B	0.80888526	6.59983069	4.36466472	0.00028219	0.11704012	0.38971666
TAGLN2	-0.9061794	4.1192284	-4.3453606	0.0002954	0.11704012	0.4360648
CADPS2	1.16711841	3.42475006	4.34471912	0.00029585	0.11704012	0.44417811
RILPL2	0.63559324	5.12415172	4.3367935	0.00030146	0.11704012	0.40283834
RSPH3	0.92615136	3.96523746	4.27881871	0.00034586	0.13013547	0.27493305
CAV2	1.24356732	2.21253439	4.25006955	0.00037025	0.13013547	-0.225215
EVL	-0.9423506	3.84335165	-4.2306695	0.00038767	0.13013547	0.20331907
RHBDF2	0.58070456	6.49036324	4.22808687	0.00039006	0.13013547	0.10433117
SPR	1.21050716	3.45410771	4.22200222	0.00039572	0.13013547	0.08409946
TMEM173	0.9288534	4.26304786	4.21954937	0.00039803	0.13013547	0.1800613
LOC653513	0.63789126	5.69962974	4.18904887	0.00042788	0.13290052	0.0881349

PDE4DIP	0.63789126	5.69962974	4.18904887	0.00042788	0.13290052	0.0881349
CPNE5	-0.619686	7.33998141	-4.1566225	0.00046208	0.13895153	-0.1267934
RAPGEF4	1.03661448	5.8732647	4.14003377	0.00048062	0.13895153	-0.0029222
VCL	0.96790267	3.16075606	4.1323392	0.00048947	0.13895153	-0.1185983
AGT	0.69527744	7.88722418	4.12515269	0.00049788	0.13895153	-0.1373748
CSRNP1	1.11639699	3.22689216	4.12059705	0.00050329	0.13895153	-0.0762934
SNHG12	0.60299302	5.50287184	4.09538331	0.00053429	0.14430468	-0.1333247
CORO1A	-0.4657135	7.68485914	-4.0489485	0.00059646	0.15766942	-0.3713834
PTP4A3	2.23793335	3.54312369	4.02308602	0.00063417	0.1641442	-0.9504971
C11orf95	-2.1736219	1.07156555	-4.0049888	0.00066196	0.16772853	-0.9498332
TSPAN7	0.55487577	6.45559377	3.99674378	0.00067502	0.16772853	-0.3870259
ASH1L	0.74979839	3.89568962	3.97513333	0.00071048	0.17307831	-0.3383428
RALB	0.93956205	3.55801259	3.95388971	0.00074715	0.17851031	-0.462536
GNAZ	-1.0395448	3.41090835	-3.9362164	0.00077908	0.18193069	-0.4590335
EPB41	-0.3835485	7.13323593	-3.9257003	0.00079872	0.18193069	-0.6136774
DTX3L	0.80338245	6.9811593	3.92218861	0.00080539	0.18193069	-0.6086029
P2RX5	-0.8169306	5.22239118	-3.9142272	0.00082072	0.18208168	-0.5338706
UNC13C	-1.0405511	3.57170558	-3.8409026	0.0009762	0.19920731	-0.6652269
OTUD5	-0.3261207	10.6320856	-3.8325817	0.0009956	0.19920731	-1.0305226
ADAMDEC1	1.05114799	3.64567527	3.82814095	0.0010061	0.19920731	-0.6484867
ARL4C	-0.4653242	7.24763872	-3.8228299	0.00101881	0.19920731	-0.9447215
ID2	0.88269555	4.26313594	3.81655613	0.00103404	0.19920731	-0.6720322
SYT1	0.92067018	4.83246635	3.811251	0.00104708	0.19920731	-0.701212
CCDC167	-0.8198365	4.8278091	-3.809735	0.00105084	0.19920731	-0.7388157
NLGN1	-0.935326	2.76236447	-3.8080262	0.00105509	0.19920731	-0.6884158
TJP2	0.89821897	4.29687135	3.80462486	0.00106361	0.19920731	-0.7007711
EHD1	-0.5887111	6.40431278	-3.8001221	0.00107499	0.19920731	-0.8586069
DNAAF1	-0.9413739	3.31420563	-3.7870099	0.00110881	0.19920731	-0.7342426
CCDC121	2.17602713	-0.5322964	3.78453847	0.0011153	0.19920731	-2.3354926
WASF1	1.18536565	2.72230165	3.7807558	0.00112531	0.19920731	-0.8435994
KCNS3	2.94830411	2.16728979	3.77069243	0.00115237	0.19920731	-2.0985443
CTTNBP2NL	2.05469303	1.34757605	3.7706703	0.00115243	0.19920731	-1.9062093
CDKN1A	0.68118114	5.1824711	3.76992868	0.00115445	0.19920731	-0.8348802
SAMHD1	0.59017378	4.29489159	3.76332411	0.0011726	0.19956646	-0.7959096
LAP3	0.78502977	6.72814382	3.75528877	0.00119505	0.20063983	-0.9588711
UNG	-0.3944345	6.62428395	-3.7255792	0.00128184	0.20931368	-1.0396993
NDST1	-0.8685063	4.28703418	-3.7185088	0.0013034	0.20931368	-0.8964536
IL16	-0.8520418	4.56256421	-3.7169939	0.00130806	0.20931368	-0.9591357
SNORD6	-1.2459903	0.90621864	-3.7150395	0.00131411	0.20931368	-1.3110504
LGALS3BP	1.75485219	1.51742165	3.70957074	0.00133116	0.20934655	-1.5102644
STIP1	-0.4712296	7.6155769	-3.6990762	0.00136451	0.21015484	-1.1404122
SEC24D	0.68109352	3.88194182	3.69733158	0.00137013	0.21015484	-0.9245064

FLNB	-0.7589179	2.7019489	-3.672861	0.00145146	0.21991424	-0.9685905
MRPS12	-0.4471582	6.13905096	-3.6654783	0.00147692	0.22107579	-1.1375005
TAGAP	0.87287449	3.78871378	3.63306978	0.00159401	0.22644937	-1.0492115
DCPS	-0.7413531	4.64486196	-3.6305356	0.00160354	0.22644937	-1.1295866
KLF6	0.69702754	6.48898849	3.63050635	0.00160365	0.22644937	-1.2019689
SEMA4D	-0.4785581	5.81889079	-3.6275236	0.00161494	0.22644937	-1.222162
BATF2	2.17359993	-0.5587911	3.62711976	0.00161648	0.22644937	-2.4804044
TMEM74B	-2.0078272	-0.0958459	-3.6250643	0.00162431	0.22644937	-2.2320659
TET1	-1.8984616	-0.4574689	-3.620872	0.00164041	0.22644937	-1.8008225
ITGB1	0.66443717	5.2040969	3.60659072	0.00169643	0.23160961	-1.1737142
JADE2	0.60171315	4.5260085	3.59976169	0.00172388	0.23279932	-1.1272555
GALNT6	2.56407013	0.77737478	3.58009752	0.0018054	0.24118613	-2.0598354
SCNN1B	-0.6871086	5.51841219	-3.5723874	0.00183839	0.24298045	-1.3103746
BTBD2	-0.7635529	3.70451402	-3.5618704	0.00188435	0.24643301	-1.1973206
HLA-DMB	0.83626431	2.90606902	3.55270987	0.0019253	0.2491657	-1.2247901
STX12	0.587245	4.26152821	3.54409928	0.00196459	0.24977965	-1.2674214
PARP9	1.36300546	5.30975246	3.53986895	0.00198418	0.24977965	-1.3166078
ZC3H12A	0.87288804	3.92715898	3.53854384	0.00199036	0.24977965	-1.2628803
KDM3A	0.88304614	5.49427294	3.52503363	0.00205442	0.25458366	-1.3796283

logFC = log2(fold-change), AveExpr = average expression, P.Value= p-value, adj.P.Val = adjusted p-value

A1.6 Top 100 differentially expressed genes in MM.1Sres vs MM.1S cells

	logFC	AveExpr	t	P.Value	adj.P.Val	B
SPINK2	3.23245459	6.39700508	24.6457404	1.40E-18	1.94E-14	32.2343954
PARP2	-4.2580234	5.47386097	-21.938729	2.05E-17	1.42E-13	29.1017618
ITGA8	-3.3385685	4.86121643	-21.486012	3.31E-17	1.53E-13	28.9473742
LINC01480	2.27199873	8.25240907	20.3605691	1.13E-16	3.92E-13	28.2390772
BHLHE41	-2.4031371	5.10619301	-18.011254	1.81E-15	5.02E-12	25.3138789
CD38	-2.1542862	6.17651265	-16.005743	2.51E-14	5.70E-11	22.8764684
TUBB2B	-4.0930712	3.67528782	-15.90707	2.88E-14	5.70E-11	21.9682456
SEL1L3	-1.5940009	6.30891764	-15.534678	4.85E-14	8.40E-11	22.2244374
SH3TC1	-3.7284757	3.64597601	-14.49258	2.21E-13	3.40E-10	20.0208944
HLA-DRA	1.70080836	9.68313973	14.3238007	2.84E-13	3.94E-10	20.3959915
CKAP4	-1.7093504	6.17276149	-13.427392	1.14E-12	1.40E-09	19.0716658
TRAF3IP3	1.28849161	8.8326511	13.359129	1.27E-12	1.40E-09	18.8915312
DPYSL3	3.67493636	4.10005337	13.3386783	1.31E-12	1.40E-09	18.6753148
ITM2A	1.49771073	6.38375794	12.9634214	2.41E-12	2.38E-09	18.3204101
LILRB4	3.45091141	4.32358193	12.7996874	3.15E-12	2.90E-09	17.965035
NUAK1	-1.9052515	4.68212765	-12.734715	3.50E-12	3.03E-09	17.9805405
TLR7	4.10610472	3.37037449	12.3354058	6.84E-12	5.36E-09	16.5429495
ID2	1.25695125	6.54537579	12.3238495	6.97E-12	5.36E-09	17.2478431
CYBB	-2.6536682	3.67191681	-12.270851	7.63E-12	5.56E-09	17.0304193
CDV3	-1.0233084	10.0293269	-12.226488	8.23E-12	5.69E-09	16.9685556
SYCP3	-1.399154	5.55942662	-12.01076	1.19E-11	7.85E-09	16.7534124
TMSB4X	1.37774903	12.1248654	11.9419344	1.34E-11	8.35E-09	16.4475056
LRMP	1.70177352	7.10801607	11.922675	1.39E-11	8.35E-09	16.5326904
HOMER3	1.57885462	8.65264835	11.5688198	2.58E-11	1.49E-08	15.832988
IER2	2.14251716	4.57249269	11.4531554	3.17E-11	1.76E-08	15.8080532
CSTB	-1.0888162	9.36036058	-11.373498	3.66E-11	1.95E-08	15.4641846
CD52	3.95001586	4.20941127	11.2165308	4.86E-11	2.49E-08	15.2993529
DUSP5	-1.3346017	7.03971775	-11.09558	6.05E-11	2.99E-08	15.031744
GPC4	2.12555915	4.10858056	10.9949845	7.28E-11	3.47E-08	14.9564249
DUSP4	1.389226	6.40303995	10.907486	8.55E-11	3.92E-08	14.7211742
GYPC	1.14178391	7.27722237	10.875116	9.08E-11	3.92E-08	14.604774
MYLK	3.1719102	3.40841322	10.8547892	9.43E-11	3.92E-08	14.5363863
C1orf21	1.24288713	7.53933095	10.8534151	9.45E-11	3.92E-08	14.5747987
TSC22D3	1.62523057	7.51679829	10.8437152	9.63E-11	3.92E-08	14.5422608
ST3GAL6	1.01205733	7.78225354	10.8183695	1.01E-10	3.99E-08	14.486427
TBC1D1	-1.3669239	5.59997839	-10.748371	1.15E-10	4.42E-08	14.4720397
NUCB2	1.34620639	5.80107023	10.6023087	1.51E-10	5.66E-08	14.2088376
MFSD12	-1.3280951	6.00782637	-10.581527	1.57E-10	5.73E-08	14.122971
CHPT1	-1.2244008	5.57872029	-10.545019	1.68E-10	5.98E-08	14.0927

GNG7	-2.3588191	3.86299202	-10.508799	1.80E-10	6.24E-08	14.0975693
CLIC2	-2.5664314	3.40009541	-10.324352	2.56E-10	8.65E-08	13.6302703
FTL	-1.2617499	9.81972078	-10.273652	2.83E-10	9.31E-08	13.3758861
XBP1	-1.1504201	9.87108421	-10.249728	2.96E-10	9.52E-08	13.3246702
HBD	2.00625462	6.90664614	10.2101585	3.19E-10	1.00E-07	13.3794328
H6PD	5.00245121	1.91736206	10.145151	3.62E-10	1.11E-07	11.458491
TCEAL9	-8.0806879	1.72886794	-10.131853	3.72E-10	1.12E-07	9.50609511
TRIB1	-1.3243712	5.94168045	-10.119624	3.81E-10	1.12E-07	13.2361305
FUCA2	-6.2294765	0.40434573	-9.9886323	4.91E-10	1.42E-07	9.3054862
HLA-DMB	2.37290123	4.20999982	9.92874056	5.53E-10	1.56E-07	12.9597751
ARL6IP4	1.04453938	6.4859844	9.81872041	6.86E-10	1.90E-07	12.604081
KCNN3	1.21282144	6.12621619	9.77822643	7.44E-10	2.02E-07	12.5417414
CHD3	2.26224661	2.85859427	9.74628033	7.92E-10	2.08E-07	12.5541247
NEK6	1.71298354	4.00864638	9.7363664	8.08E-10	2.08E-07	12.6303172
SATB1	1.92421088	3.73170271	9.73322094	8.13E-10	2.08E-07	12.6068537
PBXIP1	-0.9509344	8.0450991	-9.707861	8.55E-10	2.15E-07	12.2974039
HDAC9	1.30669077	6.08531502	9.54987933	1.17E-09	2.90E-07	12.1239965
NREP	2.15446196	3.83698167	9.49635537	1.31E-09	3.14E-07	12.1531137
PCGF3	1.93090777	3.8594958	9.49401554	1.31E-09	3.14E-07	12.1512348
SIRPA	-1.704109	3.83278521	-9.482606	1.34E-09	3.15E-07	12.1325027
RAB3D	-3.937337	2.11063831	-9.4162036	1.54E-09	3.55E-07	11.4160975
PA2G4	-0.8841949	8.49219338	-9.3673262	1.70E-09	3.85E-07	11.5741281
TNFRSF1A	-1.64374	5.05184644	-9.3529346	1.75E-09	3.91E-07	11.8002626
CHRM3	0.9205674	6.28818745	9.33011309	1.83E-09	4.03E-07	11.6215031
DDX21	-0.9455045	8.13374884	-9.318908	1.87E-09	4.05E-07	11.4852547
PCDH1	-1.6686738	4.20991933	-9.3095965	1.91E-09	4.05E-07	11.7456884
LILRA2	6.93856327	0.58579084	9.30472928	1.93E-09	4.05E-07	8.53976678
C21orf91	1.22923938	6.72432376	9.24666983	2.17E-09	4.49E-07	11.4296524
TESC	-3.2085404	2.3581648	-9.1262339	2.79E-09	5.67E-07	11.1930897
ABCG2	-5.7482126	0.19089404	-9.1014517	2.93E-09	5.88E-07	8.27898251
IFNAR2	-0.8717136	7.22538836	-9.0685966	3.14E-09	6.21E-07	10.9947795
GNPTAB	-1.098093	5.76337027	-9.0045149	3.59E-09	6.99E-07	10.9881117
SH3KBP1	1.20948739	6.48970423	8.9972205	3.64E-09	7.00E-07	10.8995569
HLA-DPB1	1.86011302	4.32891936	8.97915154	3.78E-09	7.17E-07	11.0998766
SCN3A	1.58495913	4.59543515	8.94011842	4.10E-09	7.67E-07	11.0221327
TBC1D15	-6.3441831	0.81678684	-8.9147318	4.33E-09	7.96E-07	8.06211969
MGMT	2.42842186	2.48165696	8.90976601	4.37E-09	7.96E-07	10.8090105
KRAS	0.86901989	7.48847363	8.87850411	4.67E-09	8.39E-07	10.59132
TNFAIP8	1.07645429	7.44538715	8.86727836	4.78E-09	8.48E-07	10.5749009
PLEKHO1	-1.1127161	6.84373901	-8.8592974	4.86E-09	8.51E-07	10.5945489
IRF2BP2	0.80141224	7.91639023	8.81048345	5.39E-09	9.21E-07	10.4241449
NXPE3	-0.9060758	6.5373874	-8.8101336	5.39E-09	9.21E-07	10.4961422

RNASE6	-2.9656757	2.73225933	-8.7850939	5.68E-09	9.59E-07	10.4706003
DUSP6	1.13662109	5.09594998	8.67219285	7.22E-09	1.20E-06	10.3613349
CCDC66	-1.5904622	3.93818779	-8.6481175	7.60E-09	1.24E-06	10.4371751
ODC1	-0.9553805	8.52319901	-8.6454493	7.64E-09	1.24E-06	10.0501127
PCBP2	-0.7710914	8.38962423	-8.6067822	8.30E-09	1.34E-06	9.96645024
VIM	-0.9004674	7.00540268	-8.5963645	8.48E-09	1.35E-06	9.99496645
HLA-DRB1	2.18134805	3.99054244	8.55480003	9.27E-09	1.45E-06	10.2462561
PLA2G16	-2.7602296	2.30767982	-8.5517807	9.33E-09	1.45E-06	10.0349271
ABHD2	-0.7954777	6.98263804	-8.5477127	9.41E-09	1.45E-06	9.88813344
LMAN1	-0.8726963	7.98813857	-8.5324622	9.73E-09	1.46E-06	9.81798446
DPM3	0.96275138	7.30954457	8.53155788	9.75E-09	1.46E-06	9.85652841
HLA-DPA1	1.64611253	5.75570049	8.52469545	9.89E-09	1.46E-06	9.99337081
SERPINB6	-2.8903469	2.86608261	-8.5222109	9.94E-09	1.46E-06	9.97547905
GMFG	0.85073269	8.92210348	8.43272944	1.21E-08	1.76E-06	9.57395262
CCND2	-0.867817	8.7857972	-8.4257409	1.22E-08	1.76E-06	9.55820544
CDC25A	-0.9333579	5.69487449	-8.4190361	1.24E-08	1.77E-06	9.73232241
PRXL2A	-2.368618	2.82619351	-8.4109897	1.26E-08	1.78E-06	9.86091589
ARPC3	0.77386689	7.80946869	8.35941816	1.41E-08	1.97E-06	9.45090917
RAB3B	-1.2620687	5.16274933	-8.3548934	1.43E-08	1.97E-06	9.67646076

logFC = log2(fold-change), AveExpr = average expression, P.Value= p-value, adj.P.Val = adjusted p-value

A1.7 Top 100 differentially expressed genes in LEN-treated vs DMSO-treated MM.1S cells

	logFC	AveExpr	t	P.Value	adj.P.Val	B
C1orf21	1.02879018	7.53933095	8.97950952	3.86E-09	5.35E-05	11.0440346
IRF4	-0.8724475	7.19880651	-8.5340027	9.90E-09	5.67E-05	10.0868605
KIFC3	1.23054891	4.4872034	8.43281953	1.23E-08	5.67E-05	9.96568231
CYSLTR1	0.9390451	6.97848664	7.82235836	4.70E-08	0.00013634	8.55813941
BMF	1.16986876	5.21018101	7.80113272	4.92E-08	0.00013634	8.61227704
CORO1B	2.61896174	2.31649759	7.44633459	1.10E-07	0.00022912	7.2520277
ATP2B4	1.50666148	4.2871402	7.42313877	1.16E-07	0.00022912	7.78874123
HES1	-1.0659552	4.54421607	-7.0598376	2.68E-07	0.00046435	6.94778925
ST3GAL6	0.64176209	7.78225354	6.83013699	4.60E-07	0.00063817	6.24167305
CALHM5	1.5724245	3.15580556	6.7901164	5.06E-07	0.00063817	6.29692236
PBXIP1	0.6448944	8.04509911	6.78928309	5.07E-07	0.00063817	6.10146807
DTX3L	1.27143044	4.0800523	6.68971158	6.42E-07	0.00074107	6.13544773
METTL7A	0.73033379	9.92343183	6.60494188	7.86E-07	0.00083743	5.63050989
SOX2	0.81984195	5.36815914	6.55404906	8.88E-07	0.00087839	5.74068727
CTHRC1	0.90700376	5.7322455	6.52011542	9.64E-07	0.00088937	5.65592656
ARL6IP5	0.73448963	8.4902156	6.40239951	1.28E-06	0.00110707	5.17777782
EMP2	0.70669985	5.98209049	6.3090399	1.60E-06	0.00119857	5.06734268
MYO5C	0.9791204	3.83119419	6.3018877	1.63E-06	0.00119857	5.23828381
P2RX5	-0.6228125	6.64393946	-6.2986119	1.65E-06	0.00119857	4.98740371
APOL6	0.77817399	6.43368131	6.25657154	1.82E-06	0.00126106	4.93252561
ITGA8	-0.7108585	4.86121643	-6.2236596	1.97E-06	0.00130115	4.86723815
GRN	1.02708593	5.09843754	6.16591612	2.27E-06	0.00140494	4.82546057
PLOD2	0.75184475	5.62389237	6.15488618	2.33E-06	0.00140494	4.78774706
HLA-DMB	1.48476328	4.20999982	6.06555484	2.90E-06	0.00167538	4.69178793
PARP14	0.88005461	4.49090708	5.96814877	3.69E-06	0.0020432	4.40749496
USP53	0.66942817	6.4371467	5.86668373	4.74E-06	0.00252332	3.96581936
CCDC167	-0.7812341	5.5552925	-5.8454146	5.00E-06	0.00256107	4.02379559
HLA-DRA	0.69299685	9.68313973	5.78699665	5.77E-06	0.002854	3.65364633
TIGIT	-1.1349241	3.63487193	-5.7454389	6.40E-06	0.00302251	3.95800167
LHFPL2	1.02076243	3.667565	5.73607258	6.55E-06	0.00302251	3.91787776
TPBG	1.65114749	3.04396131	5.68152479	7.50E-06	0.00334982	3.74544943
MGLL	0.86498021	4.18610904	5.63470619	8.43E-06	0.00364647	3.63336292
MME	4.08091304	1.7295839	5.6092469	8.98E-06	0.00376772	2.16869513
DOCK4	0.82247875	5.0616818	5.59077009	9.41E-06	0.00382946	3.42885071
SHROOM3	0.54748321	6.17345019	5.55679072	1.02E-05	0.00404953	3.22876677
ITGB5	0.66070849	6.92134994	5.50843362	1.16E-05	0.00420481	3.05063578
P2RY6	1.60872276	2.4614266	5.50758217	1.16E-05	0.00420481	3.32450014
BLNK	1.01145027	4.16267346	5.5014286	1.18E-05	0.00420481	3.2429626
GATA3	4.1648552	0.11673252	5.49005242	1.21E-05	0.00420481	1.22119804

WLS	0.91880231	4.71444896	5.48836918	1.22E-05	0.00420481	3.27642384
TMEM144	1.22837906	3.4573032	5.46588006	1.29E-05	0.00434	3.29657633
RAI14	0.75815392	5.21569591	5.41309535	1.47E-05	0.00483633	2.98189681
ARHGEF3	0.64839187	5.86620736	5.29469269	1.98E-05	0.0063616	2.59646676
PPP1R9A	2.10270493	2.9002908	5.27954747	2.05E-05	0.00645873	2.58752133
VPS37A	0.67892771	4.78967397	5.25612663	2.18E-05	0.00669908	2.65413321
GPC4	1.0698488	4.10858056	5.24312728	2.25E-05	0.00677174	2.76782814
DKK1	2.1263946	2.53605826	5.22812938	2.34E-05	0.00686929	2.46001697
MTMR10	0.55212481	6.0633922	5.21204979	2.43E-05	0.00686929	2.39356352
RSPH4A	1.36399081	3.15242865	5.21136027	2.44E-05	0.00686929	2.7035679
SLFN5	1.24927738	4.2064138	5.20439862	2.48E-05	0.00686929	2.66864338
SIPA1L2	1.77421234	2.17053295	5.19596563	2.53E-05	0.00687946	2.4424049
ERBIN	0.64101642	5.7939568	5.17543185	2.67E-05	0.00710615	2.32806946
IL4I1	2.25105268	3.09055271	5.14850637	2.86E-05	0.00724874	2.26387888
SH3BP5	0.83044298	3.82313661	5.1462337	2.87E-05	0.00724874	2.4562246
YPEL2	1.10974049	3.34309971	5.14536072	2.88E-05	0.00724874	2.54321004
CCDC88A	1.53596938	2.02483489	5.10898382	3.16E-05	0.00780495	2.43838361
CXCR3	0.92877567	3.95118526	5.10018245	3.23E-05	0.00784061	2.37702751
AIF1	3.52080816	-0.639876	5.0872299	3.34E-05	0.00796205	1.03465459
MAP4K4	0.58626081	5.4834685	5.05644563	3.61E-05	0.0084612	2.03957982
TGFA	0.94209229	4.1488128	5.00923835	4.06E-05	0.0093767	2.12967827
PLA2G4C	1.29477827	2.64085074	4.99301069	4.24E-05	0.0096101	2.18238161
BLVRA	0.56464457	6.20316557	4.94197696	4.82E-05	0.01076101	1.67175121
PON2	0.6524515	6.37915844	4.90356591	5.31E-05	0.01167407	1.61019817
LOC730101	0.62329634	6.70357476	4.89231033	5.47E-05	0.01182464	1.53706015
CXCL13	3.09033891	1.70950182	4.86610677	5.84E-05	0.01244344	1.15010428
ARF3	0.53025315	6.0654239	4.85352811	6.03E-05	0.0126526	1.46576692
ARL4C	-0.7445946	6.33290213	-4.8405909	6.23E-05	0.01279319	1.40431791
CTDSP2	0.54626601	7.18617438	4.83742032	6.28E-05	0.01279319	1.34508734
UBE2L6	0.77909025	4.50034934	4.75184669	7.81E-05	0.01566975	1.42687153
CXCL10	0.86854675	4.30534524	4.66864915	9.65E-05	0.01908442	1.26202399
ITGB1	0.47203617	6.35427953	4.65183576	0.00010073	0.01962177	0.9548972
ITGB7	0.50155145	12.2166908	4.64665462	0.00010206	0.01962177	0.71985772
SH3BP5-AS1	0.69511641	4.17606954	4.63341899	0.00010556	0.02001557	1.15467464
BTG1	0.44231363	9.06774822	4.61404568	0.00011089	0.02051419	0.70623817
IL23A	0.54072851	6.02884271	4.61128772	0.00011167	0.02051419	0.86785136
EPHX2	0.53231065	5.86162364	4.60791219	0.00011263	0.02051419	0.92743122
TRAPPC3L	1.27341805	3.06863232	4.57865568	0.00012134	0.02181217	1.22011419
BSPRY	0.5721185	5.64841844	4.5667826	0.00012506	0.02202782	0.77941355
SH3BGRL2	1.20131617	3.16701673	4.56470853	0.00012572	0.02202782	1.17673708
UGT2B17	0.48885879	6.2206437	4.55433662	0.00012908	0.02233406	0.72753186
BTC	2.73639492	1.43121728	4.48192275	0.00015519	0.02652012	0.5535325

ANXA4	0.94574916	3.36530433	4.44572876	0.00017015	0.02858227	0.8678654
HBEGF	1.30584872	3.15429716	4.44289358	0.00017139	0.02858227	0.90183501
DEPP1	0.95715532	3.59167306	4.42613237	0.00017885	0.02946036	0.74424202
CITED2	0.62299401	4.86806057	4.4216338	0.00018091	0.02946036	0.56133798
CAV2	0.54565396	5.70530125	4.41697821	0.00018306	0.02946459	0.43232385
CST3	0.71508281	5.48890205	4.39587777	0.00019315	0.03073141	0.43776689
AASS	1.48715324	2.51167765	4.37802667	0.00020212	0.03179296	0.75438846
UNC13C	-0.705704	4.85931265	-4.3684399	0.00020711	0.03194551	0.48523324
PDLIM3	-0.5785769	4.62872992	-4.3649228	0.00020897	0.03194551	0.46219681
PARP9	1.65499335	1.30670529	4.36295787	0.00021002	0.03194551	0.6588851
GAS6	0.75048666	8.88081854	4.33139487	0.00022756	0.03423779	0.00360576
ELAC2	-0.6440532	5.36707113	-4.3247035	0.00023146	0.03445053	0.2212148
STAP2	1.17327994	1.97550057	4.30827649	0.00024133	0.03534944	0.58736736
SHTN1	0.7609788	3.87438374	4.30619319	0.00024261	0.03534944	0.44731094
SLC30A1	0.3667717	7.2371746	4.25160741	0.00027869	0.04018362	-0.1347756
LAMC1	-0.9926316	3.23692466	-4.2404876	0.00028667	0.04090816	0.38922596
TMEM255B	0.85663151	3.57833039	4.22686179	0.00029676	0.04149933	0.29452182
PPFIBP1	1.06837391	3.01073756	4.22569028	0.00029764	0.04149933	0.38247486
CGN	1.01123996	2.66099002	4.22283624	0.00029981	0.04149933	0.33813169

logFC = log2(fold-change), AveExpr = average expression, P.Value= p-value, adj.P.Val = adjusted p-value

A1.8 Top 100 differentially expressed genes in POM-treated vs DMSO-treated MM.1S cells

	logFC	AveExpr	t	P.Value	adj.P.Val	B
CYSLTR1	1.46624018	6.97848664	12.3317469	7.13E-12	6.02E-08	17.2822424
IRF4	-1.2714224	7.19880651	-12.21444	8.70E-12	6.02E-08	17.078741
C1orf21	1.35549016	7.53933095	11.8956442	1.50E-11	6.94E-08	16.5351325
BMF	1.685052	5.21018101	11.4433123	3.33E-11	1.15E-07	15.7552871
ITGA8	-1.2171623	4.86121643	-10.360813	2.46E-10	6.17E-07	13.7803018
CORO1B	3.55928851	2.31649759	10.3167919	2.67E-10	6.17E-07	12.6469919
KIFC3	1.47576604	4.4872034	10.1993389	3.35E-10	6.63E-07	13.4810074
ARF3	1.04829816	6.0654239	9.7322997	8.36E-10	1.45E-06	12.5417478
ATP2B4	1.9134006	4.2871402	9.56449714	1.17E-09	1.80E-06	12.2343885
CTHRC1	1.26086622	5.7322455	9.17757379	2.56E-09	3.55E-06	11.474086
EMP2	1.00641094	5.98209049	9.04840742	3.35E-09	4.21E-06	11.1547165
HLA-DRA	1.06121002	9.68313973	8.89105298	4.65E-09	5.36E-06	10.7224793
P2RX5	-0.8854682	6.64393946	-8.8262007	5.32E-09	5.67E-06	10.6583039
MYO5C	1.34054865	3.83119419	8.75411897	6.20E-09	6.13E-06	10.6397811
OAF	-1.3034354	4.57247647	-8.7202642	6.66E-09	6.14E-06	10.5702643
METTL7A	0.94523909	9.92343183	8.56211269	9.32E-09	8.06E-06	10.0003318
TPBG	2.30912349	3.04396131	8.12607583	2.40E-08	1.95E-05	9.08107695
HES1	-1.2269999	4.54421607	-7.94458	3.58E-08	2.75E-05	8.89466232
P2RY6	2.25406801	2.4614266	7.91795594	3.80E-08	2.76E-05	8.60455972
CTDSP2	0.88597274	7.18617438	7.89017974	4.04E-08	2.79E-05	8.59488685
CCDC167	-1.0824554	5.5552925	-7.8649176	4.27E-08	2.82E-05	8.68937215
GRN	1.2900148	5.09843754	7.79448881	5.00E-08	3.06E-05	8.53542034
CGN	1.79690987	2.66099002	7.78699328	5.08E-08	3.06E-05	8.56627216
ITGB1	0.77921927	6.35427953	7.74868361	5.54E-08	3.18E-05	8.3341122
DTX3L	1.45901087	4.0800523	7.71606101	5.96E-08	3.18E-05	8.42583728
ST3GAL6	0.7240955	7.78225354	7.71549889	5.97E-08	3.18E-05	8.19608001
PVRIG	-2.6032413	1.32814953	-7.6241848	7.33E-08	3.52E-05	7.77238807
PLOD2	0.92475364	5.62389237	7.62228956	7.37E-08	3.52E-05	8.13968433
PBXIP1	0.72396024	8.04509911	7.62124757	7.38E-08	3.52E-05	7.93808706
ITGB5	0.90125479	6.92134994	7.54434324	8.79E-08	4.06E-05	7.83183177
SH3BP5	1.19121747	3.82313661	7.5136215	9.42E-08	4.21E-05	7.98156941
ARL6IP5	0.85626143	8.4902156	7.47008181	1.04E-07	4.50E-05	7.59569739
HLA-DMB	1.77559379	4.20999982	7.36867984	1.31E-07	5.51E-05	7.64781489
C12orf57	0.90075732	7.74183156	7.22394135	1.83E-07	7.46E-05	7.04957278
USP53	0.81485983	6.4371467	7.16339736	2.11E-07	8.34E-05	6.97760466
SHTN1	1.23058275	3.87438374	7.14527644	2.20E-07	8.46E-05	7.16953198
SH3BP5-AS1	1.0458834	4.17606954	7.08911147	2.51E-07	9.38E-05	6.99859368
WLS	1.16450929	4.71444896	7.04731383	2.76E-07	0.00010066	6.91715682
CITED2	0.97276986	4.86806057	7.02080954	2.94E-07	0.00010351	6.79463017

RAI14	0.97515184	5.21569591	7.01342922	2.99E-07	0.00010351	6.75022852
C11orf95	-2.9505048	2.38265657	-6.9772298	3.26E-07	0.00010993	6.08815323
CNTRL	-1.0353105	4.83337729	-6.9583067	3.40E-07	0.00011219	6.67495641
SPRR2A	2.41826299	1.48898598	6.86471801	4.24E-07	0.00013599	6.20577565
SERPINH1	2.60961768	1.95194595	6.85330939	4.36E-07	0.00013599	6.02019634
UNC13C	-1.1739677	4.85931265	-6.8473121	4.42E-07	0.00013599	6.45934511
RTP4	1.5444843	4.02149532	6.80590147	4.88E-07	0.00014623	6.40723797
LHFPL2	1.19941582	3.667565	6.79822513	4.97E-07	0.00014623	6.37987394
MME	4.9200108	1.7295839	6.78904038	5.07E-07	0.00014633	4.6003717
STAG3	-1.8658235	2.30488218	-6.7318201	5.81E-07	0.00016419	6.17506874
TGFA	1.24679837	4.1488128	6.71038329	6.12E-07	0.00016932	6.15518738
ZFP36L2	0.67474346	7.2072334	6.66135896	6.87E-07	0.00018656	5.73331819
DKK1	2.65120646	2.53605826	6.63484092	7.32E-07	0.00019492	5.59843073
CALHM5	1.52153411	3.15580556	6.53494344	9.30E-07	0.00024291	5.7853655
PON2	0.85836908	6.37915844	6.49006206	1.04E-06	0.00026555	5.41804273
INAFM2	0.95649947	4.88397204	6.44404773	1.16E-06	0.00029127	5.45218898
PLA2G4C	1.62449053	2.64085074	6.36054134	1.42E-06	0.00034999	5.35951948
STAT2	0.7132623	5.3460277	6.34054743	1.49E-06	0.0003609	5.11286072
DCPS	-0.6690473	6.29082766	-6.2764983	1.74E-06	0.00041429	4.87905415
TRAF3IP3	0.60545863	8.8326511	6.23695576	1.91E-06	0.00044461	4.66336359
AIF1	4.26999323	-0.639876	6.23351298	1.93E-06	0.00044461	3.37916776
ARL4C	-0.969304	6.33290213	-6.2047663	2.07E-06	0.00046903	4.6971161
GATA3	4.65108152	0.11673252	6.18070945	2.19E-06	0.00048935	2.82302812
MYB	-1.0324007	5.08220885	-6.1661672	2.27E-06	0.00049898	4.78198686
ARHGEF3	0.74750728	5.86620736	6.11583153	2.57E-06	0.00055548	4.5199996
BLVRA	0.69486	6.20316557	6.09652551	2.69E-06	0.00056213	4.43094322
PPFIBP1	1.50473978	3.01073756	6.09347212	2.71E-06	0.00056213	4.77145017
TGFBR3	1.58561713	3.03920133	6.089874	2.74E-06	0.00056213	4.75773016
VPS37A	0.78361137	4.78967397	6.08620685	2.76E-06	0.00056213	4.60093712
RNF183	1.1089617	3.26643997	6.07047171	2.87E-06	0.00057576	4.69613234
PARP14	0.89082163	4.49090708	6.02641689	3.20E-06	0.00063232	4.4764312
SOX2	0.75679969	5.36815914	6.01455153	3.29E-06	0.00064185	4.35942529
HBEGF	1.71787841	3.15429716	6.00698383	3.35E-06	0.00064481	4.5303138
TMEM255B	1.19357219	3.57833039	5.98749488	3.52E-06	0.0006672	4.4935815
GNG7	-1.0761421	3.86299202	-5.9113983	4.24E-06	0.00079389	4.19072514
AASS	1.96701498	2.51167765	5.9027557	4.34E-06	0.00080019	4.31575788
SLFN5	1.40091367	4.2064138	5.88261547	4.56E-06	0.00082515	4.25504867
TIGIT	-1.1701313	3.63487193	-5.8796586	4.59E-06	0.00082515	4.25305187
TMEM219	0.82940708	5.06658231	5.85790546	4.84E-06	0.00085956	4.00302821
CXCL13	3.67609838	1.70950182	5.84715393	4.97E-06	0.00087155	3.31305694
LOC730101	0.74202332	6.70357476	5.83714836	5.10E-06	0.00087305	3.78195341
LAMB3	2.08219538	2.094383	5.83220621	5.16E-06	0.00087305	3.98522464

DNAJC10	-0.5814163	6.80450092	-5.8313926	5.17E-06	0.00087305	3.75220161
IL27RA	-1.5633531	2.90802321	-5.8123834	5.42E-06	0.00090141	4.06743704
CCDC88A	1.73426702	2.02483489	5.80874816	5.47E-06	0.00090141	4.08916097
MGLL	0.88681674	4.18610904	5.77140058	6.00E-06	0.00097138	3.89636338
ERGIC1	-0.5978741	8.14951781	-5.7690989	6.04E-06	0.00097138	3.503297
LIG3	0.75556887	5.26239418	5.76332164	6.12E-06	0.00097408	3.7550542
TAX1BP3	1.42201771	3.21319963	5.75258723	6.29E-06	0.000989	3.94067475
RSPH4A	1.48925955	3.15242865	5.69414059	7.27E-06	0.00113074	3.83509958
IFIT3	1.95498276	1.97972842	5.6864722	7.41E-06	0.00113971	3.73203338
ST7-AS1	3.18566134	0.07419414	5.67112153	7.70E-06	0.00117047	2.69388776
FCMR	-0.7203695	5.52146758	-5.6669427	7.78E-06	0.00117047	3.48045317
IFNAR2	-0.5364424	7.22538836	-5.6541608	8.03E-06	0.00119533	3.25267298
SIDT2	-0.8793691	4.40173384	-5.6393451	8.33E-06	0.00122708	3.56840533
ATP2A3	-0.7083016	5.00263468	-5.6212254	8.72E-06	0.00126947	3.42013283
RCN1	0.70375866	5.2469342	5.61727628	8.80E-06	0.00126947	3.38005161
TK2	-1.005169	4.16546471	-5.5916396	9.39E-06	0.00133937	3.50607661
EPHX2	0.64283023	5.86162364	5.58416643	9.56E-06	0.00135067	3.25413425
TRAPPC3L	1.52487651	3.06863232	5.5611261	1.01E-05	0.00141623	3.5242419
LAP3	0.81059769	5.2713175	5.55082315	1.04E-05	0.00143863	3.19552135

logFC = log2(fold-change), AveExpr = average expression, P.Value= p-value, adj.P.Val = adjusted p-value

A1.9 Top 100 differentially expressed genes in LEN-treated vs DMSO-treated MM.1Sres cells

	logFC	AveExpr	t	P.Value	adj.P.Val	B
TGFA	1.29001303	4.1488128	5.58001044	9.58E-06	0.13257297	2.38102003
IRF4	-0.5136348	7.19880651	-5.0496127	3.64E-05	0.21050363	2.3233925
INAFM2	0.74110037	4.88397204	4.96100968	4.56E-05	0.21050363	1.91659749
MGLL	0.9023891	4.18610904	4.77768002	7.27E-05	0.251588	1.06475359
METTL7A	0.50955072	9.92343183	4.58242407	0.00011952	0.33087983	1.2227098
USP53	0.55011411	6.4371467	4.49554101	0.00014912	0.34402614	1.01975951
IL4I1	0.8058483	3.09055271	4.32019203	0.00023303	0.42492986	0.40912693
CCDC28B	0.94495442	2.29917307	4.23092058	0.00029241	0.42492986	-0.233195
PLOD2	0.49245259	5.62389237	4.22459656	0.00029714	0.42492986	0.39391215
MAP2	0.77831109	4.12915184	4.13988144	0.00036846	0.42492986	0.10543578
PARP14	0.72229048	4.49090708	4.12491666	0.00038271	0.42492986	-0.0332036
KIFC3	0.62160927	4.4872034	4.092601	0.00041539	0.42492986	-0.0171675
ST7-AS1	2.94137722	0.07419414	4.07529064	0.00043402	0.42492986	-3.3795947
CITED2	0.62980717	4.86806057	4.05428646	0.00045774	0.42492986	-0.063288
EPHX2	0.44072762	5.86162364	4.04640656	0.00046697	0.42492986	0.00082915
C1orf21	0.43938306	7.53933095	4.02643862	0.00049118	0.42492986	-0.0666999
PBXIP1	0.39293901	8.0450991	3.95333559	0.00059089	0.48112486	-0.2358587
KLF6	0.41809048	6.71854397	3.90756831	0.00066325	0.49656683	-0.3208743
GAS2L1	1.14805352	3.33920524	3.89674049	0.0006816	0.49656683	-0.9456934
JUP	0.53195839	6.0116972	3.83138112	0.00080356	0.5561417	-0.483833
PIGU	1.24530733	3.80734342	3.80033717	0.00086878	0.57265035	-0.6918566
PKIG	0.83835478	3.23061163	3.7460124	0.00099568	0.61785701	-0.947512
GRN	0.61792969	5.09843754	3.72541326	0.00104842	0.61785701	-0.7166291
P2RY6	1.0566099	2.4614266	3.71680372	0.00107127	0.61785701	-1.4245484
NR2F2	1.41437416	1.89738781	3.68930936	0.00114756	0.63538339	-1.9612289
ARL2-SNX15	0.49851667	5.8187694	3.61266484	0.00138949	0.64582615	-0.9620364
DHRS3	1.9135117	-0.5714688	3.61114618	0.00139476	0.64582615	-2.8089083
SNX15	0.49699595	5.81974854	3.60828692	0.00140473	0.64582615	-0.9716013
CXCL10	0.74245159	4.30534524	3.59882099	0.00143823	0.64582615	-1.077932
APOL6	0.43883846	6.43368131	3.58702213	0.00148108	0.64582615	-1.0440518
RTN4RL2	1.1491236	3.13370342	3.58196542	0.00149983	0.64582615	-1.3691951
DOHH	0.90230591	4.3135381	3.57432794	0.00152859	0.64582615	-1.0779009
CIB1	0.54373559	5.40960959	3.56501868	0.00156437	0.64582615	-1.0627315
ZNF219	0.95663856	2.71395424	3.55350004	0.00160977	0.64582615	-1.6511586
GGTLC2	0.57723849	4.5624323	3.54773119	0.00163299	0.64582615	-1.1033692
DUSP5	0.43505873	7.03971775	3.50398503	0.00182007	0.66768006	-1.2322391
ZC3H12A	0.46773937	5.78173172	3.49452071	0.00186321	0.66768006	-1.2283217
ZC3H14	-0.6250721	3.72673069	-3.4909048	0.00187995	0.66768006	-1.3445553
CORO1B	1.4887415	2.31649759	3.48428159	0.00191101	0.66768006	-2.3236865

SOX2	0.45063373	5.36815914	3.48040139	0.00192943	0.66768006	-1.2435851
SERF1A	-0.6899613	3.48728529	-3.4463389	0.00209878	0.6698054	-1.4743291
HES1	-0.5677307	4.54421607	-3.4424973	0.00211876	0.6698054	-1.3312898
CCNO	-2.2182659	0.41795251	-3.4376425	0.00214429	0.6698054	-3.3687222
ITGB3BP	-0.4715873	6.15608724	-3.424504	0.00221486	0.6698054	-1.3794143
RSPH3	1.10628567	2.15330508	3.38795301	0.0024233	0.6698054	-2.1609477
RMI1	-0.431399	5.39487258	-3.3787012	0.00247902	0.6698054	-1.4600082
SGK494	-1.8293337	2.31688771	-3.3752431	0.00250016	0.6698054	-2.0011375
ICK	0.73143695	3.26626676	3.37357087	0.00251045	0.6698054	-1.6555813
GLIPR2	0.50739291	5.33253795	3.37264885	0.00251613	0.6698054	-1.4754571
TRIM2	1.57902234	0.643473	3.3725757	0.00251659	0.6698054	-2.9946715
CEMIP2	0.95061821	3.8703964	3.37198853	0.00252022	0.6698054	-1.6229136
ZMYM5	-1.5969141	1.75936159	-3.3710421	0.00252608	0.6698054	-2.72232
DPH3	-0.6063751	4.47148583	-3.3648699	0.00256464	0.6698054	-1.550826
ARHGEF40	0.7888552	3.14057223	3.32845445	0.00280402	0.70686867	-1.8387388
SCMH1	0.41950086	5.308778	3.32777509	0.00280868	0.70686867	-1.5757541
TRIM59-IFT80	-0.6404235	3.75618921	-3.2960959	0.00303481	0.74405449	-1.7046352
RASA4	-0.4609789	5.1737792	-3.2921813	0.00306394	0.74405449	-1.6428947
DTX3L	0.82373067	4.0800523	3.27734663	0.00317684	0.74687084	-1.800895
CBFA2T3	0.63747151	3.60992105	3.25107859	0.00338671	0.74687084	-1.7952809
RASA3	0.33490679	7.01932235	3.23718565	0.00350306	0.74687084	-1.8433928
UBE2QL1	0.34604581	5.80738922	3.22998054	0.00356491	0.74687084	-1.8084493
PCMTD1	-0.5409237	4.58380391	-3.2236559	0.00362008	0.74687084	-1.7802813
APC	-0.5785412	4.27259568	-3.2194219	0.00365747	0.74687084	-1.807639
PPP6R2	0.34850755	5.40930111	3.21385793	0.00370717	0.74687084	-1.8192799
SLA	-1.1014494	1.45074204	-3.2094562	0.00374695	0.74687084	-2.5785507
MPP2	1.53386591	0.92017907	3.20942782	0.00374721	0.74687084	-3.0325632
RUBCN	0.41712592	6.17337044	3.20888215	0.00375217	0.74687084	-1.8511824
SERF1B	-0.6631846	3.43479964	-3.2011404	0.00382323	0.74687084	-1.9311076
ARF4-AS1	-1.377485	1.1753247	-3.1948452	0.00388197	0.74687084	-2.9930045
NUP210L	-2.6089701	-1.9241505	-3.1934216	0.00389538	0.74687084	-3.9186264
RAD51AP1	-0.4112107	5.46067415	-3.1927922	0.00390132	0.74687084	-1.8436002
TMEM173	1.49558407	0.86218874	3.18458571	0.00397958	0.74687084	-2.9202869
TNFSF13	0.50907878	4.88779077	3.17629662	0.00406016	0.74687084	-1.8768615
CHST14	-0.5313018	4.44518095	-3.1725091	0.0040975	0.74687084	-1.882937
CHST15	0.42008648	6.56944478	3.16854849	0.00413691	0.74687084	-1.9630988
SPR	0.81040159	3.42830664	3.16780735	0.00414432	0.74687084	-2.0320626
TNFSF12	0.49605102	4.90640739	3.1449206	0.00437967	0.74687084	-1.9420627
TNFSF12-TNFSF13	0.50426163	4.88547692	3.14422815	0.00438698	0.74687084	-1.9424594
R3HDM4	-0.6992829	4.20923525	-3.1415051	0.00441587	0.74687084	-1.9673602
GGT1	0.39024718	5.42582048	3.14002427	0.00443166	0.74687084	-1.9881956
FEZ2	-0.3999938	4.61983417	-3.1272654	0.00456996	0.74687084	-1.9719506

DKK1	0.89762627	2.53605826	3.12454657	0.00459996	0.74687084	-2.2754297
NAA60	-0.591279	3.57559202	-3.123618	0.00461025	0.74687084	-2.0336253
NRAV	1.64821393	0.91805346	3.12309564	0.00461605	0.74687084	-3.1464983
PLK2	0.54811486	4.02608245	3.1226305	0.00462122	0.74687084	-1.9856641
LAMTOR5-AS1	-2.4211802	-0.8263976	-3.1209184	0.00464029	0.74687084	-3.7960266
COL22A1	-2.1945299	-1.5507456	-3.1132544	0.00472661	0.74957519	-3.8096226
OR7G2	-2.2391424	-0.6954698	-3.1098539	0.0047654	0.74957519	-3.8339653
CEP19	-1.0464136	2.43812554	-3.1021784	0.00485408	0.75486425	-2.3967602
MME	1.5597529	1.7295839	3.09756976	0.00490809	0.75486425	-2.8797822
APMAP	0.46392724	6.15135593	3.08000316	0.0051193	0.7710032	-2.1308209
YPEL2	0.70794651	3.34309971	3.07691779	0.00515728	0.7710032	-2.2165342
ADCY1	-0.6002101	3.69819656	-3.071612	0.00522324	0.7710032	-2.1159344
SNORA33	-1.0555211	2.5182604	-3.0706069	0.00523583	0.7710032	-2.5078747
NGLY1	-0.3381157	6.0585849	-3.0471768	0.00553759	0.80685536	-2.1843576
GSTO2	2.41928967	0.13460618	3.04099737	0.00561991	0.81032059	-3.5570776
DEPP1	0.86445597	3.59167306	3.02996478	0.00576981	0.82150093	-2.3151783
ID1	-1.0444827	2.12292723	-3.0266101	0.00581615	0.82150093	-2.5073768
C12orf57	0.38194807	7.74183156	3.01393887	0.0059944	0.82762305	-2.3403436
DYNC1I1	-0.9253192	2.50733736	-3.0041157	0.00613617	0.82762305	-2.6351613

logFC = log2(fold-change), AveExpr = average expression, P.Value= p-value, adj.P.Val = adjusted p-value

A1.10 Top 100 differentially expressed genes in POM-treated vs DMSO-treated MM.1Sres cells

	logFC	AveExpr	t	P.Value	adj.P.Val	B
IRF4	-0.9264964	7.19880651	-8.9991025	3.63E-09	5.02E-05	11.148577
METTL7A	0.92296099	9.92343183	8.33453304	1.49E-08	0.00010321	9.70938797
PARP14	1.27875339	4.49090708	7.61227382	7.41E-08	0.00034186	8.16596716
IL4I1	1.33269392	3.09055271	7.35994233	1.32E-07	0.00045626	7.64132503
TGFA	1.63885701	4.1488128	7.25466486	1.68E-07	0.00046537	7.2823543
MAP2	1.2277751	4.12915184	6.69503636	6.26E-07	0.00117576	6.1717617
MGLL	1.22762581	4.18610904	6.68622827	6.39E-07	0.00117576	6.09520498
SH3BP5	1.46256249	3.82313661	6.66075231	6.80E-07	0.00117576	5.91897715
SNX15	0.87500978	5.81974854	6.50534067	9.86E-07	0.00145646	5.68126789
ARL2-SNX15	0.87315247	5.8187694	6.4785299	1.05E-06	0.00145646	5.61791624
HES1	-1.1357597	4.54421607	-6.3918484	1.30E-06	0.0016324	5.4746566
EPHX2	0.67545973	5.86162364	6.27539838	1.72E-06	0.00198501	5.10897878
PLOD2	0.7145243	5.62389237	6.20654156	2.04E-06	0.00216708	4.97557989
ZFYVE28	0.80224722	4.70192734	6.1492423	2.34E-06	0.00231474	4.8820935
INAFM2	0.87858404	4.88397204	5.94039389	3.91E-06	0.00343643	4.39323633
APOL6	0.7163505	6.43368131	5.92421309	4.07E-06	0.00343643	4.22184818
SOX2	0.74983557	5.36815914	5.90961098	4.22E-06	0.00343643	4.2906708
UNC13C	-0.8594322	4.85931265	-5.8255429	5.20E-06	0.00381852	4.10958511
DTX3L	1.39041637	4.0800523	5.81186299	5.38E-06	0.00381852	4.10501369
MME	2.76403087	1.7295839	5.80140593	5.52E-06	0.00381852	3.24380344
SH3BP5-AS1	1.08205854	4.17606954	5.78099	5.80E-06	0.00382574	4.0442621
CEMIP2	1.53812694	3.8703964	5.70707876	6.98E-06	0.00438863	3.86534433
P2RY6	1.52993789	2.4614266	5.67940772	7.47E-06	0.00449739	3.639078
MIR503HG	2.23167327	2.13042141	5.60558017	8.98E-06	0.00518187	2.91936406
USP53	0.66380235	6.4371467	5.46713556	1.27E-05	0.00702667	3.14160905
KLF6	0.57868154	6.71854397	5.45202791	1.32E-05	0.00702667	3.05760066
RHBDF2	0.64592524	5.51506506	5.42067417	1.43E-05	0.00721245	3.06432063
YPEL2	1.19317075	3.34309971	5.41213704	1.46E-05	0.00721245	3.15643801
OAF	-0.7583553	4.57247647	-5.3168205	1.85E-05	0.00861205	2.90809943
DUSP5	0.65272826	7.03971775	5.31425556	1.87E-05	0.00861205	2.71204778
PON2	0.64965053	6.37915844	5.14516662	2.86E-05	0.01235564	2.30613157
DHRS3	2.64478137	-0.5714688	5.13707311	2.92E-05	0.01235564	1.41051654
CCDC167	-0.6697367	5.5552925	-5.1336003	2.95E-05	0.01235564	2.36601897
GUCD1	-0.4591891	7.49507083	-5.0706641	3.45E-05	0.01353067	2.0590008
ARF3	0.58755074	6.0654239	5.06909691	3.47E-05	0.01353067	2.17427727
NEAT1	0.57341042	8.93899472	5.06337039	3.52E-05	0.01353067	1.98482574
LSAMP	2.16003215	-0.6216551	5.00309368	4.10E-05	0.01457987	1.27393263
SLC46A3	2.50929998	1.24875444	4.99558195	4.18E-05	0.01457987	1.36255589
VIM	-0.5508013	7.00540268	-4.9887358	4.25E-05	0.01457987	1.90194731

ATP2B4	0.92738123	4.2871402	4.97839968	4.37E-05	0.01457987	2.11539438
ST7-AS1	3.50732284	0.07419414	4.96860828	4.48E-05	0.01457987	-0.2136209
ZC3H12A	0.65676365	5.78173172	4.96377419	4.53E-05	0.01457987	1.902043
BLVRA	0.61830382	6.20316557	4.9607918	4.56E-05	0.01457987	1.90875552
BMF	0.69799924	5.21018101	4.95481921	4.63E-05	0.01457987	1.94728104
TRAF3IP3	0.46340001	8.8326511	4.9074094	5.23E-05	0.01608002	1.58886885
TRAPPC3L	1.08333087	3.06863232	4.84352724	6.15E-05	0.01850357	1.84339649
SSBP4	-1.4902359	2.31550604	-4.7571526	7.66E-05	0.02255986	1.53304064
THEM6	-0.7670864	3.86766818	-4.7179081	8.46E-05	0.02441022	1.50707684
PBXIP1	0.46655614	8.0450991	4.70701468	8.70E-05	0.02458441	1.13585391
CYB5A	-0.4959343	7.00260866	-4.6731032	9.49E-05	0.02626524	1.09538751
UBD	1.7360507	1.81116661	4.60616258	0.00011251	0.03020861	1.10088385
MTMR10	0.47397434	6.0633922	4.58986344	0.00011728	0.03020861	0.95085452
MRPS26	-0.5203445	6.20931565	-4.5881199	0.0001178	0.03020861	0.9438381
GLB1L	0.56404236	5.57402032	4.58795322	0.00011785	0.03020861	0.98859168
C1orf21	0.4968909	7.53933095	4.56026615	0.00012646	0.03182635	0.76790714
DCAF11	0.85956781	4.98525514	4.55139122	0.00012935	0.03197263	0.99350608
MYB	-0.7180825	5.08220884	-4.5375401	0.000134	0.03253964	0.93409546
SYCP3	-0.6052838	5.55942662	-4.5210846	0.00013973	0.03305176	0.94040926
MYO5C	0.9618518	3.83119419	4.51090243	0.0001434	0.03305176	1.06689347
RAB24	0.489385	7.50616331	4.50559704	0.00014535	0.03305176	0.63957496
GLIPR2	0.67025611	5.33253795	4.50011649	0.0001474	0.03305176	0.8167826
TNFRSF21	-2.3457626	0.80756189	-4.4983948	0.00014804	0.03305176	-0.0658273
CTDSP2	0.5045422	7.18617438	4.4737527	0.00015763	0.03406822	0.57393682
SEC24A	-0.9060082	4.02576801	-4.4727761	0.00015802	0.03406822	0.94515007
TPTEP2	0.58151092	5.52179269	4.46794643	0.00015998	0.03406822	0.68741082
HLA-DMB	0.71171575	4.20999982	4.44747297	0.00016854	0.03499153	0.77748991
ISYNA1	-1.3761179	2.15995408	-4.4455444	0.00016937	0.03499153	0.82293096
DDOST	0.54073572	6.45257223	4.41907217	0.00018118	0.03688093	0.49038431
CHPT1	-0.5794392	5.57872029	-4.4063603	0.00018714	0.03754195	0.64561886
FAM201A	1.13976568	2.58724269	4.32678586	0.00022915	0.04531294	0.6266669
DPYSL3	0.65644266	4.10005337	4.28788013	0.00025299	0.04932204	0.24442492
SPAG7	0.50783753	7.30274691	4.28199262	0.0002568	0.04937068	0.09041694
FDXACB1	-1.2152485	2.66303434	-4.2506782	0.00027809	0.05270449	0.43536873
DCPS	-0.4535674	6.29082766	-4.2455132	0.00028176	0.05270449	0.07672213
CALHM5	1.06908917	3.15580556	4.22189249	0.00029919	0.05521886	0.39871896
ATP13A1	-1.1177646	3.05471655	-4.193996	0.00032116	0.05787405	0.33473088
TMEM173	1.92026738	0.86218874	4.19304442	0.00032194	0.05787405	-0.0136426
HERPUD1	0.50642081	8.09715655	4.17833423	0.00033419	0.05787997	-0.2036157
ARHGEF25	-0.953948	3.04393169	-4.1720407	0.00033958	0.05787997	0.28596243
DDX58	1.17266249	2.826895	4.16738676	0.00034361	0.05787997	0.27048841
CCDC88A	1.8057444	2.02483489	4.16577781	0.00034502	0.05787997	0.02538177

PRELID2	1.10193925	3.3904768	4.16343857	0.00034707	0.05787997	0.25070982
DYNC1H1	0.42297488	6.17634883	4.16180944	0.00034851	0.05787997	-0.140838
CCL2	2.12053546	0.86380501	4.15492202	0.00035466	0.05787997	-0.2751199
GPAT4	0.52062585	5.61729797	4.15407045	0.00035543	0.05787997	-0.0812626
ERBIN	0.50525102	5.7939568	4.11479296	0.00039267	0.06320108	-0.1886593
CBLN2	-1.7315159	2.23423441	-4.1060584	0.00040146	0.06385428	0.0336954
NDUFA8	-0.5074361	6.73734956	-4.1016713	0.00040595	0.06385428	-0.3027824
SPR	1.02051552	3.42830664	4.07688626	0.00043227	0.06718224	0.05177353
STOM	1.76127218	2.16788587	4.0727587	0.00043682	0.06718224	-0.0727906
LMNB1	-0.5168585	7.30686323	-4.0547659	0.00045719	0.06954243	-0.465577
WNK1	-0.4642866	5.57650909	-4.0495937	0.00046321	0.06969344	-0.3096698
NDUFAF4	-0.5331859	6.01769744	-4.0376297	0.00047746	0.07106443	-0.3542212
CTHRC1	0.53677364	5.7322455	4.03135926	0.0004851	0.07141057	-0.3660164
GPR108	0.7555874	4.20232464	4.02730396	0.0004901	0.07141057	-0.1917613
GABBR1	0.81107667	4.18463159	4.00467527	0.00051898	0.07348352	-0.2370301
ARHGEF3	0.51268654	5.86620736	4.00408369	0.00051976	0.07348352	-0.445076
TCEAL4	0.53459163	5.08894223	4.00370559	0.00052026	0.07348352	-0.3650479
EMP2	0.48231424	5.98209049	3.99268507	0.00053496	0.07354263	-0.4776515
HSPG2	-3.1870118	-0.0207929	-3.9912377	0.00053692	0.07354263	-1.4455224

logFC = log2(fold-change), AveExpr = average expression, P.Value= p-value, adj.P.Val = adjusted p-value

Appendix 2: Tables of gene fold-change in MM.1S and MM.1Sres cells CRISPR screens

A2.1: Tables of top 50 enriched and top 50 depleted genes in DMSO-treated MM.1S cells at T-End vs MM.1S cells at T-0

id	neg|fdr	neg|rank	neg|goodsgrna	neg|lfc	pos|fdr	pos|rank	pos|goodsgrna	pos|lfc
RPP21	0.000825	1	4	-6.3615	1	20112	0	-6.3615
XPO5	0.000825	2	4	-6.0533	1	20111	0	-6.0533
HSPA5	0.000825	3	4	-6.5762	1	20110	0	-6.5762
API5	0.000825	4	4	-5.8878	1	20109	0	-5.8878
MTHFD1	0.000825	5	4	-5.9964	1	20108	0	-5.9964
PSMB4	0.000825	6	4	-7.757	1	20107	0	-7.757
PGAM1	0.001485	7	4	-5.3	1	20106	0	-5.3
ALDOA	0.001485	8	4	-5.1519	1	20105	0	-5.1519
PSMA5	0.001485	9	4	-7.8999	1	20104	0	-7.8999
ATP6V0C	0.001485	10	4	-8.141	1	20006	0	-8.141
CFL1	0.001485	11	4	-7.1977	1	19720	0	-7.1977
THOC6	0.001485	12	4	-4.8989	1	20103	0	-4.8989
TIPARP	0.001485	13	4	-5.9634	1	20102	0	-5.9634
DPM2	0.001485	14	4	-6.8588	1	20101	0	-6.8588
RPS3A	0.001485	15	4	-7.6478	1	20100	0	-7.6478
RPL19	0.001485	16	4	-6.7654	1	20099	0	-6.7654
MECR	0.001485	17	4	-5.5528	1	20098	0	-5.5528
LSM12	0.001485	18	4	-6.1062	1	20097	0	-6.1062
SNRPD1	0.001485	19	4	-6.7938	1	20096	0	-6.7938
EIF6	0.001485	20	4	-6.7528	1	20095	0	-6.7528
SMU1	0.001485	21	4	-6.5175	1	20094	0	-6.5175
HSPA9	0.001485	22	4	-6.9383	1	20093	0	-6.9383
LARS2	0.001485	23	4	-6.5085	1	20092	0	-6.5085
UBL5	0.001485	24	4	-7.9192	1	20091	0	-7.9192
PRMT1	0.001485	25	4	-5.3847	1	20090	0	-5.3847
RPL23A	0.001485	26	4	-7.3438	1	20089	0	-7.3438
PFDN2	0.001485	27	4	-5.7242	1	20088	0	-5.7242
POLR2K	0.001485	28	4	-5.3163	1	20087	0	-5.3163
WDR18	0.001485	29	4	-6.0879	1	20086	0	-6.0879
PLK1	0.001485	30	4	-7.1889	1	20085	0	-7.1889
DPH3	0.001485	31	4	-8.2008	1	20084	0	-8.2008
PSMB1	0.001485	32	4	-6.6864	1	20083	0	-6.6864
RPL6	0.001485	33	4	-7.575	1	20070	0	-7.575
PGD	0.001485	34	4	-7.8975	1	20082	0	-7.8975
NDUFV1	0.001485	35	4	-7.8735	1	20081	0	-7.8735
PRMT5	0.001485	36	4	-7.0467	1	20080	0	-7.0467
NFKB1	0.001485	37	4	-8.0979	1	20038	0	-8.0979

DDX54	0.001485	38	4	-7.1122	1	19590	0	-7.1122
YARS	0.001485	39	4	-6.952	1	20079	0	-6.952
MFN2	0.001485	40	4	-6.9851	1	20077	0	-6.9851
SF3B1	0.001485	41	4	-6.9097	1	20078	0	-6.9097
PGK1	0.001485	42	4	-5.2838	1	20076	0	-5.2838
HSCB	0.001485	43	4	-6.7952	1	20075	0	-6.7952
ZPR1	0.001485	44	4	-7.413	1	20074	0	-7.413
SHMT2	0.001485	45	4	-7.1955	1	20073	0	-7.1955
FAU	0.001485	46	4	-4.246	1	20072	0	-4.246
ACTR10	0.001485	47	4	-6.7524	1	20071	0	-6.7524
MBTPS1	0.001485	48	4	-5.3841	1	20069	0	-5.3841
GOSR2	0.001485	49	4	-6.1197	1	20066	0	-6.1197
USP7	0.001485	50	4	-8.1646	1	20068	0	-8.1646
ATG7	1	20062	0	2.4728	0.004082	55	4	2.4728
RBM26	1	20063	0	3.1088	0.001718	48	4	3.1088
ARRB2	1	20064	0	2.1593	0.003025	54	4	2.1593
SNX17	1	20065	0	3.2597	0.001532	34	4	3.2597
TRAFD1	1	20066	0	2.2537	0.002335	52	4	2.2537
DRG2	1	20067	0	1.5904	0.002335	51	4	1.5904
ARIH2	1	20068	0	1.6324	0.001718	49	4	1.6324
CBLL1	1	20069	0	2.7474	0.00158	47	4	2.7474
OTUB1	1	20070	0	3.2839	0.001532	42	4	3.2839
ITGAV	1	20071	0	1.9928	0.00158	45	4	1.9928
UBE2D3	1	20072	0	2.2407	0.00158	44	4	2.2407
DOCK4	1	20073	0	2.6255	0.00158	43	4	2.6255
KIAA0195	1	20074	0	2.2386	0.001532	41	4	2.2386
ITGB5	1	20075	0	2.1287	0.001532	40	4	2.1287
RAPGEF1	1	20076	0	2.0202	0.001532	39	4	2.0202
AHR	1	20077	0	1.7447	0.001532	38	4	1.7447
ELMSAN1	1	20078	0	2.1191	0.001532	37	4	2.1191
LZTR1	1	20079	0	2.5479	0.001532	36	4	2.5479
PFKL	1	20080	0	2.0823	0.001532	35	4	2.0823
PRKAB1	1	20081	0	1.9255	0.001532	33	4	1.9255
LITAF	1	20082	0	2.3728	0.001392	32	4	2.3728
FOXP1	1	20083	0	2.3696	0.001392	31	4	2.3696
ZNF652	1	20084	0	2.1969	0.001155	30	4	2.1969
ATG16L1	1	20085	0	2.3333	0.001155	29	4	2.3333
ARRDC3	1	20086	0	2.4527	0.001155	28	4	2.4527
MAZ	1	20087	0	2.8815	0.001155	27	4	2.8815
CIC	1	20088	0	2.357	0.00099	25	4	2.357
KDM6A	1	20089	0	3.0408	0.00099	24	4	3.0408
ZBTB7A	1	20090	0	4.0003	0.000675	21	4	4.0003

PDS5B	1	20091	0	2.2731	0.000861	23	4	2.2731
SPOP	1	20092	0	2.9914	0.000675	22	4	2.9914
KEAP1	1	20093	0	2.3656	0.000495	20	4	2.3656
MITF	1	20094	0	2.5234	0.000495	19	4	2.5234
PTK2B	1	20095	0	3.5719	0.000275	18	4	3.5719
GOLGA7	1	20096	0	2.9749	0.000275	17	4	2.9749
TFE3	1	20097	0	2.9917	0.000275	16	4	2.9917
NFKBIA	1	20098	0	2.8853	0.000275	15	4	2.8853
TFEB	1	20099	0	3.7676	0.000275	14	4	3.7676
TRAF2	1	20100	0	2.9064	0.000275	13	4	2.9064
ERP44	1	20101	0	3.0036	0.000275	12	4	3.0036
SIPA1L1	1	20102	0	3.1738	0.000275	11	4	3.1738
BIRC3	1	20103	0	3.3615	0.000275	10	4	3.3615
MEMO1	1	20104	0	3.847	0.000275	9	4	3.847
TLN1	1	20105	0	3.721	0.000275	8	4	3.721
ITGB1	1	20106	0	4.7383	0.000275	7	4	4.7383
VPS13C	1	20107	0	4.1565	0.000275	6	4	4.1565
CSNK2A1	1	20108	0	4.2778	0.000275	5	4	4.2778
MESDC2	1	20109	0	4.4387	0.000275	4	4	4.4387
ITGA8	1	20110	0	4.8045	0.000275	3	4	4.8045
RARA	1	20111	0	5.5664	0.000275	2	4	5.5664
YTHDF2	1	20112	0	5.1824	0.000275	1	4	5.1824

Id = gene, neg | fdr = false discovery ratio as depleted, neg | rank = rank as depleted, neg | goodsgrna = number of significantly depleted sgRNAs, neg | lfc = log2(fold-change), pos | fdr = false discovery ratio as enriched, neg | rank = rank as enriched, pos | goodsgrna = number of significantly enriched sgRNAs, pos | lfc = log2(fold-change)

A2.2. Tables of top 50 enriched and top 50 depleted genes in LEN-treated vs DMSO-treated MM.1S cells at T-End

id	neg|fdr	neg|rank	neg|good sgrna	neg|lfc	pos|fdr	pos|rank	pos|good sgrna	pos|lfc
CRBN	1	20112	0	11.942	0.00045	1	4	11.942
COPS6	1	20111	0	10.477	0.00045	2	4	10.477
COPS4	1	20071	0	9.3844	0.00045	3	3	9.3844
MBTPS1	1	20110	0	4.4914	0.00045	4	4	4.4914
COPS3	1	20102	0	9.0227	0.00045	5	3	9.0227
GPS1	1	20109	0	6.7985	0.00045	6	4	6.7985
CAND1	1	20108	0	5.7335	0.00045	7	4	5.7335
COPS5	1	18300	0	6.619	0.00045	8	3	6.619
UBE2G1	1	20107	0	4.2666	0.00045	9	4	4.2666
SCAP	1	20096	0	6.4446	0.00045	10	3	6.4446
COPS2	1	20103	0	6.56	0.00045	11	3	6.56
MBTPS2	1	20106	0	5.5547	0.002063	12	4	5.5547
NCOR1	1	20105	0	4.4957	0.004189	13	4	4.4957
EDC4	1	20104	0	3.9569	0.004597	14	4	3.9569
COPS8	1	18890	0	4.7635	0.00495	15	3	4.7635
HIST1H4F	1	11490	1	2.7951	0.031559	16	2	2.7951
C12orf49	1	20097	0	2.5907	0.046302	17	3	2.5907
DCP2	1	20086	0	2.3328	0.099835	18	3	2.3328
PDAP1	1	19934	0	3.0065	0.106566	19	3	3.0065
CAD	0.953528	4998	1	1.228	0.119991	20	3	1.228
TPI1	1	7256	1	0.94257	0.119991	21	3	0.94257
ESYT2	1	10486	2	2.1391	0.142439	22	2	2.1391
GLMN	1	20099	0	2.6412	0.142703	23	3	2.6412
MB	1	9343	2	1.5803	0.270421	24	2	1.5803
TMEM213	1	15023	1	1.5241	0.353465	25	2	1.5241
MTRNR2L5	1	6402	2	0.67079	0.366908	26	2	0.67079
SLC37A1	1	18678	0	1.8961	0.502652	27	2	1.8961
COL13A1	1	16867	1	1.3851	0.502652	28	2	1.3851
TTC21B	1	10856	2	0.47136	0.561113	29	2	0.47136
PFN3	1	16852	1	1.178	0.585551	30	2	1.178
CNGA2	1	15584	1	1.283	0.585551	31	2	1.283
LMAN1L	1	14034	2	-1.4199	0.585551	32	1	-1.4199
CDK15	1	18699	0	1.2496	0.599697	33	2	1.2496
MRPL28	0.662263	2887	3	-1.129	0.599697	34	1	-1.129
TEX40	1	9637	2	0.67372	0.599697	35	2	0.67372
SPATA31C1	0.953528	4788	1	1.2075	0.599697	36	2	1.2075
SLC38A4	0.953528	4359	3	-2.6435	0.657403	37	1	-2.6435

EPC2	1	10424	2	0.85392	0.657403	38	2	0.85392
ITPR1	1	5663	2	0.18867	0.657403	39	2	0.18867
EIF5AL1	1	7650	2	-0.55388	0.657403	40	1	-0.55388
STOML2	0.473878	2066	2	0.45664	0.657403	41	2	0.45664
EMCN	1	11786	2	0.94996	0.657403	42	2	0.94996
SOCS4	1	15305	1	0.96696	0.657403	43	2	0.96696
LDHAL6A	0.953528	4891	2	-1.5032	0.657403	44	1	-1.5032
IQCF1	1	19928	0	0.8541	0.741584	45	2	0.8541
THNSL2	1	16015	1	-0.015023	0.75043	46	1	-0.015023
MED25	1	10564	2	-1.4137	0.766436	47	1	-1.4137
PER1	1	15447	1	0.78314	0.766436	48	2	0.78314
OR5H2	1	14913	1	0.99401	0.766436	49	2	0.99401
OCIAD1	1	6098	3	-2.4372	0.766436	50	1	-2.4372
ALG12	0.001532	35	4	-1.8258	1	20087	0	-1.8258
ATP5B	0.001532	30	4	-1.5294	1	20095	0	-1.5294
BIRC5	0.001532	3	4	-1.3199	1	20089	0	-1.3199
CFLAR	0.004524	50	4	-1.0236	1	20067	0	-1.0236
COA6	0.001532	12	4	-1.0236	1	20080	0	-1.0236
COX15	0.001532	36	4	-1.0236	1	20100	0	-1.0236
COX17	0.001532	27	4	-1.0236	1	20076	0	-1.0236
DAD1	0.001532	8	4	-1.3199	1	20082	0	-1.3199
DCTN6	0.001532	28	4	-1.0236	1	20099	0	-1.0236
DNAJC9	0.001532	15	4	-1.0236	1	20094	0	-1.0236
EEF1A1	0.001532	21	4	-1.0236	1	20078	0	-1.0236
EIF1AX	0.004524	49	4	-2.1202	1	20063	0	-2.1202
EIF4A3	0.001532	17	4	-1.3199	1	20107	0	-1.3199
FDX1L	0.004524	51	4	-1.6915	1	20068	0	-1.6915
GFPT1	0.001532	33	4	-1.0236	1	20079	0	-1.0236
HARS	0.004524	45	4	-1.8238	1	20064	0	-1.8238
HSPD1	0.001532	7	4	-1.0236	1	20108	0	-1.0236
INTS1	0.001532	24	4	-1.6163	1	20085	0	-1.6163
KIAA0391	0.001532	19	4	-1.0236	1	20074	0	-1.0236
LARS2	0.004524	48	4	-1.5294	1	20062	0	-1.5294
LRPPRC	0.001532	25	4	-1.0236	1	20086	0	-1.0236
MRPS2	0.001532	1	4	-1.0236	1	20071	0	-1.0236
NDUFA11	0.001532	14	4	-1.0236	1	20090	0	-1.0236
NLE1	0.001532	2	4	-1.0236	1	20081	0	-1.0236
NOP58	0.001532	9	4	-1.0236	1	20083	0	-1.0236
PCNA	0.001532	26	4	-1.0236	1	20093	0	-1.0236
PDE12	0.001532	23	4	-1.0236	1	20098	0	-1.0236
PHB	0.001532	40	4	-1.0236	1	20111	0	-1.0236
POLR3A	0.001532	18	4	-1.0236	1	20105	0	-1.0236

PPP4C	0.001532	31	4	-1.0236	1	20072	0	-1.0236
PRPF8	0.001532	32	4	-1.3199	1	20110	0	-1.3199
PSMB1	0.001532	4	4	-1.3199	1	20103	0	-1.3199
PSMB2	0.001532	5	4	-1.0236	1	20088	0	-1.0236
RAD51	0.001532	29	4	-1.0236	1	20092	0	-1.0236
RPL10	0.004524	46	4	-1.0236	1	20065	0	-1.0236
RPL3	0.004524	43	4	-1.3199	1	20069	0	-1.3199
RPS21	0.004524	44	4	-2.1973	1	20066	0	-2.1973
RPS24	0.001532	11	4	-1.0236	1	20077	0	-1.0236
SMC2	0.004524	47	4	-1.0236	1	20070	0	-1.0236
SNRPA1	0.001532	10	4	-1.3199	1	20084	0	-1.3199
SNRPD3	0.001532	16	4	-1.0236	1	20109	0	-1.0236
TCEB2	0.001532	38	4	-1.0236	1	20096	0	-1.0236
TRAPPC1	0.001532	39	4	-1.0236	1	20097	0	-1.0236
TTC27	0.001532	41	4	-1.0236	1	20106	0	-1.0236
TUBB	0.001532	34	4	-1.0236	1	20091	0	-1.0236
TUFM	0.001532	6	4	-1.0236	1	20102	0	-1.0236
UBL5	0.001532	13	4	-1.0236	1	20075	0	-1.0236
USP7	0.001532	37	4	-1.0236	1	20101	0	-1.0236
VARS2	0.001532	20	4	-1.0236	1	20112	0	-1.0236
WASH1	0.001532	22	4	-1.0236	1	20104	0	-1.0236
XPO1	0.001532	42	4	-1.0236	1	20073	0	-1.0236

Id = gene, neg | fdr = false discovery ratio as depleted, neg | rank = rank as depleted, neg | goodsgrna = number of significantly depleted sgRNAs, neg | lfc = log2(fold-change), pos | fdr = false discovery ratio as enriched, neg | rank = rank as enriched, pos | goodsgrna = number of significantly enriched sgRNAs, pos | lfc = log2(fold-change)

A2.3. Tables of top 50 enriched and top 50 depleted genes in POM-treated vs DMSO-treated MM.1S cells at T-End

id	neg|fdr	neg|rank	neg|good sgrna	neg|lfc	pos|fdr	pos|rank	pos|good sgrna	pos|lfc
MESDC2	0.000354	1	4	-13.092	1	20112	0	-13.092
YTHDF2	0.000354	2	4	-10.425	1	20111	0	-10.425
ITGB1	0.000354	3	4	-13.063	1	20110	0	-13.063
ITGA8	0.000354	4	4	-11.958	1	20109	0	-11.958
CSNK2A1	0.000354	5	4	-11.292	1	20108	0	-11.292
ZBTB7A	0.000354	6	4	-9.472	1	20107	0	-9.472
PTK2B	0.000354	7	4	-9.8361	1	20106	0	-9.8361
MEMO1	0.000354	8	4	-9.7044	1	20105	0	-9.7044
SIPA1L1	0.000354	9	4	-8.0935	1	20104	0	-8.0935
ERP44	0.000354	10	4	-10.659	1	20103	0	-10.659
MITF	0.000354	11	4	-10.179	1	20102	0	-10.179
ARRDC3	0.000354	13	4	-9.4526	1	20101	0	-9.4526
ATG16L1	0.000354	14	4	-10.76	1	20100	0	-10.76
TLN1	0.00066	15	4	-11.055	1	20099	0	-11.055
AHR	0.001238	16	4	-7.2591	1	20098	0	-7.2591
MSI2	0.001375	17	4	-9.6589	1	20097	0	-9.6589
CIC	0.001375	18	4	-7.2173	1	20096	0	-7.2173
VPS13C	0.001563	19	4	-10.57	1	20095	0	-10.57
ZBED4	0.001575	21	4	-9.7847	1	20094	0	-9.7847
KDM6A	0.001575	22	4	-10.17	1	20093	0	-10.17
DOCK4	0.002219	23	4	-10.398	1	20085	0	-10.398
PIAS4	0.002219	24	4	-7.7954	1	20092	0	-7.7954
FAM122A	0.002219	26	4	-9.9764	1	20091	0	-9.9764
ZNF652	0.002219	27	4	-9.0374	1	20090	0	-9.0374
RAPGEF1	0.002219	28	4	-9.721	1	20089	0	-9.721
DRG2	0.00225	31	4	-7.7757	1	20088	0	-7.7757
TRAF2	0.00225	33	4	-9.8852	1	20087	0	-9.8852
ARIH2	0.002475	34	4	-9.2552	1	20086	0	-9.2552
PDS5B	0.003819	35	4	-8.3262	1	20084	0	-8.3262
OLA1	0.004299	37	4	-9.3433	1	20083	0	-9.3433
NPC2	0.004443	39	4	-8.9664	1	20082	0	-8.9664
C18orf8	0.006954	42	4	-10.3	1	20072	0	-10.3
KMT2D	0.009788	44	4	-9.2967	1	20081	0	-9.2967
TFEB	0.009791	45	4	-9.8665	1	20078	0	-9.8665
SLC5A3	0.009793	46	4	-9.3489	1	20080	0	-9.3489
LDLR	0.019095	49	4	-7.5628	1	20079	0	-7.5628
FOXP1	0.019307	50	4	-9.5946	1	20070	0	-9.5946

OR4K5	0.024294	52	4	-8.3904	1	20077	0	-8.3904
SLC30A7	0.024294	53	4	-9.3394	1	20076	0	-9.3394
ARHGAP25	0.026013	54	4	-9.2461	1	20075	0	-9.2461
HNRNPUL1	0.030499	55	4	-9.5091	1	20074	0	-9.5091
PAXIP1	0.032395	56	4	-9.3136	1	20064	0	-9.3136
TNS3	0.034056	57	4	-9.3153	1	20073	0	-9.3153
UBE2D3	0.042002	62	4	-7.4667	1	20071	0	-7.4667
GNA13	0.048101	66	4	-9.5344	1	20069	0	-9.5344
CSF2RB	0.04929	67	4	-7.1417	1	20068	0	-7.1417
ZNF598	0.04929	68	4	-9.1321	1	20067	0	-9.1321
ENDOV	0.049576	69	4	-9.2515	1	20066	0	-9.2515
RWDD1	0.04998	72	4	-8.9471	1	20065	0	-8.9471
PPM1J	0.055302	75	4	-9.3638	1	20063	0	-9.3638
controlguide963	0.023005	78	1	-15.669	1	20062	0	-15.669
SRPK1	0.418453	1187	3	-7.8031	0.930474	37	1	-7.8031
ERVMER34-1	0.44081	1362	2	-1.7299	0.930474	34	2	-1.7299
C6orf1	0.578754	3041	2	-2.5655	0.930474	48	2	-2.5655
PPP1R1B	0.584333	3081	2	-1.877	0.930474	44	2	-1.877
OGFOD2	0.815547	5868	2	-2.9038	0.930474	38	2	-2.9038
SCOC	0.819476	5921	3	-7.6197	0.930474	45	1	-7.6197
METTL18	0.833705	6073	2	-2.5553	0.930474	30	2	-2.5553
KDELC1	0.867902	6490	3	-7.2617	0.930474	35	1	-7.2617
LMOD3	0.918544	7185	2	-1.7175	0.869937	22	2	-1.7175
IRAK1	0.922661	7238	2	-2.1035	0.930474	32	2	-2.1035
HDAC5	0.932033	7365	2	-2.115	0.930474	50	2	-2.115
ZBP1	0.973731	8202	1	-2.0005	0.930474	27	2	-2.0005
RBM6	0.987255	8522	2	-2.5355	0.930474	31	2	-2.5355
THUMPD3	1	8899	2	-0.1592	0.123762	11	2	-0.1592
GPR12	1	10171	3	-5.5737	0.930474	41	1	-5.5737
SETMAR	1	10375	1	-2.0595	0.930474	36	2	-2.0595
VIT	1	10921	1	0.74242	0.077723	10	2	0.74242
SPIB	1	11101	1	-1.9247	0.930474	42	2	-1.9247
OCIAD1	1	12427	2	-6.223	0.883556	23	1	-6.223
RHBDD1	1	12785	1	-0.98088	0.697195	18	2	-0.98088
SLC37A1	1	13568	2	-1.7002	0.815417	21	2	-1.7002
MCC	1	13645	1	-2.2602	0.930474	46	2	-2.2602
C3	1	13685	1	-6.0206	0.930474	39	1	-6.0206
DCUN1D5	1	13834	1	-0.22213	0.153112	12	2	-0.22213
TSPAN16	1	14022	1	-0.15861	0.743877	19	2	-0.15861
COPS5	1	14407	1	6.8559	0.004125	6	3	6.8559
STXBP3	1	14816	1	-1.2411	0.930474	47	2	-1.2411

CEP250	1	15776	1	-6.009	0.930474	49	1	-6.009
PTCD2	1	15978	1	-1.0655	0.930474	25	2	-1.0655
CARD9	1	17036	0	-5.9794	0.930474	43	1	-5.9794
MB	1	17069	0	-0.2704	0.232673	15	2	-0.2704
PDZK1	1	17093	0	-1.0856	0.774505	20	2	-1.0856
ZACN	1	17100	0	1.0692	0.930474	40	2	1.0692
TEX40	1	17544	0	-0.46957	0.697195	17	2	-0.46957
COPS8	1	18522	0	4.8577	0.011551	9	3	4.8577
ARF1	1	18658	0	-3.2259	0.930474	28	1	-3.2259
NIPAL3	1	18662	0	1.2967	0.153112	13	2	1.2967
AAMDC	1	18806	0	-0.2267	0.577661	16	2	-0.2267
AQR	1	19404	0	-3.2445	0.928424	24	1	-3.2445
ATP5J	1	19524	0	-3.3228	0.930474	29	1	-3.3228
CYCS	1	19691	0	-1.5108	0.930474	26	1	-1.5108
CDK1	1	19697	0	-1.9154	0.930474	33	1	-1.9154
STOML2	1	19715	0	2.3603	0.153112	14	2	2.3603
COPS3	1	19884	0	7.7949	0.00165	3	3	7.7949
COPS4	1	20107	0	5.4743	0.007779	7	3	5.4743
GPS1	1	20108	0	7.0954	0.008045	8	3	7.0954
COPS2	1	20109	0	5.6948	0.004125	5	4	5.6948
CAND1	1	20110	0	2.7249	0.004125	4	4	2.7249
COPS6	1	20111	0	10.919	0.00165	2	4	10.919
CRBN	1	20112	0	12.79	0.00165	1	4	12.79

Id = gene, neg | fdr = false discovery ratio as depleted, neg | rank = rank as depleted, neg | goodsgrna = number of significantly depleted sgRNAs, neg | lfc = log2(fold-change), pos | fdr = false discovery ratio as enriched, neg | rank = rank as enriched, pos | goodsgrna = number of significantly enriched sgRNAs, pos | lfc = log2(fold-change)

A2.4: Tables of top 50 enriched and top 50 depleted genes in DMSO-treated MM.1Sres cells at T-End vs MM.1Sres cells at T-0

id	neg|fdr	neg|rank	neg|good sgrna	neg|lfc	pos|fdr	pos|rank	pos|good sgrna	pos|lfc
RPP21	0.001303	1	4	-7.0358	1	20112	0	-7.0358
MTHFD1	0.001303	2	4	-5.8507	1	20111	0	-5.8507
PRMT1	0.001303	3	4	-5.511	1	20110	0	-5.511
TKT	0.001303	4	4	-5.0475	1	20092	0	-5.0475
ANAPC11	0.001303	5	4	-3.5623	1	20109	0	-3.5623
PGAM1	0.001303	6	4	-4.1314	1	20108	0	-4.1314
CARS	0.001303	7	4	-4.434	1	20107	0	-4.434
MRPS7	0.001303	8	4	-4.6861	1	20106	0	-4.6861
ITPK1	0.001303	9	4	-3.7002	1	20105	0	-3.7002
THOC6	0.001303	11	4	-3.2713	1	20104	0	-3.2713
LUC7L3	0.001303	12	4	-5.4673	1	20103	0	-5.4673
ALDOA	0.001303	13	4	-5.7458	1	20102	0	-5.7458
RPS3A	0.001303	14	4	-7.136	1	20101	0	-7.136
EIF6	0.001303	15	4	-5.8599	1	20100	0	-5.8599
SHMT2	0.001303	16	4	-4.6556	1	20099	0	-4.6556
TOP3A	0.001303	17	4	-3.039	1	20079	0	-3.039
PSMB4	0.001303	18	4	-6.6973	1	20098	0	-6.6973
HSPA5	0.001303	20	4	-7.3749	1	20097	0	-7.3749
FAU	0.001303	21	4	-4.9249	1	20096	0	-4.9249
BUB3	0.001303	23	4	-6.8547	1	20095	0	-6.8547
PTPMT1	0.001303	25	4	-5.2597	1	20094	0	-5.2597
TAF1C	0.001303	26	4	-5.1856	1	20093	0	-5.1856
POLR2K	0.001303	27	4	-4.4018	1	20091	0	-4.4018
PRELID1	0.001303	28	4	-5.7106	1	20090	0	-5.7106
MYH9	0.001303	29	4	-4.2966	1	20089	0	-4.2966
MRPL34	0.001303	30	4	-3.0278	1	20088	0	-3.0278
RPL19	0.001303	31	4	-6.7789	1	20087	0	-6.7789
SEPHS2	0.001303	32	4	-3.7804	1	20086	0	-3.7804
NDUFV1	0.001303	33	4	-5.8754	1	20085	0	-5.8754
DPH3	0.001303	34	4	-5.2931	1	20084	0	-5.2931
RPL7	0.001303	36	4	-6.3243	1	20083	0	-6.3243
HSPA8	0.001303	37	4	-4.1062	1	20082	0	-4.1062
COG3	0.001303	38	4	-2.9245	1	20081	0	-2.9245
RPL31	0.001303	39	4	-5.8582	1	20080	0	-5.8582
CFL1	0.001303	41	4	-5.3022	1	20063	0	-5.3022
PRKDC	0.001303	42	4	-2.724	1	20078	0	-2.724
NCBP1	0.001303	43	4	-3.9553	1	20077	0	-3.9553

GINS2	0.001303	44	4	-5.8258	1	20076	0	-5.8258
PRIM1	0.001303	45	4	-4.223	1	20075	0	-4.223
GRPEL1	0.001303	47	4	-7.1359	1	20074	0	-7.1359
WDR18	0.001303	48	4	-3.9531	1	20073	0	-3.9531
XPO5	0.001303	49	4	-3.6082	1	20072	0	-3.6082
UQCRC1	0.001303	50	4	-2.8079	1	20071	0	-2.8079
MRPS25	0.001303	51	4	-4.7832	1	20070	0	-4.7832
SNUPN	0.001303	52	4	-4.6936	1	20069	0	-4.6936
HSPA9	0.001303	53	4	-5.1148	1	20068	0	-5.1148
ARCN1	0.001303	55	4	-4.7893	1	20067	0	-4.7893
RPLP0	0.001303	56	4	-6.0334	1	20066	0	-6.0334
CCND2	0.001303	57	4	-4.4109	1	20065	0	-4.4109
DCAF7	0.001451	58	4	-2.34	1	20064	0	-2.34
MRPS18A	0.001493	59	4	-5.902	1	20062	0	-5.902
RIC3	1	5112	2	-0.32449	0.275966	50	1	-0.32449
MAP3K10	1	7828	2	-0.073007	0.191301	12	1	-0.073007
CNTD2	1	8935	1	0.2809	0.207252	27	2	0.2809
SCT	1	10670	1	0.51005	0.242221	40	3	0.51005
MDH2	1	11294	1	0.81924	0.210586	36	3	0.81924
XKRY	1	14655	0	0.64206	0.207252	32	3	0.64206
ZNF410	1	14825	0	0.76294	0.207252	20	3	0.76294
AHR	1	15192	0	0.76832	0.207252	29	3	0.76832
GPR83	1	16672	0	1.5113	0.04314	6	3	1.5113
MAN2A1	1	18879	0	0.84063	0.167867	8	3	0.84063
FRYL	1	18952	0	0.76483	0.191301	13	3	0.76483
ARRDC3	1	19376	0	0.89335	0.167867	10	4	0.89335
ZNF146	1	19510	0	0.7515	0.207252	34	4	0.7515
RARA	1	19719	0	1.0292	0.04314	7	4	1.0292
TMEM31	1	20005	0	0.98863	0.235088	39	4	0.98863
NFKBIB	1	20023	0	1.204	0.207252	23	4	1.204
SPOP	1	20042	0	1.1026	0.207252	19	4	1.1026
SPTBN1	1	20080	0	0.80899	0.274752	49	4	0.80899
CLCA4	1	20081	0	0.55517	0.274752	48	4	0.55517
UST	1	20082	0	0.76118	0.269286	47	4	0.76118
controlguide506	1	20083	0	3.4981	0.203553	46	1	3.4981
GNG11	1	20084	0	0.92545	0.2668	45	4	0.92545
ZNF732	1	20085	0	0.52375	0.2668	44	4	0.52375
CALB1	1	20086	0	0.68522	0.2668	43	4	0.68522
SP4	1	20087	0	0.85516	0.262489	42	4	0.85516
GPD1L	1	20088	0	0.61769	0.260304	41	4	0.61769
GRM7	1	20089	0	0.55012	0.222153	38	4	0.55012
GPR135	1	20090	0	0.7653	0.210586	37	4	0.7653

HDAC4	1	20091	0	0.685	0.207252	35	4	0.685
AKAP4	1	20092	0	0.72268	0.207252	33	4	0.72268
UTY	1	20093	0	0.65905	0.207252	31	4	0.65905
TMEM102	1	20094	0	0.6131	0.207252	30	4	0.6131
AP1G1	1	20095	0	0.69341	0.207252	28	4	0.69341
MON1B	1	20096	0	0.76565	0.191301	14	4	0.76565
UGCG	1	20097	0	0.63987	0.207252	26	4	0.63987
TGFB1	1	20098	0	0.72291	0.207252	25	4	0.72291
JARID2	1	20099	0	0.6722	0.207252	24	4	0.6722
URAD	1	20100	0	0.59005	0.207252	22	4	0.59005
CCDC70	1	20101	0	0.69953	0.207252	21	4	0.69953
QKI	1	20102	0	0.73445	0.207252	18	4	0.73445
PDHA1	1	20103	0	0.91329	0.207252	17	4	0.91329
SECISBP2L	1	20104	0	0.96365	0.203553	16	4	0.96365
SLCO1B1	1	20105	0	0.62344	0.203553	15	4	0.62344
NFIB	1	20106	0	0.78102	0.167867	11	4	0.78102
HDAC5	1	20107	0	0.69756	0.167867	9	4	0.69756
NUDCD1	1	20108	0	1.105	0.038614	5	4	1.105
RNF167	1	20109	0	1.1223	0.038614	4	4	1.1223
BCOR	1	20110	0	1.1226	0.018152	3	4	1.1226
PDHB	1	20111	0	1.1407	0.018152	2	4	1.1407
MPC1	1	20112	0	1.6166	0.00495	1	4	1.6166

Id = gene, neg | fdr = false discovery ratio as depleted, neg | rank = rank as depleted, neg | goodsgrna = number of significantly depleted sgRNAs, neg | lfc = log2(fold-change), pos | fdr = false discovery ratio as enriched, neg | rank = rank as enriched, pos | goodsgrna = number of significantly enriched sgRNAs, pos | lfc = log2(fold-change)

A2.5. Tables of top 50 enriched and top 50 depleted genes in LEN-treated vs DMSO-treated MM.1Sres cells at T-End

id	neg|fdr	neg|rank	neg|good sgrna	neg|lfc	pos|fdr	pos|rank	pos|good sgrna	pos|lfc
MAEA	0.00495	1	4	-1.6585	1	20112	0	-1.6585
ATXN7	0.00495	2	4	-1.6552	1	20111	0	-1.6552
YPEL5	0.018152	3	4	-1.1765	1	20110	0	-1.1765
MIER3	0.018564	4	4	-1.0076	1	20109	0	-1.0076
GID8	0.020792	5	4	-1.1545	1	20103	0	-1.1545
TOP2B	0.028878	6	4	-0.92524	1	20108	0	-0.92524
MED13L	0.047383	7	3	-1.7589	1	18458	0	-1.7589
MED13	0.079758	8	4	-1.4679	1	20107	0	-1.4679
ARID3B	0.079758	9	4	-0.9869	1	19998	0	-0.9869
NFKB1	0.085959	10	4	-1.8553	1	20106	0	-1.8553
CITED2	0.085959	11	4	-1.2822	1	20105	0	-1.2822
MEF2D	0.109264	12	4	-0.84473	1	20104	0	-0.84473
G6PD	0.109264	13	4	-0.98317	1	20102	0	-0.98317
RIC3	0.146349	14	1	0.27923	1	4589	2	0.27923
CUX1	0.146349	15	4	-0.74662	1	20101	0	-0.74662
B3GAT3	0.179091	16	4	-1.0849	1	20100	0	-1.0849
LCN8	0.194893	17	4	-0.71675	1	20099	0	-0.71675
PIM2	0.194893	18	4	-1.7275	1	20098	0	-1.7275
ZNF460	0.214593	19	3	-0.77567	1	19277	0	-0.77567
DCANP1	0.214593	20	3	-0.47454	1	19225	0	-0.47454
controlguide798	0.097772	21	1	-3.1025	1	20097	0	-3.1025
PRDM1	0.214593	22	4	-1.5878	1	20079	0	-1.5878
TMEM101	0.214593	23	3	-0.76649	1	17896	0	-0.76649
WDR26	0.218441	24	4	-0.74298	1	19897	0	-0.74298
ASH1L	0.23304	25	4	-0.58945	1	20096	0	-0.58945
IFIT3	0.23304	26	4	-0.84339	1	20095	0	-0.84339
SCT	0.23304	27	3	-0.64153	1	14548	1	-0.64153
UBE2H	0.258621	28	3	-0.68058	1	18324	0	-0.68058
MPV17	0.258621	29	4	-0.96719	1	20094	0	-0.96719
TM9SF3	0.266822	30	3	-0.63086	1	19554	0	-0.63086
LZIC	0.266822	31	3	-0.62217	1	10246	1	-0.62217
PPIG	0.266822	32	4	-0.91286	1	19910	0	-0.91286
ZRSR2	0.266822	33	3	-0.65034	1	14732	1	-0.65034
KDM5C	0.266822	34	4	-1.6022	1	20093	0	-1.6022
RWDD1	0.266822	35	4	-0.88665	1	20092	0	-0.88665
CNTD2	0.266822	36	2	-0.48011	1	10378	1	-0.48011
PHF6	0.266822	37	4	-0.97971	1	20091	0	-0.97971

WDR19	0.266822	38	2	-0.65966	1	17790	0	-0.65966
SIN3B	0.266822	39	4	-0.72701	1	20090	0	-0.72701
CRAMP1L	0.266822	40	3	-0.96444	1	17985	0	-0.96444
ZNF800	0.266822	41	4	-0.60806	1	20089	0	-0.60806
GLCE	0.266822	42	3	-0.78963	1	19030	0	-0.78963
UNK	0.266822	43	3	-0.70413	1	19395	0	-0.70413
SERTAD2	0.266822	44	4	-1.392	1	20088	0	-1.392
NECAP2	0.266822	45	4	-0.57301	1	20087	0	-0.57301
SLC39A10	0.266822	46	4	-1.0029	1	20086	0	-1.0029
ZZZ3	0.266822	47	4	-0.83705	1	20085	0	-0.83705
CDIP1	0.266822	48	4	-0.42399	1	20084	0	-0.42399
SEPHS1	0.266822	49	3	-1.6506	1	19548	0	-1.6506
RAP1GAP2	0.281485	50	3	-0.67415	1	14357	1	-0.67415
TRAF2	1	20062	0	1.18	0.018477	70	4	1.18
MAP2K7	1	20063	0	0.77138	0.015443	67	4	0.77138
LRP10	1	20064	0	1.0824	0.013481	65	4	1.0824
CSNK2A1	1	20065	0	1.4312	0.003342	40	4	1.4312
KEAP1	1	20066	0	1.5281	0.003342	39	4	1.5281
NUDCD1	1	20067	0	0.83108	0.009665	63	4	0.83108
KHSRP	1	20068	0	1.3627	0.009502	62	4	1.3627
USP14	1	20069	0	1.1312	0.008197	61	4	1.1312
PGK1	1	20070	0	1.2301	0.007468	59	4	1.2301
SIPA1L1	1	20071	0	1.6035	0.007426	56	4	1.6035
PDS5B	1	20072	0	1.3032	0.004435	46	4	1.3032
PDHA1	1	20073	0	0.78585	0.006071	53	4	0.78585
CS	1	20074	0	0.98085	0.005998	52	4	0.98085
SUSD6	1	20075	0	1.063	0.005248	49	4	1.063
NOSIP	1	20076	0	1.8831	0.00429	45	4	1.8831
KDM3B	1	20077	0	0.90845	0.003938	44	4	0.90845
SMEK2	1	20078	0	1.3735	0.003799	43	4	1.3735
PBRM1	1	20079	0	1.2279	0.003799	42	4	1.2279
AGPAT5	1	20080	0	1.7293	0.003743	41	4	1.7293
MECR	1	20081	0	1.66	0.003257	38	4	1.66
FBXO11	1	20082	0	1.6124	0.002338	36	4	1.6124
KCMF1	1	20083	0	1.7506	0.002338	35	4	1.7506
UBR4	1	20084	0	2.6553	0.002184	30	4	2.6553
RAD21	1	20085	0	1.9155	0.002184	33	4	1.9155
TMEM30A	1	20086	0	1.1296	0.002184	32	4	1.1296
GPI	1	20087	0	2.7222	0.002184	31	4	2.7222
TMEM127	1	20088	0	0.85135	0.002184	29	4	0.85135
PGP	1	20089	0	1.3037	0.002184	28	4	1.3037
DDIT4	1	20090	0	1.3198	0.002184	27	4	1.3198

UBE2G2	1	20091	0	1.8787	0.002184	26	4	1.8787
SRSF5	1	20092	0	1.2672	0.002184	25	4	1.2672
YTHDF2	1	20093	0	1.6814	0.002184	23	4	1.6814
SETD1B	1	20094	0	1.2724	0.002184	22	4	1.2724
SLC16A1	1	20095	0	1.6997	0.002184	21	4	1.6997
ZBTB7A	1	20096	0	1.2778	0.002184	20	4	1.2778
TNRC18	1	20097	0	1.0946	0.002184	19	4	1.0946
BIRC6	1	20098	0	1.5338	0.001925	18	4	1.5338
ACSL4	1	20099	0	1.5829	0.001925	17	4	1.5829
DCP2	1	20100	0	1.9672	0.001925	16	4	1.9672
ZFP36L2	1	20101	0	2.4877	0.001925	15	4	2.4877
NPRL3	1	20102	0	2.3273	0.001925	14	4	2.3273
COPS4	1	20103	0	2.2738	0.001925	13	4	2.2738
FUBP1	1	20104	0	1.2204	0.001925	12	4	1.2204
RARA	1	20105	0	1.1426	0.001925	10	4	1.1426
LZTR1	1	20106	0	2.8226	0.000619	6	4	2.8226
STAG2	1	20107	0	1.9327	0.000619	8	4	1.9327
UBA6	1	20108	0	1.7083	0.000619	5	4	1.7083
METAP2	1	20109	0	3.0028	0.000619	4	4	3.0028
UBE2D3	1	20110	0	3.3646	0.000619	3	4	3.3646
CAND1	1	20111	0	2.7786	0.000619	2	4	2.7786
CRBN	1	20112	0	1.7411	0.000619	1	4	1.7411

Id = gene, neg | fdr = false discovery ratio as depleted, neg | rank = rank as depleted, neg | goodsgrna = number of significantly depleted sgRNAs, neg | lfc = log2(fold-change), pos | fdr = false discovery ratio as enriched, neg | rank = rank as enriched, pos | goodsgrna = number of significantly enriched sgRNAs, pos | lfc = log2(fold-change)

A2.6. Tables of top 50 enriched and top 50 depleted genes in POM-treated vs DMSO-treated MM.1Sres cells at T-End

id	neg|fdr	neg|rank	neg|good sgrna	neg|lfc	pos|fdr	pos|rank	pos|good sgrna	pos|lfc
ANP32B	0.00165	1	4	-2.5636	1	20112	0	-2.5636
ATXN7	0.00165	2	4	-2.0942	1	20111	0	-2.0942
MIER3	0.00165	3	4	-2.2216	1	20110	0	-2.2216
MAEA	0.003536	4	4	-1.8139	1	20109	0	-1.8139
MEF2D	0.003536	5	4	-1.4896	1	20108	0	-1.4896
NSUN2	0.003536	6	4	-1.8663	1	20107	0	-1.8663
YPEL5	0.003536	7	4	-1.6317	1	20080	0	-1.6317
WDR26	0.00495	8	4	-1.5509	1	20093	0	-1.5509
TOP2B	0.00495	9	4	-1.8795	1	20106	0	-1.8795
ZNF800	0.00495	10	4	-1.1808	1	20105	0	-1.1808
MED13L	0.00495	11	4	-2.3409	1	20097	0	-2.3409
RING1	0.00495	12	3	-1.4233	1	19570	0	-1.4233
SETBP1	0.00495	13	4	-1.9205	1	20104	0	-1.9205
PHF6	0.00495	14	4	-1.7042	1	20103	0	-1.7042
ZNF460	0.00495	15	4	-1.3575	1	20095	0	-1.3575
QRICH1	0.005879	16	4	-1.5726	1	20102	0	-1.5726
PRKCE	0.00728	17	4	-1.1209	1	20101	0	-1.1209
CUX1	0.007426	18	4	-1.1903	1	19928	0	-1.1903
ARID3B	0.009119	19	4	-1.7899	1	20100	0	-1.7899
PCGF1	0.009158	20	4	-0.97657	1	20099	0	-0.97657
MED13	0.010576	21	4	-2.6359	1	19935	0	-2.6359
G6PD	0.010576	22	4	-1.3238	1	20090	0	-1.3238
LARP1	0.01356	23	4	-1.1471	1	20098	0	-1.1471
TSPYL1	0.020421	24	4	-0.98532	1	20096	0	-0.98532
MORF4L1	0.02396	25	4	-0.85861	1	20049	0	-0.85861
CHD8	0.026085	26	3	-1.8471	1	18550	0	-1.8471
SFMBT1	0.029153	27	4	-1.0278	1	19797	0	-1.0278
RANBP9	0.036245	28	3	-1.3675	1	19704	0	-1.3675
GNAI2	0.040457	29	4	-0.78961	1	20094	0	-0.78961
DCANP1	0.049041	30	3	-0.75668	1	18258	0	-0.75668
SEPHS1	0.049041	31	4	-2.4497	1	20083	0	-2.4497
MKLN1	0.049041	32	4	-1.7278	1	20053	0	-1.7278
NFKB1	0.066157	33	4	-1.3383	1	20092	0	-1.3383
MAP3K10	0.06662	34	1	-0.14297	1	18607	0	-0.14297
YWHAE	0.06662	35	4	-2.7629	1	20091	0	-2.7629
HSPA4	0.067794	36	4	-1.0404	1	20089	0	-1.0404
SREK1	0.067835	37	4	-1.1945	1	19903	0	-1.1945

CDK2	0.069177	38	4	-1.3165	1	20088	0	-1.3165
ZNF142	0.074876	39	4	-1.0137	1	20087	0	-1.0137
RPS6KB1	0.074876	40	4	-1.4361	1	20086	0	-1.4361
KDM5A	0.07957	41	4	-1.253	1	20085	0	-1.253
PLAC1	0.08074	42	2	-0.42755	1	8269	1	-0.42755
CARM1	0.083258	43	3	-1.8824	1	19387	0	-1.8824
SIN3B	0.083258	44	4	-1.1552	1	20084	0	-1.1552
FAM122A	0.084674	45	4	-0.81086	1	20082	0	-0.81086
RBBP6	0.084674	46	3	-1.6226	1	19093	0	-1.6226
RAB22A	0.084674	47	4	-0.6487	1	20081	0	-0.6487
TMEM31	0.084674	48	3	-0.79682	1	18984	0	-0.79682
PIM2	0.088806	49	4	-3.5066	1	20069	0	-3.5066
MON2	0.094059	50	4	-0.90393	1	20079	0	-0.90393
DEPDC5	1	20062	0	1.7382	0.000908	57	4	1.7382
TKT	1	20063	0	4.2932	0.000396	24	4	4.2932
GPS1	1	20064	0	3.3942	0.000908	56	4	3.3942
SOX2	1	20065	0	1.8804	0.000908	55	4	1.8804
GLMN	1	20066	0	2.3786	0.000908	51	4	2.3786
ILF3	1	20067	0	2.7018	0.000908	50	4	2.7018
ZBTB7A	1	20068	0	1.5069	0.000908	49	4	1.5069
SRSF7	1	20069	0	3.0988	0.000908	48	4	3.0988
NUDCD1	1	20070	0	1.5146	0.000908	47	4	1.5146
HSD17B12	1	20071	0	2.8812	0.000908	46	4	2.8812
GPI	1	20072	0	2.9799	0.000908	45	4	2.9799
SETD1B	1	20073	0	1.6093	0.000908	44	4	1.6093
PDS5B	1	20074	0	1.6668	0.000908	43	4	1.6668
DCP2	1	20075	0	2.8066	0.000908	42	4	2.8066
RC3H1	1	20076	0	2.038	0.000908	41	4	2.038
NOSIP	1	20077	0	2.9936	0.000866	40	4	2.9936
LUC7L2	1	20078	0	2.2103	0.000866	38	4	2.2103
VCPIP1	1	20079	0	1.7818	0.000669	37	4	1.7818
ACSL4	1	20080	0	2.2778	0.000669	36	4	2.2778
PBRM1	1	20081	0	2.309	0.000669	34	4	2.309
SRSF5	1	20082	0	1.8468	0.000669	33	4	1.8468
CSNK2A1	1	20083	0	1.7368	0.000669	32	4	1.7368
FUBP1	1	20084	0	1.6301	0.000669	31	4	1.6301
CFAP20	1	20085	0	3.5881	0.000669	30	4	3.5881
PCBP2	1	20086	0	3.8132	0.000669	29	4	3.8132
CBLL1	1	20087	0	2.7894	0.000669	28	4	2.7894
KCMF1	1	20088	0	3.1637	0.000669	27	4	3.1637
C19orf43	1	20089	0	2.3743	0.000571	26	4	2.3743
EDC4	1	20090	0	3.4298	0.000215	20	4	3.4298

PDAP1	1	20091	0	4.2973	0.000396	25	4	4.2973
BIRC6	1	20092	0	2.2183	0.000215	23	4	2.2183
C12orf49	1	20093	0	3.0471	0.000215	22	4	3.0471
UBE2G2	1	20094	0	2.8128	0.000215	21	4	2.8128
TRAF2	1	20095	0	2.0034	0.000215	19	4	2.0034
YTHDF2	1	20096	0	3.035	0.000215	18	4	3.035
STAG2	1	20097	0	2.5471	0.000215	16	4	2.5471
SLC25A1	1	20098	0	3.1814	0.000215	15	4	3.1814
COPS7A	1	20099	0	2.4238	0.000215	14	4	2.4238
UBR4	1	20100	0	4.373	0.000215	13	4	4.373
NPRL3	1	20101	0	3.4845	0.000215	12	4	3.4845
COPS4	1	20102	0	3.7337	0.000215	11	4	3.7337
METAP2	1	20103	0	4.5155	0.000215	10	4	4.5155
UBE2G1	1	20104	0	3.3963	0.000215	9	4	3.3963
NCOR1	1	20105	0	3.8633	0.000215	8	4	3.8633
UBE2D3	1	20106	0	4.748	0.000215	7	4	4.748
UBA6	1	20107	0	2.9159	0.000215	6	4	2.9159
TNRC18	1	20108	0	2.5549	0.000215	5	4	2.5549
COPS7B	1	20109	0	4.1462	0.000215	4	4	4.1462
RARA	1	20110	0	2.5244	0.000215	3	4	2.5244
CRBN	1	20111	0	4.2752	0.000215	2	4	4.2752
CAND1	1	20112	0	5.7092	0.000215	1	4	5.7092

Id = gene, neg | fdr = false discovery ratio as depleted, neg | rank = rank as depleted, neg | goodsgrna = number of significantly depleted sgRNAs, neg | lfc = log2(fold-change), pos | fdr = false discovery ratio as enriched, neg | rank = rank as enriched, pos | goodsgrna = number of significantly enriched sgRNAs, pos | lfc = log2(fold-change)

Appendix 3: Tables of significantly enriched proteins in proteomics assays

A3.1 Significantly enriched proteins in HEK293T BioID2-CRBN expressing cells vs HEK293T BioID2 expressing cells

This table shows proteins and their average enrichment (AveExpr) that are enriched only in HEK293T BioID2-expressing cells and significant for FDR (adj.P.value) < 0.05.

id	AveExpr	adj.P.Val
CRBN	18.8399704	9.38E-11
COPS7A	16.3931786	3.21E-10
NSFL1C	19.9845053	5.27E-08
TXNL1	19.1944137	1.17E-07
COPS7B	15.5245741	1.76E-07
RANBP1	19.2317052	2.12E-07
RPS27A;UBC;UBB;UBA52	21.4613571	8.19E-07
CUL4B	17.4109077	9.58E-07
HNRNPF	18.1797735	9.58E-07
DCUN1D1	14.3056801	1.15E-06
COPS3	13.9610048	1.15E-06
BTF3	19.3647048	3.70E-06
EIF4G3	18.4745671	4.84E-06
DCUN1D5	14.33796	5.70E-06
NACA	23.062221	1.43E-05
ACACB	20.4187614	1.54E-05
PSMD4	16.9500287	4.06E-05
SRP54	21.3522361	6.66E-05
CCT8	20.8411211	8.35E-05
DIS3	19.0991774	0.00011176
MCCC1	24.6245783	0.00011276
USP5	16.8186415	0.00011425
PC	26.5276818	0.00014781
PCCA	25.0669568	0.00015792
NUP98	16.4730266	0.0002656
PRDX4	17.4341985	0.00031083
ACACA	26.5797816	0.00031262
HNRNPH1	17.7698833	0.00035775
UBE2M	20.5029374	0.00041666
HDLBP	19.9284481	0.00083479
VCPIP1	16.6328878	0.00138329
HLCS	18.3021266	0.00188974
NEDD8;NEDD8-MDP1	14.9375606	0.00275803

DCUN1D4	19.2085513	0.00609573
RAN	21.2589684	0.00611033
EIF4G2	18.5471958	0.0099776
PSMD9	12.9339805	0.01111121
PIH1D1	14.3524166	0.01496445
ST13;ST13P4;ST13P5	17.0354566	0.01763157
CCNB1	14.7602573	0.01822059
NMT1	16.0574403	0.01907574
BTF3L4	15.5413244	0.02756624
ENSA	18.4158314	0.02783508
UBFD1	16.5811532	0.03634472
PPP2R5C	14.1982208	0.03905394
PDIA6	16.57145	0.04270599
RPL17;RPL17-C18orf32	16.1338795	0.04988043

A3.2 Significantly enriched proteins in OPM2-BioID2-CRBN (Experiment 1)

This table shows proteins and their average enrichment (AveExpr) whose differential enrichment across different conditions is significant for FDR (adj.P.value) < 0.2.

id	AveExpr	adj.P.Val
DVL2	20.171	0
DVL1;DVL1P1	20.205	0
IKZF1	19.47	0.008
UQCRH	15.656	0.008
RRM2	17.913	0.008
HNRNPA0	17.032	0.008
IGJ;JCHAIN	16.64	0.008
CFDP1	15.484	0.013
CTAG1A;CTAG1B	16.651	0.021
HSPA1B;HSPA1A	18.884	0.023
IKZF3	15.455	0.027
WEE1	15.442	0.03
IRAK1	15.783	0.034
PSMD8	16.861	0.05
PLAA	18.005	0.05
IMMT	17.211	0.058
G3BP2	19.194	0.058
CCT3	20.512	0.094
MATR3	14.833	0.107
ANXA7	15.377	0.111
G3BP1	20.333	0.121
EIF3C;EIF3CL	17.793	0.145
FAM208A	14.972	0.145
SUPT16H	15.032	0.145
EIF4A1	19.121	0.145
SON	14.885	0.158
ATP5B	17.315	0.158
MYH9	24.97	0.16
YWHAB	14.822	0.166
VCPIP1	19.332	0.166
UBE2O	15.383	0.166
CTTN	19.455	0.187
SRRM2	18.255	0.187

PSME1	15.401	0.199

A3.3 Significantly enriched proteins in OPM2-BioID2-CRBN (Experiment 2)

This table shows proteins and their average enrichment (AveExpr) whose differential enrichment across different conditions is significant for FDR (adj.P.value) < 0.05.

id	AveExpr	adj.P.Val
HNRNPA0	13.7666654	5.13E-19
DVL2	13.2679788	1.42E-14
DVL1;DVL1P1	12.9405192	1.50E-12
IKZF1	13.1453706	2.13E-12
MYH9	17.1711419	4.27E-12
IGJ;JCHAIN	13.6286077	8.03E-11
FLNA	15.6457322	8.03E-11
RRM2	13.2544616	1.03E-10
HSPA1A;HSPA1B	14.4239544	1.29E-09
G3BP1	15.3493486	5.57E-09
PKP2	12.6307952	5.57E-09
CHORDC1	16.3597987	2.28E-07
UBTF	12.9366595	8.52E-07
HNRNPA2B1	15.6902558	1.87E-06
RPS27A;UBC;UBB;UBA52	18.8902232	4.77E-06
RBM27	15.533873	4.77E-06
HSPH1	13.1244027	4.77E-06
CAMSAP1	12.6918223	6.50E-06
DNAJB1	16.8511538	8.01E-06
RANBP2	14.4499137	8.18E-06
CUL4A	14.2881247	8.39E-06
CSNK1A1;CSNK1A1L	12.2862572	1.73E-05
MYL6;MYL6B	11.5512078	1.87E-05
CCDC58	12.3884511	2.02E-05
HBS1L	13.9151742	3.64E-05
HSPE1	15.2756867	6.83E-05
CTTN	12.4860364	9.04E-05
MKI67	11.7078247	0.00013265
SNRNP27	13.3846411	0.00016969
DCUN1D4	12.7367234	0.00020758
NCL	15.2050165	0.00033165
HRNR	18.6741542	0.00048755
U2SURP	13.4545749	0.00052659

NPM1	15.045817	0.00067882
HDLBP	14.5432889	0.00072933
RPL18A	15.3606108	0.00091155
IMMT	12.6936798	0.00100001
EIF3C;EIF3CL	12.6189144	0.00101178
GEMIN5	13.4607597	0.00108965
RANGAP1	13.4706575	0.00108965
PNN	15.8518056	0.00108965
NACA	17.7108725	0.00121407
RUVBL2	19.5219017	0.00127809
LRMP	13.0592802	0.00131203
PCCB	14.4306668	0.00151392
VIM	16.1362371	0.00203934
MAP4	14.5219431	0.00278505
ARL6IP4	16.5808632	0.00278505
EDC4	12.6581343	0.00283043
AARS	14.9697414	0.00327602
CCT3	13.4736581	0.00327927
PRRC2C	12.8675552	0.00361316
SPTBN1	11.8682505	0.00454337
PRKDC	12.3883381	0.00454337
HNRNPC	11.851498	0.00464387
CBX3	13.3731328	0.00476425
RBBP6	12.0583516	0.00488212
NUP50	12.9501278	0.00488212
BCCIP	12.2107847	0.00488212
PLAA	12.0089394	0.00488212
CKAP5	13.3291801	0.00547992
LUC7L2	16.7281898	0.00547992
IGLL5;IGLC1;IGLC6	16.2560736	0.00592653
MCM4	13.9201079	0.00619835
HBB;HBD	12.7758049	0.00687378
PDAP1	12.934872	0.00824009
HBA1;HBA2	11.9432389	0.00861386
NUP98	13.9038861	0.00865158
CASP8	11.627165	0.00932655
GFPT1	11.5359555	0.01031406
CRBN	18.9374591	0.01050182

CGN	11.8092652	0.01155043
PTK2B	12.4605611	0.01868455
LBR	13.5153944	0.01944677
TPM4	11.2486762	0.01944677
HNRNPL	11.8405214	0.02002875
MCCC1	21.5528185	0.0233409
VCPIP1	11.8734132	0.02629867
ATIC	11.4593513	0.02825411
TIMM44	11.3009924	0.02988179
CCT8	16.8817507	0.03065346
RPS21	11.5464369	0.03234524
NSUN2	11.5332637	0.03275633
GPKOW	13.4061917	0.03423302
GSPT1	12.7199342	0.03474661
SRP68	11.4589644	0.03611015
CCT5	16.067382	0.0362544
SF3B1	13.266646	0.0362544
HIST1H2AC;HIST1H2AD;HIST2H2AA3; HIST1H2AH;HIST1H2AB;HIST3H2A; HIST2H2AC;H2AFJ;HIST1H2AJ; HIST1H2AG;H2AFV;H2AFX;H2AFZ;HIST1H2AA	14.153984	0.0362544
HSPB1	15.789497	0.03903487
DHX29	14.4897538	0.04065637
FUS;TAF15	12.9726085	0.04128655
PCCA	21.5870837	0.04128655
COPB2	12.2077136	0.04128655
RPS11	12.1861787	0.04168851
RPS15A	14.1010986	0.04168851
DDX46	14.1044299	0.04240169
NUP153	12.4620497	0.04593029
CALML5	17.8639067	0.04687507
KIAA0196	15.547307	0.0472104
FAM192A;NIP30	12.1147821	0.04958245

References

1. Palumbo, A. & Anderson, K. Multiple Myeloma. *The New England Journal of Medicine* **364**, 1046–1060 (2011).
2. Becker, N. Multiple Myeloma. 25–35 (2011) doi:10.1007/978-3-540-85772-3_2.
3. Alexander, D. D. *et al.* Multiple myeloma: A review of the epidemiologic literature. *International Journal of Cancer* **120**, 40–61 (2007).
4. Pan, S. Y., Johnson, K. C., Ugnat, A.-M., Wen, S. W. & Mao, Y. Association of Obesity and Cancer Risk in Canada. *American Journal of Epidemiology* **159**, 259–268 (2004).
5. Birmann, B. M., Giovannucci, E., Rosner, B., Anderson, K. C. & Colditz, G. A. Body Mass Index, Physical Activity, and Risk of Multiple Myeloma. *Cancer Epidemiology Biomarkers & Prevention* **16**, 1474–1478 (2007).
6. Schinasi, L. H. *et al.* Multiple myeloma and family history of lymphohaematopoietic cancers: Results from the International Multiple Myeloma Consortium. *British Journal of Haematology* **175**, 87–101 (2016).
7. Grass, S. *et al.* Association of a dominantly inherited hyperphosphorylated paraprotein target with sporadic and familial multiple myeloma and monoclonal gammopathy of undetermined significance: a case–control study. *The Lancet Oncology* **10**, 950–956 (2009).
8. Grass, S. *et al.* Paraproteins of familial MGUS/multiple myeloma target family-typical antigens: hyperphosphorylation of autoantigens is a consistent finding in familial and sporadic MGUS/MM. *Blood* **118**, 635–637 (2011).
9. Preuss, K.-D. *et al.* Hyperphosphorylation of autoantigenic targets of paraproteins is due to inactivation of PP2A. *Blood* **118**, 3340–3346 (2011).
10. Preuss, K.-D. *et al.* Sumoylated HSP90 is a dominantly inherited plasma cell dyscrasias risk factor. *Journal of Clinical Investigation* **125**, 316–323 (2014).
11. Weinhold, N. *et al.* The CCND1 c.870G>A polymorphism is a risk factor for t(11;14)(q13;q32) multiple myeloma. *Nature Genetics* **45**, 522–525 (2013).
12. Chubb, D. *et al.* Common variation at 3q26.2, 6p21.33, 17p11.2 and 22q13.1 influences multiple myeloma risk. *Nature Genetics* **45**, 1221–1225 (2013).
13. consortium, T. P. *et al.* Identification of multiple risk loci and regulatory mechanisms influencing susceptibility to multiple myeloma. *Nature Communications* **9**, 3707 (2018).
14. Wei, X. *et al.* Germline mutations in lysine specific demethylase 1 (LSD1/KDM1A) confer susceptibility to multiple myeloma. *Cancer Research* **78**, canres.1900.2017 (2018).
15. Cook, L. & Macdonald, D. H. C. Management of paraproteinaemia. *Postgraduate Medical Journal* **83**, 217–223 (2007).

16. Pandey, S. & Kyle, R. A. Unusual myelomas: A review of IgD and IgE variants. *ONCOLOGY (United States)* vol. 27 (2013).
17. Bergsagel, P. L. Where We Were, Where We Are, Where We Are Going: Progress in Multiple Myeloma. *American Society of Clinical Oncology Educational Book* 199–203 (2014) doi:10.14694/edbook_am.2014.34.199.
18. Kyle, R. A. *et al.* Prevalence of Monoclonal Gammopathy of Undetermined Significance. *New England Journal of Medicine* **354**, 1362–1369 (2006).
19. Wadhera, R. K. & Rajkumar, S. V. Prevalence of monoclonal gammopathy of undetermined significance: a systematic review. *Mayo Clinic proceedings* **85**, 933–942 (2010).
20. Rajkumar, S. V. Multiple myeloma: 2016 update on diagnosis, risk-stratification, and management. *American Journal of Hematology* **91**, 719–734 (2016).
21. Rajkumar, S. V. Multiple myeloma: 2018 update on diagnosis, risk-stratification, and management. *American Journal of Hematology* **93**, 1091–1110 (2018).
22. Palumbo, A. *et al.* Revised International Staging System for Multiple Myeloma: A Report From International Myeloma Working Group. *J Clin Oncol* **33**, 2863–2869 (2015).
23. Hari, P. N. *et al.* Is the international staging system superior to the Durie–Salmon staging system? A comparison in multiple myeloma patients undergoing autologous transplant. *Leukemia* **23**, 1528–1534 (2009).
24. Oyajobi, B. O. Multiple myeloma/hypercalcemia. *Arthritis Research & Therapy* **9**, S4 (2007).
25. Hameed, A., Brady, J. J., Dowling, P., Clynes, M. & O'Gorman, P. Bone disease in multiple myeloma: pathophysiology and management. *Cancer growth and metastasis* **7**, 33–42 (2014).
26. Weiss, G. & Goodnough, L. T. Anemia of Chronic Disease. *The New England Journal of Medicine* **352**, 1011–1023 (2005).
27. Silvestris, F., Tucci, M., Cafforio, P. & Dammacco, F. Fas-L up-regulation by highly malignant myeloma plasma cells: role in the pathogenesis of anemia and disease progression. *Blood* **97**, 1155–1164 (2001).
28. Heaney, J. L. J. *et al.* Characterisation of immunoparesis in newly diagnosed myeloma and its impact on progression-free and overall survival in both old and recent myeloma trials. *Leukemia* **32**, 1727–1738 (2018).

29. Sørrig, R. *et al.* Immunoparesis in newly diagnosed Multiple Myeloma patients: Effects on overall survival and progression free survival in the Danish population. *PLoS ONE* **12**, (2017).
30. Kyrtsonis, M.-C., Mouzaki, A. & Maniatis, A. Mechanisms of polyclonal hypogammaglobulinaemia in multiple myeloma (MM). *Medical Oncology* **16**, 73–77 (1999).
31. Fahey, J. L., Barth, W. F. & Solomon, A. Serum Hyperviscosity Syndrome. *JAMA: The Journal of the American Medical Association* **192**, 464 (1965).
32. Hutchison, C. A. *et al.* The pathogenesis and diagnosis of acute kidney injury in multiple myeloma. *Nature Reviews Nephrology* vol. 8 43–51 (2012).
33. Weinstock, M. & Ghobrial, I. M. Extramedullary multiple myeloma. *Leukemia & Lymphoma* **54**, 1135–1141 (2012).
34. Larrea, C. F. de *et al.* Plasma cell leukemia: consensus statement on diagnostic requirements, response criteria and treatment recommendations by the International Myeloma Working Group. *Leukemia* **27**, 780–791 (2012).
35. Nahi, H. *et al.* Incidence, characteristics, and outcome of solitary plasmacytoma and plasma cell leukemia. Population-based data from the Swedish Myeloma Register. *European Journal of Haematology* **99**, 216–222 (2017).
36. Caers, J. *et al.* Diagnosis, treatment, and response assessment in solitary plasmacytoma: updated recommendations from a European Expert Panel. *Journal of Hematology & Oncology* **11**, 10 (2018).
37. Rajkumar, S. V. Updated Diagnostic Criteria and Staging System for Multiple Myeloma. *American Society of Clinical Oncology educational book / ASCO. American Society of Clinical Oncology. Meeting* **35**, e418–23 (2016).
38. Oertel, M. *et al.* Impact of radiation dose on local control and survival in extramedullary head and neck plasmacytoma. *Radiation Oncology* **14**, 63 (2019).
39. Mheidly, K. *et al.* New insights in the treatment of patients with solitary bone plasmacytoma. *Leukemia & Lymphoma* **60**, 2810–2813 (2019).
40. Waal, E. G. M. de *et al.* Progression of a solitary plasmacytoma to multiple myeloma. A population-based registry of the northern Netherlands. *British Journal of Haematology* **175**, 661–667 (2016).
41. Desport, E. *et al.* AL Amyloidosis. *Orphanet Journal of Rare Diseases* **7**, 54 (2012).
42. Dember, L. M. Amyloidosis-Associated Kidney Disease. *Journal of the American Society of Nephrology* **17**, 3458–3471 (2006).

43. Busslinger, M. Transcriptional Control of Early B Cell Development1. *Annual Review of Immunology* **22**, 55–79 (2004).
44. Igarashi, H., Gregory, S. C., Yokota, T., Sakaguchi, N. & Kincade, P. W. Transcription from the RAG1 Locus Marks the Earliest Lymphocyte Progenitors in Bone Marrow. *Immunity* **17**, 117–130 (2002).
45. Meffre, E., Casellas, R. & Nussenzweig, M. C. Antibody regulation of B cell development. *Nature Immunology* **1**, 379–385 (2000).
46. Geisberger, R., Lamers, M. & Achatz, G. The riddle of the dual expression of IgM and IgD. *Immunology* **0**, 060526021554006–??? (2006).
47. Pieper, K., Grimbacher, B. & Eibel, H. B-cell biology and development. *Journal of Allergy and Clinical Immunology* **131**, 959–971 (2013).
48. Mesin, L., Ersching, J. & Victora, G. D. Germinal Center B Cell Dynamics. *Immunity* **45**, 471–482 (2016).
49. Stebegg, M. *et al.* Regulation of the Germinal Center Response. *Frontiers in Immunology* **9**, 2469 (2018).
50. Li, Z., Woo, C. J., Iglesias-Ussel, M. D., Ronai, D. & Scharff, M. D. The generation of antibody diversity through somatic hypermutation and class switch recombination. *Genes & Development* **18**, 1–11 (2004).
51. Muramatsu, M. *et al.* Class Switch Recombination and Hypermutation Require Activation-Induced Cytidine Deaminase (AID), a Potential RNA Editing Enzyme. *Cell* **102**, 553–563 (2000).
52. Sciammas, R. *et al.* Graded Expression of Interferon Regulatory Factor-4 Coordinates Isotype Switching with Plasma Cell Differentiation. *Immunity* **25**, 225–236 (2006).
53. Nutt, S. L., Taubenheim, N., Hasbold, J., Corcoran, L. M. & Hodgkin, P. D. The genetic network controlling plasma cell differentiation. *Seminars in Immunology* **23**, 341–349 (2011).
54. Dominguez-Sola, D. *et al.* The proto-oncogene MYC is required for selection in the germinal center and cyclic reentry. *Nature Immunology* **13**, 1083–1091 (2012).
55. Nutt, S. L., Hodgkin, P. D., Tarlinton, D. M. & Corcoran, L. M. The generation of antibody-secreting plasma cells. *Nature Reviews Immunology* **15**, 160–171 (2015).
56. Willis, S. N. *et al.* Transcription Factor IRF4 Regulates Germinal Center Cell Formation through a B Cell–Intrinsic Mechanism. *The Journal of Immunology* **192**, 3200–3206 (2014).

57. Ochiai, K. *et al.* Transcriptional Regulation of Germinal Center B and Plasma Cell Fates by Dynamical Control of IRF4. *Immunity* **38**, 918–929 (2013).
58. Teng, Y. *et al.* IRF4 negatively regulates proliferation of germinal center B cell-derived Burkitt's lymphoma cell lines and induces differentiation toward plasma cells. *European Journal of Cell Biology* **86**, 581–589 (2007).
59. Tarlinton, D. B-cell memory: are subsets necessary? *Nature Reviews Immunology* **6**, 785–790 (2006).
60. Shaffer, A. L. *et al.* Blimp-1 Orchestrates Plasma Cell Differentiation by Extinguishing the Mature B Cell Gene Expression Program. *Immunity* **17**, 51–62 (2002).
61. Shapiro-Shelef, M. *et al.* Blimp-1 Is Required for the Formation of Immunoglobulin Secreting Plasma Cells and Pre-Plasma Memory B Cells. *Immunity* **19**, 607–620 (2003).
62. Tellier, J. *et al.* Blimp-1 controls plasma cell function through the regulation of immunoglobulin secretion and the unfolded protein response. *Nature Immunology* **17**, 323–330 (2016).
63. Lohr, J. G. *et al.* Widespread genetic heterogeneity in multiple myeloma: implications for targeted therapy. *Cancer cell* **25**, 91–101 (2014).
64. Leung-Hagesteijn, C. *et al.* Xbp1s-Negative Tumor B Cells and Pre-Plasmablasts Mediate Therapeutic Proteasome Inhibitor Resistance in Multiple Myeloma. *Cancer Cell* **24**, 289–304 (2013).
65. Shaffer, A. L. *et al.* IRF4 addiction in multiple myeloma. *Nature* **454**, 226–231 (2008).
66. Georgopoulos, K., Moore, D. & Derfler, B. Ikaros, an early lymphoid-specific transcription factor and a putative mediator for T cell commitment. *Science* **258**, 808–812 (1992).
67. John, L. B. & Ward, A. C. The Ikaros gene family: Transcriptional regulators of hematopoiesis and immunity. *Molecular Immunology* **48**, 1272–1278 (2011).
68. Yoshida, T. & Georgopoulos, K. Ikaros fingers on lymphocyte differentiation. *International Journal of Hematology* **100**, 220–229 (2014).
69. Sun, L. *et al.* Expression of dominant-negative Ikaros isoforms in T-cell acute lymphoblastic leukemia. *Clinical Cancer Research* **5**, 2112–2120 (1999).
70. Sun, L. *et al.* Expression of dominant-negative and mutant isoforms of the antileukemic transcription factor Ikaros in infant acute lymphoblastic leukemia. *Proceedings of the National Academy of Sciences* **96**, 680–685 (1999).
71. Nakase, K. *et al.* Dominant negative isoform of the Ikaros gene in patients with adult B-cell acute lymphoblastic leukemia. *Cancer research* **60**, 4062–4065 (2000).

72. Zhang, J. *et al.* Harnessing of the nucleosome-remodeling-deacetylase complex controls lymphocyte development and prevents leukemogenesis. *Nature Immunology* **13**, 86–94 (2011).
73. Bottardi, S. *et al.* The IKAROS Interaction with a Complex Including Chromatin Remodeling and Transcription Elongation Activities Is Required for Hematopoiesis. *PLoS Genetics* **10**, e1004827 (2014).
74. Oravecz, A. *et al.* Ikaros mediates gene silencing in T cells through Polycomb repressive complex 2. *Nature Communications* **6**, 8823 (2015).
75. Koipally, J. & Georgopoulos, K. Ikaros Interactions with CtBP Reveal a Repression Mechanism That Is Independent of Histone Deacetylase Activity. *Journal of Biological Chemistry* **275**, 19594–19602 (2000).
76. Koipally, J., Renold, A., Kim, J. & Georgopoulos, K. Repression by Ikaros and Aiolos is mediated through histone deacetylase complexes. *The EMBO Journal* **18**, 3090–3100 (1999).
77. Georgopoulos, K. The making of a lymphocyte: The choice among disparate cell fates and the IKAROS enigma. *Genes and Development* vol. 31 439–450 (2017).
78. Hu, Y. *et al.* Superenhancer reprogramming drives a B-cell–epithelial transition and high-risk leukemia. *Genes & Development* **30**, 1971–1990 (2016).
79. Powell, M. D., Read, K. A., Sreekumar, B. K. & Oestreich, K. J. Ikaros Zinc Finger Transcription Factors: Regulators of Cytokine Signaling Pathways and CD4+ T Helper Cell Differentiation. *Frontiers in Immunology* **10**, 1299 (2019).
80. Thomas, R. M. *et al.* Ikaros Silences T-bet Expression and Interferon-γ Production during T Helper 2 Differentiation. *Journal of Biological Chemistry* **285**, 2545–2553 (2010).
81. Wong, L. Y., Hatfield, J. K. & Brown, M. A. Ikaros Sets the Potential for Th17 Lineage Gene Expression through Effects on Chromatin State in Early T Cell Development. *Journal of Biological Chemistry* **288**, 35170–35179 (2013).
82. Heller, J. J. *et al.* Restriction of IL-22–Producing T Cell Responses and Differential Regulation of Regulatory T Cell Compartments by Zinc Finger Transcription Factor Ikaros. *The Journal of Immunology* **193**, 3934–3946 (2014).
83. Read, K. A. *et al.* Integrated STAT3 and Ikaros Zinc Finger Transcription Factor Activities Regulate Bcl-6 Expression in CD4+ Th Cells. *The Journal of Immunology* **199**, 2377–2387 (2017).

84. Ana, C. L. de, Arakcheeva, K., Agnihotri, P., Derosia, N. & Winandy, S. Lack of Ikaros Deregulates Inflammatory Gene Programs in T Cells. *The Journal of Immunology* **202**, 1112–1123 (2019).
85. Wang, J. H. *et al.* Aiolos regulates B cell activation and maturation to effector state. *Immunity* **9**, 543–553 (1998).
86. Cortés, M. & Georgopoulos, K. Aiolos Is Required for the Generation of High Affinity Bone Marrow Plasma Cells Responsible for Long-Term Immunity. *Journal of Experimental Medicine* **199**, 209–219 (2004).
87. Hung, K.-H. *et al.* Aiolos collaborates with Blimp-1 to regulate the survival of multiple myeloma cells. *Cell Death & Differentiation* **23**, 1175–1184 (2016).
88. Ochiai, K. *et al.* Zinc finger–IRF composite elements bound by Ikaros/IRF4 complexes function as gene repression in plasma cell. *Blood Advances* **2**, 883–894 (2018).
89. Lu, G. *et al.* The Myeloma Drug Lenalidomide Promotes the Cereblon-Dependent Destruction of Ikaros Proteins. *Science* **343**, 305–309 (2014).
90. Krönke, J. *et al.* Lenalidomide Causes Selective Degradation of IKZF1 and IKZF3 in Multiple Myeloma Cells. *Science* **343**, 301–305 (2014).
91. XU, Z. *et al.* DNA Lesions and Repair in Immunoglobulin Class Switch Recombination and Somatic Hypermutation. *Annals of the New York Academy of Sciences* **1050**, 146–162 (2005).
92. Corre, J., Munshi, N. & Avet-Loiseau, H. Genetics of multiple myeloma: another heterogeneity level? *Blood* **125**, 1870–1876 (2015).
93. Corradini, P., Boccadoro, M., Voena, C. & Pileri, A. Evidence for a bone marrow B cell transcribing malignant plasma cell VDJ joined to C mu sequence in immunoglobulin (IgG)- and IgA-secreting multiple myelomas. *The Journal of Experimental Medicine* **178**, 1091–1096 (1993).
94. Taylor, B. J. *et al.* Analysis of clonotypic switch junctions reveals multiple myeloma originates from a single class switch event with ongoing mutation in the isotype-switched progeny. *Blood* **112**, 1894–1903 (2008).
95. Chesi, M. *et al.* AID-Dependent Activation of a MYC Transgene Induces Multiple Myeloma in a Conditional Mouse Model of Post-Germinal Center Malignancies. *Cancer Cell* **13**, 167–180 (2008).
96. Kuehl, W. M. & Bergsagel, P. L. Early Genetic Events Provide the Basis for a Clinical Classification of Multiple Myeloma. *ASH Education Program Book* **2005**, 346–352 (2005).

97. Walker, B. A. *et al.* Characterization of IGH locus breakpoints in multiple myeloma indicates a subset of translocations appear to occur in pregerminal center B cells. *Blood* **121**, 3413–3419 (2013).

98. Bergsagel, P. L. & Kuehl, W. M. Chromosome translocations in multiple myeloma. *Oncogene* **20**, 5611–5622 (2001).

99. Barwick, B. G., Gupta, V. A., Vertino, P. M. & Boise, L. H. Cell of Origin and Genetic Alterations in the Pathogenesis of Multiple Myeloma. *Frontiers in Immunology* **10**, 1121 (2019).

100. Jin, Y. *et al.* Active enhancer and chromatin accessibility landscapes chart the regulatory network of primary multiple myeloma. *Blood* **131**, 2138–2150 (2018).

101. Huang, M. *et al.* dbCoRC: a database of core transcriptional regulatory circuitries modeled by H3K27ac ChIP-seq signals. *Nucleic Acids Research* **46**, D71–D77 (2017).

102. Conery, A. R. *et al.* Bromodomain inhibition of the transcriptional coactivators CBP/EP300 as a therapeutic strategy to target the IRF4 network in multiple myeloma. *eLife* **5**, e10483 (2016).

103. Gabay, M., Li, Y. & Felsher, D. W. MYC Activation Is a Hallmark of Cancer Initiation and Maintenance. *Cold Spring Harbor Perspectives in Medicine* **4**, a014241 (2014).

104. Dang, C. V. MYC on the Path to Cancer. *Cell* **149**, 22–35 (2012).

105. McMahon, S. B., Buskirk, H. A. van, Dugan, K. A., Copeland, T. D. & Cole, M. D. The Novel ATM-Related Protein TRRAP Is an Essential Cofactor for the c-Myc and E2F Oncoproteins. *Cell* **94**, 363–374 (1998).

106. Liu, X., Vorontchikhina, M., Wang, Y.-L., Faiola, F. & Martinez, E. STAGA Recruits Mediator to the MYC Oncoprotein To Stimulate Transcription and Cell Proliferation. *Molecular and Cellular Biology* **28**, 108–121 (2007).

107. Kanazawa, S., Soucek, L., Evan, G., Okamoto, T. & Peterlin, B. M. c-Myc recruits P-TEFb for transcription, cellular proliferation and apoptosis. *Oncogene* **22**, 5707–5711 (2003).

108. Vervoorts, J. *et al.* Stimulation of c-MYC transcriptional activity and acetylation by recruitment of the cofactor CBP. *EMBO reports* **4**, 484–490 (2003).

109. Seoane, J., Le, H.-V. & Massagué, J. Myc suppression of the p21Cip1 Cdk inhibitor influences the outcome of the p53 response to DNA damage. *Nature* **419**, 729–734 (2002).

110. Herold, S. *et al.* Negative Regulation of the Mammalian UV Response by Myc through Association with Miz-1. *Molecular Cell* **10**, 509–521 (2002).

111. Li, Z. *et al.* A global transcriptional regulatory role for c-Myc in Burkitt's lymphoma cells. *Proceedings of the National Academy of Sciences* **100**, 8164–8169 (2003).
112. Jovanović, K. K. *et al.* Targeting MYC in multiple myeloma. *Leukemia* **32**, 1295–1306 (2018).
113. Shou, Y. *et al.* Diverse karyotypic abnormalities of the c-myc locus associated with c-myc dysregulation and tumor progression in multiple myeloma. *Proceedings of the National Academy of Sciences* **97**, 228–233 (2000).
114. Network, M. C. *et al.* MYC dysregulation in the progression of multiple myeloma. *Leukemia* 1–5 (2019) doi:10.1038/s41375-019-0543-4.
115. Holien, T., Våtsveen, T. K., Hella, H., Waage, A. & Sundan, A. Addiction to c-MYC in multiple myeloma. *Blood* **120**, 2450–2453 (2012).
116. Kumar, S. *et al.* Trisomies in multiple myeloma: impact on survival in patients with high-risk cytogenetics. *Blood* **119**, 2100–2105 (2012).
117. Pandey, S. *et al.* Impact Of FISH Abnormalities On Response To Lenalidomide In Patients With Multiple Myeloma. *Blood* **122**, 3210 (2013).
118. Decaux, O. *et al.* Prediction of Survival in Multiple Myeloma Based on Gene Expression Profiles Reveals Cell Cycle and Chromosomal Instability Signatures in High-Risk Patients and Hyperdiploid Signatures in Low-Risk Patients: A Study of the Intergroupe Francophone du Myélome. *Journal of Clinical Oncology* **26**, 4798–4805 (2008).
119. Chin, M. *et al.* Prevalence and timing of TP53 mutations in del(17p) myeloma and effect on survival. *Blood cancer journal* **7**, e610 (2017).
120. Gabrea, A., Bergsagel, P. L. & Kuehl, W. M. Distinguishing primary and secondary translocations in multiple myeloma. *DNA Repair* **5**, 1225–1233 (2006).
121. Kuehl, W. M. & Bergsagel, P. L. Molecular pathogenesis of multiple myeloma and its premalignant precursor. *Journal of Clinical Investigation* **122**, 3456–3463 (2012).
122. Dutta, A. K. *et al.* Subclonal evolution in disease progression from MGUS/SMM to multiple myeloma is characterised by clonal stability. *Leukemia* **33**, 457–468 (2018).
123. Furukawa, Y. & Kikuchi, J. Molecular pathogenesis of multiple myeloma. *International Journal of Clinical Oncology* **20**, 413–422 (2015).
124. Mikulasova, A. *et al.* The spectrum of somatic mutations in monoclonal gammopathy of undetermined significance indicates a less complex genomic landscape than that in multiple myeloma. *Haematologica* **102**, 1617–1625 (2017).
125. Samur, A. A. *et al.* Deciphering the chronology of copy number alterations in Multiple Myeloma. *Blood Cancer Journal* **9**, 39 (2019).

126. Abe, M., Hiura, K., Ozaki, S., Kido, S. & Matsumoto, T. Vicious cycle between myeloma cell binding to bone marrow stromal cells via VLA-4–VCAM-1 adhesion and macrophage inflammatory protein-1α and MIP-1β production. *Journal of Bone and Mineral Metabolism* **27**, 16–23 (2009).
127. Michigami, T. *et al.* Cell-cell contact between marrow stromal cells and myeloma cells via VCAM-1 and alpha(4)beta(1)-integrin enhances production of osteoclast-stimulating activity. *Blood* **96**, 1953–1960 (2000).
128. Fowler, J. A., Mundy, G. R., Lwin, S. T. & Edwards, C. M. Bone Marrow Stromal Cells Create a Permissive Microenvironment for Myeloma Development: A New Stromal Role for Wnt Inhibitor Dkk1. *Cancer Research* **72**, 2183–2189 (2012).
129. Yaccoby, S. *et al.* Myeloma interacts with the bone marrow microenvironment to induce osteoclastogenesis and is dependent on osteoclast activity. *British Journal of Haematology* **116**, 278–290 (2002).
130. Edwards, C. M., Zhuang, J. & Mundy, G. R. The pathogenesis of the bone disease of multiple myeloma. *Bone* **42**, 1007–1013 (2008).
131. Yaccoby, S. *et al.* Antibody-based inhibition of DKK1 suppresses tumor-induced bone resorption and multiple myeloma growth in vivo. *Blood* **109**, 2106–2111 (2006).
132. Vacca, A. & Ribatti, D. Bone marrow angiogenesis in multiple myeloma. *Leukemia* **20**, 193–199 (2005).
133. Giuliani, N., Storti, P., Bolzoni, M., Palma, B. D. & Bonomini, S. Angiogenesis and multiple myeloma. *Cancer microenvironment : official journal of the International Cancer Microenvironment Society* **4**, 325–337 (2011).
134. Rajkumar, S. V. *et al.* Bone marrow angiogenesis in 400 patients with monoclonal gammopathy of undetermined significance, multiple myeloma, and primary amyloidosis. *Clinical Cancer Research* **8**, 2210–2216 (2002).
135. Ribatti, D. & Vacca, A. New Insights in Anti-Angiogenesis in Multiple Myeloma. *International Journal of Molecular Sciences* **19**, 2031 (2018).
136. Ribatti, D., Nico, B. & Vacca, A. Importance of the bone marrow microenvironment in inducing the angiogenic response in multiple myeloma. *Oncogene* **25**, 4257–4266 (2006).
137. Panchabhai, S. *et al.* Tumor-associated macrophages and extracellular matrix metalloproteinase inducer in prognosis of multiple myeloma. *Leukemia* **30**, 951–954 (2015).

138. Veirman, K. de *et al.* Myeloid-Derived Suppressor Cells as Therapeutic Target in Hematological Malignancies. *Frontiers in Oncology* **4**, 349 (2014).
139. Moreau, P. *et al.* Multiple myeloma: ESMO Clinical Practice Guidelines for diagnosis, treatment and follow-up. *Annals of Oncology* **28**, iv52–iv61 (2017).
140. Moreau, P., Attal, M. & Facon, T. Frontline therapy of multiple myeloma. *Blood* **125**, 3076–3084 (2015).
141. Attal, M. *et al.* Lenalidomide, Bortezomib, and Dexamethasone with Transplantation for Myeloma. *New England Journal of Medicine* **376**, 1311–1320 (2017).
142. Kumar, S. K. *et al.* Multiple Myeloma, Version 3.2017, NCCN Clinical Practice Guidelines in Oncology. *Journal of the National Comprehensive Cancer Network* **15**, 230–269 (2017).
143. Korde, N. *et al.* Treatment With Carfilzomib-Lenalidomide-Dexamethasone With Lenalidomide Extension in Patients With Smoldering or Newly Diagnosed Multiple Myeloma. *JAMA Oncology* **1**, 746 (2015).
144. Sonneveld, P. *et al.* Bortezomib Induction and Maintenance Treatment in Patients With Newly Diagnosed Multiple Myeloma: Results of the Randomized Phase III HOVON-65/ GMMG-HD4 Trial. *Journal of Clinical Oncology* **30**, 2946–2955 (2012).
145. McCarthy, P. L. *et al.* Lenalidomide Maintenance After Autologous Stem-Cell Transplantation in Newly Diagnosed Multiple Myeloma: A Meta-Analysis. *Journal of clinical oncology : official journal of the American Society of Clinical Oncology* **35**, 3279–3289 (2017).
146. O'Donnell, E. K. *et al.* A phase 2 study of modified lenalidomide, bortezomib and dexamethasone in transplant-ineligible multiple myeloma. *British Journal of Haematology* **182**, 222–230 (2018).
147. Mohty, M. & Harousseau, J.-L. Treatment of autologous stem cell transplant-eligible multiple myeloma patients: ten questions and answers. *Haematologica* **99**, 408–416 (2014).
148. Hamed, R. al, Bazarbachi, A. H., Malard, F., Harousseau, J.-L. & Mohty, M. Current status of autologous stem cell transplantation for multiple myeloma. *Blood Cancer Journal* **9**, 44 (2019).
149. Kumar, S. K. *et al.* Improved survival in multiple myeloma and the impact of novel therapies. *Blood* **111**, 2516–2520 (2008).
150. Bjorklund, C. C. *et al.* Iberdomide (CC-220) is a potent cereblon E3 ligase modulator with antitumor and immunostimulatory activities in lenalidomide- and pomalidomide-

resistant multiple myeloma cells with dysregulated CRBN. *Leukemia* 1–5 (2019) doi:10.1038/s41375-019-0620-8.

151. Herndon, T. M. *et al.* U.S. Food and Drug Administration Approval: Carfilzomib for the Treatment of Multiple Myeloma. *Clinical Cancer Research* **19**, 4559–4563 (2013).
152. Dimopoulos, M. A. *et al.* Elotuzumab plus lenalidomide/dexamethasone for relapsed or refractory multiple myeloma: ELOQUENT-2 follow-up and post-hoc analyses on progression-free survival and tumour growth. *British Journal of Haematology* **178**, 896–905 (2017).
153. Dimopoulos, M. A. *et al.* Daratumumab, Lenalidomide, and Dexamethasone for Multiple Myeloma. *New England Journal of Medicine* **375**, 1319–1331 (2016).
154. Palumbo, A. *et al.* Daratumumab, Bortezomib, and Dexamethasone for Multiple Myeloma. *The New England Journal of Medicine* **375**, 754–766 (2016).
155. Lokhorst, H. M. *et al.* Targeting CD38 with Daratumumab Monotherapy in Multiple Myeloma. *The New England Journal of Medicine* **373**, 1207–1219 (2015).
156. Fedele, P. L. *et al.* IMiDs through loss of Ikaros and Aiolos primes myeloma cells for daratumumab mediated killing by upregulation of CD38. *Blood* **132**, 2166–2178 (2018).
157. Martin, T. *et al.* A phase 1b study of isatuximab plus lenalidomide and dexamethasone for relapsed/refractory multiple myeloma. *Blood* **129**, 3294–3303 (2017).
158. Richardson, P. G. *et al.* Isatuximab plus pomalidomide/dexamethasone versus pomalidomide/dexamethasone in relapsed/refractory multiple myeloma: ICARIA Phase III study design. *Future Oncology* **14**, 1035–1047 (2018).
159. Trudel, S. *et al.* Targeting B-cell maturation antigen with GSK2857916 antibody–drug conjugate in relapsed or refractory multiple myeloma (BMA117159): a dose escalation and expansion phase 1 trial. *The Lancet Oncology* **19**, 1641–1653 (2018).
160. Tai, Y.-T. *et al.* Novel anti-B-cell maturation antigen antibody-drug conjugate (GSK2857916) selectively induces killing of multiple myeloma. *Blood* **123**, 3128–3138 (2014).
161. Hipp, S. *et al.* A novel BCMA/CD3 bispecific T-cell engager for the treatment of multiple myeloma induces selective lysis in vitro and in vivo. *Leukemia* **31**, 1743–1751 (2016).
162. Cho, S.-F. *et al.* Anti-BCMA BiTE® AMG 701 Potently Induces Specific T Cell Lysis of Human Multiple Myeloma (MM) Cells and Immunomodulation in the Bone Marrow Microenvironment. *Blood* **132**, 592 (2018).

163. Topp, M. S. *et al.* Evaluation of AMG 420, an anti-BCMA bispecific T-cell engager (BiTE) immunotherapy, in R/R multiple myeloma (MM) patients: Updated results of a first-in-human (FIH) phase I dose escalation study. *Journal of Clinical Oncology* **37**, 8007 (2019).
164. San-Miguel, J. F. *et al.* Panobinostat plus bortezomib and dexamethasone versus placebo plus bortezomib and dexamethasone in patients with relapsed or relapsed and refractory multiple myeloma: a multicentre, randomised, double-blind phase 3 trial. *The Lancet Oncology* **15**, 1195–1206 (2014).
165. Chari, A. *et al.* A phase 2 study of panobinostat with lenalidomide and weekly dexamethasone in myeloma. *Blood Advances* **1**, 1575–1583 (2017).
166. Touzeau, C., Maciag, P., Amiot, M. & Moreau, P. Targeting Bcl-2 for the treatment of multiple myeloma. *Leukemia* **32**, 1899–1907 (2018).
167. Leisch, M., Egle, A. & Greil, R. Plitidepsin: a potential new treatment for relapsed/refractory multiple myeloma. *Future Oncology* **15**, 109–120 (2019).
168. Aplidin (plitidepsin) is a novel anti-myeloma agent with potent anti-resorptive activity mediated by direct effects on osteoclasts. *Oncotarget* **10**, 2709–2721 (2019).
169. Mitsiades, C. S. *et al.* Aplidin, a Marine Organism-Derived Compound with Potent Antimyeloma Activity In vitro and In vivo. *Cancer Research* **68**, 5216–5225 (2008).
170. Raje, N. *et al.* Anti-BCMA CAR T-Cell Therapy bb2121 in Relapsed or Refractory Multiple Myeloma. *New England Journal of Medicine* **380**, 1726–1737 (2019).
171. Rajkumar, S. V. & Kumar, S. Multiple Myeloma: Diagnosis and Treatment. *Mayo Clinic Proceedings* **91**, 101–119 (2016).
172. Group, M. T. C. Combination chemotherapy versus melphalan plus prednisone as treatment for multiple myeloma: an overview of 6,633 patients from 27 randomized trials. Myeloma Trialists' Collaborative Group. *Journal of Clinical Oncology* **16**, 3832–3842 (1998).
173. Attal, M. *et al.* A Prospective, Randomized Trial of Autologous Bone Marrow Transplantation and Chemotherapy in Multiple Myeloma. *New England Journal of Medicine* **335**, 91–97 (1996).
174. Franks, M. E., Macpherson, G. R. & Figg, W. D. Thalidomide. *The Lancet* **363**, 1802–1811 (2004).
175. Jørgensen, M. B., Kristensen, H. K. & Buch, N. H. Thalidomide-induced Aplasia of The Inner Ear. *The Journal of Laryngology & Otology* **78**, 1095–1101 (1964).
176. Mellin, G. W. & Katzenstein, M. The Saga of Thalidomide. *New England Journal of Medicine* **267**, 1238–1244 (1962).

177. Lenz, W. & Knapp, K. Thalidomide Embryopathy. *Archives of Environmental Health: An International Journal* **5**, 14–19 (1962).
178. Vargesson, N. Thalidomide-induced teratogenesis: History and mechanisms. *Birth Defects Research Part C: Embryo Today: Reviews* **105**, 140–156 (2015).
179. Fratta, I. D., Sigg, E. B. & Maiorana, K. Teratogenic effects of thalidomide in rabbits, rats, hamsters, and mice. *Toxicology and Applied Pharmacology* **7**, 268–286 (1965).
180. Teo, S. K. *et al.* Thalidomide in the treatment of leprosy. *Microbes and Infection* **4**, 1193–1202 (2002).
181. D'Amato, R. J., Loughnan, M. S., Flynn, E. & Folkman, J. Thalidomide is an inhibitor of angiogenesis. *Proceedings of the National Academy of Sciences* **91**, 4082–4085 (1994).
182. Singhal, S. *et al.* Antitumor Activity of Thalidomide in Refractory Multiple Myeloma. *New England Journal of Medicine* **341**, 1565–1571 (1999).
183. Rajkumar, S. V., Blood, E., Vesole, D., Fonseca, R. & Greipp, P. R. Phase III Clinical Trial of Thalidomide Plus Dexamethasone Compared With Dexamethasone Alone in Newly Diagnosed Multiple Myeloma: A Clinical Trial Coordinated by the Eastern Cooperative Oncology Group. *Journal of Clinical Oncology* **24**, 431–436 (2006).
184. Facon, T. *et al.* Melphalan and prednisone plus thalidomide versus melphalan and prednisone alone or reduced-intensity autologous stem cell transplantation in elderly patients with multiple myeloma (IFM 99–06): a randomised trial. *The Lancet* **370**, 1209–1218 (2007).
185. Gay, F. *et al.* Lenalidomide plus dexamethasone versus thalidomide plus dexamethasone in newly diagnosed multiple myeloma: a comparative analysis of 411 patients. *Blood* **115**, 1343–1350 (2009).
186. Richardson, P. G. *et al.* Pomalidomide, bortezomib, and dexamethasone for patients with relapsed or refractory multiple myeloma previously treated with lenalidomide (OPTIMISMM): a randomised, open-label, phase 3 trial. *The Lancet Oncology* **20**, 781–794 (2019).
187. List, A. *et al.* Lenalidomide in the Myelodysplastic Syndrome with Chromosome 5q Deletion. *New England Journal of Medicine* **355**, 1456–1465 (2006).
188. Ghobrial, I. M. & Rajkumar, S. V. Management of thalidomide toxicity. *The journal of supportive oncology* vol. 1 194–205 (2003).
189. Petrucci, M., Cesini, L. & Grammatico, S. Managing treatment-related peripheral neuropathy in patients with multiple myeloma. *Blood and Lymphatic Cancer: Targets and Therapy* **Volume 6**, 37–47 (2016).

190. Richardson, P. G. *et al.* Immunomodulatory drug CC-5013 overcomes drug resistance and is well tolerated in patients with relapsed multiple myeloma. *Blood* **100**, 3063–3067 (2002).
191. Raedler, L. A. Pomalyst (Pomalidomide) Received a New Indication for Patients with Relapsed and/or Refractory Multiple Myeloma. *American health & drug benefits* **9**, 111–4 (2016).
192. Giagounidis, A. *et al.* Practical recommendations on the use of lenalidomide in the management of myelodysplastic syndromes. *Annals of hematology* **87**, 345–352 (2008).
193. Li, S. *et al.* IMiD compounds affect CD34+ cell fate and maturation via CRBN-induced IKZF1 degradation. *Blood Advances* **2**, 492–504 (2018).
194. Liu, A. *et al.* Immunomodulatory drugs downregulate IKZF1 leading to expansion of hematopoietic progenitors with concomitant block of megakaryocytic maturation. *Haematologica* **103**, haematol.2018.188227 (2018).
195. Accaoui, R. el, Shamseddeen, W. & Taher, A. Thalidomide and thrombosis. *Thrombosis and Haemostasis* **97**, 1031–1036 (2007).
196. Hirsh, J. Risk of Thrombosis With Lenalidomide and Its Prevention With Aspirin. *Chest* **131**, 275–277 (2007).
197. Lopez-Girona, A. *et al.* Lenalidomide downregulates the cell survival factor, interferon regulatory factor-4, providing a potential mechanistic link for predicting response. *British Journal of Haematology* **154**, 325–336 (2011).
198. K. Gandhi, A. *et al.* Dexamethasone Synergizes with Lenalidomide to Inhibit Multiple Myeloma Tumor Growth, But Reduces Lenalidomide-Induced Immunomodulation of T and NK Cell Function. *Current Cancer Drug Targets* **10**, 155–167 (2010).
199. Mitsiades, N. *et al. Apoptotic signaling induced by immunomodulatory thalidomide analogs in human multiple myeloma cells: therapeutic implications*. https://ashpublications.org/blood/article-pdf/99/12/4525/1686185/h81202004525.pdf (2002).
200. Mitsiades, N. *et al.* Biologic sequelae of nuclear factor–κB blockade in multiple myeloma: therapeutic applications. *Blood* **99**, 4079–4086 (2002).
201. Bolzoni, M. *et al.* Immunomodulatory drugs lenalidomide and pomalidomide inhibit multiple myeloma-induced osteoclast formation and the RANKL/OPG ratio in the myeloma microenvironment targeting the expression of adhesion molecules. *Experimental Hematology* **41**, 387–397.e1 (2013).

202. Yabu, T. *et al.* Thalidomide-induced antiangiogenic action is mediated by ceramide through depletion of VEGF receptors, and is antagonized by sphingosine-1-phosphate. *Blood* **106**, 125–134 (2005).
203. Luisi, A. de *et al.* Lenalidomide Restrains Motility and Overangiogenic Potential of Bone Marrow Endothelial Cells in Patients with Active Multiple Myeloma. *Clinical Cancer Research* **17**, 1935–1946 (2011).
204. Lu, L. *et al.* The anti-cancer drug lenalidomide inhibits angiogenesis and metastasis via multiple inhibitory effects on endothelial cell function in normoxic and hypoxic conditions. *Microvascular Research* **77**, 78–86 (2009).
205. Geitz, H., Handt, S. & Zwingenberger, K. Thalidomide selectively modulates the density of cell surface molecules involved in the adhesion cascade. *Immunopharmacology* **31**, 213–221 (1996).
206. Henry, J. Y. *et al.* Enhanced cross-priming of naive CD8 + T cells by dendritic cells treated by the IMiDs ® immunomodulatory compounds lenalidomide and pomalidomide. *Immunology* **139**, 377–385 (2013).
207. Neuber, B. *et al.* Lenalidomide Enhances Antigen-Specific Activity and Decreases CD45RA Expression of T Cells from Patients with Multiple Myeloma. *The Journal of Immunology* **187**, 1047–1056 (2011).
208. Galustian, C. *et al.* The anti-cancer agents lenalidomide and pomalidomide inhibit the proliferation and function of T regulatory cells. *Cancer Immunology, Immunotherapy* **58**, 1033–1045 (2008).
209. Neuber, B. *et al.* Lenalidomide overcomes the immunosuppression of regulatory CD8+CD28- T-cells. *Oncotarget* **8**, 98200–98214 (2017).
210. Lagrue, K., Carisey, A., Morgan, D. J., Chopra, R. & Davis, D. M. Lenalidomide augments actin remodeling and lowers NK-cell activation thresholds. *Blood* **126**, 50–60 (2015).
211. Hsu, A. K. *et al.* The immunostimulatory effect of lenalidomide on NK-cell function is profoundly inhibited by concurrent dexamethasone therapy. *Blood* **117**, 1605–1613 (2011).
212. Wu, L. *et al.* Lenalidomide Enhances Natural Killer Cell and Monocyte-Mediated Antibody-Dependent Cellular Cytotoxicity of Rituximab-Treated CD20 + Tumor Cells. (2008) doi:10.1158/1078-0432.CCR-07-4405.
213. Otáhal, P. *et al.* Lenalidomide enhances antitumor functions of chimeric antigen receptor modified T cells. *OncoImmunology* **5**, e1115940 (2016).

214. Wang, X. *et al.* Lenalidomide enhances the function of CS1 chimeric antigen receptor redirected T cells against multiple myeloma. *Clinical Cancer Research* **24**, clincanres.0344.2017 (2017).
215. Higgins, J. J., Hao, J., Kosofsky, B. E. & Rajadhyaksha, A. M. Dysregulation of large-conductance Ca2+-activated K+ channel expression in nonsyndromal mental retardation due to a cereblon p.R419X mutation. *neurogenetics* **9**, 219–223 (2008).
216. Ito, T. *et al.* Identification of a Primary Target of Thalidomide Teratogenicity. *Science* **327**, 1345–1350 (2010).
217. Zhu, Y. X. *et al.* Cereblon expression is required for the antimyeloma activity of lenalidomide and pomalidomide. *Blood* **118**, 4771–4779 (2011).
218. Heintel, D. *et al.* High expression of cereblon (CRBN) is associated with improved clinical response in patients with multiple myeloma treated with lenalidomide and dexamethasone. *British Journal of Haematology* **161**, 695–700 (2013).
219. Kortüm, K. M. *et al.* Targeted sequencing of refractory myeloma reveals a high incidence of mutations in CRBN and Ras pathway genes. (2016) doi:10.1182/blood-2016-02-698092.
220. Jones, J. R. *et al.* Clonal evolution in myeloma: The impact of maintenance lenalidomide and depth of response on the genetics and sub-clonal structure of relapsed disease in uniformly treated newly diagnosed patients. *Haematologica* **104**, 1440–1450 (2019).
221. Gooding, S. *et al.* Multiple cereblon genetic changes are associated with acquired resistance to lenalidomide or pomalidomide in multiple myeloma. *Blood* **137**, 232–237 (2021).
222. Varshavsky, A. Regulated protein degradation. in *Trends in Biochemical Sciences* vol. 30 283–286 (Elsevier, 2005).
223. Goldberg, A. L. Protein degradation and protection against misfolded or damaged proteins. *Nature* vol. 426 895–899 (2003).
224. Ye, Y. & Rape, M. Building ubiquitin chains: E2 enzymes at work. *Nature Reviews Molecular Cell Biology* **10**, 755–764 (2009).
225. Fischer, E. S. *et al.* Structure of the DDB1–CRBN E3 ubiquitin ligase in complex with thalidomide. *Nature* **512**, 49–53 (2014).
226. Petroski, M. D. & Deshaies, R. J. Function and regulation of cullin–RING ubiquitin ligases. *Nature Reviews Molecular Cell Biology* **6**, 9–20 (2005).
227. Fischer, E. S. *et al.* The Molecular Basis of CRL4DDB2/CSA Ubiquitin Ligase Architecture, Targeting, and Activation. *Cell* **147**, 1024–1039 (2011).

228. Licht, J. D., Shortt, J. & Johnstone, R. From Anecdote to Targeted Therapy: The Curious Case of Thalidomide in Multiple Myeloma. *Cancer Cell* **25**, 9–11 (2014).
229. Eisenmann, K. M. *et al.* 5q- myelodysplastic syndromes: Chromosome 5q genes direct a tumor-suppression network sensing actin dynamics. *Oncogene* vol. 28 3429–3441 (2009).
230. Krönke, J. *et al.* Lenalidomide induces ubiquitination and degradation of CK1α in del(5q) MDS. *Nature* **523**, 183–188 (2015).
231. Eichner, R. *et al.* Immunomodulatory drugs disrupt the cereblon-CD147-MCT1 axis to exert antitumor activity and teratogenicity. *Nature Medicine* **22**, 735–743 (2016).
232. Muramatsu, T. JB Review Basigin (CD147), a multifunctional transmembrane glycoprotein with various binding partners Takashi Muramatsu*. doi:10.1093/jb/mvv127.
233. Petzold, G., Fischer, E. S. & Thomä, N. H. Structural basis of lenalidomide-induced CK1α degradation by the CRL4CRBN ubiquitin ligase. *Nature* **532**, 127–130 (2016).
234. Petzold, G., Fischer, E. S. & Thomä, N. H. Structural basis of lenalidomide-induced CK1α degradation by the CRL4 CRBN ubiquitin ligase. *Nature* **532**, 127–130 (2016).
235. Chamberlain, P. P. *et al.* Structure of the human Cereblon-DDB1-lenalidomide complex reveals basis for responsiveness to thalidomide analogs. *Nature Structural and Molecular Biology* **21**, 803–809 (2014).
236. Sievers, Q. L. *et al.* Defining the human C2H2 zinc finger degrome targeted by thalidomide analogs through CRBN. *Science* **362**, eaat0572 (2018).
237. Fink, E. C. *et al.* CrbnI391V is sufficient to confer in vivo sensitivity to thalidomide and its derivatives in mice. *Blood* **132**, 1535–1544 (2018).
238. Gemechu, Y. *et al.* Humanized cereblon mice revealed two distinct therapeutic pathways of immunomodulatory drugs. *Proceedings of the National Academy of Sciences* **115**, 201814446 (2018).
239. Sievers, Q. L., Gasser, J. A., Cowley, G. S., Fischer, E. S. & Ebert, B. L. Genome-wide screen identifies cullin-RING ligase machinery required for lenalidomide-dependent CRL4CRBN activity. *Blood* **132**, 1293–1303 (2018).
240. Liu, J. *et al.* A genome-scale CRISPR-Cas9 screening in myeloma cells identifies regulators of immunomodulatory drug sensitivity. *Leukemia* **33**, 171–180 (2019).
241. Shalem, O. *et al.* Genome-scale CRISPR-Cas9 knockout screening in human cells. *Science* **343**, 84–87 (2014).

242. Cope, G. A. & Deshaies, R. J. COP9 signalosome: A multifunctional regulator of SCF and other cullin-based ubiquitin ligases. *Cell* vol. 114 663–671 (2003).
243. Petroski, M. D. & Deshaies, R. J. Mechanism of Lysine 48-Linked Ubiquitin-Chain Synthesis by the Cullin-RING Ubiquitin-Ligase Complex SCF-Cdc34. *Cell* **123**, 1107–1120 (2005).
244. Enchev, R. I., Schulman, B. A. & Peter, M. Protein neddylation: Beyond cullin-RING ligases. *Nature Reviews Molecular Cell Biology* vol. 16 30–44 (2015).
245. Meir, M. *et al.* The COP9 signalosome is vital for timely repair of DNA double-strand breaks. *Nucleic Acids Research* **43**, 4517–4530 (2015).
246. Chung, D. & Dellaire, G. The role of the COP9 signalosome and neddylation in DNA damage signaling and repair. *Biomolecules* **5**, 2388–2416 (2015).
247. Dubiel, D., Rockel, B., Naumann, M. & Dubiel, W. Diversity of COP9 signalosome structures and functional consequences. *FEBS Letters* vol. 589 2507–2513 (2015).
248. Chamovitz, D. A. Revisiting the COP9 signalosome as a transcriptional regulator. *EMBO Reports* **10**, 352–358 (2009).
249. Duda, D. M. *et al.* Structural Insights into NEDD8 Activation of Cullin-RING Ligases: Conformational Control of Conjugation. *Cell* **134**, 995–1006 (2008).
250. Song, T. *et al.* CRL4 antagonizes SCFFbxo7-mediated turnover of cereblon and BK channel to regulate learning and memory. *PLOS Genetics* **14**, e1007165 (2018).
251. Bjorklund, C. C. *et al.* Rate of CRL4CRBN substrate Ikaros and Aiolos degradation underlies differential activity of lenalidomide and pomalidomide in multiple myeloma cells by regulation of c-Myc and IRF4. *Blood Cancer Journal* **5**, e354–e354 (2015).
252. An, J. *et al.* PSILAC mass spectrometry reveals ZFP91 as IMiD-dependent substrate of the CRL4 CRBN ubiquitin ligase. *Nature Communications* **8**, 1–11 (2017).
253. Donovan, K. A. *et al.* Thalidomide promotes degradation of SALL4, a transcription factor implicated in Duane radial ray syndrome. *eLife* **7**, (2018).
254. Lyu, Y. L. *et al.* Topoisomerase II Mediated DNA Double-Strand Breaks: Implications in Doxorubicin Cardiotoxicity and Prevention by Dexrazoxane. *Cancer Research* **67**, 8839–8846 (2007).
255. Subramanian, A. *et al. Gene set enrichment analysis: A knowledge-based approach for interpreting genome-wide expression profiles*. www.pnas.orgcgidoi10.1073pnas.0506580102 (2005).
256. Ran, F. A. *et al.* Genome engineering using the CRISPR-Cas9 system. *Nature Protocols* **8**, 2281–2308 (2013).

257. Lampert, F. *et al.* The multi-subunit GID/CTLH E3 ligase promotes proliferation and targets the transcription factor Hbp1 for degradation. *eLife* **7**, e35528 (2018).
258. Maitland, M. E. R. *et al.* The mammalian CTLH complex is an E3 ubiquitin ligase that targets its subunit muskelin for degradation. *Scientific Reports* **9**, (2019).
259. Rodríguez-Navarro, S. Insights into SAGA function during gene expression. *EMBO Reports* vol. 10 843–850 (2009).
260. Ramachandran, S. *et al.* The SAGA Deubiquitination Module Promotes DNA Repair and Class Switch Recombination through ATM and DNAPK-Mediated γH2AX Formation. *Cell Reports* **15**, 1554–1565 (2016).
261. Madabhushi, R. The roles of DNA topoisomerase IIβ in transcription. *International Journal of Molecular Sciences* vol. 19 (2018).
262. Chen, S. H., Chan, N.-L. & Hsieh, T. New Mechanistic and Functional Insights into DNA Topoisomerases. *Biochemistry* **82**, 139–170 (2013).
263. Nitiss, J. L. DNA topoisomerase II and its growing repertoire of biological functions. *Nature Reviews Cancer* **9**, 327–337 (2009).
264. Ju, B.-G. *et al.* A Topoisomerase IIß-Mediated dsDNA Break Required for Regulated Transcription. *Science* **312**, 1798–1802 (2006).
265. Roy, S. *et al.* Redefining the transcriptional regulatory dynamics of classically and alternatively activated macrophages by deepCAGE transcriptomics. *Nucleic Acids Research* **43**, 6969–6982 (2015).
266. Kim, Y. *et al.* The MEF2D transcription factor mediates stress-dependent cardiac remodeling in mice. *Journal of Clinical Investigation* **118**, 124–132 (2008).
267. Feliciano, Y. M. S. *et al.* PHF6 regulates phenotypic plasticity through chromatin organization within lineage-specific genes. *Genes and Development* **31**, 973–989 (2017).
268. Bobbs, A. *et al.* ARID3B directly regulates ovarian cancer promoting genes. *PLoS ONE* **10**, (2015).
269. Hulea, L. & Nepveu, A. CUX1 transcription factors: From biochemical activities and cell-based assays to mouse models and human diseases. *Gene* vol. 497 18–26 (2012).
270. Poss, Z. C., Ebmeier, C. C. & Taatjes, D. J. The Mediator complex and transcription regulation. *Critical Reviews in Biochemistry and Molecular Biology* vol. 48 575–608 (2013).
271. Derwish, R., Paterno, G. D. & Gillespie, L. L. Differential HDAC1 and 2 Recruitment by Members of the MIER Family. *PLOS ONE* **12**, e0169338 (2017).

272. Yang, S. *et al.* ANP32B deficiency impairs proliferation and suppresses tumor progression by regulating AKT phosphorylation. *Nature Publishing Group* **7**, (2016).
273. Jiang, L. *et al.* Identification and experimental validation of G protein alpha inhibiting activity polypeptide 2 (GNAI2) as a microRNA-138 target in tongue squamous cell carcinoma. *Human Genetics* **129**, 189–197 (2011).
274. Tcherkezian, J. *et al.* Proteomic analysis of cap-dependent translation identifies LARP1 as a key regulator of 5'TOP mRNA translation. *Genes and Development* **28**, 357–371 (2014).
275. Tuorto, F. *et al.* RNA cytosine methylation by Dnmt2 and NSun2 promotes tRNA stability and protein synthesis. *Nature Structural and Molecular Biology* **19**, 900–905 (2012).
276. Cappellini, M. D. & Fiorelli, G. *Seminar Glucose-6-phosphate dehydrogenase defi ciency*. *www.thelancet.com* vol. 371 www.thelancet.com (2008).
277. Meyers, R. M. *et al.* Computational correction of copy number effect improves specificity of CRISPR-Cas9 essentiality screens in cancer cells. *Nature Genetics* **49**, 1779–1784 (2017).
278. Brinkman, E. K., Chen, T., Amendola, M. & van Steensel, B. Easy quantitative assessment of genome editing by sequence trace decomposition. *Nucleic Acids Research* **42**, 168 (2014).
279. Gurova, K. New hopes from old drugs: Revisiting DNA-binding small molecules as anticancer agents. *Future Oncology* vol. 5 1685–1704 (2009).
280. Karpinich, N. O., Tafani, M., Rothman, R. J., Russo, M. A. & Farber, J. L. The Course of Etoposide-induced Apoptosis from Damage to DNA and p53 Activation to Mitochondrial Release of Cytochrome c*. (2002) doi:10.1074/jbc.M110629200.
281. Burma, S., Chen, B. P., Murphy, M., Kurimasa, A. & Chen, D. J. ATM Phosphorylates Histone H2AX in Response to DNA Double-strand Breaks. *Journal of Biological Chemistry* **276**, 42462–42467 (2001).
282. Jirkovský, E. *et al.* Pharmacokinetics of the Cardioprotective Drug Dexrazoxane and Its Active Metabolite ADR-925 with Focus on Cardiomyocytes and the Heart. *Journal of Pharmacology and Experimental Therapeutics* **364**, 433–446 (2017).
283. Gandhi, A. K. *et al.* Measuring cereblon as a biomarker of response or resistance to lenalidomide and pomalidomide requires use of standardized reagents and understanding of gene complexity. *British Journal of Haematology* **164**, 233–244 (2013).

284. Ianevski, A., He, L., Aittokallio, T. & Tang, J. SynergyFinder: a web application for analyzing drug combination dose-response matrix data. doi:10.1093/bioinformatics/btx162.

285. Klemm, S. L., Shipony, Z. & Greenleaf, W. J. Chromatin accessibility and the regulatory epigenome. doi:10.1038/s41576-018-0089-8.

286. Savitski, M. M. *et al.* Multiplexed Proteome Dynamics Profiling Reveals Mechanisms Controlling Protein Homeostasis. *Cell* **173**, 260-274.e25 (2018).

287. Maity, R. *et al.* Cereblon (CRBN) Splice Isoform Lacking Exon 10 Attenuates Lenalidomide-Mediated Degradation of Aiolos and Is Upregulated in Immunomodulatory Drugs (IMiDs) Resistant Myeloma (MM) Patients. *Blood* **124**, 639–639 (2014).

288. Ménard, A. *et al.* Cereblon (CRBN) Splicing Could Influence Response To IMiDs : A New PCR Strategy to Easily Detect and Semi-Quantify Loss Of The IMiDs Binding Domain. *Blood* **122**, 3107–3107 (2013).

289. Dimopoulos, K. *et al.* Dual inhibition of DNMTs and EZH2 can overcome both intrinsic and acquired resistance of myeloma cells to IMiDs in a cereblon-independent manner. *Molecular Oncology* **12**, 180–195 (2018).

290. Easwaran, H., Tsai, H. C. & Baylin, S. B. Cancer Epigenetics: Tumor Heterogeneity, Plasticity of Stem-like States, and Drug Resistance. *Molecular Cell* vol. 54 716–727 (2014).

291. Prior, I. A., Lewis, P. D. & Mattos, C. A Comprehensive Survey of Ras Mutations in Cancer. (2012) doi:10.1158/0008-5472.CAN-11-2612.

292. Zhang, L., Tai, Y. T., Ho, M. Z. G., Qiu, L. & Anderson, K. C. Interferon-alpha-based immunotherapies in the treatment of B cell-derived hematologic neoplasms in today's treat-to-target era. *Experimental Hematology and Oncology* vol. 6 20 (2017).

293. Friedman, R. L. & Stark, G. R. α-interferon-induced transcription of HLA and metallothionein genes containing homologous upstream sequences. *Nature* **314**, 637–639 (1985).

294. Keskinen, P., Ronni, T., Matikainen, S., Lehtonen, A. & Julkunen, I. Regulation of HLA class I and II expression by interferons and influenza A virus in human peripheral blood mononuclear cells. *Immunology* **91**, 421–429 (1997).

295. Herzog, V. A. *et al.* Thiol-linked alkylation of RNA to assess expression dynamics. *Nature Methods* **14**, 1198–1204 (2017).

296. Natsume, T., Kiyomitsu, T., Saga, Y. & Kanemaki, M. T. Rapid Protein Depletion in Human Cells by Auxin-Inducible Degron Tagging with Short Homology Donors. *Cell Reports* **15**, 210–218 (2016).

297. Cavadini, S. *et al.* Cullin-RING ubiquitin E3 ligase regulation by the COP9 signalosome. *Nature* **531**, 598–603 (2016).

298. Yamamoto, H. *et al.* NCoR1 is a conserved physiological modulator of muscle mass and oxidative function. *Cell* **147**, 827–839 (2011).

299. Uusküla-Reimand, L. *et al.* Topoisomerase II beta interacts with cohesin and CTCF at topological domain borders. *Genome Biology* **17**, 182 (2016).

300. Bunch, H. *et al.* Transcriptional elongation requires DNA break-induced signalling. *Nature Communications* **6**, 1–12 (2015).

301. Canela, A. *et al.* Topoisomerase II-Induced Chromosome Breakage and Translocation Is Determined by Chromosome Architecture and Transcriptional Activity. *Molecular Cell* **75**, 252–266.e8 (2019).

302. Wiseman, L. R. & Spencer, C. M. Dexrazoxane. A review of its use as a cardioprotective agent in patients receiving anthracycline-based chemotherapy. *Drugs* vol. 56 385–403 (1998).

303. Wei, S. *et al.* Lenalidomide promotes p53 degradation by inhibiting MDM2 auto-ubiquitination in myelodysplastic syndrome with chromosome 5q deletion. *Oncogene* **32**, 1110–1120 (2012).

304. Zhou, L. & Xu, G. Cereblon attenuates DNA damage-induced apoptosis by regulating the transcription-independent function of p53. *Cell Death and Disease* **10**, 1–13 (2019).

305. Palumbo, A. *et al.* Second primary malignancies with lenalidomide therapy for newly diagnosed myeloma: A meta-analysis of individual patient data. *The Lancet Oncology* **15**, 333–342 (2014).

306. Schroeder, P. E., Davidson, J. N. & Hasinoff, B. B. Dihydroorotase catalyzes the ring opening of the hydrolysis intermediates of the cardioprotective drug dexrazoxane (ICRF-187). *Drug Metabolism and Disposition* **30**, 1431–1435 (2002).

307. Roux, K. J., Kim, D. I., Raida, M. & Burke, B. A promiscuous biotin ligase fusion protein identifies proximal and interacting proteins in mammalian cells. *Journal of Cell Biology* **196**, 801–810 (2012).

308. Kim, D. I. *et al.* An improved smaller biotin ligase for BioID proximity labeling. *Molecular Biology of the Cell* **27**, 1188–1196 (2016).

309. Roux, K. J., Kim, D. I., Burke, B. & May, D. G. BioID: A Screen for Protein-Protein Interactions. *Current Protocols in Protein Science* **91**, 19.23.1-19.23.15 (2018).
310. Gibson, D. G. *et al.* Enzymatic assembly of DNA molecules up to several hundred kilobases. *Nature Methods* **6**, 343–345 (2009).
311. Lazar, C., Gatto, L., Ferro, M., Bruley, C. & Burger, T. Accounting for the Multiple Natures of Missing Values in Label-Free Quantitative Proteomics Data Sets to Compare Imputation Strategies. *Journal of Proteome Research* **15**, 1116–1125 (2016).
312. Tong, L. Structure and function of biotin-dependent carboxylases. *Cellular and Molecular Life Sciences* vol. 70 863–891 (2013).
313. Jitrapakdee, S. *et al.* Structure, mechanism and regulation of pyruvate carboxylase. *Biochemical Journal* vol. 413 369–387 (2008).
314. Mitsiades, N. *et al.* Molecular sequelae of proteasome inhibition in human multiple myeloma cells. *Proceedings of the National Academy of Sciences* **99**, 14374–14379 (2002).
315. Lin, Y. H. *et al.* LIMCH1 regulates nonmuscle myosin-II activity and suppresses cell migration. *Molecular Biology of the Cell* **28**, 1054–1065 (2017).
316. Pecci, A., Ma, X., Savoia, A. & Adelstein, R. S. MYH9: Structure, functions and role of non-muscle myosin IIA in human disease. *Gene* vol. 664 152–167 (2018).
317. Protter, D. S. W. & Parker, R. Principles and Properties of Stress Granules. *Trends in Cell Biology* vol. 26 668–679 (2016).
318. Ivanov, P., Kedersha, N. & Anderson, P. Stress Granules and Processing Bodies in Translational Control. *Cold Spring Harbor Perspectives in Biology* **11**, a032813 (2019).
319. Youn, J. Y. *et al.* High-Density Proximity Mapping Reveals the Subcellular Organization of mRNA-Associated Granules and Bodies. *Molecular Cell* **69**, 517-532.e11 (2018).
320. Amen, T. & Kaganovich, D. Stress granules sense metabolic stress at the plasma membrane and potentiate recovery by storing active Pkc1. *Science Signaling* **13**, (2020).
321. Aulas, A. *et al.* G3BP1 promotes stress-induced RNA granule interactions to preserve polyadenylated mRNA. *Journal of Cell Biology* **209**, 73–84 (2015).
322. Kido, K. *et al.* Airid, a novel proximity biotinylation enzyme, for analysis of protein–protein interactions. *eLife* **9**, (2020).
323. Sebastian, S. *et al.* Multiple myeloma cells' capacity to decompose H2O2 determines lenalidomide sensitivity. *Blood* **129**, 991–1007 (2017).
324. Sopko, R. *et al.* Mapping pathways and phenotypes by systematic gene overexpression. *Molecular Cell* **21**, 319–330 (2006).

325. Hideshima, T. *et al. The Proteasome Inhibitor PS-341 Inhibits Growth, Induces Apoptosis, and Overcomes Drug Resistance in Human Multiple Myeloma Cells 1*. *CANCER RESEARCH* vol. 61 (2001).

326. Sabatier, P., Saei, A. A., Wang, S. & Zubarev, R. A. Dynamic Proteomics Reveals High Plasticity of Cellular Proteome: Growth-Related and Drug-Induced Changes in Cancer Cells are Comparable. *Proteomics* **18**, (2018).

327. Branon, T. C. *et al.* Efficient proximity labeling in living cells and organisms with TurboID. *Nature Biotechnology* **36**, 880–898 (2018).

328. Clevers, H. Wnt/β-Catenin Signaling in Development and Disease. *Cell* **127**, 469–480 (2006).

329. Qiang, Y.-W. *et al.* Myeloma-derived Dickkopf-1 disrupts Wnt-regulated osteoprotegerin and RANKL production by osteoblasts: a potential mechanism underlying osteolytic bone lesions in multiple myeloma. *Blood* **112**, 196–207 (2008).

330. Qiang, Y.-W., Shaughnessy, J. D. & Yaccoby, S. Wnt3a signaling within bone inhibits multiple myeloma bone disease and tumor growth. *Blood* **112**, 374–382 (2008).

331. Creyghton, M. P. *et al.* Histone H3K27ac separates active from poised enhancers and predicts developmental state. *Proceedings of the National Academy of Sciences of the United States of America* **107**, 21931–21936 (2010).

332. Udeshi, N. D., Mertins, P., Svinkina, T. & Carr, S. A. Large-scale identification of ubiquitination sites by mass spectrometry. *Nature Protocols* **8**, 1950–1960 (2013).

333. Xu, G. & Jaffrey, S. R. Proteomic identification of protein ubiquitination events. *Biotechnology and Genetic Engineering Reviews* **29**, 73–109 (2013).

334. Fan, Z. *et al.* CDK13 cooperates with CDK12 to control global RNA polymerase II processivity. *Science Advances* **6**, eaaz5041 (2020).

335. Woerner, A. C. *et al.* Cytoplasmic protein aggregates interfere with nucleocytoplasmic transport of protein and RNA. *Science* **351**, 173–176 (2016).

336. Dermit, M., Dodel, M. & Mardakheh, F. K. Methods for monitoring and measurement of protein translation in time and space. *Molecular BioSystems* vol. 13 2477–2488 (2017).

337. Chang, C. te, Bercovich, N., Loh, B., Jonas, S. & Izaurralde, E. The activation of the decapping enzyme DCP2 by DCP1 occurs on the EDC4 scaffold and involves a conserved loop in DCP1. *Nucleic Acids Research* **42**, 5217–5233 (2014).

338. Gray, R. S., Roszko, I. & Solnica-Krezel, L. Planar Cell Polarity: Coordinating Morphogenetic Cell Behaviors with Embryonic Polarity. *Developmental Cell* vol. 21 120–133 (2011).

339. Zhang, L. *et al.* A lateral signalling pathway coordinates shape volatility during cell migration. *Nature Communications* **7**, (2016).

340. Kelley, M. J., Jawien, W., Ortel, T. L. & Korczak, J. F. Mutation of MYH9, encoding non-muscle myosin heavy chain A, in May-Hegglin anomaly. *Nature Genetics* **26**, 106–108 (2000).

341. Gekas, C. *et al.* Mef2C is a lineage-restricted target of Scl/Tall and regulates megakaryopoiesis and B-cell homeostasis. *Blood* **113**, 3461–3471 (2009).

342. Fournier, M. J., Gareau, C. & Mazroui, R. The chemotherapeutic agent bortezomib induces the formation of stress granules. *Cancer Cell International* **10**, 12 (2010).

343. Winter, G. E. *et al.* Phthalimide conjugation as a strategy for in vivo target protein degradation. *Science* **348**, 1376–1381 (2015).

344. Patil, A., Manzano, M. & Gottwein, E. CK1a and IRF4 are essential and independent effectors of immunomodulatory drugs in primary effusion lymphoma. *Blood* **132**, 577–586 (2018).

345. Hu, Y. *et al.* CSNK1α1 mediates malignant plasma cell survival. *Leukemia* **29**, 474–482 (2015).

346. Manni, S. *et al.* Inactivation of CK1α in multiple myeloma empowers drug cytotoxicity by affecting AKT and ß-catenin survival signaling pathways. *Oncotarget* **8**, 14604–14619 (2017).

347. Fionda, C. *et al.* The IMiDs targets IKZF-1/3 and IRF4 as novel negative regulators of NK cell-activating ligands expression in multiple myeloma. *Oncotarget* **6**, 23609–23630 (2015).

348. Buettner, F. *et al.* Computational analysis of cell-to-cell heterogeneity in single-cell RNA-sequencing data reveals hidden subpopulations of cells. *Nature Biotechnology* **33**, 155–160 (2015).

349. Jaitin, D. A. *et al.* Massively parallel single-cell RNA-seq for marker-free decomposition of tissues into cell types. *Science* **343**, 776–779 (2014).

350. Chen, S. *et al.* Genome-wide CRISPR screen in a mouse model of tumor growth and metastasis. *Cell* **160**, 1246–1260 (2015).

351. Canela, A. *et al.* Genome Organization Drives Chromosome Fragility. *Cell* **170**, 507–521.e18 (2017).

352. Sharma, S. *et al.* Involvement of Hepcidin in the Anemia of Multiple Myeloma. *Clinical Cancer Research* **14**, 3262–3267 (2008).

353. Bjorklund, C. C. *et al.* Evidence of a role for activation of Wnt/β-catenin signaling in the resistance of plasma cells to lenalidomide. *Journal of Biological Chemistry* **286**, 11009–11020 (2011).

354. Steele, B. M. *et al.* WNT-3a modulates platelet function by regulating small GTPase activity. *FEBS Letters* **586**, 2267–2272 (2012).

355. Steele, B. M. *et al.* Canonical Wnt signaling negatively regulates platelet function. *Proceedings of the National Academy of Sciences of the United States of America* **106**, 19836–19841 (2009).

356. Zhang, Y. K. *et al.* WNT signaling underlies the pathogenesis of neuropathic pain in rodents. *Journal of Clinical Investigation* **123**, 2268–2286 (2013).

357. Kleiger, G. & Mayor, T. Perilous journey: a tour of the ubiquitin–proteasome system. *Trends in Cell Biology* **24**, 352–359 (2014).